SYNTHESIS, STUDY, AND CATALYSIS OF NEW DIMETHYL-PHOSPHINE LIGANDS

by

ALEXANDER JACOB KENDALL

A DISSERTATION

Presented to the Department of Chemistry and Biochemistry
and the Graduate School of the University of Oregon
in partial fulfillment of the requirements
for the degree of
Doctor of Philosophy

March 2016

DISSERTATION APPROVAL PAGE

Student: Alexander Jacob Kendall

Title: Synthesis, Study, and Catalysis of New Dimethyl-Phosphine Ligands

This dissertation has been accepted and approved in partial fulfillment of the requirements for the Doctor of Philosophy degree in the Department of Chemistry and Biochemistry by:

Shannon Boettcher	Chairperson
David R. Tyler	Advisor
Victoria DeRose	Core Member
Mark Reed	Institutional Representative

and

Scott L. Pratt	Dean of the Graduate School

Original approval signatures are on file with the University of Oregon Graduate School.

Degree awarded March 2016

DISSERTATION ABSTRACT

Alexander Jacob Kendall

Doctor of Philosophy

Department of Chemistry and Biochemistry

March 2016

Title: Synthesis, Study, and Catalysis of New Dimethyl-Phosphine Ligands

Two new general synthetic routes to phosphines were developed. The first method described directly converts phosphonates to phosphine oxides using organometallic nucleophiles. This reaction proceeds through a five-coordinate phosphorus intermediate. The second synthetic method uses a deprotonated secondary phosphine oxide for nucleophilic addition to an alkyl halide to form a tertiary phosphine oxide. This reaction proceeds through a standard S_N2 mechanism, however in extreme cases a competitive electron transfer reaction was observed.

These syntheses were used to make a new dimethyl phosphine (MeJPhos). This phosphine was used as a ligand for metal complexes and compared against a series of structurally related (JohnPhos) phosphines. MeJPhos was found to be the strongest electron donor in the series MeJPhos, EtJPhos, ^{i}PrJPhos, CyJPhos, and ^{t}BuJPhos.

These ligands were then used to study structural effects of ligands on Buchwald-Hartwig cross-coupling catalysis. It was found that only ^{t}BuJPhos performed catalytically. This observation is likely due to the smaller steric profile of the other JohnPhos ligands. Specifically, it is the inability to perform the reductive elimination step of the catalytic cycle that prevents turnover.

Ozonolysis was used to oxidize alkenes to aldehydes directly. Typically with ozonolysis, a secondary ozonide is formed as the product that must be chemically reacted in a subsequent step. By trapping out the immediate chemical precursor to the secondary ozonide with water, the formation of secondary ozonides was avoided. This method produced aldehydes directly from aryl alkenes in good to excellent yields.

This dissertation includes previously published and unpublished coauthored material.

CURRICULUM VITAE

NAME OF AUTHOR: Alexander Jacob Kendall

GRADUATE AND UNDERGRADUATE SCHOOLS ATTENDED:

University of Oregon, Eugene OR
Western Washington University, Bellingham WA

DEGREES AWARDED:

Doctor of Philosophy, Chemistry, 2016, University of Oregon
Master of Science, Chemistry, 2011, University of Oregon
Bachelor of Science, Chemistry, 2010, Western Washington University

AREAS OF SPECIAL INTEREST:

Organophosphorus synthesis
Inorganic Chemistry
Organometallic Chemistry
Small Molecule Catalysis

PROFESSIONAL EXPERIENCE:

Teaching Assistant for University of Oregon Materials Science Institute Masters Organic Synthesis and Organometallic Laboratory

Teaching Assistant for the University of Oregon Organic and General Chemistry Laboratory

GRANTS, AWARDS, AND HONORS:

National Science Foundation Graduate Research Fellowship (2011-2016)

"Synthesis of Triply Chiral Phosphine Ligands." ACS Petroleum Research Fund ND. 2014-2016.

PUBLICATIONS:

"Steric and Electronic Influences of Buchwald-Type Alkyl JohnPhos Ligands." Kendall, A. J.; Zakharov, L. N.; Tyler, D. R. Inorganic Chemistry, 2016, in press, 10.1021/acs.inorgchem.5b02996.

"Highly efficient biphasic ozonolysis of alkenes using a high-throughput film-shear flow reactor." Kendall, A.J., Barry, J. T.; Seidenkranz, D. T.; Ryerson, A.; Hiatt, C.; Salazar, C. A.; Bryant, D. J.; Tyler, D. R. Tetrahedron Letters, 2016, 57, 1342-1345.

"Heteroleptic Organophosphine Synthesis." Kendall, A. J. and Professor David R. Tyler. Dalton Transactions, 2015, 44 (28), 12473-12483.

"Direct Conversion of Phosphonates to Phosphine Oxides: An Improved Synthetic Route to Phosphines Including the First Synthesis of Methyl JohnPhos." Kendall, A. J.; Salazar, C. A.; Martino, P. F.; Tyler, D. R. Organometallics, 2014, 33 (21), pp 6171–6178.

"Nitrogen Activation." Tyler, D. R.; Balesdent, C. G.; Kendall, A. J. In Comprehensive Inorganic Chemistry II (Second Edition); Reedijk, J.; Poeppelmeier, K., Eds.; Elsevier: Amsterdam, 2013; pp. 525–552.

"Synthesis and Stabilization of a Monomeric Iron(II) Hydroxo Complex via Intramolecular Hydrogen Bonding in the Secondary Coordination Sphere." Kendall, A. J.; Zakharov, L. N.; Gilbertson, J. D. Inorg. Chem., 2010, 49 (19), pp 8656–8658.

ACKNOWLEDGMENTS

I would like to express my greatest gratitude and appreciation for the love and support of my amazing wife, Brittany M. Sadro. Without her support through graduate school and parenthood, I would have fallen into shadow. I would also like to acknowledge Professor David R. Tyler for his support and guidance throughout the last 6 years. In addition, special thanks are due to Dr. Alec Brown and Justin Barry whose insight and ideas were always available. I also thank the undergraduates and graduate students I've had the pleasure to work with. I would like to acknowledge the National Science Foundation (NSF) Research Experiences for Undergraduates program, the NSF Graduate Research Fellowship (DGE-8029517), the Donors of the American Chemical Society Petroleum Research Fund (ACS PRF 53962-ND3), The University of Oregon Graduate School, and the University of Oregon Material Science Institute for financial support.

Dedicated to Leonard Nimoy: Live long and prosper.

TABLE OF CONTENTS

Chapter Page

I. A REVIEW OF THE MODERN SYNTHETIC ROUTES TO HETEROLEPTIC PHOSPHINES 1

1.1. Introduction 1

1.2. Heteroleptic Phosphine Synthesis 6

1.3. Looking Forward 25

1.4. Summary 26

1.5. Notes 27

1.6. Coauthored Material 27

1.7. Bridge 28

II. THE DIRECT CONVERSION OF PHOSPHONATES TO PHOSPHONATES TO PHOSPHINE OXIDES: AN IMPROVED SYNTHETIC ROUTE TO PHOSPHINES INCLUDING THE FIRST SYNTHESIS OF METYL JOHNPHOS 30

2.1. Introduction 30

2.2. Results and Discussion 33

2.3. Conclusions 47

2.4. Experimental Section 47

2.5. Summary 54

2.6. Bridge 55

III. IMPROVED GENERAL SYNTHETIC ROUTE TO ALKYL-DIMETHYLPHOSPHINES 56

Chapter Page

3.1. Introduction 56

3.2. Results and Discussion 57

3.3. Conclusions 65

3.4. Experimental 65

3.5. Summary 71

3.6. Notes 71

3.7. Bridge 72

IV. STERIC AND ELECTRONIC INFLUENCES OF BUCHWALD-TYPE ALKYL-JOHNPHOS LIGANDS 73

4.1. Introduction 73

4.2. Results and Discussion 75

4.3. Conclusions 97

4.4. Experimental Section 99

4.5. Summary 109

4.6. Notes 110

4.7. Bridge 110

V. BUCHWALD-HARTWIG CROSS-COUPLING CATALYSIS OF PALLADIUM-JOHNPHOS COMPLEXES 111

5.1. Introduction 111

5.2. Results and Discussion 112

5.3. Conclusions 131

5.4. Experimental 133

Chapter Page

5.5. Summary 134

5.6. Bridge 135

VI. OTHER SYNTHESES, DATA, AND REACTIONS 136

6.1. Introduction 136

6.2. Highly Efficient Biphasic Ozonolysis of Alkenes Using a High-Throughput Film-Shear Flow Reactor 136

6.3. Iron-Phosphine Complexes for Nanoparticle Coordination 146

6.4. Nickel DMeOPrPE Complexes for PNNL Collaboration 156

6.5. Summary 158

6.6. Concluding Summary 160

APPENDICES 161

A. SUPPORTING INFORMATION FOR CHAPTER II 161

B. SUPPORTING INFORMATION FOR CHAPTER III 296

C. SUPPORTING INFORMATION FOR CHAPTER IV 335

D. SUPPORTING INFORMATION FOR CHAPTER V 355

E. SUPPORTING INFORMATION FOR CHAPTER VI 367

F. TABULATED CRYSTALLOGRAPHIC DATA 390

REFERENCES CITED 513

LIST OF FIGURES

Figure Page

1.1. Examples of (a) classic heteroleptic phosphines and (b) designer heteroleptic phosphines 2

1.2. Nomenclature for common organophosphorus species relevant to the synthesis of heteroleptic phosphines 4

1.3. Definition of the three general types of phosphines: a) homoleptic, b) heteroleptic, and c) asymmetric. Examples are shown in the boxes 5

2.1. A Buchwald-type phosphine 31

2.2. ^{1}H NMR observed signals in select regions for (a) MeMgCl and (b) MeMgBr reacting with PhP(O)(OMe)$_2$ in THF-d_8 36

3.1. General scheme showing how H-phosphonate and H-phosphine oxide can form a phosphinite anion and subsequently, a tertiary phosphine oxide 58

3.2. ^{31}P{^{1}H} NMR overlay showing crude reaction mixtures after SPO deprotonation and EtI quench 59

3.3. Deprotonation of SPO to form the intermediate phosphinite anion followed by reaction with an electrophile to a tertiary phosphine oxide (^{31}P{^{1}H} NMR shifts noted) 64

4.1. (a) Buchwald-type ligand structural features and their proposed effects on the palladium complex and catalytic properties for cross-coupling reactions. (b) The mechanism of Buchwald-Hartwig cross-coupling 74

Figure Page

4.2. Structures, names, and abbreviated names of the R-JohnPhos ligands studied in this report 75

4.3. ORTEP crystal structure of MeJPhos (all H atoms refined)..... 76

4.4. Time-resolved infrared spectroscopy of the carbonyl region for photolysis of $Cr^0(CO)_6$ in THF solution with (a) ^{t}BuJPhos, (b) CyJPhos, (c) ^{i}PrJPhos, (d) EtJPhos, and (e) MeJPhos 79

4.5. Relative percent σ-donating and π-accepting data for $Cr^0(CO)_5$(R-JohnPhos) complexes 82

4.6. ORTEP crystal structure of *trans*-$Cr^0(CO)_4(MeJPhos)_2$ (all H atoms refined) ... 84

4.7. Selected bond distances from crystal structure data of *trans*-$Cr^0(CO)_4(PEt_3)_2$, *trans*-$Cr^0(CO)_4(PPh_3)_2$, and *trans*-$Cr^0(CO)_4(MeJPhos)_2$..... 85

4.8. ORTEP crystal structure of $Pd^0(MeJPhos)_2(\eta^2$-dba) (all H atoms refined)..... 88

4.9. Selected bond distances, bond angles, and torsion angles from crystal structure data of $Pd^0(MeJPhos)_2(\eta^2$-dba), $Pd^0(PCy_3)_2(\eta^2$-dba), and $Pd^0(PPh_3)_2(\eta^2$-dba)..... 89

4.10. ORTEP crystal structures of (a) *trans*-$Pd^{II}(Cl)_2(MeJPhos)_2$ (all H atoms refined), and (b) *trans*-$Pd^{II}(Cl)_2(^i$PrJPhos)$_2$ (all H atoms refined)..... 90

4.11. Phosphorus-palladium bond distances from crystal structure data for 16 representative phosphines..... 92

4.12. Structural and geometric parameters defining the symmetric deformation coordinate (S4') 93

Figure Page

4.13. Phosphorus S4' values from crystal structure data for 16 representative phosphines..... 94

4.14. Visual representation of the $\%V_{bur}$ steric calculation..... 95

4.15. $\%V_{bur}$ calculations from crystal structure data for 16 representative phosphines..... 97

5.1. Buchwald-Hartwig aryl amination mechanism with catalyst properties highlighted 112

5.2. Phosphine ligands that form active catalysts with palladium to perform Buchwald-Hartwig cross-coupling 112

5.3. Preliminary rate data for scout reaction 118

5.4. (a) Rate data for Buchwald-Hartwig amination with Me-, Et-, Cy-, and ^{t}BuJPhos ligands. (b) Zoom-in of Figure..... 120

6.1. Criegee mechanism of ozonolysis showing traditional ozonolysis product pathway (top route) and the Dussault modification of *in situ* H_2O reduction 137

6.2. General setup of biphasic ozonolysis using the film-shear reactor..... 138

6.3. Resonance stabilization of aryl conjugated carbonyl oxide..... 143

6.4. TEM of PbS (oleic acid capped) after attempted exchange of ligand shell with *trans*-$FeCl_2$(DpPSMePE)$_2$ 150

LIST OF TABLES

Table Page

1.1. H-Phosphonate reaction with Grignard reagents to form either H-phosphine oxides or heteroleptic phosphine oxides 20

2.1. Organometallic reagent screening 34

2.2. Sodium salt screen for halogen abstraction 37

2.3. Leaving group study for phenylphosphonate derivatives 38

2.4. Alkyl phosphonate study and Grignard reagent study 39

2.5. Aryl phosphonate study 40

2.6. Reaction of PhP(O)(OMe)Me and MeMgCl with reaction additives 43

3.1. Reaction scope of deprotonated SPOs for nucleophilic substitution 59

3.2. Reaction scope of alkyl halides and triflates for nucleophilic substitution 60

3.3. Bidentate phosphine oxide pre-ligand synthesis 63

4.1. Assigned CO stretches and force constants for the $Cr^{0}(CO)_{5}$(R-JohnPhos) complexes 80

4.2. Relative σ-donating and π-accepting ability of the R-JohnPhos ligands using the Graham treatment 80

4.3. Crystallographic Data for Me-JohnPhos 101

4.4. Crystallographic Data for *trans*-$Cr^{0}(CO)_{4}(MeJPhos)_{2}$ 104

4.5. Crystallographic Data for *trans*-$Pd^{II}(Cl)_{2}(MeJPhos)_{2}$ 105

Table Page

4.6. Crystallographic Data for *trans*-$Pd^{II}(Cl)_2(^{i}PrJPhos)_2$ 107

4.7. Crystallographic Data for $Pd^{0}(MeJPhos)_2(\eta^2\text{-dba})$ 108

5.1. Preliminary Suzuki cross-coupling catalysis 115

5.2. Preliminary Buchwald-Hartwig amination catalysis 117

5.3. Competitive cross-coupling screening for Me-, Cy-, and ^{t}BuJPhos 128

5.4. Preliminary Buchwald-Hartwig amination catalysis 129

5.5. Pd(0)$(MeJPhos)_2(\eta^2\text{-dba})$ catalysis 130

5.6. cis-Pd(II)$(TMEDA)Cl_2$ and MeJPhos catalysis 132

6.1. Gram/multi-gram scale ozonolysis of aryl alkenes 140

6.2. Product distributions for ozonolysis of aryl alkenes 141

6.3. Screening conditions for alkyl olefin ozonolysis 142

6.4. Crystallographic Data for 1,2-bis(bis(4-(methylthio)phenyl)phosphino)ethane (DpPSMePE) 152

6.5. Crystallographic Data for 1,2-bis(bis(4-(methylthio)phenyl)phosphineborane)-ethane $(DpPSMePE(BH_3)_2)$ 153

6.6. Crystallographic Data for $(\mu\text{-DpPSMePE-}\kappa P{:}\kappa P')_2(FeCl_2)_2$ 154

6.7. Crystallographic Data for trans-$FeCl_2(DpPSMePE)_2$ 155

LIST OF SCHEMES

Scheme Page

1.1. Generation of heteroleptic phosphine precursors from PCl_3 using amine protecting groups to achieve selective stoichiometry. M-R = organometallic nucleophile 9

1.2. Common conditions for unintended dehydrocoupling during a) generation of a phosphide intermediate and b) reduction of phosphonates 10

1.3. Generation of a phosphide dianion as an intermediate in the synthesis of a heteroleptic phosphine 11

1.4. An example of how the generation of a phosphide from PH_3 will selectively make secondary phosphines 12

1.5. Fluoride-induced desilylation of a silylphosphine to generate a phosphide, which undergoes a two-step reaction to generate a complex heteroleptic phosphine in a one-pot reaction 13

1.6. Silyl-modified Michaelis-Arbuzov reaction of $P(OEt)_3$ with an alkyl bromide .. 14

1.7. Radical chain mediated hydrophosphination of a P-H bond across an alkene. ... 15

1.8. An example of Buchwald-Hartwig-type Pd-catalyzed cross-coupling of an aryl chloride with a secondary phosphine..... 16

1.9. Indirect conversion of a phosphonate to a phosphine oxide going through a phosphonic dichloride intermediate 18

Scheme Page

1.10. Direct conversion of a phosphonate to a phosphine oxide showing the proposed intermediates to (top) coordination salt oligomers in the presence of halides and (bottom) a phosphine oxide in the absence of halides 19

1.11. H-Phosphine oxides as nucleophiles for alkene conjugated carbonyls showing a) zinc-mediated Michael addition to the alkene and b) calcium-mediated direct carbonyl addition 22

1.12. Phosphine oxide α-methyl carbanion generation for C-C bond formation β to the phosphorus 23

1.13. Mn(III)-mediated radical acetoxyphosphorylation of alkenes with both H-phosphine oxides and H-phosphonates 23

1.14. An example of Pd-catalyzed cross-coupling of an aryl halide with a secondary P(V) species 24

2.1. Synthetic routes from phosphonates to heteroleptic phosphines 32

2.2. Proposed steps and intermediates in the side reaction of $PhP(O)(OMe)_2$ with Grignard reagents 36

2.3. Theoretical stepwise double-displacement mechanism of phosphonate conversion to phosphine oxide 41

2.4. Proposed reaction pathway for the reaction of phosphonates with Grignard reagents 45

Scheme Page

2.5. a) Synthesis of dppp using the phosphonate to phosphine oxide single step reaction as the key step (*isolated as the mono-hydrate.) b) Synthesis of Methyl JohnPhos, a new Buchwald-type ligand 46

3.1. Electron transfer mechanism, favoring di-*tert*-butylphosphinic bromide formation over standard S_N2 products 65

4.1. *In situ* synthesis of $Cr^0(CO)_5PR_3$ species (boxed for clarity) also showing a secondary carbonyl expulsion leading to *trans*-$Cr^0(CO)_4(PR_3)_2$ 78

5.1. General reaction for synthesis of JohnPhos palladacycle 122

5.2. General reaction for synthesis of $Pd^0(RJPhos)_2(\eta^2\text{-dba})$ complex 123

5.3. Synthesis of Pd(0)(RJPhos)(η^2-dba)-type species with ^{t}BuJPhos (top) and MeJPhos (bottom) ligands 124

5.4. Buchwald precatalyst synthesis 125

5.5. Proposed mechanism of Buchwald precatalyst synthesis from Scheme 5.4 126

5.6. Synthesis towards pseudo-halide Buchwald precatalyst 127

6.1. Synthesis of DpPSMePE ligand 147

6.2. Synthesis of *trans*-$FeCl_2(DpPSMePE)_2$ and (μ-DpPSMePE-$\kappa P:\kappa P')_2(FeCl_2)_2$ complexes 148

6.3. Attempted synthesis of a hydride complex from *trans*-$FeCl_2(DpPSMePE)_2$ 148

6.4. Attempted coordination of *trans*-$FeCl_2(DpPSMePE)_2$ to PbS nanoparticle 149

CHAPTER I

A REVIEW OF THE MODERN SYNTHETIC ROUTES TO HETEROLEPTIC PHOSPHINES

1.1. Introduction

The challenging nature of phosphine chemistry has thwarted the development of new phosphine ligands. In consequence, phosphine syntheses remain virtually unchanged after nearly a century of research.[1-3] It is astounding how little progress has been made in the development of new phosphine syntheses when contrasted with the importance of phosphines in modern inorganic chemistry. This situation is changing, however, because a revival of research in organophosphine synthesis has recently begun, bringing with it the promise of new inorganic complexes, catalysts,[4] materials,[5] medicinal compounds,[6] and organic reagents.[7–9]

Since their discovery in 1847[10,11] and their development throughout the first half of the 20th century, phosphines have established themselves as an essential class of ligands for organometallic and inorganic chemistry. Twentieth century inorganic chemists identified phosphines as superb ligands for transition metals and exploited them to great effect. Phosphine-metal complexes have been the fulcrum for an astounding number of influential processes and studies that have shaped chemistry and the world today.[12,13]

Early phosphine syntheses were hindered by the exceptional air-sensitivity of alkyl phosphines and a general lack of air-free techniques. By the mid-20th century, a rigorous set of air-free protocols was standard in inorganic laboratories and the synthesis

of phosphines developed into standardized procedures.[13] Aryl phosphines, usually triphenyl phosphine (PPh_3), became commonplace as ligands owing to their air-stability and ease of synthesis.

Phosphine chemistry entered a golden age during the 1960's through 1980's when classics were established in the field. Exemplary phosphines that emerged out of this era include 1,2-bis(diphenylphosphino)ethane (dppe)[14], 1,1'-bis(diphenylphosphino)ferrocene (dppf)[15], and 2,2'-bis(diphenylphosphino)-1,1'-binaphthalene (BINAP)[16] (Figure 1.1a). Of late, the application of phosphines has seen a resurgence with modern "designer" phosphines[‡] that display complex or chiral architecture such as 4,5-bis(diphenylphosphino)-9,9-dimethylxanthene (Xantphos),[17] (*S*)-1-[(R_P)-2-(dicyclohexylphosphino)ferrocenyl]ethyldicyclohexylphosphine (Josi-Phos),[18] and 2-dicyclohexylphosphino-2′,6′-dimethoxybiphenyl **(**SPhos)[19] (Figure 1.1b).

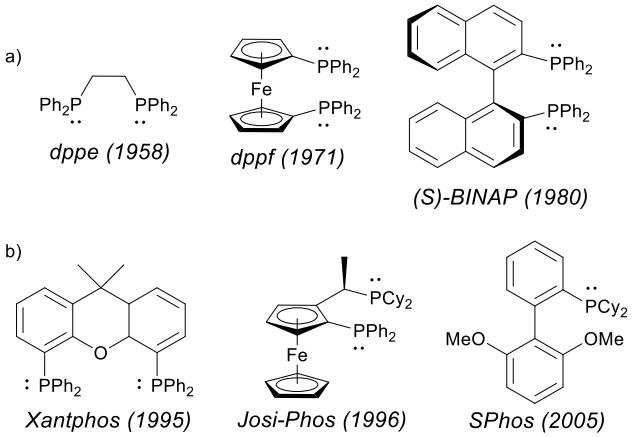

Figure 1.1. Examples of (a) classic heteroleptic phosphines and (b) designer heteroleptic phosphines.

The power of designer phosphines is nicely illustrated by Pd-catalyzed cross-coupling reactions in which designer phosphines are often required to form active

catalytic Pd(0) complexes.[20] The identity of the phosphine ligand can change what products are formed in a reaction by changing the catalytic cycle. For example, PCy_3 forms $(L)_2Pd(0)$ complexes and stabilizes Pd(0/II) oxidation states, while P^tBu_3 forms lower coordination number catalytic complexes $(LPd(I)X)_2$ and LPd(0) and stabilizes Pd(0/I) oxidation states. The different coordination modes and oxidation states for these complexes change the cross-coupling chemoselectivity.[21] Proutiere *et al.* showed that the hybrid heteroleptic phosphine $P(^tBu)_2(^iPr)$ forms $(LPd(I)X)_2$, LPd(0), and $L_2Pd(0)$ complexes, which allows modulation of chemoselectivity based on how many equivalents of ligand are used.[22,23] The ability to design a phosphine for directed influence at a metal center in a tailored fashion is a key advent in inorganic and organometallic chemistry. Developing new syntheses of phosphines drives these fields toward new frontiers.

This perspective will discuss synthetic strategies to make heteroleptic phosphines. Both modern and classic strategies to make heteroleptic phosphines will be assessed with a focus on modern synthetic approaches. This perspective should serve as a primer for organophosphorus chemistry and its application to phosphine syntheses.

1.1.1. Nomenclature

When discussing organophosphorus chemistry, a nomenclature is necessary to facilitate organophosphorus's many common forms. Although the nomenclature is somewhat cumbersome, it is an essential part of discussing the chemistry and is reviewed in Figure 1.2.

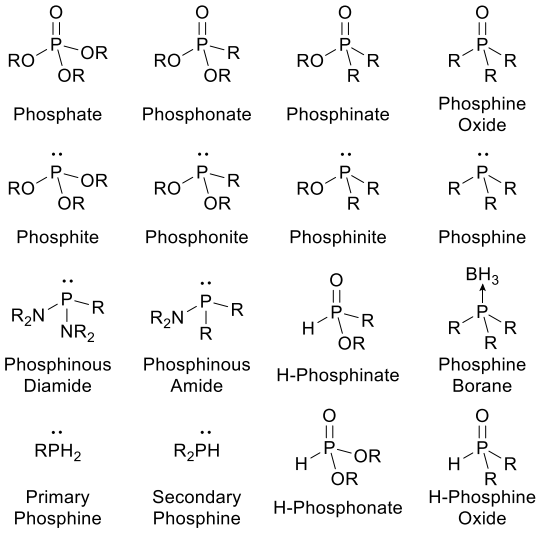

Figure 1.2. Nomenclature for common organophosphorus species relevant to the synthesis of heteroleptic phosphines.

1.1.2. Types of phosphines

For this perspective, it is helpful to divide phosphines into three categories: 1) homoleptic phosphines, 2) heteroleptic phosphines, and 3) asymmetric (or P-chiral) phosphines (Figure 1.3). Homoleptic phosphines have three identical organic substituents on phosphorus, such as PPh_3. Heteroleptic phosphines are defined as having the general structure R_2PR^1, where R and R^1 are distinct. Asymmetric phosphines have three distinct groups connected to phosphorus which, due to the large inversion barrier of a phosphine lone pair,[24] make these phosphines chiral.

Despite the severely limited architectures available with homoleptic phosphines, they are good "general-use" ligands. P- chiral phosphines are useful in asymmetric syntheses, although they are incredibly laborious to synthesize and thus generally impractical. (However, an excellent body of research has been done and is continuing on this subject.[25-27]) In contrast to homoleptic and asymmetric phosphines, heteroleptic phosphines are both synthetically accessible and tailorable. Furthermore, heteroleptic

phosphines make excellent polydentate phosphines and can also be chiral (*e.g.*, (+)-DIOP, Figure 1.2). In comparison to P-chiral phosphines, it is often easier to synthetically install controlled chirality in one of the R groups of a heteroleptic phosphine. Chiral heteroleptic phosphine syntheses can therefore take advantage of well-established main-group chemistry to achieve ligand chirality while avoiding the laborious drawbacks of a P-chiral phosphine synthesis. Overall, heteroleptic phosphines represent a ligand class that is exceptional in versatility and practicality for both synthesis and performance.[1]

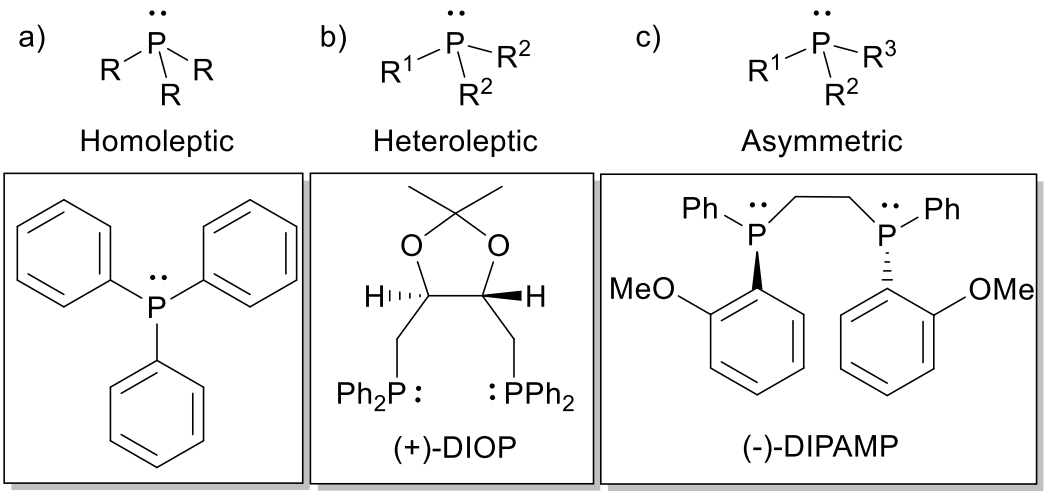

Figure 1.3. Definition of the three general types of phosphines: a) homoleptic, b) heteroleptic, and c) asymmetric. Examples are shown in the boxes below.

1.1.3. General considerations in phosphine synthesis

Phosphines have their drawbacks. Compared to most ligands, phosphines are: readily oxidized (O_2-instability), difficult to handle (they are profoundly malodorous and pyrophoric), and typically extremely difficult to purify (due to instability on silica, non-crystallinity, and very high boiling points). These qualities are more pronounced with alkyl phosphines than with aryl phosphines, which has made the synthesis and study of

aryl phosphines more attractive, even though alkyl phosphines often have more favorable properties.

The convoluted nature of phosphorus syntheses arises from several factors including stable oxidation states of III and V, multiple coordination modes (up to 6 coordinate), pseudo-rotations, radical chemistry, and lower redox potentials (*e.g.*, both dehydrocoupling and oxidation are much easier for P species than N analogues).[28,29] These factors make organophosphorus chemistry considerably more sensitive to reaction conditions than typical first-row main-group chemistry.

Syntheses can also be complicated by the Lewis basicity of phosphines. The basicity of phosphines can be tailored by changing the electronics of the substituents at phosphorus. More electron-withdrawing groups at phosphorus or π-conjugated groups increase the π-accepting ability of the phosphine, and thus decrease the σ-donating (*i.e.* basicity) ability of the phosphorus lone pair.[30-33] Alkyl phosphines are much better σ-donors and much weaker π-acceptors than aryl phosphines. Protonated tertiary phosphines typically have pK_a's from ~2 to 8,[34] making them moderately basic to acidic – something to keep in mind if using an acidic workup.

1.2. Heteroleptic phosphine synthesis

The synthesis of heteroleptic phosphines can be broken down into two general routes: those involving P(III), or trivalent phosphorus, and those involving P(V), or oxidized tetravalent phosphorus. Because P(III) species are typically air-sensitive and P(V) species are not, these two general synthetic approaches are very different. Each category is further divided into electrophilic chemistry, nucleophilic chemistry, radical

chemistry, and metal-mediated chemistry. Herein, the general strategies will be discussed in the context of their strengths and limitations based on our laboratory's experience and the recent scientific literature.

1.2.1. Phosphorus (III) syntheses

P(III) molecules are readily oxidized by molecular oxygen and most species must be handled rigorously air-free. Trivalent phosphorus species are slow to oxidize in O_2 if they are sufficiently kinetically or thermodynamically stabilized. For example, Barder *et al.* showed that sterically shielding the lone pair of phosphines kinetically slows oxidation considerably.[35] With respect to thermodynamics, oxidation of P(III) can be controlled by the lone-pair's ability to participate in O_2 chemistry. When electronegative or electron-withdrawing groups are bonded to the P(III), the basicity of the phosphine is decreased and oxidation is prevented (*e.g.*, PCl_3 and PPh_3 are O_2-stable, whereas $PhPCl_2$ and PEt_3 are not). Syntheses starting from P(III) precursors typically require air-free techniques from start to finish – increasing the time and labor required. However, the advantage of a P(III) synthesis is that a reduction step from P(V) to P(III) is not necessary.

1.2.1.1. Phosphorus(III) electrophiles

Electrophilic P(III) species are typically derived from P-Cl molecules. Trichlorophosphine (PCl_3) is a readily available starting material and relatively O_2-stable, and for these reasons it serves as a convenient starting point for most phosphine syntheses. For a heteroleptic phosphine synthesis, however, PCl_3 has significant synthetic

drawbacks. Directly generating the heteroleptic $RPCl_2$ or R_2PCl species from PCl_3 is not trivial because controlling the number of nucleophiles that will add to PCl_3 is very difficult. This lack of selectivity is likely caused by the extreme electrophilicity of P-Cl species. Even carefully selected reaction conditions still yield the desired product in a mixture. In and of itself, this would not normally be problematic except for the difficulty in isolating the product out of the mixture. To avoid this lack of selectivity, a typical work-around is to "protect" electrophilic sites with amide fragments (Scheme 1.1).[36] This approach is higher yielding but has the drawbacks of requiring several extra synthetic steps (protection/deprotection) while maintaining O_2 and H_2O free conditions for the phosphinous amide or phosphinous diamide intermediate. In addition, the purification can still be challenging.[§]

Purifications of P-Cl compounds are difficult for several reasons: 1) incompatibility with silica, 2) $RPCl_2$ and R_2PCl species are considerably more O_2 sensitive than PCl_3, and 3) incompatibility with H_2O. These compounds must therefore undergo air-free distillation for purification, typically requiring large-scale reactions (>10 grams).

1.2.1.2. Nucleophiles from trivalent phosphorus

Using nucleophiles generated from trivalent phosphorus species is another strategy for P-C bond formation. Secondary and primary phosphines are easily deprotonated by organometallic reagents (pK_a typically ~25-35)[37] to produce phosphide species (Equation 1.1). Phosphides are transient and quite nucleophilic, making this strategy good for reluctant electrophiles. Careful stoichiometry must be observed with

Scheme 1.1. Generation of heteroleptic phosphine precursors from PCl_3 using amine protecting groups to achieve selective stoichiometry. M-R = organometallic nucleophile.

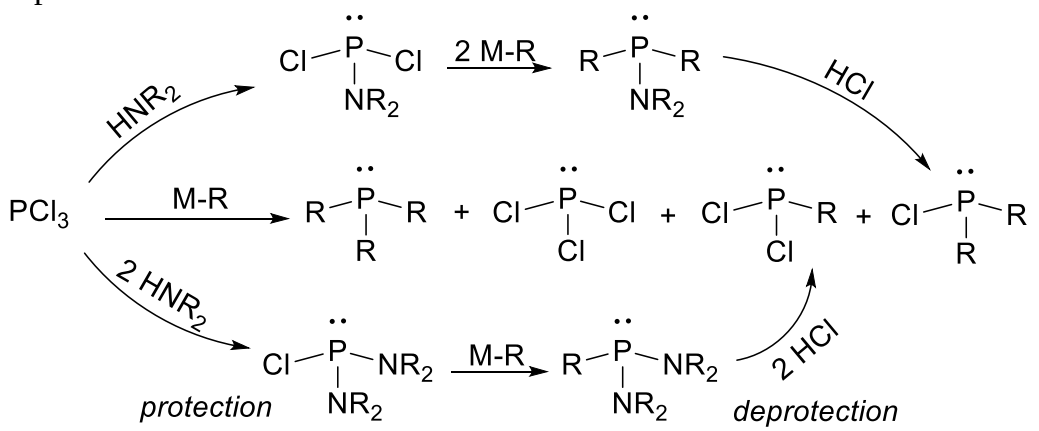

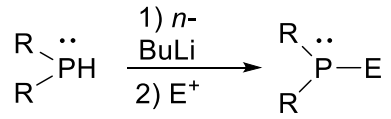

(1.1)

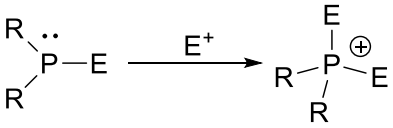

(1.2)

electrophiles using this synthetic approach or over-alkylation may occur at the phosphine lone-pair, producing the persistent and stable phosphonium species (Equation 1.2).

A side reaction that often occurs instead of phosphide anion generation is dehydrocoupling of primary or secondary phosphines (Scheme 1.2a). Under reducing conditions and in the presence of trace metals or Lewis acids, reduction of the phosphorus to a P-P bond can occur in competition with deprotonation. This is common when deprotonating either primary or secondary alkyl phosphines. Dehydrocoupling of phosphines is also common when reducing an alkyl phosphorus species (*i.e.*, an alkyl phosphonate or phosphinate) to a primary or secondary phosphine (Scheme 1.2b). The P-P species thus generated is often difficult to remove from reaction mixtures and contributes to side reactions. Dehydrocoupling can be promoted with transition metal catalysts[38] as well as strong Lewis acids.[39]

Scheme 1.2. Common conditions for unintended dehydrocoupling during a) generation of a phosphide intermediate and b) reduction of phosphonates.

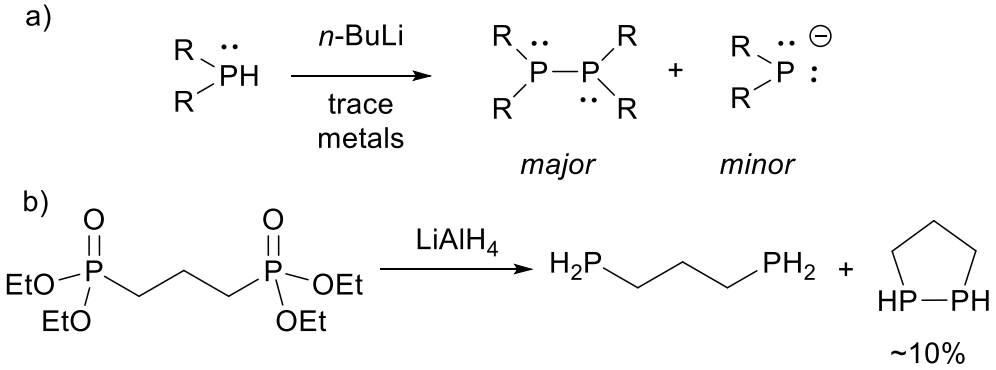

Dehydrocoupling is rarely a problem with aryl phosphines or sterically hindered phosphines. For example, Ficks *et al.* showed the binapthyl phosphine (*S*)-H-MOP can be

synthesized using a primary phosphine precursor that is notably O_2-stable (Scheme 1.3).[40] The large biaryl group allows the phosphorus di-anion to be generated as an intermediate. Though they are somewhat rare, there are several known O_2-stable primary phosphines.[41] Tertiary phosphines made from these O_2-stable primary phosphines are also typically oxygen resistant. Bulky aryl phosphines are good candidates for phosphide generation because the anions are typically more persistent and do not undergo side reactions as readily as alkyl phosphines.

Scheme 1.3. Generation of a phosphide dianion as an intermediate in the synthesis of a heteroleptic phosphine.

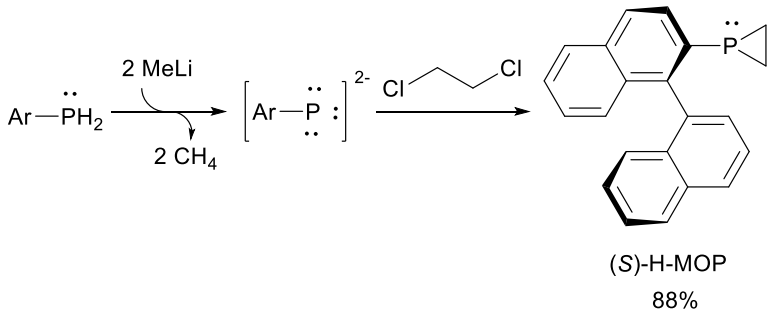

Phosphine gas (PH_3), typically used to make homoleptic phosphines, can also be used to generate heteroleptic phosphines. Note that PH_3 gas is extremely dangerous due to its acute toxicity (>1 ppm) and highly pyrophoric nature.[42] Nonetheless, PH_3 can be generated on-site using red phosphorus and $NaOH/H_2O$. When PH_3 is bubbled through strongly basic media (KOH in dimethylsulfoxide), the phosphide (PH_2^-) species is generated and can be used to add across aryl or heteroaryl conjugated unsaturated hydrocarbons.[43] The pK_a values of PH_3 and RPH_2 are low enough that these species are deprotonated under the reaction conditions, Scheme 1.4. (Note: the pK_a of R_2PH is too

high, making the secondary phosphine the product of the reaction in these cases.) The advantage of this approach is the selectivity of P-C bond formation at the terminal carbon (due to resonance stabilization of the carbanion at the benzyl position) and strict double addition to form a secondary phosphine selectively and in good yields.

Scheme 1.4. An example of how the generation of a phosphide from PH_3 will selectively make secondary phosphines.

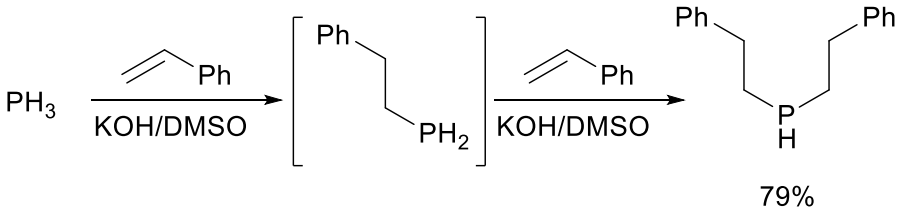

A modern approach to generating the phosphide anion is fluoride-induced desilylation. Starting with a silylphosphine, the phosphide can be generated by the introduction of a fluoride anion. This approach has been exploited to great effect by the Hayashi group (Scheme 1.5).[44] The silylphosphine can be generated from either an electrophilic (*e.g.*, P-Cl) or a nucleophilic (*e.g.*, phosphide anion) phosphorus source and a silicon precursor. The resulting silylphosphine is more easily handled, purified, and stored than P-H or P-Cl precursors. The gentle *in situ* formation of a phosphide anion provides better kinetic control over the reactivity, excellent selectivity, and yields. Using fluoride to generate the phosphide is gentle enough to carry out in the presence of electrophiles, unlike organometallic generation of phosphides where electrophiles must be introduced in a second step. The *in situ* procedure allows for cascade or multi-step

reactions to take place in one-pot, generating selective and complex architectures from simple precursors.[44]

Scheme 1.5. Fluoride-induced desilylation of a silylphosphine to generate a phosphide, which undergoes a two-step reaction to generate a complex heteroleptic phosphine in a one-pot reaction.

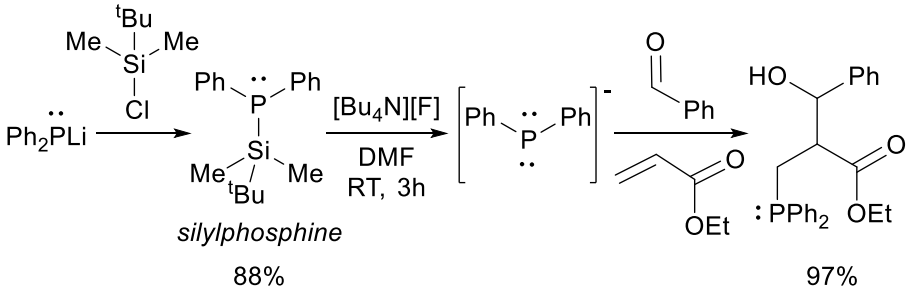

1.2.1.3. Phosphorus(III) nucleophiles

Perhaps the most well-known strategy to synthetically incorporate phosphorus into a molecule is the Michaelis-Arbuzov reaction, which converts an alkyl phosphite and alkyl halide to a phosphonate. This reaction takes advantage of a phosphite's ability to act as a modest nucleophile for P-C functionalization. The Michaelis-Arbuzov reaction has been thoroughly studied and is discussed in-depth elsewhere.[45] In practice, Michaelis-Arbuzov reactions require high temperatures (~130°C) and generally harsh conditions. A valuable modification to the Michaelis-Arbuzov is to first silylate the phosphite (using catalytic (5%) trimethylsilylhalide), which lowers the activation barrier for reactivity considerably (Scheme 1.6).[46] This modification also helps mitigate side reactions of phosphite with the alkyl halide (*e.g.*, EtBr in Scheme 1.6) generated during the reaction. The alkyl halide generated in the reaction must still be systematically removed (typically

using a Dean-Stark apparatus), which is easier at lower temperatures where the side reaction is slower.

Scheme 1.6. Silyl-modified Michaelis-Arbuzov reaction of $P(OEt)_3$ with an alkyl bromide.

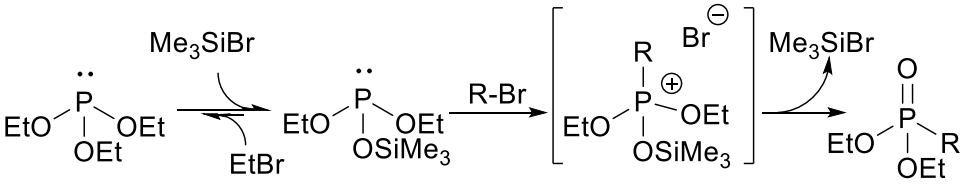

1.2.1.4. Radicals from trivalent phosphorus

P-H bonds can be readily homolyzed using standard non-peroxide radical initiators such as azobisisobutyronitrile (AIBN), Scheme 1.7a.[47] The phosphine radical is exceptionally stable for a radical species and undergoes well-behaved radical chemistry. Access to this radical chemistry makes hydrophosphination across unsaturated hydrocarbons a very reliable reaction (Scheme 1.7). Often times, discrete species with few side reactions can be isolated from a radical reaction with primary or secondary phosphines with alkenes. Regioselectivity for this radical reaction is anti-Markovnikov. A low effective concentration of radicals helps mitigate unfavorable termination steps (Scheme 1.7d). Electron-rich alkenes tend to react under milder conditions than electron-poor alkenes. For heteroleptic phosphine syntheses, this strategy requires either a primary or a secondary phosphine as a precursor and produces ethylene-linked functionalization at the phosphorus (PCH_2CH_2R).

Scheme 1.7. Radical chain mediated hydrophosphination of a P-H bond across an alkene. Desired product is boxed for clarity.

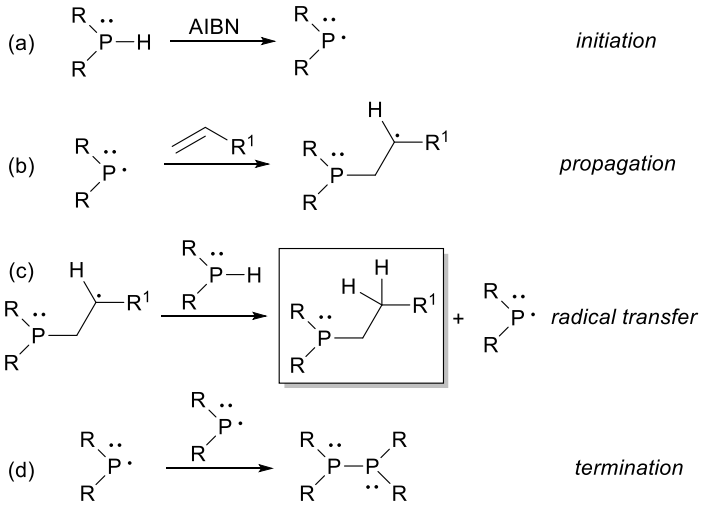

1.2.1.5. Cross-coupling trivalent phosphorus

For aryl P-C functionalization, palladium-mediated cross-coupling is an emerging field. Akin to Buchwald-Hartwig cross-coupling, trivalent phosphorus cross-coupling allows secondary phosphines to be coupled to aryl halides. In a seminal study, Surry *et al.* were able to cross-couple a myriad of secondary phosphines (both alkyl and aryl) with aryl chlorides using the commercially available bidentate phosphine, 1,1'-bis-(diisopropylphosphino)ferrocene (DiPPF), for the palladium catalyst (Scheme 1.8). Bidentate phosphines are typically required for palladium mediated H-phosphine oxide[48] and H-phosphonate[49] cross-couplings.¶ This reaction is particularly useful because aryl chlorides are both cheaper and more amenable to late-stage functionalization than aryl bromides. The only limitation to this study is that the secondary phosphines were all *sec*-alkyl or aryl derivatives.

Scheme 1.8. An example of Buchwald-Hartwig-type Pd-catalyzed cross-coupling of an aryl chloride with a secondary phosphine. Catalytic steps are: 1) oxidative addition, 2) ligand exchange, 3) deprotonation, and 4) reductive elimination. L = DiPPF (a bidentate phosphine).

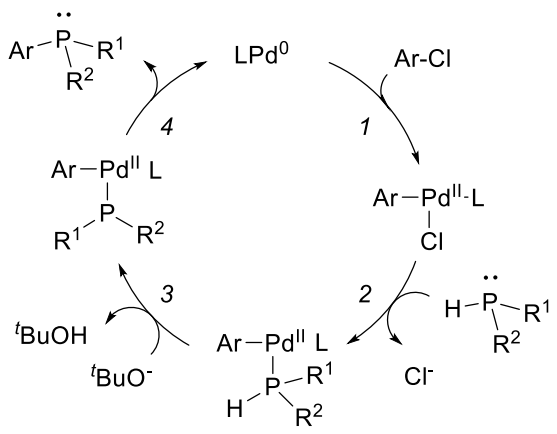

1.2.2. Phosphorus (V) syntheses

In the preparation of heteroleptic phosphines, it is often synthetically advantageous to start with an oxidized form of phosphorus. Phosphorus(V) species are typically tetravalent with a formal double bond at phosphorus; examples include phosphates, phosphonates, phosphinates, etc. (Figure 1.1). Phosphorus(V) starting materials can also be highly cost-effective because they are typically much cheaper and more varied than P(III) precursors. Phosphorus(V) synthetic chemistry is currently undergoing a modernization with a renewed interest in developing milder conditions and broader substrates for synthesis.[50]

Starting a synthesis with P(V) species is attractive for several reasons: 1) O_2 stability, 2) H_2O stability, and 3) silica stability. Benchtop chemistry can be used in these syntheses. This approach typically culminates in a tertiary phosphine oxide that is reduced to the desired phosphine, generating the air-sensitive product at the end of the synthesis. In its own right, P(V) reduction to P(III) is a growing field. However, there are

currently many ways to reduce phosphine oxides to phosphines using a wide range of reagents and conditions.[51–53] Thus, reduction is typically not a difficult step in phosphine synthesis as long as it is substrate-compatible. For brevity, the P(V) compounds discussed here will focus on oxo-P(V) derivatives, that is, $R_3P(O)$ species. The analogous phosphorus sulfide ($R_3P{=}S$) and phosphorus imine ($R_3P{=}NR$) derivatives have also been studied; however, they are less synthetically relevant.

1.2.2.1. Phosphorus(V) electrophiles

As a starting material, trichlorophosphine oxide ($P(O)Cl_3$) offers few advantages over PCl_3 so $P(O)Cl_3$ is typically not used. On the other hand, phosphonic dichlorides ($RP(O)Cl_2$) and phosphinic chlorides ($R_2P(O)Cl$) can be used as P(V) electrophiles. These species are not generated directly from $P(O)Cl_3$, rather from the chlorination of phosphonates ($RP(O)(OR)_2$) or phosphinates ($R_2P(O)(OR)$). Most synthetic methods do not isolate these chlorinated species, rather they are reacted after *in situ* generation. Generally, phosphorus pentachloride (PCl_5) or trimethylsilylchloride (TMSCl) followed by oxalyl chloride ($(COCl)_2$) is used for chlorination (Scheme 1.9).‖ These chlorination conditions are strongly acidic, which are not amenable to many functional groups. Chlorination can be problematic in its own right because of the undesirable and highly reactive by-products generated and harsh conditions required. The lack of isolation or purification of the chlorinated intermediate as standard procedure shows the difficulty in handling these compounds. Yields vary wildly, though our experience has been that very low yields (<20%) should be expected for this two-step conversion to heteroleptic phosphine oxides.

Scheme 1.9. Indirect conversion of a phosphonate to a phosphine oxide going through a phosphonic dichloride intermediate.

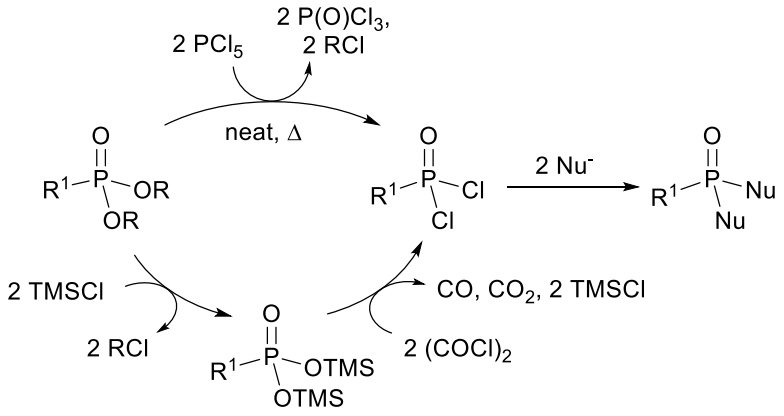

For decades, the question of why phosphonates cannot undergo direct nucleophilic attack (akin to an ester) had gone unanswered. Attempts at direct conversion of phosphonates to phosphine oxides using organometallic reagents were unsuccessful. Grignard reagents offered the best results: low yields (~20%) of phosphine oxide with complete consumption of starting material.[54,55]

A recent development in our laboratory showed that direct and high-yielding P-C functionalization at phosphonates was possible without decomposition or the need for multistep chlorination.[56] In a typical reaction of a Grignard reagent with phosphonate, a pentavalent phosphorus intermediate quickly reacts with free halide in solution to form coordination salt oligomers (Scheme 1.10, top route). This reaction is mechanistically similar to the Michaelis-Arbuzov reaction and accounts for the complete consumption of phosphonate starting material and low yields of phosphine oxide. By removing the free halide from solution using a sodium salt (sodium trifluoromethanesulfonate), oligomer formation was eliminated and yields improved dramatically (Scheme 1.10, bottom route). This direct conversion of a phosphonate to a phosphine oxide is considerably simpler,

higher yielding, and has a large substrate scope compared to the traditional two-step chlorination route (Scheme 1.9).

Scheme 1.10. Direct conversion of a phosphonate to a phosphine oxide showing the proposed intermediates to (top) coordination salt oligomers in the presence of halides and (bottom) a phosphine oxide in the absence of halides.

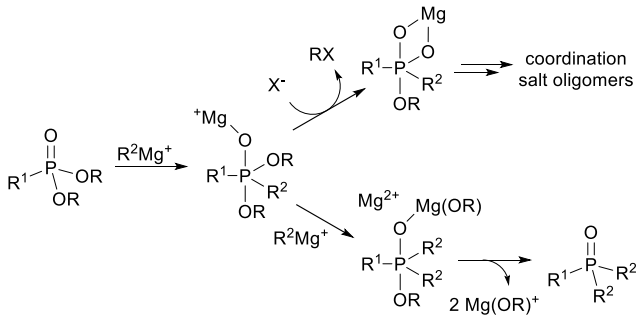

1.2.2.2. Tetravalent phosphorus electrophiles

In a related reaction, H-phosphonates can be used as a convenient starting material to make H-phosphine oxides and tertiary phosphine oxides using Grignard reagents (Table 1.1). Several well-established protocols can be used to directly convert H-phosphonates to heteroleptic phosphine oxides. It is notable that unlike phosphonates, H-phosphonates do not undergo side reactions with halogens in solution (similar to Scheme 1.10 top route). Rather, the first equivalent of Grignard reagent acts to deprotonate the H-phosphonate, generating the anion, which quickly and exothermically reacts with two additional Grignard reagents to form the deprotonated phosphinous anion (Table 1.1). The phosphorus anion reacts with soft electrophiles at the phosphorus to generate a tertiary phosphine oxide.[57] The synthesis of a wide range of phosphine oxides can be made this way from simple starting materials. Oxophilic electrophiles such as

TMSCl can be used to generate the phosphinite by reacting at the oxygen instead of the phosphorus.

Table 1.1. H-Phosphonate reaction with Grignard reagents to form either H-phosphine oxides or heteroleptic phosphine oxides. [a]From reference 57, [b]From: L. R. Doyle, A. Heath, C. H. Low and A. E. Ashley, *Adv. Synth. Catal.*, 2014, **356**, 603-608.

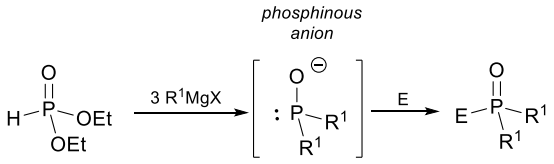

R^1	E	Product	Isolated Yield
Me	H^+	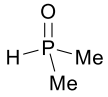	63[a]
Et	H^+	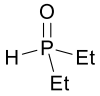	52[a]
Ph	$C_{12}H_{25}Br$	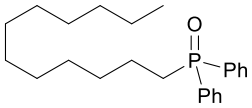	88[a]
Me	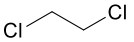	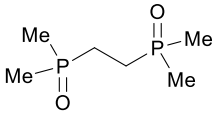	84[b]
Et	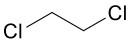	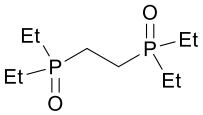	78[b]
^{i}Pr	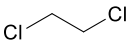	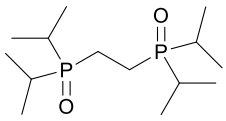	76[b]
^{i}Bu	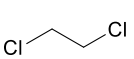	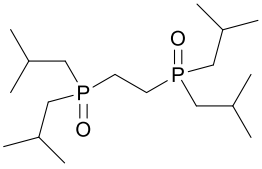	92[b]
^{t}Bu		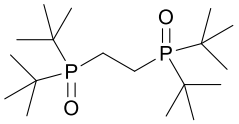	85[b]

1.2.2.3. Nucleophiles from tetravalent phosphorus

Generating a phosphide-type anion from an oxidized phosphorus species is almost exclusively done by deprotonating an H-phosphorus precursor. This methodology works well, although the persistence of the phosphorus anion generated *in situ* varies depending on the identity of the H-phosphorus precursor, solvent, and cation. In general, cryogenic conditions and organometallic bases produce good yields of products, though this must be experimentally determined for reliable yields. This strategy can also be applied to secondary phosphine-boranes.[58]

H-phosphonates (pK_a ~9-23) are more acidic than H-phosphinates (pK_a ~20-23), which in turn are more acidic than H-phosphine oxides (pK_a ~21-27).[37] As one would expect, electron withdrawing groups and aromatic moieties at phosphorus lower the pK_a, whereas alkyl and electron donating groups raise the pK_a. If the proton is acidic enough, sometimes KOH/DMSO or $Ca(OH)_2$/DMF mixtures are basic enough to generate the phosphorus anion. As first noted by Hays, unless an oxophilic electrophile (*e.g.*, silyl chloride) is used, the phosphorus is the predominant nucleophile, not the oxygen.[57] The P-C bond formation can selectively undergo Michael-type addition to ketone conjugated alkenes (Scheme 1.11a)[59,60] or direct carbonyl addition (Scheme 1.11b),[61] depending on the catalyst or the phosphorus cation. This simple strategy can be used to great effect, especially for chiral syntheses.

1.2.2.4. Nucleophiles from α-methyl carbanion

α-Methyl phosphine oxides can be deprotonated using organolithiates in conjunction with *N*,*N*,*N*′,*N*′-tetramethylethane-1,2-diamine (TMEDA) to generate an α-

carbanion. This carbanion can be reacted with an electrophile, creating a C-C bond β to the phosphorus (Scheme 1.12). This is especially advantageous when R = CH_3. From trimethyl phosphine oxide, alkyl dimethyl phosphine oxides can be directly generated. Though this approach is equally valid with alkyl phosphines,[62] the hydrogens at the α-carbon become considerably more acidic (and carbanion better behaved) when using the phosphine oxide, phosphine borane, or phosphine sulfide (R_3P=S).[63] This approach is not valid for phosphonates or phosphinates because of the electrophilic nature of the P-OR bond which reacts quickly with alkyl lithiates.

Scheme 1.11. H-Phosphine oxides as nucleophiles for alkene conjugated carbonyls showing a) zinc-mediated Michael addition to the alkene and b) calcium-mediated direct carbonyl addition.

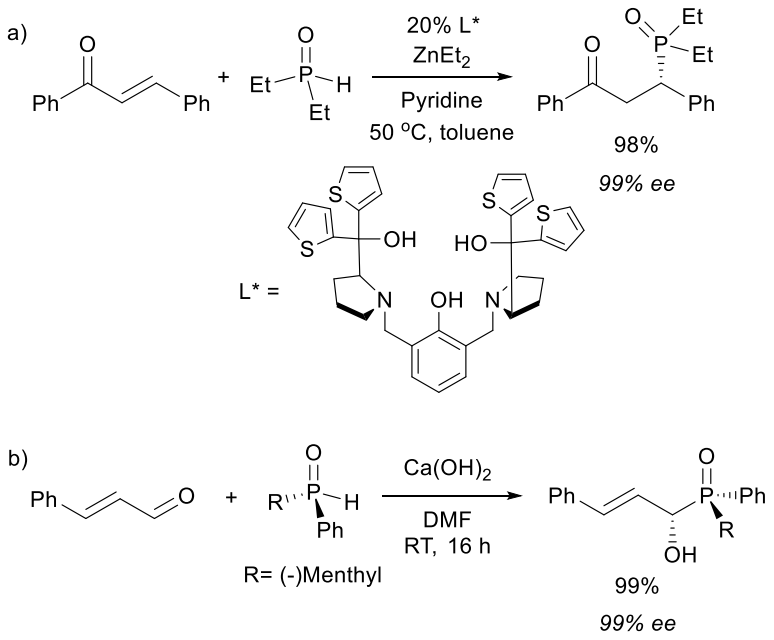

Scheme 1.12. Phosphine oxide α-methyl carbanion generation for C-C bond formation β to the phosphorus.

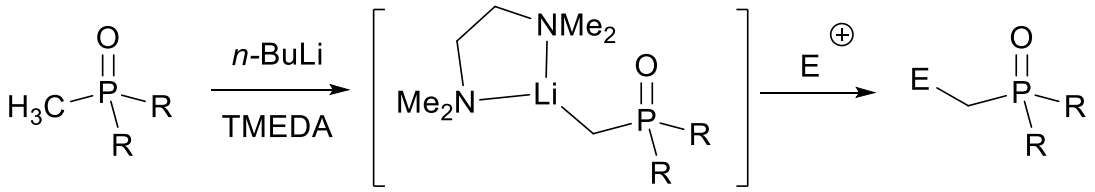

1.2.2.5. Radical from tetravalent phosphorus

H-Phosphonates, H-phosphinates, and H-phosphine oxides undergo radical chemistry in a nearly identical fashion to secondary and primary phosphines. A major step forward in this field was the discovery of metal-mediated radical acetoxyphosphorylation. The simultaneous installation of two functional groups across unsaturated alkenes produces more complex architectures in one step compared to standard hydrophosphination. In a preliminary finding by Zhou *et al.*, both H-phosphine oxides and H-phosphonates can be added regioselectively with an acetoxy group across conjugated alkenes (Scheme 1.13).[64]

Scheme 1.13. Mn(III)-mediated radical acetoxyphosphorylation of alkenes with both H-phosphine oxides and H-phosphonates.

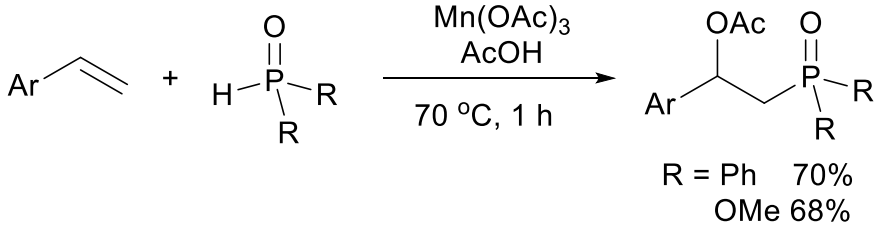

1.2.2.6 Cross-coupling tetravalent phosphorus

One of the quickly growing subfields in organophosphorus chemistry is the development of H-phosphonate,[48,65–69] H-phosphinate,[70,71] and H-phosphine oxide cross-coupling reactions[72–74] to form P-C bonds (Scheme 1.14). There has been serious interest in these transformations during the last decade and these reactions are now standard practice in organophosphorus synthesis. Cross-couplings to form P-C bonds are more sensitive to conditions than "typical" C-C bond-forming reactions, with phosphine oxides often being more finicky than phosphonates. Typically, several literature preparations must be screened before a cross-coupling reaction has been optimized for any specific substrate. Both palladium[75] and nickel[76] cross-coupling protocols for H-phosphonates, H-phosphinates, and H-phosphine oxides are reasonably robust across a variety of substrates. In spite of these advances, cross-coupling of P-H species is still in need of standard protocols that are universally reliable and mechanistically well understood.

Scheme 1.14. An example of Pd-catalyzed cross-coupling of an aryl halide with a secondary P(V) species. Catalytic steps are: 1) oxidative addition, 2) P(V)-P(III) tautomerization, 3) ligand exchange, 4) deprotonation, and 5) reductive elimination. L is typically a bidentate phosphine ligand.

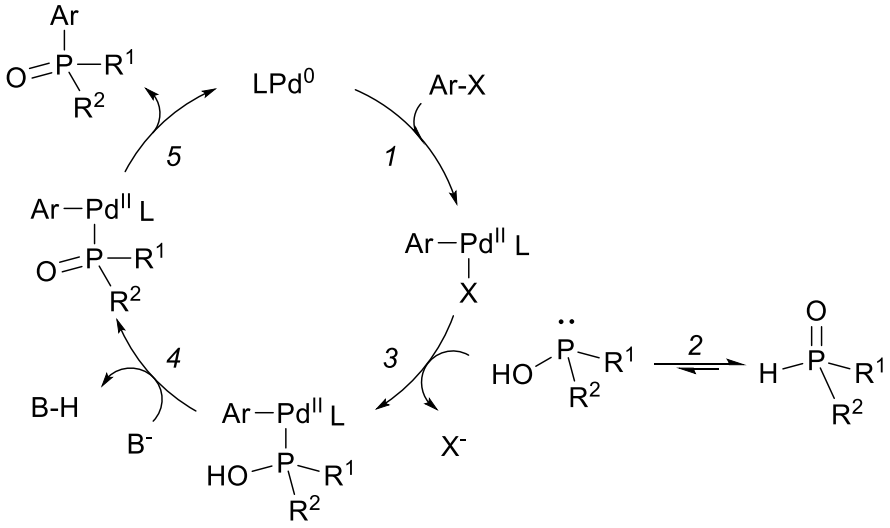

1.3. Looking forward

Although the modern organophosphorus chemist has more synthetic tools than ever before, the ability to make P-C bonds as easily as first-row main-group bonds to carbon is still a distant dream. The differences in first- and second-row main-group chemistry provide a high degree of variance in reactivity and sensitivity to subtle changes in conditions. The exploitation of these differences is the fuel that drives phosphine chemistry toward new and seminal discoveries.

One such area of research uses borane as a protecting group for phosphines.[49] This approach is an excellent way to take advantage of air- and silica-stability of phosphine-boranes. Also, phosphine boranes are easily deprotected to yield phosphines. (Heating with amines will typically free the phosphine.) Considering the diversity of chemistry discussed in this Perspective, it is readily apparent that borane-protected phosphorus syntheses have been minimally exploited.[77,78] Typically, borane is used as a late-stage protecting group; however, it could be used throughout the synthesis. The ability of phosphine-borane derivatives of phosphinites and phosphonites to undergo nucleophilic attack or be deprotonated to a phosphide is not well established. Cross-coupling of phosphine-boranes is also an underdeveloped field that shows much promise for the future of organophosphine synthesis.

The ability to gently and selectively reduce P(V) species to P(III) is an ongoing challenge for chemists. In a recent example of research in this area, the Gilheany group showed the ability to reduce P=O bonds while retaining the weaker (more easily reduced) P-N bonds of aminophosphine oxides.[79] Selective reduction of P(V) was thought impossible based on the large discrepancy in bond strengths and reduction potentials of

P=O and P-N bonds. The ability to selectively reduce P=O bonds will grant access to more diverse functionality at P(V) precursors and will open up new routes to heteroleptic phosphines. As such, the development of selective reduction for P(V) species will continue to be a key area of modern phosphine chemistry.

The last decade has seen a renewed interest in organophosphorus chemistry. New chemistries for reliable P(III) and P(V) syntheses of heteroleptic phosphines have emerged. Many chemists, however, still rely on traditional P-Cl derived synthetic routes and aryl phosphines for research. The new synthetic methods grant access to ligands like alkyl phosphines that currently represent an underutilized class of heteroleptic phosphines due to the considerable synthetic hurdles associated with their synthesis. As new syntheses of heteroleptic phosphines come online, inorganic and organometallic chemistry will surely flourish. The new organophosphorus synthetic methods will also have a serious impact on other fields including medicinal chemistry, biochemistry, materials science, solid state chemistry, and catalysis. From a global perspective, the new syntheses will serve to expand our understanding of the idiosyncratic nature of second-row main-group chemistry.

1.4. Summary

This dissertation describes synthetic developments in the area of organophosphine chemistry and application of new dimethyl-functionalized phosphines. Chapter II describes a new methodology to use phosphonates as electrophilic phosphorus(V) reagents for organometallic nucleophiles. Chapter III describes a new methodology to use H-phosphine oxides as nucleophiles for alkyl halides. Chapter IV is an examination

of a series of phosphine ligands (JohnPhos ligands) for their steric and electronic properties when coordinated to transition metals. Chapter V explores Buchwald-Hartwig cross-coupling with JohnPhos ligands. Finally, in Chapter VI, iron-phosphine complexes, other phosphine reactions, and preliminary findings are reported.

1.5. Notes

‡ Designer ligands have structures that are strictly tailored for a specific chemical purpose. Typically, these ligands represent synthetically fine-tuned structures because they evolved from previously studied structures.

§ Preliminary work with 2,2'-biphenol as a bidentate P-Cl protecting group has also shown promise, where the P-O bond is sensitive to organolithiates, but not organomagnesium reagents.[80]

¶ The Tavs Reaction is another trivalent phosphorus cross-coupling reaction. It serves as an alternative to H-phosphonate cross-coupling and uses alkyl phosphites with aryl halides to form aryl phosphonates.[81]

‖ Thionyl chloride also works well as a chlorinating agent for phosphonates to phosphinic dichlorides.

1.6. Coauthored material

This dissertation includes previously published and unpublished coauthored material.

1.6.1. Previously published coauthored material

Chapter I of my thesis is a modified form of a published paper. I conceived of and wrote the manuscript. Coauthor includes David R. Tyler.

Chapter II of my thesis is a modified form of a published paper. I developed the project, did the majority of the chemistry, and wrote the manuscript. Coauthors include Chase A. Salazar, Patrick F. Martino and David R. Tyler.

1.6.2. Unpublished coauthored material

Chapter III is a modified form of a paper to be submitted for publication. I developed the project, did the majority of the chemistry, and wrote the manuscript. Coauthors include Daniel T. Seidenkranz and David R. Tyler.

Chapter IV is a modified form of a paper submitted for publication. I conceived of the project, performed the chemistry, and wrote the manuscript.. Coauthors include Lev Zakharov and David R. Tyler.

Chapter VI is a modified form of a paper to be submitted for publication. I directed the project, developed the theory, interpreted the data, and wrote the manuscript. Coauthors include Justin T. Barry, Daniel T. Seidenkranz, Ajay Ryerson, Colin Hiatt, Chase A. Salazar, Dillon J. Bryant, and David R. Tyler.

1.7. Bridge

In this chapter, a brief overview of organophosphorus chemistry is discussed. This discussion is meant to set the stage for the next two chapters which deal with

organophosphine synthesis using new synthetic methods. The motivation for the development of these methods was largely derived from the discussion in this chapter.

CHAPTER II

THE DIRECT CONVERSION OF PHOSPHONATES TO PHOSPHINE OXIDES: AN IMPROVED SYNTHETIC ROUTE TO PHOSPHINES INCLUDING THE FIRST SYNTHESIS OF METHYL JOHNPHOS

2.1. Introduction

2.1.1. Coauthored material

Chapter II of my dissertation is a modified form of a published paper. I developed the project, did the majority of the chemistry, and wrote the manuscript. Coauthors include Chase A. Salazar, Patrick F. Martino and David R. Tyler. Citation for the article: Kendall, A. J.; Salazar, C. A.; Martino, P. F.; Tyler, D. R. *Organometallics*, **2014**, *33* (21), pp 6171–6178.

2.1.2. History of phosphines

The use of heteroleptic phosphine ligands – in particular Buchwald-type phosphines (Figure 2.1) – has enjoyed great success for a diverse array of catalytic transformations.[1,2] The synthesis of heteroleptic phosphines, however, is laborious and requires air- and water-free techniques for most of their multi-step syntheses.[3–5] The intermediates can be difficult to purify due to their instability on silica (e.g. P-Cl bonds) or the exceptional volatility of primary-, secondary-, and alkyl-phosphines. In addition, commercially available sources of phosphine precursor compounds can be prohibitively

expensive for preparatory scale chemistry. For these reasons, traditional syntheses are limited to bulky groups on phosphorus and are plagued by low yields.

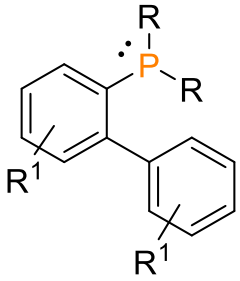

Figure 2.1. A Buchwald-type phosphine.

Heteroleptic phosphines incorporating methyl moieties ($RPMe_2$) are exceptionally rare due to the harsh reaction conditions and difficult purification and handling necessary to access both potential precursors: chlorodimethylphosphine,[6] and $RPCl_2$ species from either PCl_3 or $ClP(NEt_2)_2$.[7-9] This problem becomes especially prevalent during exploratory chemistry in which reactions are poorly optimized, ultimately limiting phosphine ligand design and development.

A more common motif for modern ligand design is the inclusion of a diphenylphosphino-, di-*tert*-butylphosphino-, or dicyclohexylphosphino- moiety. This is best demonstrated by Buchwald-type ligands which have a diverse array of biaryl structures, but all share a narrow set of phosphine functionalization (Figure 2.1, R typically = Ph, *t*-Bu, Cy).[10] The precursors for these phosphines are commercially avaliable,[11] easier to handle (i.e. higher boiling points or melting points) and the resulting phosphines are relatively air stable.[12] Synthetically this choice is convenient, however, can be unfavorable because as ligands smaller alkyl phosphines remain better electron donors and form considerably shorter phosphine-metal bonds.[13-16] For instance, dimethyl

Buchwlad-type ligands (e.g. Methyl Johnphos, Figure 2.1, R = Me, R^1 = H) have never been synthesized, even though as ligands they would be excellent at stabilizing high oxidation states of metals and would impart greater catalytic activity in many cases.[17,18]

The synthesis of phosphines from phosphonates is an alternative to traditional phosphine syntheses. However, current routes rely on molecules with P-Cl or P-H bonds (Scheme 2.1, top and bottom routes). The synthesis of phosphine oxides from phosphonates in a single step (Scheme 2.1, middle route) offers a tantalizingly simple and selective pathway because of its respective air-, water-, and silica-stability. In addition, phosphonates can be easily synthesized from alkyl or aryl halides using the Arbuzov reaction[19] or H-phosphonate cross-coupling reactions.[20] Despite this, phosphine oxide synthesis from phosphonates (Scheme 2.1, middle route) is a low yielding (typically <25%)[21] reaction and consequently this conversion is not used in phosphine synthesis.

Scheme 2.1. Synthetic routes from phosphonates to heteroleptic phosphines.

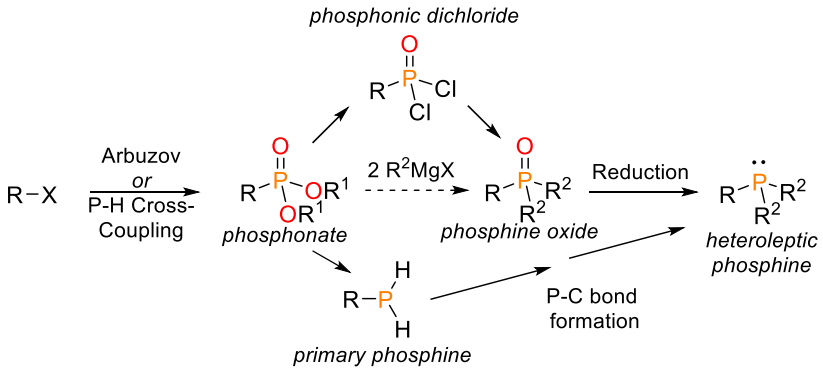

The goal of this work was to develop a synthetic method to access heteroleptic tertiary phosphines, namely those with a dimethylphosphino- moiety that avoids air- and

water-sensitive intermediates, with the key step being the direct conversion of phosphonates to phosphine oxides (Scheme 2.1, middle route).

We herein report the first facile and high yielding synthesis of phosphine oxides directly from phosphonates as well as the first synthesis of Methyl JohnPhos.

2.2. Results and discussion

Two approaches were investigated for the direct conversion of phosphonates to phosphine oxides: (1) activating the phosphonate for nucleophilic attack; and (2) determining the reaction mechanism in order to discern ways of increasing the yields.

2.2.1. Activation of the phosphonate

A variety of organometallic reagents were screened for the direct conversion of phosphonates to phosphine oxides (Table 2.1). Grignard reagents proved to be the best candidates for this reaction while organo-zincates were non-reactive and organo-lithiates were too reactive, giving numerous undesirable products. Grignard reagents are widely commercially available as well as easy to synthesize and handle, providing convenient methods for preparation.

Lewis acid additives were screened in the expectation that they would increase the electrophilicity of the phosphonate through coordination – analogous to Lewis acid catalyzed nucleophilic ester substitution. Similar work by Hays suggested the viability of this approach.[22] After a rigorous Lewis acid screening (Appendix A, Table A3), the highest yield achieved was 54% of phosphine oxide when using lutetium triflate ($Lu(OTf)_3$). Although this yield was promising it was still lower than desired. The

phosphonate was completely consumed in the reaction, demonstrating a substantial side reaction was the major reason for the low yields.

Table 2.1. Organometallic reagent screening. [a]NMR yields, [b]GC yields, and [c]isolated yield.

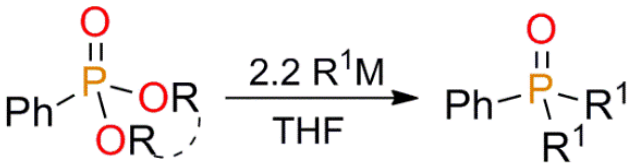

Entry	R	R^1M	Temp. (°C)	%Yield
1	Me	MeMgBr	50	23[b]
2	Me	$ZnEt_2$	66	<0.1[a]
3	Me	MeMgBr·LiCl	50	32[a]
4	Me	MeLi	-78	15[a]
5	Me	MeMgBr· 0.2 $Lu(OTf)_3$	66	54[c]
6 *	CH_2CH_2	MeMgBr	66	32[a]

* cyclic ester 2-phenyl-1,3,2-dioxaphospholane 2-oxide

To determine if activating the phosphonate was truly a viable strategy for increasing the phosphine oxide yields, the cyclic phosphonate 2-phenyl-1,3,2-dioxaphospholane 2-oxide (Table 2.1, entry 6) was synthesized. The ring strain (estimated 5.2 kcal/mol) of this phosphonate has been shown to increase the rate of hydration compared with an acyclic analogue.[23] Assuming the ring strain would increase the rate of nucleophilic substitution, we reacted this cyclic phosphonate with MeMgBr. The cyclic phosphonate was unable to out-compete the side reaction (Table 2.1, entry 6), suggesting side reaction and not phosphonate activation, is the major the problem in optimizing the reaction.

2.2.2. Identifying the side reaction

While studying the reaction of MeMgBr with $PhP(O)(OMe)_2$, a 23% yield of $PhP(O)Me_2$ was obtained; however, 77% of the starting material in the reaction was unaccounted for by gas chromatography (Appendix A, Figure A2). These results suggested a non-volatile by-product is responsible for the low yields in the reaction. NMR spectroscopy was used to observe the reaction in solution over time in a sealed NMR tube affixed with a J. Young valve. Surprisingly, as many as seven phosphorus species, (converting into two discrete peaks) were observed by ^{31}P NMR spectroscopy over the course of 24 hours (Appendix A, Figure A6).

These final species observed in the NMR spectra are likely the phosphine oxide and another thermodynamic by-product of the reaction. ^{1}H NMR spectroscopy revealed a considerable accumulation of C_2H_6 (^{1}H NMR, δ = 0.85 ppm in THF-d_8, Figure 2.2b) in addition to MeBr (^{1}H NMR, δ = 2.65 ppm in THF-d_8) transiently appearing in solution when MeMgBr was used. The C_2H_6 generation had a clear induction period and increased proportionally to the loss of both MeBr and MeMgBr. The production of MeBr *in-situ* would logically be followed by the production of C_2H_6 from reaction with active MeMgBr. To confirm the identity of these assignments, the experiment was repeated with MeMgCl in the expectation that MeCl would be observed (Figure 2.2a). Indeed, the reaction yielded traces of MeCl (^{1}H NMR, δ = 3.02 ppm in THF-d_8), no observable peak at 2.65 ppm, and again a buildup of C_2H_6.

Mikulski and coworkers observed phosphonates under nearly the same conditions used for this study reacted with metal halides to cause an Arbuzov-like decomposition of the phosphonates into alkyl halides and metal-phosphonate salts and oligomers.[26] Our

observations corroborate this mechanism (Scheme 2.2). This side reaction accounts for the low yields of phosphine oxide with high conversion of starting material, as well as the inability to characterize the side products of the reaction by GC. To test if the side reaction (Scheme 2.2) could be prevented, $PhP(O)(OPh)_2$ was reacted with MeMgBr with the assumption that the ipso-carbon of the phenoxide leaving group (P-OPh) is unable to undergo the reaction described by Mikulski. The reaction proceeded cleanly and in quantitative yield, confirming the identity of the side reaction. These results are also

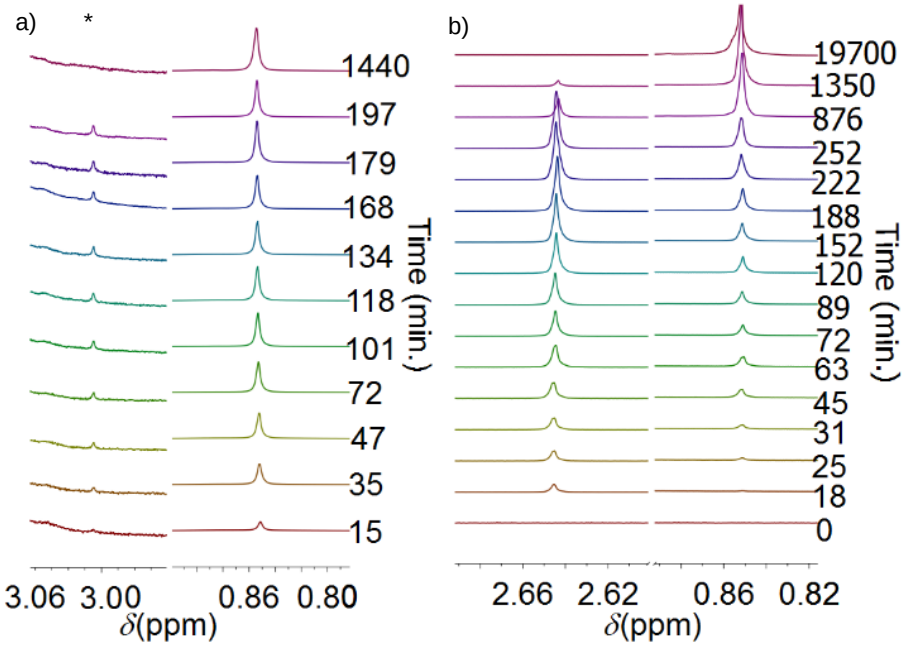

Figure 2.2. ^1H NMR observed signals in select regions for (a) MeMgCl and (b) MeMgBr reacting with $PhP(O)(OMe)_2$ in THF-d_8. The signals correspond with C_2H_6 at δ = 0.85 ppm,[24] MeBr δ = 2.65 ppm,[25] and MeCl δ = 3.02 ppm.[25] *Vertical scale enhanced by 4x for clarity.

Scheme 2.2. Proposed steps and intermediates in the side reaction of $PhP(O)(OMe)_2$ with Grignard reagents.

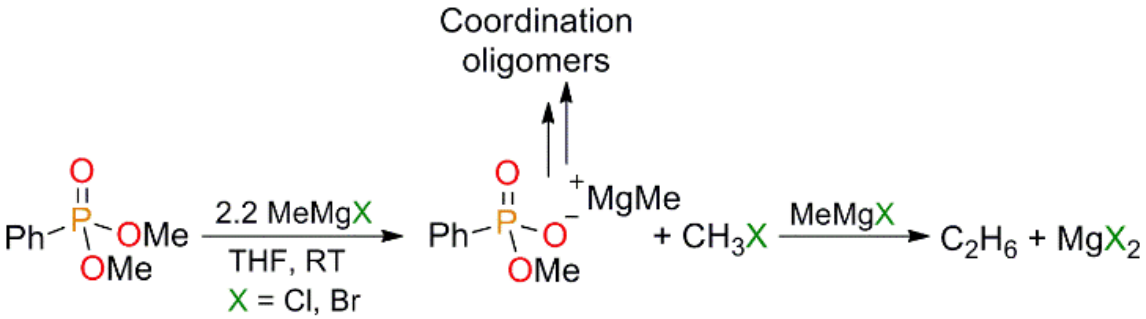

corroborated by literature that observes high yields with similar diphenylphosphonates.[21] It should be noted that these types of phosphonates are only synthetically accessible through P-Cl precursors, and therefore are not a synthetic improvement over traditional phosphine syntheses.

2.2.3. Eliminating the side reaction

To generalize the reaction for all phosphonates lacking the P-OPh group, *in-situ* halide abstraction agents were screened (Table 2.2). Stoichiometric addition of a sodium salt should remove the Grignard halide from the reaction medium before it can decompose the phosphonate into coordination oligomers, thereby preventing the side reaction. The addition of sodium triflate (NaOTf) to the reaction precipitated NaBr. This observation was accompanied by a 75% yield of the phosphine oxide. The ^{19}F chemical shift of the OTf anion remained constant throughout the reaction, suggesting the OTf anion is acting as a non-coordinating ion. Silver(I) salts (Appendix A, Table A3) were not satisfactory as abstracting agents due to their additional redox chemistry (likely from transmetallation) followed by silver(0) precipitation.

Table 2.2. Sodium salt screen for halogen abstraction. [a]NMR yields. (Isolated yields).

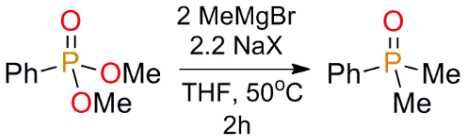

X	% Conversion[a]	% Yield[a]
OTf	>99	75 (73)
BF_4	45	23
BPh_4	56	32

Experimentally, the addition of NaOTf provided for higher yields and much cleaner reaction mixtures. After reaction workup, only phosphonate and phosphine oxide were observed, which were easily separated using aqueous washes. The discrepancy between the yield and conversion can be attributed to hydrolysis of the phosphonate during workup – producing a water-soluble phosphonic acid. Using NaOTf as an *in-situ* abstracting agent essentially eliminates the side reaction and provides consistently high yields of products that are easily purified.

2.2.4. Reaction scope

To assess the general scope of the reaction, the phosphonate leaving groups (P-OR) were varied (Table 2.3). Bulkier leaving group substituents on the phosphonate lowered the overall yields. This trend follows for all leaving groups except phenoxide (Table 2.3, entry 5), which may be due to the ability of phenoxide to delocalize the negative charge, which electronically stabilizes the leaving group.

Table 2.3. Leaving group study for phenylphosphonate derivatives. (-)MenOH = (1R,2S,5R)-2-isopropyl-5-methylcyclohexanol. [a]NMR yields.

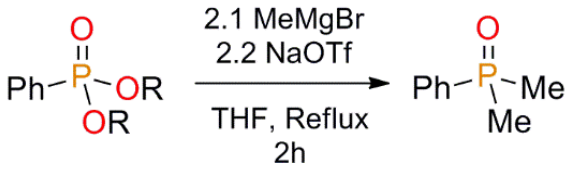

Entry	OR	% Yield[a]
1	OMe	75
2	OEt	58
3	O*i*Pr	35
4	O*t*Bu	<0.1
5	OPh	>99
6	O(-)Men	<0.1

Alkyl phosphonate derivatives were then studied (Table 2.4, Entries 1-3). In general, alkyl phosphonates gave much lower yields than the phenyl analogues. For the phenyl phosphonates, (Table 2.4, Entries 4-10) the phosphine oxide yields correspond reasonably well with the steric influence of the Grignard reagent, i.e., bulkier Grignards provided diminished yields.

Table 2.4. Alkyl phosphonate study and Grignard reagent study. [a]NMR yields.

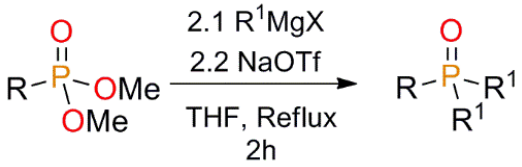

Entry	R	R^1MgX	% Yield[a]
1	*n*-Hex	MeMgBr	33
2	*n*-Hex	PhMgBr	7
3	Me	PhMgBr	38
4	Ph	MeMgBr	75
5	Ph	PhMgBr	87
6	Ph	EtMgBr	61
7	Ph	*i*-PrMgCl	11
8	Ph	*n*-BuMgCl	45
9	Ph	CyMgCl	5
10	Ph	*t*-BuMgCl	<0.1

To complete the substrate study, the effects of changing the electronics of aryl phosphonates were explored. Across a diverse range of electronic and steric influences, yields of phosphine oxides ranged from good to excellent (Table 2.5). The substituent position on the ring had little effect on the yields, with the exception that *ortho*-substituted groups generally had higher yields. A clear trend arises when comparing yields from Table 2.3 (Entries 1-3) with yields from Table 2.5 (Entries 8-10), namely that the *ortho*-phenyl substituent has a positive influence on the yields of the reaction. In addition, dimethyl(2-bromophenyl)phosphine oxide is obtained in good yield, which could act as a precursor for a diverse array of new phosphines by means of later functionalization at the bromide (Table 2.5, entry 13).

Table 2.5. Aryl phosphonate study. [a]NMR Yields.

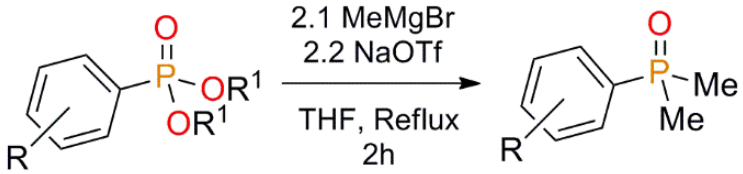

Entry	R	OR^1	% Yield[a]
1	4-OMe	OMe	78
2	3-OMe	OMe	82
3	2-OMe	OMe	77
4	4-F	OMe	52
5	3-F	OMe	72
6	2-F	OMe	67
7	4-Ph	OMe	83
8	2-Ph	OMe	91
9	2-Ph	OEt	49
10	2-Ph	OiPr	56
11	2-Me	OMe	84
12	2-Cl	OMe	65
13	2-Br	OMe	72

To complete the substrate study, the effects of changing the electronics of aryl phosphonates were explored. Across a diverse range of electronic and steric influences, yields of phosphine oxides ranged from good to excellent (Table 2.5). The substituent position on the ring had little effect on the yields, with the exception that *ortho*-substituted groups generally had higher yields. A clear trend arises when comparing yields from Table 2.3 (Entries 1-3) with yields from Table 2.5 (Entries 8-10), namely that the *ortho*-phenyl substituent has a positive influence on the yields of the reaction. In addition, dimethyl(2-bromophenyl)phosphine oxide is obtained in good yield, which could act as a precursor for a diverse array of new phosphines by means of later functionalization at the bromide (Table 2.5, entry 13).

2.2.5. Mechanistic considerations

The reaction of a Grignard reagent with a phosphonate proceeds by two double-displacement reactions. When the equivalents of the Grignard reagent were reduced (Appendix A, Figure A9), the reaction preferred double addition to a single phosphorus center over single addition. This result suggests the first displacement by the Grignard reagent is slow, followed by fast displacement a second time. Also, increasing the amount of Grignard reagent past the stoichiometric requirement (two equivalents) did not afford significantly higher yields of phosphine oxide.

A stepwise double displacement model suggests the logical intermediate is a phosphinate (Scheme 2.3). Although no evidence by NMR spectroscopy or GC for this intermediate was observed, it is likely transient and very short lived.

Scheme 2.3. Theoretical stepwise double-displacement mechanism of phosphonate conversion to phosphine oxide.

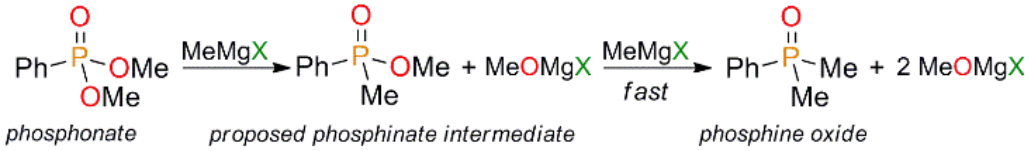

To test whether a phosphinate is an intermediate in the reaction as proposed in Scheme 2.3, PhP(O)(OMe)Me was prepared and reacted with MeMgCl with the expectation that it would react readily if it is a transient intermediate in the reaction. A series of reactions were run to simulate the *in-situ* reactive conditions for the phosphinate (Table 2.6).

Surprisingly, the phosphinate is completely non-reactive with MeMgCl (Table 2.6, entry 1). When NaOTf was added, the phosphinate reacted cleanly with MeMgCl to produce modest yields of phosphine oxide product (Table 2.6, entry 2). The abstraction of the halide from the Grignard reagent produces the MeMgOTf reagent, which has been shown to have slightly enhanced reactivity but with a stronger steric sensitivity than MeMgX (X= Cl, Br, I).[27] This is corroborated by our observations that the MeMgOTf reagent is more nucleophilic than MeMgCl and reacts with phosphinates, but has a strong sensitivity to leaving group (P-OR) steric influence (as seen in Table 2.3).

When the phosphinate was reacted with MeMgCl in the presence of a stoichiometric amount of MeOMgCl (the species resulting from the first Grignard displacement), complete consumption of the MeMgCl without production of phosphine oxide was observed (Table 2.6, entry 3). This result is somewhat inconclusive because the observed reaction could be attributed to the phosphinate producing coordination

oligomers or it could be an unrelated coincidental reaction. MeOMgCl does not react with PhP(O)(OMe)Me by itself, and no C_2H_6 was observed by NMR spectroscopy (Appendix A, Figure A11) for any reaction of Grignards with phosphinates.

To determine whether the phosphinate is truly an intermediate in the reaction of phosphonates with Grignard reagents, one final reaction was carried out (Table 2.6, entry 4). Stoichiometric NaOTf was added to the reaction of phosphinate with MeOMgCl and MeMgCl with the assumption that if the phosphinate is an intermediate, these reaction conditions should prevent the coordination oligomers and provide a high yield of phosphine oxide similar to that observed in Table 2.2.

Table 2.6. Reaction of PhP(O)(OMe)Me and MeMgCl with reaction additives. [a]NMR Yields.

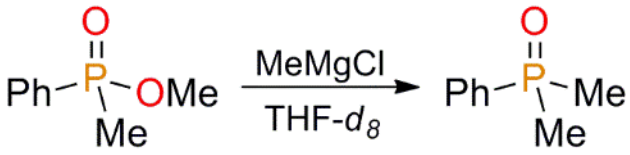

Entry	Reaction Additive	%Conversion	% Yield[a]
1	-	< 0.1	< 0.1
2	1.1 NaOTf	29	28
3	1 MeOMgCl	> 99	< 0.1
4	2.2 NaOTf, 1 MeOMgCl	> 99	< 0.1

The addition of NaOTf did not yield any phosphine oxide product (Table 2.6, entry 4). There was no observable difference between Table 2.6 entries 3 and 4, suggesting the reactions observed under these conditions are in fact coincidental and likely stem from phosphinate coordination events in solution.

The results of these reactions can be summarized as follows: (a) no C_2H_6 was produced in any reaction of PhP(O)(OMe)Me with MeMgCl; (b) MeMgCl does not react with PhP(O)(OMe)Me by itself; (c) no spectroscopic evidence for phosphinates in the reaction were observed; (d) under conditions that provided excellent yields for phosphine oxides from phosphonates (Table 2.6, entries 2 and 4), either no phosphine oxide was produced or it was produced in substantially smaller yields than observed with the phosphonate. It is concluded from these results that the phosphinate does not – under any comparable conditions – produce product competently enough to be an intermediate in the reaction. These results rule out the phosphinate as an intermediate in the reaction of phosphonates with Grignard reagents (Scheme 2.3).

Because a phosphinate is not the intermediate in Scheme 2.3, a five-coordinate phosphorus intermediate is likely formed (Scheme 2.4). Specifically, it is hypothesized the first Grignard reagent reacts to yield a short-lived, five-coordinate intermediate that reacts quickly to yield either coordination oligomers or phosphine oxide. Similar five-coordinate species are well documented. [28-32]

Steric influence near the P-C bond of the phosphonate increases the yield of the reaction. This inverse steric trend is attributed to steric deterrence of product inhibition by phosphine oxides coordinating active Grignard species. Product inhibition accounts for the observation of incomplete conversion of starting material even with an excess of the Grignard reagent present and longer reaction times for most phosphonates studied. This notion is also corroborated by the observation that alkyl phosphonates (Table 2.4, Entries 1-3) had lower yields than aryl phosphonates. Alkyl phosphine oxides are harder Lewis bases and less sterically hindered, and therefore better product inhibitors for Grignard

reagents. To test this hypothesis, a variety of Lewis bases were added to the reaction of PhP(O)(OMe)2 with MeMgBr, resulting in significantly lower yields and conversions (Appendix A, Table A4).

Scheme 2.4. Proposed reaction pathway for the reaction of phosphonates with Grignard reagents. RDS = rate determining step.

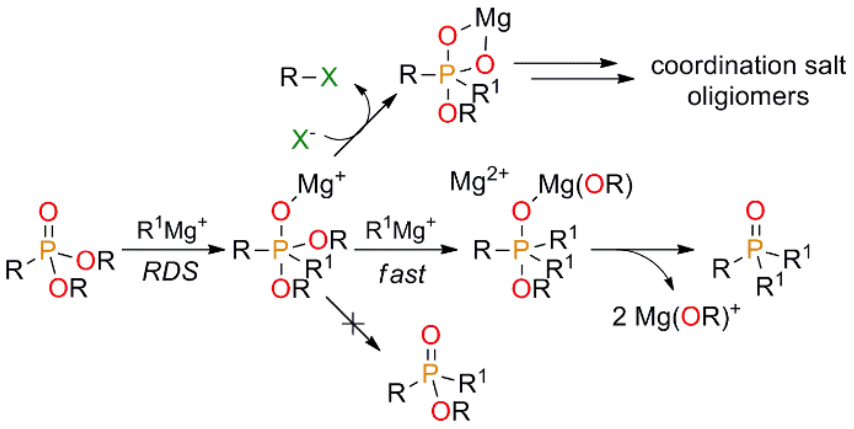

2.2.6. Phosphine synthesis

To highlight the usefulness of this reaction, a new method to synthesize phosphines directly from phosphonates is presented. This method utilizes all air-stable intermediates, readily available starting materials, and Grignard reagents for direct P-C functionalization.

The classic and commercially available bidentate phosphine ligand 1,3-bis(diphenylphosphino)propane (dppp) was synthesized using nearly all benchtop

techniques (Scheme 2.5a). The overall yield of the three-step synthesis was 60% starting from the alkyl bromide. The commercial synthesis of dppp has been well established;[33-35] however, stoichiometric amounts of sodium metal are required. Although PhMgBr was used for the synthesis in Scheme 2.5a, other aryl Grignard reagents could also be used to make novel dppp derivatives that are not commercially available.

A new Buchwald-type ligand featuring a dimethyl phosphine moiety (Scheme 2.5b) was also synthesized. Dimethyl aryl phosphine derivatives are very laborious to synthesize, thus the traditional syntheses of similar phosphines rely on heavier and more electronically stabilized phosphorus precursors. For this reason, dimethyl-Buchwald-type ligands have, to the best of our knowledge, never been synthesized. As shown in Scheme 2.5b, the first synthesis of [1,1'-biphenyl]-2-yldimethylphosphine or methyl JohnPhos was achieved in a three-step reaction with a 52% overall yield using inexpensive chemicals starting from the aryl bromide. The reaction is also easily scalable. This new method for heteroleptic phosphine synthesis provides several advantages over traditional routes, requiring no air-free techniques, facile purification of products, and considerably higher yields.[36]

While the choice to use aluminum-hydride sources (Scheme 2.5) as reducing agents was one made out of synthetic convenience, there is a considerable body of literature reporting alternative reducing agents that are mild and selective reducing agents for converting phosphine oxides to phosphines.[37-42] In all, these provide an extremely mild route for the overall synthesis of the targeted phosphines. Finally, a diverse array of functionalization can be appended using any number of commercially available or custom-made Grignard reagents.

Scheme 2.5. a) Synthesis of dppp using the phosphonate to phosphine oxide single step reaction as the key step (*isolated as the mono-hydrate.) b) Synthesis of Methyl JohnPhos, a new Buchwald-type ligand. All isolated yields.

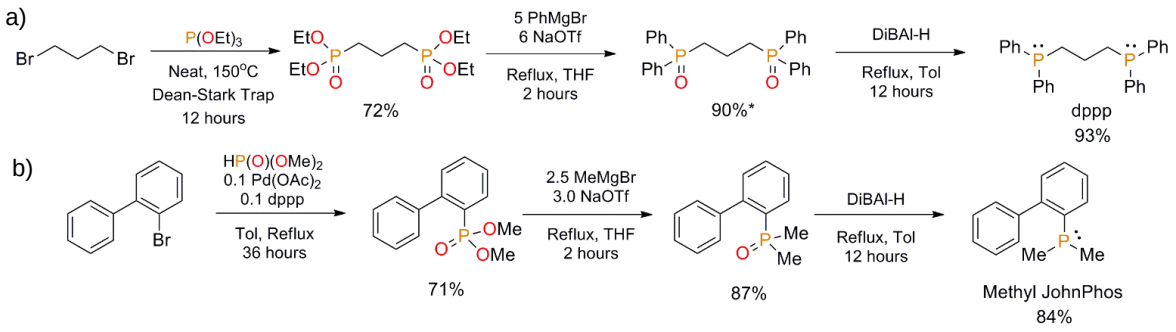

2.3. Conclusions

This work demonstrates a new, robust, and diverse method for synthesizing phosphine ligands that can be used to generate both known and novel heteroleptic phosphine ligands accessed through air-, water-, and silica-stable intermediates. Specifically, an improved method for the conversion of phosphonates into phosphine oxides using Grignard reagents was developed for the synthesis of phosphines. Normally, this reaction is plagued by a halide-mediated rearrangement of the phosphonate into thermodynamically inert oligomeric salts (Scheme 2.4). By precipitating the halide *in-situ*, vastly improved yields of the phosphine oxide were observed. Abstracting the halide from the Grignard reagent also appears to activate the Grignard for reactivity with otherwise non-reactive substrates such as phosphinates.

The reaction proceeds through a short-lived 5-coordinate intermediate, rather than a 4-coordinate phosphinate intermediate. It is also notable that this reaction proceeds with an inverse steric influence likely derived from the ability to prevent product inhibition of the phosphine oxide with the active Grignard reagent.

2.4. Experimental section

2.4.1. General considerations

Unless stated otherwise, reactions were conducted in oven-dried glassware under an atmosphere of nitrogen. Diethylether and tetrahydrofuran (THF) were dried using a DriSolv system using CuO and molecular sieves under argon. All other reaction solvents were purified and dried according to the literature.[43] All commercially obtained reagents were used as received unless otherwise specified. Synthesized organomagnesium reagents were titrated before use using either diphenylacetic acid[44] or No-D NMR spectroscopy[45] to determine concentration and were stored Ar at room temperature. Thin-layer chromatography (TLC) was visualized using low wavelength ultraviolet light (UV) for all aryl species or phosphomolybdic acid otherwise. Gas chromatography (GC) was performed on an Agilent Technologies 6850 Series II Gas Chromatograph. ^{1}H NMR spectra were recorded on a 300 or 500 MHz Varian spectrometer (^{1}H 300.09 MHz or 500.02 MHz, respectively) and are reported relative to deuterated solvent signals or an internal reference. Data for ^{1}H NMR spectra are reported as follows: chemical shift (δ ppm), multiplicity, coupling constant (Hz) and relative integration. ^{31}P{^{1}H} NMR spectra were recorded on a 300 or 500 MHz Varian spectrometer (^{31}P 121.48 MHz or 202.13 MHz, respectively) and are reported relative to the external standard of 0.1% H_3PO_4 in D_2O at 0 ppm. Infrared spectra were recorded using Nicolet Magna-550 Fourier Transform Infrared Spectrophotometer with diamond crystal ATR attachment.

The Biomolecular Mass Spectrometry Core of the Environmental Health Sciences Core Center at Oregon State University provided the high resolution mass spectra. The

project described was supported, in part, by award number P30ES000210 from the NIEHS, NIH.

2.4.2. Synthesis of phosphonates, phosphinates, and other reagents

All syntheses are described in detail in the Appendix A along with the relevant literature references. Text describing all syntheses; ^{1}H-, ^{31}P-, ^{19}F-, ^{13}C-NMR and IR spectra of starting materials and products; and data for selected additional experiments are available in Appendix A.

2.4.3. Reaction of phosphonates with organomagnesium and sodium triflate

All NMR yields were run (at least) in duplicate. For a typical reaction: a mixture of phosphonate (0.30 mmol) with NaOTf (0.67 mmol, 113.7 mg) stirring under a nitrogen atmosphere in a 5 mL round-bottom flask with a jacketed reflux condenser (set to 0 ^{o}C) was added 3.00 mL of THF with hexamethylbenzene (HMB) from a stock solution, containing 135.2 mg of HMB or 0.833 mmol in 25.00 mL of THF. The NaOTf was allowed to completely dissolve at room temperature before the flask was cooled to 0 ^{o}C with an ice bath. Organomagnesium reagent (0.63 mmol in an ethereal solvent) was added drop wise (generally 1 drop per 10 seconds) in a manner that the drops of reagent contacted the 0 ^{o}C cooling jacket wall before dripping down into the flask – effectively precooling each drop. A white precipitate immediately formed. After complete addition of organomagnesium, the reaction was allowed to stir at 0 ^{o}C for 2 minutes, then heated to reflux in an oil bath for 2 hours.

To quench the reaction, the flask was cooled to 0 ^{o}C, then poured into a separatory funnel with 5 mL of 0.1 M H_2SO_4. The round bottom flask was washed out with 5 mL of 0.1 M H_2SO_4 and added to the separatory funnel. The mixture was not allowed to sit for more than 2 minutes (polymerization of THF can occur) before the round bottom flask was rinsed out with 5 mL of dichloromethane and then added to the separatory funnel. The aqueous layer was washed three times 5 mL of dichloromethane. The combined organic layers were dried over Na_2SO_4 for several hours, then filtered, and dried *in vacuo*. The residue from the organic layer dissolved into deuterated chloroform and analyzed by NMR spectroscopy. All NMR yields reported were performed in at least duplicate with yields matching within +/-3%. A representative labeled spectrum from each is shown in the SI.

Slow addition rates of the organo-magnesium reagent are important for the best reproducibility. A very low effective magnesium concentration compared to phosphonate (i.e. a very slow addition rate) at cold temperatures (i.e. 0 ^{o}C) yields the most reproducible and highest yields. Reaction times for substrates may vary, however all reactions discussed were observed to be complete after 2 hours – longer reaction times sometimes led to lower yields. The workup of the reaction is also sensitive, responding best to a sulfuric acid quench followed by serial dichloromethane extractions (this step is necessary because phosphine oxides are very water soluble).

2.4.4. Synthesis of dppp

2.4.4.1. tetraethyl propane-1,3-diylbis(phosphonate)

A mixture of 1,3-dibromopropane (8.6445 g, 42 mmol) and triethylphosphite (16.50 g, 100 mmol) in a round bottom flask attached to a Dean-Stark apparatus were heated to 170 ^{o}C for 12 hours. The collection arm slowly collected bromoethane as confirmed by NMR spectroscopy. The reaction mixture was cooled to room temperature and directly fractionally distilled. The distillation yielded diethyl ethylphosphonate (35 ^{o}C at 400 mTorr), followed by triethylphosphate (55 ^{o}C at 400 mTorr) followed by a colorless oil of pure product (135-150 ^{o}C at 1000 mTorr), 9.7179 g, 72.3% yield. Properties matched literature values.[46] ^{1}H NMR (300 MHz, $CDCl_3$) δ 4.27 – 3.85 (m, 8H), 2.12 – 1.68 (m, 6H), 1.31 (t, *J* = 7.0 Hz, 12H). ^{31}P NMR (121 MHz, $CDCl_3$) δ 30.59.

2.4.4.2. propane-1,3-diylbis(diphenylphosphine oxide)

To a solution of tetraethyl propane-1,3-diylbis(phosphonate) (1.0277 g, 3.16 mmol) and sodium trifluoromethanesulfonate (4.421 g, 25 mmol) in THF (35 mL) at 0 ^{o}C was added phenylmagnesium bromide (11.0 mL, 1.73 M, 19 mmol) drop wise over 15 minutes. The reaction was then brought to reflux for 2 hours. The reaction mixture was cooled to 0 ^{o}C and quenched with 0.1 M H_2SO_4 (40 mL). The reaction mixture was washed with dichloromethane (3 x 35 mL), then the organics were collected and dried over Na_2SO_4. The organics were filtered and dried *in vacuo*, yielding a slightly yellow-clear extremely viscous paste. The paste was triturated with both H_2O and pentane to afford a slurry of fluffy off-white crystalline solid, propane-1,3-diylbis(diphenylphosphine oxide)•H_2O (1.3160 g, 90% yield). ^{1}H NMR (300 MHz, $CDCl_3$) δ 7.76 – 7.62 (m, 8H), 7.46 (m, 12H), 2.50 (dt, *J* = 10.8, 7.6 Hz, 4H), 2.28 (H_2O, s, 2H), 2.00 (dq, *J* = 20.0, 12.8, 9.6 Hz, 2H). ^{31}P NMR (121 MHz, $CDCl_3$) δ 32.59.

2.4.4.3. 1,3-bis(diphenylphosphino)propane

Under an inert atmosphere, propane-1,3-diylbis(diphenylphosphine oxide)•H_2O (50.0 mg, 0.11 mmol) was added to diisobutylaluminum hydride (161.2 mg, 1.1 mmol) and toluene (up to 0.5 mL) in a heavy-walled unregulated pressure vessel. The reaction mixture was allowed to vent overnight before being sealed and heated to 150 ^oC for 12 hours. The reaction mixture was allowed to cool, then (under an atmosphere of N_2) quenched with degassed 0.1M HCl and diluted out with diethyl ether (20 mL). The aqueous layer was washed with ether (3 x 10 mL). The collected organics were dried over Na_2SO_4, then filtered and dried *in vacuo*, affording very pure dppp as an off white crystalline solid (41.3 mg, 93% yield). Properties were identical to a purchased standard. ^1H NMR (300 MHz, $CDCl_3$) δ 7.51 – 7.23 (m, 10H), 2.24 (t, *J* = 7.8 Hz, 4H), 1.65 (tt, *J* = 16.1, 8.7 Hz, 1H). ^{31}P NMR (121 MHz, $CDCl_3$) δ -17.36.

2.4.5. Synthesis of methyl JohnPhos

2.4.5.1. dimethyl [1,1'-biphenyl]-2-ylphosphonate.

A 250 mL round bottomed flask fitted with a reflux condenser was charged with 2-bromobiphenyl (2.0225 g, 8.6 mmol), diisopropylethylamine (2.0700 g, 18 mmol), dimethylphosphonate (5.0800 g, 46 mmol), palladium(II) acetate (190.5 mg, 0.8 mmol), and 1,3-bis(diphenylphosphino)propane (696.3 mg, 1.7 mmol), dissolved in dry toluene (100 mL), and heated to reflux for 36 hours. The reaction was cooled to room temperature and diluted with EtOAc (100 mL). The organic layer was washed with saturated $NaHCO_3$ (3 x 100 mL) solution, then once with brine (100 mL). The organic layer was dried over Na_2SO_4, filtered, and the solvent was removed *in vacuo* yielding a

crude yellow oil with residual white solids. The crude product was purified by flash column chromatography (60 mesh silica, EtOAc with 1% triethyl amine, R_f = 0.6) yielding a hygroscopic crystalline white solid (1.5868 g, 71.1% yield). Properties were identical to the literature values.[47] MP (under Argon) 59-61 ^oC. ^1H NMR (500 MHz, $CDCl_3$) δ 8.03 (dd, *J* = 14.2, 7.7 Hz, 1H), 7.58 (t, *J* = 7.6 Hz, 1H), 7.50 – 7.32 (m, 7H), 3.51 (d, *J* = 11.2 Hz, 6H). ^{13}C NMR (126 MHz, $CDCl_3$) δ 141.32 (d, *J* = 4.4 Hz), 133.92 (d, *J* = 9.6 Hz), 132.13 (d, *J* = 3.0 Hz), 131.33 (d, *J* = 14.3 Hz), 129.12 , 127.55 (d, *J* = 2.8 Hz), 126.94 (d, *J* = 14.6 Hz), 126.06 (d, *J* = 188.2 Hz), 52.35 (d, *J* = 6.2 Hz). ^{31}P NMR (202 MHz, $CDCl_3$) δ 20.82.

2.4.5.2. [1,1'-biphenyl]-2-yldimethylphosphine oxide

To a solution of dimethyl [1,1'-biphenyl]-2-ylphosphonate (95.1 mg, 1.8 mmol) and sodium trifluoromethanesulfonate (150.0 mg, 4.2 mmol) in THF (4 mL) at 0 ^oC was added methylmagnesium bromide (0.32 mL, 3.0 M, 4.0 mmol) drop wise over 5 minutes. The reaction was then brought to reflux for 2 hours. The reaction mixture was cooled to 0 ^oC and quenched with 0.1 M H_2SO_4 (4 mL). The reaction mixture was washed with dichloromethane (3 x 4 mL), then the organics were collected and dried over Na_2SO_4. The mixture was filtered and dried *in vacuo* to afford a pure product as a crystalline solid (72.6 mg, 87% yield). ^1H NMR (300 MHz, $CDCl_3$) δ 8.16 (ddd, *J* = 12.9, 6.4, 2.4 Hz, 1H), 7.61 – 7.49 (m, 2H), 7.48 – 7.34 (m, 5H), 7.34 – 7.27 (m, 1H), 1.40 (d, *J* = 13.1 Hz, 6H). ^{13}C NMR (126 MHz, $CDCl_3$) δ 144.48 (d, *J* = 9.9 Hz), 141.26 (d, *J* = 3.5 Hz), 132.07 (d, *J* = 8.3 Hz), 131.24 (d, *J* = 2.5 Hz), 131.08 (d, *J* = 10.0 Hz), 129.66, 128.17, 128.09, 127.47 (d, *J* = 10.8 Hz), 18.98 (d, *J* = 71.6 Hz). ^{31}P NMR (121 MHz, $CDCl_3$) δ

35.02. HRMS (ES^+-TOF) m/z: $[M+Na]^+$ Calcd. for $C_{14}H_{15}ONaP$ 253.0751; found 253.0758.

2.4.5.3. [1,1'-biphenyl]-2-yldimethylphosphine

Under an inert atmosphere of N_2, [1,1'-biphenyl]-2-yldimethylphosphine oxide (368.0 mg, 1.6 mmol) was added to diisobutylaluminum hydride (1.2116g, 8.0 mmol) and toluene (5 mL) in a heavy-walled unregulated pressure vessel. The reaction mixture was allowed to vent overnight before being sealed and heated to 150 ^oC for 12 hours. The reaction mixture was allowed to cool, then (under an atmosphere of N_2) quenched with degassed 0.1M HCl and diluted with diethyl ether (20 mL). The aqueous layer was washed with ether (3 x 20 mL). The collected organics were dried over Na_2SO_4, then filtered and dried *in vacuo*, affording a very pure [1,1'-biphenyl]-2-yldimethylphosphine as a colorless crystalline solid (288.3 mg, 84% yield). ^1H NMR (500 MHz, $CDCl_3$) δ 7.37 (ddd, *J* = 7.0, 4.1, 1.9 Hz, 1H), 7.29 – 7.25 (m, 4H), 7.25 – 7.19 (m, 3H), 7.11 (ddd, *J* = 6.2, 3.9, 2.1 Hz, 1H), 0.97 (d, *J* = 3.8 Hz, 6H). ^{13}C NMR (126 MHz, $CDCl_3$) δ 146.69 (d, *J* = 23.1 Hz), 142.00 (d, *J* = 4.3 Hz), 140.49 (d, *J* = 18.3 Hz), 129.82 (d, *J* = 3.9 Hz), 129.58 (d, *J* = 4.3 Hz), 128.89, 127.83, 127.20 (d, *J* = 21.2 Hz), 14.04 (d, *J* = 13.8 Hz). ^{31}P NMR (202 MHz, $CDCl_3$) δ -51.86. HRMS (EI^+-JEOL MStation) m/z: $[M]^+$ Calcd. for $C_{14}H_{15}P$ 214.09114; found 214.09049.

2.5. Summary

The synthesis of tertiary phosphine oxides from phosphonates was achieved reliably and in good-to-excellent yields using stoichiometric amounts of alkyl or aryl

Grignard reagents and sodium trifluoromethanesulfonate (NaOTf). In the absence of the NaOTf additive, covalent coordination oligomers of magnesium and phosphorus species dominate the reaction – producing very low yields of phosphine oxide, but high conversions of the phosphonate starting material. Mechanistic studies revealed that a five-coordinate phosphorus species – not a phosphinate – is the reaction intermediate. A diverse array of phosphonates was converted to phosphine oxides using a variety of Grignard reagents for direct carbon-phosphorus functionalization. This new methodology especially simplifies the synthesis of dimethylphosphino ($RPMe_2$)-type phosphines by using air-, water-, and silica-stable intermediates. To highlight this reaction, a new Buchwald-type ligand ([1,1'-biphenyl]-2-yldimethylphosphine or Methyl JohnPhos) as well as a classic bidentate phosphine bis(diphenylphosphino)propane (dppp) were synthesized in excellent yields.

2.6. Bridge

In this chapter, a new synthetic method for making phosphine oxides is presented. This approach uses the phosphorus moiety as an electrophile. The next chapter will discuss using a phosphorus moiety as a nucleophile for similar phosphine oxide syntheses. These two approaches represent a new way to synthesize aryl and alkyl dimethyl phosphines.

CHAPTER III

IMPROVED GENERAL SYNTHETIC ROUTE TO ALKYL-DIMETHYLPHOSPHINES

3.1. Introduction

3.1.1. Coauthored material

Chapter III is a modified form of a paper to be submitted for publication. I developed the project, did the majority of the chemistry, and wrote the manuscript. Coauthors include Daniel T. Seidenkranz and David R. Tyler.

3.1.2. Introduction

Despite the importance of phosphines in modern inorganic chemistry, catalysts, materials, medicinal compounds, and organic reagents, the challenging nature of phosphine chemistry continues to thwart the development of new phosphines.[1–3] Alkyl dimethylphosphines, a severely under-represented class of phosphines, have been the focus of research in our laboratory. Their outstanding ligand properties are overshadowed by their synthetic inaccessibility due to air-, water-, and silica-instability of many of the precursors and intermediates for traditional syntheses.[4] We sought to develop a synthesis for alkyl-dimethylphosphines (similar to our development of aryl-dimethylphosphine synthesis) that focuses on air-, water-, and silica-stable precursors.[5]

3.2. Results and discussion

3.2.1. Preliminary results

Secondary phosphine oxides[6–8] are an excellent synthon for making tertiary phosphine oxides, but to our knowledge have only been used as cross-coupling partners to form P-aryl bonds or P-alkyl bonds via radical chemistry.[9,10] Based on an early report by Hays[11] and later Doyle[12] in which H-phosphonates are directly converted to tertiary phosphine oxides (Figure 3.1, top route), we believed it possible to isolate the phosphinite anion intermediate and use it directly. The Hays method is a two-step, one-pot reaction with poor yields, egregious workup conditions, and very limited substrates.[‡] We sought to produce the nucleophilic phosphinite anion directly from a secondary phosphine oxide (SPO) to avoid these severely unfavorable reaction conditions.

Initial attempts to deprotonate the SPO with a Grignard reagent to generate the same phosphinite anion as Hays were not successful. Grignard reagents promoted disproportionation of the SPO rather than deprotonation, which was very surprising given that the pK_a range for SPOs is 21-27.[13] This result suggests that the formation and subsequent stability of the phosphinite anion is sensitive to choice of base.

A brief screening of bases for SPO deprotonation confirms the sensitivity of deprotonation to choice of base, with only KHMDS and NaHMDS producing product both quantitatively and cleanly (Figure 3.2). Based on the results from Figure 3.2, it is likely that a combination of cation, conjugate acid, and kinetics of deprotonation all contribute to KHMDS and NaHMDS being the most effective base. It is also notable that at times up to 24 hours after the phosphinite anion had been generated, the same clean conversions to triethylphopshine oxide from reaction with ethyl iodide were observed

with these bases. This result suggests that the phosphinite anion formed with NaHMDS or KHMDS is stable at room temperature (under N_2) and not prone to disproportionation for at least a day.

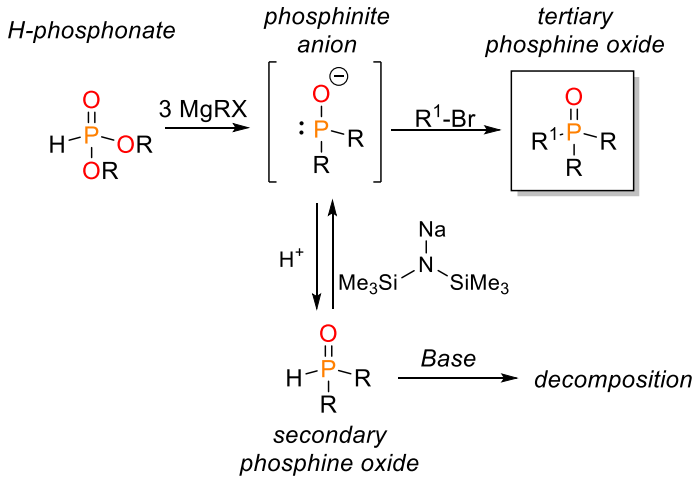

Figure 3.1. General scheme showing how H-phosphonate and H-phosphine oxide can form a phosphinite anion and subsequently, a tertiary phosphine oxide.

3.2.2. Substrate scope

To determine the generality of the reaction, a series of SPOs were deprotonated using NaHMDS and reacted with a terminal alkyl bromide (Table 3.1). All were very clean reactions – with no observable elimination products or side reactions. Note that no purification was necessary; the purity of the crude reaction mixtures was >98% in every case. Because of the incredible polarity of the phosphine oxide and non-polar alkyl halide, separation of the reaction components with water and organic solvents provides excellent purification.

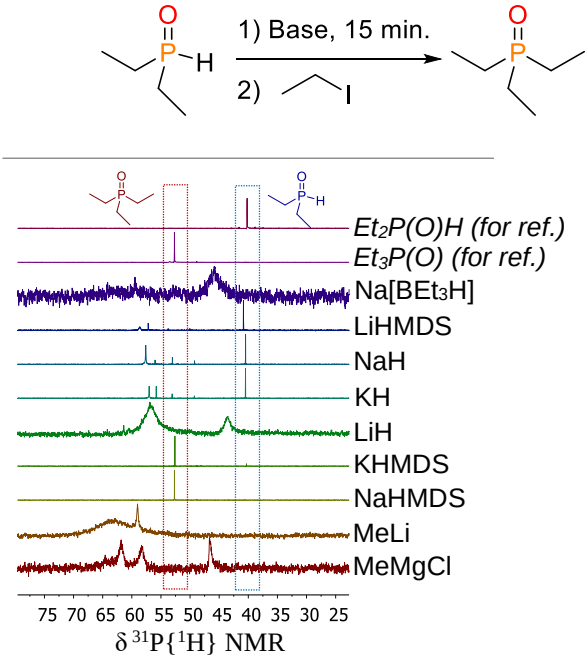

Figure 3.2. $^{31}P\{^{1}H\}$ NMR overlay showing crude reaction mixtures after SPO deprotonation and EtI quench.

Table 3.1. Reaction scope of deprotonated SPOs for nucleophilic substitution. [a]Average of two isolated yields.

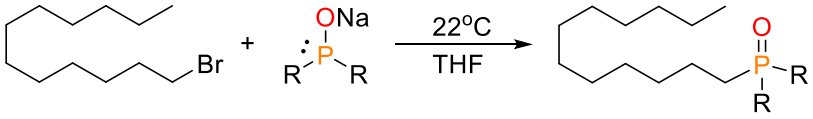

R	Yield[a]
Me	93
Et	95
^{i}Pr	89
^{t}Bu	94

Next, we explored the reactivity of dimethyl phosphinite anion with a series of electrophiles (Table 3.2). Primary chlorides and bromides as well as secondary bromides were converted to tertiary phosphine oxides in excellent yields. Benzyl bromides and chlorides were also high yielding. The primary triflate (Table 3.2, entry 3) was completely consumed with no evidence of product formation. The secondary triflate

(Table 3.2, entry 10) was completely unreactive with no appreciable conversion. As well, secondary chlorides were resistant to conversion in refluxing THF (Table 3.2, entry 5). The identity of the leaving group appears to play a significant electronic role with better electrophiles being more readily reacted with the phosphinite anion.

Slightly increasing the steric hindrance of the electrophile to a secondary carbon (Table 3.2, entries 4-10) only grants reactivity with bromides. Even so, reactivity is only observed at the less sterically hindered *sec*-butyl- and cyclopentylbromide (Table 3.2, entries 6 and 7) compared with slightly more sterically hindered cyclohexyl- and 2-adamantylbromides (Table 3.2, entries 8 and 9). The surprising chemoselectivity of the phosphinite anion likely arises predominantly from steric hindrance with a slight electronic influence.

Table 3.2. Reaction scope of alkyl halides and triflates for nucleophilic substitution. [a]Average of two isolated yields. [a]All average of two isolated yields. [b]Quantitiative conversion. [c]No conversion observed. [d]Refluxing THF for 16 hours, no conversion observed. [e]Reacted at 0 ^{o}C for 2 hours.

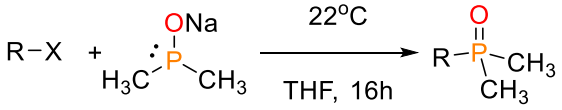

Entry	Electrophile	Yield[a] (%)
1	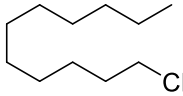	92
2	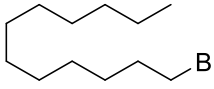	93

Table 3.2. (continued)

Entry	Electrophile	Yield[a] (%)
3	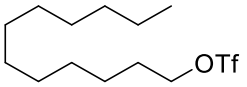	0[b]
4	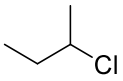	0[c]
5	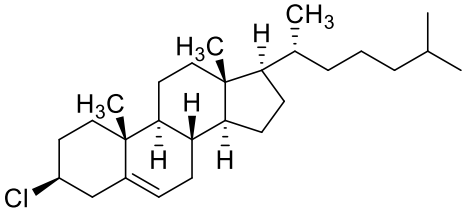	0[d]
6	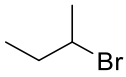	76
7	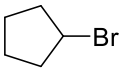	86
8	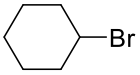	0[c]
9	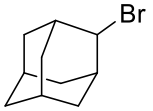	0[c]
10	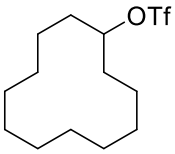	0[c]
11	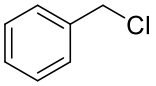	80[e]
12	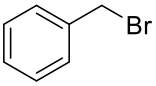	86[e]

3.2.3. Ligand precursors

With the general scope of reactivity well established, a series of unique dimethyl phosphine ligand precursors (phosphine oxides) were synthesized (Table 3.3). Bis-electrophiles were readily converted into bidentate phosphine precursors. Though a handful of bis(dimethylphosphine) ligands have been made – they are typically synthesized under arduous synthetic conditions.[14–17] Table 3.3 represents an exceptionally simple and straightforward method for synthesizing a series of bidentate phosphine precursors. These phosphine oxide precursors are air-, water-, and silica-stable compounds that typically exist as crystalline solids. A single step reduction will yield the air-sensitive alkyl dimethylphosphine product.[18–20]

3.2.4. Mechanistic considerations

In agreement with data from Hays, the intermediate after SPO deprotonation appears to be best described as a phosphinite anion with a $^{31}P\{^{1}H\}$ shift to a single resonance at 121.60 ppm from 22.51 ppm (Figure 3.3, R = ^{i}Pr). The nucleophilicity of the phosphinite anion prefers P-attack over O-attack for most electrophiles. Two notable exceptions are benzyl bromides (a small amount of side reactivity attributed to competitive O-attack) and oxophilic electrophiles such as chlorosilanes. This observation suggests that the hard oxygen nucleophile is cation passivated and only attacks strongly electrophilic or oxophilic substrates. In almost all other cases, bond formation was observed at the phosphorus.

Table 3.3. Bidentate phosphine oxide pre-ligand synthesis. [a]Average of two isolated yields.

Entry	Substrate	Product	Yield[a] (%)
1	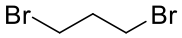	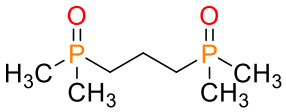	78
2	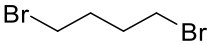	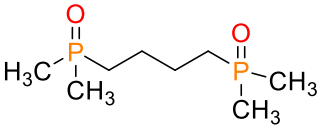	67
3	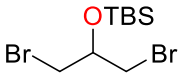	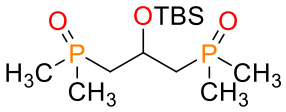	84
4	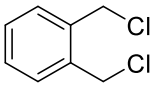	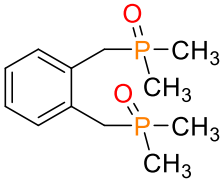 dts2.084, dts2.116	87
5	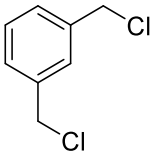	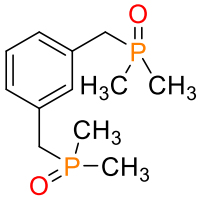 dts2.085, dts2.117	87

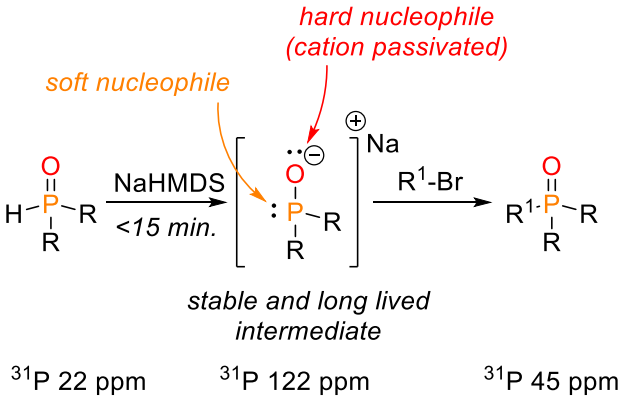

Figure 3.3. Deprotonation of SPO to form the intermediate phosphinite anion followed by reaction with an electrophile to a tertiary phosphine oxide ($^{31}P\{^{1}H\}$ NMR shifts noted).

Based on the trends in Table 3.2, the reaction very likely proceeds via an S_N2 mechanism. This mechanism explains the chemoselectivity. It is likely that steric sensitivity is predominantly responsible for reactivity with non-sterically hindered secondary bromides, but reluctance to react with secondary chlorides and sterically hindered secondary bromides.

We have also observed the ability of di-*tert*-butylphosphine oxide to perform electron transfer chemistry (Scheme 3.1). In the extreme case of di-*tert*-butylphopshinite anion reacting with benzylbromide, di-*tert*-butylphosphinic bromide was isolated along with 1,2-diphenylethane (Scheme 3.1). This observation suggests that in these extreme cases a competitive electron transfer can occur. We are still investigating this reaction; however, it offers a resourceful new way to synthesize di-*tert*-butylphosphinic bromide. Notably, in these cases the primary product of the reaction is a phosphinic bromide species which is not observed in other cases.

Scheme 3.1. Electron transfer mechanism, favoring di-*tert*-butylphosphinic bromide formation over standard S_N2 products.

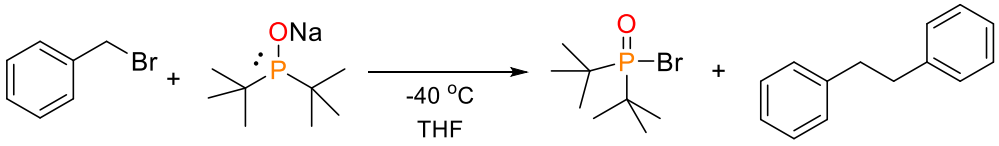

3.3. Conclusions

In conclusion, we have developed a straight-forward approach to synthesize tertiary phosphine oxides directly from SPOs. The deprotonation of these SPOs was extremely sensitive to the identity of the base. NaHMDS was found to be the best choice to quickly and selectively produce a single species: the stable phosphinite anion. The phosphinite anion acts as a nucleophile predominantly through the phosphorus, not the oxygen. The reactivity of the phosphinite anion is very sensitive to steric hindrance and likely proceeds through an S_N2 mechanism. The reactivity was very clean, favoring P-addition to electrophiles over elimination. No purification was necessary for almost all the substrates studied.

3.4. Experimental

3.4.1. General Considerations

Unless stated otherwise, reactions were conducted in oven-dried glassware under an atmosphere of nitrogen using either standard Schlenk techniques or a dribox maintained at < 1.0 ppm O_2. Diethyl ether and tetrahydrofuran (THF) were dried using a DriSolv system using CuO and molecular sieves under argon. All other reaction solvents were purified and dried according to the literature.[21] All commercially obtained reagents were used as received unless otherwise specified. Synthesized organomagnesium

reagents were titrated before use using either diphenyl acetic acid[22] or No-D NMR spectroscopy[23] to determine concentration and were stored under Ar at room temperature. Thin-layer chromatography (TLC) was visualized using low wavelength ultraviolet light (UV) for all aryl species or phosphomolybdic acid. ^{1}H NMR spectra were recorded on a 300 or 500 MHz Varian spectrometer (^{1}H 300.09 MHz or 500.02 MHz, respectively) and are reported relative to deuterated solvent signals or an internal reference. Data for ^{1}H NMR spectra are reported as follows: chemical shift (δ ppm), multiplicity, coupling constant (Hz) and relative integration. ^{31}P{^{1}H} NMR spectra were recorded on a 300 or 500 MHz Varian spectrometer (^{31}P 121.48 MHz or 202.13 MHz, respectively) and are reported relative to the external standard of 0.1% H_3PO_4 in D_2O at 0 ppm.
Secondary phosphine oxides were synthesized as previously reported (see Appendix B).

3.4.2. General synthetic procedure

3.4.2.1. Mono-phosphine oxides

To a stirring degassed solution of dialkylphosphine oxide (1.1 equivalents per electrophile, 0.2 M in THF) was added sodium bis(trimethylsilyl)amide (1 equivalent per dialkylphosphine oxide, c.a. 1.9 M in THF) dropwise at room temperature and allowed to stir for 15 minutes. The solution became turbid as the phosphinite anion formed. A degassed solution of alkyl halide (1 equivalent, 0.2 M in THF) was added dropwise to the phosphinite anion mixture. A white precipitate formed. The reaction mixture was stirred at room temperature for 1-16 hours. To quench the mixture, the equivalent volume of H_2O was added and the mixture was extracted five times with equal volumes of

dichloromethane. The combined organics were dried over Na_2SO_4, filtered, and solvent was removed under vacuum.

3.4.2.2. Bis-phosphine oxides

To a stirring degassed solution of dialkylphosphine oxide (0.95 equivalents per electrophile, 0.2 M in THF) was added sodium bis(trimethylsilyl)amide (1 equivalent per dialkylphosphine oxide, c.a. 1.9 M in THF) dropwise at room temperature and allowed to stir for 15 minutes. The solution became turbid as the phosphinite anion formed. A degassed solution of bis-alkyl halide (0.47 equivalents, 0.2 M in THF) was added dropwise to the phosphinite anion mixture. A white precipitate formed. The reaction mixture was stirred at room temperature for 1-16 hours. Bis-phosphine oxide workup. To quench the mixture, the equivalent volume of H_2O was added and the mixture was extracted five times with equal volumes of dichloromethane. The aqueous layer was evaporated to salts and extracted into chloroform with stirring. The resulting mixture was filtered through diatomaceous earth and the solvent was removed under vacuum. If further purification was necessary, flash chromatography on neutral alumina using chloroform and isopropanol mixtures were used.

3.4.3. Spectroscopic data for phosphine oxides

Dodecyldimethylphosphine oxide. Dimethylphosphine oxide (34.4 mg, 0.44 mmol), dodecyl bromide (100.0 mg, 0.40 mmol). Isolated as a pure white crystalline solid (96.6 mg, 93.4%). ^{1}H NMR (300 MHz, Chloroform-*d*) δ 1.76 – 1.47 (m, 3H), 1.43 (d, J = 12.5

Hz, 7H), 1.22 (d, *J* = 4.5 Hz, 18H), 0.96 – 0.70 (m, 3H). ^{31}P NMR (121 MHz, cdcl$_3$) δ 42.44.

Dodecyldiethylphosphine oxide. Diethylphosphine oxide (46.8 mg, 0.44 mmol), dodecyl bromide (100.0 mg, 0.40 mmol). Isolated as a pure white crystalline solid (99.8 mg, 96.4%). ^{1}H NMR (300 MHz, Chloroform-*d*) δ 1.75 – 1.42 (m, 5H), 1.42 – 1.27 (m, 6H), 1.22 (s, 16H), 1.12 (dt, *J* = 15.8, 7.7 Hz, 5H), 0.92 – 0.76 (m, 3H). ^{31}P NMR (121 MHz, cdcl$_3$) δ 51.59.

Dodecyldiisopropylphosphine oxide. Diisopropylphosphine oxide (46.8 mg, 0.44 mmol), dodecyl bromide (100.0 mg, 0.40 mmol). Isolated as a colorless oil (113.2 mg, 93.6%). ^{1}H NMR (300 MHz, Chloroform-*d*) δ 2.01 (dhept, *J* = 10.9, 7.2 Hz, 2H), 1.72 – 1.51 (m, 4H), 1.33 (d, *J* = 26.2 Hz, 1H), 1.25 (s, 18H), 1.23 – 1.11 (m, 12H), 0.92 – 0.81 (m, 3H). ^{31}P NMR (121 MHz, cdcl$_3$) δ 55.87.

Di-*tert*-butyl(dodecyl)phosphine oxide. Di-*tert*-butylphosphine oxide (46.8 mg, 0.44 mmol), dodecyl bromide (100.0 mg, 0.40 mmol). Isolated as a white crystalline solid (128.9 mg, 97.5%). ^{1}H NMR (300 MHz, Chloroform-*d*) δ 1.75 – 1.55 (m, 4H), 1.42 – 1.07 (m, 36H), 0.87 (t, *J* = 7.0, 5.9 Hz, 3H). ^{31}P NMR (121 MHz, cdcl$_3$) δ 59.42.

sec-Butyldimethylphosphine oxide. Dimethylphosphine oxide (50.0 mg, 0.64 mmol), 2-bromobutane (96.6 mg, 0.71 mmol). Isolated as a white crystalline solid (73.1 mg, 76.6%). ^{1}H NMR (300 MHz, Chloroform-*d*) δ 1.74 (ddddd, *J* = 80.5, 14.3, 10.7, 7.3, 3.7

Hz, 2H), 1.43 (dd, *J* = 12.2, 4.1 Hz, 6H), 1.29 (dtd, *J* = 13.5, 6.7, 3.2 Hz, 1H), 1.16 (dd, *J* = 17.0, 7.2 Hz, 3H), 1.04 (t, *J* = 7.4 Hz, 3H). ^{31}P NMR (121 MHz, Chloroform-*d*) δ 48.72.

Undecyldimethylphosphine oxide. Dimethylphosphine oxide (50 mg, 0.64 mmol), 1-chloroundecane (111.1 mg, 0.58 mmol). Isolated as a white crystalline solid (127.7 mg, 91.9%). ^{1}H NMR (300 MHz, Chloroform-*d*) δ 1.72 – 1.45 (m, 2H), 1.40 (d, *J* = 12.5 Hz, 6H), 1.36 – 1.23 (m, 6H), 1.20 (d, *J* = 5.1 Hz, 12H), 0.89 – 0.73 (m, 3H). ^{31}P NMR (121 MHz, Chloroform-*d*) δ 42.44.

Cyclopentyldimethylphosphine oxide. Dimethylphosphine oxide (50.0 mg, 0.64 mmol), bromocyclopentane (86.8 mg, 0.58 mmol). Isolated as a white crystalline solid (76.4 mg, 87.2%). ^{1}H NMR (300 MHz, Chloroform-*d*) δ 2.10 – 1.80 (m, 3H), 1.80 – 1.50 (m, 6H), 1.41 (d, *J* = 12.2 Hz, 6H). ^{31}P NMR (121 MHz, Chloroform-*d*) δ 46.03.

Benzyldimethylphosphine oxide. Dimethylphosphine oxide (50.0 mg, 0.64 mmol), benzylchloride (73.7 mg, 0.58 mmol) or benzylbromide (99.6 mg, 0.58 mmol). Isolated as a white crystalline solid (78.3mg, 79.9% and 84.4 mg, 86.2%, respectively). ^{1}H NMR (300 MHz, Chloroform-*d*) δ 7.39 – 7.17 (m, 4H), 3.16 (d, *J* = 15.5 Hz, 2H), 1.43 (d, *J* = 12.6 Hz, 6H). ^{31}P NMR (121 MHz, Chloroform-*d*) δ 40.96.

Propane-1,3-diylbis(dimethylphosphine oxide). Dimethylphosphine oxide (50 mg, 0.64 mmol), 1,3-dibromopropane (136.8 mg, 0.67 mmol). Isolated as a white crystalline solid

(97.9 mg, 78.0%). ^{1}H NMR (300 MHz, Chloroform-*d*) δ 2.08 – 1.76 (m, 6H), 1.48 (d, *J* = 12.5 Hz, 12H). ^{31}P NMR (121 MHz, Chloroform-*d*) δ 41.43.

Butane-1,4-diylbis(dimethylphosphine oxide). Dimethylphosphine oxide (50 mg, 0.64 mmol), 1,4-dibromobutane (144.7 mg, 0.67 mmol). Isolated as a white crystalline solid (90.5 mg, 67.3%). ^{1}H NMR (300 MHz, Chloroform-*d*) δ 1.85 – 1.61 (m, 8H), 1.46 (d, *J* = 12.9 Hz, 12H). ^{31}P NMR (121 MHz, Chloroform-*d*) δ 41.70.

(2-((tert-butyldimethylsilyl)oxy)propane-1,3-diyl)bis(dimethylphosphine oxide). Dimethylphosphine oxide (50 mg, 0.64 mmol), tert-butyl((1,3-dibromopropan-2-yl)oxy)dimethylsilane (222.5 mg, 0.67 mmol). Isolated as a white crystalline solid (174.9 mg, 83.7%). ^{1}H NMR (300 MHz, Chloroform-*d*) δ 4.66 (dp, *J* = 15.2, 7.2, 6.2 Hz, 1H), 2.47 (ddd, *J* = 15.0, 10.4, 7.0 Hz, 2H), 2.05 (ddd, *J* = 15.1, 10.6, 4.7 Hz, 2H), 1.66 – 1.41 (m, 12H), 0.87 (s, 9H), 0.11 (s, 6H). ^{31}P NMR (121 MHz, Chloroform-*d*) δ 39.48.

(1,2-phenylenebis(methylene))bis(dimethylphosphine oxide). Dimethylphosphine oxide (50.0 mg, 0.64 mmol), 1,2-bis(bromomethyl)benzene (176.9 mg, 0.67 mmol). Isolated as a white crystalline solid (144.0 mg, 87.1%). ^{1}H NMR (500 MHz, Chloroform-*d*) δ 7.25 – 7.13 (m, 4H), 3.49 (d, *J* = 12.8 Hz, 4H), 1.48 (d, *J* = 12.3 Hz, 12H). ^{31}P NMR (202 MHz, Chloroform-*d*) δ 41.39.

(1,3-phenylenebis(methylene))bis(dimethylphosphine oxide). Dimethylphosphine oxide (50.0 mg, 0.64 mmol), 1,3-bis(bromomethyl)benzene (176.9 mg, 0.67 mmol). Isolated as

a white crystalline solid (144.3 mg, 87.3%). ^{1}H NMR (500 MHz, Chloroform-*d*) δ 7.30 (t, *J* = 7.6 Hz, 1H), 7.21 – 7.10 (m, 3H), 3.13 (d, *J* = 14.8 Hz, 4H), 1.44 (d, *J* = 12.5 Hz, 12H). ^{31}P NMR (202 MHz, Chloroform-*d*) δ 40.37.

3.5. Summary

The synthesis of alkyl tertiary phosphine oxides directly from SPOs was described. The deprotonation of alkyl SPOs is extremely sensitive to the identity of the base. NaHMDS was found to be the best choice to quickly and selectively produce a stable phosphinite anion. The phosphinite anion is nucleophilic towards common organic electrophiles predominantly through the phosphorus, not the oxygen. Very few side reactions or elimination reactions were observed. The phosphinite anion is sensitive to steric hindrance and likely proceeds through an S_N2 mechanism.

3.6. Notes

‡Requires 4 hours of refluxing THF, typical yields <60% for primary alkyl bromides, typical workup includes rigorously slow addition with K_2CO_3 (aq) to a vigorously stirred solution of product to prevent gelation of Mg salts, followed by several multi-liter washes with boiling MeOH (when performed on the preparative scale) over a fine precipitate cake , including multiple filtrations and drying steps – all before compound purification.

3.7. Bridge

This chapter of my dissertation discusses new synthetic methods to make dimethyl phosphine oxides. The utility of phosphine oxides is in their reduced form as ligands for metal complexes. The next chapter will discuss several ligands synthesized using this chemistry and their properties as metal complexes.

CHAPTER IV

STERIC AND ELECTRONIC INFLUENCES OF BUCHWALD-TYPE ALKYL-JOHNPHOS LIGANDS

4.1. Introduction

4.1.1. Coauthored material

Chapter IV is a modified form of a paper submitted for publication. I developed the project, did all of the chemistry, and wrote the manuscript. Coauthors include Lev N. Zakharov and David R. Tyler.

4.1.2. Introduction to phosphines

The advent of designer phosphines in the last two decades has led to a portfolio of homogenous metal catalytic systems that impart distinctive reactivity using subtle structural variations in the phosphines.[1] Buchwald-type ligands have been particularly successful at forming highly active palladium catalysts for cross-coupling while exemplifying how subtle structural variations create critical reactivity differences at a palladium center (Figure 4.1).[2–4] Due to limitations in traditional phosphine synthetic methods, typical commercially available phosphine ligands are limited to bulky functional groups.[5] Consequently, the synthesis of dimethyl-functionalized designer phosphine ligands is rare.[6] In fact, the dimethyl phosphine derivatives of most commercially available phosphine ligands have yet to be reported (e.g., dimethyl phosphino- DIOP, -BINAP, -SPhos,[‡] etc.).[7] Such ligands would potentially provide better catalysts or, at the very least, conclusive information about electronic and structural

trends for ligand design. The omission of the dimethyl phosphine moiety in modern ligand design has been partly compensated for by predictive calculations;[8–11] however, many of these calculations have yet to be validated by experiment.

The recent preparation of [1,1'-biphenyl]-2-yldimethylphosphine (Methyl-JohnPhos; MeJPhos for short) by our laboratory has given us the opportunity to study a representative series of alkyl- JohnPhos ligands.[12] Buchwald ligands have long been valued for two design features, namely a strong σ-donating dialkyl-phosphine and a sterically demanding biphenyl moiety.[13] Though Buchwald-type ligands have been thoroughly studied for their properties by derivatization of the biphenyl moiety, very little effort has gone into determining effects of the alkyl groups at phosphorus.[14–17] Because only larger alkyl groups (*tert*-butyl, *cyclo*-hexyl, adamantyl, etc.) have been studied, it is not clear how small alkyl groups on the phosphine affect metal complex reactivity.

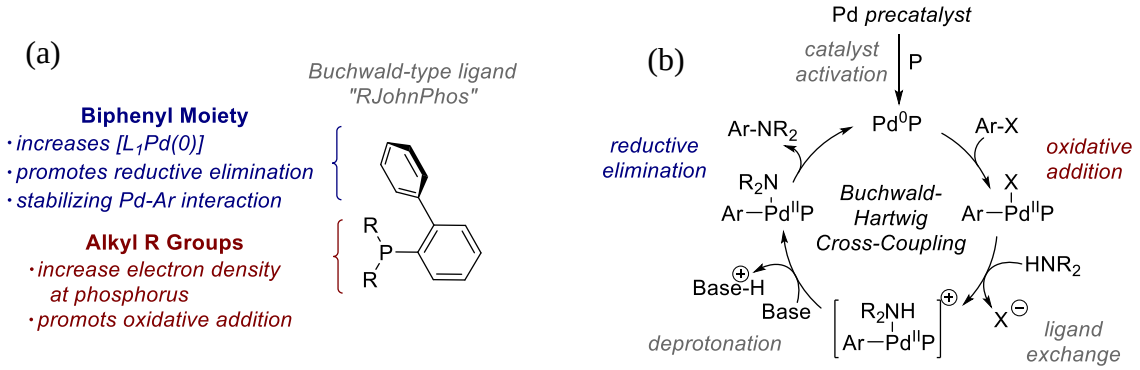

Figure 4.1. (a) Buchwald-type ligand structural features and their proposed effects on the palladium complex and catalytic properties for cross-coupling reactions.[13] (b) The mechanism of Buchwald-Hartwig cross-coupling.[18]

To investigate the effect of the alkyl groups, we synthesized and investigated a range of Buchwald-type ligands (Figure 4.2), with an emphasis on how the ligands

contribute to the electronic and structural properties of metal complexes. We hypothesized that a shorter phosphorus-metal bond distance for the smaller R-JohnPhos ligands could provide superior σ-donation (which is necessary for difficult oxidative additions at Pd metal centers, Figure 4.1b) while retaining enough steric hindrance at the biphenyl moiety (which is necessary for reductive eliminations in Pd cross-coupling reactions, Figure 4.1b). We report here the results of our study on Buchwald-type ligands with smaller alkyl groups and the implications for structure-function relationships.

4.2. Results and discussion

A complete series of alkyl-JohnPhos ligands (referred to as R-JohnPhos ligands from here forward) was synthesized (MeJPhos, EtJPhos, and ^{i}PrJPhos) or purchased (CyJPhos and ^{t}BuJPhos; Figure 4.2). These served as a representative collection of alkyl groups at the phosphorus while maintaining the *o*-biphenyl moiety.

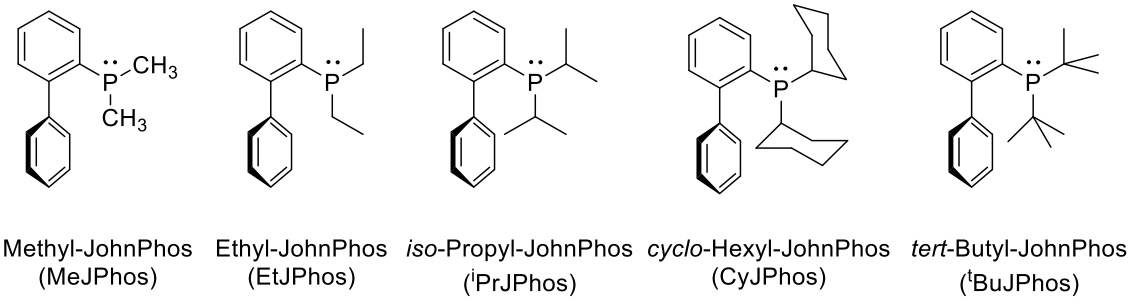

Figure 4.2. Structures, names, and abbreviated names of the R-JohnPhos ligands studied in this report.

4.2.1. Methyl-JohnPhos

Given that MeJPhos has not been studied before, its properties are briefly discussed here. MeJPhos is a low melting (55-56 °C) crystalline solid. The crystal structure exhibits a slightly distorted trigonal pyramid at phosphorus and a dihedral angle of 66.8° for the biphenyl (Figure 4.3). Based on the ∠C-P-C bond angles (100.3°, 102.7°, and 98.7°; Figure 4.3), there is relatively little steric strain in the solid state. It is notable that both as a solid and in solution, MeJPhos resists oxidation by O_2. Experimentally, after 85 hours under 1 atm of O_2, only 8% of a sample in C_6D_6 solution was oxidized (Appendix C, Figure C1). In comparison to $PPhMe_2$ (a non-*o*-biphenyl structural analogue), this oxidation is approximately 10^3 slower. Other Buchwald-type ligands displayed almost identical oxygen stability as MeJPhos. It is noted that the reasons for O_2 stability in Buchwald-type ligands have been studied.[19]

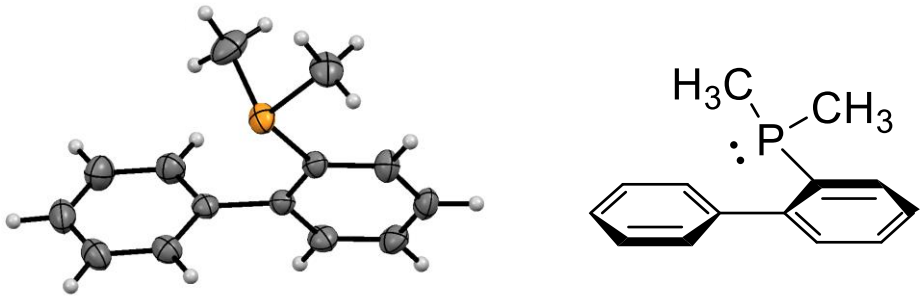

Figure 4.3. ORTEP crystal structure of MeJPhos (all H atoms refined). The biphenyl torsion angle is 66.8° and the ∠C-P-C bond angles are 100.3°, 102.7°, and 98.7°. Thermal ellipsoids are drawn at 50% probability.

4.2.2. Electronic analysis

In general, Buchwald-type ligands are known for their strong σ-donation, especially when compared to triaryl phosphine ligands (e.g. PPh_3).[3] All phosphines with an aryl substituent are also capable of some π-accepting from the metal, although the π-accepting interaction is weaker than the σ-donation. Both the σ- and π-electronic influences at a metal center play crucial roles in determining reactivity. Therefore, it is important to understand the degree to which both σ-basicity and π-acidity of the phosphine affect a metal. The traditional Tolman $Ni^0(CO)_3PR_3$ complexes used to measure the electronic parameters of ligands are straightforward to synthesize (in a room temperature reaction) and can be compared against a large body of literature.[20] However, for our study Tolman's method is disadvantageous because of both the acute toxicity of $Ni^0(CO)_4$ and the convolution of the σ- and π-ligand/metal interactions. To quantify both the π-acidity and σ-basicity of the R-JohnPhos ligands in Figure 4.2, a series of pseudo-octahedral chromium carbonyl complexes ($Cr^0(CO)_5PR_3$) was chosen to serve as spectroscopic proxies for the Ni complexes. The $Cr^0(CO)_5PR_3$ complexes can be compared directly to the $Ni^0(CO)_3PR_3$ complexes by using a well-established linear relationship using ^{13}C NMR and IR data.[21,22] Solution measurements were chosen to avoid aberrations caused by crystal packing forces of solid-state measurements.

The $Cr^0(CO)_5PR_3$ complexes for MeJPhos, EtJPhos, ^{i}PrJPhos, CyJPhos and ^{t}BuJPhos were generated in-situ by irradiation ($\lambda > 254$ nm) of $Cr^0(CO)_6$ and the ligand in THF with a high-pressure mercury arc lamp in a CaF_2 cell (Scheme 4.1). Substitution quickly occurred.

This transformation was monitored over time by infrared spectroscopy to determine the stretching frequencies of the carbonyl ligands in the $Cr^0(CO)_5PR_3$ product. From these spectra, $Cr^0(CO)_5PR_3$ (the first species to form) was easily de-convoluted from the *trans*-$Cr^0(CO)_4(PR_3)_2$ complex that formed subsequently.

Scheme 4.1. *In-situ* synthesis of $Cr^0(CO)_5PR_3$ species (boxed for clarity) also showing a secondary carbonyl expulsion leading to *trans*-$Cr^0(CO)_4(PR_3)_2$.

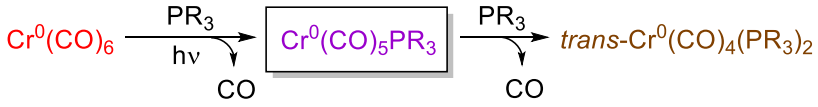

As shown in Figure 4.4, irradiation of $Cr^0(CO)_6$ in the presence of ligand produced the $Cr^0(CO)_5PR_3$ species (where PR_3 = R-JohnPhos), with carbonyl absorption peaks assigned according to known values of analogous solution-phase chromium complexes.[23–26] The vibrational force constants were calculated using the Cotton-Kraihanzel model (Appendix C, Figure C2).[24] Note that the Cotton-Kraihanzel calculations do not provide absolute force constants, but rather relative force constants for similar complexes. Therefore, the accuracy of the absolute force constants is not as relevant as the relative force constants. The comparison of relative force constants is both quantitative and meaningful.[27] The results of the calculations are summarized in Table 4.1.

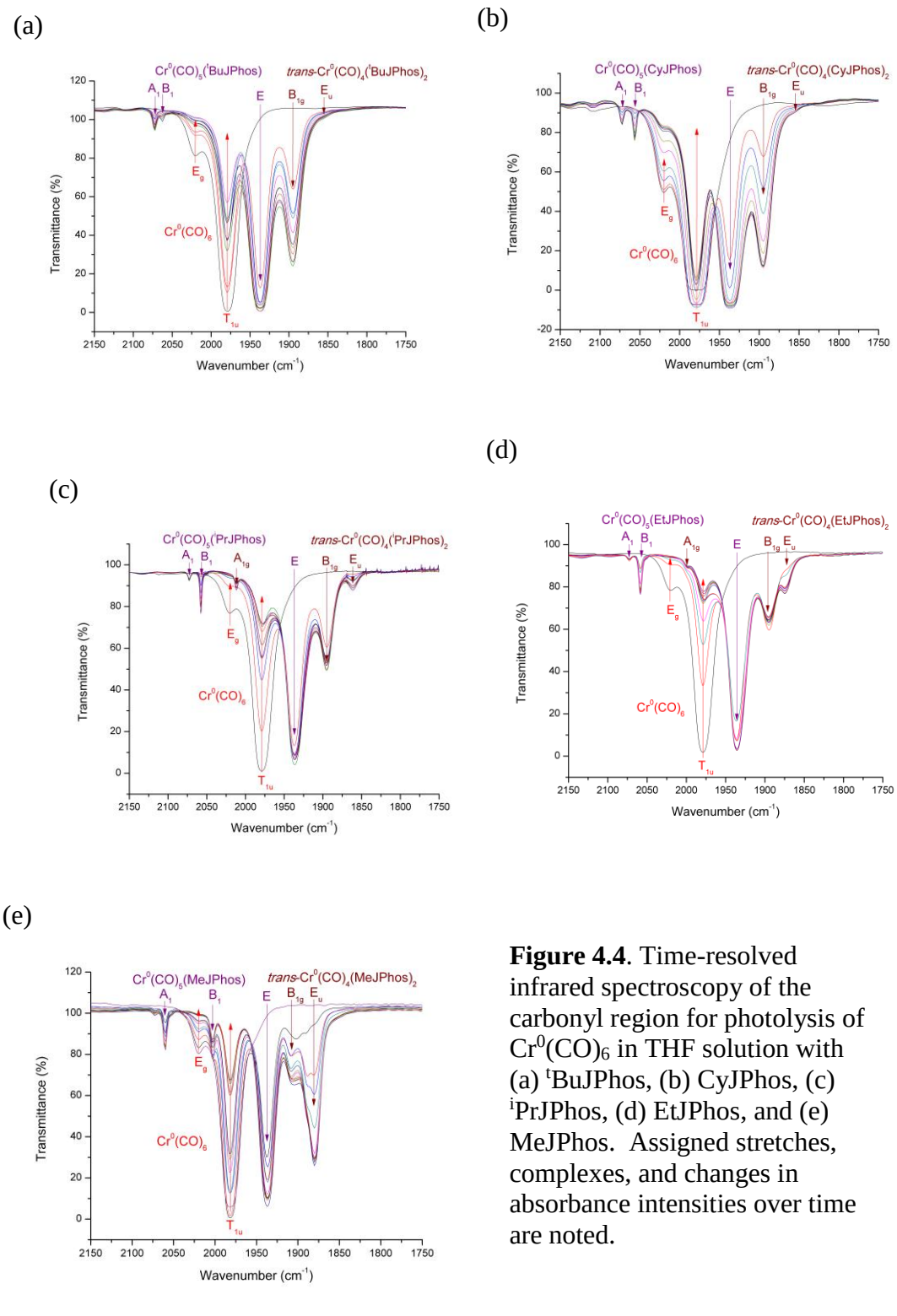

Figure 4.4. Time-resolved infrared spectroscopy of the carbonyl region for photolysis of $Cr^0(CO)_6$ in THF solution with (a) ^{t}BuJPhos, (b) CyJPhos, (c) ^{i}PrJPhos, (d) EtJPhos, and (e) MeJPhos. Assigned stretches, complexes, and changes in absorbance intensities over time are noted.

Table 4.1. Assigned CO stretches and force constants for the $Cr^0(CO)_5$(R-JohnPhos) complexes. A_1, B_1, and E are assigned CO stretches (in cm^{-1}); k_1 = stretching force constant for CO group *trans* to the phosphine (mdynes/Å), k_2 = stretching force constant for CO groups *cis* to the phosphine (mdynes/Å), and k_i = CO-CO interaction force constant (mdynes/Å).

	MeJPhos	**EtJPhos**	**^{i}PrJPhos**	**CyJPhos**	**^{t}BuJPhos**
A_1	2059.6	2072.5	2072.8	2072.1	2072.1
B_1	2003.2	2058.5	2057.6	2056.7	2062.5
E	1937.5	1935.3	1936.4	1937.1	1937.1
k_1	15.5	15.8	15.8	15.8	15.4
k_2	16.2	17.1	17.1	17.1	17.2
k_i	0.52	0.99	0.98	0.96	1.01

The Graham treatment[27] (eqs 4.1 and 4.2) of these force constants was used to quantify the relative σ-basicity and π-acidity of the R-JohnPhos ligands. These data are summarized in Table 4.2.

$$\Delta k_1 = \Delta\sigma + 2\Delta\pi \qquad (4.1)$$

$$\Delta k_2 = \Delta\sigma + \Delta\pi \qquad (4.2)$$

Table 4.2. Relative σ-donating and π-accepting ability of the R-JohnPhos ligands using the Graham treatment of the force constants for the $Cr^0(CO)_5$(R-JohnPhos) complexes in Table 4.1 (relative to ^{t}BuJPhos). The Δk_1, Δk_2, $\Delta\pi$, and $\Delta\sigma$ values are reported in mdynes/Å. The %$\Delta\pi$, and %$\Delta\sigma$ values were normalized over the value of the ^{t}BuJPhos k_2 force constant (the strongest CO bond measured in this system).

	Δk_1	**Δk_2**	**$\Delta\pi$**	**$\Delta\sigma$**	**% $\Delta\pi$**	**% $\Delta\sigma$**
MeJPhos	0.321	0.974	-0.653	1.63	-3.80	9.47
EtJPhos	0.0414	0.0666	-0.0252	0.0918	-0.15	0.53
^{i}PrJPhos	0.0346	0.0819	-0.0473	0.129	-0.28	0.75
CyJPhos	0.0326	0.0965	-0.0639	0.160	-0.37	0.93
^{t}BuJPhos	0	0	0	0	0	0

Several interesting trends appear in the data shown in Table 4.2. First, as expected, the σ-donating and π-accepting abilities for each ligand have an inverse relationship with each other based on the mathematical treatment. Second, a surprising finding is the "zigzag" shape of the σ-donating and π-accepting trends moving from MeJPhos to ^{t}BuJPhos (Figure 4.5), which is seemingly counterintuitive. The zigzag results indicate there are at least two competing factors driving the trends.

The obvious electronic contributor to phosphine σ-donating ability is the electron donating ability of the R groups, which follows the trend: Me < Et < ^{i}Pr ~ Cy < ^{t}Bu.[20] However, the observed ordering in Figure 4.5 (MeJPhos >> CyJPhos > ^{i}PrJPhos > EtJPhos > ^{t}BuJPhos) is in contrast to the common assumption that more electron donating groups at phosphorus cause the phosphine to be a stronger σ-donor. Thus, the electron-donating abilities of the R groups appear to play only a minor role in determining the σ-donating ability of the R-JohnPhos ligands.

Because a higher electron density at phosphorus fails to explain the electronic trend of the R-JohnPhos ligands, it is likely that steric factors account for the discrepancy. Steric influences that affect the electron donating ability at phosphorus manifest in two distinct ways for metal complexes: (1) steric hindrance between the metal complex and phosphine resulting in longer P-Cr bonds, a phenomenon known as "front strain", and (2) sterically induced geometric distortions at phosphorus changing the electronics of the lone pair and reducing the ability of the phosphine to σ-donate, known as "back strain".[28,29] The front strain of a phosphine with the $Cr^{0}(CO)_{5}$ moiety in $Cr^{0}(CO)_{5}PR_{3}$ is expected to be reasonably minimal (although it is not completely disregarded as playing a minor role in longer P-Pd bonds), suggesting that back strain at phosphorus is responsible

for the R-JohnPhos trend in σ-donation. Specifically, it is suggested that the steric hindrance of the R groups on the R-JohnPhos ligands forces the geometry at P to change, leading to more p-character in the HOMO, and thus poorer overlap with the metal center (*vide infra*). The phenomenon of bulky alkyl groups causing back strain (and thus weaker basicity) for amines is well established.[29] Though phosphine basicity is typically less affected by back strain than amines,[30] it can clearly manifest itself in phosphines, as for example in the unpredictable pK_a shifts for *ortho*-substituted aryl phosphines.[31,32]

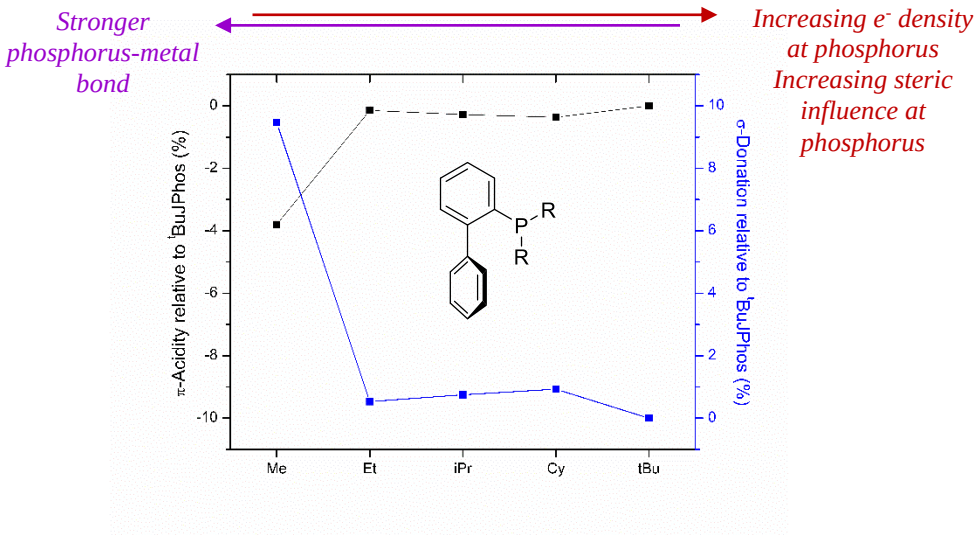

Figure 4.5. Relative percent σ-donating and π-accepting data for $Cr^0(CO)_5$(R-JohnPhos) complexes from Table 4.2.

Overall, it is suggested that the trend in σ-donation can be rationalized as two competing factors: 1) increasing electron density at phosphorus from MeJPhos to ^{t}BuJPhos, which gives the slight positive slope from EtJPhos to CyJPhos (Figure 4.5), and 2) stronger P-Cr bond overlap (increasing from ^{t}BuJPhos to MeJPhos) due to steric factors (mostly due to decreasing back strain), which significantly affects the σ-donation

of MeJPhos and ^{t}BuJPhos. To explore this hypothesis further, we turned to solid-state structural data for a closer analysis of R-JohnPhos-metal bonding.

4.2.3. Solid state structural analysis

4.2.3.1. Chromium(0) complexes

We set out to structurally characterize the $Cr^0(CO)_5$(MeJPhos) complex because of the significant electronic difference we observed compared between MeJPhos and the other R-JohnPhos ligands. Unfortunately, attempts to crystallize the $Cr^0(CO)_5$(MeJPhos) complex were unsuccessful; only the *trans*-$Cr^0(CO)_4(MeJPhos)_2$ complex (Figure 4.6) was isolable. This crystal structure was compared to other chromium-phosphine complexes and yielded striking results (Figure 4.7). Surprisingly, the *trans*-$Cr^0(CO)_4(MeJPhos)_2$ complex has a shorter P-Cr bond distance than the analogous *trans*-$Cr^0(CO)_4(PEt_3)_2$ complex. This result is surprising for two reasons: 1) PEt_3 is a stronger σ-donor than MeJPhos (vide infra) which should result in shorter P-Cr bonds, and 2) common metrics to quantify ligand sterics (e.g., the Tolman cone angle[20] and the percent buried volume[33]) show the PEt_3 ligand is considerably smaller than the MeJPhos ligand (Appendix C, Table C1).

The elongation of the carbonyl C≡O bonds in the *trans*-$Cr^0(CO)_4(PR_3)_2$ complexes (due to back-bonding from the metal) can be used to determine the σ-donating ability of the phosphine ligands. The carbonyl bond distances show that MeJPhos (C-O bond distance 1.148 Å) is bracketed between PEt_3 (1.161 Å) and PPh_3 (1.149 Å) in its σ-donating ability, as expected for an aryl-alkyl mixed phosphine. From these data, it is

concluded that the σ-donating ability of the ligands doesn't explain the shorter P-Cr bond distance for MeJPhos compared to PEt_3.

The short P-Cr bond in *trans*-$Cr^0(CO)_4(MeJPhos)_2$ appears to be the result of steric interactions between the ligand and pseudo-octahedral metal complex. Even though the average steric profile of PEt_3 and MeJPhos (as measured by the Tolman cone angle and the percent buried volume) show MeJPhos to be larger overall, the local steric influence of the -PMe_2 moiety must be smaller compared to the local steric influence of the PEt_3 ligand in order to form shorter P-Cr bonds. This observation suggests MeJPhos is capable of retaining a large overall steric profile while sustaining strong and short bonds to metal complexes.

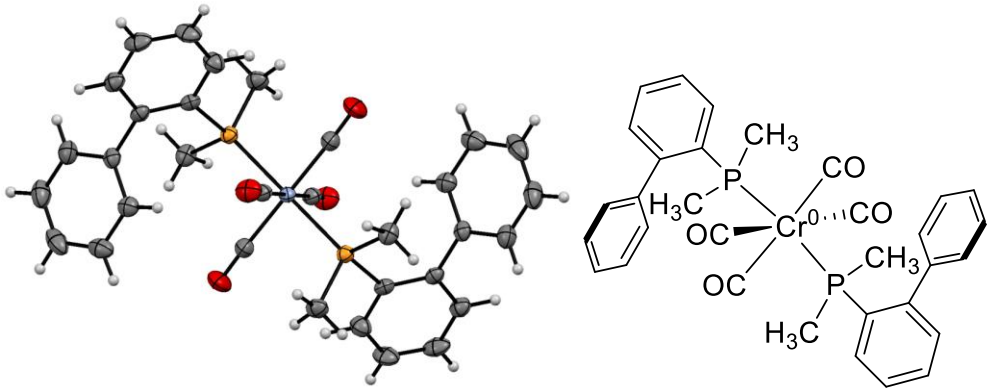

Figure 4.6. ORTEP crystal structure of *trans*-$Cr^0(CO)_4(MeJPhos)_2$ (all H atoms refined). Thermal ellipsoids are drawn at 50% probability.

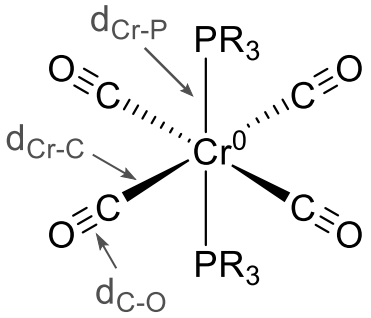

	d_{P-Cr} (Å)	d_{C-Cr} (Å)	d_{C-O} (Å)
MeJPhos	2.319	1.882	1.148
PEt_3	2.329	1.865	1.161
PPh_3	2.356	1.884	1.149

Figure 4.7. Selected bond distances from crystal structure data of *trans*-$Cr^0(CO)_4(PEt_3)_2$, *trans*-$Cr^0(CO)_4(PPh_3)_2$, and *trans*-$Cr^0(CO)_4$(MeJPhos)$_2$.

4.2.3.2 Palladium(0) complexes

To further explore the validity of the strong σ-donation and proposed steric explanation for the $Cr^0(CO)_5$(MeJPhos) and *trans*-$Cr^0(CO)_4$(MeJPhos)$_2$ complexes, the Pd^0(MeJPhos)$_2$(η^2-dba) complex was prepared and examined (Figure 4.8). Because $Pd^0(PR_3)_2$(η^2-dba)-type complexes can serve as cross-coupling pre-catalysts, determining if steric and electronic trends for MeJPhos are general across different metal complexes has significant implications vis-à-vis catalysis. We expected that the significant electronic difference between MeJPhos and the other R-JohnPhos ligands would manifest as measurable structural features. The structure of Pd^0(MeJPhos)$_2$(η^2-dba) displays a *cis*-conformation of two MeJPhos ligands on a trigonal planar palladium center. This structure was compared to two known structures, $Pd^0(PCy_3)_2$(η^2-dba) and $Pd^0(PPh_3)_2$(η^2-dba) (Figure 4.9).[34] Three structural features were notable: 1) the C-Pd bond distances in the MeJPhos complex are much shorter than in the analogous PCy_3 or PPh_3 complexes), 2) the P-Pd bond distances in the MeJPhos complex are also considerably shorter than in

the analogous PCy_3 or PPh_3 complexes, and 3) the "bite angle" (the angle between the two phosphorus atoms and palladium, Figure 4.9. $\theta_{P\text{-}Pd\text{-}P}$) is much smaller than in the analogous PCy_3 or PPh_3 complexes.

Activation of the C=C bond by the palladium is another metric that is often used to determine the electron density at the palladium; however, it is dependent on in-plane conjugation of the adjacent phenyl ring. Unfortunately, it is difficult to de-convolute the effects of back-bonding (elongation of the C=C bond) from effects of phenyl ring conjugation (which is correlated to the dihedral angle, φ, between the C=C plane and the adjacent phenyl ring)[35] because both contribute significantly to the electronic nature of the C=C bond and because φ is inconsistent across the three crystal structures. Thus, the C=C bond distance is not a conclusive metric for these molecules. Likewise, hybridization at the ethylene carbons could not be used to determine activation because the hydrogen atoms were not refined for the $Pd^0(PCy_3)_2(\eta^2\text{-dba})$ and $Pd^0(PPh_3)_2(\eta^2\text{-dba})$ complexes.

Evidence of activation at the C=C bond may also be drawn from the η^2-Pd-(C=C) bond distance. Stronger back-bonding between the palladium and ethylene fragment will yield a shorter η^2-Pd-(C=C) bond distance. The $Pd^0(MeJPhos)_2(\eta^2\text{-dba})$ complex has a considerably shorter η^2-Pd-(C=C) bond distance (average C-Pd bond distance of 2.135 Å) than the analogous PCy_3 (2.175 Å) or PPh_3 (2.163 Å) complexes. Overall, these findings support the hypothesis that MeJPhos is an especially strong σ-donor, even when compared to PCy_3 or PPh_3. This observation for the $Pd^0(PR_3)_2(\eta^2\text{-dba})$ complexes may be due to front strain at the P-Pd^0 coordination site for the larger PCy_3 and PPh_3 ligands perturbing σ-orbital overlap between the phosphorus and palladium.

The short P-Pd^0 distances and narrow "bite angle" (Figure 4.9, $\theta_{P\text{-}Pd\text{-}P}$) of MeJPhos (average P-$Pd^0$ bond distance of 2.301 Å, $\theta_{P\text{-}Pd\text{-}P}$ = 105.7°) compared to the analogous PCy_3 (2.175 Å, 115.6°) or PPh_3 (2.163 Å, 114.9°) complexes suggest a very small steric profile (small front strain) at the phosphorus. In fact, to our knowledge $Pd^0(MeJPhos)_2(\eta^2\text{-dba})$ makes the narrowest "bite angle" of any bis-monodentate complex of this type. This suggestion is also supported by comparison to bidentate phosphine palladium dba complexes ($Pd^0(P_2)(\eta^2\text{-dba})$, where P_2 is a bidentate phosphine), which have much smaller bite angles because the phosphines are tethered. Rings formed by the bidentate phosphines and palladium in $Pd^0(P_2)(\eta^2\text{-dba})$ complexes typically have the following bite angles: 5-membered rings, ~88°; 6-membered rings, ~99°; and 8-membered rings, ~112°.[36–41] Bis-monodentate phosphine "bite angles" are wider still. The $Pd^0(MeJPhos)_2(\eta^2\text{-dba})$ complex has a "bite angle" (105.7°) approximately equivalent to a 7-membered ring with palladium. The -PMe_2 moieties can make close contacts with the metal and position themselves relatively close to each other despite MeJPhos being a sterically demanding ligand overall. (Appendix C, Table C1.) In summary, the ability of the MeJPhos ligand to form a closer P-Pd^0 bond in a sterically competitive environment likely leads to the superb σ-donation of MeJPhos in comparison to PCy_3 or PPh_3. These findings also suggest MeJPhos is particularly suited to form palladium complexes that would perform difficult oxidative additions if employed in cross-coupling catalysis (Figure 4.1).

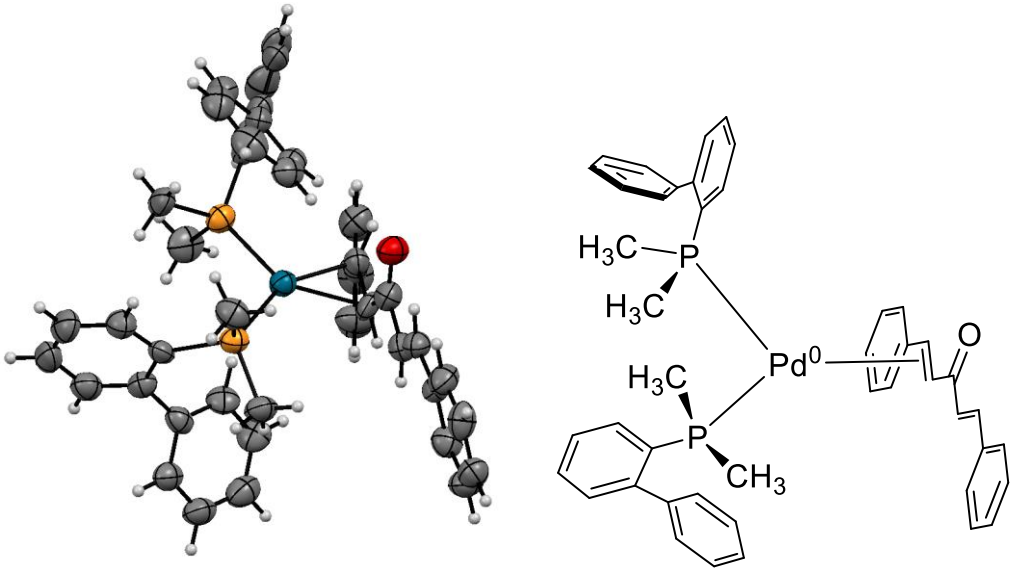

Figure 4.8. ORTEP crystal structure of $Pd^0(MeJPhos)_2(\eta^2\text{-dba})$ (all H atoms refined). Thermal ellipsoids are drawn at 50% probability.

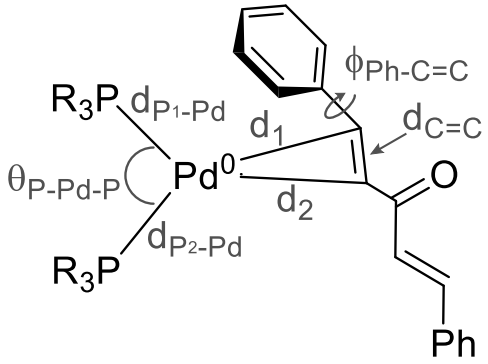

PR_3	d_{P1-Pd} (Å)	d_{P2-Pd} (Å)	d_1 (Å)	d_2 (Å)	$d_{C=C}$ (Å)	θ_{P-Pd-P} (°)	$\varphi_{Ph-C=C}$ (°)
MeJPhos	2.304	2.297	2.123	2.146	1.417	105.70	14.3
PCy_3	2.364	2.384	2.159	2.190	1.450	115.59	27.1
PPh_3	2.331	2.343	2.154	2.172	1.393	114.88	19.0

Figure 4.9. Selected bond distances, bond angles, and torsion angles from crystal structure data of $Pd^0(MeJPhos)_2(\eta^2\text{-dba})$, $Pd^0(PCy_3)_2(\eta^2\text{-dba})$, and $Pd^0(PPh_3)_2(\eta^2\text{-dba})$.

4.2.3.3 Palladium(II)-phosphorus bond lengths (front strain)

Sixteen *trans*-$Pd^{II}(Cl)_2(PR_3)_2$ complexes (PR_3 = various phosphines and R-JohnPhos ligands) were also analyzed to better understand structural differences induced by R-JohnPhos ligands. Most of the 16 crystal structures were obtained through the Cambridge Crystallographic Data Centre (Appendix C, Table C1). The solid state structures of *trans*-$Pd^{II}(Cl)_2(MeJPhos)_2$ and *trans*-$Pd^{II}(Cl)_2(^iPrJPhos)_2$ were obtained in this work (Figure 4.10).

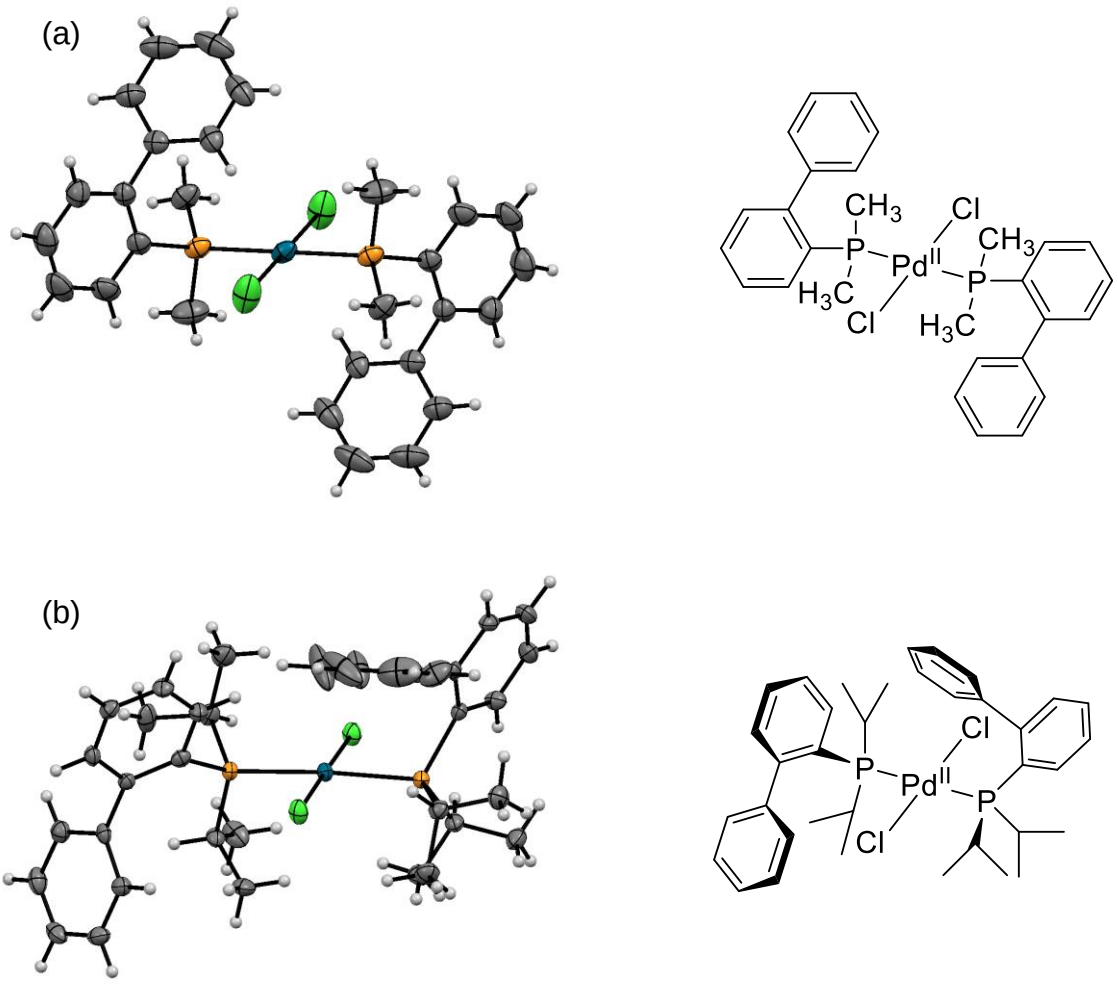

Figure 4.10. ORTEP crystal structures of (a) *trans*-$Pd^{II}(Cl)_2(MeJPhos)_2$ (all H atoms refined), and (b) *trans*-$Pd^{II}(Cl)_2(^{i}PrJPhos)_2$ (all H atoms refined). Thermal ellipsoids are drawn at 50% probability.

The analysis found the following. First, P-Pd^{II} bond lengths varied from ~2.18 to 2.40 Å (Figure 4.11). Based on the other data discussed above, it is not surprising that MeJPhos makes the shortest bond (2.319 Å) Pd^{II} among the R-JohnPhos ligands. This bond distance is the fourth shortest bond of the 16 measured, behind PEt_3, PMe_3, and $PPhEt_2$. The short P-Pd^{II} bond distance for MeJPhos supports the notion that front strain for MeJPhos is very small, especially compared to the other R-JohnPhos ligands. Note

that ^{t}BuJPhos is absent from Figure 4.1. This absence is due to the inability of ^{t}BuJPhos to form the *trans*-$Pd^{II}(Cl)_2(^{t}BuJPhos)_2$ complex (even with considerable synthetic effort on our part). The inability of the complex to form is likely due to extreme steric crowding about the Pd^{II} center. Qualitatively, this complex likely has a longer P-Pd^{II} bond than the other R-JohnPhos ligands, consistent with the σ-donor trends discussed above.

PEt_3 forms a notably shorter P-Pd^{II} bond than MeJPhos in the square planar *trans*-$Pd^{II}(Cl)_2(PR_3)_2$ complexes, which is in contrast to the case (*vide supra*) of P-Cr bond lengths for the analogous *trans*-$Cr^0(CO)_4(PR_3)_2$ complexes. This observation suggests that front strain between the ligand and metal complex is the reason that MeJPhos has a shorter bond than PEt_3 in the *trans*-$Cr^0(CO)_4(PR_3)_2$ complexes discussed above. There is inherently less front strain between a ligand and square planar metal complex than with an analogous octahedral complex. In general, therefore, MeJPhos appears to form short phosphorus-metal bonds in coordination complexes, but especially so compared to other phosphine ligands in metal complexes with steric crowding (e.g., *trans*-$Cr^0(CO)_4(PR_3)_2$ and $Pd^0(PR_3)_2(\eta^2\text{-dba})$).

4.2.3.4. Phosphine back strain on palladium(II)

The geometric distortion at the phosphorus was calculated from crystal structure data for the 16 *trans*-$Pd^{II}(Cl)_2(PR_3)_2$ complexes. The distortion is directly analogous to back strain experienced by sterically crowded amines.[29] For phosphines, this geometric distortion is measured using the symmetric deformation coordinate or S4' (Figure

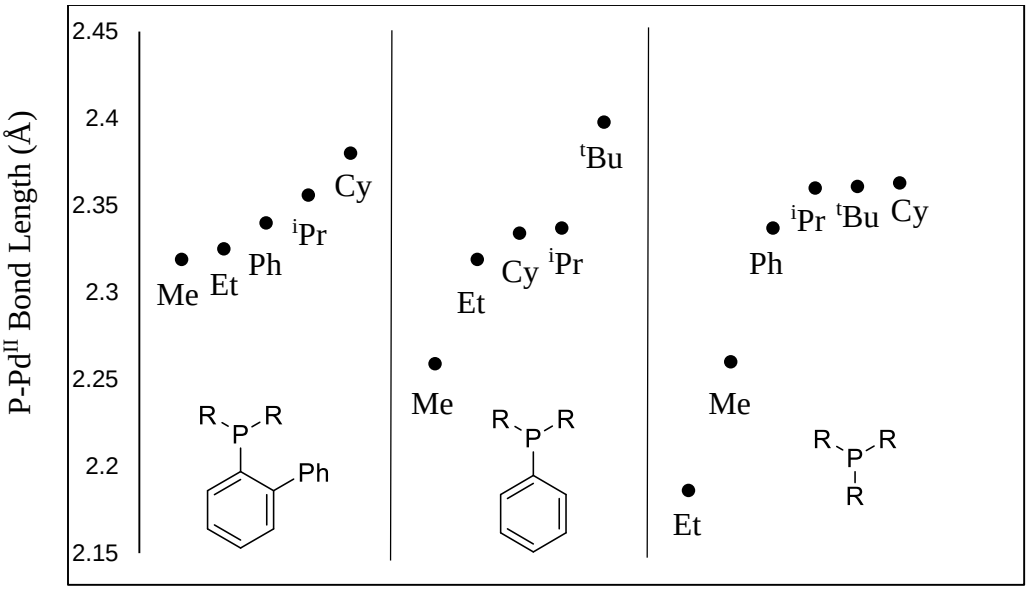

Figure 4.11. Phosphorus-palladium bond distances from crystal structure data for 16 representative phosphines (including MeJPhos, EtJPhos, PhJPhos, ^{i}PrJPhos, and CyJPhos) on Pd^{II}.

4.12).[28,42] The S4' value is the angular difference between the three ligand ∠C-P-C angles and ∠C-P-Pd angles. The distortion from trigonal pyramidal at the phosphorus directly correlates to the hybridization of the lone pair. More distortion towards trigonal planar, caused by sterically bulky R groups at phosphorus, forces the lone pair (HOMO) into a p-like orbital that in turn has poorer overlap with the metal.[43] This distortion occurs when strong steric influence at phosphorus forces the geometry to be more planar, which results in near-zero or negative S4' values. Conversely, when the substituents directly bonded to phosphorus have low steric influence, there is little distortion and the lone pair is allowed to occupy an sp^3-like orbital which has strong overlap and directionality to donate to a metal center, which results in larger S4' values. For the phosphines in Figure 4.13, the S4' values range from 8.6° to 35.3°.

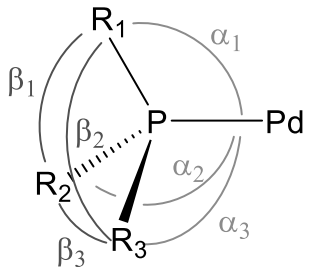

Figure 4.12. Structural and geometric parameters defining the symmetric deformation coordinate (S4'). S4' = ($\alpha_1 + \alpha_2 + \alpha_3$) - ($\beta_1 + \beta_2 + \beta_3$).

The calculations show PhJPhos, EtJPhos, and MeJPhos all have relatively large S4' values (29.77°, 29.26°, and 27.96° respectively). These compare very well with low steric profile phosphines like $PPhMe_2$ (32.81°) and PMe_3 (35.33°). This finding is in stark contrast to the larger CyJPhos, which has a considerable S4' value (16.91°). Again, although ^{t}BuJPhos is not available for analysis here, it likely has a low S4' value based on the two *tert*-butyl groups at phosphorus. The most analogous ligand to ^{t}BuJPhos, $PPh(^tBu)_2$ has an S4' value of 18.36°. ^{t}BuJPhos very likely has an S4' value below 18.36°, which qualitatively gives it the smallest S4' value among the R-JohnPhos ligands. The S4' values show that back strain is likely a major contributor to the structural/electronic relationship between the R-JohnPhos ligands and the metal center. The back strain is especially pronounced in R-JohnPhos ligands for the larger and more electron donating alkyl groups such as ^{t}Bu and Cy. It is proposed that the significant back strain of the larger R-JohnPhos ligands is a major influence in the poor σ-donating ability of ^{t}BuJPhos compared to the other R-JohnPhos ligands.

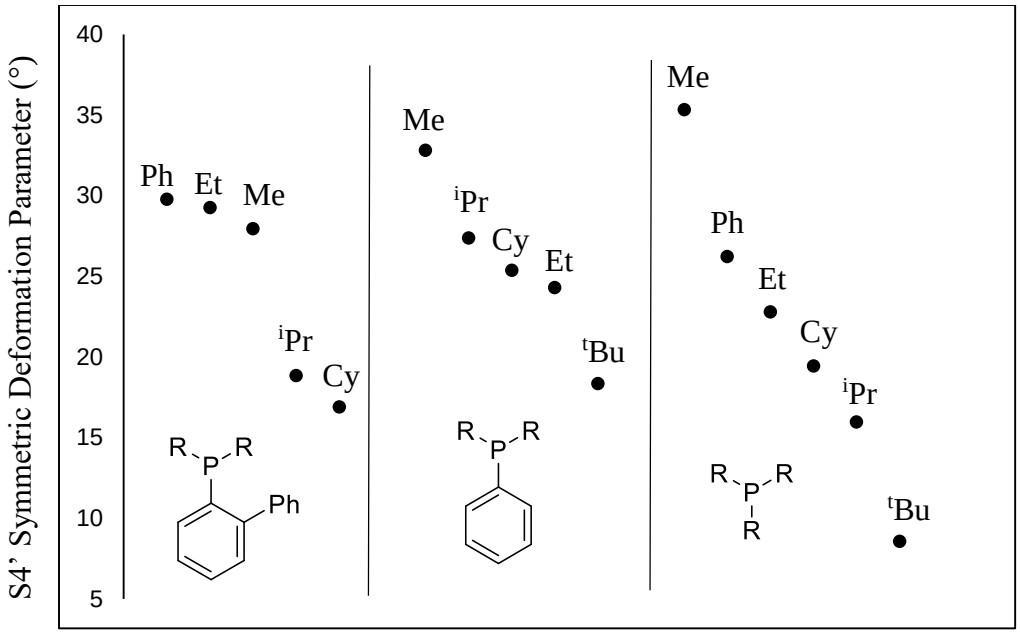

Figure 4.13. Phosphorus S4' values from crystal structure data for 16 representative phosphines (including MeJPhos, EtJPhos, PhJPhos, ^{i}PrJPhos, and CyJPhos) on Pd^{II}.

4.2.3.5. Overall steric profile of phosphines on palladium(II)

Finally, crystal structure data for the 16 *trans*-$Pd^{II}(Cl)_2(PR_3)_2$ complexes was used to calculate the overall steric influence of each phosphine ligand. Though many steric metrics exist,[44] we chose to employ the percent buried volume calculation ($\%V_{bur}$).[33,45] This steric metric is related to front strain, but distinct in that it measures the influence of the entire ligand on the coordination sphere of the metal (even the distally located moieties that may not affect front strain). This steric analysis has been especially successful at determining steric profiles for structurally elaborate, large, and unsymmetrical ligands (e.g., N-heterocyclic carbenes and Buchwald-type ligands). The $\%V_{bur}$ is defined as the percent of the total volume of a sphere around the metal that is occupied by a ligand (Figure 4.14). The sphere has a defined radius of 3.5 Å from the

metal center which represents the potential coordination sphere space around the metal. The $\%V_{bur}$ calculation is well suited for crystal structure analysis because it uses a three-dimensional spatial model, so actual crystal structure data can be used to determine steric influence between the ligand and the metal. The $\%V_{bur}$ calculations were obtained using the Samb*V*ca (Salerno molecular buried volume calculation) software developed by Cavallo and co-workers (available as an online tool.)[46]

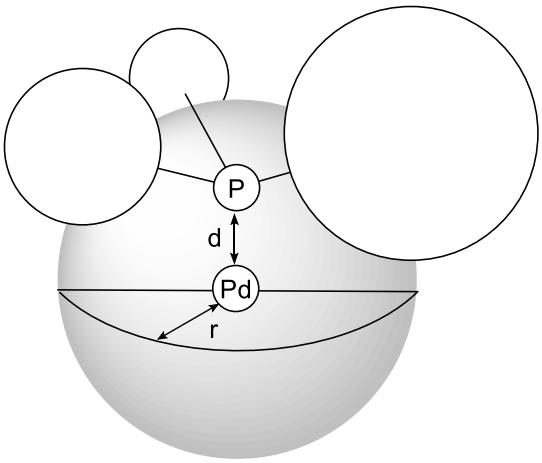

Figure 4.14. Visual representation of the $\%V_{bur}$ steric calculation. For the 16 crystal structures analyzed, d = the crystallographic P-Pd bond distance (Å) (Figure 4.11), r = 3.5 Å, Samb*V*ca mesh spacing = 0.05, all H-atoms are included, and bond radii were scaled by 1.17 (as recommended by Cavallo).[45]

For the 16 complexes analyzed, $\%V_{bur}$ varied from 23.6% to 35.0% (Figure 4.15). Two observations stand out for the $\%V_{bur}$ values calculated: (1) the steric size of the R groups on $PPh(R)_2$ and PR_3 ligands trends reasonably well with the overall $\%V_{bur}$, while the R-JohnPhos series does not; and (2) the R-JohnPhos ligands generally have a large $\%V_{bur}$ (average of 33.6%) with a narrow range (32.7%-35.0%) compared with the $PPh(R)_2$ and PR_3 ligands. The discrepancy in the correlation between $\%V_{bur}$ and the size

of R for the R-JohnPhos ligands is partly due to P-Pd^{II} bond distances (with shorter bond distances increasing the $\%V_{bur}$ value). For example, even though *cyclo*-hexyl groups are much larger than methyl groups, CyJPhos ($\%V_{bur}$ 32.7% and P-Pd^{II} distance 2.380 Å) is slightly smaller than MeJPhos ($\%V_{bur}$ 32.8% and P-Pd^{II} distance 2.319 Å). Because bond distance alone doesn't explain the discrepancy across all the R-JohnPhos ligands, it is likely the *o*-biphenyl moiety also has a dominating effect on the $\%V_{bur}$ values for the R-JohnPhos ligands, as seen in the narrow range of values compared with the $PPh(R)_2$ and PR_3 ligands. That is to say, changing the R group on the R-JohnPhos ligands has a nominal effect on the overall steric profile because the $\%V_{bur}$ is mostly dependent on the *o*-biphenyl moiety's steric influence.

The overall steric profile of a ligand relates to its ability to perform reductive eliminations during cross-coupling (Figure 4.1). It is believed that a combination of both large steric profile ($\%V_{bur}$) and strong σ-donation are the primary factors responsible for ligands' success in forming catalytically active Pd species.[18] In Buchwald-Hartwig cross-coupling, the oxidative addition is typically the rate-limiting step in the catalytic cycle (especially so with aryl-chlorides).[47] It is known that ^{t}BuJPhos, CyJPhos, and $P(^{t}Bu)_3$ can perform Buchwald-Hartwig cross-coupling reactions with aryl-chlroides.[47,48] MeJPhos appears to be an excellent candidate for Buchwald-Hartwig cross-coupling reactions with aryl-chlorides because it has a $\%V_{bur}$ in the range of other ligands known to form catalytically active species (i.e. CyJPhos 32.7%, MeJPhos 32.8%, and $P(^{t}Bu)_3$ 36.5%) and it is a very strong σ-donor.

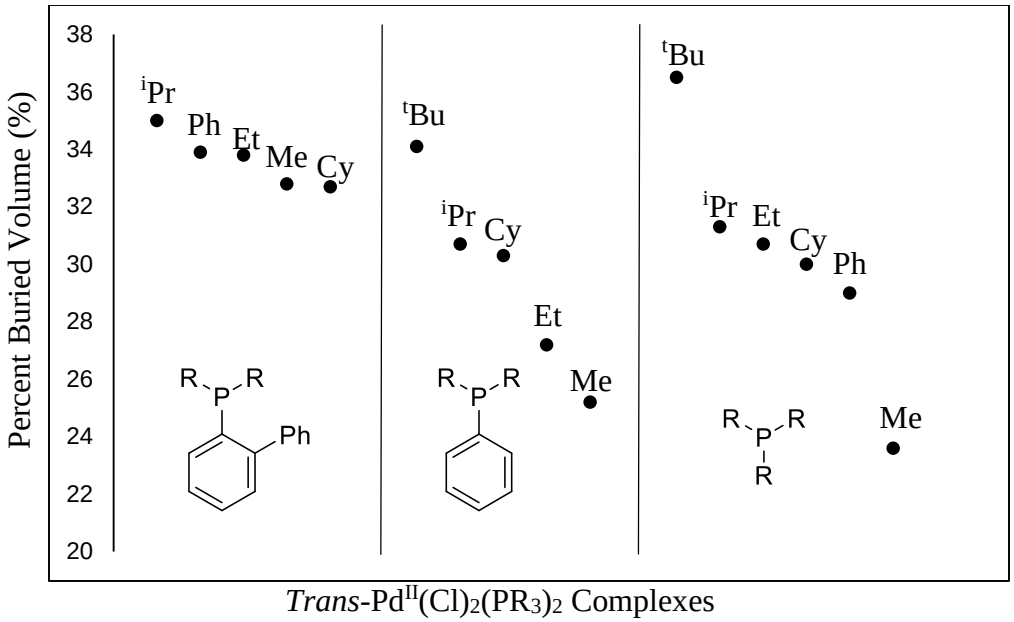

Trans-$Pd^{II}(Cl)_2(PR_3)_2$ Complexes

Figure 4.15. *%V*$_{bur}$ calculations from crystal structure data for 16 representative phosphines (including MeJPhos, EtJPhos, PhJPhos, ^{i}PrJPhos, and CyJPhos) on Pd^{II}.

4.3. Conclusions

The σ-donating ability of the R-JohnPhos ligands (where R = Me, Et, ^{i}Pr, Cy, ^{t}Bu) follow the trend ^{t}BuJPhos < EtJPhos < ^{i}PrJPhos < CyJPhos << MeJPhos. If this ordering were to follow a trend based solely on the electron-donating abilities of the R groups (Me < Et < ^{i}Pr ~ Cy < ^{t}Bu) then MeJPhos would be the weakest σ-donor rather than the strongest donor. The conclusion is that factors other than the σ-donating ability of the R group contribute to the net donor ability of these phosphine ligands. The σ-donor ordering is proposed to arise from competition between the intrinsic electron-donating ability of the R groups (increasing from MeJPhos to ^{t}BuJPhos) and steric interactions (increasing from MeJPhos to ^{t}BuJPhos) that decrease the electron-donating ability of the phosphine. The steric interactions that affect the electronic contributions of the ligand to the metal can be divided into categories: (1) steric interactions between the metal moiety

and the phosphine (front strain, as measured by the P-Pd^{II} bond distance), and (2) a distortion of the hybridization at phosphorus caused by interactions of the R groups (back strain, as measured by the S4' value). Both categories of steric interactions appear to play a significant role in determining phosphorus-metal bond distances and σ-donating ability for the R-JohnPhos ligands. Only MeJPhos appears to benefit from low back strain *and* low front strain. Consequently, MeJPhos can form close metal contacts and small "bite angles" (for bisphosphine complexes). Because the methyl groups are intrinsically poorer electron donating groups than the other R groups, it is concluded that MeJPhos is a much stronger σ-donor than the other R-JohnPhos ligands primarily for steric reasons.

Another important conclusion of this study is that the σ-donating abilities of the R-JohnPhos ligands are very sensitive to the back strain generated by alkyl groups at phosphorus. Back strain, of course, does affect the basicity of amines, but it is not a factor that is typically associated with phosphine donor ability. The R-JohnPhos ligands are unusual in this regard. As discussed in the text, other *ortho*-functionalized aryl phosphines likely have a similar dependency of σ-donating ability on back strain.

Overall, the -PMe_2 moiety of MeJPhos appears to be special in its ability to form short phosphorus-metal bonds while avoiding back strain. The *o*-biphenyl moiety serves to maintain an overall steric profile comparable to larger ligands (e.g. CyJPhos). Consequently, the -PMe_2 moiety has a small S4' distortion, excellent σ-donation to metals, and maintains a large %V_{bur}. This conclusion suggests that the -PMe_2 moiety is a powerful way to incorporate strong σ-donation into "designer" phosphines while retaining other advantageous structural and reactivity properties. For example, MeJPhos

benefits from both the large steric profile of the *o*-biphenyl and the oxygen resistance that is typical of Buchwald-type ligands.

Finally, because of its strong σ-donating properties and overall size, it is hypothesized that MeJPhos will be an ideal ligand for Pd Buchwald-Hartwig cross-coupling catalysts. Catalytic cross-coupling studies using this ligand are reported in Chapter V.

4.4. Experimental section

4.4.1. General considerations

Unless stated otherwise, reactions were conducted in oven-dried glassware under an atmosphere of nitrogen using either standard Schlenk techniques or a dribox maintained at < 1.0 ppm O_2. Diethyl ether and tetrahydrofuran (THF) were dried using a DriSolv system using CuO and molecular sieves under argon. All other reaction solvents were purified and dried according to the literature.[49] All commercially obtained reagents were used as received unless otherwise specified. Synthesized organomagnesium reagents were titrated before use using either diphenyl acetic acid[50] or No-D NMR spectroscopy[51] to determine concentration and were stored under Ar at room temperature. Thin-layer chromatography (TLC) was visualized using low wavelength ultraviolet light (UV) for all aryl species or phosphomolybdic acid. ^{1}H NMR spectra were recorded on a 300 or 500 MHz Varian spectrometer (^{1}H 300.09 MHz or 500.02 MHz, respectively) and are reported relative to deuterated solvent signals or an internal reference. Data for ^{1}H NMR spectra are reported as follows: chemical shift (δ ppm), multiplicity, coupling constant (Hz) and relative integration. ^{31}P{^{1}H} NMR spectra were recorded on a 300 or

500 MHz Varian spectrometer (^{31}P 121.48 MHz or 202.13 MHz, respectively) and are reported relative to the external standard of 0.1% H_3PO_4 in D_2O at 0 ppm. Infrared spectra were recorded using Nicolet Magna-550 Fourier Transform Infrared Spectrophotometer using an air-free fluorite prism solution cell with a 0.1 mm cell thickness. All phosphines were either synthesized as previously reported (*vide infra*) or purchased. In the cases of [1,1'-biphenyl]-2-yldicyclohexylphosphine (CyJPhos) and [1,1'-biphenyl]-2-yldi-*tert*-butylphosphine (^{t}BuJPhos), the ligands were purchased from Strem Chemicals, Inc. and used without further purification.

4.4.2. X-ray crystallography

Diffraction intensities were collected at 173 K ($Pd^0(MeJPhos)_2(\eta^2$-dba), *trans*-$Cr^0(CO)_4(MeJPhos)_2$ and *trans*-$Pd^{II}(Cl)_2(^iPrJPhos)_2$) and 200 K (Me-JohnPhos, *trans*-$Pd^{II}(Cl)_2(MeJPhos)_2$) on a Bruker Apex2 CCD diffractometer using MoKα (Me-JohnPhos, *trans*-$Pd^{II}(Cl)_2(MeJPhos)_2$, *trans*-$Pd^{II}(Cl)_2(^iPrJPhos)_2$) and Cu K$\alpha$ ($Pd^0(MeJPhos)_2(\eta^2$-dba), *trans*-$Cr^0(CO)_4(MeJPhos)_2$) radiation (λ= 0.71073 Å and 1.54178 Å, respectively). Diffraction for $Pd^0(MeJPhos)_2(\eta^2$-dba) and *trans*-$Cr^0(CO)_4(MeJPhos)_2$ were weak, so a strong Incoatec *I*μ*S* Cu source was used. Data for these two crystals were collected up to $2\theta_{max}$ = 133.0°, but only reflections with $2\theta_{max}$ = 110.0° have been used in the refinement for $Pd^0(MeJPhos)_2(\eta^2$-dba), due to very weak reflections at the high angles. Even with such restrictions, the appropriate number of reflections per refined parameters were used. Space groups were determined based on systematic absences (*trans*-$Pd^{II}(Cl)_2(MeJPhos)_2$) and intensity statistics. Absorption corrections were applied by SADABS.[54] Structures were solved by direct methods and

Fourier techniques, then refined on F^2 using full matrix least-squares procedures. All non-H atoms were refined with anisotropic thermal parameters. H atoms in all structures were found from the residual density maps and refined with isotropic thermal parameters without any restrictions except those in $Pd^0(MeJPhos)_2(\eta^2\text{-dba})$ which were refined in calculated positions in a rigid group model. All calculations were performed by the Bruker SHELXL-2013 package.[55]

4.4.3 Synthesis of ligands

4.4.3.1. [1,1'-biphenyl]-2-yldimethylphosphine (MeJPhos)

The synthesis of MeJPhos has been described by our laboratory previously.[12] MeJPhos was isolated as a white crystalline solid. ^{1}H NMR (500 MHz, $CDCl_3$) δ 7.37 (ddd, J = 7.0, 4.1, 1.9 Hz, 1H), 7.29 – 7.25 (m, 4H), 7.25 – 7.19 (m, 3H), 7.11 (ddd, J = 6.2, 3.9, 2.1 Hz, 1H), 0.97 (d, J = 3.8 Hz, 6H). ^{31}P{^{1}H} NMR (202 MHz, $CDCl_3$) δ -51.86. The compound was further characterized by single crystal XRD (Table 4.3).

Table 4.3. Crystallographic Data for Me-JohnPhos. Additional parameters: crystal dimensions = 0.25 x 0.21 x 0.14 mm, $F(000)$ = 456, $2\theta_{max}$ = 56.0°, 26879 reflections, 5817 independent reflections [R_{int} = 0.0452], R1 = 0.0390, wR2 = 0.0922 and GOF = 1.012 for 5817 reflections (392 parameters) with I>2σ(I), R1 = 0.0563, wR2 = 0.1045 and GOF = 1.012 for all reflections, max/min residual electron density +0.277/-0.258 eÅ^3.

Formula = $C_{14}H_{15}P$	
Formula weight = 214.23 g/mol a = 7.9111(5) Å	Space group = P-1
b = 11.4369(8) Å	T = 200(2) K
c = 13.9141(9) Å	λ = 0.71073 Å
α = 78.752(3)°, β = 80.116(3)°, γ = 79.644(3)°	D_c = 1.183 Mg/m^3
V = 1202.40(14) Å^3	μ(Mo) = 0.193 mm^{-1}
Z = 4, Z' = 2	$R(F_o)$ = 3.90%
Crystal system = triclinic	$R_w(F_o)$ = 9.22%

4.4.3.2. [1,1'-biphenyl]-2-yldiethylphosphine (EtJPhos).

The synthesis of EtJPhos has been previously described.[16] To a 25 mL Schlenk flask was added 2-bromobiphenyl (0.9474 g, 4.0 mmol) and then charged with 6 mL Et_2O. The solution was then freeze-pump-thawed three times and back-filled with N_2. The solution was cooled to -10 °C and freshly titrated *n*-BuLi (4.40 mL, 0.93 M in hexanes, 4.04 mmol) was added dropwise over 15 minutes. The solution turned yellow upon *n*-BuLi addition, and white precipitate formed after ~1.5 mL were added. The mixture was allowed to stir at -10 °C for 3 hours. A solution of $PCl(Et)_2$ (504.0 mg, 4.01 mmol, in ~1.0 mL of Et_2O) was added dropwise over 20 minutes. The mixture turned orange-red and a considerable precipitate formed. The mixture was allowed to stir and warm to room temperature overnight. The mixture was quenched on silica and directly loaded onto a flash-chromatography column for purification (60 mesh silica, either Et_2O R_f=0.9 or hexanes R_f=0.4 can be used) to yield colorless oil (678.1 mg, 70.0% yield). ^{1}H NMR (300 MHz, Benzene-d_6) δ 7.45 (dddd, J = 8.1, 5.0, 2.3, 1.2 Hz, 3H), 7.40 – 7.31 (m, 1H), 7.28 – 7.06 (m, 5H), 1.52 – 1.27 (m, 4H), 0.84 (dt, J = 14.3, 7.6 Hz, 6H). ^{31}P{^{1}H} NMR (121 MHz, Benzene-d_6) δ -26.76.

4.4.3.3. [1,1'-biphenyl]-2-yldiisopropylphosphine (^{i}PrJPhos).

The synthesis of ^{i}PrJPhos has been previously described.[52] To a 25 mL Schlenk flask was added 2-bromobiphenyl (0.9380 g, 4.0 mmol) and then charged with 6 mL Et_2O. The solution was then freeze-pump-thawed three times and back-filled with N_2. The solution was cooled to -10 °C and freshly titrated *n*-BuLi (2.0 mL, 2.06 M in hexanes, 4.04 mmol) was added dropwise over 15 minutes. The solution turned yellow

upon *n*-BuLi addition, and white precipitate formed after ~1.5 mL were added. The mixture was allowed to stir at -10 °C for 3 hours. A solution of $PCl(^{i}Pr)_2$ (625.0 mg, 4.01 mmol, in ~1.0 mL of Et_2O) was added dropwise over 20 minutes. The mixture turned pink-red and a considerable precipitate formed. The mixture was allowed to stir and warm to room temperature overnight. The mixture was quenched on silica and directly loaded onto a flash-chromatography column for purification (60 mesh silica, either Et_2O R_f=0.8 or hexanes R_f=0.3 can be used) to yield colorless crystalline solid (734.0 mg, 68.1% yield). ^{1}H NMR (500 MHz, Benzene-d_6) δ 7.50 – 7.38 (m, 3H), 7.26 (dddd, *J* = 21.0, 7.7, 5.0, 2.3 Hz, 2H), 7.18 – 7.10 (m, 4H), 1.85 (heptd, *J* = 7.0, 1.4 Hz, 2H), 0.98 – 0.86 (m, 12H). $^{31}P\{^1H\}$ NMR (202 MHz, Benzene-d_6) δ -5.29.

4.4.4. Synthesis of metal complexes

4.4.4.1. Trans-$Cr^0(CO)_4$(MeJPhos)$_2$

Under and inert atmosphere of N_2, $Cr^0(CO)_6$ (25.0 mg, 114 μmol) with MeJPhos (31.2 mg, 137 μmol) and THF-d_8 (0.5 mL) were added to a J-Young adapted NMR tube. The sample was frozen and the headspace was replaced with Ar. The sample was heated to 60 °C for 8 hours, observed by NMR, then freeze-pump-thawed, backfilled with Ar, and allowed to heat for another 8 hours at 60 °C. After the complete conversion by ^{31}P NMR, the now yellow solution was vacuumed to dryness and triturated with hexanes, leaving a residue of yellow solids. These solids were taken up into THF and allowed to crystalize by slow evaporation under N_2, yielding 40.4 mg (60%) of yellow crystalline *trans*-$Cr^0(CO)_4$(MeJPhos)$_2$. The compound was further characterized by single crystal XRD (Table 4.4).

Table 4.4. Crystallographic Data for *trans*-$Cr^0(CO)_4(MeJPhos)_2$. Additional parameters: crystal dimensions = 0.10 x 0.07 x 0.02 mm, $F(000)$ = 308, $2\theta_{max}$ = 133.0°, 8026 reflections, 2550 independent reflections [R_{int} = 0.0429], R1 = 0.0354, wR2 = 0.0908 and GOF = 1.057 for 2550 reflections (238 parameters) with I>2σ(I), R1 = 0.0395, wR2 = 0.0934 and GOF = 1.057 for all reflections, max/min residual electron density +0.290/-0.262 eÅ^3.

Formula = $C_{32}H_{30}CrO_4P_2$	
Formula weight = 592.50 g/mol a = 7.3216(3) Å	Space group = *P*-1
b = 9.6435(4) Å	T = 173(2) K
c = 11.8158(4) Å	λ = 1.54178 Å
α = 67.621(2)°, β = 72.584(2)°, γ = 76.173(2)°	D_c = 1.350 Mg/m^3
V = 728.64(5) Å^3	μ(Cu) = 4.553 mm^{-1}
Z = 1, Z' = 0.5	$R(F_o)$ = 3.54%
Crystal system = triclinic	$R_w(F_o)$ = 9.08%

4.4.4.2. Trans-$Pd^{II}(Cl)_2(MeJPhos)_2$

$Pd^{II}Cl_2$ (58.0 mg, 0.30 mmol) was added to dry THF (2.0 mL) and stirred vigorously. A solution of MeJPhos (140 mg, 0.60 mmol, 2 mL THF, c.a. 300 mM) was added dropwise to the stirring slurry and allowed to stir overnight at room temperature. The solution went from a purple slurry to a yellow slurry. The mixture was filtered through diatomaceous earth and reduced via vacuum to a yellow-white solid. This mixture was taken up into a minimal amount of THF (c.a. 0.5 mL) and dropped into hexanes to precipitate a flocculent yellow solid. This solid was collected and recrystallized by layering a saturated THF solution with hexanes, yielding a yellow crystalline solid (161.6 mg, 68.8%). ^{1}H NMR (500 MHz, Benzene-d_6) δ 7.85 – 7.76 (m, 1H), 7.70 – 7.61 (m, 1H), 7.27 (t, J = 7.7 Hz, 1H), 7.17 – 7.00 (m, 2H), 1.26 (t, J = 3.4 Hz, 3H). ^{13}C NMR (126 MHz, Benzene-d_6) δ 145.77 – 144.89 (m), 141.63 (t, J = 1.5 Hz), 133.14 – 132.49 (m), 132.16 (d, J = 22.5 Hz), 131.04 – 130.49 (m), 129.86 , 129.43 ,

128.46 , 127.96 , 127.76 , 126.49 (t, J = 4.4 Hz), 112.49 , 12.76 (t, J = 15.5 Hz). $^{31}P\{^{1}H\}$ NMR (202 MHz, Benzene-d_6) δ -3.10. The compound was further characterized by single crystal XRD (Table 4.5).

Table 4.5. Crystallographic Data for *trans*-$Pd^{II}(Cl)_2(MeJPhos)_2$. Additional parameters: crystal dimensions = 0.27 x 0.16 x 0.08 mm, $F(000)$ = 616, $2\theta_{max}$ = 56.0°, 19508 reflections, 4177 independent reflections [R_{int} = 0.0425], R1 = 0.0376, wR2 = 0.0818 and GOF = 1.024 for 4177 reflections (211 parameters) with I>2σ(I), R1 = 0.0583, wR2 = 0.0930 and GOF = 1.024 for all reflections, max/min residual electron density +0.799/-0.703 eÅ^3.

Formula = $C_{28}H_{30}Cl_2P_2Pd$	
Formula weight = 605.76 g/mol a = 11.6418(13) Å	Space group = $P2_1/n$
b = 7.1671(8) Å	T = 200(2) K
c = 16.4230(17) Å	λ = 0.71073 Å
α = 90°, β = 92.638(5)°, γ = 90°	D_c = 1.470 Mg/m^3
V = 1368.8(3) Å^3	μ(Mo) = 1.005 mm^{-1}
Z = 2, Z' = 0.5	$R(F_o)$ = 3.76%
Crystal system = triclinic	$R_w(F_o)$ = 8.18%

4.4.4.3. Trans-$Pd^{II}(Cl)_2(EtJPhos)_2$

$Pd^{II}Cl_2$ (71.2 mg, 0.4 mmol) was added to dry THF (5 mL) and stirred vigorously. A solution of EtJPhos (193.9 mg, 0.8 mmol, 5 mL THF, c.a. 160 mM) was added dropwise to the stirring slurry and allowed to stir overnight at room temperature. The solution went from a purple slurry to a red-orange slurry. The mixture was filtered through diatomaceous earth and reduced via vacuum to a red-orange oil. This mixture was taken up into a minimal amount of THF (c.a. 1 mL) and dropped into hexanes to precipitate a flocculent orange solid. This solid was collected and recrystallized by layering a saturated THF solution with hexanes, yielding a yellow-orange crystalline

solid (123.0 mg, 46.3%). ^{1}H NMR (500 MHz, Chloroform-*d*) δ 7.95 (d, *J* = 7.4 Hz, 4H), 7.66 (t, *J* = 7.5 Hz, 4H), 7.58 (q, *J* = 10.5, 9.0 Hz, 6H), 7.47 – 7.33 (m, 4H), 1.95 (ddt, *J* = 327.6, 14.2, 7.6 Hz, 8H), 1.16 (dt, *J* = 18.5, 7.7 Hz, 12H). ^{31}P NMR (202 MHz, Chloroform-*d*) δ 32.87.

4.4.4.4. Trans-$Pd^{II}(Cl)_2(^{i}PrJPhos)_2$

$Pd^{II}Cl_2$ (32.8 mg, 0.18 mmol) was added to dry THF (2 mL) and stirred vigorously. A solution of ^{i}PrJPhos (99.7 mg, 0.40 mmol, 2 mL THF, c.a. 200 mM) was added dropwise to the stirring slurry and allowed to stir overnight at room temperature. The solution went from a purple slurry to a yellow slurry. The mixture was filtered through diatomaceous earth and reduced via vacuum to a yellow-white solid. This mixture was taken up into a minimal amount of THF (c.a. 0.5 mL) and dropped into hexanes to precipitate a flocculent light-yellow solid. This solid was collected and recrystallized by layering a saturated THF solution with hexanes, yielding a yellow crystalline solid (88.2 mg, 61.4%). ^{1}H NMR (500 MHz, Benzene-d_6) δ 8.09 (q, *J* = 6.1 Hz, 2H), 7.75 (d, *J* = 7.3 Hz, 4H), 7.24 – 7.08 (m, 8H), 7.08 – 7.00 (m, 4H), 2.77 – 2.57 (m, 4H), 1.24 (dq, *J* = 146.2, 7.4 Hz, 24H). ^{31}P{^{1}H} NMR (202 MHz, Benzene-d_6) δ 42.42 (broad). The compound was further characterized by single crystal XRD (Table 4.6).

Table 4.6. Crystallographic Data for *trans*-$Pd^{II}(Cl)_2(^iPrJPhos)_2$. Additional parameters: crystal dimensions = 0.14 x 0.13 x 0.07 mm, $F(000) = 744$, $2\theta_{max} = 56.0°$, 35568 reflections, 8457 independent reflections [$R_{int} = 0.0964$], R1 = 0.0466, wR2 = 0.0820 and GOF = 1.017 for 8457 reflections (370 parameters) with $I>2\sigma(I)$, R1 = 0.0955, wR2 = 0.0984 and GOF = 1.017 for all reflections, max/min residual electron density +0.559/-0.989 eÅ^3.

Formula = $C_{36}H_{46}Cl_2P_2Pd$	
Formula weight = 717.97 g/mol a = 11.0565(18) Å	Space group = *P*-1
b = 12.827(2) Å	T = 173(2) K
c = 13.891(2) Å	λ = 0.71073 Å
α = 71.824(3)°, β = 73.300(3)°, γ = 70.806(3)°	D_c = 1.378 Mg/m^3
V = 1729.8(5) Å^3	μ(Mo) = 0.807 mm^{-1}
Z = 2, Z' = 0	$R(F_o)$ = 4.66%
Crystal system = triclinic	$R_w(F_o)$ = 8.20%

4.4.4.5. $Pd^0(MeJPhos)_2(\eta^2$-dba)

To a solution of freshly recrystalized[53] $Pd^0{}_2(dba)_3$•$CHCl_3$ (87.0 mg, 80 μmol, 2 mL THF, c.a. 40 mM) was added dropwise a solution of MeJPhos (70.0 mg, 320 μmol, 2 mL THF, c.a. 160 mM). Note that if stoichiometry is less than 2:1 phosphine to Pd, a green insoluble polymeric solid results. The mixture was allowed to stir overnight at room temperature. The brown-red solution was filtered through diatomaceous earth and reduced via vacuum to a brown-red sludge. This mixture was taken up into a minimum amount of Et_2O (c.a. 0.5 mL) and diluted with hexanes to 20 mL resulting in a brown-red solution. Note that the target complex is insoluble in hexanes, but will oil under almost all crystallization conditions (any trace solvent except pure hexanes). The Et_2O/hexanes mixture was then left to evaporate slowly (the Et_2O evaporates first) yielding deep red crystals ($Pd^0(MeJPhos)_2(\eta^2$-dba)) in a yellow solution (displaced dba) which can be decanted to purity. Crystals should be washed several times with hexanes to ensure any residual dba has been rinsed away. This procedure reliably produced product in excellent

yields (116.9 mg, 95.0%). The complex can also be isolated using gradient column chromatography (60 mesh silica, CH_3CN R_f=0.9). ^{1}H NMR (300 MHz, Benzene-d_6) δ 8.00 (d, J = 15.7 Hz, 1H), 7.86 – 7.65 (m, 8H), 7.37 – 6.69 (m, 21H), 5.21 – 4.71 (m, 2H), 0.92 (dd, J = 93.2, 5.3 Hz, 6H), 0.71 – 0.59 (m, 6H). ^{31}P{^{1}H} NMR (121 MHz, Benzene-d_6) δ -12.47 (d, J = 5.8 Hz), -14.61 (d, J = 5.8 Hz). The compound was further characterized by single crystal XRD (Table 4.7).

Table 4.7. Crystallographic Data for $Pd^0(MeJPhos)_2(\eta^2$-dba). Additional parameters: crystal dimensions = 0.07 x 0.04 x 0.02 mm, $F(000)$ = 796, $2\theta_{max}$ = 110.0°, 11800 reflections, 4684 independent reflections [R_{int} = 0.0824], R1 = 0.0700, wR2 = 0.1649 and GOF = 1.023 for 4684 reflections (442 parameters) with I>2σ(I), R1 = 0.0889, wR2 = 0.1755 and GOF = 1.023 for all reflections, max/min residual electron density +0.450/-1.114 eÅ^3.

Formula = $C_{45}H_{44}OP_2Pd$	
Formula weight = 769.14 g/mol a = 11.1180(6) Å	Space group = P-1
b = 11.4477(6) Å	T = 173 K
c = 15.4317(9) Å	λ = 1.54178 Å
α = 81.426(2) °, β = 78.935(2) °, γ = 79.538(2) °	D_c = 1.357 Mg/m^3
V = 1882.20(18) Å^3	μ(Cu) = 5.030 mm^{-1}
Z = 2, Z' = 0	$R(F_o)$ = 7.00%
Crystal system = triclinic	$R_w(F_o)$ = 16.49%

4.4.5. Time resolved infrared spectroscopy and photolysis of chromium complexes

Under an inert atmosphere of N_2, $Cr^0(CO)_6$ (2.2 mg, 10 μmol) and the R-JohnPhos ligand (10 μmol) were added to a 1.00 mL volumetric flask. The flask was filled to the 1.00 mL mark with THF and mixed until all solids were dissolved. The colorless solution was injected into a fluorite prism liquid IR cell and sealed with air-free Teflon stoppers. Photolysis was performed by sequential exposure of the window of the

cell (6” from refocusing lens) for varying times (4 seconds to 144 seconds) to broadband UV from a high-pressure Hg arc lamp followed by immediate collection of IR spectra. All solutions turned yellow upon exposure to UV radiation. Displayed spectra are THF subtracted from a blank using the same fluorite prism liquid cell and baseline corrected.

4.4.6. Additional information

Text describing detailed mathematical treatment of carbonyl absorbance data, calculations of carbonyl force constants, tabulated crystallographic data, Tolman cone angle calculations, percent buried volume calculations, ^{1}H- and ^{31}P-spectra of new complexes, and data for selected additional experiments is provided in Appendix C.

4.5. Summary

The electron donating and steric properties of Buchwald-type ligands ([1,1'-biphenyl]-2-yldi(alkyl)phosphine; R-JohnPhos, where R = Me, Et, ^{i}Pr, Cy, ^{t}Bu) were determined. The π-acidity and σ-donating properties of the R-JohnPhos ligands were quantified using a Cotton-Kraihanzel analysis on the $Cr^{0}(CO)_{5}$(R-JohnPhos) complexes. Somewhat surprisingly, the σ-donating ability of the R-JohnPhos ligands follow the trend ^{t}Bu-JohnPhos < Et-JohnPhos < ^{i}Pr-JohnPhos < Cy-JohnPhos << Me-JohnPhos. This ordering is proposed to arise from competition between the intrinsic electron-donating ability of the R groups (Me < Et < ^{i}Pr ~ Cy < ^{t}Bu) and steric interactions (front and back strain) that decrease the electron-donating ability of the phosphine. X-ray crystallographic data of 22 metal complexes (general forms: *trans*-$Cr^{0}(CO)_{4}(PR_{3})_{2}$, $Pd^{0}(PR_{3})_{2}(\eta^{2}$-dba), and *trans*-$Pd^{II}(Cl)_{2}(PR_{3})_{2}$) were also analyzed to help explain the

electronic trends measured for the R-JohnPhos ligands. The R-JohnPhos ligands are exceptionally sensitive to back strain compared to typical phosphines, and the strong σ-donating ability of the Methyl-JohnPhos ligand is attributed to its ability to avoid both front strain and back strain. Consequently, the -PMe_2 moiety allows for very short phosphorus-metal bond distances. Because of the sterically dominating *o*-biphenyl and close phosphorus-metal bond distances, MeJPhos maintains a large overall steric profile that is actually larger than CyJPhos as measured by percent buried volume ($\%V_{bur}$). Overall, the -PMe_2 moiety is a powerful way to incorporate strong σ-donation into "designer" phosphines while retaining other advantageous structural and reactivity properties.

4.6. Notes

‡DIOP = (2,3-O-isopropylidene-2,3-dihydroxy-1,4-bis(diphenylphosphino)butane), BINAP = (2,2'-bis(diphenylphosphino)-1,1'-binaphthyl), and SPhos = 2-Dicyclohexylphosphino-2′,6′-dimethoxybiphenyl.

4.7. Bridge

This chapter discusses the steric and electronic properties for a series of five phosphine ligands. These properties are intrinsically interesting; however, how these properties relate to catalysis is the goal of this work. The next chapter will discuss catalysis in the context of ligand structure and properties as discussed in this chapter.

CHAPTER V

BUCHWALD-HARTWIG CROSS-COUPLING CATALYSIS OF PALLADIUM-JOHNPHOS COMPLEXES

5.1. Introduction

5.1.1. History

Though C_{Ar}-C bond forming cross-coupling reactions have been known for the better half of a century, C_{Ar}-N bond forming cross-coupling (Buchwald-Hartwig) is a more recent discovery.[1,2] The first example C_{Ar}-N cross-coupling was reported by Migita and coworkers in 1983, using aminostannane and phenyl bromide.[3] Three years later, C_{Ar}-N bond formation from a free amine (R_2NH) was reported by Yagupol'skii.[4] These reports both went largely overlooked until 1995, when both Buchwald[5] and Hartwig[6] independently developed a method to cross-couple free amines and aryl halides using strong bases such as lithium bis(trimethylsilyl)amide and potassium *tert*-butoxide with palladium catalysts. Although the cross-coupling substrates have been established over a broad range of coupling partners, the identity of the catalyst is still limited to a narrow range of ligands and metals (Figure 5.1).[7]

In general, very sterically large bidentate or pseudo-bidentate ligands are required that also have strong sigma-donating properties (Figure 5.2).[8] The form of the ligand facilitates two competing factors: (1) strong electron donation to facilitate oxidative addition, and (2) extreme steric hindrance to promote the active species as well as reductive elimination. Aspects of a catalyst that accelerate the rate of either oxidative addition or reductive elimination will inherently decelerate the rate of the opposite

through the law of microscopic reversibility.[9] Thus, only a finely tuned range of catalysts has been discovered.

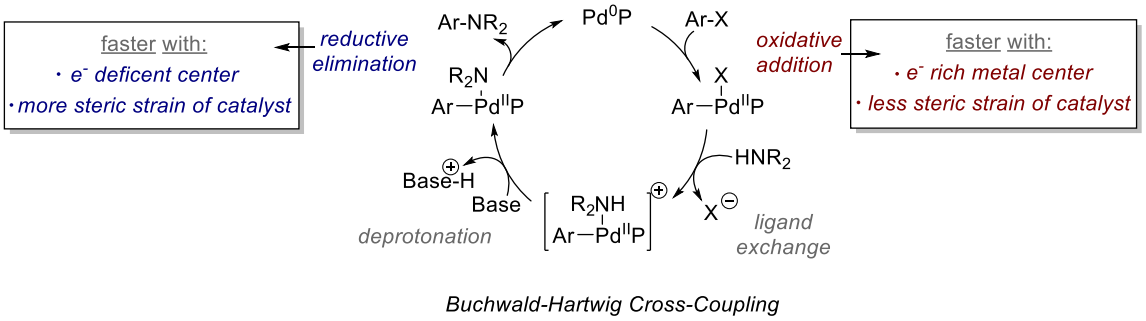

Figure 5.1. Buchwald-Hartwig aryl amination mechanism with catalyst properties highlighted.

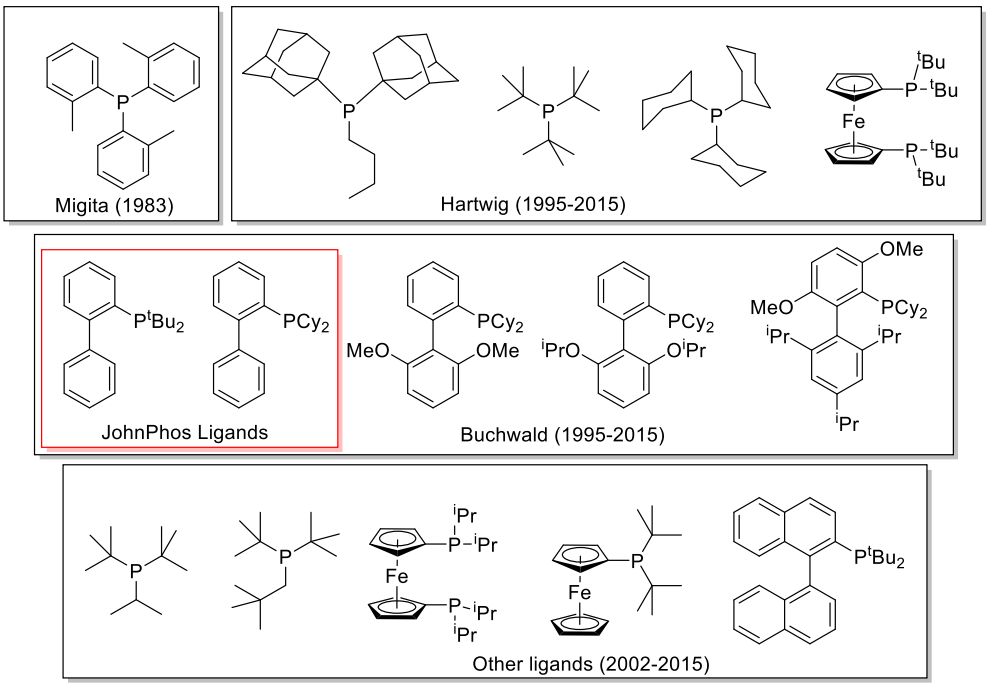

Figure 5.2. Phosphine ligands that form active catalysts with palladium to perform Buchwald-Hartwig cross-coupling. Highlighted in red are the simplest Buchwald-type ligands known to form active catalysts, ^{t}Bu- and CyJohnPhos.

The exact nature of how and why these ligands form catalytic species with palladium is still largely speculative and, at best, qualitative.[10] The *ab initio* design of new ligands, and thus new catalysts, has been throttled because of this fact. Instead of designing new ligands and catalysts, serendipity and high-throughput screening are employed to discover new active catalysts.[11]

5.1.2. The rate limiting step

In a catalytic cycle, as with any chemical reaction, the emphasis for improvement is directed at the turnover frequency, or TOF (addressing the rate-limiting step of the reaction),[12] and the turnover number, or TON (addressing the longevity of the catalyst).[13] Typically for Buchwald-Hartwig cross-coupling, the overall TOF is slow due to the considerable electronegativity differences between the carbon and nitrogen coupling partners. Thus, much research has aimed at improving the TOF of the catalytic cycle – especially for electronically deactivated substrates.[14] For a given Buchwald-Hartwig amination, any of the four steps (Figure 5.1) can be rate limiting. For electronically deactivated substrates, however, oxidative addition is typically the rate determining step.[9] (Although multiple active catalytic species that form allow concentrations of additives or base to affect the rate, the dominant factor for the TOF is the ability of the catalyst to perform oxidative addition).[15] Electronically reluctant coupling partners exhibit one or more of several properties: (1) electron rich through resonance, (2) sterically demanding, (3) thermodynamically inert bonds that are oxidatively added to(e.g., Ar-Cl, Ar-F, Ar-H, etc.).

Although many studies have been performed to determine rates and the rate limiting steps of Buchwald-Hartwig cross-couplings,[15] no kinetic or rate data have been published on Buchwald-type ligands. The purpose of this study was to determine how the alkyl substituents on the simplest Buchwald-type ligands (see Chapter IV, Figure 4.2) affects catalytic rates. The steric and electronic contributions measured for these ligands (Me-, Et-, ^{i}Pr-, Cy-, and ^{t}Bu-JohnPhos) in Chapter IV can be related to catalytic TOF.

5.2. Results and discussion

5.2.1. Preliminary catalysis

To independently synthesize biaryl species and probe non-Buchwald-Hartwig cross-coupling, initial reaction conditions for a Suzuki cross-coupling were attempted. The reactions (based on literature) were met with failure (Table 5.1). Preliminary observations suggested the identity of the purchased phenylboronic acid was actually phenylboroxine (the dehydrated boro-ester trimer). The independent synthesis of boronic acid and subsequent reaction still failed to produce measurable yields with several alkyl JohnPhos (RJPhos) ligands.

Buchwald-Hartwig amination conditions were screened for feasibility of determining rates (Table 5.2). The reaction conditions were drawn from an early study by Buchwald et al.[14] Satisfactorily, the reactions provided excellent yields for morpholine and deactivated aryl chlorides.

Table 5.1. Preliminary Suzuki cross-coupling catalysis. [a]Isolated yields after 8 hours. Concentrations of reagents: phenylboronic acid = 1.5 M, aryl chloride = 1.0 M, KF = 2.0 M, with 4.0 mol% $Pd(OAc)_2$ and 8.0 mol% RJPhos.

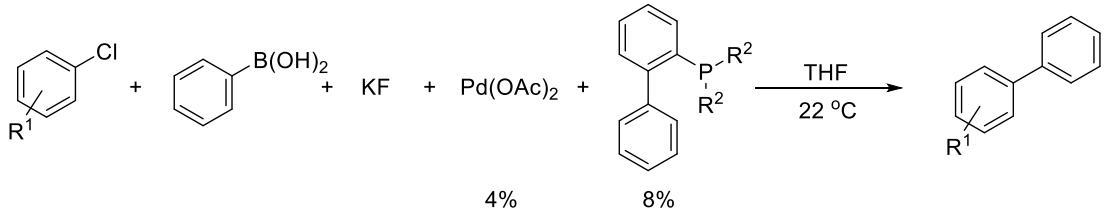

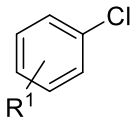	**R^2**	**Yield (%)[a]**
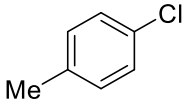	^{t}Bu	11.3
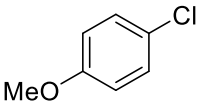	^{t}Bu	10.1
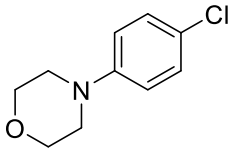	^{t}Bu	6.0
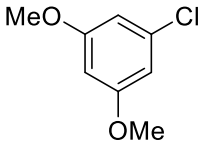	^{t}Bu	<1
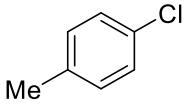	Me	<1
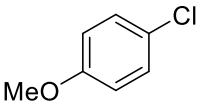	Me	<1

Table 5.1. (continued)

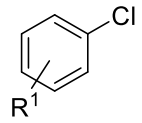	**R^2**	**Yield (%)[a]**
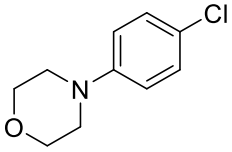	Me	<1
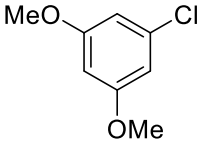	Me	<1
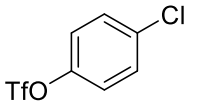	Me	<1

A series of reaction rates were measured using time point sampling with combined NMR and GC-MS quantification of both yield and conversion. The kinetic data were measured to gauge a reasonable catalytic loading, concentration, and lapse of time (Figure 5.3). The rates were determined by concentration of product over time. The data showed that over a span of approximately 8 hours the reaction was complete at room temperature.

Table 5.2. Preliminary Buchwald-Hartwig amination catalysis. [a]Isolated yields after 8 hours. Concentrations of reagents: amine = 1.2 M, aryl chloride = 1.0 M, NaO^tBu = 1.4 M, with 4.0 mol% $Pd(OAc)_2$ and 8.0 mol% ^{t}BuJPhos.

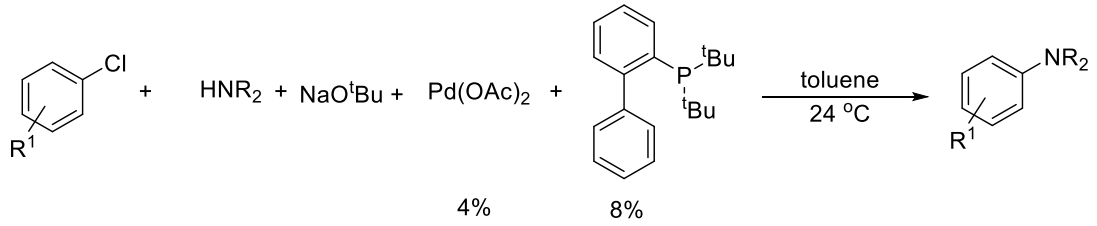

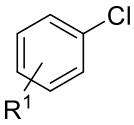	**HNR_2**	**Yield (%)[a]**
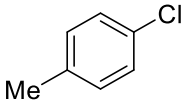	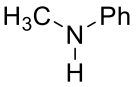	<1
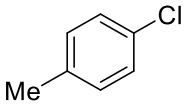	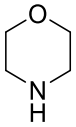	73
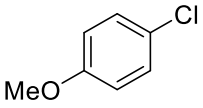	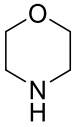	79

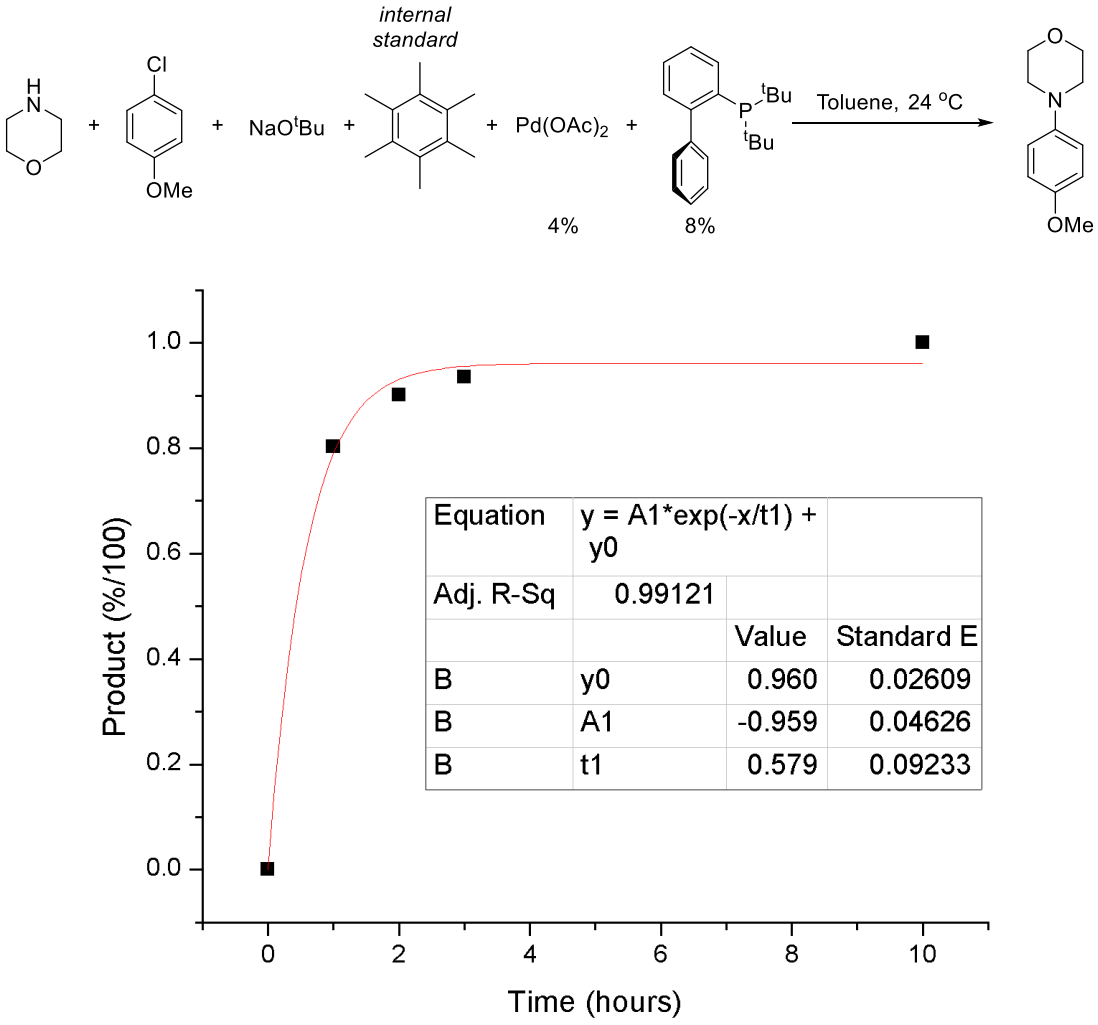

Figure 5.3. Preliminary rate data for scout reaction. Concentrations of reagents: morpholine = 1.2 M, p-chloroanisole = 1.0 M, NaO^{t}Bu = 1.4 M, hexamethylbenzene 0.083 M, with 4.0 mol% Pd(OAc)$_2$ and 8.0 mol% ^{t}BuJPhos. Yields determined by ^{1}H NMR and GC-MS.

5.2.2. Ligand catalysis comparison

Kinetics were measured (Figure 5.4 for four JohnPhos ligands (Me-, Et-, Cy-, and ^{t}BuJPhos) under similar conditions from those reported in Figure 5.3. Surprisingly, only the ^{t}BuJPhos performed catalytically. These data are surprising for two reasons: (1) CyJPhos is a literature reported ligand for this catalysis and (2) the catalytic activity

"turns-on" with the ^{t}BuJPhos with no intermediate catalysis from Cy-, Et-, and MeJPhos. The drastic difference in catalysis is derived from very subtle structural differences of the ligands. Because the electronic differences are extremely small compared to the steric profile differences of the ligands (see Chapter IV), it is empirically deduced that the structure of the ligand for Buchwald-Hartwig amination requires a minimum steric profile to perform catalytically (greater than CyJPhos). The need for a minimum steric profile of the ligand to perform catalytically could derive from one or more factors: (1) inept catalyst formation due to ligand size, (2) failed palladium activation, (3) ligand equilibrium to inactive metal complex, and (4) inability to perform one of the catalytic steps (such as reductive elimination) due to ligand size.

5.2.3. Precatalyst study

The first possibility addressed for the inactivity of the Me-, Et-, and CyJPhos ligands was formation of the active catalyst. The catalytic data in Figure 5.4 were obtained by allowing a brief pre-coordination of $Pd(OAc)_2$ and the phosphine, followed by addition to the reaction vessel. It is possible that an active catalyst was never formed for the Me-, Et-, and CyJPhos complexes. This could be the result of either stoichiometry between Pd and the phosphine ($(L)_2Pd(0)$ complexes are known be inactive until ligand dissociation),[16] or the failure to reduce palladium (II) to palladium (0) *in situ*.[17] To address both of these potential complications, "precatalysts" were synthesized. A

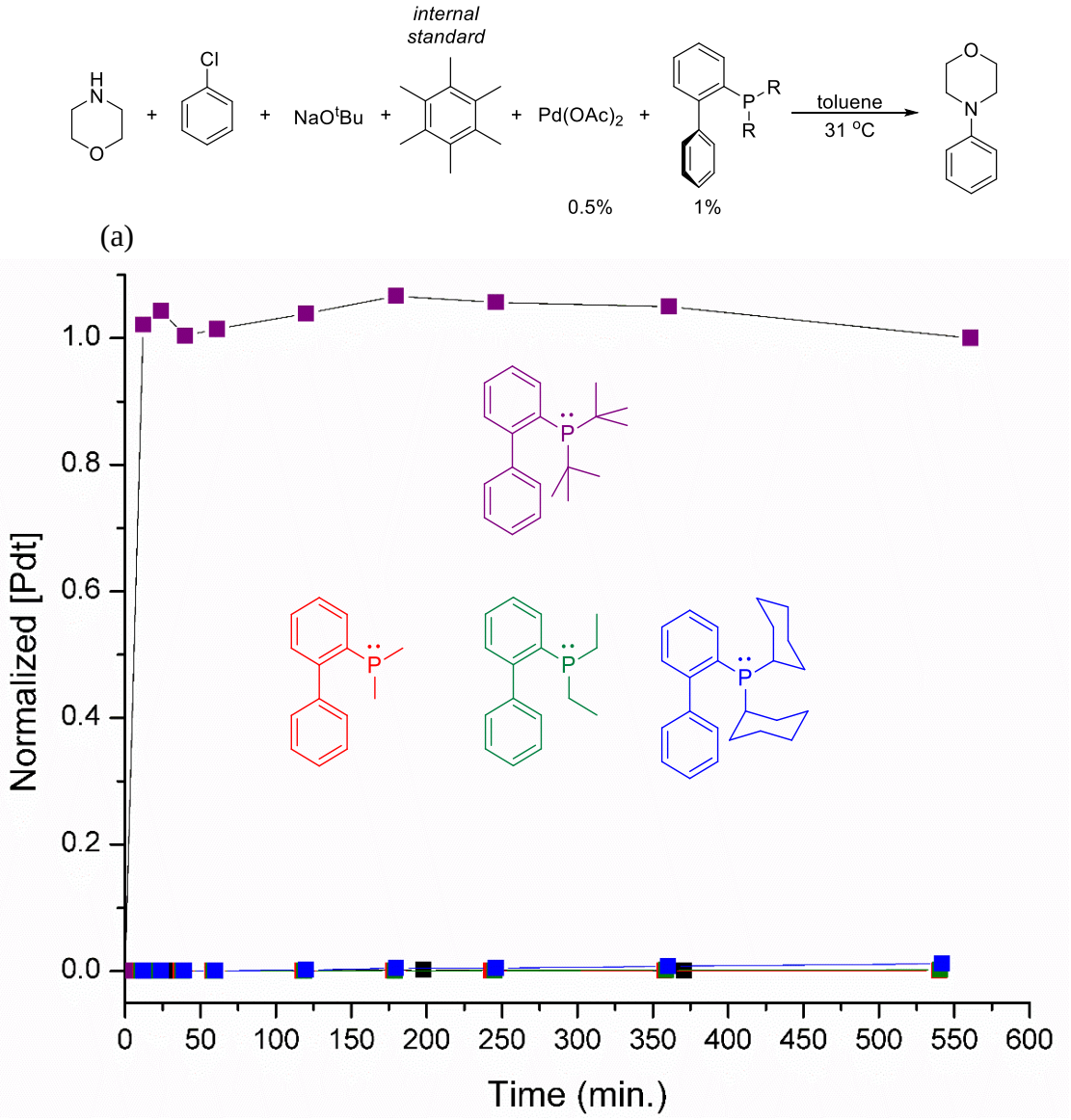

Figure 5.4. (a) Rate data for Buchwald-Hartwig amination with Me-, Et-, Cy-, and ^{t}BuJPhos ligands. (b; next page) Zoom-in of Figure 5.4a. Black trace represents a control with no ligand present. Concentrations of reagents: morpholine = 1.2 M, chlorobenzene = 1.0 M, NaO^{t}Bu = 1.4 M, hexamethylbenzene 0.083 M, with 0.5 mol% Pd(OAc)$_2$ and 1.0 mol% R-JohnPhos. Yields determined by ^{1}H NMR and GC-MS.

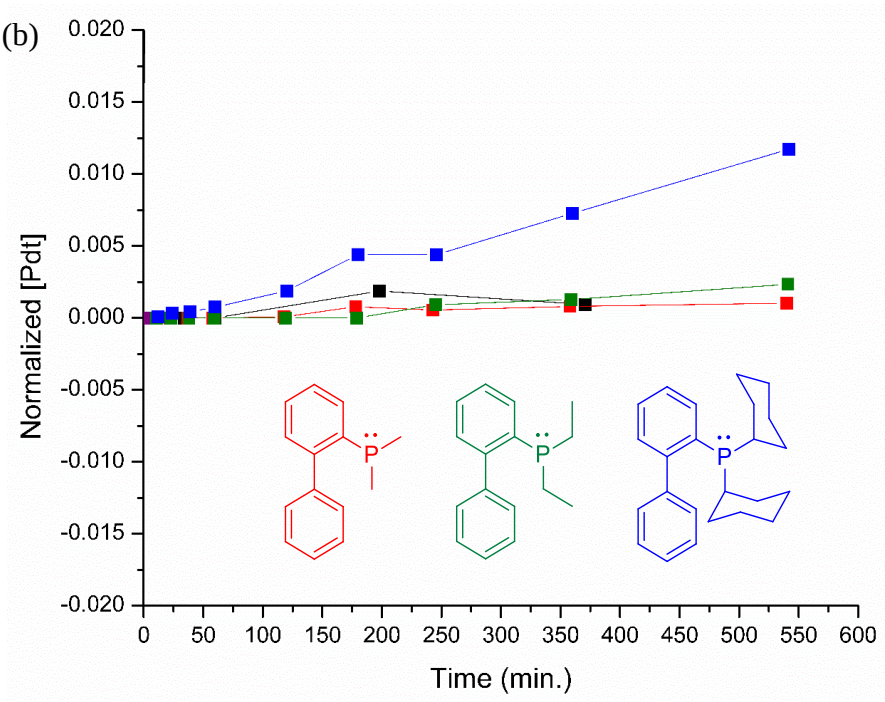

Figure 5.4. (continued)

precatalyst is a stable form of an immediate precursor to active catalyst. Typically, adding the precatalyst to the reaction medium results in selective and rapid formation of the active catalyst (LPd(0) in this case).

5.2.3.1. Palladium acetate "palladacycle"

A report by Buchwald et al. describes the formation of a precatalyst using ^{t}BuJPhos and palladium acetate to make a palladacycle that is catalytically active for Buchwald-Hartwig aminations of aryl chlorides (Scheme 5.1).[18] Although palladium is in the 2+ oxidation state, it is easily reduced by reductive elimination of the aryl ring on the ligand to form a catalytically active LPd(0) species *in situ*.

Scheme 5.1. General reaction for synthesis of JohnPhos palladacycle.

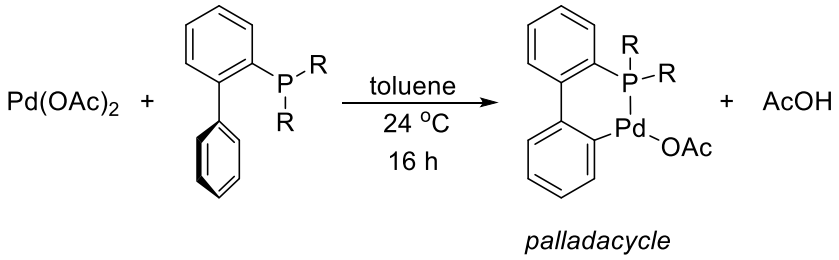

The coordination of ^{t}BuJPhos to $Pd(OAc)_2$ and consequent conversion to the palladacycle was achieved as reported. Me-, Et-, ^{i}Pr-, and CyJPhos did not react with $Pd(OAc)_2$ to form discrete species. MeJPhos formed at least seven distinct species which were intractably inseparable. These results suggested that the palladacycle was not a good precatalyst target to study catalysis across the JohnPhos ligands.

5.2.3.2. Palladium(0) dibenzylideneacetone complexes

A common strategy for cross-coupling precatalysts is to use a reduced form of palladium to synthesize a precatalyst complex. Pd(0) precursors like $Pd_2(dba)_3$ (dba = dibenzylideneacetone) are chemically stable sources of Palladium (0). Because dba is a weakly coordinating ligand and is easily displaced by stronger coordinating ligands such as phosphines, precatalysts can easily be synthesized (Scheme 5.2). Once in solution, simple ligand dissociation is required to form an active (LPd(0)) catalyst.

Scheme 5.2. General reaction for synthesis of $Pd^0(RJPhos)_2(\eta^2\text{-dba})$ complex.

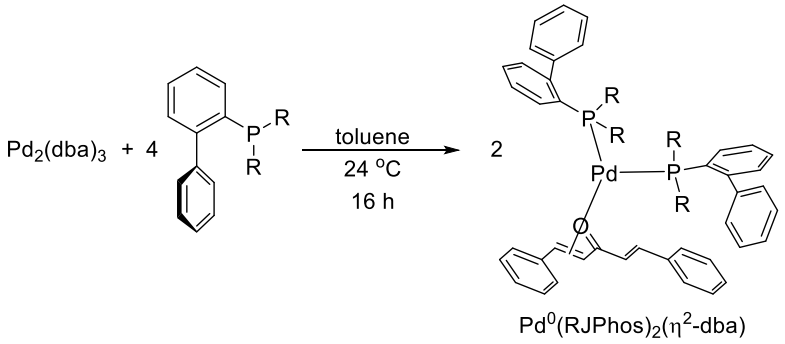

MeJPhos reacted discretely to form the $Pd^0(MeJPhos)_2(\eta^2\text{-dba})$ as shown in Scheme 5.2 (see Chapter IV). Unfortunately, Et-, ^{i}Pr-, Cy-, and ^{t}BuJPhos did not all form the same species. Rather, Me- and EtJPhos formed $Pd^0(RJPhos)_2(\eta^2\text{-dba})$ complexes while Cy- and ^{t}BuJPhos formed Pd(0)(RJPhos-κ*P*:κ*C*)(η^2-dba) type species and ^{i}PrJPhos formed a mixture. The inconsistent coordination is likely from a competition of 1:1 phosphine to palladium versus 2:1 phosphine to palladium as the R groups become more sterically demanding than methyl groups.

To address the inconsistent coordination stoichiometry aforementioned, the mono-phosphine complexes (Pd(0)(RJPhos)(η^2-dba)-type species) were considered as synthetic targets. The feasibility of synthesizing these types of complexes has president with a ^{t}BuJPhos.[19] The reported synthesis of Pd(0)(^{t}BuJPhos-κ*P*:κ*C*)(η^2-dba) was easily reproduced (Scheme 5.3, top route). Attempted synthesis under the same conditions with MeJPhos yielded a green solid insoluble in all common solvents (including DMSO). Attempts to heat the green solid in non-coordinating and coordinating solvents only yielded decomposition to palladium black. This green solid was likely a coordination polymer wherein the sub-valent palladium coordinates to another molecule's

uncoordinated dba alkene and forms long chains of poly-Pd(0)(MeJPhos)-μ-(η^2-dba)$_2$ (Scheme 5.3, bottom route). As with the Pd^0(RJPhos)$_2$(η^2-dba) complexes, it appears that the difference in R groups' steric profile leads to vastly differing coordination geometries and resulting complexes. This point is perhaps best highlighted with Scheme 5.3. Due to the inconsistent coordination complexes formed by these ligands, this approach at forming precatalysts was determined to be impractical for this study.

Scheme 5.3. Synthesis of Pd(0)(RJPhos)(η^2-dba)-type species with ^{t}BuJPhos (top) and MeJPhos (bottom) ligands.

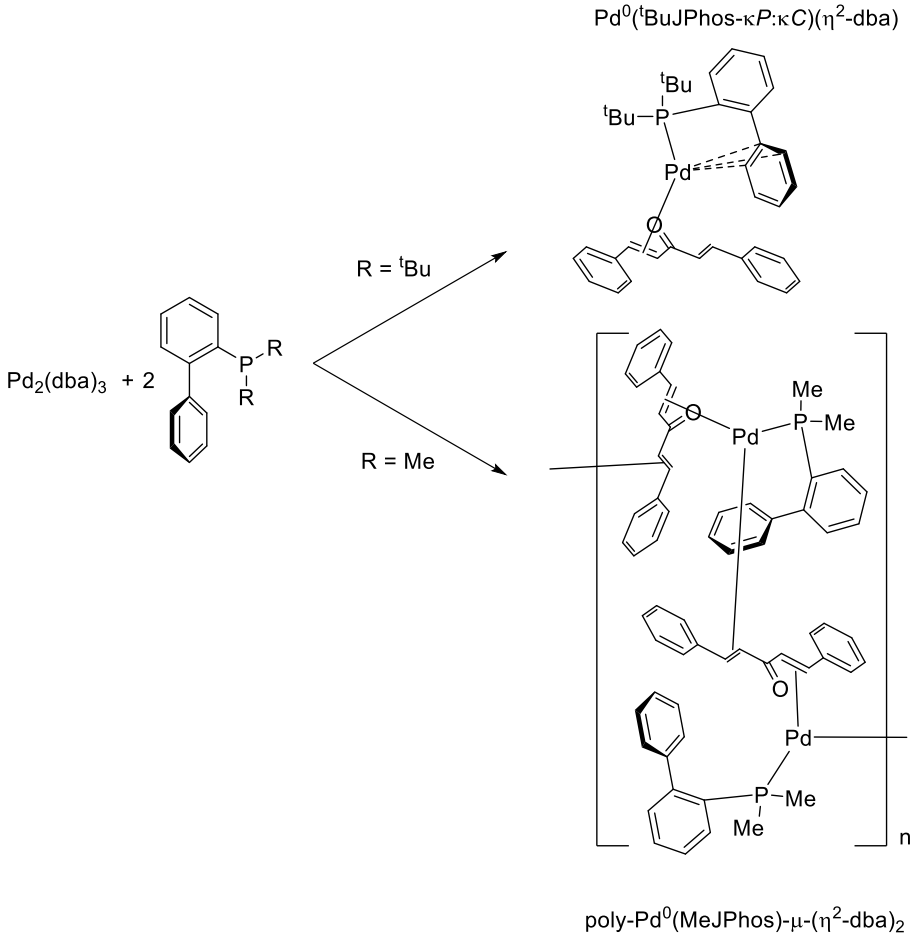

5.3.3.3. Buchwald precatalysts

Buchwald precatalysts were developed by Buchwald et al. to address many of the synthetic problems associated with the stability and activation of precatalysts for Buchwald-Hartwig amination.[20] The synthesis is straightforward (Scheme 5.4); however, it has only been used with 2-Dicyclohexylphosphino-2',6'-dimethoxybiphenyl (SPhos) type phosphines. To determine if the synthesis was viable for JohnPhos-type Buchwald ligands, a preliminary reaction using CyJPhos to generate the Buchwald precatalyst (Scheme 5.4, Buchwald precatalyst R = Cy) was carried out. This initial exploratory reaction provided a discrete species that was isolated in decent yield. When Me-, Et-, ^{i}Pr-, and ^{t}BuJPhos were screened under similar conditions; however, non-discrete species formed with a considerable amount of palladium decomposition to palladium black. Varying both time and temperature of the reaction did not have any considerable effect on the results.

Scheme 5.4. Buchwald precatalyst synthesis.

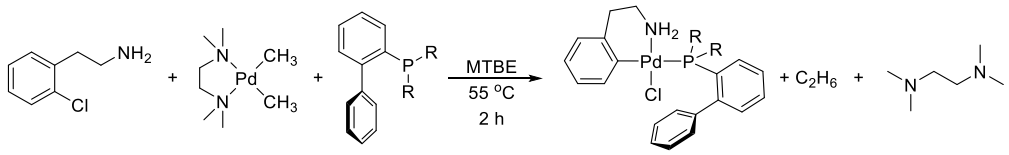

Buchwald precatalyst

The reactions using the Me-, Et-, ^{i}Pr-, and ^{t}BuJPhos ligands to generate Buchwald precatalysts likely failed due to a kinetics mismatch in the formation of the precatalyst complex (Scheme 5.4, Buchwald precatalyst). In order to form the precatalyst complex,

the several intermediates and kinetic steps must all work synergistically to produce the precatalyst (Scheme 5.5). Although it is unclear why the Me-, Et-, ^{i}Pr-, and ^{t}BuJPhos ligands failed to form discrete species, the problem could potentially be mitigated with a derivative chemical reaction in which the aryl chloride is replaced with a pseudo-halide. A pseudo-halide would facilitate faster oxidative addition to the Pd(0) species formed during the precatalyst formation (Scheme 5.5, final step). It is possible that a slow oxidative addition to the aryl chloride (for the Me-, Et-, ^{i}Pr-, and ^{t}BuJPhos ligands) allowed enough time for the Pd^{0} complex to ligand dissociate and aggregate as palladium black.

Scheme 5.5. Proposed mechanism of Buchwald precatalyst synthesis from Scheme 5.4.

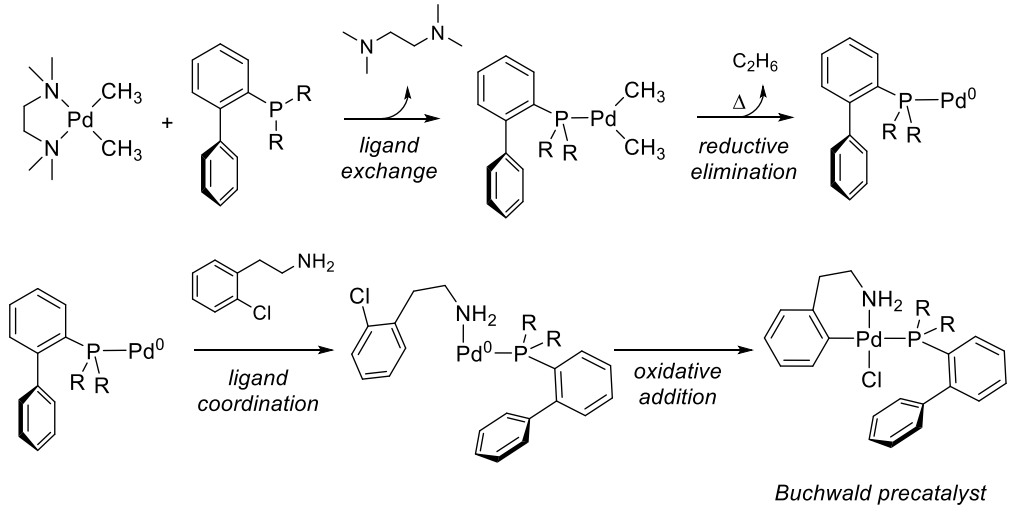

Early investigations into using a pseudo-halide in lieu of an aryl chloride for the synthesis of a Buchwald catalyst were undertaken. The direct synthesis of such a precursor molecule was attempted (Scheme 5.6, top route) based on a report by Kaboudin

et al.;[21] however, it was found to be non-reactive for the 2-(2-aminoethyl)anisole substrate. An alternative synthetic route was briefly explored (Scheme 5.6, bottom route) and found to be feasible. Notably, 2-(2-aminoethyl)phenol (~$300/g BOC Sciences) was isolated in excellent yields from 2-(2-aminoethyl)anisole (~$4/g TCI) using refluxing HBr on the 25g scale. Ultimately, the Buchwald precatalyst approach was left unfinished in favor of other experiments.

Scheme 5.6. Synthesis towards pseudo-halide Buchwald precatalyst.

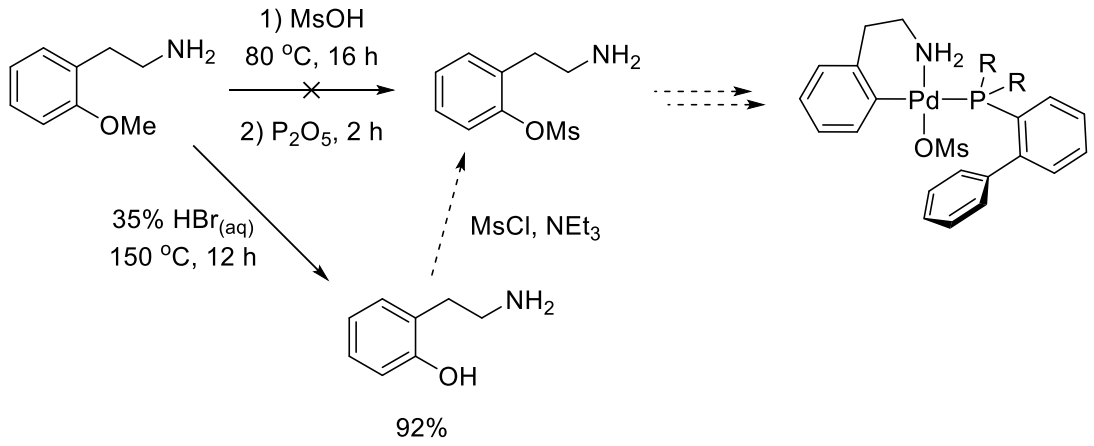

5.2.4. Other catalysis

A variety of Buchwald-Hartwig amination reactions were screened for reactivity across several of the JohnPhos ligands – with a special emphasis on MeJPhos.

5.2.4.1. Competitive cross-coupling

Buchwald-Hartwig aminations are known to proceed via either Pd 0/2+ (two electron) catalytic cycles or Pd 0/1+ (one electron) catalytic cycles. A simple test for this

reactivity is competitive cross-coupling with an aryl halogen and a pseudo-halide. Pseudo-halides do not undergo cross-coupling via one electron catalytic cycles at an appreciable rate compared to aryl halides, so analysis of the product distribution for a competition reaction (with aryl chlorides and pseudo-halides) can lend insight into the catalytic process.[22] The attempt to probe of Me-, Cy-, and ^{t}BuJPhos under the conditions in Table 5.3 produced a stoichiometric side reaction in all cases.

Table 5.3. Competitive cross-coupling screening for Me-, Cy-, and ^{t}BuJPhos. [a]Isolated yields after 8 hours. Concentrations of reagents: amine = 1.2 M, aryl chloride = 1.0 M, NaO^{t}Bu = 1.4 M, with 4.0 mol% Pd(OAc)2 and 8.0 mol% RJPhos.

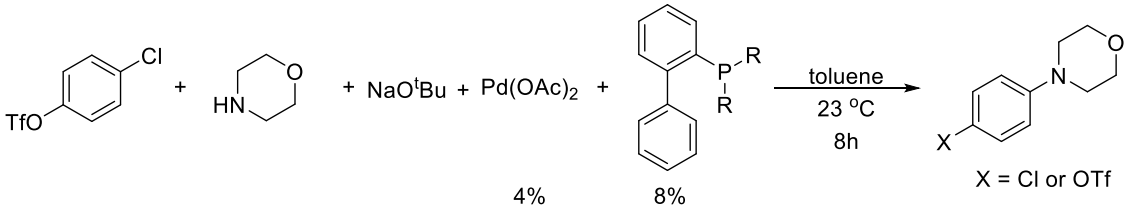

R	*X= Cl* Yield (%)[a]	*X= OTf* Yield (%)[a]
Me	<1	<1
Cy	<1	<1
^{t}Bu	<1	<1

5.2.4.2. Pd(II)Cl$_2$ complexes

Although rare, PdCl$_2$ complexes have been reported to act as precatalysts for Buchwald-Hartwig aminations.[23] The *trans*-PdCl$_2$(RJPhos)$_2$ complexes (R= Me, Et, ^{i}Pr) were all synthesized (see Chapter IV) and screened under the reaction conditions in Table 5.4. No catalysis was observed for the *trans*-PdCl$_2$(RJPhos)$_2$ complexes at room

temperature. This is likely due to the inability to form Pd(0) complexes *in situ* with the $Pd(II)Cl_2$ precursors.

Table 5.4. Preliminary Buchwald-Hartwig amination catalysis. [a]NMR yields after 16 hours. Concentrations of reagents: amine = 1.2 M, aryl chloride = 1.0 M, NaO^tBu = 1.4 M, HMB = 0.083 M, with 4.0 mol% $PdCl_2(RJPhos)_2$.

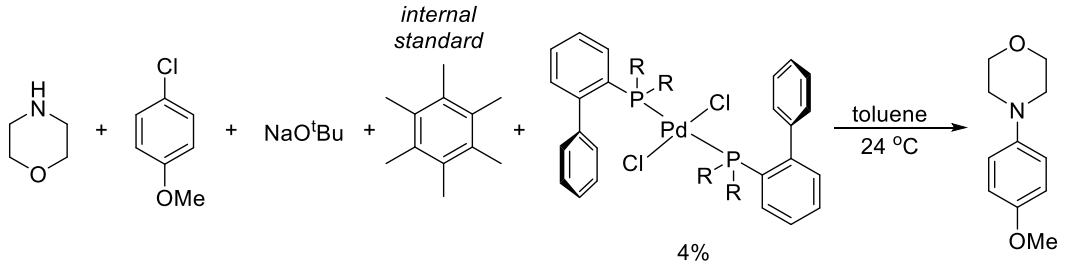

R	Yield (%)[a]
Me	<1
Et	<1
iPr	<1

5.2.4.3. Pd(0)(MeJPhos)$_2$(η^2-dba) catalysis

Catalysis screened over a host of aryl halides (both activated and deactivated) using Pd(0)(MeJPhos)$_2$(η^2-dba) as a catalyst yielded stoichiometric or sub-stoichiometric TONs (Table 5.5). These data show that the Pd(0)(MeJPhos)$_2$(η^2-dba) complex is not catalytic for room temperature Buchwald-Hartwig aminations. The absence of catalysis can be attributed to either ligand equilibrium to an inactive metal complex (favoring $L_2Pd(0)$ instead of LPd(0)) or the inability of the complex to perform one of the catalytic steps (such as reductive elimination).

Table 5.5. Pd(0)(MeJPhos)$_2$(η^2-dba) catalysis. [a]NMR yields after 16 hours. Concentrations of reagents: amine = 1.2 M, aryl halide = 1.0 M, NaO^{t}Bu = 1.4 M, HMB = 0.083 M, with 0.1 mol% Pd(0)(MeJPhos)$_2$(η^2-dba).

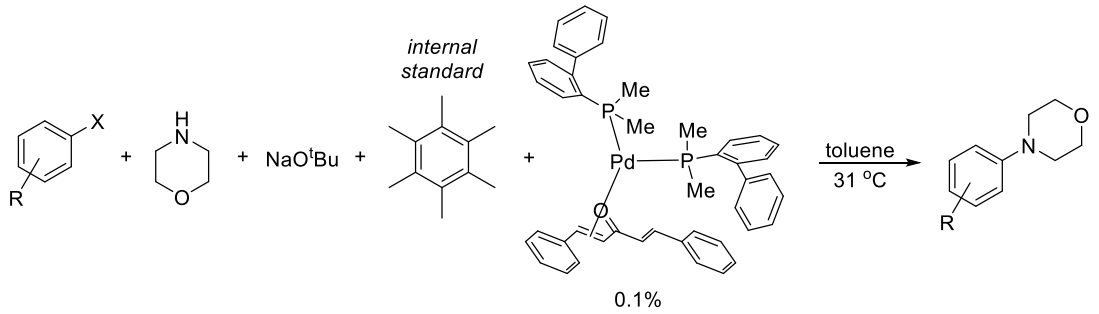

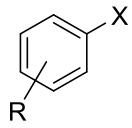	**TON[a]**
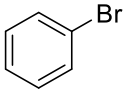	1.1
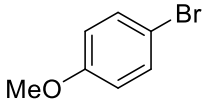	<0.1
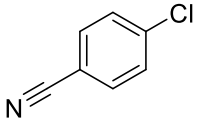	1.2
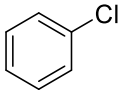	<0.1
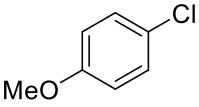	<0.1

5.2.4.4. cis-Pd(II)(TMEDA)Cl_2 catalysis

The *cis*-Pd(II)(TMEDA)Cl_2 complex (used in Scheme 5.4) was used as a precatalyst by coordination with the MeJPhos ligand. When added to a reaction and heated, these conditions should liberate LPd(0) – the active catalyst. Over several substrates and conditions, only stoichiometric yields of Griseofulvin with morpholine were achieved (Table 5.6). Notably because stoichiometric yields are observed, it is likely that the catalytic cycle is stalling at one of the steps, and thus not providing TONs >1. Excitingly, Griseofulvin is an incredibly deactivated aryl chloride and a small yield was observed, suggesting the oxidative addition – even to very deactivated aryl chlorides is possible with MeJPhos. However, without the ability to complete multiple turnovers, catalysis with MeJPhos remains evasive.

5.3. Conclusions

The influence of the identity of the R groups for RJohnPhos ligands on Buchwald-Hartwig amination show a strong dependence on steric profile compared with electronic contributions. In fact, only the largest JohnPhos ligand that was studied performed catalytically (^{t}BuJPhos). This observation suggests that a minimum steric profile of the ligand is necessary to facilitate catalytic turnover. The reason for this steric necessity is still unclear, although it likely derives from the inability to perform reductive elimination. Because a comparison across all of the JohnPhos ligands couldn't be made for any precatalysts, only generalities can be made. These data point out the necessity to balance both electronic and steric factors for an effective Buchwald-Hartwig amination

Table 5.6. *cis*-Pd(II)(TMEDA)Cl_2 and MeJPhos catalysis. [a]NMR yields after 16 hours. Concentrations of reagents: amine = 1.2 M, aryl chloride = 1.0 M, NaHMDS = 1.4 M, HMB = 0.083 M, with 2 mol% *cis*-Pd(II)(TMEDA)Cl_2 and 2 mol% MeJPhos.

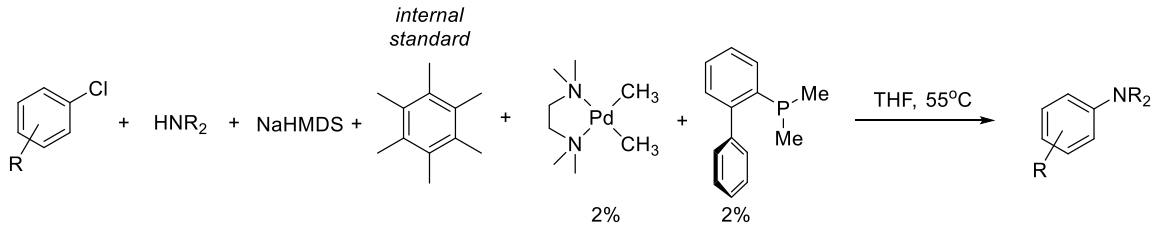

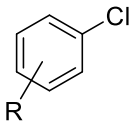	**HNR_2**	**Yield(%)[a]**
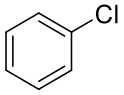	$HNPh_2$	<0.1
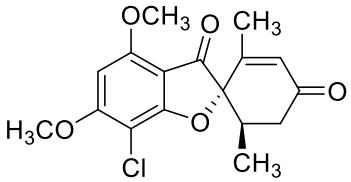	$HNPh_2$	<0.1
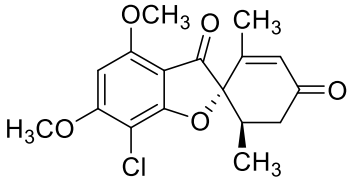	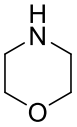	2

ligand. Even very subtle steric and electronic differences cause dramatic differences in catalysis.

Notably, MeJPhos complexes can perform stoichiometric cross-coupling of very deactivated aryl chlorides (suggesting favorable electronics of the ligand); however, these complexes do not perform catalytically. It is possible that a more sterically demanding ligand derivative similar to MeJPhos would overcome the minimum steric profile "barrier" and perform catalytically.

5.4. Experimental

5.4.1. General considerations

Unless stated otherwise, reactions were conducted in freshly aqua regia cleaned and oven-dried glassware under an atmosphere of nitrogen using either standard Schlenk techniques or a dribox maintained at < 1.0 ppm O_2. Diethyl ether and tetrahydrofuran (THF) were dried using a DriSolv system using CuO and molecular sieves under argon. All other reaction solvents were purified and dried according to the literature.[24] All commercially obtained reagents were used as received unless otherwise specified. Thin-layer chromatography (TLC) was visualized using low wavelength ultraviolet light (UV) for all aryl species or phosphomolybdic acid. ^{1}H NMR spectra were recorded on a 300 or 500 MHz Varian spectrometer (^{1}H 300.09 MHz or 500.02 MHz, respectively) and are reported relative to deuterated solvent signals or an internal reference. Data for ^{1}H NMR spectra are reported as follows: chemical shift (δ ppm), multiplicity, coupling constant (Hz) and relative integration. $^{31}P\{^{1}H\}$ NMR spectra were recorded on a 300 or 500 MHz Varian spectrometer (^{31}P 121.48 MHz or 202.13 MHz, respectively) and are reported relative to the external standard of 0.1% H_3PO_4 in D_2O at 0 ppm.

5.4.2. General catalysis

5.4.2.1. Isolated yield catalysis

All reagents except for palladium and the ligand were added to the reaction vessel and dissolved in the appropriate solvent. A freshly prepared stock solution of palladium and ligand was volumetrically added to the reaction medium. The reaction vessel was sealed and stirred for 16 hours. The reaction medium was then filtered through celite-

silica with Et_2O. The solvent was removed using vacuum. The crude reaction mixture was according to literature.[6,14,18]

5.4.2.2. NMR yield catalysis

All reagents except for palladium and the ligand were added to the reaction vessel and dissolved in the appropriate solvent. A freshly prepared stock solution of palladium and ligand was volumetrically added to the reaction medium. The reaction vessel was sealed and stirred for 16 hours. The reaction medium was then filtered through diatomaceous earth-silica with Et_2O. The solvent was removed using vacuum. ^{1}H NMR spectroscopy was used to determine the yield against an internal standard of known concentration. If GC-MS was also used, the NMR sample was diluted to 100 ppm using HPLC grade solvent, and analyzed by GC-MS.

5.4.3. Synthesis

The synthesis of Palladacycles,[18] Pd(0)(RJPhos)$_2$(η^2-dba) (see Chapter IV), Pd(0)(^{t}BuJPhos-κ*P*:κ*C*)(η^2-dba),[19] and Buchwald preligands[20] were synthesized according to the literature preparations.

5.5. Summary

Buchwald-type JohnPhos phosphine ligands were used to study Buchwald-Hartwig amination catalysis. Specifically, the effects of the alkyl groups at phosphorus were compared to determine whether electronic or steric effects dominate the reactivity during the catalytic cycle. Trials with $Pd(OAc)_2$ and two equivalents of JohnPhos ligand

performed catalytically with ^{t}BuJPhos only. Several attempts were made to synthesize precatalysts and catalyst precursors that could help narrow down why all but one of the JohnPhos ligands failed to perform catalytically. Unfortunately, no other direct comparison was possible due to synthetic difficulties. In general, the data suggest that the JohnPhos ligands were stalling in the catalytic cycle at the reductive elimination step. This stalling is likely due to steric profile of the ligand. Notably, MeJPhos – the most electron rich ligand – was able to stoichiometrically cross-couple Griseofulvin (an extremely electronically deactivated aryl chloride). Catalysis with Me-, Et-, ^{i}Pr-, and CyJPhos have yet to be observed.

5.6. Bridge

This chapter of my dissertation discusses catalytic trials screened for several JohnPhos ligands. The purpose of the catalysis is the synthesis of new and interesting organic chemicals. The goal of catalysis is to make a chemoselective transformation with low energy input. Another approach to the same problem is to start with high energy reagents and control the reaction. This approach will be discussed in Chapter VI with the ozonolysis of alkenes.

CHAPTER VI

OTHER SYNTHESES, DATA, AND REACTIONS

6.1. Introduction

6.1.1. Coauthored material

Chapter VI of my dissertation is a modified form of a published paper. I directed the project, developed the theory, interpreted the data, and wrote the manuscript. Coauthors include Justin T. Barry, Daniel T. Seidenkranz, Ajay Ryerson, Colin Hiatt, Chase A. Salazar, Dillon J. Bryant, and David R. Tyler.

6.1.2. Introduction to chapter VI

This chapter represents a series of projects that stand loosely related to previous chapters. In and of itself, this represents a considerable body of work. It is therefore consolidated here as a chapter.

6.2. Highly efficient biphasic ozonolysis of alkenes using a high-throughput film-shear flow reactor

6.2.1. Introduction to ozonolysis

The use of ozone to oxidize alkenes (ozonolysis) is a powerful tool in modern organic chemistry.[1–3] Ozone has many advantages over other common strong oxidants: high atom economy, absence of metals or hyper-valent iodine, and the straightforward synthesis of ozone from O_2. These factors make ozonolysis ideal for many industrial

processes.[4] However, the use of ozonolysis both industrially and in research labs is limited because of the cryogenic temperatures (-40°C) typically required, dangerous intermediates and byproducts that are produced stoichiometrically, and the necessity of a secondary reduction step (using Me_2S, PPh_3, Pt/H_2, BH_3, $NaBH_4$, Zn/HOAc, $LiAlH_4$, etc.) to form ketones, aldehydes, or alcohols.[3] Several approaches have been developed to address these inherent drawbacks. Flow chemistry has been used to minimize the concentration of dangerous intermediates and cryogenic temperatures; however, the reactions still require a secondary quench step of the reaction mixture.[5–10] Another approach, pioneered by Dussault et. al, prevents secondary ozonide (SOZ) formation by using an *in situ* reduction of the carbonyl oxide intermediate with water as the reductant (Figure 6.1).[11,12] This approach allows for a single-step reaction using ozone and water to oxidize alkenes into aldehydes and ketones directly while avoiding a secondary step and strong reducing agents that may be incompatible with the rest of the molecule. Batch reactions and water-miscible polar organic solvents (containing 5% water) were used by Dussault and coworkers, limiting the usefulness of this method for large scale syntheses. Also, when a biphasic system using phase transfer catalysis was attempted, *in situ*

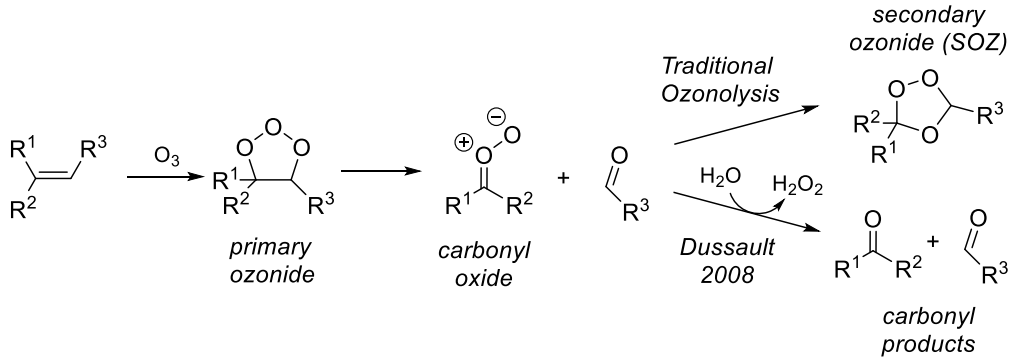

Figure 6.1. Criegee mechanism[13] of ozonolysis showing traditional ozonolysis product pathway (top route) and the Dussault modification[11] of *in situ* H_2O reduction (bottom route).

water reduction was never observed.[14]

6.2.2. Experimental

To expand the approach of *in situ* carbonyl oxide reduction with water, while taking advantage of the safety and scalability of flow ozonolysis, we developed a high-throughput, flow method using a Synthetron™ S3T1 film-shear reactor.[15] A film-shear reactor is a device with a rotating disk (the rotor) placed at an adjustable distance 20-300 μm from a stationary disk (the stator). The rotor spins at speeds up to 10^4 rpm, and two streams containing the reactants are introduced between the two disks. Contact of the reactants within the narrow gap results in intense shear with consequent intimate mixing of the reactants.

As shown in Figure 6.2, the reaction system is comprised of a plug-flow organic/aqueous mixture that is sheared in the reaction chamber with ozone. The shear

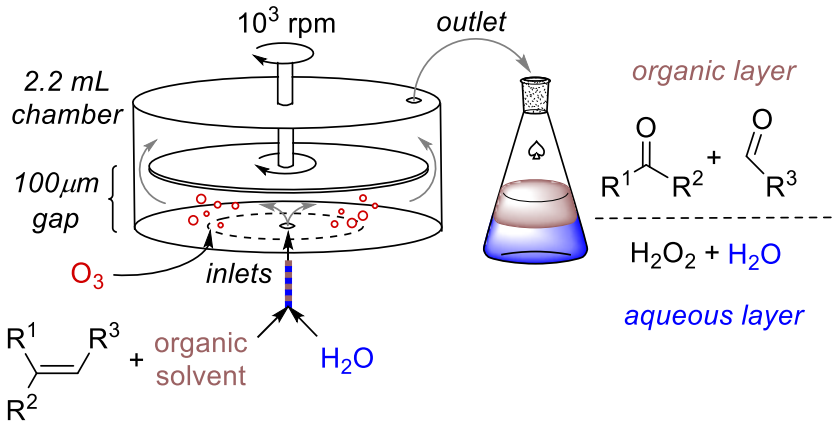

Figure 6.2. General setup of biphasic ozonolysis using the film-shear reactor. [a]A more detailed diagram of the reactor setup is provided in Appendix E, Figure E1.

force increases the interface of H_2O and the organic phase.[16–20] In addition, the mass-transport of ozone into solution benefits from the reactor microfluidics and shear mixing.[21–23] Upon exiting the reactor, the reaction mixture self-separates, with the desired products in the organic phase and H_2O_2 in the aqueous phase.

Preliminary optimizations using isoeugenol found that EtOAc was an excellent solvent and that quantitative conversion to vanillin was achieved at a molar flow rate of 1.0 mmol/min (Appendix E, Figure E2). This molar flow rate is approximately eight times faster than has been previously reported in more conventional microfluidic systems.[24] It is also notable that the residence time in the reactor is 8 seconds. Even with a very short residence time, ozone reacted with greater than 70% efficiency (1.4 eq. of O_3 per 1.0 eq. of isoeugenol, see Appendix E).

The substrate scope of the film-shear ozonolysis system was determined next. When aryl conjugated alkenes were screened, predominantly aldehyde or ketone products were observed. We were then able to run six substrates on the gram/multi-gram scale with good yields of the aldehyde or ketone (Table 6.1). Note that no secondary quench was used before these isolations. These results demonstrate several important attributes of our ozonolyis method: (1) it can effectively mix biphasic media to react the carbonyl oxide with water during ozonolysis, (2) it is scalable to multi-gram reaction scale while retaining good yields, (3) aldehydes and ketones can be directly attained from alkenes in flow without a secondary quench step, and (4) reaction times of <10 seconds.

To further understand the reaction profile with the aryl substrates, we screened an additional four aryl alkenes to determine the ratio of SOZ to carbonyl (Table 6.2). These

data help determine how effective the *in situ* water reduction is for each substrate. In addition, 1-decene was screened under a variety of conditions (Table 6.3). The aryl alkenes afforded much higher ratios of carbonyl to SOZ compared to alkyl alkenes. In fact, the dominant product of the reaction with 1-decene was SOZ under a variety of

Table 6.1. Gram/multi-gram scale ozonolysis of aryl alkenes. [a]Isolated yields.

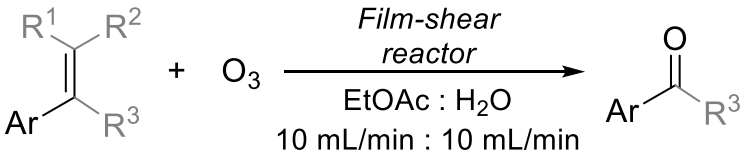

Entry	Substrate	Product	Yield (%)[a]
1	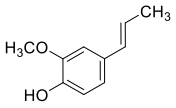	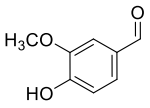	49
2	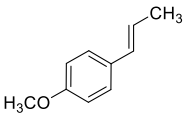	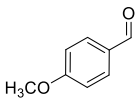	81
3		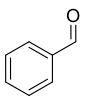	72
4	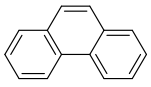	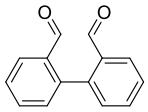	64
5	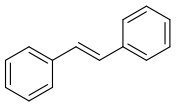	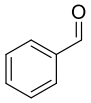	79
6	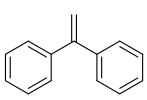	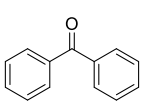	35

Table 6.2. Product distributions for ozonolysis of aryl alkenes. [a] Determined by ^{1}H NMR from the crude reaction mixture.

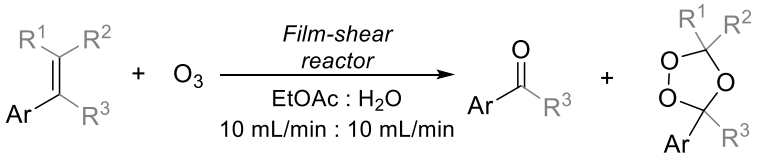

Entry	Substrate	Ratio of carbonyl : SOZ[a]
1	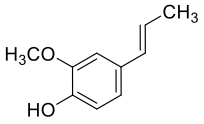	>99:1
2	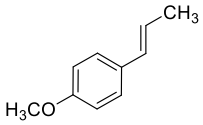	>99:1
3		7.6:1
4	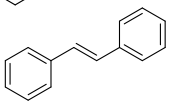	33:1
5	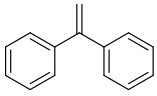	2.8:1
6	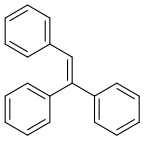	3.4:1
7	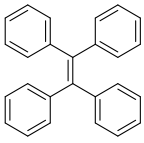	3.5:1
8	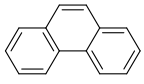	3.6:1
9		1:1.8
10	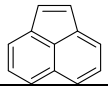	1:17

Table 6.3. Screening conditions for alkyl olefin ozonolysis.[a] TEABr = tetraethylammonium bromide. [b]See Experimental section and Appendix E, Figure E1 for details on method. [c]As determined by ^{1}H NMR with 1,1,2,2-tetrachloroethane or hexamethyl benzene as an internal standard.

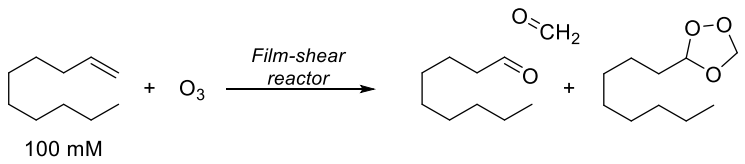

100 mM

Entry	Phases			Flow Rates[b] (mL/min)				Yield (%)[c]	
	Organic	Aqueous	Additives[a]	Organic	Aqueous	Shear RPM (x1000)	Conversion (%)[c]	Aldehyde	SOZ
1	EtOAc	H_2O	-	10	80	2.0	>99	10	38
2	EtOAc	H_2O	-	15	80	2.0	>99	8	37
3	EtOAc	H_2O	-	20	80	2.0	>99	7	36
4	Hexanes	H_2O	-	10	80	2.0	>99	11	38
5	Hexanes	0.1 M $H_2SO_{4(aq)}$	-	10	80	3.6	>99	10	35
6	Hexanes	1.0 M $H_2SO_{4(aq)}$	-	10	80	3.6	>99	4	41
7	Hexanes	H_2O	3 eq. TEABr	10	10	3.6	>99	11	44
8	Hexanes	H_2O	50% MeOH	10	10	3.6	>99	1	36
9	Hexanes	H_2O	3 eq. TBABr	10	10	3.6	>99	13	65
10	Hexanes	H_2O	50% EtOH	10	10	3.6	>99	3	40
11	Hexanes	0.1 M $H_2SO_{4(aq)}$	50% EtOH	10	10	3.6	>99	3	42

conditions (Table 6.3). (Even with aqueous oxidants, various acids, phase transfer catalysts, and alcohol solvents, SOZ was the predominant product.)

The discrepancy between the alkyl and aryl alkene ozonolysis products is likely due to a difference in the stabilities of the carbonyl oxide intermediates. Although the rate-determining step in ozonolysis is the initial attack of the ozone on the alkene, the nature of the intermediates that follow determine which product(s) form. It is likely that the lifetime of the carbonyl oxide (10^{-3} to 10^{-5} seconds)[25] plays a dominant role in product distributions observed in these cases. For alkyl carbonyl oxides, rearrangement to SOZ is

preferred due to the short lifetime of the carbonyl oxide intermediate. However, with aryl conjugated alkenes, benzylic resonance stabilization (Figure 6.3) of the carbonyl oxide may contribute to a more persistent intermediate, allowing enough time for the intermediate to react with water, thus making the product-determining step favor carbonyl products. This explanation also explains the large bias for isoeugenol and anethole (entries 1 and 2) toward carbonyl products over SOZs, because they have electron rich aryl rings that provide additional stabilization of the delocalized cation of the carbonyl oxide intermediate.

Most of the aryl alkenes in Table 6.2 have a ratio biasing strongly towards aldehyde or ketone as products. Notably, cyclic alkenes (Entries 8-10) are more prone to form SOZs with decreasing degrees of freedom (from entries 8 to 10) for the corresponding carbonyl oxide intermediate. The tethered carbonyl and carbonyl oxide pair favor SOZ formation if there is a strong enough entropic bias preferring intramolecular reaction (leading to SOZ) over intermolecular reduction (leading to carbonyl products directly). Notably, phenanthrene (Table 6.2, entry 8) still produces a majority of carbonyl products even though it is a tethered alkene.

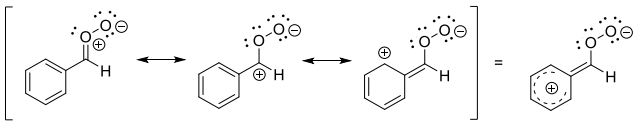

Figure 6.3. Resonance stabilization of aryl conjugated carbonyl oxide.

6.2.3. Conclusions to ozonolysis

In conclusion, we have developed a method for flow ozonolysis using a film-shear reactor. H_2O acts as a mild *in situ* reductant of the carbonyl oxide intermediate, yielding ketones and aldehydes directly. This flow reactor has a molar flow rate eight times faster than previously reported flow ozonolysis systems and is currently only limited by the rate of ozone production, with reaction times of 8 seconds. The excellent reaction rates and molar flow rates are attributed to superb mixing of the reactants within the film-shear reaction chamber. Alkyl olefins likely produce a carbonyl oxide intermediate that is too short lived to effectively react with water, preferring the formation of SOZs. The longer lifetimes of aryl conjugated carbonyl oxides are responsible for the excellent selectivity and reactivity of aryl conjugated olefins, which generally prefer carbonyl products over SOZs. Overall, the film-shear reactor system described here provides a direct route to carbonyl products from aryl alkenes without any secondary quench with scalable (multi-gram) flow chemistry.

We are currently using this method to investigate aryl alkyne ozonolysis, as well as stoichiometric ozone delivery to multi-olefin substrates.

6.2.4. Experimental for ozonolysis

6.2.4.1. General considerations.

All reaction solvents were purchased (ACS reagent grade or HPLC grade) and used without further purification. All commercially obtained reagents were used as received (≥95%) unless otherwise specified. Thin-layer chromatography (TLC) was visualized using low wavelength ultraviolet light (UV) for all aryl species, 2,4-

dinitrophenylhydrazine stain, or phosphomolybdic acid.[26] ^{1}H NMR spectra were recorded on a 300 or 500 MHz Varian spectrometer (^{1}H 300.09 MHz or 500.02 MHz, respectively) and are reported relative to deuterated solvent signals or an internal reference. Data for ^{1}H NMR spectra are provided in Appendix E and reported as follows: chemical shift (δ ppm), multiplicity, coupling constant (Hz) and relative integration.

6.2.4.2. Standard ozonolysis procedure

The syringe pumps and the film-shear reactor were primed by running 50 mL EtOAc at 10 mL/min and 50 mL deionized H_2O at 10ml/min with the rotor running at 2000 RPM. This procedure was repeated with pure oxygen also flowing at 0.8 L/min The film-shear reaction chamber was cooled to 0°C with a recirculator.

Both a 0.10 M solution of alkene in EtOAc at 0°C and deionized water at 0°C were pumped into a "T" valve (10 mL/min each) generating the plug-flow that entered the film-shear reactor. Ozone was sparged through the reaction chamber at 0.8 L/min.

A product flask was primed with 2 molar equivalents of a sodium sulfite solution to quench any hydrogen peroxide produced. The resulting product mixture was collected in a fume hood (CAUTION! residual ozone, formaldehyde, and hydrogen peroxide may be present as an aerosol; perform only in a well ventilated hood). The pH was adjusted to 3 using 3 M $HCl_{(aq)}$. The two resulting layers were separated. The aqueous layer was washed three times with 15 mL of EtOAc, then the organic layers were combined, dried over Na_2SO_4, filtered, and the solvent was removed under vacuum. The products were purified as noted in Appendix E.

6.3. Iron-phosphine complexes for nanoparticle coordination

6.3.1. Introduction

Iron tetraphosphine complexes have been reported to bind and activate dinitrogen as a ligand.[27,28] A limiting feature in these complexes is that electron transfer to nitrogen is very difficult. In previous work, Gilbertson et al. showed that sub-stoichiometric ammonia can be generated from N_2 with exogenous proton sources and the electrons from an iron (0) complex.[29] Two major inhibitions to performing this chemistry catalytically are: (1) competing proton reduction to form H_2, and the inability to redox cycle back to iron (0) without an exogenous reductant.

The goal of this study was to synthesize an iron tetraphosphine metal complex that could bind N_2, as well as coordinate to a nanoparticle in the secondary coordination sphere. The nanoparticle could act as an electron reservoir for electron transfer to the iron complex to facilitate catalytic dinitrogen reduction at the iron center.[30,31]

6.3.2. Design of the system

PbS nanoparticles (oleic acid capped) are known to have accessible redox properties, and thus, seemed an ideal target tethering partner.[32] These nanoparticles are also well studied and reliable to synthesize with low size distributions.[33]

For the iron complex, a bidentate aryl phosphine was chosen. A slightly derivative dppe (1,2-ethylenebis(diphenylphosphine)) ligand was chosen with soft coordination sites (-SMe) functionalized in the *para*-positions. The thioether coordination sites are very soft compared to the phosphines. This feature ensures the phosphines coordinate iron rather than the thioether.

6.3.3. Results and discussion

The bidentate phosphine ligand 1,2-bis(bis(4-methylthio)phenyl)phosphino)ethane or DpPSMePE was synthesized using 1,2-bis(dichlorophosphino)ethane and a lithiated aryl ring (Scheme 6.1). The resulting crystalline solid was then coordinated to iron (Scheme 6.2). Although the primary reaction product was the expected *trans*-$FeCl_2(DpPSMePE)_2$, a small amount the bridged di-iron species (μ-DpPSMePE-κ*P*:κ*P'*)$_2(FeCl_2)_2$ was also formed. Though a minor species, its presence demonstrates to the extreme steric strain about an octahedral center with two DpPSMePE ligands in the equatorial positons.

Scheme 6.1. Synthesis of DpPSMePE ligand.

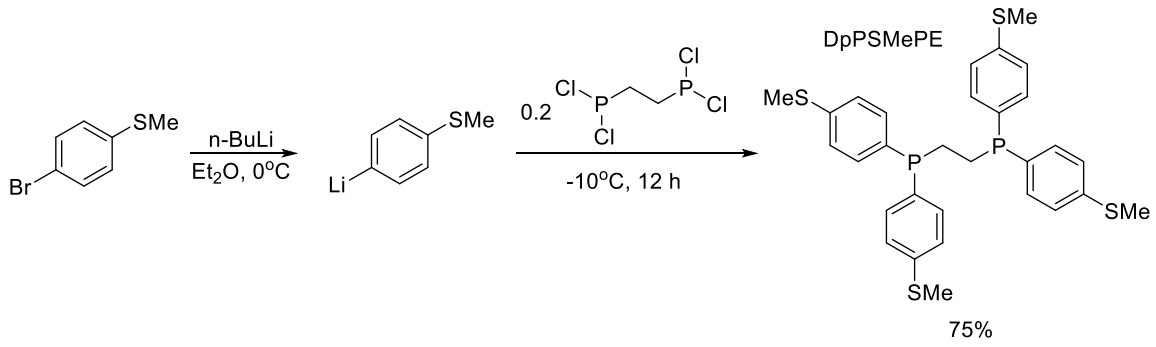

Attempts to make a hydride complex (a precursor for the nitrogen binding complex described by both Leigh[34] and Gilbertson[29]) using a modified Leigh anion-hydride exchange produced an orange solid (Scheme 6.3). Further investigation showed total dissociation of the ligands from the complex and metal reduction to bulk iron (0). The phosphine ligands coordinated free borane in solution. The resulting orange solid was the phosphine-borane adduct of the free ligand.

Scheme 6.2. Synthesis of *trans*-$FeCl_2$(DpPSMePE)$_2$ and (μ-DpPSMePE-κ*P*:κ*P′*)$_2$($FeCl_2$)$_2$ complexes.

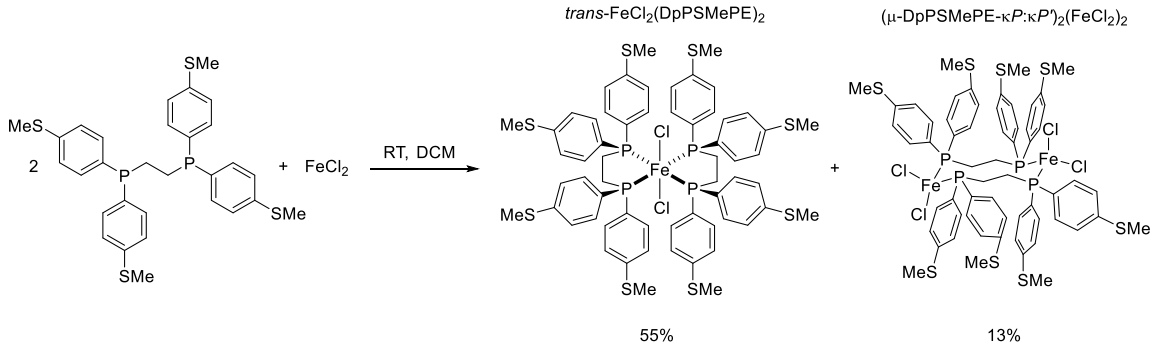

Scheme 6.3. Attempted synthesis of a hydride complex from *trans*-$FeCl_2$(DpPSMePE)$_2$.

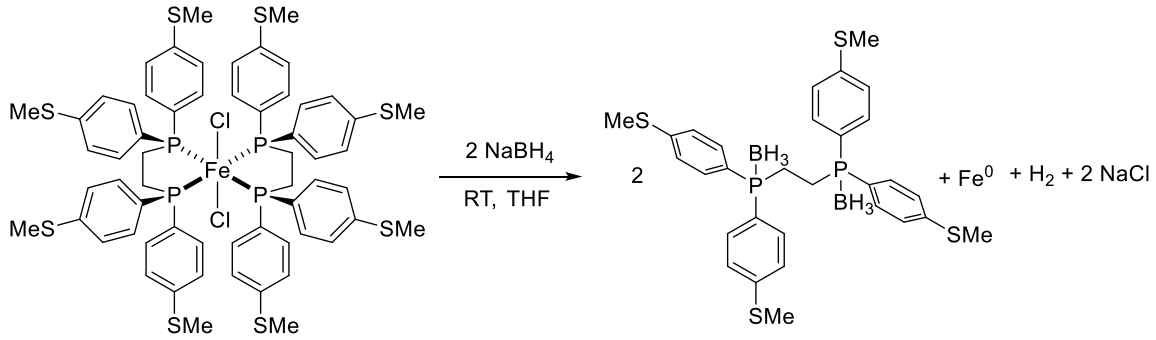

Finally, *trans*-$FeCl_2$(DpPSMePE)$_2$ was screened for ligand exchange with the PbS nanoparticle ligand shell (Scheme 6.4). Several attempts were made including using a multi-phase exchange with sodium 3-mercaptopropane-1-sulfonate (MPS) as ligand shell transfer reagent. Unfortunately, no TEM (Figure 6.4) or spectroscopic evidence (λ_{max} at 1390 nm for PbS starting materials remained un-shifted) supported the coordination of the complex to the nanoparticles.

Scheme 6.4. Attempted coordination of *trans*-$FeCl_2(DpPSMePE)_2$ to PbS nanoparticle.

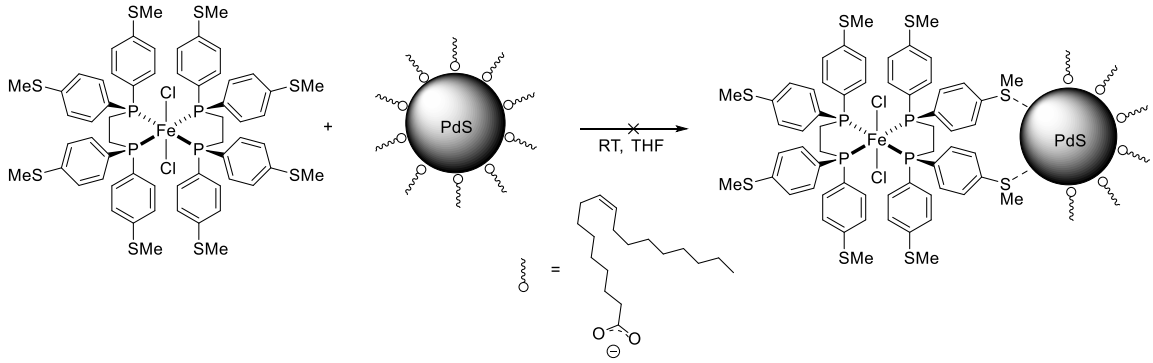

6.3.4. Summary and conclusions of iron complexes for nanoparticle coordination

The synthesis, isolation, and characterization of the new *trans*-$FeCl_2(DpPSMePE)_2$, an octahedral high-spin (S = 2) complex, was achieved. Attempts to react *trans*-$FeCl_2(DpPSMePE)_2$ with $NaBH_4$ were met with decomposition. It is likely that the inherent strain of the ligands on the complex and lability of the ligands are responsible for the non-robust coordination complex. Attempts at coordination of *trans*-$FeCl_2(DpPSMePE)_2$ to PdS nanoparticles was unsuccessful.

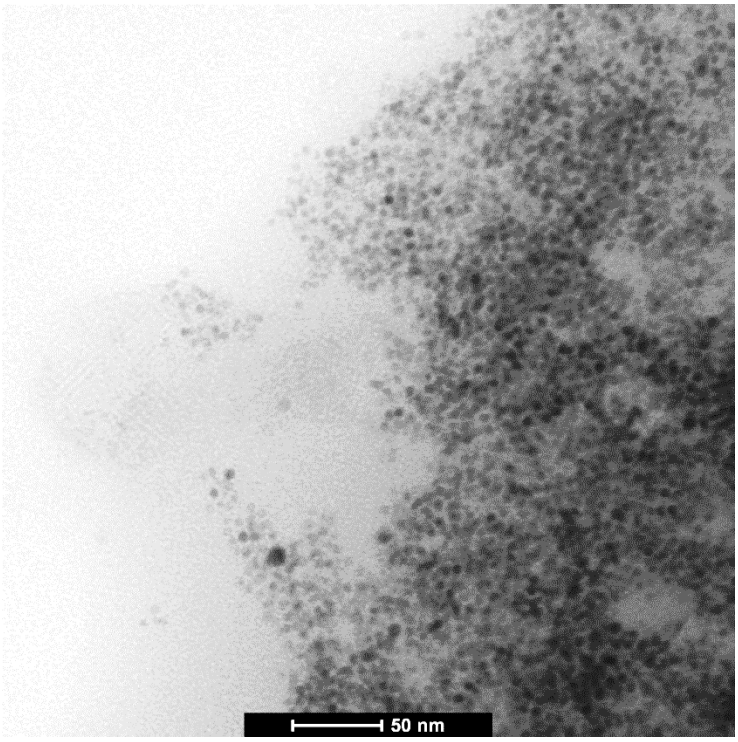

Figure 6.4. TEM of PbS (oleic acid capped) after attempted exchange of ligand shell with *trans*-$FeCl_2(DpPSMePE)_2$. Note that distance between particles is consistent with oleic acid ligand shell, not the *trans*-$FeCl_2(DpPSMePE)_2$ complex.

6.3.5. Experimental details

6.3.5.1. General considerations

Unless stated otherwise, reactions were conducted in oven-dried glassware under an atmosphere of nitrogen using either standard Schlenk techniques or a dribox maintained at < 1.0 ppm O_2. Diethyl ether and tetrahydrofuran (THF) were dried using a DriSolv system using CuO and molecular sieves under argon. All other reaction solvents were purified and dried according to the literature.[35] All commercially obtained reagents were used as received unless otherwise specified. Synthesized organomagnesium reagents were titrated before use using either diphenyl acetic acid[36] to determine

concentration and were stored under Ar at room temperature. Thin-layer chromatography (TLC) was visualized using low wavelength ultraviolet light (UV) for all aryl species or phosphomolybdic acid. ^{1}H NMR spectra were recorded on a 300 or 500 MHz Varian spectrometer (^{1}H 300.09 MHz or 500.02 MHz, respectively) and are reported relative to deuterated solvent signals or an internal reference. Data for ^{1}H NMR spectra are reported as follows: chemical shift (δ ppm), multiplicity, coupling constant (Hz) and relative integration. ^{31}P{^{1}H} NMR spectra were recorded on a 300 or 500 MHz Varian spectrometer (^{31}P 121.48 MHz or 202.13 MHz, respectively) and are reported relative to the external standard of 0.1% H_3PO_4 in D_2O at 0 ppm. A Titan 80-300 cryo transmission electron microscope was used to determine nanoparticle morphology and dispersity.

6.3.5.1. X-ray crystallography

Diffraction intensities were collected at 173 K on a Bruker Apex2 CCD diffractometer using MoKα (λ= 0.71073 Å). Absorption corrections were applied by SADABS.[37] Structures were solved by direct methods and Fourier techniques, then refined on F^2 using full matrix least-squares procedures. All non-H atoms were refined with anisotropic thermal parameters. H atoms in all structures were found from the residual density maps and refined with isotropic thermal parameters without any restrictions or which were refined in calculated positions in a rigid group model. All calculations were performed by the Bruker SHELXL-2013 package.[38] See Tables 6.4-6.7 for additional crystallographic details.

Table 6.4. Crystallographic Data for 1,2-bis(bis(4-(methylthio)phenyl)phosphino)ethane (DpPSMePE).

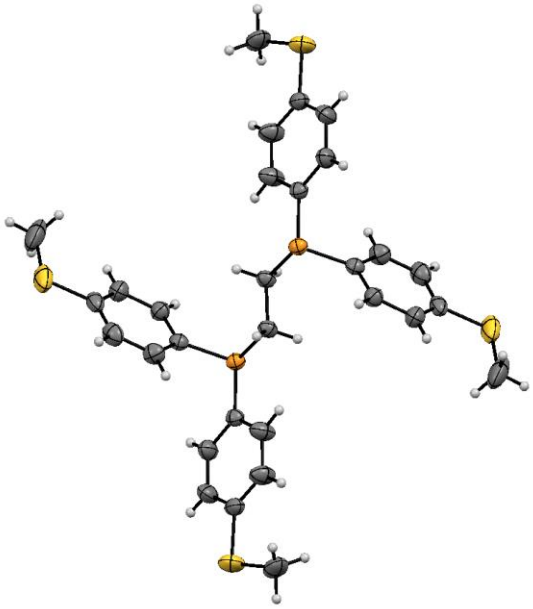

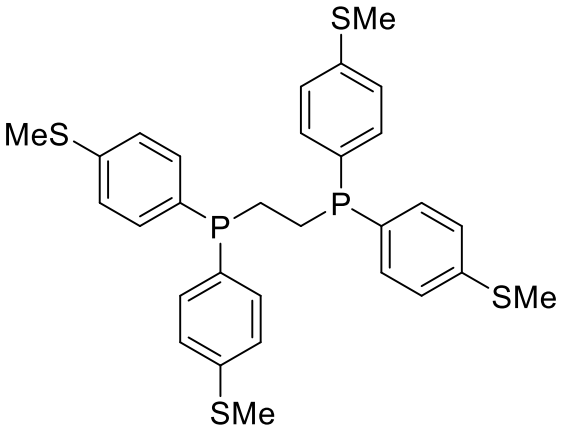

Formula = C30 H32 P2 S4	
Formula weight = 582.74 g/mol a = 11.6057(19) Å	Space group = P2(1)/c
b = 5.2265(9) Å	T = 173(2) K
c = 24.290(4) Å	λ = 0.71073 Å
α = 90°, β = 94.509(3)°, γ = 90°	D_c = 1.318 Mg/m^3
V = 1468.8(4) Å^3	μ(Mo) = 0.451 mm^{-1}
Z = 2, Z' = 2	R(F_o) = 3.33%
Crystal system = Monoclinic	R_w(F_o) = 2.77%

Table 6.5. Crystallographic Data for 1,2-bis(bis(4-(methylthio)phenyl)phosphineborane)ethane (DpPSMePE$(BH_3)_2$).

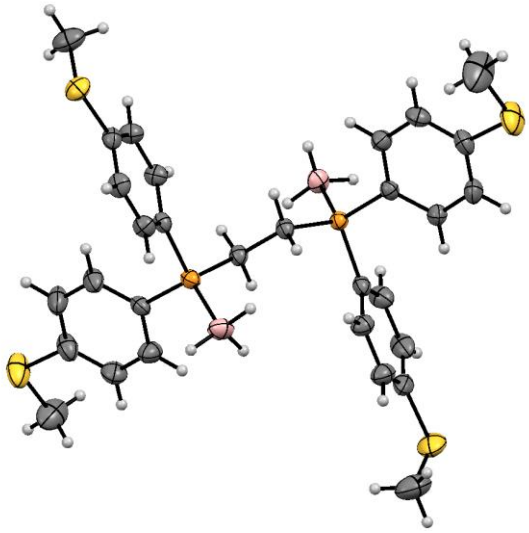

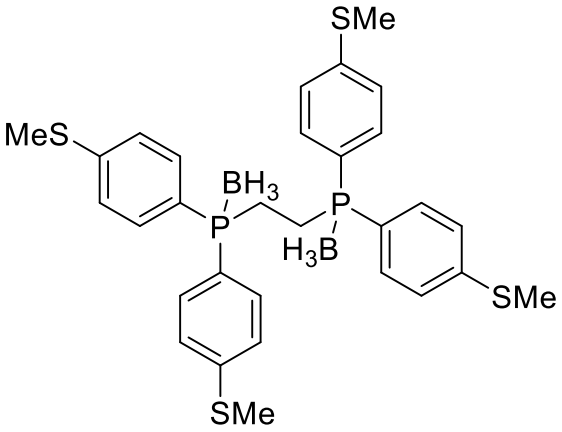

Formula = C30 H38 B2 P2 S4	
Formula weight = 610.40 g/mol a = 11.9406(14) Å	Space group = P2(1)/c
b = 19.391(2) Å	T = 173(2) K
c = 14.1165(17) Å	λ = 0.71073 Å
α = 90°, β = 101.172(2)°, γ = 90°	D_c = 1.264 Mg/m^3
V = 3206.6(7) Å^3	μ(Mo) = 0.415 mm^{-1}
Z = 4, Z' = 0	$R(F_o)$ = 2.95%
Crystal system = Monoclinic	$R_w(F_o)$ = 2.13%

Table 6.6. Crystallographic Data for (μ-DpPSMePE-κ*P*:κ*P′*)$_2$(FeCl$_2$)$_2$.

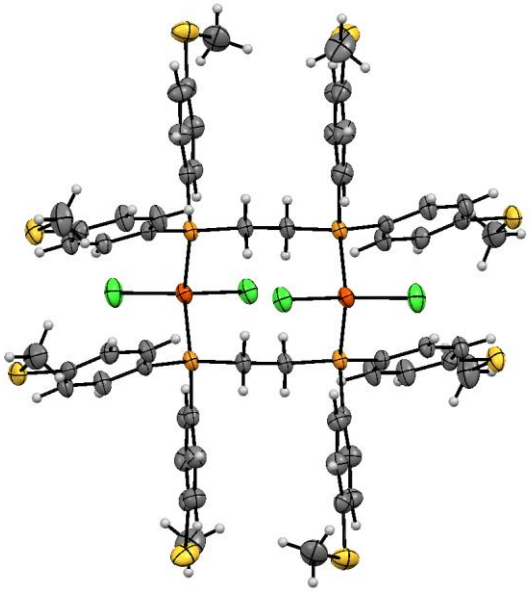

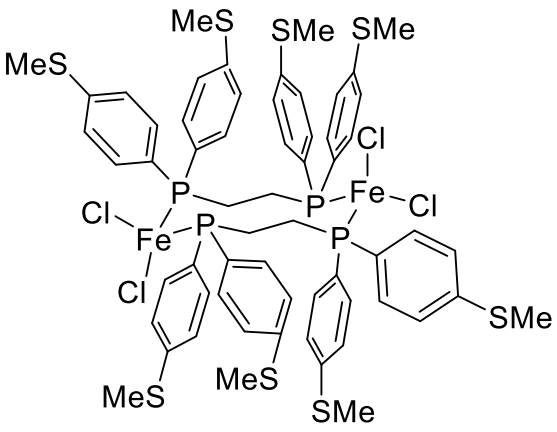

Formula = C62 H68 Cl8 Fe2 P4 S8	
Formula weight = 1588.82 g/mol a = 20.0248(17)Å	Space group = C2/c
b = 14.5159(12)Å	T = 173(2) K
c = 25.819(2)Å	λ = 0.71073 Å
α = 90°, β = 104.0440(10)°, γ = 90°	D_c = 1.450 Mg/m^3
V = 7280.6(10) Å^3	μ(Mo) = 1.047 mm^{-1}
Z = 4, Z' = 2	R(F_o) = 3.09%
Crystal system = Monoclinic	R_w(F_o) = 2.41%

Table 6.7. Crystallographic Data for *trans*-$FeCl_2(DpPSMePE)_2$.

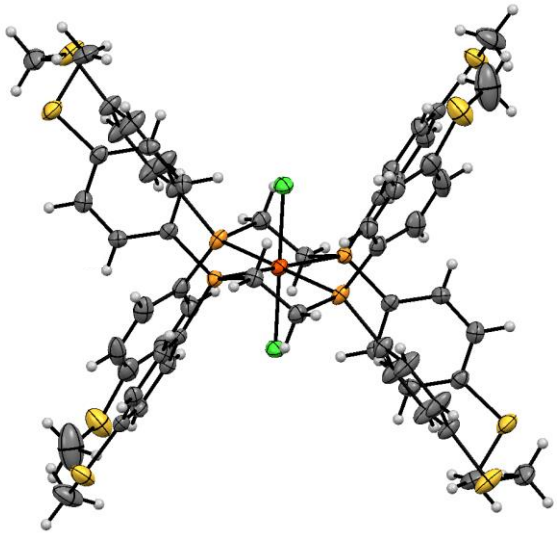

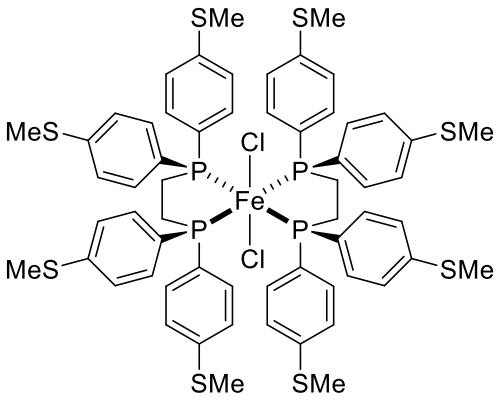

Formula = C61 H66 Cl4 Fe P4 S8	
Formula weight = 1377.15 g/mol a = 10.5589(13) Å	Space group = P-1
b = 11.7579(14) Å	T = 173(2) K
c = 28.178(3) Å	λ = 0.71073 Å
α = 92.397(2)°, β = 97.465(2)°, γ = 110.261(2)°	D_c = 1.412 Mg/m^3
V = 3239.8(7) Å^3	μ(Mo) = 0.793 mm^{-1}
Z = 2, Z' = 0	$R(F_o)$ = 4.28%
Crystal system = Triclinic	$R_w(F_o)$ = 6.20%

6.3.5.2. Synthesis of DpPSMePE

To a solution of p-bromomercaptoanisole (3.8649g, 19 mmol) in 20 mL Et_2O, was added *n*-BuLi (1.6 M, 13.1 mL, 21 mmol) dropwise at 0°C. The mixture was allowed to stir for one hour, then cooled to -10°C. A solution of 1,2-bis(dichlorophosphino)ethane (0.8823 g, 3.8 mmol) in 20 mL Et_2O was added dropwise to the mixture and allowed to warm up to room temperature overnight. The reaction mixture was quenched with 0.1 M $HCl_{(aq)}$ solution and extracted with DCM three times.

The organic layers were combined and dried over Na_2SO_4, then filtered and vacuum dried to produce a white crystalline solid (1.6544g, 74.6%). ^{1}H NMR (300 MHz, Chloroform-*d*) δ 7.21-7.16 (m, 16H), 2.45 (s, 12H), 2.02 (m, 4H). ^{31}P{^{1}H} NMR (121 MHz, Chloroform-*d*) δ -14.6.

6.3.5.3. Synthesis of trans-$FeCl_2$(DpPSMePE)$_2$ and (μ-DpPSMePE-κP:κP′)$_2$($FeCl_2$)$_2$

To a solution of DpPSMePE (450.0 mg, 0.8 mmol) in THF was added anhydrous $FeCl_2$ (51.4 mg, 0.4 mmol). The mixture was allowed to stir overnight. The mixture was filtered through celite, then precipitated by vapor diffusion of Et_2O. This process yielded two products, green crystals of (μ-DpPSMePE-κ*P*:κ*P*′)$_2$($FeCl_2$)$_2$ (65.0 mg, 13.2%), and pink needle crystals of *trans*-$FeCl_2$(DpPSMePE)$_2$ (276.1 mg, 55.0%). Solution state Evan's method was used to measure the paramagnetic moment of the *trans*-$FeCl_2$(DpPSMePE)$_2$ complex to be μ_{eff} = 4.55 BM (*S* = 2 or 4 unpaired e^-).

6.4. Nickel DMeOPrPE complexes for PNNL collaboration

6.4.1. Introduction for nickel complexes

In a collaboration with Pacific Northwest National Laboratory (PNNL), three new nickel(II) 1,2-bis(bis(3-methoxypropyl)phosphino)ethane (DMeOPrPE) complexes were synthesized. They are currently being studied for catalysis with H_2 and CO_2 by PNNL.

6.4.2. Experimental for nickel complexes

6.4.2.1. Synthesis of Ni(II)(DMeOPrPE)$_2$Br$_2$

To an blue/brown suspension of $NiBr_2$•3(H_2O) (541.6 mg, 2.0 mmol, in 3.0 mL THF, c.a. 600 mM) was added a solution of DMeOPrPE (1.6025 g, 4.2 mmol, in 13.0 mL THF, c.a. 300 mM) dropwise. The mixture slowly clarified and turned dark brown/red. The solution was allowed to stir for 16 hours at room temperature. The red/brown solution was purified by dropwise addition of the crude solution into cold Et_2O, causing a red oil precipitation. The Et_2O layer was decanted off and the red oil was collected as the pure complex (1.7469 g, 85.6%). ^{1}H NMR (300 MHz, Chloroform-*d*) δ 3.44 (t, *J* = 5.7 Hz, 16H), 3.32 (s, 24H), 2.30 – 2.02 (m, 22H), 1.94 – 1.72 (m, 18H). ^{31}P{^{1}H} NMR (121 MHz, Chloroform-*d*) δ 52.02. HRMS (ES+-TOF) m/z: [M^+] calcd for $[C_{36}H_{80}BrNiO_8P_4]^+$ 901.3341; found 901.3334.

6.4.2.2. Synthesis of [Ni(II)(DMeOPrPE)$_2$] 2[BF$_4$]

To a solution of Ni(II)(DMeOPrPE)$_2$Br$_2$ (0.8830 g, 0.9 mmol) in 50 mL THF was added a solution of $AgBF_4$ (375.1 mg, 1.9 mmol, in 10 mL THF, c.a. 200 mM) dropwise at room temperature. The red solution turned turbid yellow upon addition. The mixture was allowed to stir at room temperature for 5 hours. The mixture was then filtered. The resulting filtrate was reduced under vacuum and taken up into a minimal amount of THF (5.0 mL) and added dropwise into cold Et_2O, causing an orange oil precipitation. The Et_2O layer was decanted off and the orange oil was collected as the pure complex (534.5 mg, 59.6%). ^{1}H NMR (500 MHz, Chloroform-*d*) δ 3.57 – 3.40 (m, 16H), 3.34 (s, 24H), 2.44 – 1.96 (m, 22H), 1.96 – 1.66 (m, 18H). ^{11}B NMR (160 MHz, Chloroform-*d*) δ -0.77

. $^{31}P\{^{1}H\}$ NMR (202 MHz, Chloroform-*d*) δ 55.96. HRMS (ES+-TOF) m/z: [M^+] calcd for $[C_{36}H_{80}BF_4NiO_8P_4]^+$ 909.4193; found 909.4200.

6.4.2.3. Synthesis of [Ni(II)(DMeOPrPE)$_2$] 2[OTf]

To a solution of Ni(II)(DMeOPrPE)$_2$Br$_2$ (0.8830 g, 0.9 mmol) in 50 mL THF was added a solution of NaOTf (341.0 mg, 2.0 mmol, in 10 mL THF, c.a. 200 mM) dropwise at room temperature. The red solution turned turbid upon addition. The mixture was heated for 5 hours at reflux, then cooled and filtered. The resulting filtrate was reduced under vacuum and taken up into $CHCl_3$ (5.0 mL) at which point more precipitates formed. This mixture was again filtered, then the filtrate was added dropwise into cold Et_2O, causing a red oil precipitation. The Et_2O layer was decanted off and the red oil was collected as the pure complex (0.8100 g, 80.2%). ^{1}H NMR (500 MHz, Chloroform-*d*) δ 3.44 (t, *J* = 5.8 Hz, 20H), 3.33 (s, 24H), 2.31 – 1.94 (m, 24H), 1.94 – 1.61 (m, 12H). ^{19}F NMR (471 MHz, Chloroform-*d*) δ -78.20. $^{31}P\{^{1}H\}$ NMR (202 MHz, Chloroform-*d*) δ 51.96 . HRMS (ES+-TOF) m/z: [M^+] calcd for $[C_{38}H_{80}F_3NiO_8P_4S]^+$ 1011.2779; found 1011.2783.

6.5. Summary

6.5.1. Ozonolysis

A new method for ozonolysis of alkenes using a continuous flow film-shear reactor was developed. The reactor uses a shearing microfluidic mixing chamber to provide biphasic mixing of an organic phase and aqueous phase with ozone gas. The H_2O acts as an *in situ* reducing agent for the carbonyl oxide intermediate, providing ketones

and aldehydes directly from the reaction mixture. Flow rates of up to 1.0 mmol/min (alkene) with an ozone reaction efficiency of >70% were achieved. Aryl conjugated olefins reacted to form carbonyl species in good yields on a multi-gram scale; however, alkyl olefins reacted with ozone to predominantly form secondary ozonides. The discrepancy in product distributions between alkyl and aryl olefins likely originates from the electronic stability of the carbonyl oxide intermediate, which is longer lived for aryl derivatives due to conjugation.

6.5.2. Iron-Phosphine complexes

The synthesis of a bidentate phosphine, DpPSMePE, for coordination to both iron (through the phosphines) and subsequent outer-sphere coordination to PdS nanoparticles (through distal -SMe moieties) was successful. Coordination to iron yielded two distinct coordination complexes: *trans*-$FeCl_2(DpPSMePE)_2$ and (μ-DpPSMePE-κ*P*:κ*P*′)$_2(FeCl_2)_2$. The *trans*-$FeCl_2(DpPSMePE)_2$ complex is a high-spin, (μ_{eff} = 4.55 BM) with 4 unpaired e^-. Unfortunately, both the attempted formation of a hydride complex and coordination to PbS nanoparticles were met with failure.

6.5.3. Nickel DMeOPrPE Complexes

The synthesis and characterization of a three new nickel complexes ($Ni(II)(DMeOPrPE)_2Br_2$, $[Ni(II)(DMeOPrPE)_2]$ 2[BF_4], and $[Ni(II)(DMeOPrPE)_2]$ 2[OTf]) was accomplished. These complexes were sent to a collaborator at PNNL for catalytic study.

6.6. Concluding summary

Two new general synthetic routes to phosphines were developed. The first method described directly converts phosphonates to phosphine oxides using organometallic nucleophiles. This reaction proceeds through a five-coordinate phosphorus intermediate. The second synthetic method uses a deprotonated secondary phosphine oxide for nucleophilic addition to an alkyl halide to form a tertiary phosphine oxide. This reaction proceeds through a standard S_N2 mechanism, however in extreme cases a competitive electron transfer reaction was observed.

These syntheses were used to make a new dimethyl phosphine (MeJPhos). This phosphine was used as a ligand for metal complexes and compared against a series of structurally related (JohnPhos) phosphines. MeJPhos was found to be the strongest electron donor in the series MeJPhos, EtJPhos, ^{i}PrJPhos, CyJPhos, and ^{t}BuJPhos. These ligands were then used to study structural effects of ligands on Buchwald-Hartwig cross-coupling catalysis. It was found that only tBuJPhos performed catalytically. This observation is likely due to the smaller steric profile of the other JohnPhos ligands. Specifically, it is the inability to perform the reductive elimination step of the catalytic cycle that prevents turnover.

Ozonolysis was used to oxidize alkenes to aldehydes directly. Typically with ozonolysis, a secondary ozonide is formed as the product that must be chemically reacted in a subsequent step. By trapping out the immediate chemical precursor to the secondary ozonide with water, the formation of secondary ozonides was avoided. This method produced aldehydes directly from aryl alkenes in good to excellent yields.

APPENDIX A

SUPPORTING INFORMATION FOR CHAPTER II

A.1. General Considerations

Unless stated otherwise, reactions were conducted in oven-dried glassware under an atmosphere of nitrogen. Diethylether and tetrahydrofuran were dried using a DriSolv system using CuO and molecular sives under argon, all other reaction solvents were purified and dried according to literature.[1] All commercially obtained reagents were used as received unless otherwise specified. Organomagnesium reagents synthesized were titrated before use using either diphenylacetic acid[2] or no-d NMR[3] to determine molarity and stored under an atmosphere of argon gas at room temperature. Thin-layer chromatography (TLC) was visualized using low wavelength ultraviolet light (UV) for all aryl species or phosphomolybdic acid. Gas chromatography (GC) was performed on an Agilent Technologies 6850 Series II. ^{1}H NMR spectra were recorded on a Varian spectrometer (at 300.09 MHz or 500.02 MHz) and are reported relative to the residual solvent signals or the internal standard. Data for ^{1}H NMR spectra are reported as follows: chemical shift (δ ppm), multiplicity, coupling constant (Hz) and integration. ^{31}P{^{1}H} NMR spectra were recorded on a Varian spectrometer (at 121.48 MHz or 202.13 MHz) and are reported relative to an external standard of 0.1% H_3PO_4 in D_2O at 0 ppm. Infrared spectra were taken using Nicolet Magna-550 Fourier Transform Infrared Spectrophotometer in ATR mode.

The Biomolecular Mass Spectrometry Core of the Environmental Health Sciences Core Center at Oregon State University provided the high resolution mass spectra. The project described was supported, in part, by award number P30ES000210 from the NIEHS, NIH.

Acronyms used herein: dichloromethane (DCM), saturated NaCl/H_2O (brine), tetrahydrofuran (THF), room temperature (RT ~ 17 ^oC), trifluoromethanesulfonate (OTf), nuclear magnetic resonance (NMR), deionized water (DI H_2O), ethyl acetate (EtOAc), acetate (OAc), trifluoroacetate (OAc_F), thin-layer chromatography (TLC), low wavelength ultraviolet light (UV), gas chromatography (GC).

A.2. Optimizing Parent Reaction Conditions

A.2.1. GC Calibration.

Samples were injected at 300 ^oC (160 psi, 91 mL/min). The oven initial temperature was 100 ^oC which was ramped 10 ^oC/min until 150 ^oC; upon reaching the final temperature, it was held for 4 minutes. The pressure inside the column was 16 psi the whole time until the post-run burn. This successfully separated decane (0.72 minutes), dimethylphenylphosphonate (1.45 minutes), and dimethylphenylphosphine oxide (2.02 minutes).

Standard concentrations of phenyldimethyl phosphonate and phenyldimethylphosphine oxide were prepared using volumetric flasks and in dimethylformamide. Each sample had 50 mM of decane as an internal standard. Values for concentration ranged from 1 mM analyte to 150 mM analyte to determine the limit of

detection. All samples were prepared and run at least in duplicate. Both the dimethylphenylphosphonate and the dimethylphenylphosphine oxide calibrations produced response curves with R^2>0.98.

A.2.2. Solvent Screen and Time Trials

A round bottomed flask containing solvent (93 mL) was charged with dimethyl phenylphosphonate (1.8681 g, 10 mmol) and decane (0.7146 g, 5 mmol). A 1.0 mL aliquot of the reaction mixture was sampled for a time=0 point. The flask was then charged with methylmagnesium chloride solution in THF (7.30 mL, 3.0 M, 22 mmol). Aliquots for GC analysis were taken and quenched with isopropanol (until gas formation ceased).

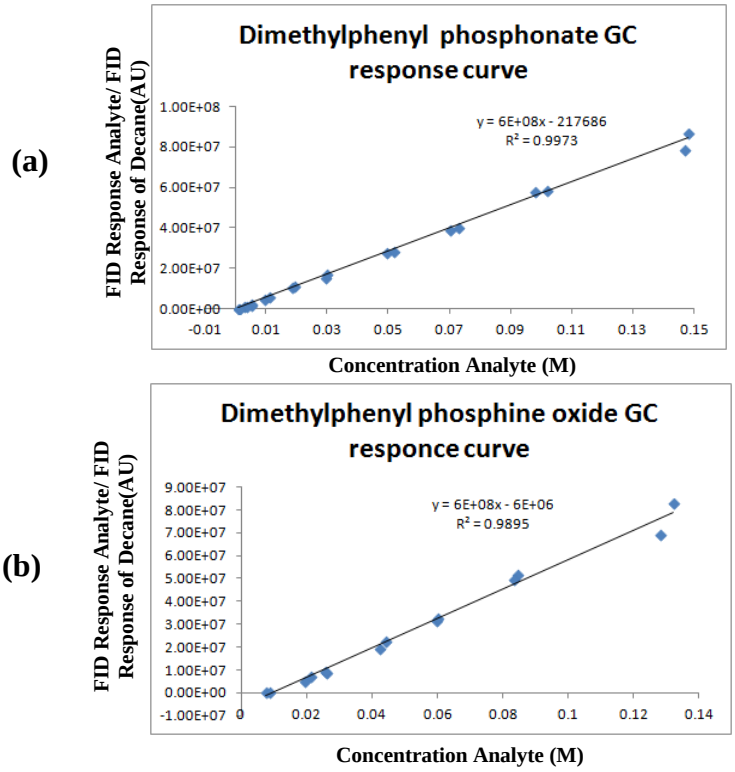

Figure A1. GC Response Curves for (a) dimethylphenyl phosphonate and (b) dimethylphosphine oxide.

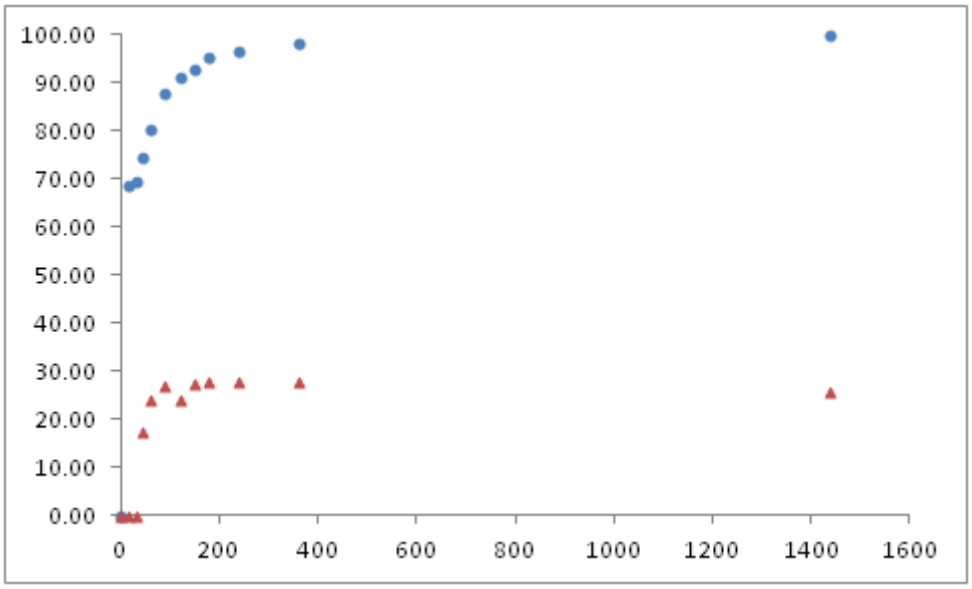

Figure A2. Conversion of dimethyl phenylphosphonate to dimethylphenylphosphine oxide in THF at RT (%Conversion in blue, %yield in red, x=minutes, y=%)

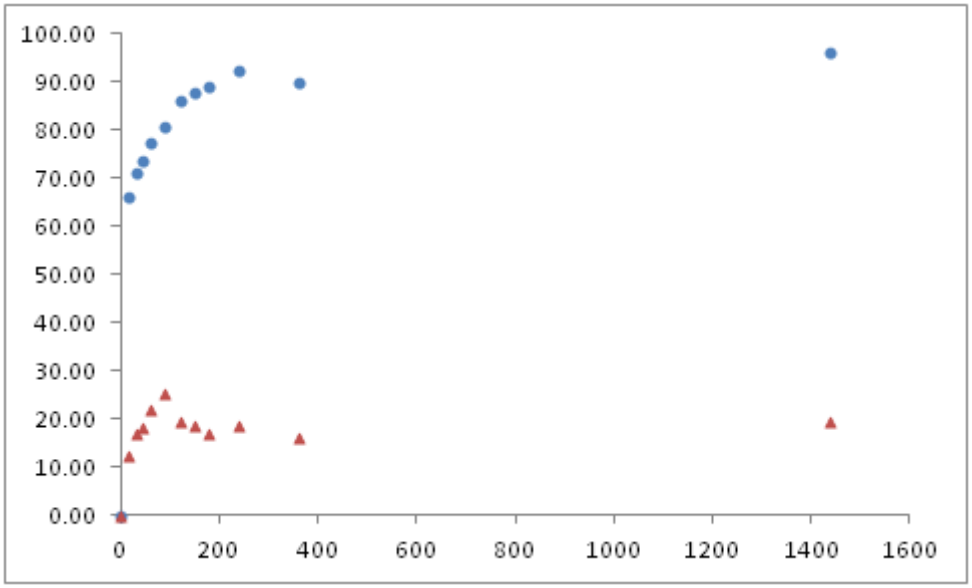

Figure A3. Conversion of dimethyl phenylphosphonate to dimethylphenylphosphine oxide in glyme at RT (%Conversion in blue, %yield in red, x=minutes, y=%)

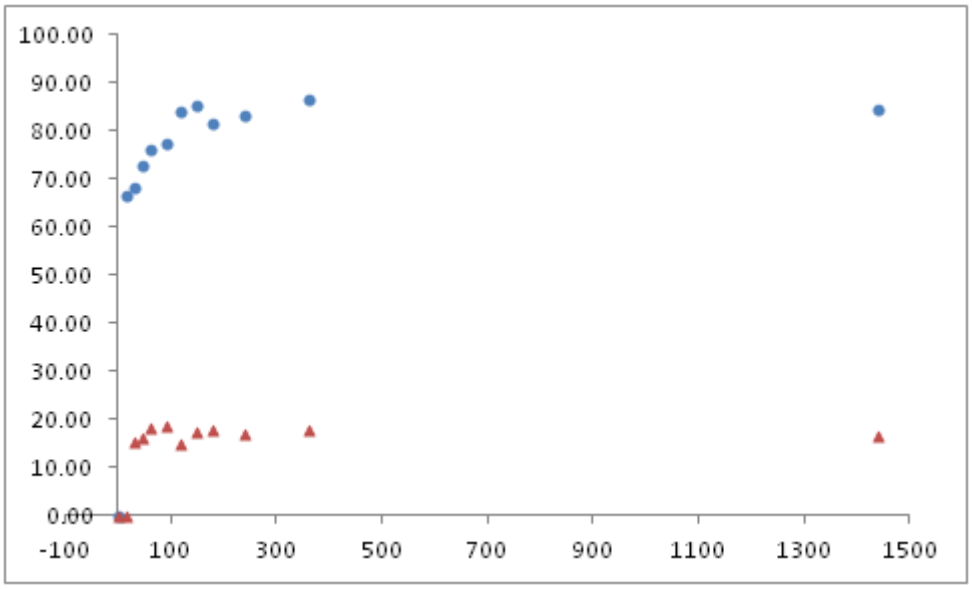

Figure A4. Conversion of phenyldimethylphosphonate to dimethylphenylphosphine oxide in dioxane at RT (%Conversion in blue, %yield in red, x=minutes, y=%)

Table A1. Solvent Screen for Grignards

Solvent	% Conv	% Yield
THF	98	28
Et_2O*	-	-
1,4-dioxane	87	18
glyme	90	16
Reactions run at RT, yields after 6 hours. *Phosphonate and phosphine oxide insoluble in Et_2O.		

Table A2. Grignard screening for temperature of addition.

Temperature (ºC)	%yield
0	<10
20	12
50	23
67	24
Based on GC Analysis after 6 hours	

A.2.3. Organometallic Nucleophile Screen

A.2.3.1. Methyllithium at -78 ºC

Methyllithium (420 µL, 1.02 mmol) was added drop wise to dimethyl phenylphosphonate in 3 mL of THF at -78˚C. The solution was stirred for 2 hours then stirred for 10 hours at room temperature. The solution was quenched with 250 µL saturated sodium bicarbonate (aq). The organic layer was dried with sodium sulfate, the solvent was removed via vacuum, and the crude reaction mixture was analyzed by NMR. $^{31}P\{^{1}H\}$ NMR (121 MHz, $CDCl_3$) δ 43.77, 39.14, 34.31, 34.10, 32.26, 30.82, 30.06.

A.2.3.2. Diethylzinc at Reflux

A 15 mL 3-necked round bottom flask was affixed with a reflux condenser and was charged with THF (6 mL) and diethylzinc (142 mg, 1.15 mmol) via syringe. Dimethyl phenylphosphonate (80 µL, 0.5 mmol) was then added via syringe. The mixture was refluxed while stirring for 24 hours. 12 hours into the reaction the mixture was quenched with 3 M hydrochloric acid (aq) and turned yellow upon quenching. The organic layer was dried with sodium sulfate for 45 minutes, then was filtered through a

short pipet plug of diatomaceous earth and rinsed with DCM (4 mL, 66 mmol). The solvent was removed under reduced pressure. The oil was taken up into deuterated chloroform and determined to be only starting material. $^{31}P\{^{1}H\}$ NMR (121 MHz, chloroform-D) δ 21.75.

A.3. Lewis-Acid Screening

A.3.1. GC analysis.

To a 20 mL scintillation vial charged with 5 mL of THF, decane (0.25 mmol, 35.6 mg) 0.20 equivalents Lewis acid, and dimethyl phenylphosphonate (93.1 mg, 0.5 mmol), was added MeMgBr (3.0 M, 350 µL, 1.05 mmol) drop wise at room temperature. The mixture was allowed to stir at 25 ^{o}C for 12 hours, then quenched with K_2CO_3/H_2O. DCM was used to extract out product, which was analyzed by GC.

A.3.2. NMR analysis.

To a 20 mL scintillation vial charged with 5 mL of THF, hexamethylbenzene (0.17 mmol, 26.8 mg) 0.20 equivalents Lewis acid, and dimethyl phenylphosphonate (93.1 mg, 0.5 mmol), was added MeMgBr (3.0 M, 350 µL, 1.05 mmol) drop wise at room temperature. The mixture was allowed to stir at 50 ^{o}C for 8 hours, then quenched with K_2CO_3/H_2O. DCM was used to extract out product. The organic layer was reduced via vacuum. The resulting mixture was taken back up into deuterated chloroform with hexamethylbenzene as an internal standard (at 11 mM) and analyzed via NMR spectroscopy.

A.3.3. Isolated yield.

To a 20 mL scintillation vial charged with 5 mL of THF, 0.20 equivalents Lewis acid, and dimethyl phenylphosphonate (93.1 mg, 0.5 mmol), was added MeMgBr (3.0 M, 350 µL, 1.05 mmol) drop wise at room temperature. The mixture was allowed to stir at 50 °C for 8 hours, then quenched with K_2CO_3/H_2O. DCM was used to extract out product. The organic layer had solvent removed via vacuum, yielding 41.6 mg (54%) of pure white crystals of dimethylphenylphosphine oxide.

Table A3. Lewis acid runs. All additives run at 20% metal loading. [a]Measured by GC after 12 hours at RT. [b]Measured by NMR after 8 hours at 50 °C. [c]Isolated yield after 8 hours at 50 °C.

Lewis acid	**% yield**
$AgOAc_F$	29[b]
$AlCl_3$	<10[a]
CsI	21[b]
$Cu(OTf)_2$	<10[a]
$Dy(OTf)_3$	12[a]
$Eu(OTf)_3$	12[a]
$FeCl_2$	<10[a]
$FeCl_3$	16[a]
$Gd(OTf)_3$	12[a]
$Ho(OTf)_3$	12[a]
La(OTf)3	20[b]
Lu(OTf)3	54[c]
$MgCl_2$	13[a]
MgO	11[a]
$MnBr_2$	<10[a]
$Nd(OTf)_3$	14[a]
$Pr(OTf)_3$	11[a]
RbCl	20[a]
$Sm(OTf)_3$	<10[a]
$Sm(OTf)_3$	14[a]
$Tb(OTf)_3$	12[a]
$Ti(OEt)_4$	18[a]
$Tm(OTf)_3$	13[a]
$ZrCl_4$	<10[a]

A.4. NMR Experiments

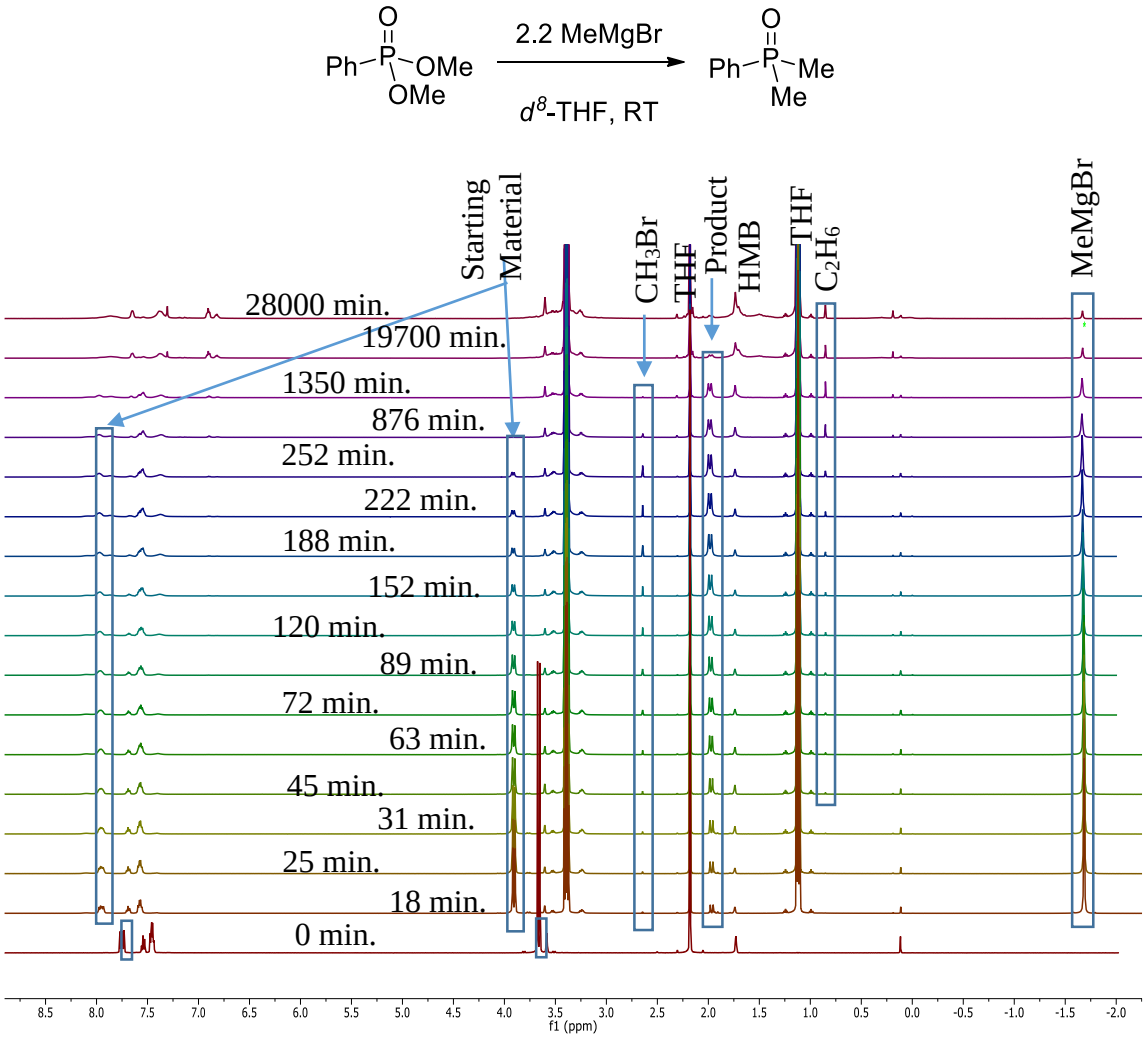

Figure A5. ^{1}H NMR of dimethyl phenylphosphonate and MeMgBr over time

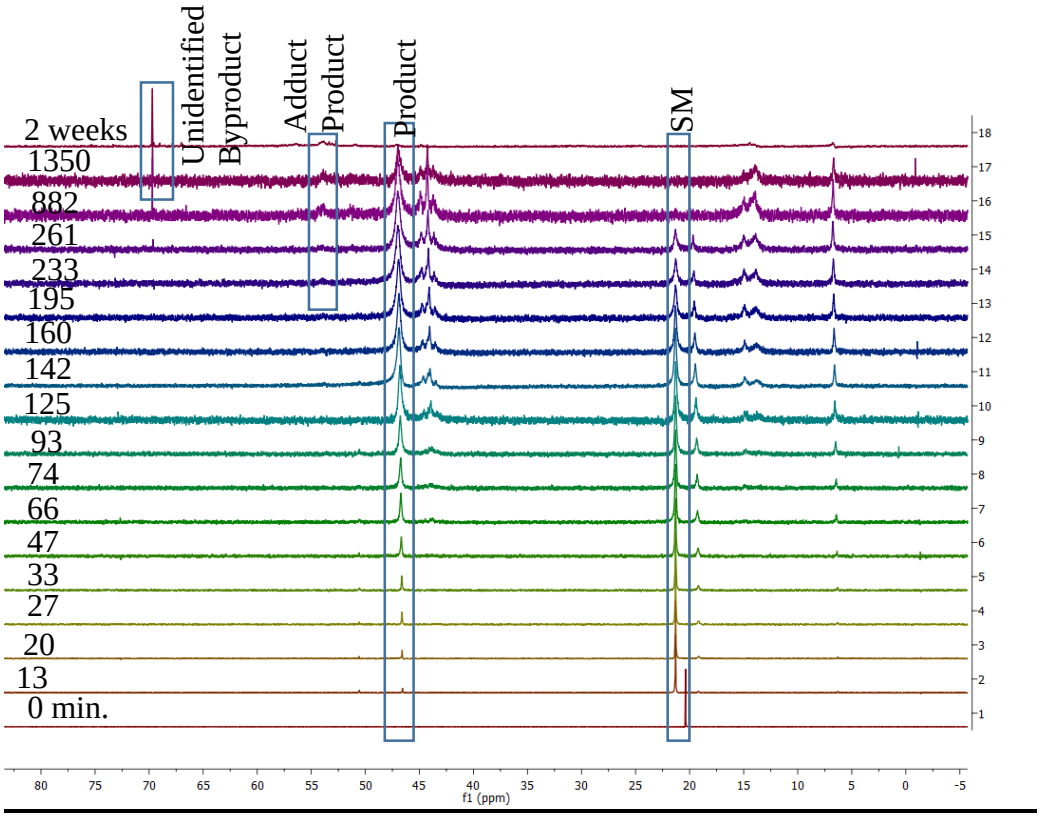

Figure A6. $^{31}P\{^{1}H\}$ NMR of dimethyl phenylphosphonate and MeMgBr over time

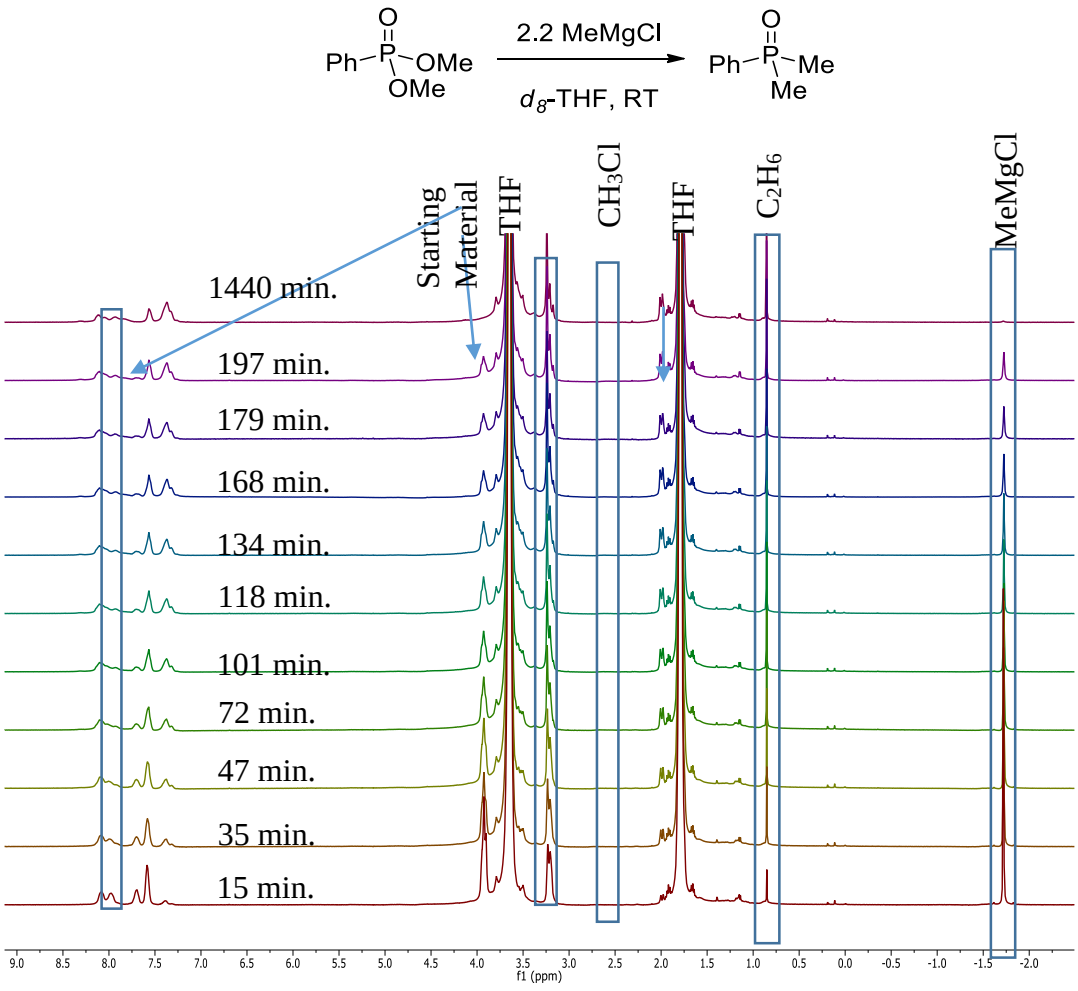

Figure A7. ^{1}H NMR of Dimethyl phenylphosphonate and MeMgCl over time

A.5. Synthesis of Precursors

A.5.1. Phosphine Oxides as Standards

A.5.1.1. General Procedure

Unless otherwise stated, the phosphine oxides below were synthesized according to the following procedure. To a 20 mL scintillation vial containing 10 mL of THF at either 0 ^{o}C or -15 ^{o}C was added 0.10 mL (0.51 mmol) phenylphosphonic dichloride, followed by 2.2 equivalents of the organomagnesium reagent drop wise. The reaction mixture was allowed to stir for 1 hour at 0 ^{o}C, followed by 1h at 22 ^{o}C. The reaction was quenched with 5 mL 0.1 M H_2SO_4, then 10 mL of DCM was added. The two phases were separated and the aqueous was back washed with another 10 mL of DCM. The combined organic layers were dried over Na_2SO_4, filtered, and the solvent removed via vacuum. Some compounds were further purified via column chromatography.

A.5.1.2. Dimethylphenylphosphine oxide

To dimethyl(phenyl)phosphine (20 mL, 0.1 M, 2.0 mmol) in THF at 0 ^{o}C was added H_2O_2 (30% wt/wt in H_2O, 0.40 mL, 3 mmol). After 3 hours at room temperature, the solvent was removed and the crude oil was purified by sublimation, yielding very hygroscopic white crystals (280.6 mg, 91% yield). Properties matched previously reported values.[4] ^{1}H NMR (300 MHz, chloroform-d) δ 7.75 (dd, *J* = 11.9, 6.2, 1.7 Hz, 2H), 7.58 – 7.44 (m, 3H), 1.78 (d, *J* = 13.1 Hz, 6H). $^{31}P\{^{1}H\}$ NMR (121 MHz, chloroform-d) δ 36.20.

A.5.1.3. Diethyl phenylphosphine oxide

^{1}H NMR (300 MHz, chloroform-d) δ 7.70 – 7.58 (m, 2H), 7.52 – 7.36 (m, 2H), 2.04 – 1.74 (m, 34), 1.07 (dtd, *J* = 17.1, 7.6, 2.0 Hz, 6H). ^{13}C NMR (126 MHz, chloroform-d) δ 131.74 (d, *J* = 92.4 Hz), 131.51 (d, *J* = 2.6 Hz), 130.53 (d, *J* = 8.7 Hz), 128.59 (d, *J* = 11.1 Hz), 22.25 (d, *J* = 69.5 Hz), 5.53 (d, *J* = 5.1 Hz). ^{31}P{^{1}H} NMR (121 MHz, chloroform-d) δ 45.45. HRMS (ES^{+}-TOF) m/z: [M]$^{+}$ Calcd. for $C_{10}H_{16}OP$ 183.0937; Found 183.0939.

A.5.1.3. Diisopropylphenylphosphine oxide

Properties matched previously reported values.[6] ^{1}H NMR (300 MHz, chloroform-d) δ 7.69 (dd, *J* = 7.3, 3.5 Hz, 2H), 7.58 – 7.42 (m, 3H), 2.42 – 2.21 (m, 2H), 1.14 (dddd, *J* = 45.0, 15.9, 7.2, 3.2 Hz, 12H). ^{31}P{^{1}H} NMR (121 MHz, chloroform-d) δ 51.01.

A.5.1.4. Di(n-butyl)phenylphosphine oxide

Properties matched previously reported values.[7] ^{1}H NMR (300 MHz, chloroform-d) δ 7.67 (ddd, *J* = 12.7, 6.4, 2.0 Hz, 2H), 7.53 – 7.39 (m, 3H), 2.06 – 1.71 (m, 4H), 1.70 –1.25 (m, 8H), 0.84 (td, *J* = 7.0, 1.9 Hz, 6H). ^{31}P{^{1}H} NMR (121 MHz, chloroform-d) δ 40.59.

A.5.1.5. Dicyclohexylphenylphosphine oxide

Properties matched literature values.[8] ^{1}H NMR (300 MHz, chloroform-d) δ 7.71 – 7.58 (m, 2H), 7.46 (d, *J* = 7.8 Hz, 3H), 2.12 – 1.93 (m, 4H), 1.92 – 1.48 (m, 8H), 1.42 – 0.97 (m, 10H). ^{31}P{^{1}H} NMR (121 MHz, chloroform-d) δ 45.56 .

A.5.1.6. Di(phenylethynyl)phenylphosphine oxide

Properties matched literature values.[9] ^{1}H NMR (300 MHz, chloroform-d) δ 8.17 – 8.03 (m, 2H), 7.59 (p, *J* = 4.5, 3.5 Hz, 9H), 7.50 – 7.31 (m, 4H). ^{31}P{^{1}H} NMR (121 MHz, chloroform-d) δ -19.42 .

A.5.1.7. Triphenylphosphine oxide

Properties matched literature values.[10] ^{1}H NMR (300 MHz, chloroform-d) δ 7.68 (ddt, *J* = 11.8, 8.3, 1.6 Hz, 6H), 7.60 – 7.40 (m, 9H). ^{31}P{^{1}H} NMR (121 MHz, chloroform-d) δ 29.17.

A.5.2. Synthesis of Organomagnesium reagents

A.5.2.1. Tert-butylmagnesium bromide

A three necked round bottom flask was equipped with a reflux condenser (set to 0 ^{o}C), a mechanical overhead stirrer (strongly recommended), and an addition funnel. The round bottom flask was charged with THF (105 mL) and magnesium turnings (4.9200 g, 0.2 mol) and stirred vigorously while heating to gentle reflux. A small crystal of iodine (~20 mg) was added to the mixture. The addition funnel was charged with *tert*-butyl bromide (25.00 g, 0.18 mol) and added in small aliquots until the yellow color of the solution clarified. External heat was removed from the reaction apparatus. The addition rate of the *tert*-butyl bromide was drop wise, but fast enough to maintain a reflux from the exothermic reaction. Once all the *tert*-butyl bromide had been added, the mixture was maintained at reflux via external heat for 2 hours. The mixture was cooled to room temperature and cannula filtered to a dry Schlenk flask. The solution concentration was

determined as discussed in the general procedures, yielding a 1.15 M light grey solution of *tert*-butylmagnesium bromide.

A.5.2.2. Cyclohexylmagnesium chloride

A three necked round bottom flask was equipped with a reflux condenser (set to 0 ^{o}C), a mechanical overhead stirrer (strongly recommended), and an addition funnel. The round bottom flask was charged with THF (420 mL) and magnesium turnings (23.2010 g, 0.93 mol) and stirred vigorously while heating to gentle reflux. A small crystal of iodine (~20 mg) was added to the mixture. The addition funnel was charged with chlorocyclohexane (100.0 mL, 0.84 mol) and added in small aliquots until the yellow color of the solution clarified. External heat was removed from the reaction apparatus. The addition rate of the chlorocyclohexane was drop wise, but fast enough to maintain a reflux from the exothermic reaction. Once all the chlorocyclohexane had been added, the mixture was maintained at reflux via external heat for 2 hours. The mixture was cooled to room temperature and cannula filtered to a dry Schlenk flask. The solution concentration was determined as discussed in the general procedures, yielding a 1.73 M dark grey solution of cyclohexylmagnesium chloride.

A.5.3. Synthesis of H-Phosphonate

A.5.3.1. Diisopropylphosphonate

The preparation from Mirzaei et al. was found to be exceptionally useful in the synthesis of this molecule.[11] In a partially evacuated two necked round bottomed flask fitted with a reflux condenser (set to -10 ^{o}C) and addition funnel, isopropyl alcohol (29.0

mL, 380 mmol) dissolved in dichloromethane (4.0 mL) at 0 ºC was added. The addition funnel was charged with trichlorophosphine (11.0 mL, 125 mmol) in dichloromethane (4.0 mL). While stirring at 0 ºC, the addition funnel contents was added to the flask drop wise at a rate of 0.5 mL/min, then allowed to warm up to room temperature overnight. Volatiles were removed via vacuum, and out of the crude reaction mixture was distilled pure product (300 mTorr, 30-33 ºC), yielding a colorless oil (16.6160 g, 80.0 % yield). ^{1}H NMR (300 MHz, chloroform-d) δ 6.82 (d, *J* = 687.7 Hz, 1H), 4.71 (ddt, *J* = 12.4, 8.6, 6.2 Hz, 2H), 1.34 (dd, *J* = 6.2, 1.9 Hz, 12H). ^{31}P{^{1}H} NMR (121 MHz, chloroform-d) δ 4.43 (d, *J* = 7.0 Hz).

A.5.4. Synthesis of Aryl Phosphinate

A.5.4.1. Methyl methyl(phenyl)phosphinate

Methanol (5 mL, 3.95 mmol) in 20 mL THF was added drop wise over 3 hours to a solution of dichlorophenylphosphine (10.0183 g, 55.97 mmol) and pyridine (18 mL, 0.996 mol) in 100 mL of hexanes at 0 ˚C. Solution stirred for 1 hour then stirred for an additional 35 hours at room temperature. The pyridine hydrochloride precipitate was filtered, the solvent was evaporated, and the resulting oil was distilled to remove the hydrolyzed side product. This product, dimethyl phenlyphosphonite, was distilled at 51˚C at 1000 mtorr (4.9449g, 52.1% yield). ^{31}P{^{1}H} NMR (202 MHz, chloroform-d) δ 160.6, and was telescoped without further purification. Dimethyl phenylphosphonite (4.9449g, 29.06 mmol) in iodomethane (360 µL, 5.78 mmol) was refluxed for two hours. The methyl methyl(phenyl)phosphinate product was purified through column chromatography with 30% Hex: 70% Acetone as the mobile phase with an R_f of 0.09. Product was a clear

oil with a 73.0% yield. Properties matched literature values.[12] ^{1}H NMR (500 MHz, chloroform-d) δ 7.84 – 7.75 (m, 2H), 7.63 – 7.40 (m, 3H), 3.61 (dd, *J* = 11.5, 2.6 Hz, 3H), 1.72 – 1.57 (m, 3H). ^{13}C NMR (126 MHz, chloroform-d) δ 132.34 (d, *J* = 2.9 Hz), 131.31 (d, *J* = 10.3 Hz), 131.06 (d, *J* = 127.0 Hz), 128.69 (d, *J* = 12.7 Hz), 51.01 (d, *J* = 6.3 Hz), 15.54 (d, *J* = 103.2 Hz). ^{31}P{^{1}H} NMR (202 MHz, chloroform-d) δ 43.98.

A.5.5. Synthesis of Alkyl phosphonates

A.5.5.1. Dimethyl methylphosphonate

A mixture of iodomethane (0.1 mL, 1.6 mmol) in trimethylphosphite (0.8 mL, 6.5 mmol)) in a round bottom flask attached to a Dean-Stark apparatus was heated to 100 ^{o}C for 12 hours. The collection arm slowly collected iodomethane as confirmed by NMR. The reaction mixture was cooled to room temperature and directly fractionally distilled. The distillation yielded crude dimethyl methylphosphonate (52-55 ^{o}C at 2000 mTorr), which was further purified via Kendallrohr (Figure A8) to yield pure product (637.2 mg, 79.0% yield). Properties matched literature values.[13] ^{1}H NMR (300 MHz, chloroform-d) δ 3.71 (dd, *J* = 10.7, 2.0 Hz, 6H), 1.45 (dd, *J* = 17.1, 2.3 Hz, 3H). ^{31}P{^{1}H} NMR (121 MHz, chloroform-d) δ 33.16 .

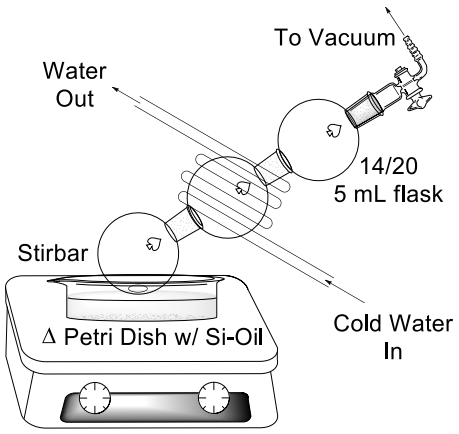

Figure A8. Kendallrohr distillation apparatus.

A.5.5.2. Diethyl n-hexylphosphonate

A mixture of 1-bromohexane (7.1906 g, 45 mmol) and triethylphosphite (21.6559 g, 126 mmol) in a round bottom flask attached to a Dean-Stark apparatus were heated to 170 ^{o}C for 12 hours. The collection arm slowly collected bromoethane as confirmed by NMR. The reaction mixture was cooled to room temperature and directly fractionally distilled. The distillation yielded diethyl ethylphosphonate (35 ^{o}C at 400 mTorr), followed by triethylphosphate (55 ^{o}C at 400 mTorr), followed by pure diethyl hexylphosphonate (65-75 ^{o}C at 1000 mTorr), 8.8600 g, 95.0% yield. Properties matched previously reported values.[14] ^{1}H NMR (300 MHz, chloroform-d) δ 4.08 (m, 4H), 1.83 – 1.47 (m, 4H), 1.47 – 1.18 (m, 12H), 0.96 – 0.79 (m, 3H). ^{31}P{^{1}H} NMR (121 MHz, chloroform-d) δ 32.63.

A.5.5.2. Tetraethyl propane-1,3-diylbis(phosphonate)

A mixture of 1,3-dibromopropane (8.6445 g, 42 mmol) and triethylphosphite (16.50 g, 100 mmol) in a round bottom flask attached to a Dean-Stark apparatus were

heated to 170 °C for 12 hours. The collection arm slowly collected bromoethane as confirmed by NMR. The reaction mixture was cooled to room temperature and directly fractionally distilled. The distillation yielded diethyl ethylphosphonate (35 °C at 400 mTorr), followed by triethylphosphate (55 °C at 400 mTorr) followed by a colorless oil of pure product (135-150 °C at 1000 mTorr), 9.7179 g, 72.3% yield. Properties matched literature values.[15] ^{1}H NMR (300 MHz, chloroform-d) δ 4.27 – 3.85 (m, 8H), 2.12 – 1.68 (m, 6H), 1.31 (t, *J* = 7.0 Hz, 12H). ^{31}P{^{1}H} NMR (121 MHz, chloroform-d) δ 30.59.

A.5.6. Synthesis of Aryl phosphonates

A.5.6.1. 2-Phenyl-1,3,2-dioxaphospholane 2-oxide

A solution of ethylene glycol (318.42 mg, 5.48 mmol) and triethylamine (2.1780 g, 21.52 mmol) in THF (81 mL) was added drop wise over 2 hours into a 0˚C solution of phenylphosphonic dichloride (1.002 g, 5.14 mmol) in THF (80 mL). The mixture's temperature slowly rose to room temperature and stirred for 8 hours. The precipitant was filtered and the solution extracted with dichloromethane and water. The organic layer was dried over sodium sulfate and rotary evaporation was used to remove the solvent. The resulting oil was purified through column chromatography using ethyl acetate as the mobile phase. The resulting product was a white solid (65.9 mg, 7.6% yield). Properties matched literature values.[16] ^{1}H NMR (300 MHz, $CDCl_3$) 7.77 (dd, *J* = 14.2, 7.7 Hz, 2H), 7.56 (t, *J* = 7.5 Hz, 1H), 7.50-7.36 (m, 2H), 4.66 - 4.49 (m, 2H), 4.49 - 4.30 (m, 2H). ^{31}P{^{1}H} NMR (121 MHz, $CDCl_3$) δ 36.66.

A.5.6.2.Diisopropyl phenylphosphonate

To a stirring solution of phenylphosphonic dichloride (7.5 mL, 51 mmol) in hexanes (50mL) at 0 ^{o}C, was added a solution of isopropanol (20 mL, 255 mmol) and triethylamine (19 mL, 150 mmol) in hexanes (50 mL) drop wise over 1 hour. Once the addition was complete, the mixture was refluxed for 12 hours. The reaction was quenched with saturated $NaHCO_3$ (50 mL), then taken up into EtOAc (50 mL) and washed twice with equal volumes of saturated $NaHCO_3$, followed by brine. The organic layer was then dried over Na_2SO_4, filtered, and solvent removed via vacuum, yielding a crude oil. This crude product was fractionally distilled at 72-78 ^{o}C at 300 mTorr, yielding a colorless oil (12.7270 g, 93.0% yield). Properties matched literature values.[10] ^{1}H NMR (300 MHz, chloroform-d) δ 8.02 – 7.76 (m, 2H), 7.70 – 7.38 (m, 3H), 5.09 (dqq, *J* = 12.8, 6.5, 3.9, 3.4 Hz, 2H), 1.48 (ddd, *J* = 9.3, 6.2, 2.7 Hz, 12H). ^{31}P{^{1}H} NMR (121 MHz, chloroform-d) δ 27.45.

A.5.6.3. Ditertbutyl phenylphosphonate

To a stirring slurry of potassium tert-butoxide (3.050 g, 112 mmol) in diethyl ether (50 mL) at 0 ^{o}C, was added phenylphosphonic dichloride (1.60 mL, 10.2 mmol) drop wise. After complete addition, the solution was allowed to stir at 0 ^{o}C for 1 hour, then was brought to reflux overnight. Reaction was quenched with DI H_2O, and washed three times against 50 mL of DI H_2O. The ether layer was dried over Na_2SO_4. After filtration, solvent was removed via vacuum, yielding a crude oil. The crude material was purified by flash column chromatography (silica, 60 mesh, 1:1 Hexanes:EtOAc, R_f = 0.4) yielding a hygroscopic crystalline white solid (1.7858 g, 64.4% yield). Properties

matched literature values.[17] MP (under Ar) 46-49 °C. ^{1}H NMR (500 MHz, chloroform-d) δ 7.85 – 7.74 (m, 2H), 7.47 (t, *J* = 7.5 Hz, 1H), 7.41 (dt, *J* = 11.4, 5.4 Hz, 2H), 1.47 (s, 18H). ^{13}C NMR (126 MHz, chloroform-d) δ 133.99 (d, *J* = 192.6 Hz), 131.45 (d, *J* = 9.7 Hz), 131.19 (d, *J* = 3.0 Hz), 128.00 (d, *J* = 15.1 Hz), 82.27 , 30.46 (d, *J* = 4.1 Hz). ^{31}P{^{1}H} NMR (202 MHz, chloroform-d) δ 9.87.

A.5.6.4. Diphenyl phenylphosphonate

A two neck 250 mL round bottom flask fitted with a reflux condenser (0 °C) and an addition funnel was charged with phenylphosphonic dichloride (4.75 mL, 33.3 mmol) in THF (50 mL) then brought to 0 °C. The addition funnel was charged with a lithium phenoxide solution (1.0 M in THF, 100 mL, 100 mmol) and added drop wise to the reaction mixture. Upon completion of addition, the reaction was brought to reflux overnight. The reaction mixture was then cooled and quenched with 50 mL DI H_2O. Next, 100 mL of EtOAc was added, and the organic layer was washed two times against equivalent volume DI H_2O, followed by brine. The organic layer was dried over Na_2SO_4, filtered, and solvent removed via vacuum to yield a crude orange solid. The product was recrystallized out of the crude by taking up into hot Et_2O and adding hexanes. Beautiful white needle crystals were obtained in excellent purity, which were then filtered and washed with cold hexanes, yielding product (8.2750 g, 80.2% yield). Properties matched literature values.[18] ^{1}H NMR (300 MHz, chloroform-d) δ 8.05 – 7.93 (m, 2H), 7.68 – 7.58 (m, 1H), 7.58 – 7.48 (m, 2H), 7.37 – 7.26 (m, 5H), 7.26 – 7.10 (m, 5H). ^{31}P{^{1}H} NMR (121 MHz, chloroform-d) δ 11.69.

A.5.6.5. Bis((1R,2S,5R)-2-isopropyl-5-methylcyclohexyl) phenylphosphonate

To a 100 mL round bottom flask equipped with a reflux condenser (0 °C) containing a slurry of potassium hyrdride (30% wt/wt dispersion in mineral oil, 1.5769 g, 11.4 mmol) in Et_2O (50 mL) at 0 °C was added (1*R*,2*S*,5*R*)-(−)-Menthol (1.8700 g, 12.0 mmol) in Et_2O (10 mL) drop wise. Formation of a gas was observed. The mixture was allowed to stir at 0 °C for 1 hour, then brought to reflux for 1 hour. While refluxing, phenylphosphonic dichloride (0.73 mL, 5.1 mmol) was added drop wise. After complete addition, the reaction was refluxed overnight. The reaction was cooled to room temperature and washed against equal volumes of DI H_2O two times, 0.1 M KOH two times, followed by brine, then dried over Na_2SO_4. The mixture was filtered and solvent removed via vacuum, yielding a crude oil/solid mixture. The crude material was purified by flash column chromatography (silica, 60 mesh, gradient 100% Hexanes (R_f = 0.0) to 100% EtOAc (R_f = 0.5)) yielding a very viscous oil (1.2501 g, 58.1% yield). Properties matched literature values.[19] ^{1}H NMR (500 MHz, chloroform-d) δ 7.85 – 7.78 (m, 2H), 7.51 (td, *J* = 7.3, 1.6 Hz, 1H), 7.43 (td, *J* = 7.6, 4.2 Hz, 2H), 4.20 (dtdd, *J* = 124.7, 11.0, 7.3, 4.4 Hz, 2H), 3.41 (tt, *J* = 9.7, 4.1 Hz, 1H), 2.44 – 2.35 (m, 1H), 2.29 (pd, *J* = 7.0, 2.5 Hz, 1H), 2.17 (pt, *J* = 6.9, 3.5 Hz, 1H), 2.13 – 2.01 (m, 1H), 1.97 (dtd, *J* = 12.1, 4.0, 2.1 Hz, 1H), 1.85 (pd, *J* = 7.1, 2.4 Hz, 1H), 1.72 – 1.53 (m, 6H), 1.52 – 1.34 (m, 5H), 1.33 – 0.98 (m, 5H), 0.98 – 0.76 (m, 18H), 0.39 (d, *J* = 6.9 Hz, 2H). ^{13}C NMR (126 MHz, chloroform-d) δ 131.83 (d, *J* = 3.1 Hz), 131.75 (d, *J* = 9.7 Hz), 130.35 (d, *J* = 190.3 Hz), 128.10 (d, *J* = 14.9 Hz), 77.70 (d, *J* = 6.6 Hz), 71.54 , 50.16 , 48.72 (d, *J* = 6.6 Hz), 48.63 (d, *J* = 7.1 Hz), 45.09 , 43.25 (d, *J* = 63.8 Hz), 34.56 , 34.13 (d, *J* = 3.2 Hz), 31.64 (d, *J* = 4.4 Hz), 31.51 , 25.86 , 25.47 (d, *J* = 27.7 Hz), 23.16 , 22.77 (d, *J* = 7.6 Hz), 22.23 , 21.96

(d, *J* = 11.8 Hz), 21.04 (d, *J* = 18.1 Hz), 21.02 , 16.12 , 15.46 (d, *J* = 86.2 Hz). $^{31}P\{^{1}H\}$ NMR (202 MHz, chloroform-d) δ 16.33.

A.5.6.6. Dimethyl o-tolylphosphonate

A 50 mL round bottom flask containing 1-iodo-2-methylbenzene (1.0168 g, 4.5 mmol), dimethyl phosphonate (1.5579 g, 15 mmol), N,N-diisopropylethylamine (2.6169 g, 20 mmol), 1,3-bis(diphenylphosphino)propane (189.0 mg, 0.46 mmol), and palladium(II) acetate (116.1 mg, 0.47 mmol) was charged with 25 mL toluene and refluxed for 48 hours. The reaction mixture was then cooled to room temperature and quenched with DI H_2O (25 mL). The reaction was taken up into 25 mL EtOAc and washed three times with equivalent volumes of saturated $NaHCO_3$, followed by brine. The organic layer was dried over Na_2SO_4, filtered, and dried via vacuum, yielding a crude oil. The crude material was purified by flash column chromatography (silica, 60 mesh, 4% triethylamine in EtOAc (R_f=0.5)) yielding a colorless oil (213.3 mg, 24.3% yield). Properties matched literature values.[20] ^{1}H NMR (300 MHz, chloroform-d) δ 7.38 (m, 2H), 7.04 – 6.84 (m, 2H), 6.84 – 6.57 (m, 5H), 3.47 – 3.02 (m, 12H), 2.03 (d, *J* = 7.8 Hz, 6H). $^{31}P\{^{1}H\}$ NMR (121 MHz, chloroform-d) δ 21.94.

A.5.6.7. Diethyl (2-chlorophenyl)phosphonate

A round-bottom flask fitted with a Dean-Stark apparatus was charged with 1-chloro-2-iodobenzene (4.9510 g, 20.9 mmol), triethylphosphite (5.7372 g, 33.1 mmol), and palladium on carbon (30% wt/wt, 145 mg, 0.02 equivalents palladium). The reaction was heated to 175 ^{o}C for 12 hours. The collection arm slowly collected iodoethane as

confirmed by NMR. The reaction mixture was cooled to room temperature and directly fractionally distilled. The distillation yielded diethyl ethylphosphonate (35 ^{o}C at 400 mTorr), followed by triethylphosphate (55 ^{o}C at 400 mTorr) followed by a colorless oil of pure product (100-112 ^{o}C at 500 mTorr), 4.1300 g, 80.0% yield. Properties matched literature values.[21] ^{1}H NMR (500 MHz, chloroform-d) δ 8.01 (ddd, *J* = 14.6, 7.3, 1.5 Hz, 1H), 7.50 – 7.42 (m, 2H), 7.35 (ddt, *J* = 8.6, 6.4, 3.0 Hz, 1H), 4.26 – 4.06 (m, 4H), 1.35 (t, *J* = 7.1 Hz, 6H). ^{13}C NMR (126 MHz, chloroform-d) δ 136.85 (d, *J* = 3.0 Hz), 135.93 (d, *J* = 7.8 Hz), 133.57 (d, *J* = 2.6 Hz), 130.78 (d, *J* = 10.2 Hz), 127.46 (d, *J* = 190.5 Hz), 126.40 (d, *J* = 13.7 Hz), 62.54 (d, *J* = 5.5 Hz), 16.29 (d, *J* = 6.5 Hz). ^{31}P{^{1}H} NMR (202 MHz, chloroform-d) δ 14.49.

A.5.6.8. 2-Bromophenyl trifluoromethanesulfonate

To a stirring mixture of 2-bromophenol (15.1340 g, 88 mmol) and pyridine (17.9346 g, 220 mmol) in DCM (50 mL) at 0 ^{o}C was added trifluoromethanesulfonic anhydride (25.00 g, 89 mmol) drop wise. The addition caused fuming in the flask. After the slow addition, the reaction was allowed to stir at room temperature overnight. The reaction was quenched with 0.1 M H_2SO_4, then taken up into 100 mL of EtOAc and washed twice with equal volumes saturated $NaHCO_3$, followed by brine. The organic layer was dried over Na_2SO_4, filtered, and solvent removed via vacuum, yielding a crude oil. The crude product was distilled at 41-51 ^{o}C at 450 mTorr, to yield a colorless oil (24.2469 g, 90.6% yield). Properties matched literature values.[22] ^{1}H NMR (300 MHz, chloroform-d) δ 7.72 (dd, *J* = 8.0, 1.6 Hz, 1H), 7.48 – 7.34 (m, 2H), 7.28 (td, *J* = 7.5, 7.0, 2.0 Hz, 1H). ^{19}F NMR (282 MHz, chloroform-d) δ -73.37.

A.5.6.9. Dimethyl (2-bromophenyl)phosphonate

A 100 mL round bottom flask containing 2-bromophenyl trifluoromethanesulfonate (1.0020 g, 3.3 mmol), dimethyl phosphonate (546.3 mg, 5.0 mmol), N,N-diisopropylethylamine (696.8 mg, 5.0 mmol), 1,3-bis(diphenylphosphino)propane (73.0 mg, 0.16 mmol), and palladium(II) acetate (18.0 mg, 0.08 mmol) was charged with 50 mL toluene and refluxed for 48 hours. The reaction mixture was then cooled to room temperature and quenched with DI H_2O (50 mL). The reaction was taken up into 50 mL EtOAc and washed three times with equivalent volumes of saturated $NaHCO_3$, followed by brine. The organic layer was dried over Na_2SO_4, filtered, and dried via vacuum, yielding a crude mixture. The crude material was purified by flash column chromatography (silica, 60 mesh, 4% triethylamine in EtOAc (R_f=0.5)) yielding a colorless oil (493.3 mg, 56.5% yield). Properties matched literature values.[23] ^{1}H NMR (500 MHz, chloroform-d) δ 8.09 – 7.89 (m, 1H), 7.67 (ddd, *J* = 7.0, 5.1, 2.3 Hz, 1H), 7.46 – 7.33 (m, 2H), 3.81 (d, *J* = 11.4 Hz, 6H). ^{13}C NMR (126 MHz, chloroform-d) δ 136.41 (d, *J* = 8.0 Hz), 134.37 (d, *J* = 11.4 Hz), 133.85 (d, *J* = 2.8 Hz), 128.34 (d, *J* = 193.8 Hz), 126.97 (d, *J* = 13.8 Hz), 125.16 (d, *J* = 4.2 Hz), 53.00 (d, *J* = 5.6 Hz). ^{31}P{^{1}H} NMR (202 MHz, chloroform-d) δ 17.83.

A.5.6.10. 2-Fluorophenyl trifluoromethanesulfonate

To a stirring mixture of 2-fluorophenol (1.0533 g, 8.9 mmol) and pyridine (1.6541 g, 17.4 mmol) in DCM (15 mL) at 0 ^{o}C was added trifluoromethanesulfonic anhydride (1.80 mL, 10.7 mmol) drop wise. The addition caused fuming in the flask. After the slow addition, the reaction was allowed to stir at room temperature overnight. The

reaction was quenched with 0.1 M H_2SO_4, then taken up into 25 mL of EtOAc and washed twice with equal volumes saturated $NaHCO_3$, followed by brine. The organic layer was dried over Na_2SO_4, filtered, and solvent removed via vacuum, yielding a crude orange oil. The crude product was distilled at 26 ^oC at 650 mTorr, to yield a colorless oil (1.7966 g, 83.3% yield). Properties matched literature values.[24] ^1H NMR (300 MHz, chloroform-d) δ 7.34 – 7.24 (m, 1H), 7.23 – 7.10 (m, 1H). ^{19}F NMR (282 MHz, chloroform-d) δ -72.70 , -112.01 – -112.53 (m).

A.5.6.11. Dimethyl (2-fluorophenyl)phosphonate

A 100 mL round bottom flask containing 2-fluorophenyl trifluoromethanesulfonate (1.3097 g, 5.3 mmol), dimethyl phosphonate (2.1044 g, 18 mmol), N,N-diisopropylethylamine (3.0531 g, 23 mmol), 1,3-bis(diphenylphosphino)propane (224.9 mg, 0.53 mmol), and palladium(II) acetate (135.3 mg, 0.55 mmol) was charged with 50 mL toluene and refluxed for 48 hours. The reaction mixture was then cooled to room temperature and quenched with DI H_2O (50 mL). The reaction was taken up into 50 mL EtOAc and washed three times with equivalent volumes of saturated $NaHCO_3$, followed by brine. The organic layer was dried over Na_2SO_4, filtered, and dried via vacuum, yielding a crude mixture. The crude material was purified by flash column chromatography (silica, 60 mesh, 4% triethylamine in EtOAc (R_f=0.5)) yielding a colorless oil (660.0 mg, 61.2% yield). ^1H NMR (500 MHz, chloroform-d) δ 7.85 (dddd, *J* = 14.3, 8.0, 6.4, 1.8 Hz, 1H), 7.56 (ddd, *J* = 7.5, 5.5, 1.9 Hz, 1H), 7.25 (td, *J* = 7.3, 3.0 Hz, 1H), 7.14 (td, *J* = 8.9, 6.2 Hz, 1H), 3.82 (d, *J* = 11.5 Hz, 6H). $^{13}C\{^1H\}$ NMR (126 MHz, chloroform-d) δ 163.66 (d, *J* = 253.2 Hz), 135.81 –

134.67 (m), 124.53 (dd, *J* = 14.0, 3.5 Hz), 116.48 (dd, *J* = 22.5, 8.2 Hz), 114.50 , 53.26 (d, *J* = 5.7 Hz). ^{19}F NMR (471 MHz, chloroform-d) δ -103.78 (dt, *J* = 10.5, 5.9 Hz). ^{31}P{^{1}H} NMR (202 MHz, chloroform-d) δ 16.80. HRMS (ES^{+}-TOF) m/z: [M+Na]$^{+}$ Calcd. for $C_8H_{10}O_3FNaP$ 227.0249; Found 227.0240.

A.5.6.12. Dimethyl (3-fluorophenyl)phosphonate

A 100 mL round bottom flask containing 1-bromo-3-fluorobenzene (1.0409 g, 5.5 mmol), dimethyl phosphonate (1.8366 g, 16 mmol), N,N-diisopropylethylamine (2.9471 g, 23 mmol), 1,3-bis(diphenylphosphino)propane (217.8 mg, 0.53 mmol), and palladium(II) acetate (120.6 mg, 0.54 mmol) was charged with 50 mL toluene and refluxed for 48 hours. The reaction mixture was then cooled to room temperature and quenched with DI H_2O (50 mL). The reaction was taken up into 50 mL EtOAc and washed three times with equivalent volumes of saturated $NaHCO_3$, followed by brine. The organic layer was dried over Na_2SO_4, filtered, and dried via vacuum, yielding a crude mixture. The crude material was purified by flash column chromatography (silica, 60 mesh, 4% triethylamine in EtOAc (R_f=0.5)) yielding a colorless oil (680.1 mg, 60.6% yield). ^{1}H NMR (500 MHz, chloroform-d) δ 7.59 (dd, *J* = 12.9, 7.5 Hz, 1H), 7.54 – 7.42 (m, 2H), 7.27 (td, *J* = 8.7, 2.6 Hz, 1H), 3.78 (d, *J* = 11.1 Hz, 6H). ^{13}C{^{1}H} NMR (126 MHz, chloroform-d) δ 161.77 – 161.61 (m), 161.94 – 161.78 (m), 162.77 (dd), 130.89 (dd, *J* = 17.7, 7.5 Hz), 129.88 (dd, *J* = 189.8, 6.2 Hz), 127.95 (dd, *J* = 9.2, 3.3 Hz), 163.76 – 163.60 (m), 120.15 (dd, *J* = 21.1, 3.1 Hz), 119.08 (dd, *J* = 22.5, 10.4 Hz), 53.19 (d, *J* = 5.6 Hz), 163.93 – 163.77 (m). ^{19}F NMR (471 MHz, chloroform-d) δ -111.32 (qd,

J = 8.6, 5.4 Hz). $^{31}P\{^{1}H\}$ NMR (202 MHz, chloroform-d) δ 19.45 (d, *J* = 8.9 Hz). HRMS (ES^{+}-TOF) m/z: $[M+Na]^{+}$ Calcd. for $C_8H_{10}O_3FNaP$; 227.0249, Found 227.0250.

A.5.6.13. 4-Fluorophenyl trifluoromethanesulfonate

To a stirring mixture of 4-fluorophenol (1.0934 g, 8.9 mmol) and pyridine (1.6645 g, 17.4 mmol) in DCM (15 mL) at 0 ºC was added trifluoromethanesulfonic anhydride (1.80 mL, 10.7 mmol) drop wise. The addition caused fuming in the flask. After the slow addition, the reaction was allowed to stir at room temperature overnight. The reaction was quenched with 0.1 M H_2SO_4, then taken up into 25 mL of EtOAc and washed twice with equal volumes saturated $NaHCO_3$, followed by brine. The organic layer was dried over Na_2SO_4, filtered, and solvent removed via vacuum, yielding a crude orange oil. The crude product was distilled at 23 ºC at 650 mTorr, to yield a colorless oil (1.8872 g, 86.9% yield). Properties matched literature values.[24] ^{1}H NMR (300 MHz, chloroform-d) δ 7.35 – 7.22 (m, 1H), 7.22 – 7.10 (m, 1H). ^{19}F NMR (282 MHz, chloroform-d) δ -72.70 , -112.29 (d, *J* = 7.5 Hz).

A.5.6.14. Dimethyl (4-fluorophenyl)phosphonate

A 100 mL round bottom flask containing 4-fluorophenyl trifluoromethanesulfonate (1.3149 g, 5.3 mmol), dimethyl phosphonate (2.0249 g, 17 mmol), N,N-diisopropylethylamine (3.3254 g, 24 mmol), 1,3-bis(diphenylphosphino)propane (236.4 mg, 0.60 mmol), and palladium(II) acetate (125.0 mg, 0.55 mmol) was charged with 50 mL toluene and refluxed for 48 hours. The reaction mixture was then cooled to room temperature and quenched with DI H_2O (50 mL). The

reaction was taken up into 50 mL EtOAc and washed three times with equivalent volumes of saturated $NaHCO_3$, followed by brine. The organic layer was dried over Na_2SO_4, filtered, and dried via vacuum, yielding a crude mixture. The crude material was purified by flash column chromatography (silica, 60 mesh, 4% triethylamine in EtOAc (R_f=0.4)) yielding a colorless oil (735.7 mg, 68.0% yield). Properties matched literature values.[20] ^{1}H NMR (500 MHz, chloroform-d) δ 7.88 – 7.74 (m, 2H), 7.17 (td, *J* = 8.6, 3.3 Hz, 2H), 3.76 (d, *J* = 11.1 Hz, 6H). $^{13}C\{^1H\}$ NMR (126 MHz, chloroform-d) δ 165.83 (dd, *J* = 253.9, 3.9 Hz), 134.86 (dd, *J* = 11.4, 8.8 Hz), 123.38 (dd, *J* = 193.7, 3.4 Hz), 116.29 (dd, *J* = 21.5, 16.3 Hz), 53.07 (d, *J* = 5.5 Hz). ^{19}F NMR (471 MHz, chloroform-d) δ -105.46 (td, *J* = 9.0, 4.6 Hz). $^{31}P\{^1H\}$ NMR (202 MHz, chloroform-d) δ 20.64.

A.5.6.15. Dimethyl (2-methoxyphenyl)phosphonate

A 100 mL round bottom flask containing 1-bromo-2-methoxybenzene (1.0129 g, 5.3 mmol), dimethyl phosphonate (1.9812 g, 16 mmol), N,N-diisopropylethylamine (3.3762 g, 24 mmol), 1,3-bis(diphenylphosphino)propane (275.3 mg, 0.60 mmol), and palladium(II) acetate (152.6 mg, 0.60 mmol) was charged with 50 mL toluene and refluxed for 48 hours. The reaction mixture was then cooled to room temperature and quenched with DI H_2O (50 mL). The reaction was taken up into 50 mL EtOAc and washed three times with equivalent volumes of saturated $NaHCO_3$, followed by brine. The organic layer was dried over Na_2SO_4, filtered, and dried via vacuum, yielding a crude mixture. The crude material was purified by flash column chromatography (silica, 60 mesh, 4% triethylamine in EtOAc (R_f=0.3)) yielding a colorless oil (782.1 mg, 68.3%

yield). Properties matched literature values.[25] ^{1}H NMR (300 MHz, chloroform-d) δ 7.81 (ddd, *J* = 14.9, 7.6, 1.8 Hz, 1H), 7.58 – 7.46 (m, 1H), 7.07 – 6.90 (m, 2H), 3.92 (s, 3H), 3.80 (d, *J* = 11.3 Hz, 6H). ^{13}C{^{1}H} NMR (126 MHz, chloroform-d) δ 161.61 (d, *J* = 2.8 Hz), 135.47 (d, *J* = 7.2 Hz), 134.83 (d, *J* = 2.1 Hz), 120.76 (d, *J* = 14.5 Hz), 115.72 (d, *J* = 186.9 Hz), 111.51 (d, *J* = 9.5 Hz), 56.26, 53.14 (d, *J* = 5.7 Hz). ^{31}P{^{1}H} NMR (121 MHz, chloroform-d) δ 20.37 .

A.5.6.16. Dimethyl (3-methoxyphenyl)phosphonate

A 100 mL round bottom flask containing 1-bromo-3-methoxybenzene (1.0245 g, 5.3 mmol), dimethyl phosphonate (2.0145 g, 17 mmol), N,N-diisopropylethylamine (2.749 g, 22 mmol), 1,3-bis(diphenylphosphino)propane (241.5 mg, 0.60 mmol), and palladium(II) acetate (135.9 mg, 0.59 mmol) was charged with 50 mL toluene and refluxed for 48 hours. The reaction mixture was then cooled to room temperature and quenched with DI H_2O (50 mL). The reaction was taken up into 50 mL EtOAc and washed three times with equivalent volumes of saturated $NaHCO_3$, followed by brine. The organic layer was dried over Na_2SO_4, filtered, and dried via vacuum, yielding a crude mixture. The crude material was purified by flash column chromatography (silica, 60 mesh, 4% triethylamine in EtOAc (R_f=0.4)) yielding a colorless oil (744.1 mg, 65.0% yield). Properties matched literature values.[25] ^{1}H NMR (500 MHz, chloroform-d) δ 7.43 – 7.29 (m, 3H), 7.10 (dt, *J* = 7.3, 2.3 Hz, 1H), 3.85 (s, 3H), 3.77 (d, *J* = 11.1 Hz, 6H). ^{13}C{^{1}H} NMR (126 MHz, chloroform-d) δ 159.85 (d, *J* = 19.1 Hz), 130.17 (d, *J* = 17.8 Hz), 128.45 (d, *J* = 187.5 Hz), 124.39 (d, *J* = 9.2 Hz), 119.45 (d, *J* = 3.3 Hz), 116.71 (d, *J*

= 11.3 Hz), 55.78, 53.06 (d, *J* = 5.5 Hz). $^{31}P\{^{1}H\}$ NMR (202 MHz, chloroform-d) δ 21.49.

A.5.6.17. 4-Methoxyphenyl trifluoromethanesulfonate

To a stirring mixture of 4-methoxyphenol (1.0137 g, 8.6 mmol) and pyridine (1.6807 g, 17.4 mmol) in DCM (15 mL) at 0 ^{o}C was added trifluoromethanesulfonic anhydride (1.80 mL, 10.7 mmol) drop wise. The addition caused fuming in the flask. After the slow addition, the reaction was allowed to stir at room temperature overnight. The reaction was quenched with 0.1 M H_2SO_4, then taken up into 25 mL of EtOAc and washed twice with equal volumes saturated $NaHCO_3$, followed by brine. The organic layer was dried over Na_2SO_4, filtered, and solvent removed via vacuum, yielding a crude orange oil. The crude product was distilled at 48 ^{o}C at 640 mTorr, to yield a colorless oil (1.8444 g, 81.4% yield). Properties matched literature values.[24] ^{1}H NMR (300 MHz, chloroform-d) δ 7.24 – 7.16 (m, 2H), 6.97 – 6.88 (m, 2H), 3.83 (d, *J* = 1.0 Hz, 3H). ^{19}F NMR (282 MHz, chloroform-d) δ -72.76 .

A.5.6.18. Dimethyl (4-methoxyphenyl)phosphonate

A 100 mL round bottom flask containing 4-methoxyphenyl trifluoromethanesulfonate (1.3616 g, 5.3 mmol), dimethyl phosphonate (2.0350 g, 17 mmol), N,N-diisopropylethylamine (3.0562 g, 22 mmol), 1,3-bis(diphenylphosphino)propane (230.7 mg, 0.60 mmol), and palladium(II) acetate (130.8 mg, 0.56 mmol) was charged with 50 mL toluene and refluxed for 48 hours. The reaction mixture was then cooled to room temperature and quenched with DI H_2O (50 mL). The

reaction was taken up into 50 mL EtOAc and washed three times with equivalent volumes of saturated $NaHCO_3$, followed by brine. The organic layer was dried over Na_2SO_4, filtered, and dried via vacuum, yielding a crude mixture. The crude material was purified by flash column chromatography (silica, 60 mesh, 4% triethylamine in EtOAc (R_f=0.3)) yielding a colorless oil (952.1 mg, 83.1% yield). Properties matched literature values.[20] ^{1}H NMR (300 MHz, chloroform-d) δ 7.74 (dd, *J* = 12.8, 8.6 Hz, 2H), 6.97 (dt, *J* = 9.6, 4.7 Hz, 2H), 3.85 (s, 3H), 3.74 (d, *J* = 11.1 Hz, 6H). ^{13}C{^{1}H} NMR (126 MHz, chloroform-d) δ 163.35 (d, *J* = 3.3 Hz), 134.22 (d, *J* = 11.4 Hz), 118.32 (d, *J* = 195.9 Hz), 114.42 (d, *J* = 16.0 Hz), 55.66, 52.85 (d, *J* = 5.6 Hz). ^{31}P{^{1}H} NMR (121 MHz, chloroform-d) δ 22.58.

A.5.6.19. Dimethyl [1,1'-biphenyl]-2-ylphosphonate.

A 250 mL round bottomed flask fitted with a reflux condenser with 2-bromobiphenyl (2.0225 g, 8.6 mmol), diisopropylethylamine (2.0700 g, 18 mmol), dimethylphosphonate (5.0800 g, 46 mmol), palladium(II) acetate (190.5 mg, 0.8 mmol), and 1,3-bis(diphenylphosphino)propane (696.3 mg, 1.7 mmol) dissolved in toluene (100 mL) was heated to reflux for 36 hours. The reaction was cooled to room temperature and diluted with 100 mL EtOAc. The organic layer was washed three times with saturated $NaHCO_3$ solution, then once with brine. The organic layer was dried over Na_2SO_4, filtered, and the solvent was removed via vacuum yielding a crude yellow oil with residual white solids. The crude product was purified by flash column chromatography (silica, 60 mesh, EtOAc with 1% triethyl amine, R_f = 0.6) yielding a hygroscopic crystalline white solid (1.5868 g, 71.1% yield). Properties matched literature values.[26]

MP (under Argon) 59-61 ºC. ^{1}H NMR (500 MHz, chloroform-d) δ 8.03 (dd, *J* = 14.2, 7.7 Hz, 1H), 7.58 (t, *J* = 7.6 Hz, 1H), 7.50 – 7.32 (m, 7H), 3.51 (d, *J* = 11.2 Hz, 6H). ^{13}C NMR (126 MHz, chloroform-d) δ 141.32 (d, *J* = 4.4 Hz), 133.92 (d, *J* = 9.6 Hz), 132.13 (d, *J* = 3.0 Hz), 131.33 (d, *J* = 14.3 Hz), 129.12 , 127.55 (d, *J* = 2.8 Hz), 126.94 (d, *J* = 14.6 Hz), 126.06 (d, *J* = 188.2 Hz), 52.35 (d, *J* = 6.2 Hz). ^{31}P{^{1}H} NMR (202 MHz, chloroform-d) δ 20.82.

A.5.6.20. Diethyl [1,1'-biphenyl]-2-ylphosphonate

A 250 mL round bottomed flask fitted with a reflux condenser with 2-bromobiphenyl (2.0825 g, 8.6 mmol), diisopropylethylamine (1.9905 g, 18 mmol), diethylphosphonate (4.7905 g, 34 mmol), palladium(II) acetate (193.0 mg, 0.9 mmol), and 1,3-bis(diphenylphosphino)propane (495.6 mg, 1.3 mmol) dissolved in toluene (100 mL) was heated to reflux for 36 hours. The reaction was cooled to room temperature and diluted with 100 mL EtOAc. The organic layer was washed three times with saturated $NaHCO_3$ solution, then once with brine. The organic layer was dried over Na_2SO_4, filtered, and the solvent was removed via vacuum yielding a crude yellow oil. The crude product was purified by vacuum transfer (500 mTorr, 135 ºC) yielding a viscous colorless oil (1.9818 g, 79.4% yield). Properties matched literature values.[27] ^{1}H NMR (300 MHz, chloroform-d) δ 8.16 – 7.95 (m, 1H), 7.71 – 7.23 (m, 6H), 4.09 – 3.63 (m, 3H), 1.13 (td, *J* = 7.1, 2.2 Hz, 6H). ^{13}C NMR (126 MHz, chloroform-d) δ 146.05 (d, *J* = 9.9 Hz), 141.46 (d, *J* = 4.2 Hz), 133.81 (d, *J* = 9.6 Hz), 131.93 (d, *J* = 3.0 Hz), 131.35 (d, *J* = 14.1 Hz), 129.34 , 127.45 (d, *J* = 6.2 Hz), 126.99 (d, *J* = 187.1 Hz), 126.86 (d, *J* = 14.6 Hz), 61.79 (d, *J* = 6.0 Hz), 16.07 (d, *J* = 6.9 Hz). ^{31}P{^{1}H} NMR (121 MHz, chloroform-d) δ 18.11.

A.5.6.21. Diisopropyl [1,1'-biphenyl]-2-ylphosphonate[28]

A 100 mL round bottomed flask fitted with a reflux condenser with 2-bromobiphenyl (2.0244 g, 8.6 mmol), anhydrous potassium carbonate (3.7000 g, 26 mmol), diisopropylphosphonate (2.2255 g, 13.1 mmol), palladium(II) acetate (205.1 mg, 0.9 mmol), and 1,3-bis(diphenylphosphino)propane (356.3 mg, 0.9 mmol) dissolved in dimethylformamide (50 mL) was heated to 100 ^{o}C for 2 hours. The reaction was cooled to room temperature and diluted with 100 mL EtOAc. The organic layer was washed two times with saturated ammonium chloride solution, two times with saturated lithium chloride solution, and once with brine. The organic layer was dried over Na_2SO_4, filtered, and the solvent was removed via vacuum yielding a crude oil with white solids. The crude product was purified by flash column chromatography (silica, 60 mesh, Et_2O with 1% triethyl amine, R_f = 0.3) yielding a viscus faintly yellow oil (1.3123 g, 47.5% yield). Properties matched literature values.[28] ^{1}H NMR (500 MHz, chloroform-d) δ 8.09 (dd, *J* = 14.6, 7.7 Hz, 1H), 7.54 (td, *J* = 7.5, 1.7 Hz, 1H), 7.50 – 7.41 (m, 3H), 7.41 – 7.29 (m, 4H), 4.65 – 4.50 (m, *J* = 6.3 Hz, 2H), 1.15 (dd, *J* = 21.6, 6.1 Hz, 12H). ^{13}C NMR (126 MHz, chloroform-d) δ 145.92 (d, *J* = 9.6 Hz), 141.72 , 133.60 (d, *J* = 9.9 Hz), 131.63 (d, *J* = 3.0 Hz), 131.45 (d, *J* = 14.1 Hz), 129.73 , 128.51 (d, *J* = 188.8 Hz), 127.27 (d, *J* = 11.5 Hz), 126.68 (d, *J* = 14.9 Hz), 70.67 (d, *J* = 6.4 Hz), 23.81 (dd, *J* = 15.9, 4.5 Hz). ^{31}P{^{1}H} NMR (202 MHz, chloroform-d) δ 16.14. HRMS (ES^{+}-TOF) m/z: $[M]^{+}$ Calcd. for $C_{18}H_{24}O_3P$ 319.1461; Found 319.1463.

A.5.6.22. Dimethyl [1,1'-biphenyl]-4-ylphosphonate

A 50 mL round bottom flask containing 4-bromo-1,1'-biphenyl (1.0069 g, 4.5 mmol), dimethyl phosphonate (1.5086 g, 13.6 mmol), N,N-diisopropylethylamine (2.3224 g, 18.3 mmol), 1,3-bis(diphenylphosphino)propane (298.0 mg, 0.72 mmol), and palladium(II) acetate (107.6 mg, 0.46 mmol) was charged with 25 mL toluene and refluxed for 48 hours. The reaction mixture was then cooled to room temperature and quenched with DI H_2O (25 mL). The reaction was taken up into 25 mL EtOAc and washed three times with equivalent volumes of saturated $NaHCO_3$, followed by brine. The organic layer was dried over Na_2SO_4, filtered, and dried via vacuum, yielding a crude oil. The crude material was purified by flash column chromatography (silica, 60 mesh, 4% triethylamine in EtOAc (R_f=0.5)) yielding a colorless oil (603.7 mg, 36.0% yield). Properties matched literature values.[26] ^{1}H NMR (300 MHz, chloroform-d) δ 7.95 – 7.82 (m, 2H), 7.77 – 7.66 (m, 2H), 7.66 – 7.57 (m, 2H), 7.54 – 7.35 (m, 3H), 3.80 (d, *J* = 11.1 Hz, 2H). ^{13}C NMR (126 MHz, chloroform-d) δ 145.50 , 139.90 , 132.44 (d, *J* = 10.2 Hz), 128.97 , 128.24 , 127.30 , 127.28 (d, *J* = 15.4 Hz), 125.45 (d, *J* = 190.1 Hz), 52.74 (d, *J* = 5.5 Hz). ^{31}P{^{1}H} NMR (121 MHz, chloroform-d) δ 21.80.

A.6. Reaction of Phosphonates with Organomagnesium and Sodium Triflate

A.6.1. General Considerations

All NMR yields were run in at least duplicate. For a typical run: To a mixture of phosphonate (0.30 mmol) with NaOTf (0.67 mmol, 113.7 mg) stirring under a nitrogen atmosphere in a 5 mL round-bottom flask with a jacketed reflux condenser attached (set

to 0 °C) was added 3.00 mL of THF with hexamethylbenzene (from a stock solution, containing 135.2 mg of HMB or 0.833 mmol in 25.00 mL of THF). The NaOTf was allowed to completely dissolve at room temperature before the flask was cooled to 0 °C with an ice bath. Organomagnesium reagent (0.63 mmol in an ethereal solvent) was added very slowly drop wise (generally 1 drop per 10 seconds) in a manner that the drops of reagent contacted the 0 °C cooling jacket wall before dripping down into the flask – precooling each drop. A white precipitate immediately formed. After complete addition of organomagnesium, the reaction was allowed to stir at 0 °C for 2 minutes, then heated to reflux in an oil bath for 2 hours. To quench, the reaction was cooled to 0 °C, then poured into a separatory funnel with 5 mL of 0.1 M H_2SO_4. The round bottom flask was washed out with 5 mL of 0.1 M H_2SO_4 and added to the separatory funnel. The mixture was not allowed to sit for more than 2 minutes (polymerization of THF can occur) before the round bottom flask was rinsed out with 5 mL of DCM and added to the separatory funnel. The aqueous layer was washed three times 5 mL of DCM. The combined organic layers were dried over Na_2SO_4 for several hours, then filtered, and solvent removed via vacuum. The residue from the organic layer was taken up into deuterated chloroform and analyzed by NMR. All NMR yields reported were performed in at least duplicate with yields matching within +/-3%. A representative labeled spectrum from each is displayed below.

Note: Addition rates of the organo-magnesium reagent have considerable consequences on the outcome of the reaction. It has been determined through painstaking trial and error that a very low effective magnesium concentration compared to phosphonate (i.e. a very slow addition rate) at cold temperatures (i.e. 0 °C) yields the

most reproducible and highest yields. Reaction times for substrates may vary, however all were observed to be done after 2 hours – longer reaction times sometimes led to lower yields. The workup of the reaction is also sensitive, responding best to a sulfuric acid quench followed by serial DCM extractions (phosphine oxides are very water soluble).

A.6.2. Equivalents study

Reactions were run using the general setup as noted above, with any changes noted in the figure below (Figure A9).

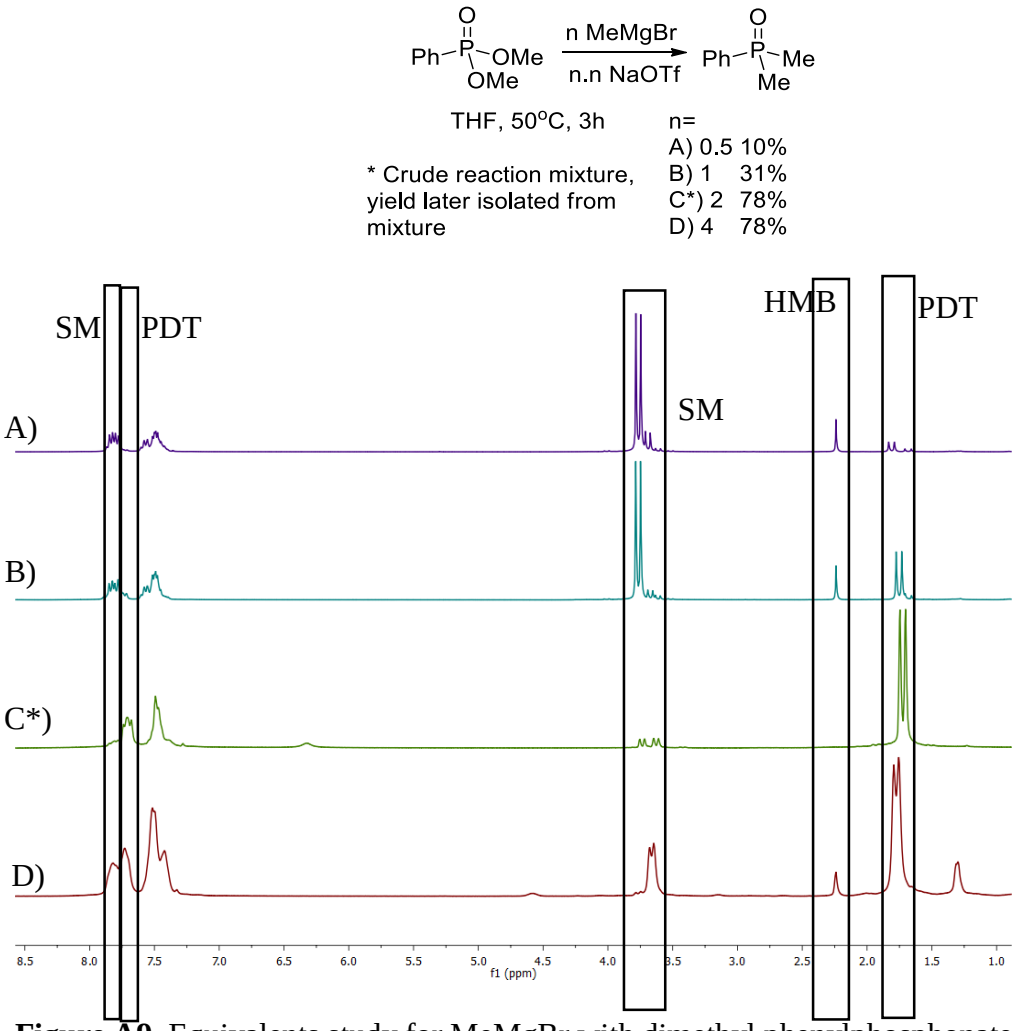

Figure A9. Equivalents study for MeMgBr with dimethyl phenylphosphonate and NaOTf.

A.6.3. Optimization study

Reactions were run using the general setup as noted above, with any changes noted in the figure below (Figure A10).

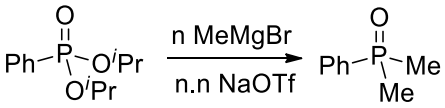

A) 67°C, THF, 6h	n= 2	35%
B)	4	35%
C)	6	23%
D) 100°C, Bomb, THF, 24h	2	33%
E) 67°C, Dioxane, 6h	2	24%
F) 101°C, Dioxane, 20h	2	22%
G) 67°C, THF, 6h*	2	5%

*phosphonate added to grignard dropwise

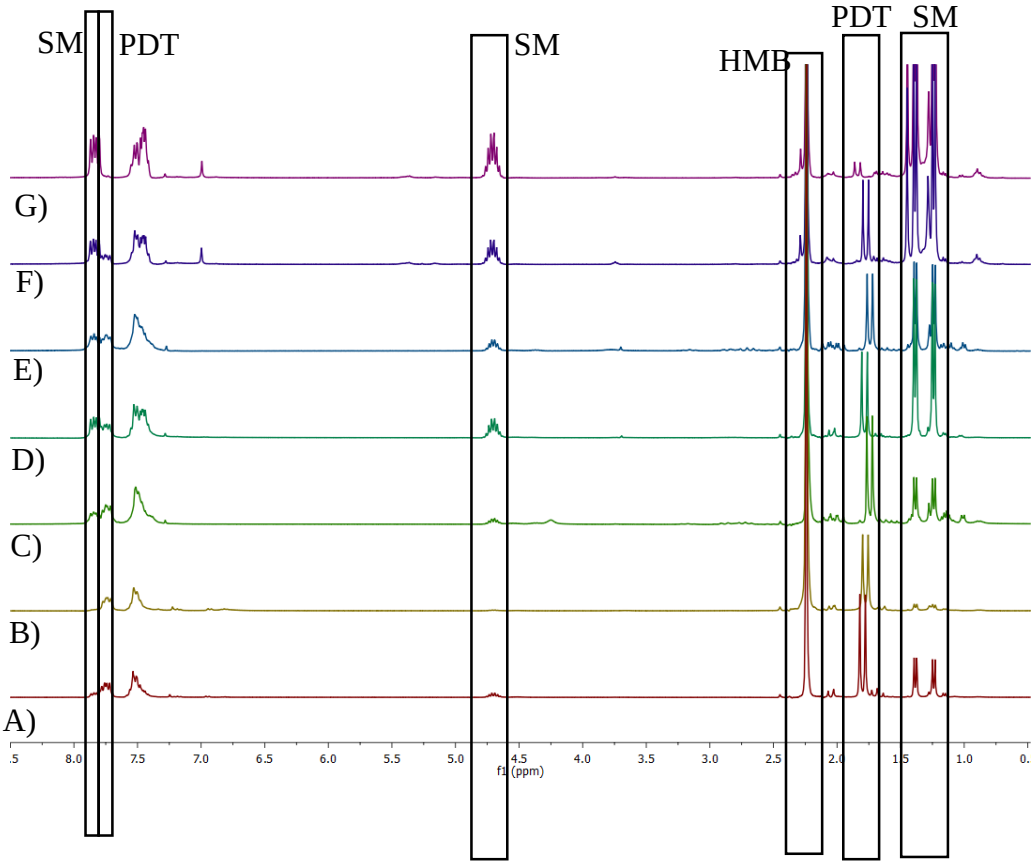

Figure A10. Extreme reaction condition screening to enhance yields

A.6.4. Phosphonate Leaving Group Study

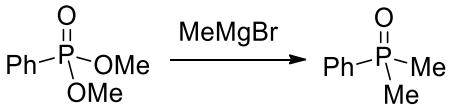

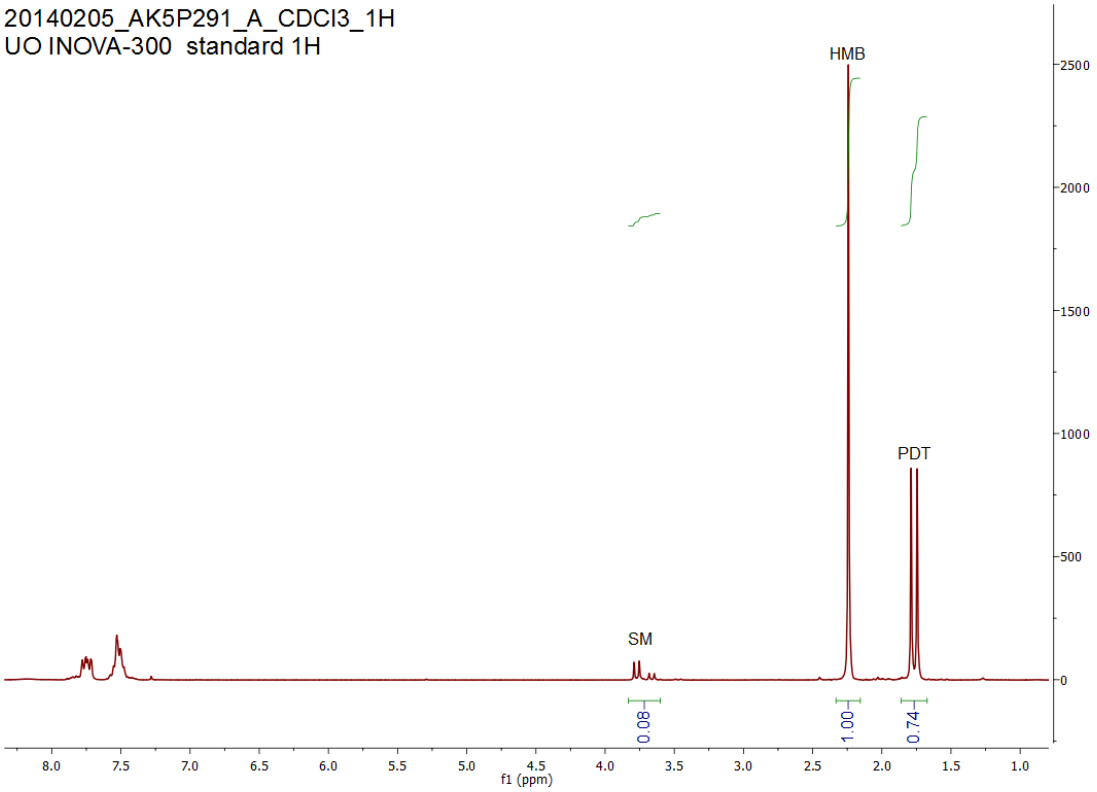

Figure A11. Methoxy leaving groups.

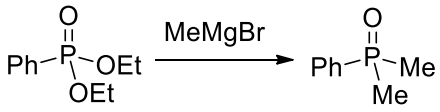

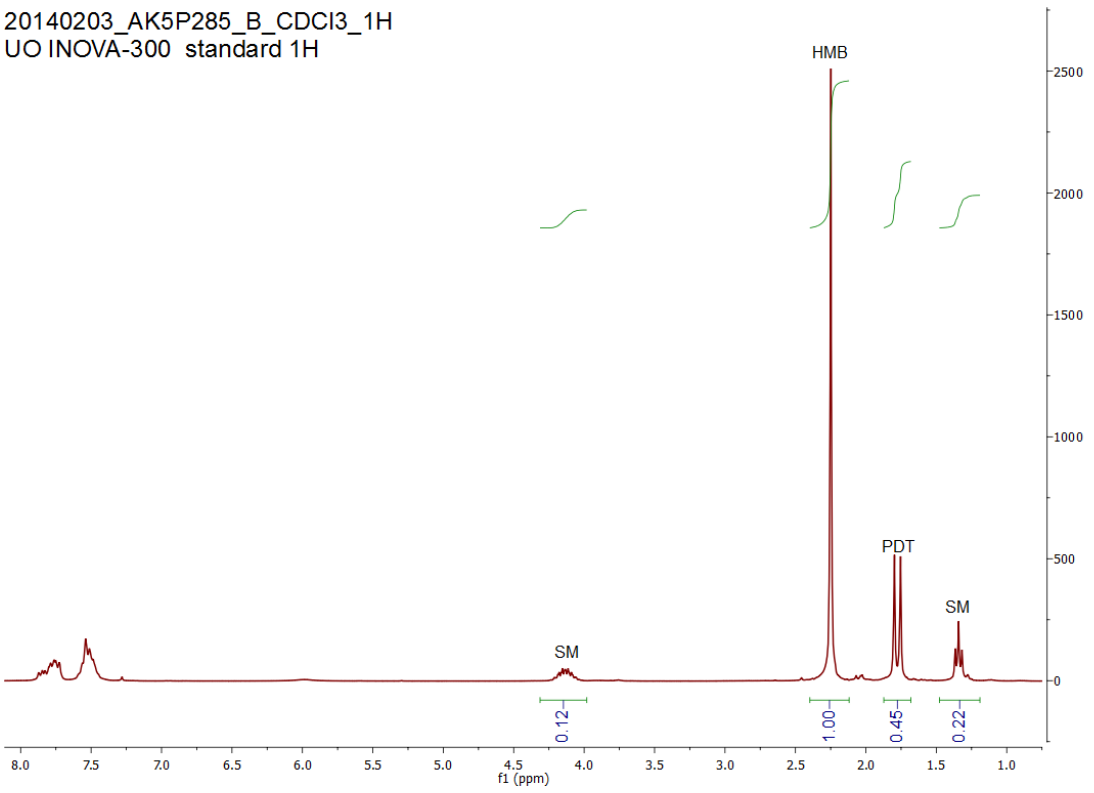

Figure A12. Ethoxy leaving groups.

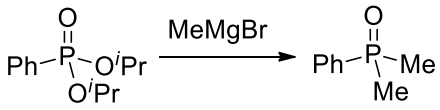

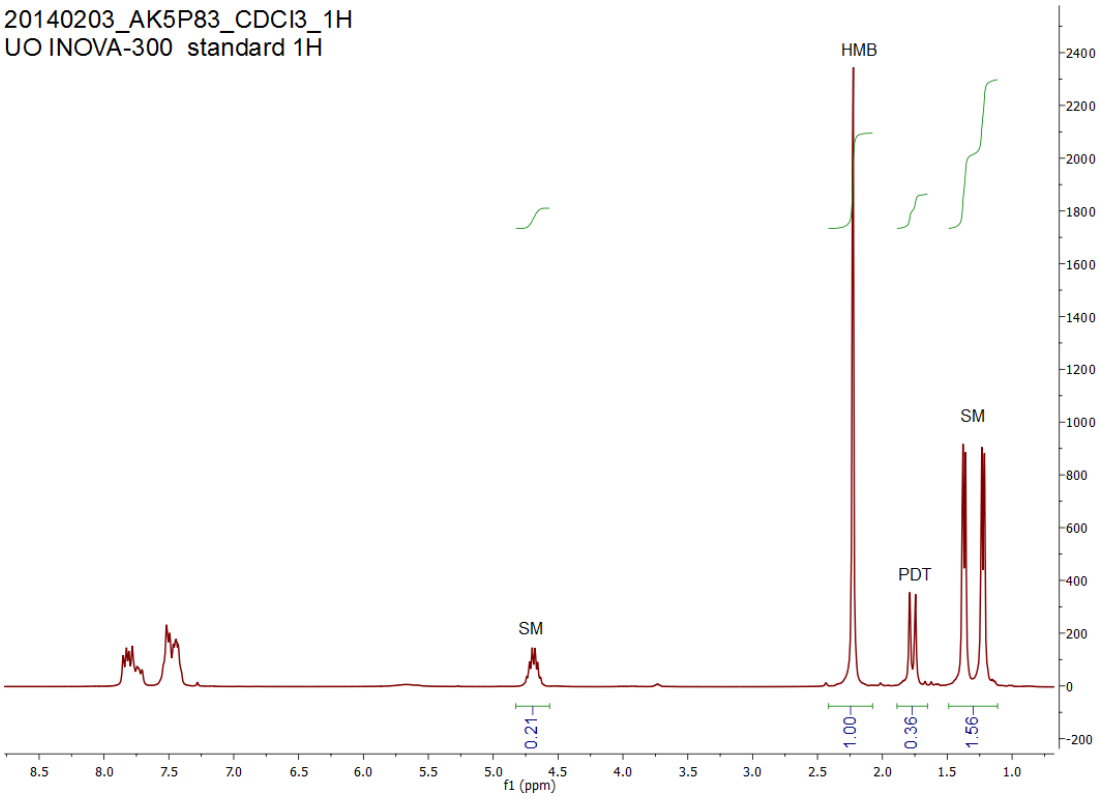

Figure A13. Isopropoxy leaving groups.

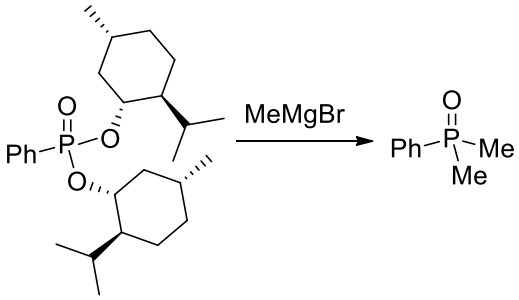

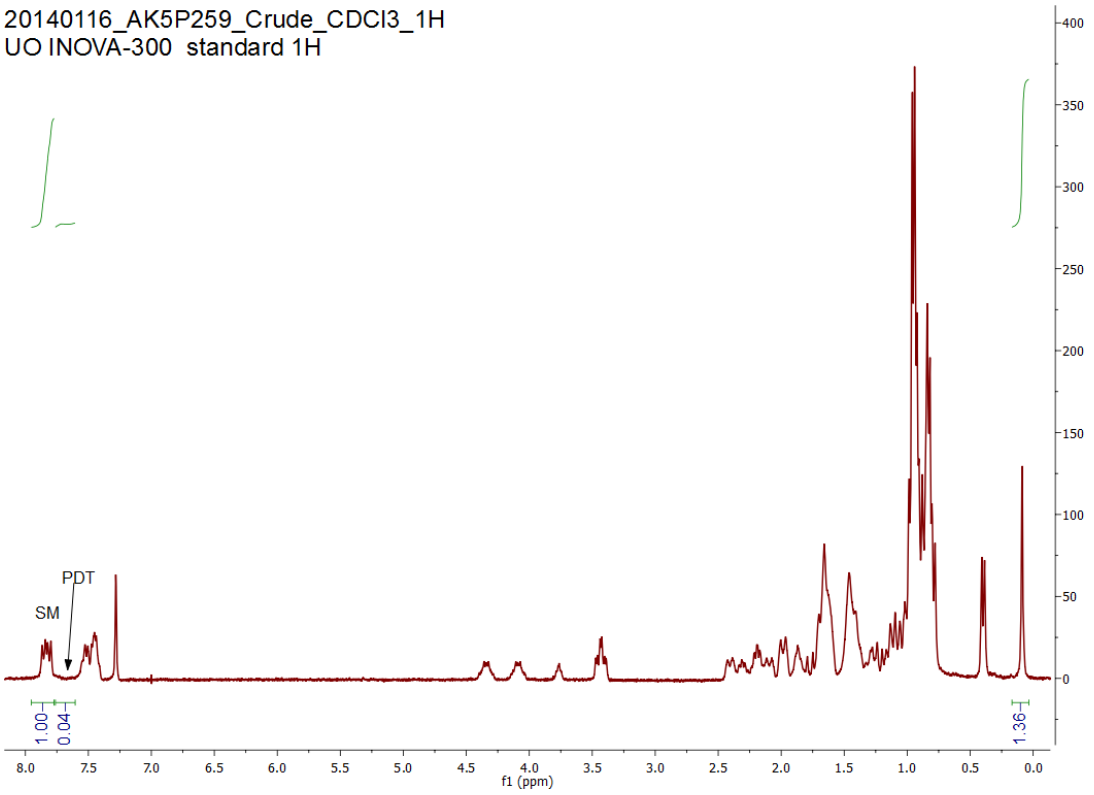

Figure A14. Menthoxide leaving groups.

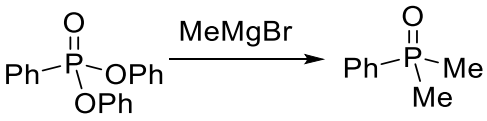

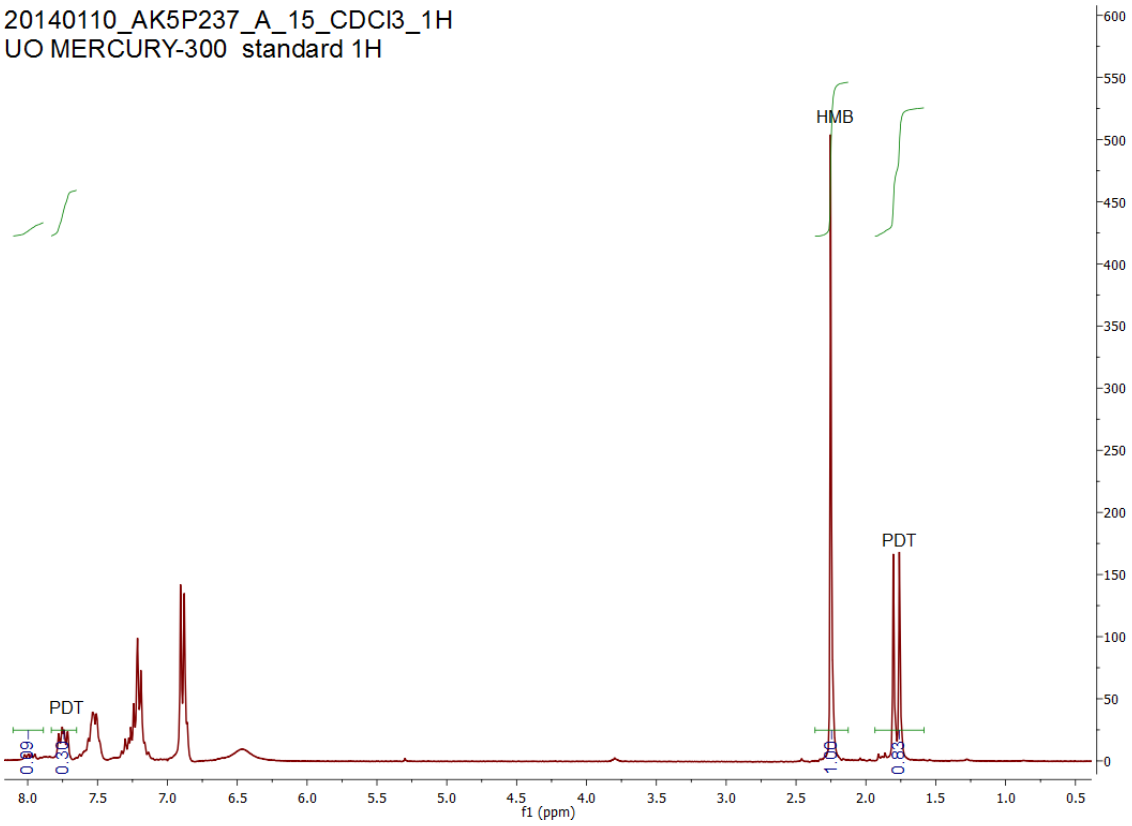

Figure A15. Phenoxy leaving groups.

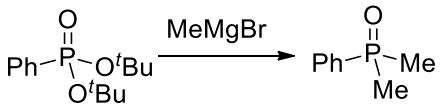

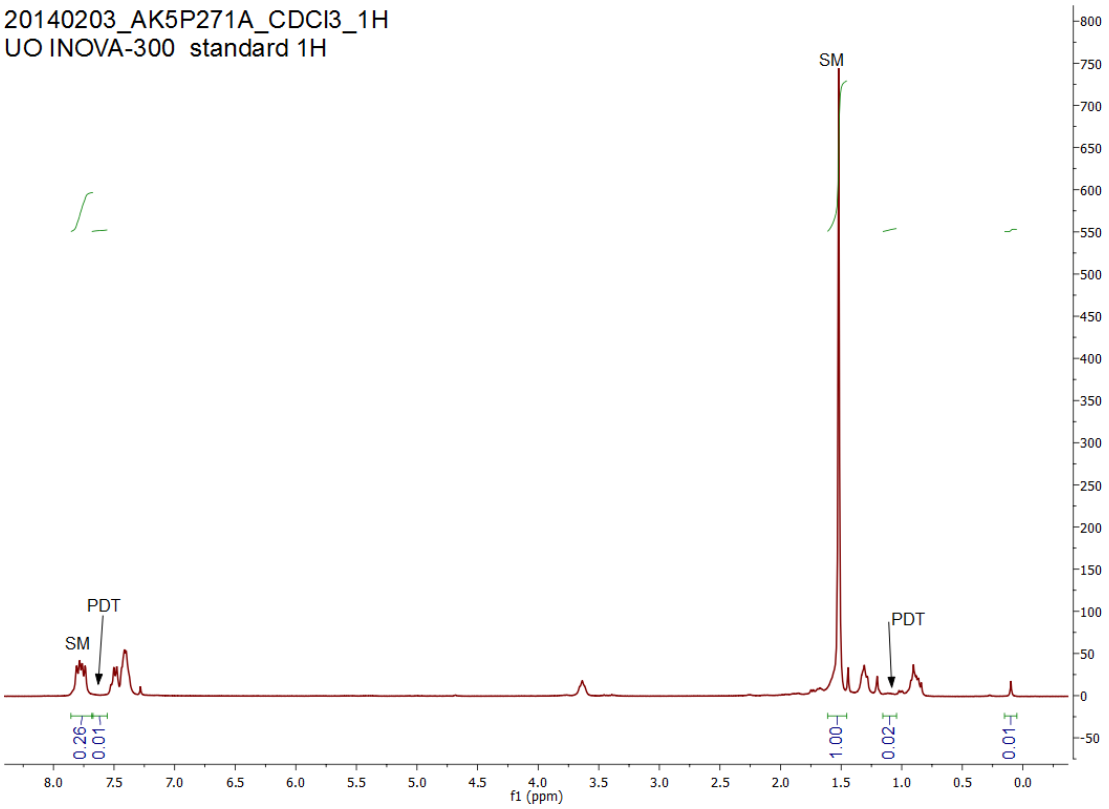

Figure A16. *tert*-Butoxy leaving groups.

A.6.5. Alkyl phosphonate study

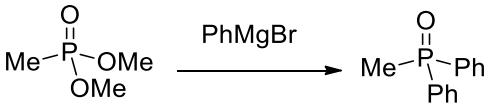

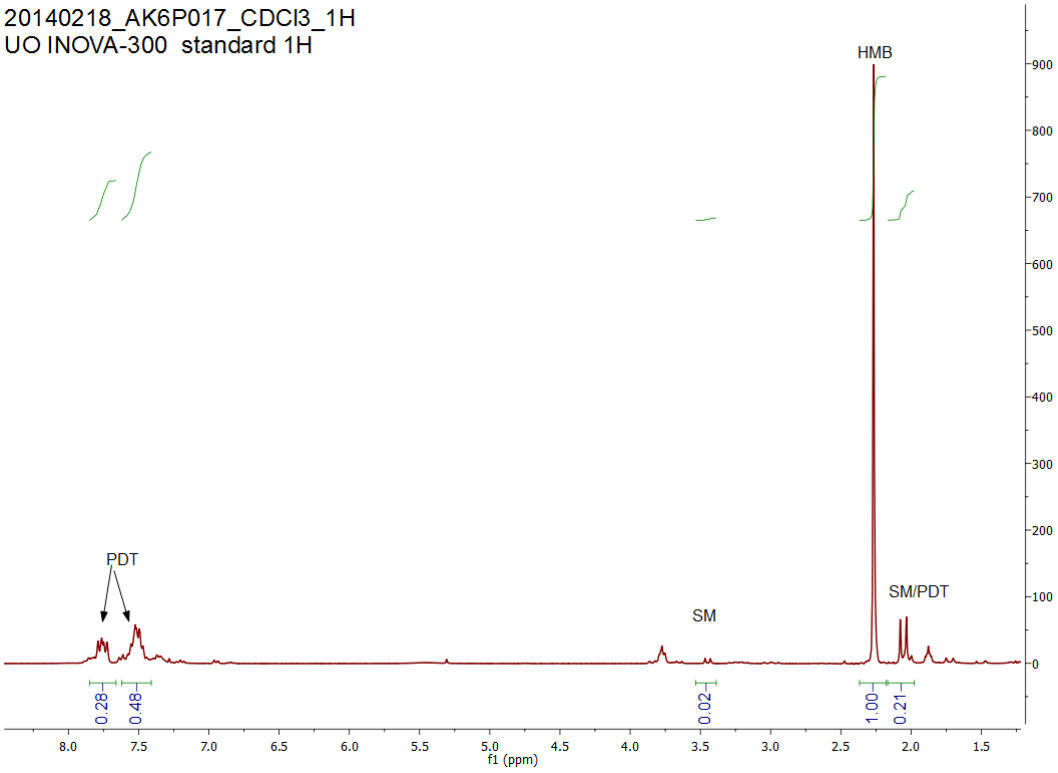

Figure A17. Dimethyl methylphopshonate reacting with phenylmagnesium bromide.

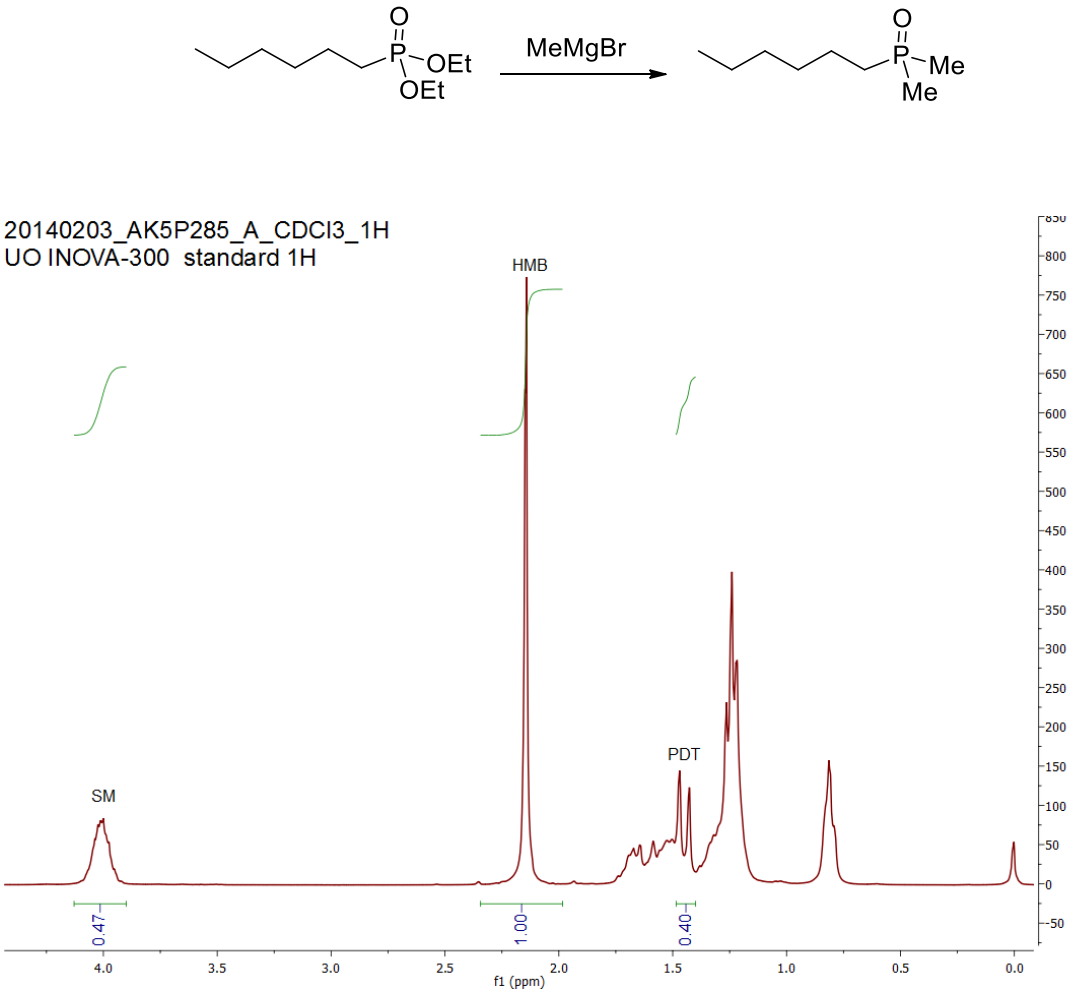

Figure A18. Diethyl *n*-hexylphosphonate reacting with methylmagnesium bromide.

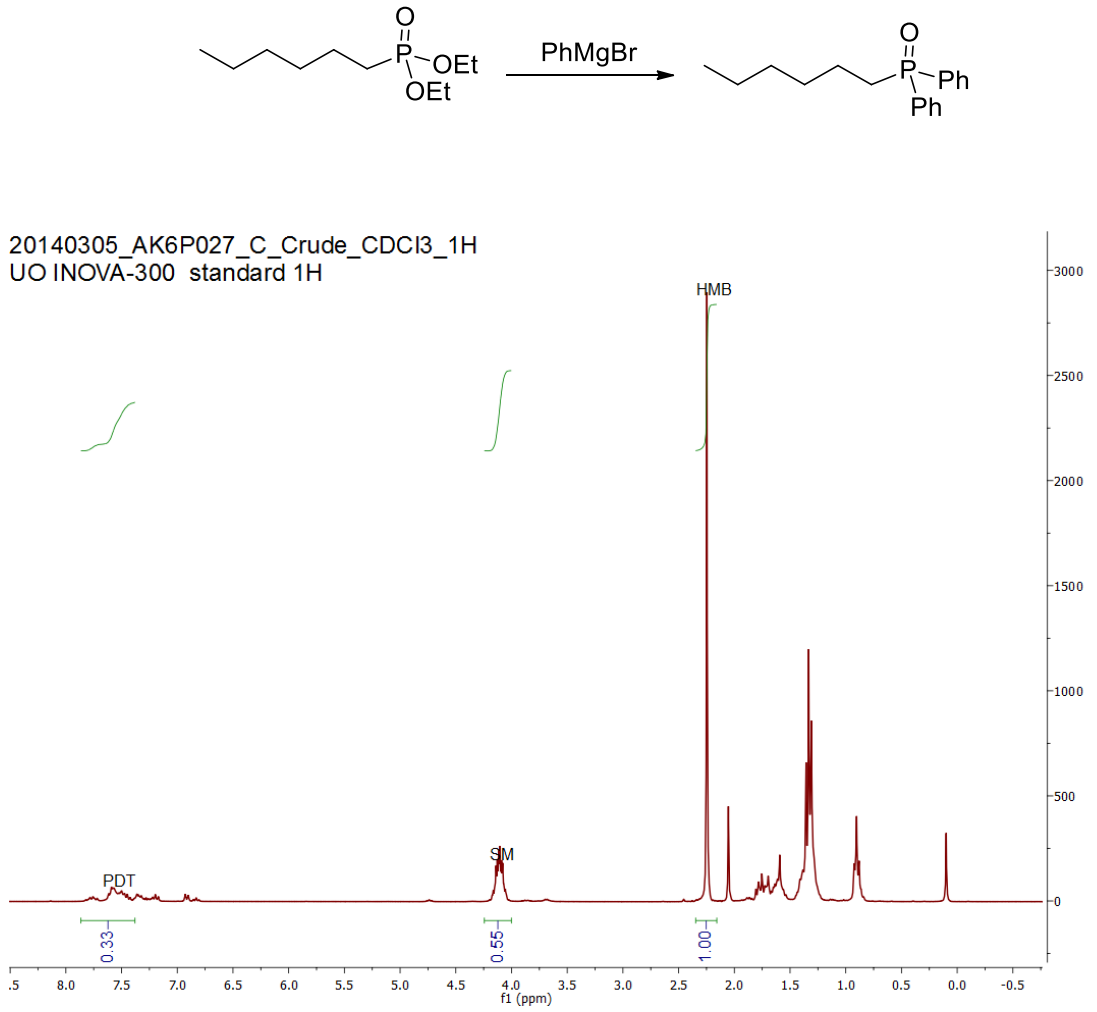

Figure A19. Diethyl *n*-hexylphosphonate reacting with phenylmagnesium bromide.

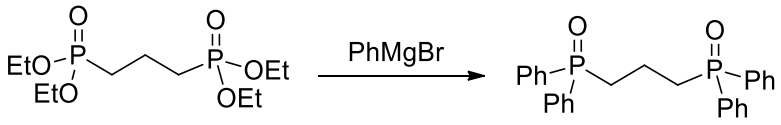

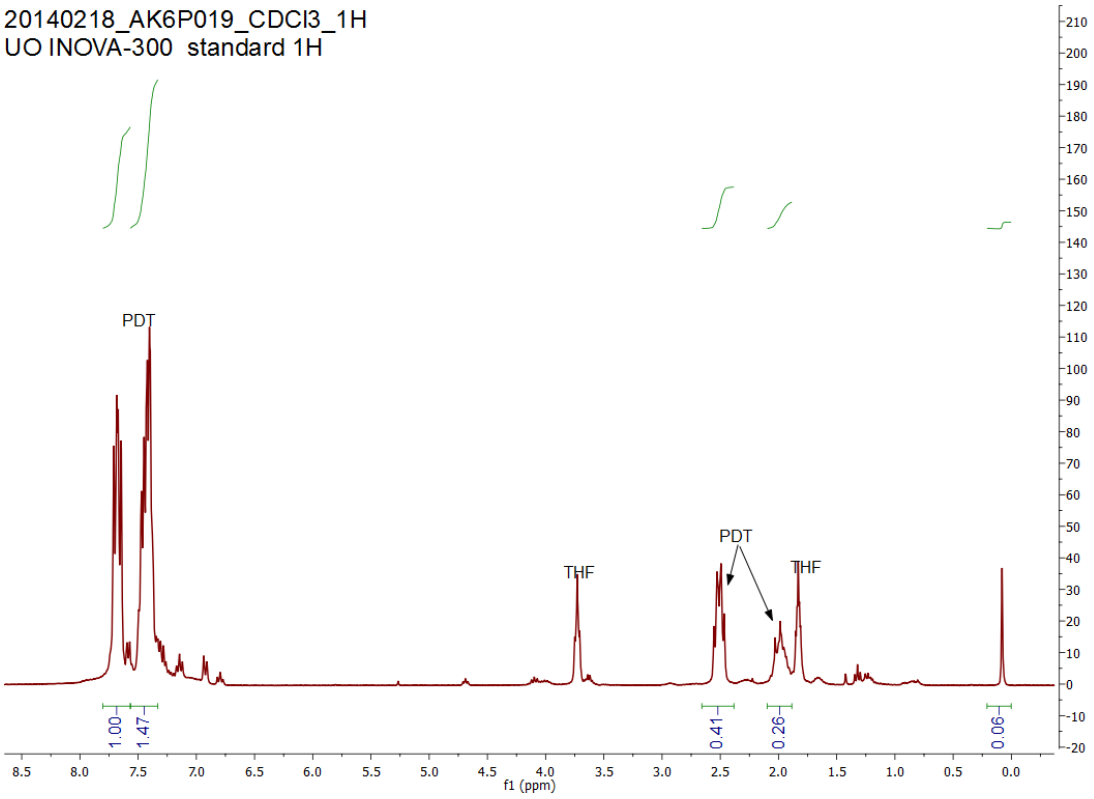

Figure A20. 1,3-Bis(diethyl phosphonate)propane reacting with phenylmagnesium bromide.

A.6.6. Aryl phosphonate study

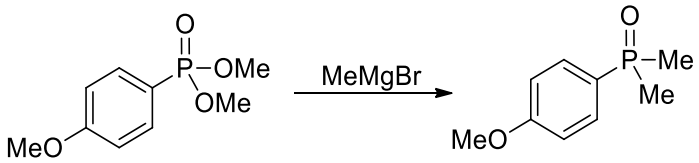

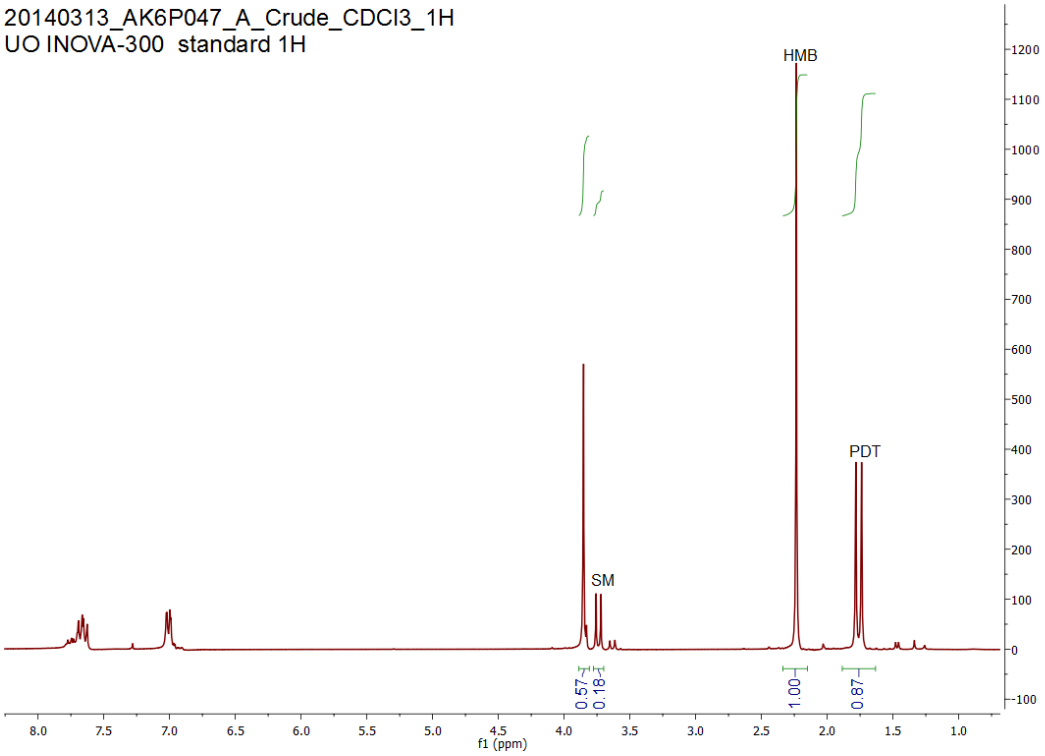

Figure A21. Dimethyl (*p*-methoxybenzene)phosphonate reacting with methylmagnesium bromide.

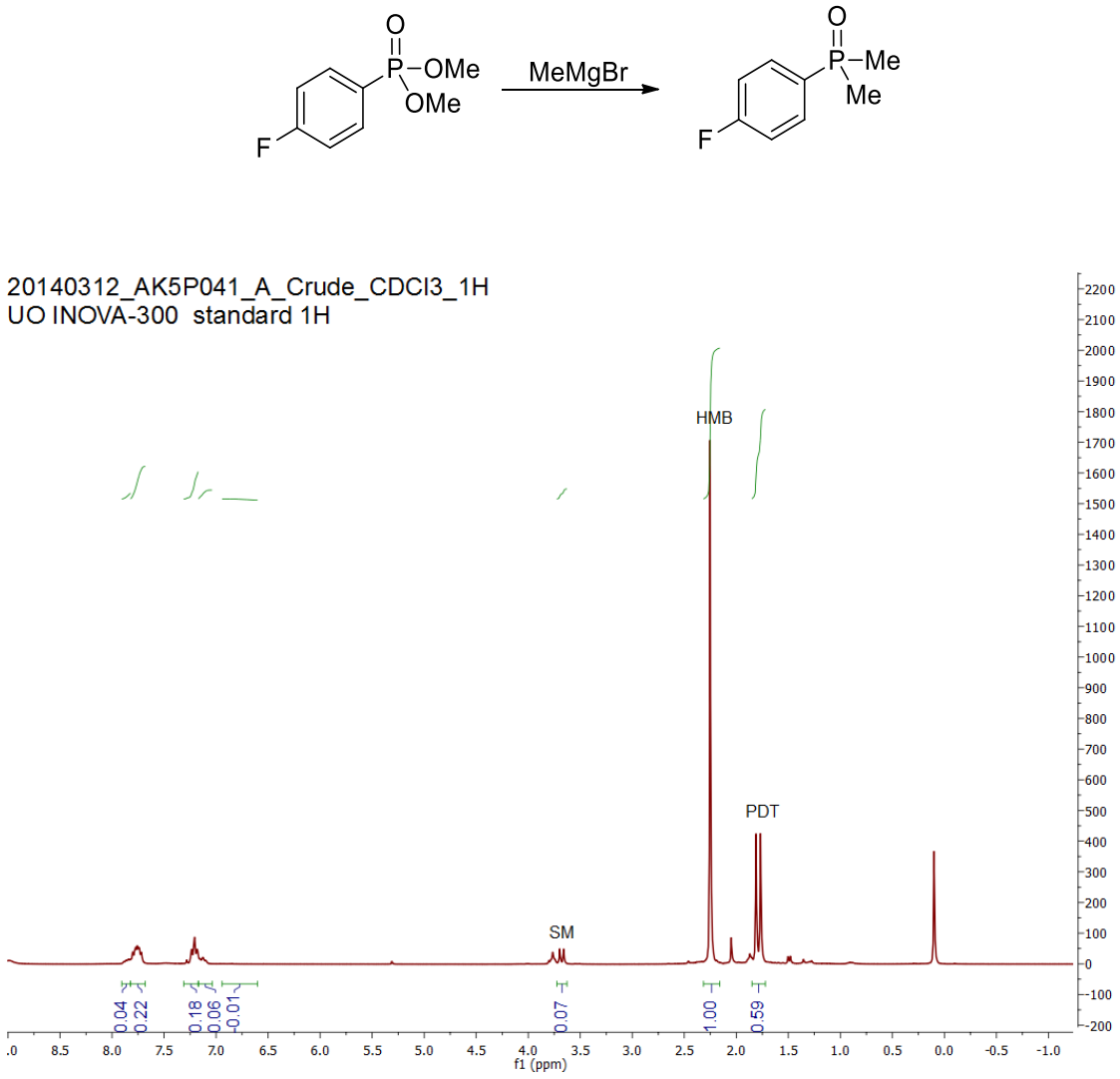

Figure A22. Dimethyl (*p*-fluorobenzene)phosphonate reacting with methylmagnesium bromide.

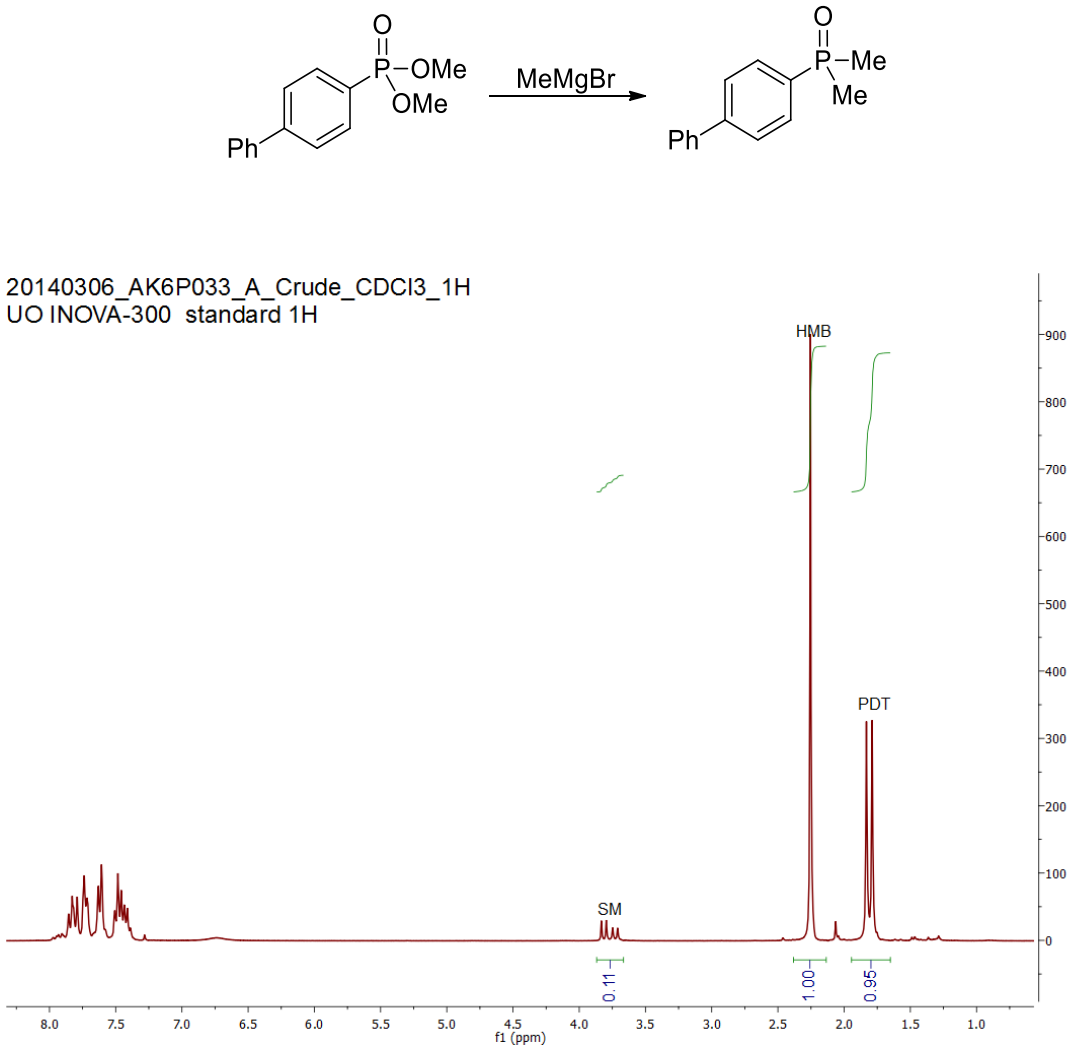

Figure A23. Dimethyl (*p*-biphenyl)phosphonate reacting with methylmagnesium bromide.

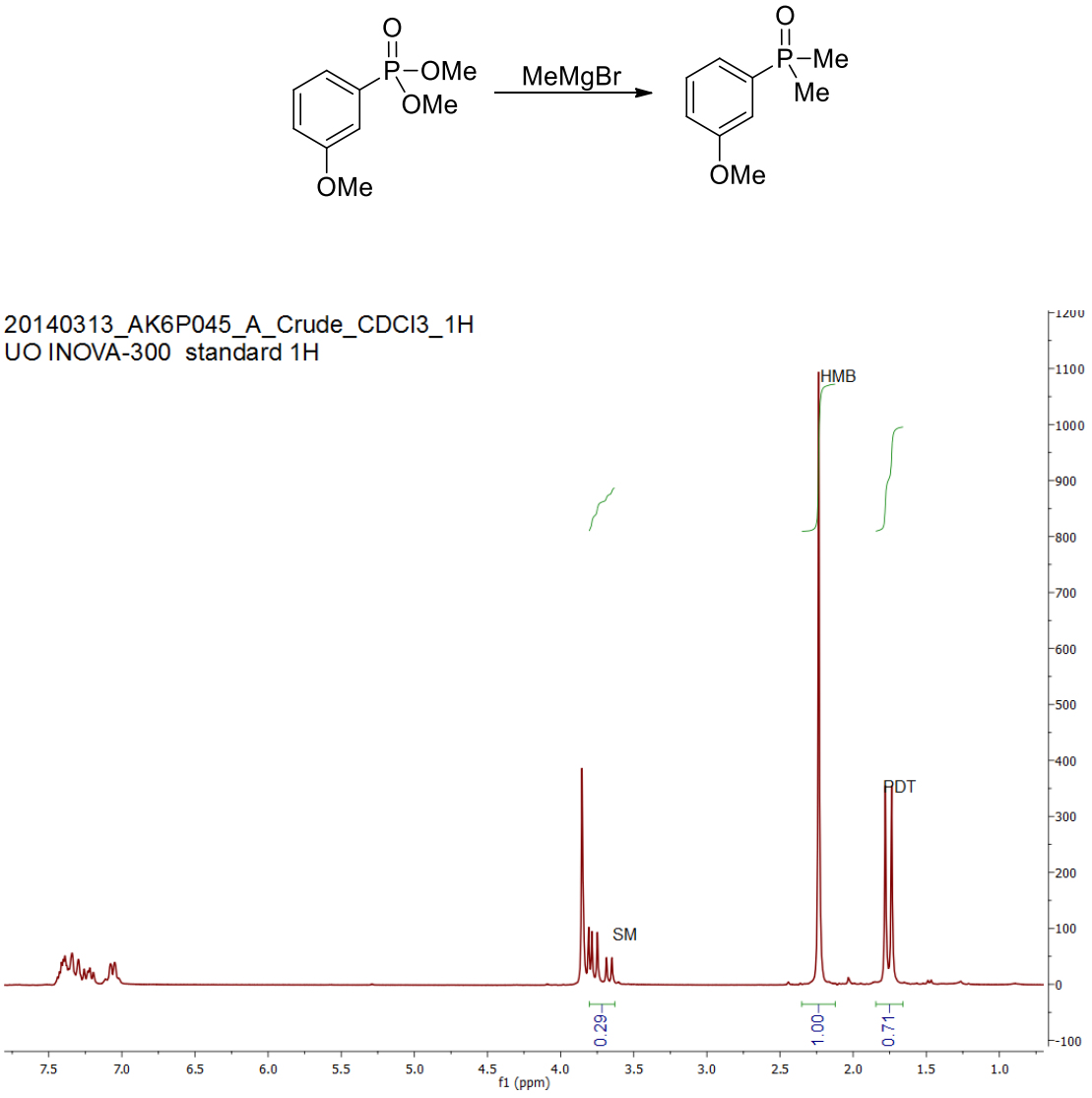

Figure A24. Dimethyl (*m*-methoxybenzene)phosphonate reacting with methylmagnesium bromide.

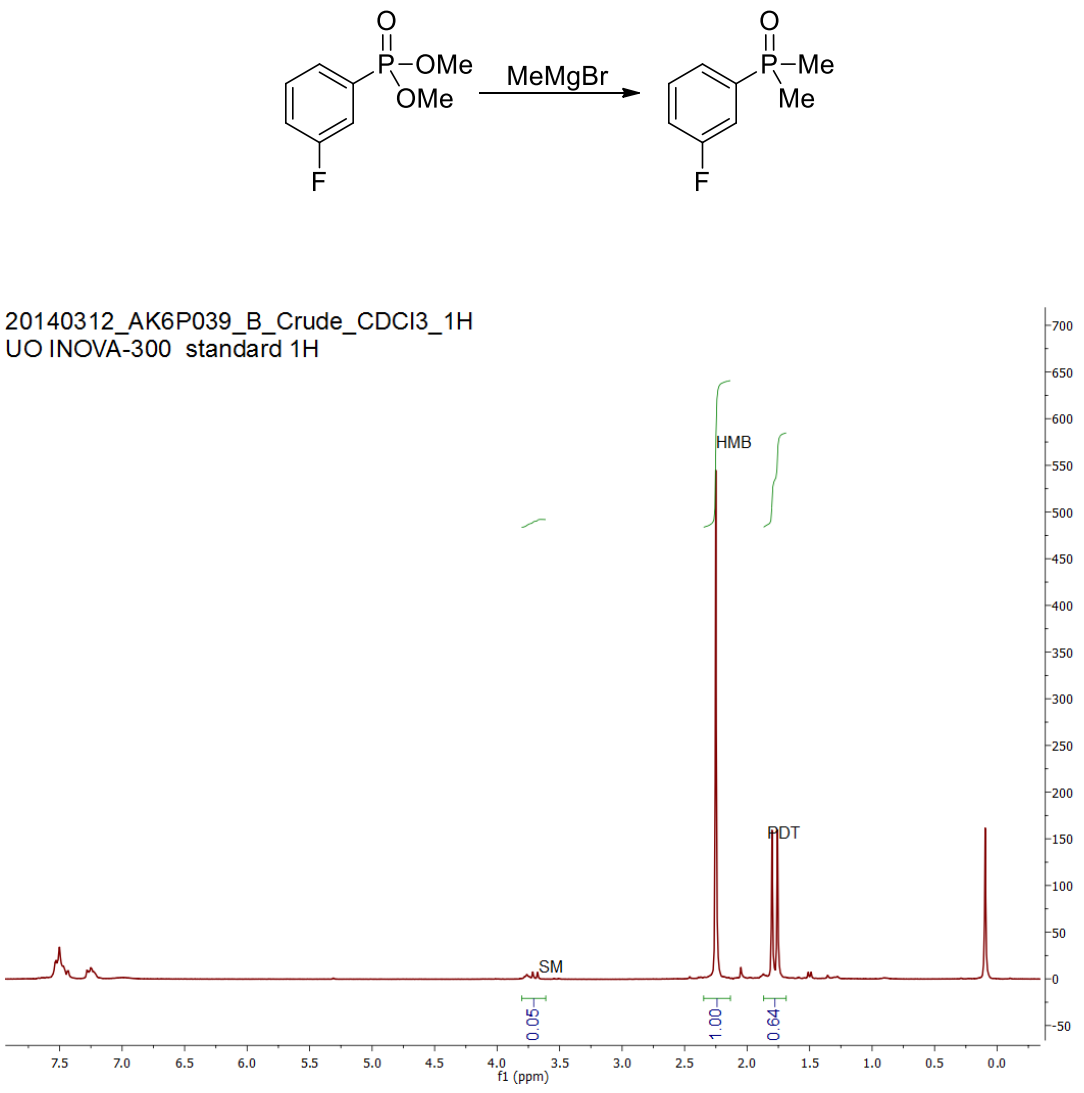

Figure A25. Dimethyl (*m*-fluorobenzene)phosphonate reacting with methylmagnesium bromide.

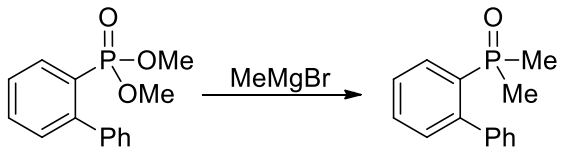

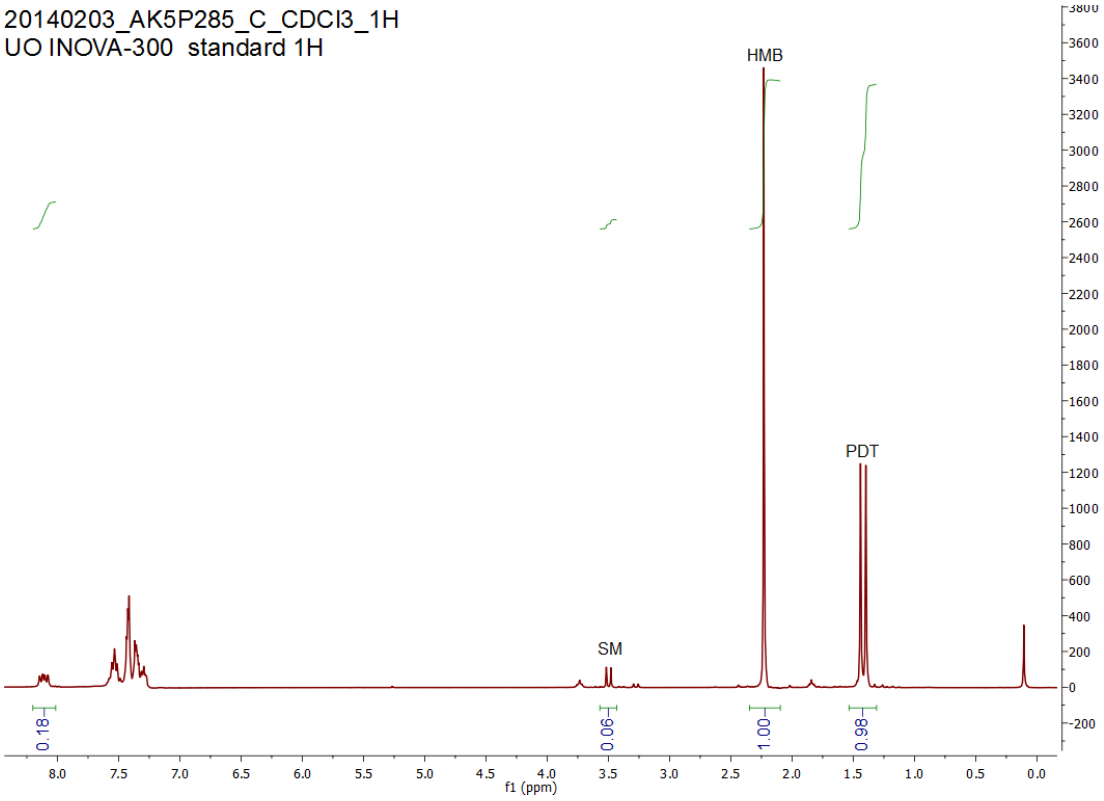

Figure A26. Dimethyl (*o*-biphenyl)phosphonate reacting with methylmagnesium bromide.

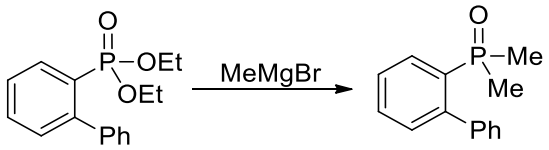

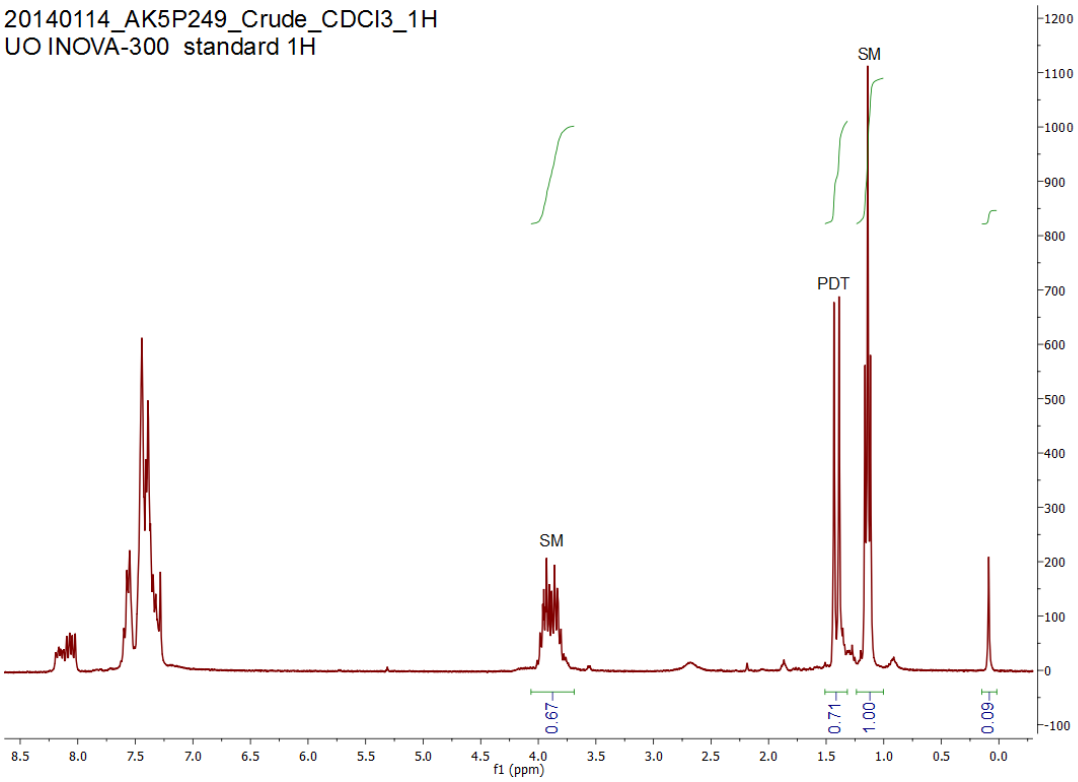

Figure A27. Diethyl (*o*-biphenyl)phosphonate reacting with methylmagnesium bromide.

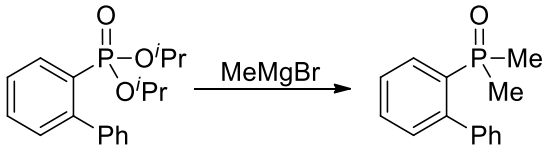

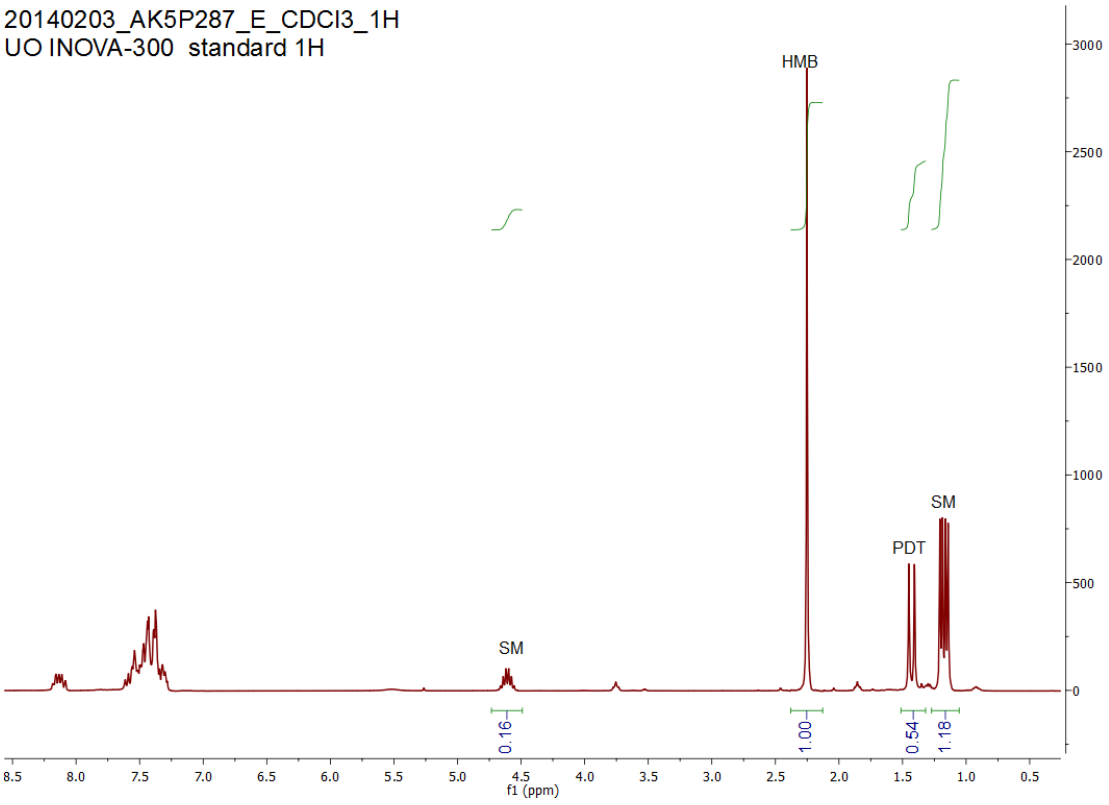

Figure A28. Diisopropyl (*o*-biphenyl)phosphonate reacting with methylmagnesium bromide.

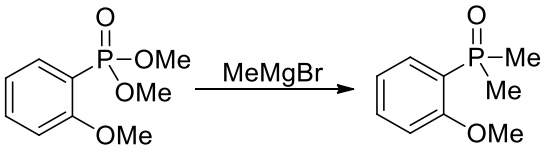

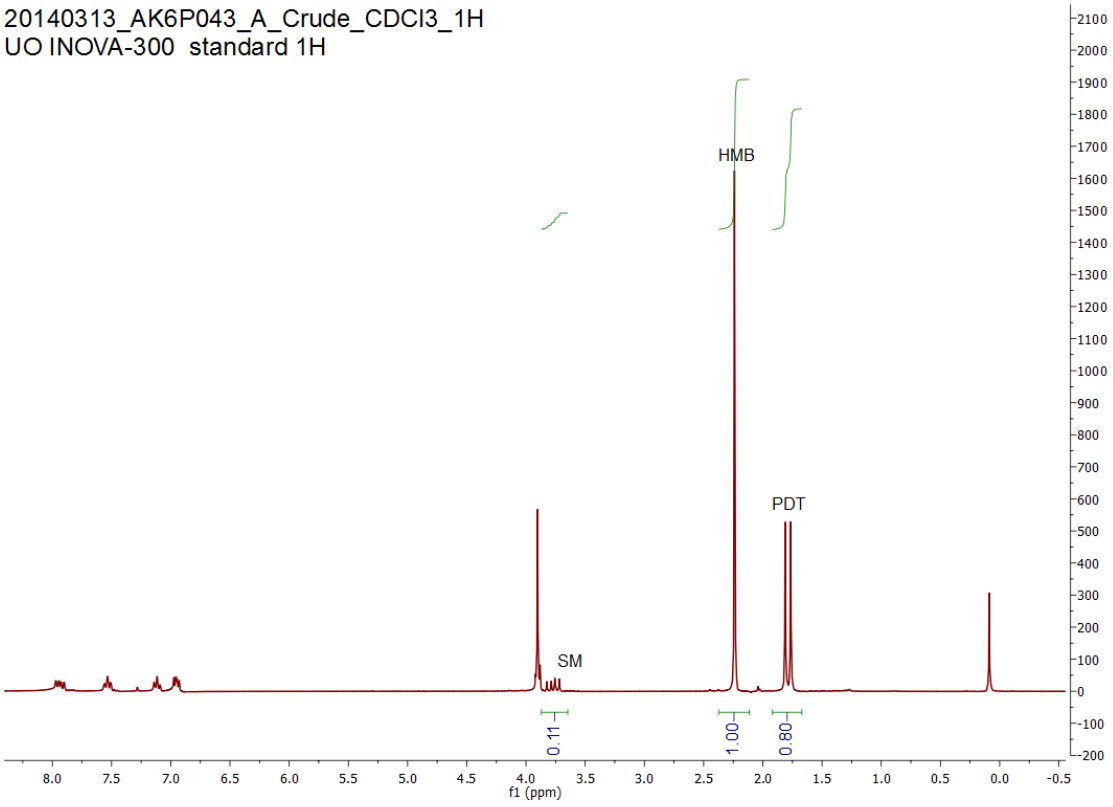

Figure A29. Dimethyl (*o*-methoxybenzene)phosphonate reacting with methylmagnesium bromide.

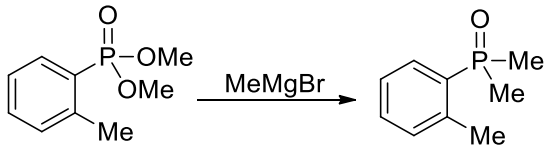

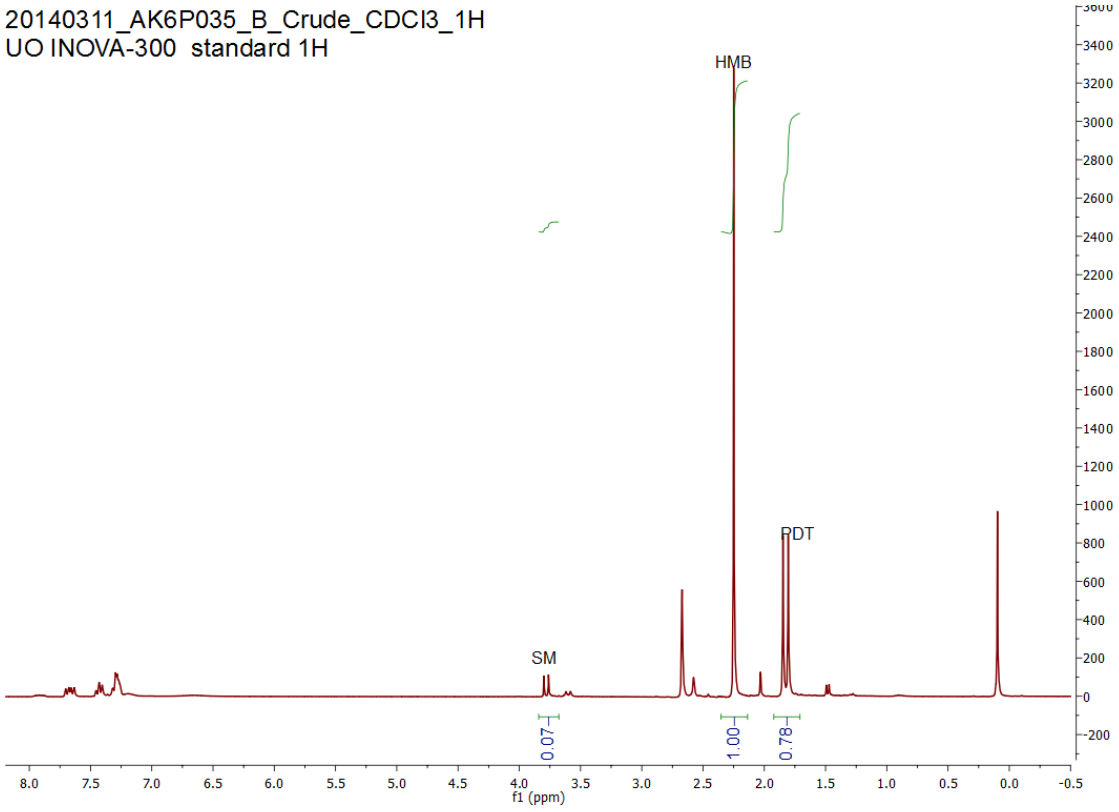

Figure A30. Dimethyl (*o*-tolyl)phosphonate reacting with methylmagnesium bromide.

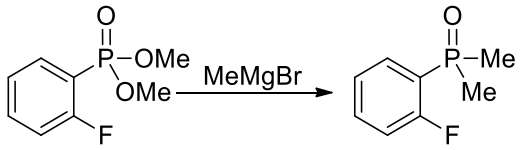

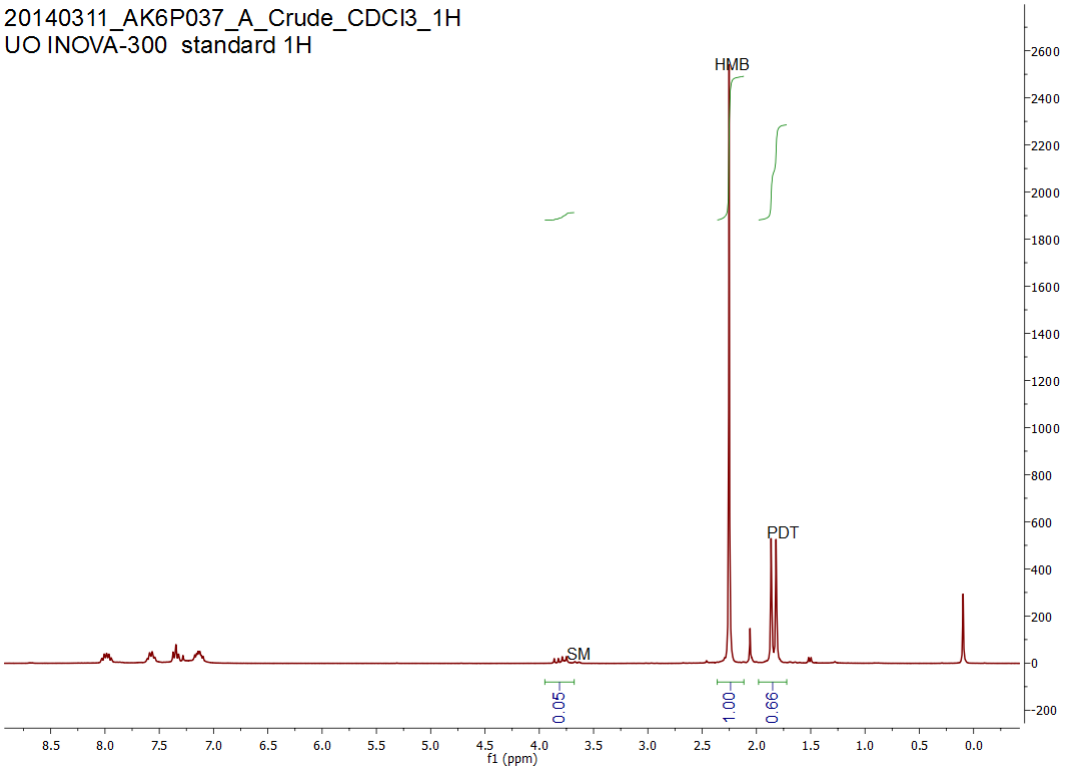

Figure A31. Dimethyl (*o*-fluorobenzene)phosphonate reacting with methylmagnesium bromide.

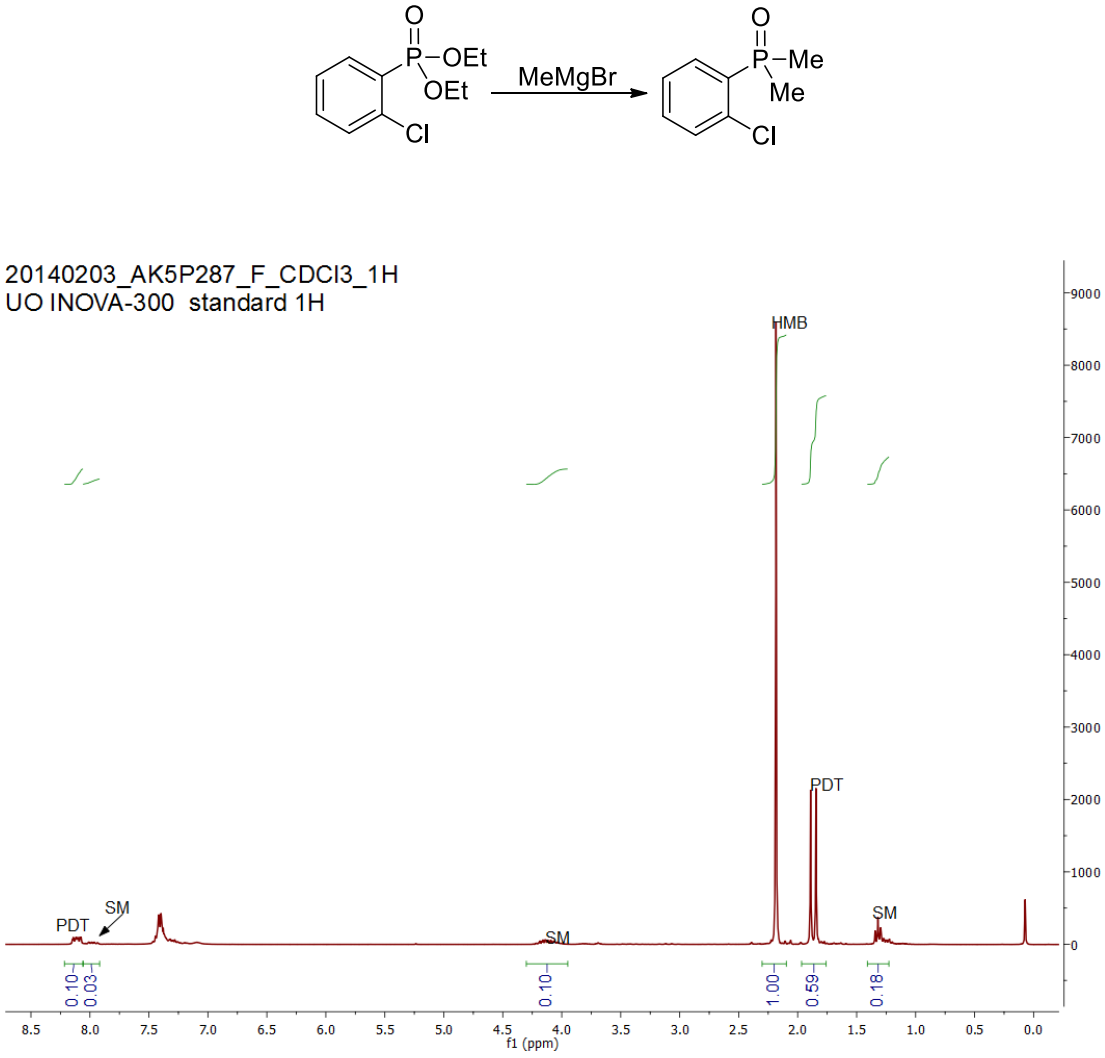

Figure A32. Diethyl (*o*-chlorobenzene)phosphonate reacting with methylmagnesium bromide.

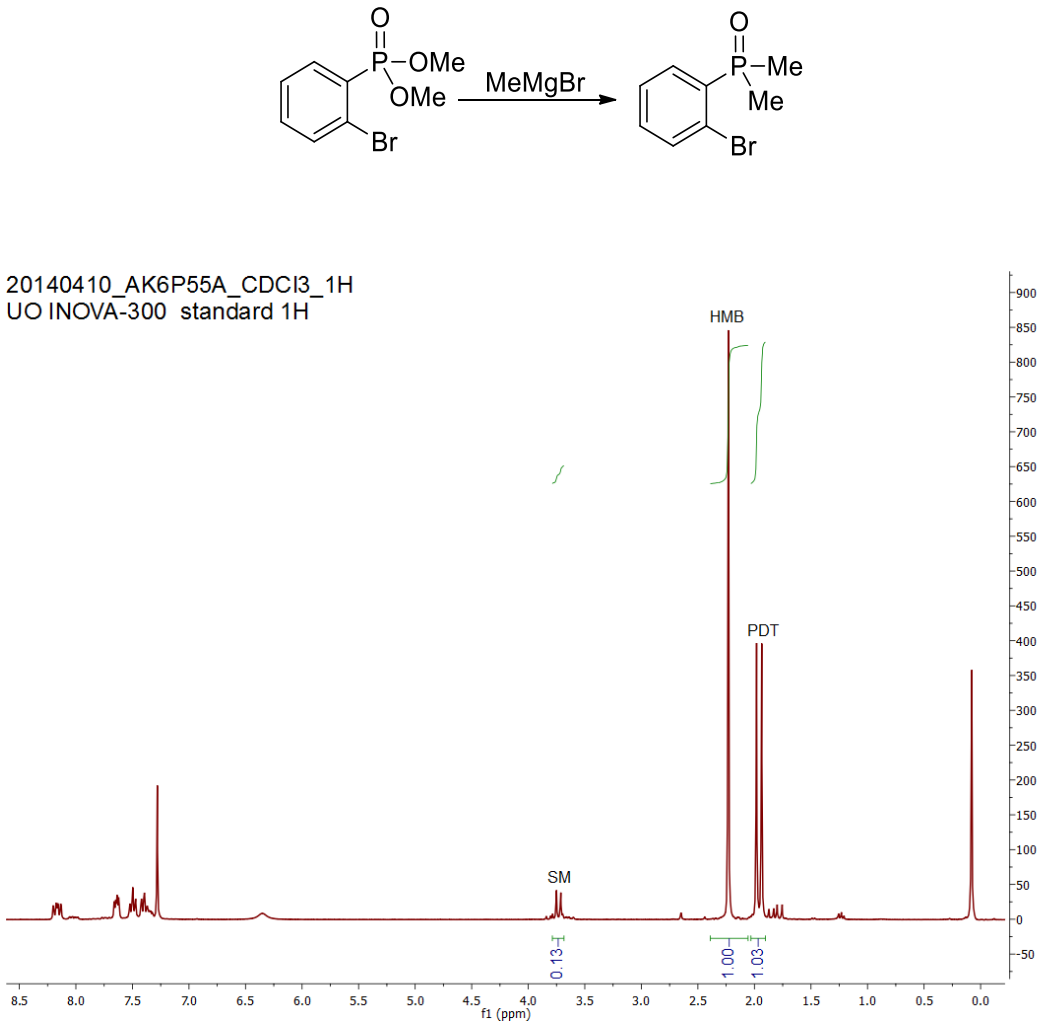

Figure A33. Dimethyl (*o*-bromobenzene)phosphonate reacting with methylmagnesium bromide.

A.6.7. Organomagnesium Study

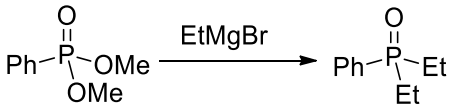

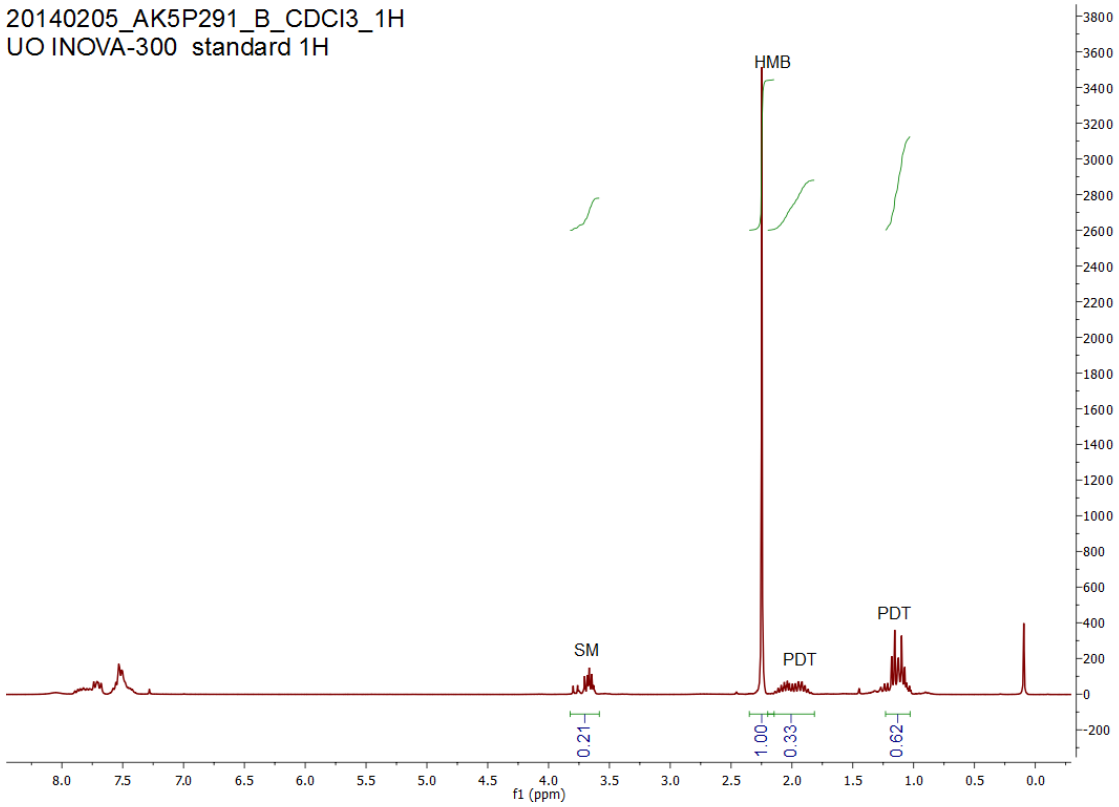

Figure A34. Dimethyl phenylphoshphonate reacting with ethylmagnesium bromide.

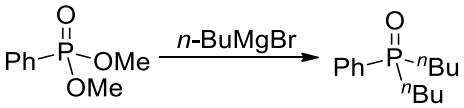

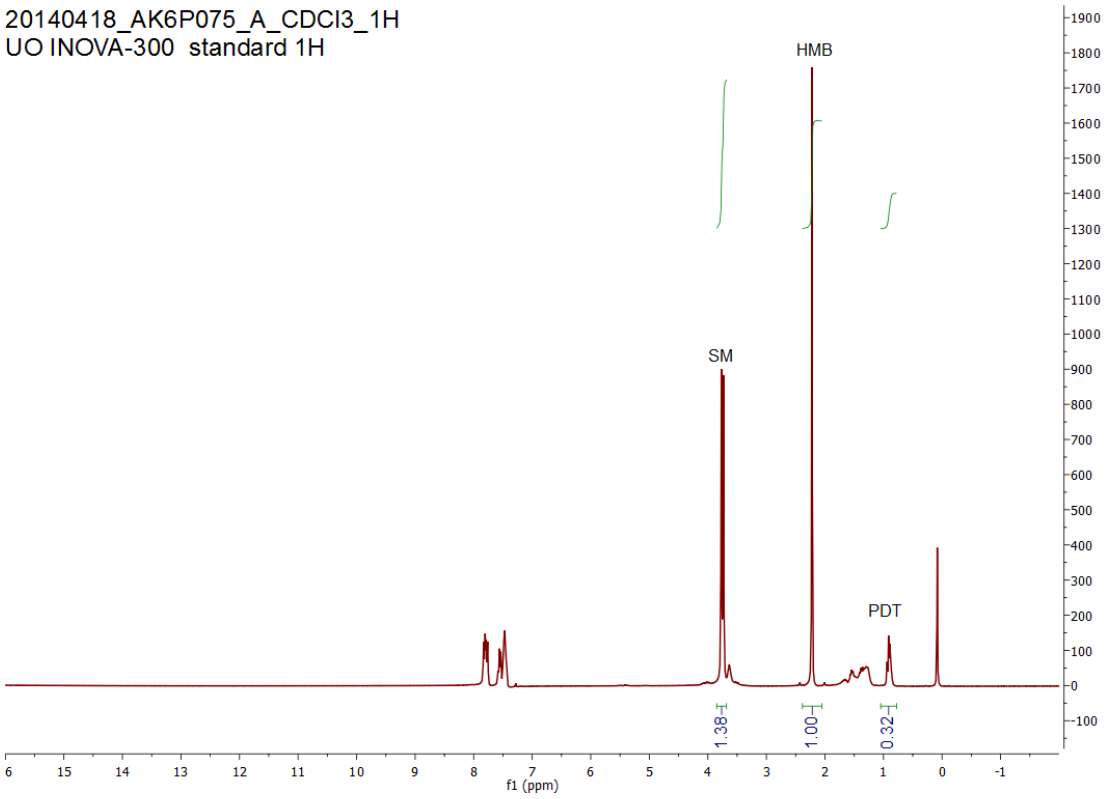

Figure A35. Dimethyl phenylphoshphonate reacting with *n*-butylmagnesium bromide.

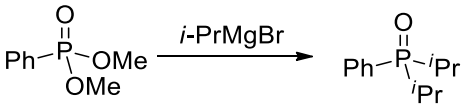

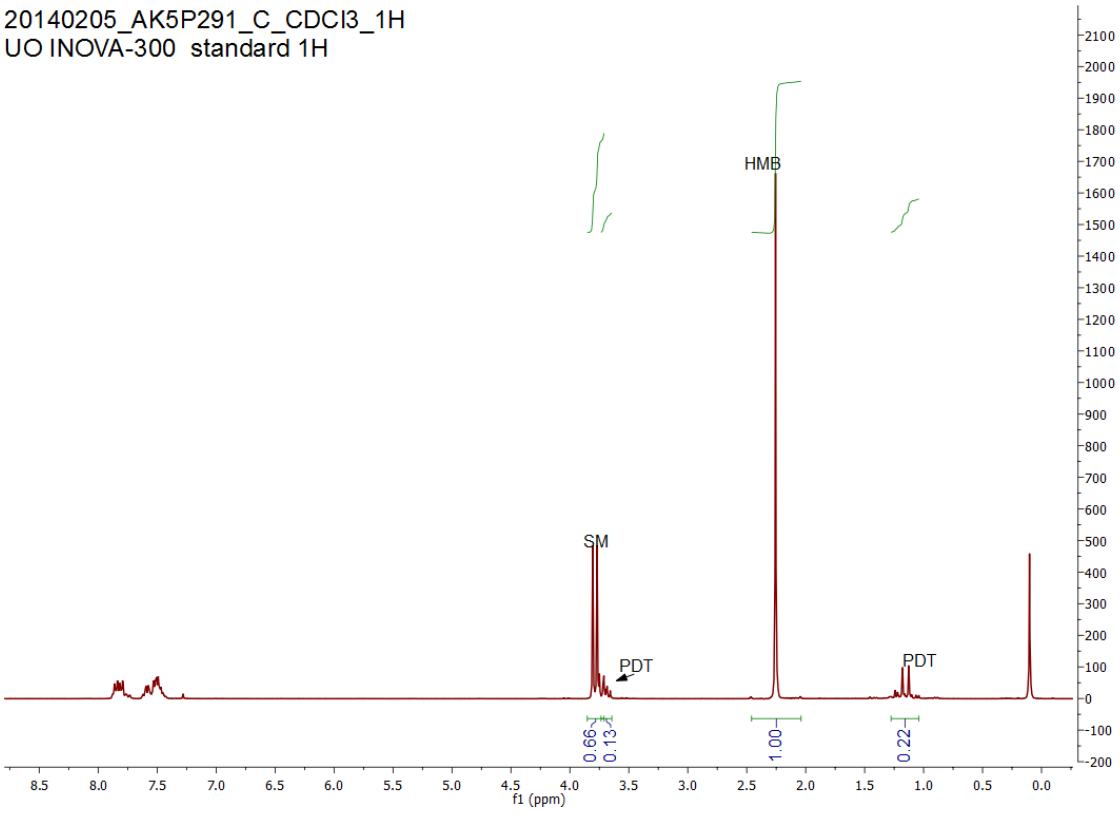

Figure A36. Dimethyl phenylphoshphonate reacting with isopropylmagnesium bromide.

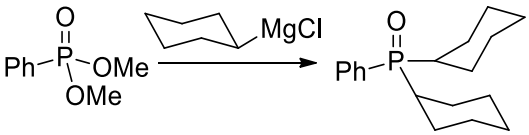

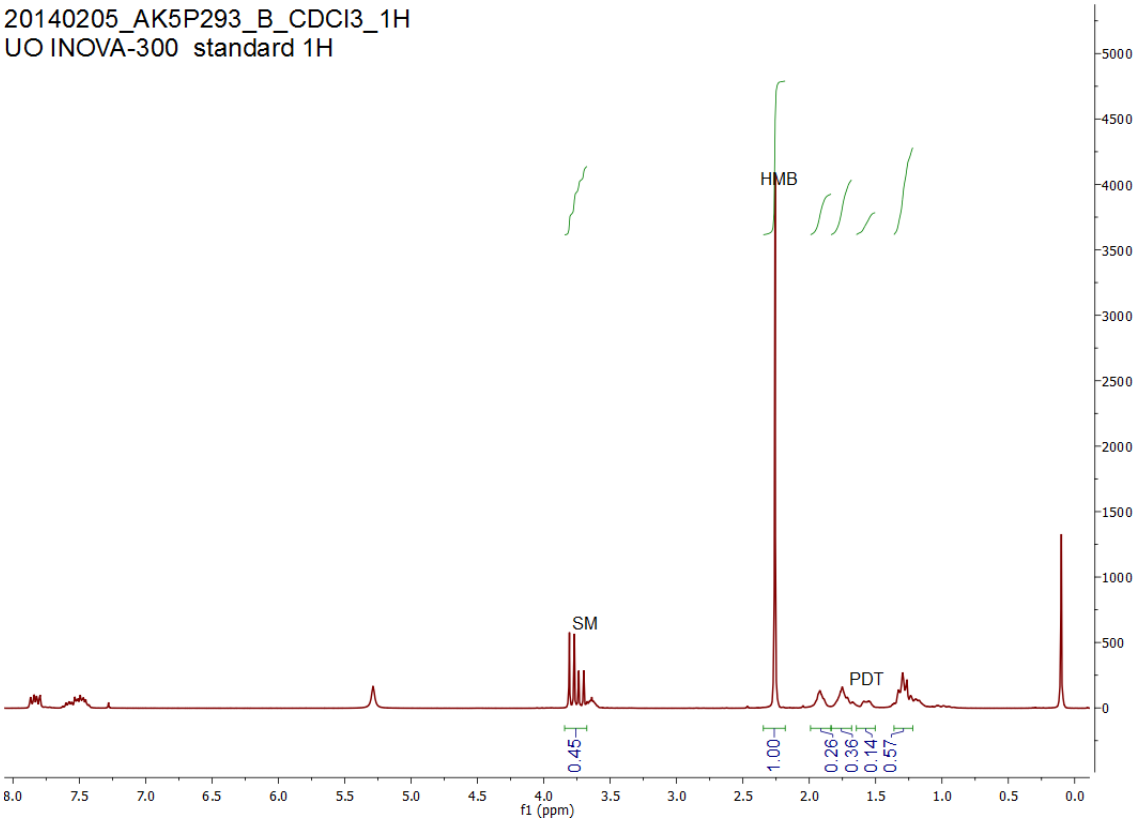

Figure A37. Dimethyl phenylphoshphonate reacting with *cyclo*-hexylmagnesium bromide.

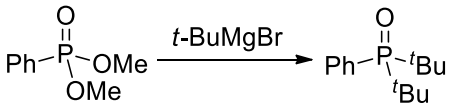

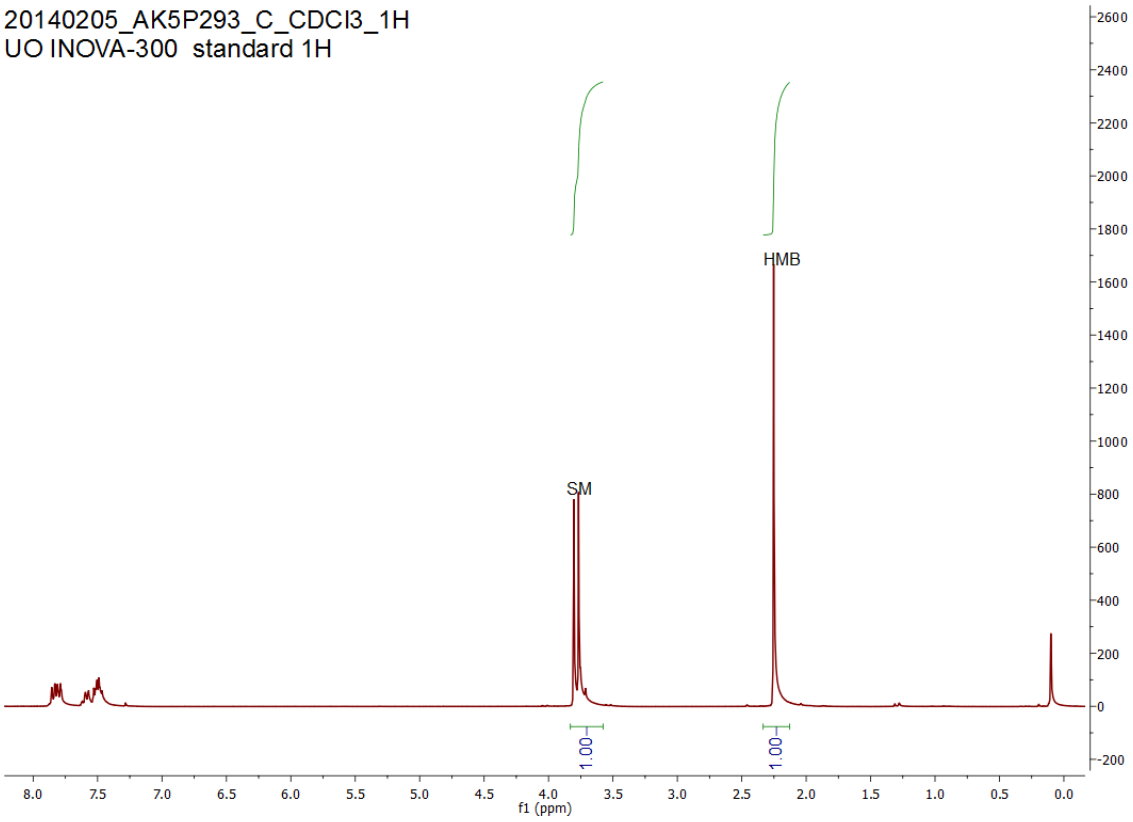

Figure A38. Dimethyl phenylphoshphonate reacting with *tert*-butylmagnesium bromide.

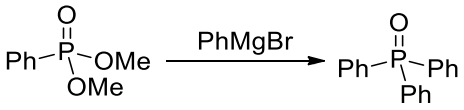

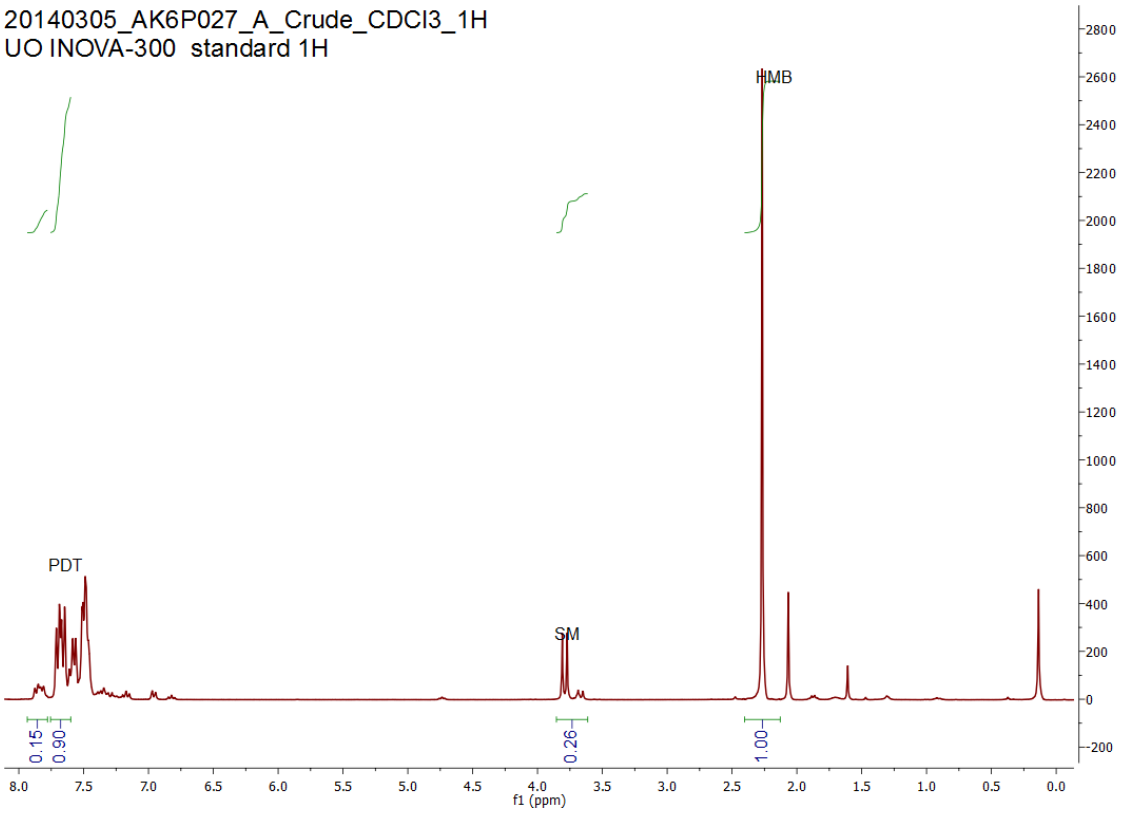

Figure A39. Dimethyl phenylphoshphonate reacting with phenylmagnesium bromide.

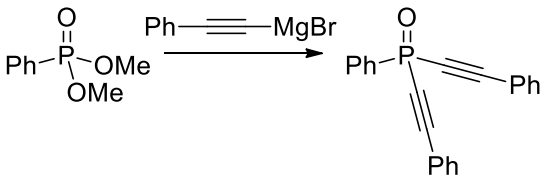

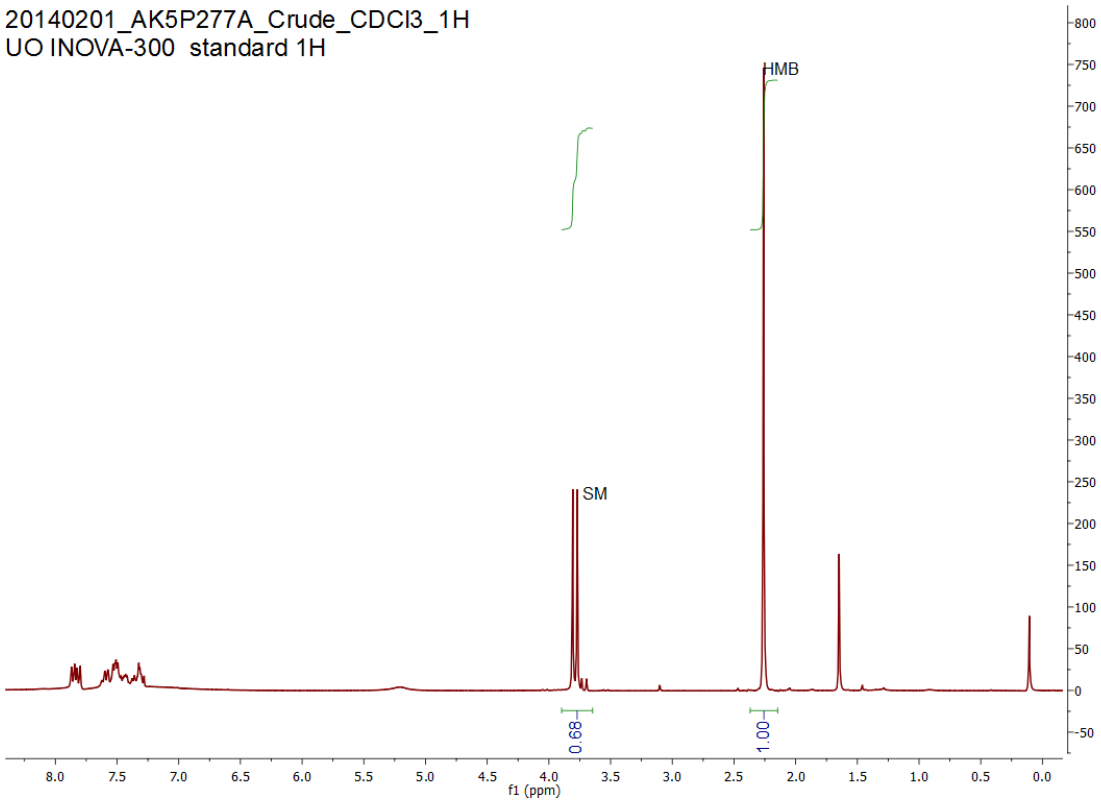

Figure A40. Dimethyl phenylphoshphonate reacting with phenylethynylmagnesium bromide.

A.6.8. Phosphinate study

Reactions were run using the general setup as noted above, with any changes noted in the figure below (Figure A41).

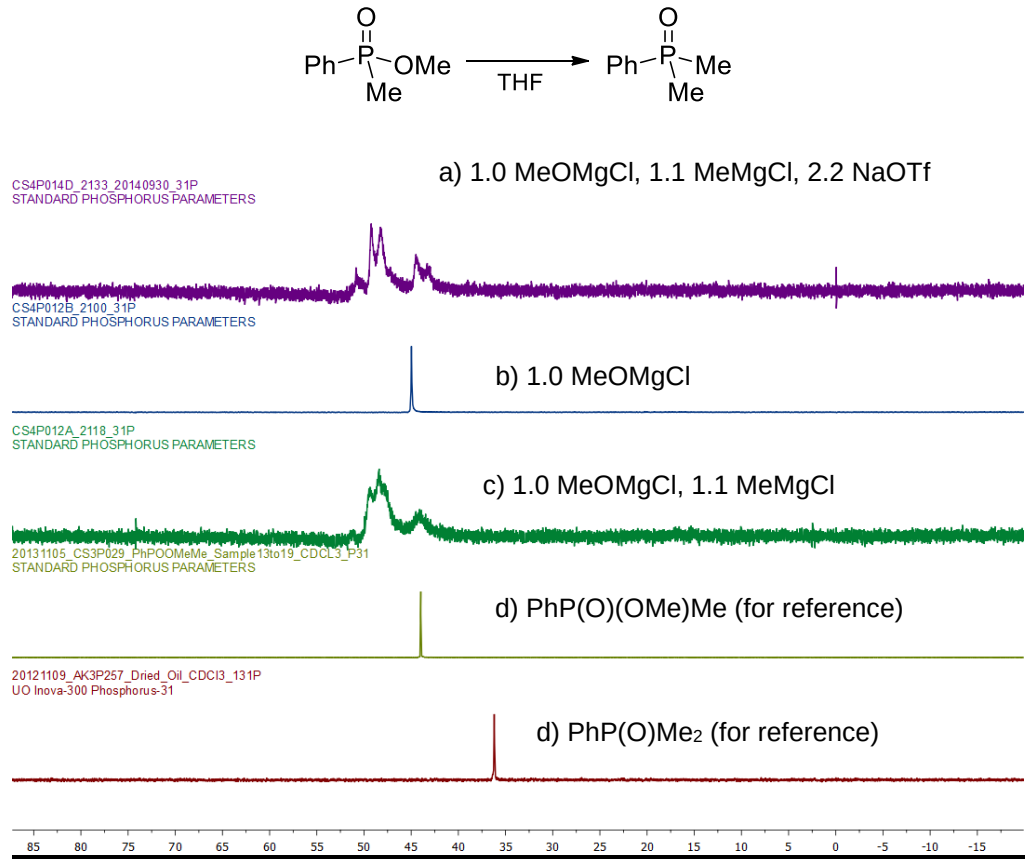

Figure A41. $^{31}P\{^{1}H\}$ analysis of PhP(O)(OMe)Me reacting under different conditions to determine phosphine oxide yield

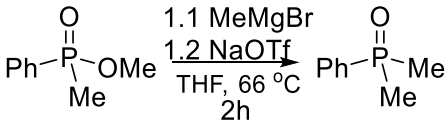

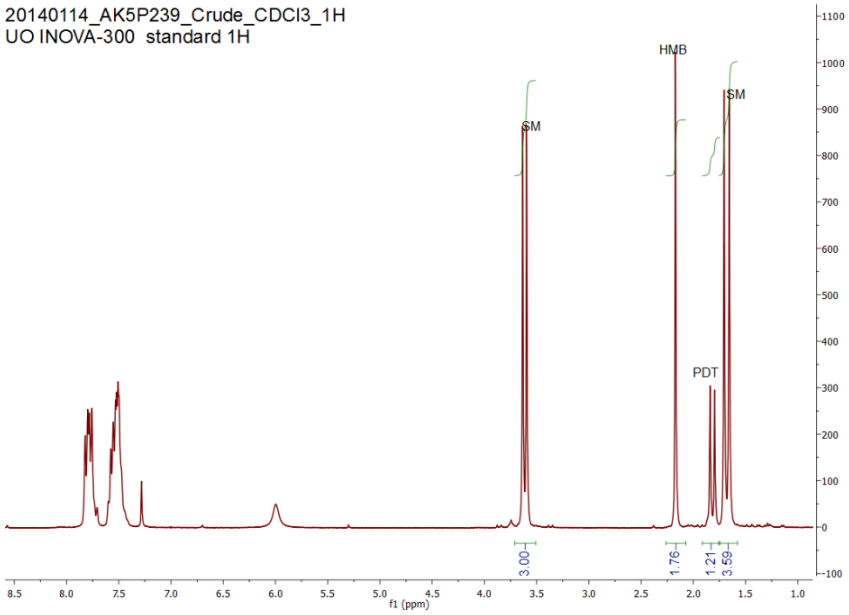

Figure A42. Methyl methyl phenylphosphinate reacting with methylmagnesium bromide in the presence of sodium triflate.

A.6.9. Ligand syntheses

A.6.9.1. [1,1'-Biphenyl]-2-yldimethylphosphine oxide

To a solution of dimethyl [1,1'-biphenyl]-2-ylphosphonate (95.1 mg, 1.8 mmol) and sodium trifluoromethanesulfonate (150.0 mg, 4.2 mmol) in THF (4 mL) at 0 °C was added methylmagnesium bromide (0.32 mL, 3.0 M, 4.0 mmol) drop wise over 5 minutes. The reaction was then brought to reflux for 2 hours. The reaction mixture was cooled to 0 °C and quenched with 0.1 M H_2SO_4 (4 mL). The reaction mixture was washed with

DCM three times (4 mL each), then the organics were collected and dried over Na_2SO_4. The mixture was filtered and dried via vacuum to afford pure product as a crystalline solid (72.6 mg, 87% yield). ^{1}H NMR (300 MHz, chloroform-d) δ 8.16 (ddd, *J* = 12.9, 6.4, 2.4 Hz, 1H), 7.61 – 7.49 (m, 2H), 7.48 – 7.34 (m, 5H), 7.34 – 7.27 (m, 1H), 1.40 (d, *J* = 13.1 Hz, 6H). ^{13}C NMR (126 MHz, chloroform-d) δ 144.48 (d, *J* = 9.9 Hz), 141.26 (d, *J* = 3.5 Hz), 132.07 (d, *J* = 8.3 Hz), 131.24 (d, *J* = 2.5 Hz), 131.08 (d, *J* = 10.0 Hz), 129.66, 128.17, 128.09, 127.47 (d, *J* = 10.8 Hz), 18.98 (d, *J* = 71.6 Hz). ^{31}P{^{1}H} NMR (121 MHz, chloroform-d) δ 35.02. HRMS (ES$^+$-TOF) m/z: $[M+Na]^+$ Calcd. for $C_{14}H_{15}ONaP$ 253.0751; Found 253.0758.

A.6.9.2. [1,1'-Biphenyl]-2-yldimethylphosphine

Under an inert atmosphere, [1,1'-biphenyl]-2-yldimethylphosphine oxide (368.0 mg, 1.6 mmol) was added to diisobutylaluminum hydride (1.2116g, 8.0 mmol) and toluene (up to 6 mL) in a heavy walled unregulated pressure vessel. The reaction mixture was allowed to off-gas overnight before being sealed and heated to 150 °C for 12 hours. The reaction mixture was allowed to cool, then (under an atmosphere of N_2) quenched with degassed 0.1M HCl and diluted out with diethyl ether (20 mL). The aqueous layer was washed 3x with ether. Collected organics were dried over Na_2SO_4, then filtered and dried under vacuum, affording very pure [1,1'-biphenyl]-2-yldimethylphosphine as a colorless crystalline solid (288.3 mg, 84% yield). ^{1}H NMR (500 MHz, chloroform-d) δ 7.37 (ddd, *J* = 7.0, 4.1, 1.9 Hz, 1H), 7.29 – 7.25 (m, 4H), 7.25 – 7.19 (m, 3H), 7.11 (ddd, *J* = 6.2, 3.9, 2.1 Hz, 1H), 0.97 (d, *J* = 3.8 Hz, 6H). ^{13}C NMR (126 MHz, chloroform-d) δ 146.69 (d, *J* = 23.1 Hz), 142.00 (d, *J* = 4.3 Hz), 140.49 (d, *J* = 18.3 Hz), 129.82 (d, *J* =

3.9 Hz), 129.58 (d, *J* = 4.3 Hz), 128.89, 127.83, 127.20 (d, *J* = 21.2 Hz), 14.04 (d, *J* = 13.8 Hz). $^{31}P\{^{1}H\}$ NMR (202 MHz, chloroform-d) δ -51.86. HRMS (EI^{+}-JEOL MStation) m/z: $[M]^{+}$ Calcd. for $C_{14}H_{15}P$ 214.09114; Found 214.09049.

A.6.9.3. Propane-1,3-diylbis(diphenylphosphine oxide)

To a solution of tetraethyl propane-1,3-diylbis(phosphonate) (1.0277 g, 3.16 mmol) and sodium trifluoromethanesulfonate (4.421 g, 25 mmol) in THF (35 mL) at 0 °C was added phenylmagnesium bromide (11.0 mL, 1.73 M, 19 mmol) drop wise over 15 minutes. The reaction was then brought to reflux for 2 hours. The reaction mixture was cooled to 0 °C and quenched with 0.1 M H_2SO_4 (40 mL). The reaction mixture was washed with DCM three times (35 mL each), then the organics were collected and dried over Na_2SO_4. The organics were filtered and evaporated to dryness, yielding a slightly yellow clear extremely viscous paste. This was triturated with both H_2O and pentane to afford a slurry of fluffy off-white crystalline solid, or propane-1,3-diylbis(diphenylphosphine oxide)●monohydrate (1.3160 g, 90% yield). ^{1}H NMR (300 MHz, chloroform-d) δ 7.76 – 7.62 (m, 8H), 7.46 (m, 12H), 2.50 (dt, *J* = 10.8, 7.6 Hz, 4H), 2.28 (H_2O, s, 2H), 2.00 (dq, *J* = 20.0, 12.8, 9.6 Hz, 2H). $^{31}P\{^{1}H\}$ NMR (121 MHz, chloroform-d) δ 32.59.

A.6.9.4. 1,3-Bis(diphenylphosphino)propane

Under an inert atmosphere, propane-1,3-diylbis(diphenylphosphine oxide)●monohydrate (50.0 mg, 0.11 mmol) was added to diisobutylaluminum hydride (161.2 mg, 1.1 mmol) and toluene (up to 0.5 mL) in a heavy walled unregulated pressure

vessel. The reaction mixture was allowed to off-gas overnight before being sealed and heated to 150 °C for 12 hours. The reaction mixture was allowed to cool, then (under an atmosphere of N_2) quenched with degassed 0.1M HCl and diluted out with diethyl ether (20 mL). The aqueous layer was washed 3x with ether. Collected organics were dried over Na_2SO_4, then filtered and dried under vacuum, affording very pure as an off white crystalline solid (41.3 mg, 93% yield). Properties matched a purchased standard. ^{1}H NMR (300 MHz, chloroform-d) δ 7.51 – 7.23 (m, 10H), 2.24 (t, *J* = 7.8 Hz, 4H), 1.65 (tt, *J* = 16.1, 8.7 Hz, 1H). ^{31}P{^{1}H} NMR (121 MHz, chloroform-d) δ -17.36.

A.6.10. Other Experiments

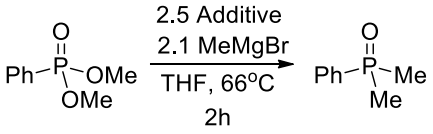

Additive	% Conv.	% Yield[a]
Me_3P=O	77	12
cyHex_3P=O	68	<0.1
KO*t*Bu	65	<0.1

Figure A43. Lewis base effects on reactivity. Hydrolysis products observed for all reactions upon workup.

A.7. Additional spectra

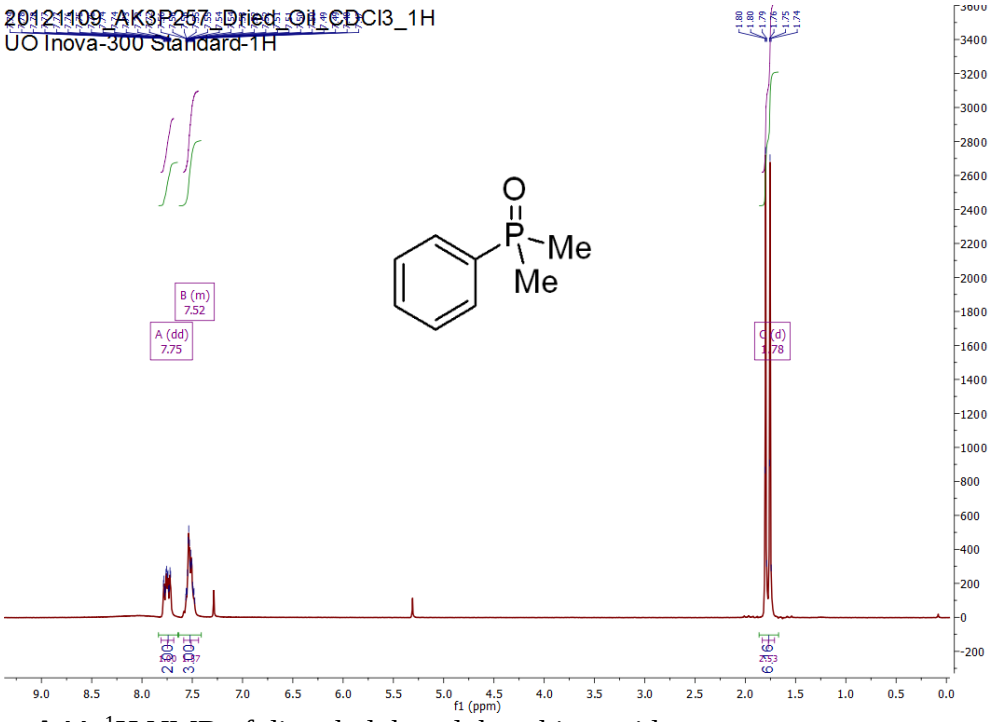

Figure A44. ^{1}H NMR of dimethylphenylphosphine oxide

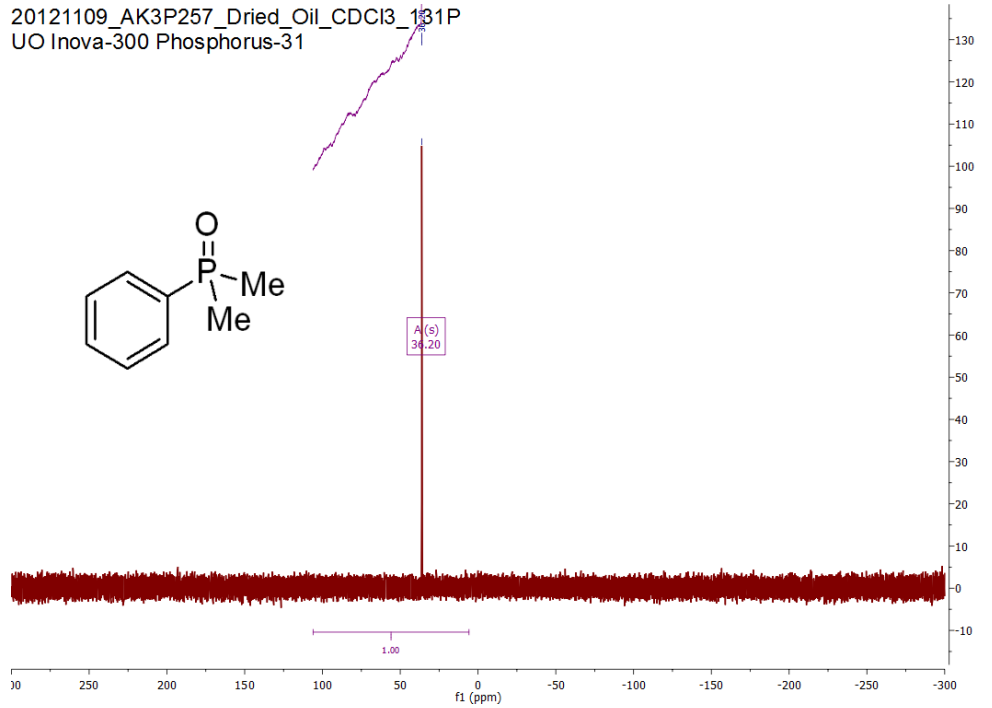

Figure A45. ^{31}P{^{1}H} NMR of dimethylphenylphosphine oxide

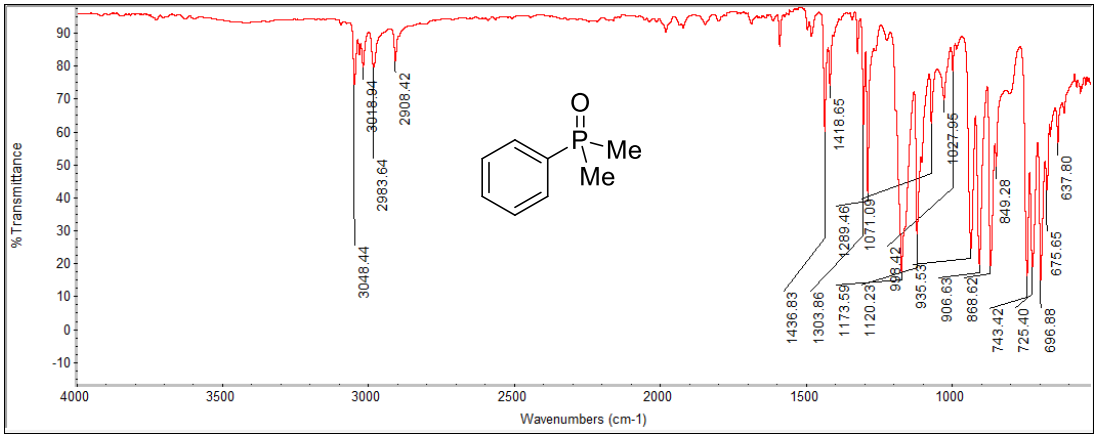

Figure A46. Infrared absorption spectrum of dimethylphenylphosphine oxide

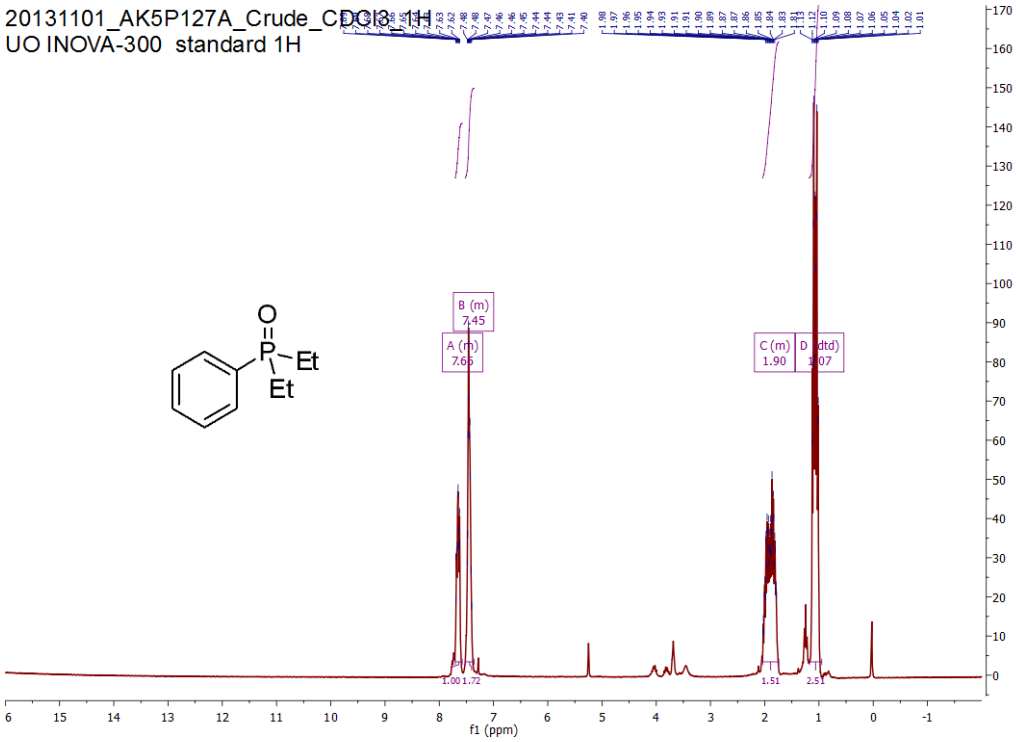

Figure A47. ^{1}H NMR of diethylphenylphosphine oxide

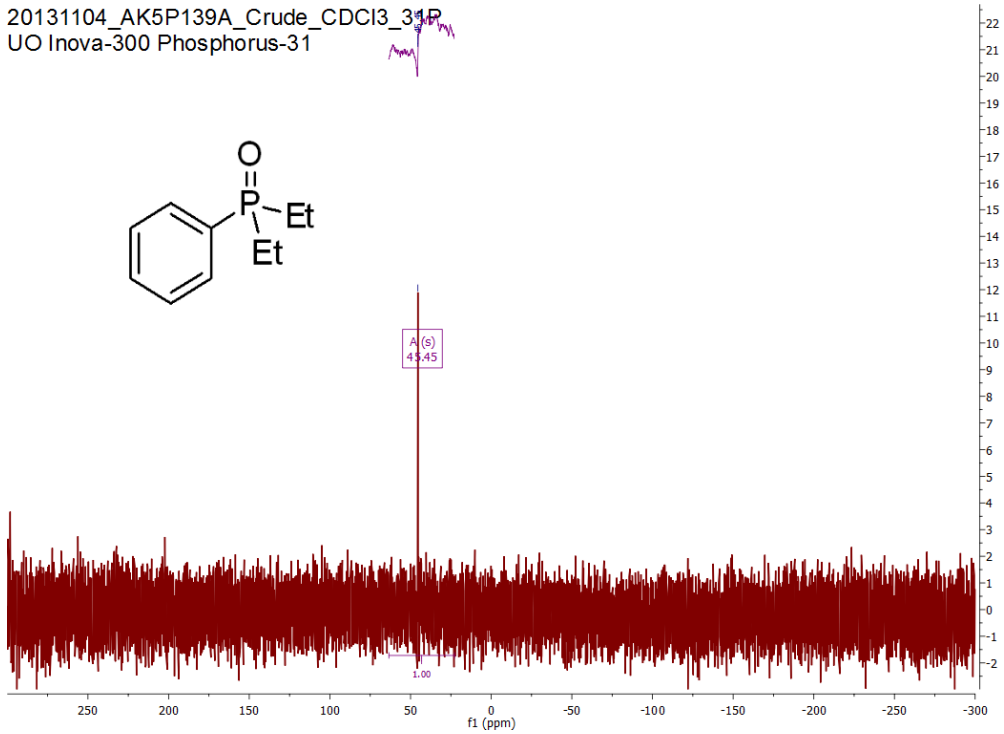

Figure A48. $^{31}P\{^{1}H\}$ NMR of diethylphenylphosphine oxide

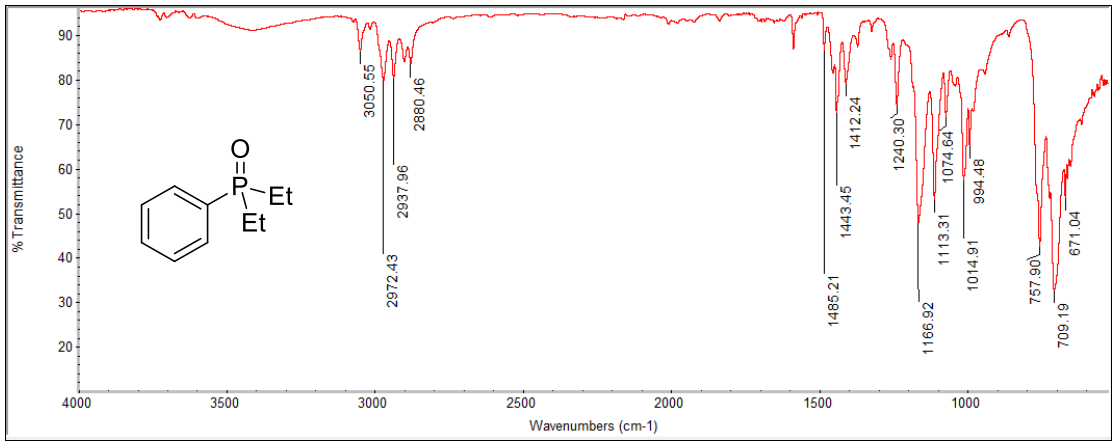

Figure A49. Infrared absorption spectrum of diethylphenylphosphine oxide

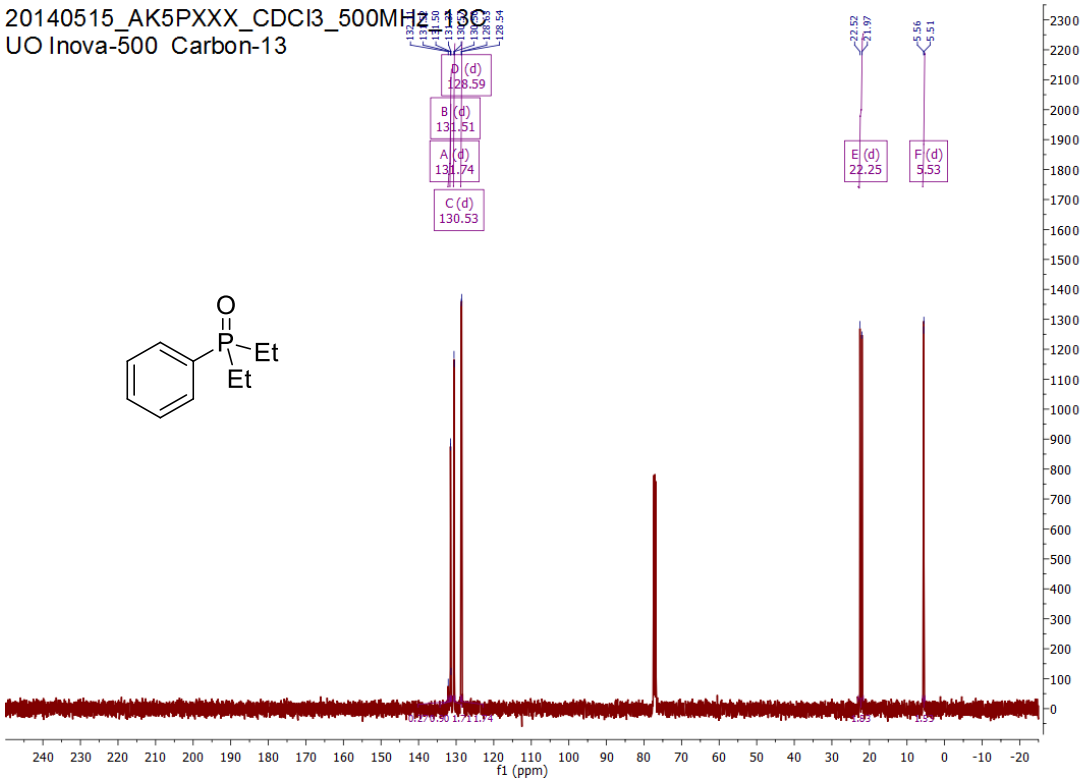

Figure A50. ^{13}C NMR of diethylphenylphosphine oxide

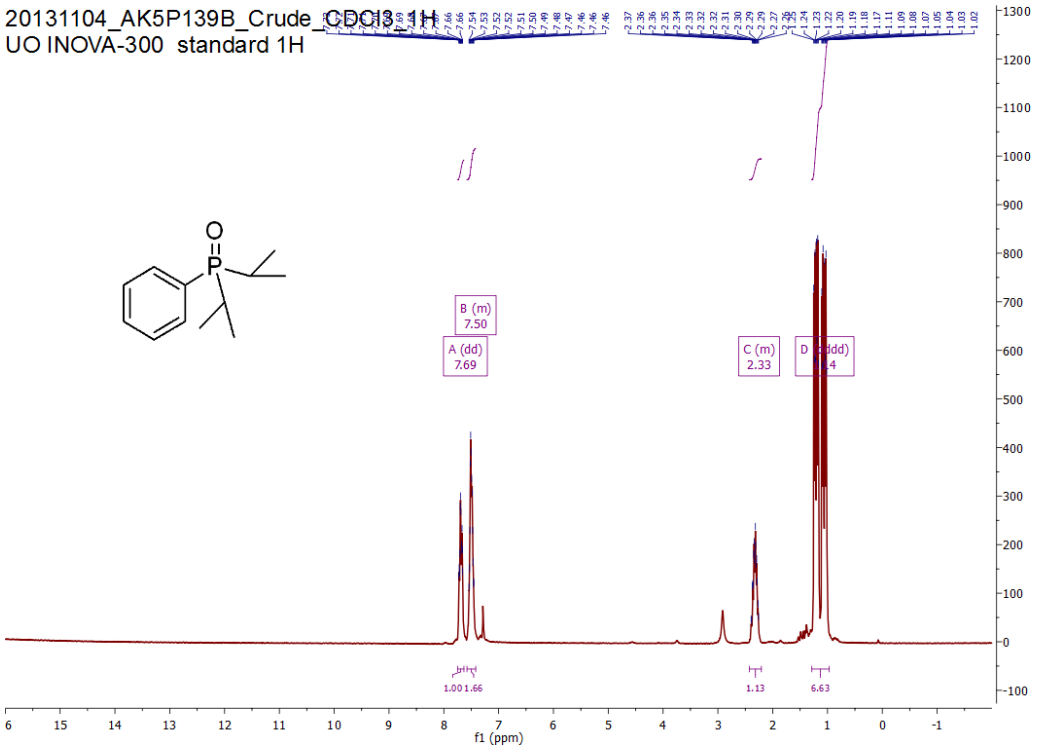

Figure A51. ^{1}H NMR of diisopropylphenylphosphine oxide

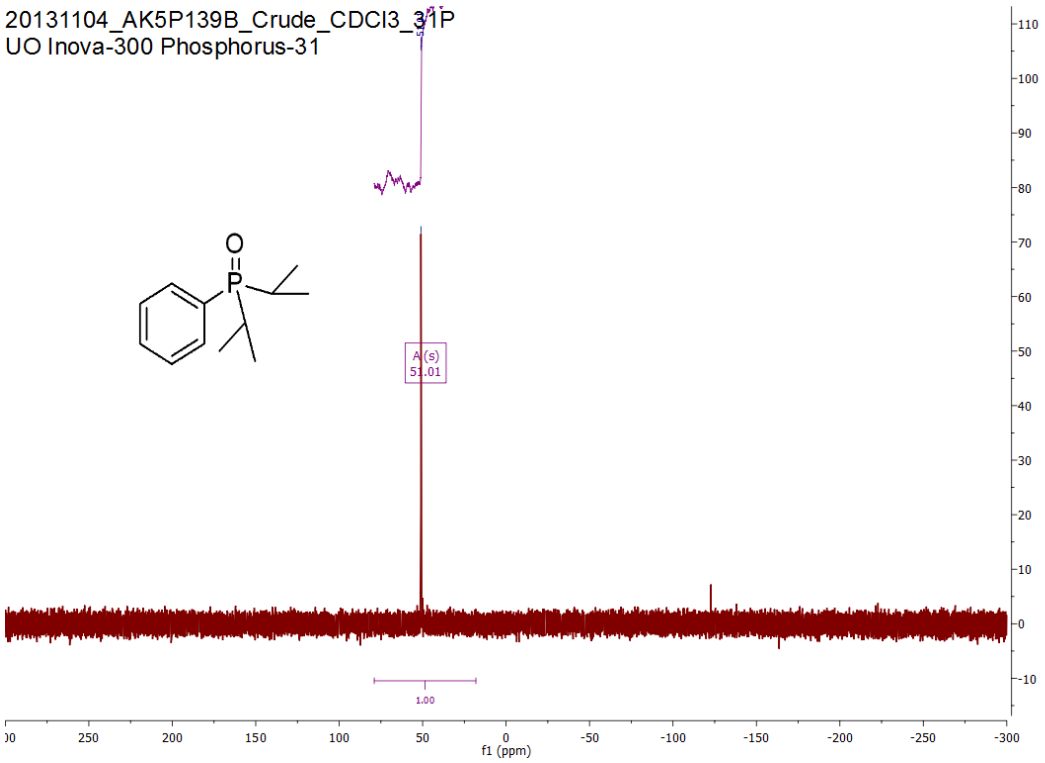

Figure A52. $^{31}P\{^{1}H\}$ NMR of diisopropylphenylphosphine oxide

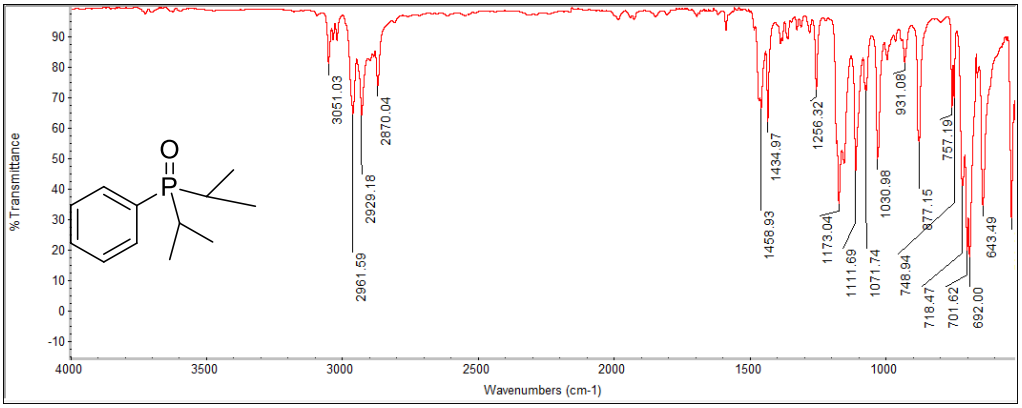

Figure A53. Infrared absorption spectrum of diisopropylphenylphosphine oxide

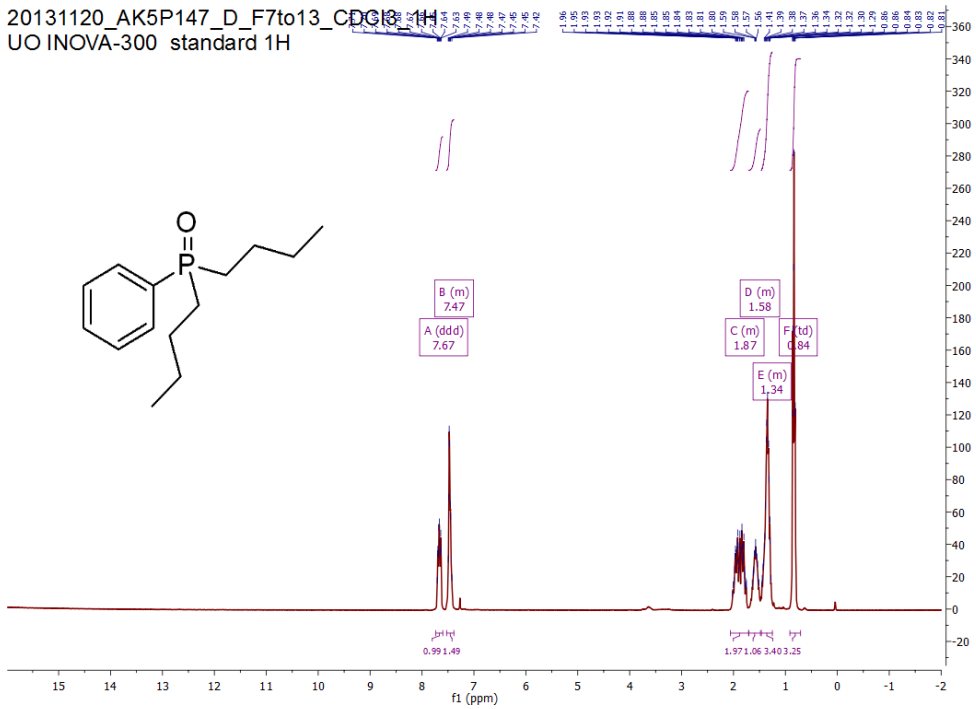

Figure A54. ^{1}H NMR of di(*n*-butyl)phenylphosphine oxide

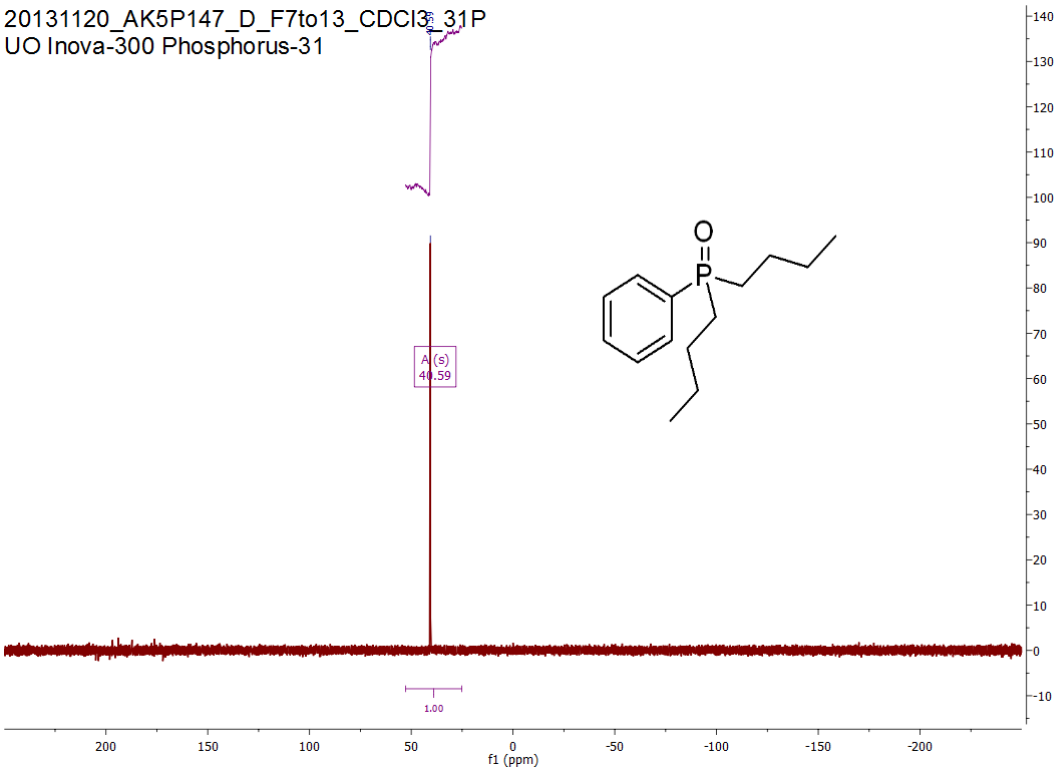

Figure A55. ^{31}P{^{1}H} NMR of di(*n*-butyl)phenylphosphine oxide

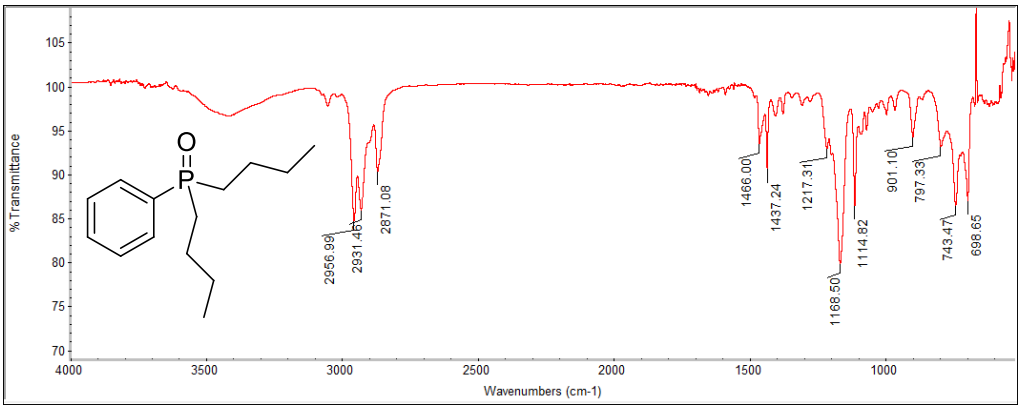

Figure A56. Infrared absorption spectrum of di(*n*-butyl)phenylphosphine oxide

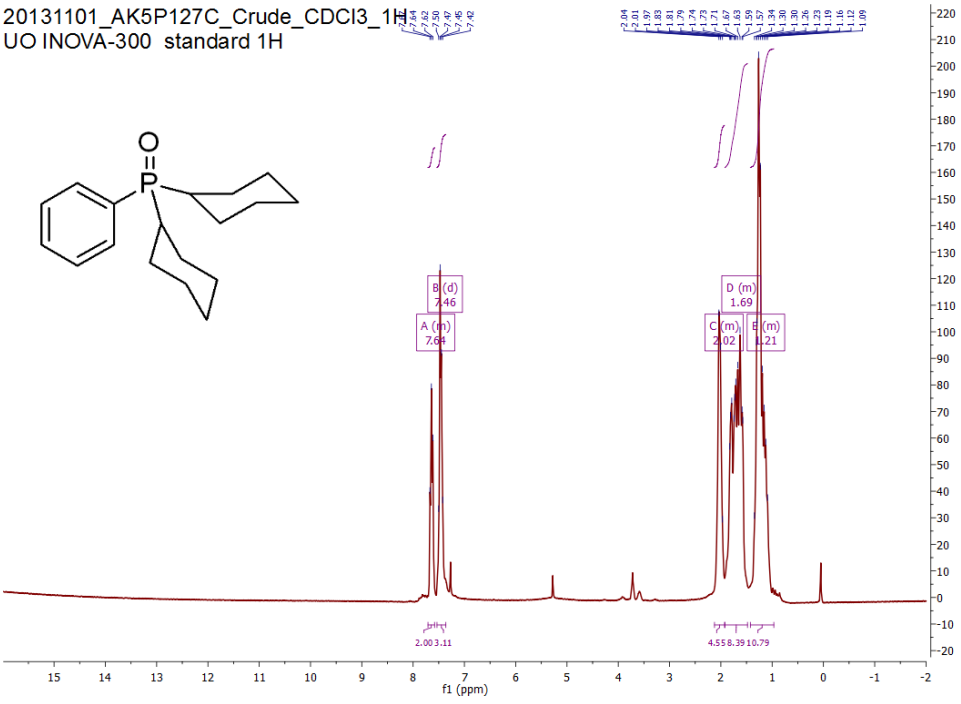

Figure A57. ^{1}H NMR of di(*cyclo*-hexyl)phenylphosphine oxide

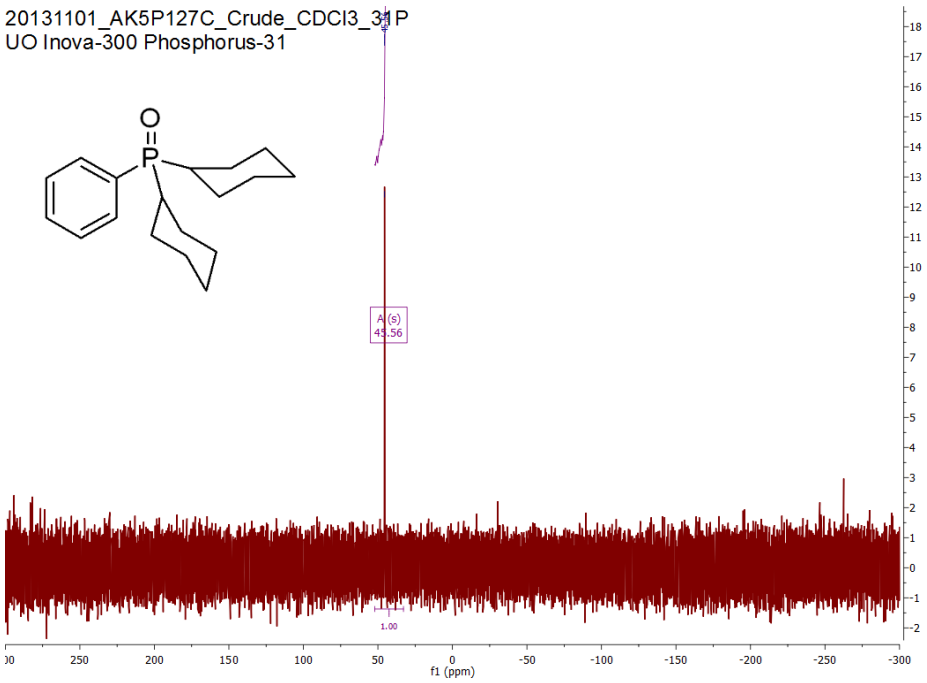

Figure A58. $^{31}P\{^{1}H\}$ NMR of di(*cyclo*-hexyl)phenylphosphine oxide

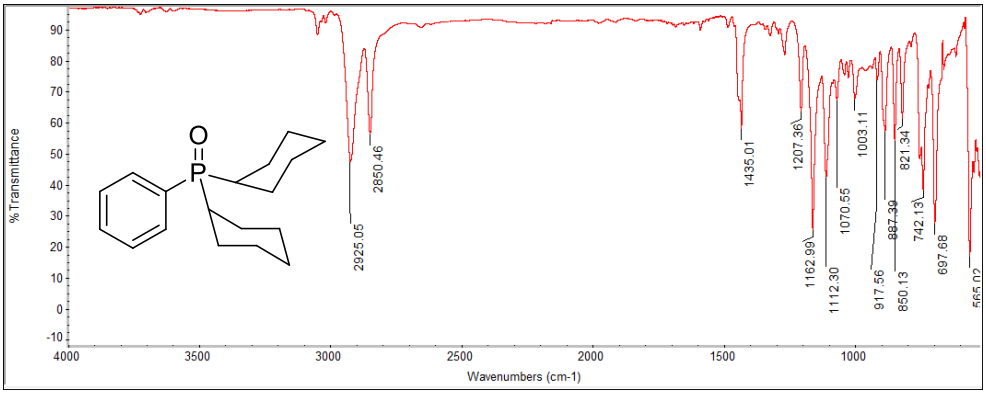

Figure A59. Infrared absorption spectrum of di(*cyclo*-hexyl)phenylphosphine oxide

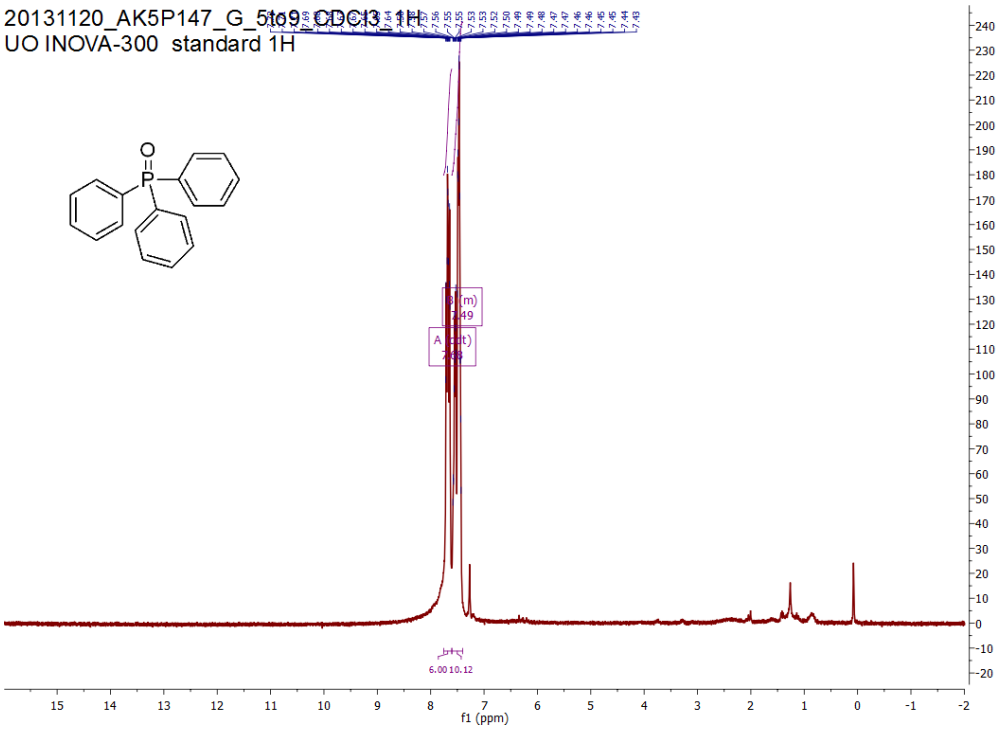

Figure A60. ^{1}H NMR of triphenylphosphine oxide.

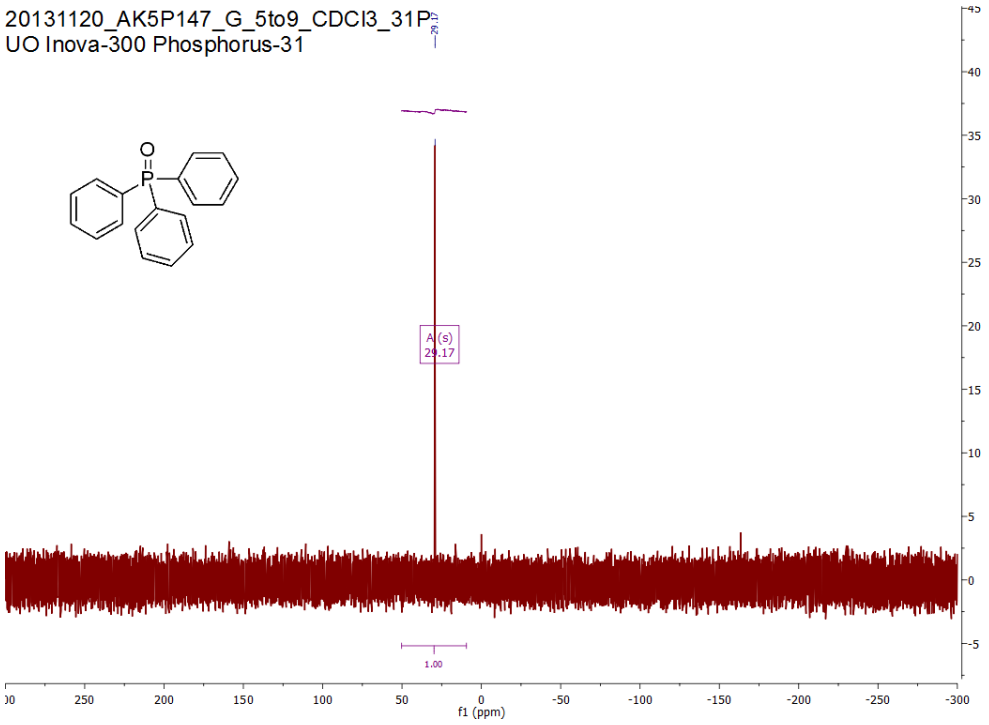

Figure A61. ^{31}P{^{1}H} NMR of triphenylphosphine oxide.

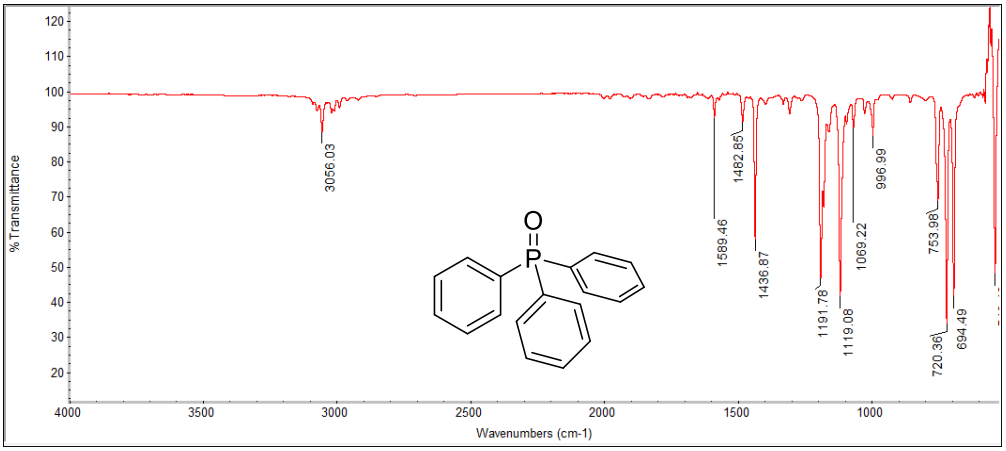

Figure A62. Infrared absorption spectrum of triphenylphosphine oxide.

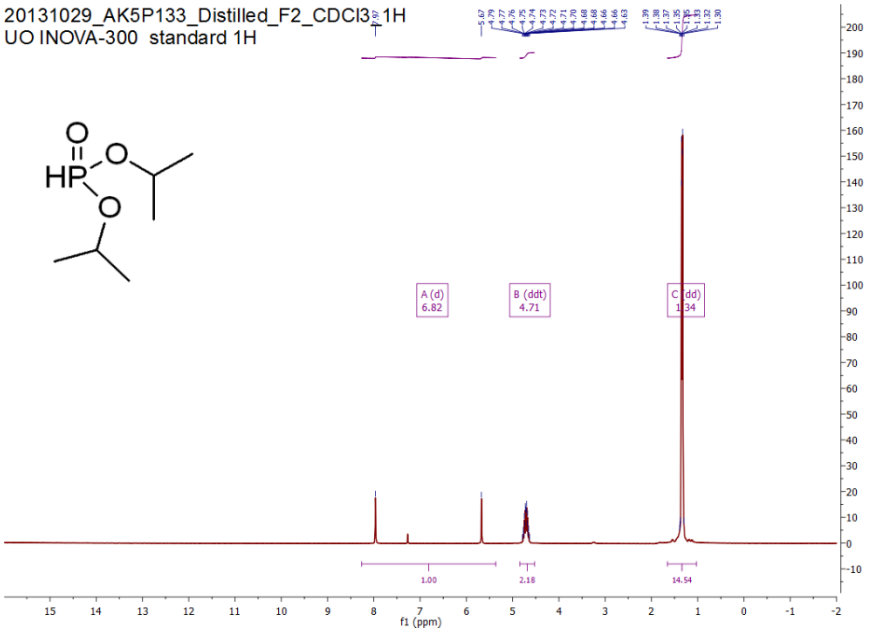

Figure A63. ^{1}H NMR of diisopropylphosphine oxide.

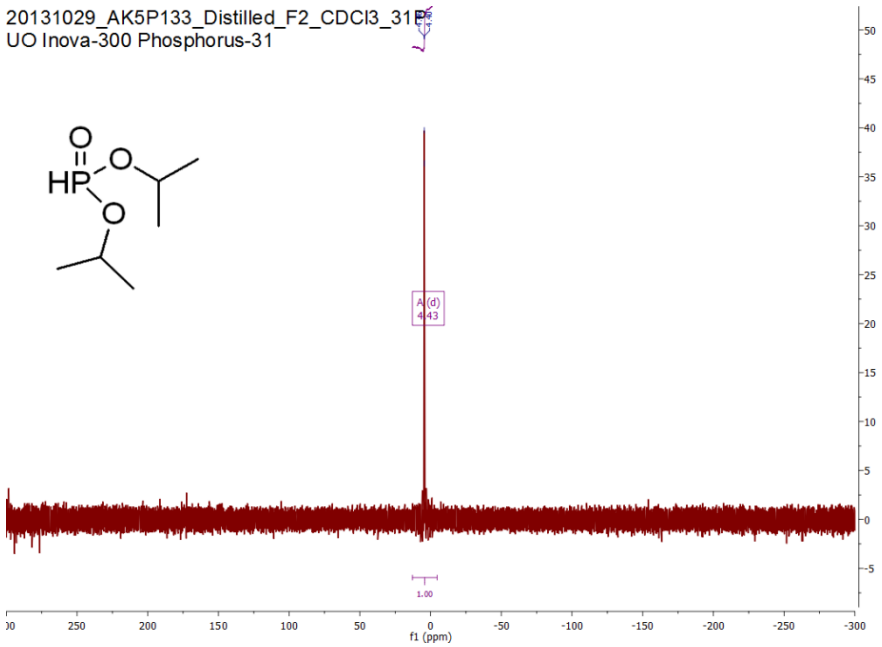

Figure A64. $^{31}P\{^{1}H\}$ NMR of diisopropylphosphine oxide.

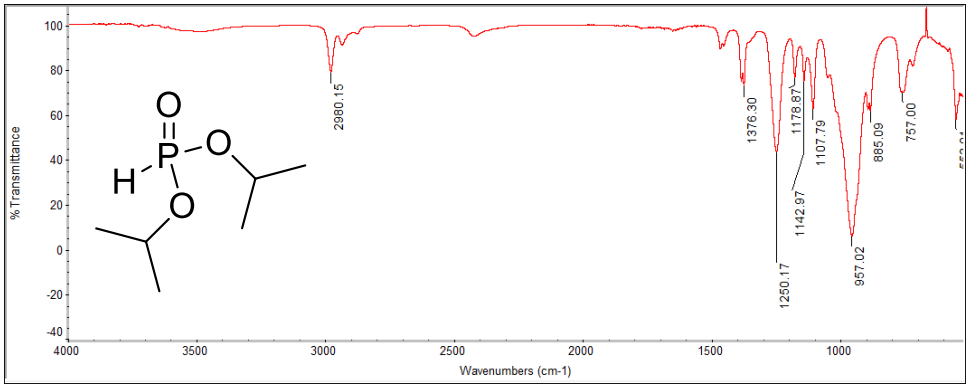

Figure A65. Infrared absorption spectrum of diisopropylphosphine oxide.

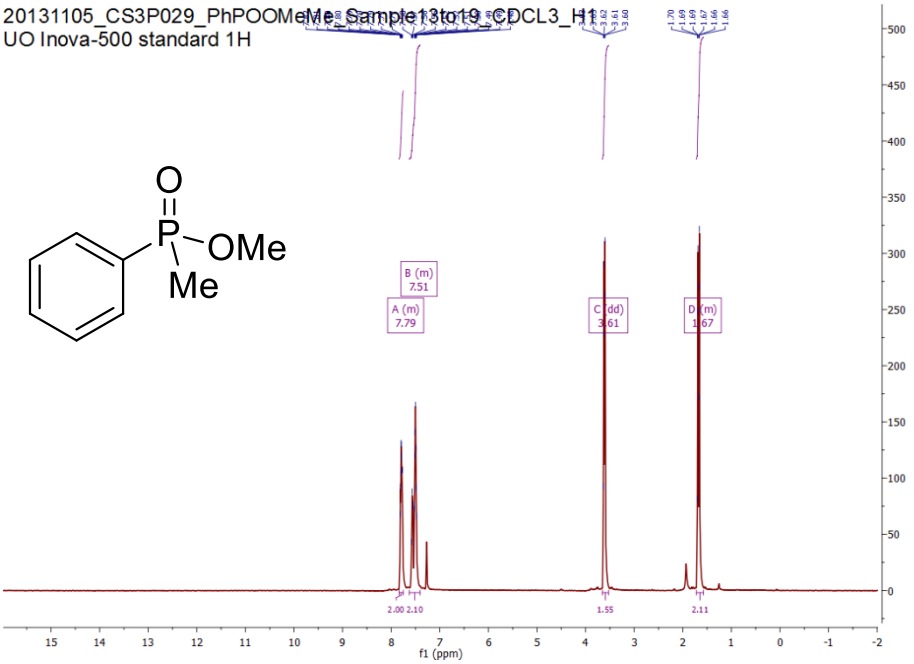

Figure A66. ^{1}H NMR of methyl methylphenylphosphinate

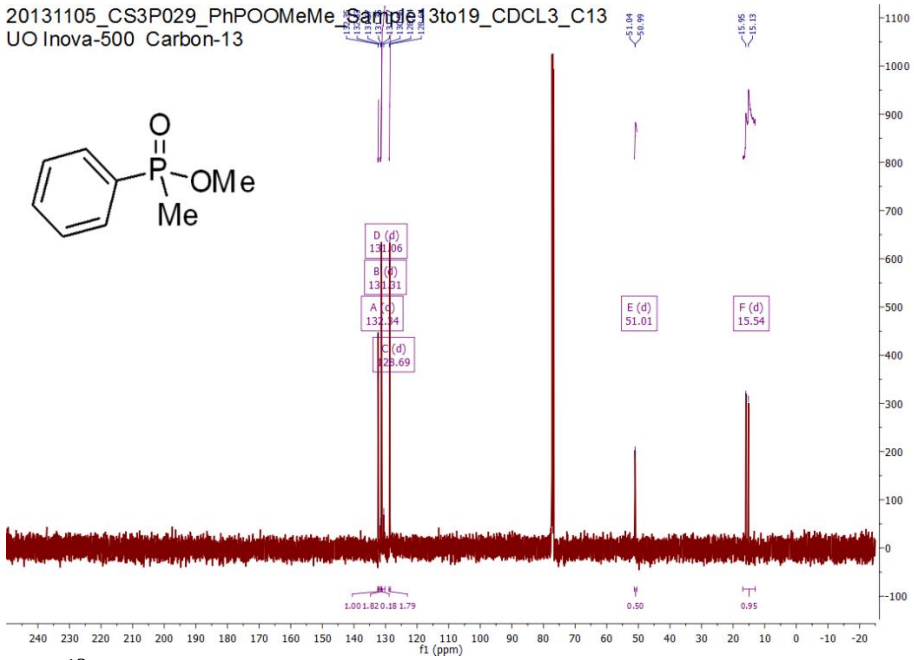

Figure A67. ^{13}C NMR of methyl methylphenylphosphinate.

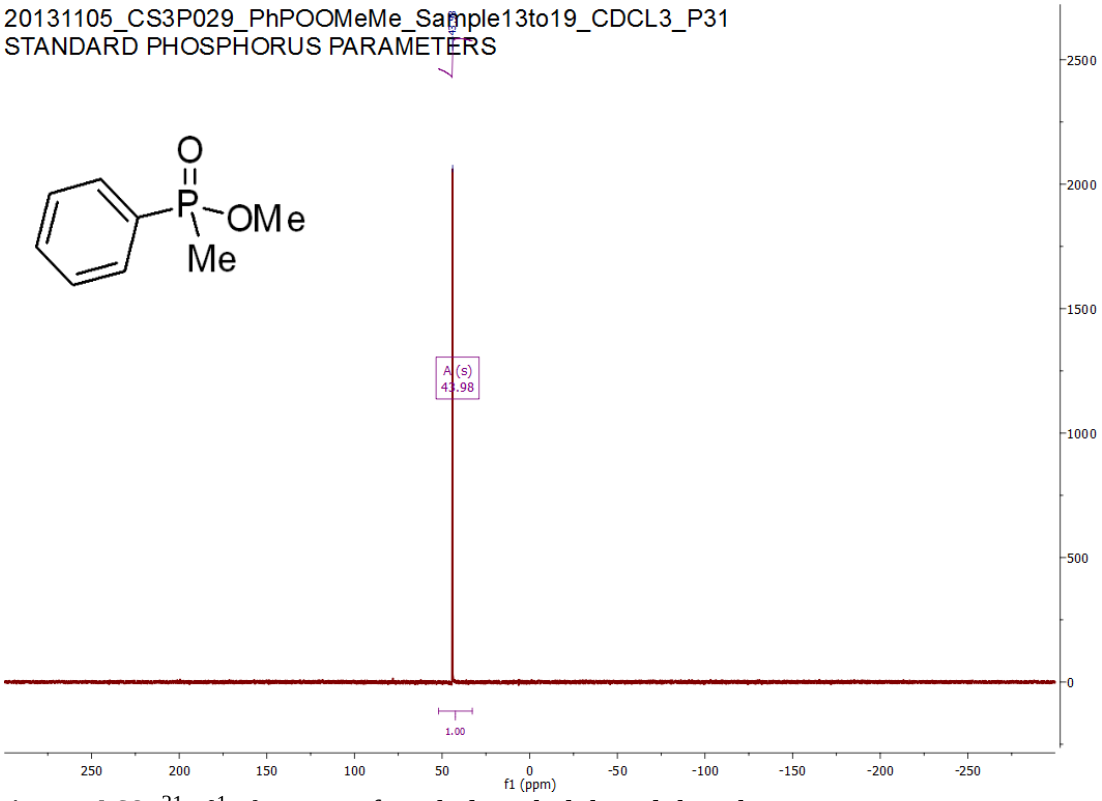

Figure A68. $^{31}P\{^{1}H\}$ NMR of methyl methylphenylphosphinate.

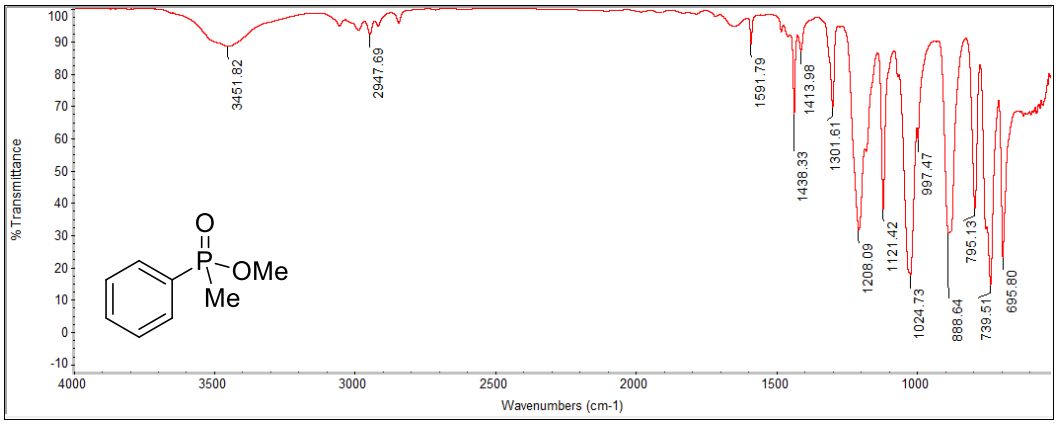

Figure A69. Infrared absorption spectrum of methyl methylphenylphosphinate.

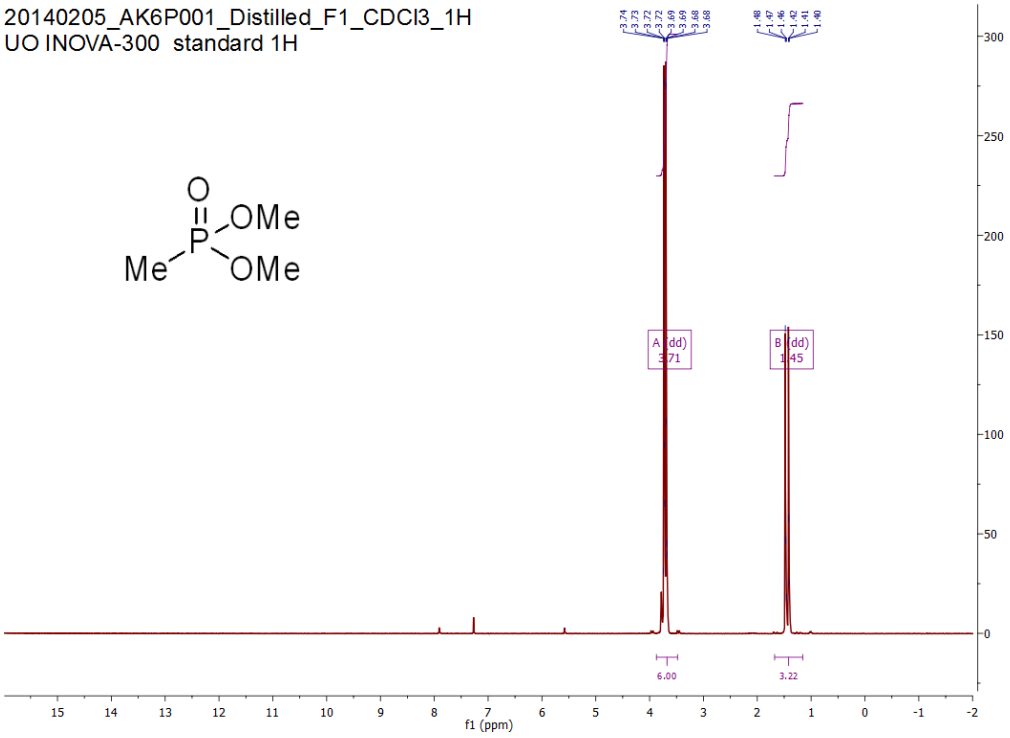

Figure A70. ^{1}H NMR of dimethyl methylphosphonate.

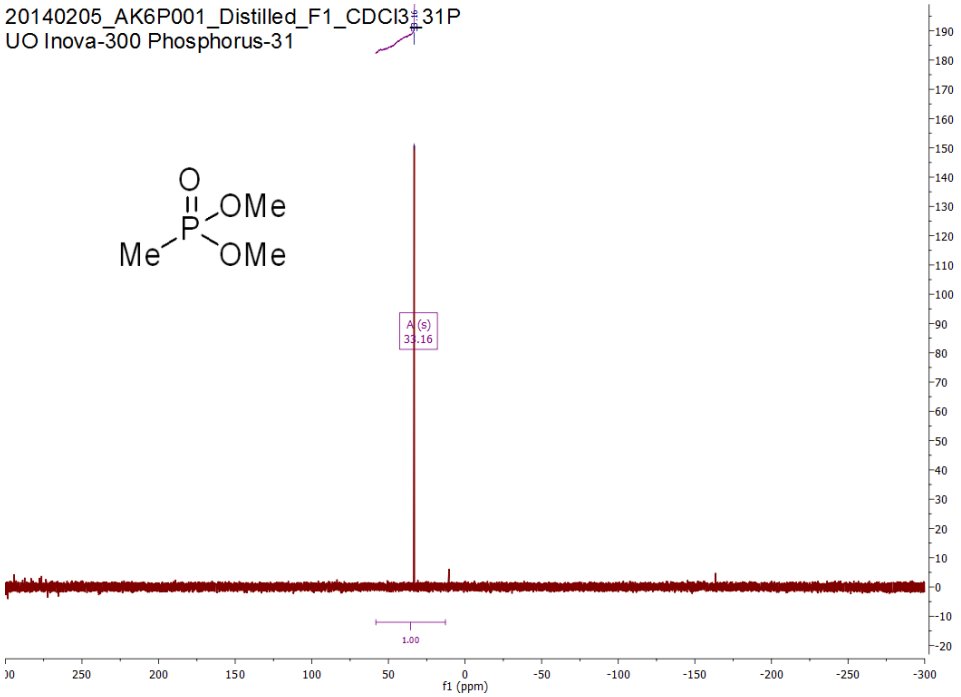

Figure A71. ^{31}P{^{1}H} NMR of dimethyl methylphosphonate.

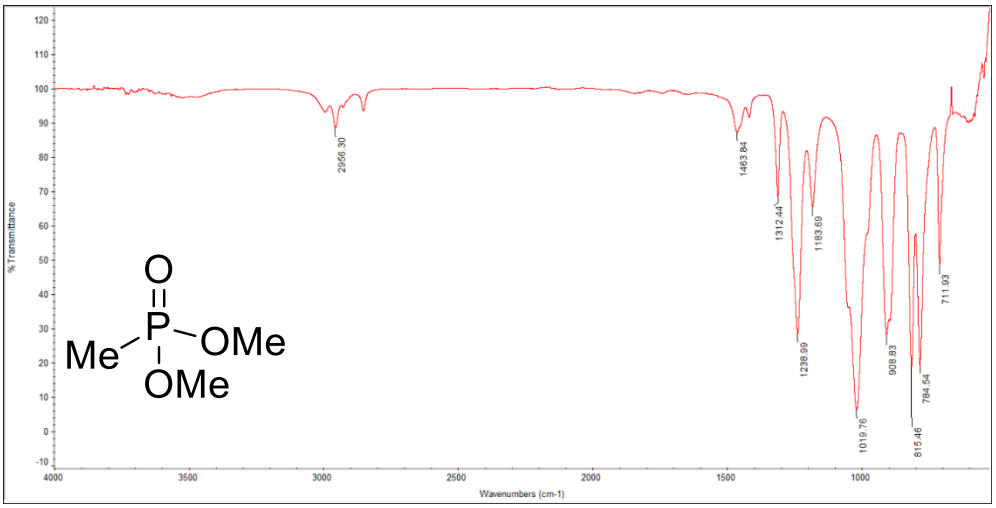

Figure A72. Infrared absorption spectrum of dimethyl methylphosphonate.

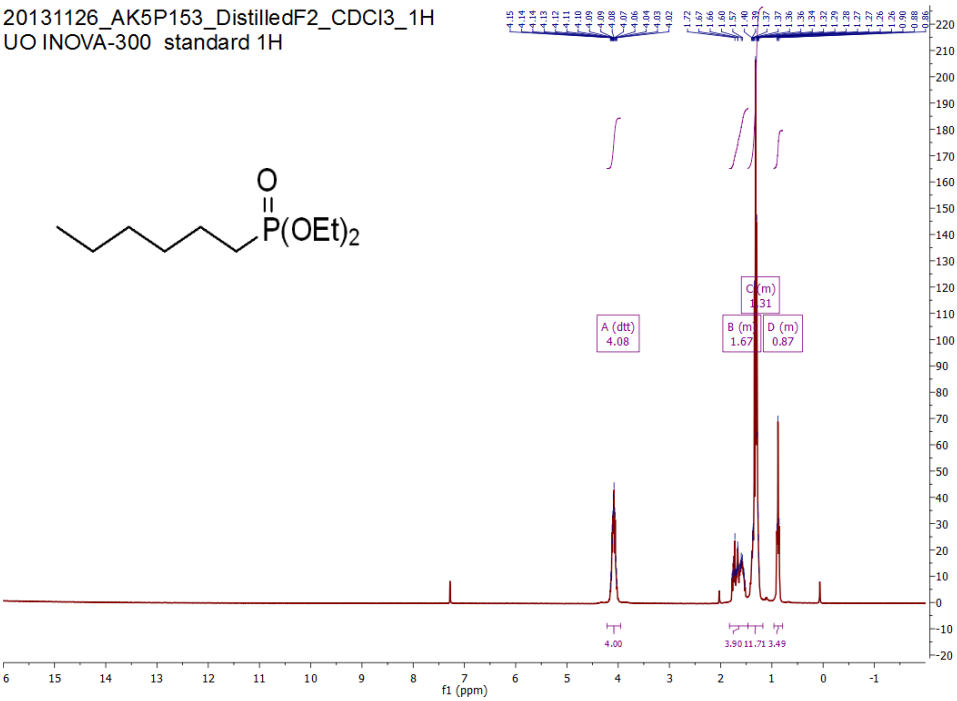

Figure A73. ^{1}H NMR of diethyl *n*-hexylphosphonate.

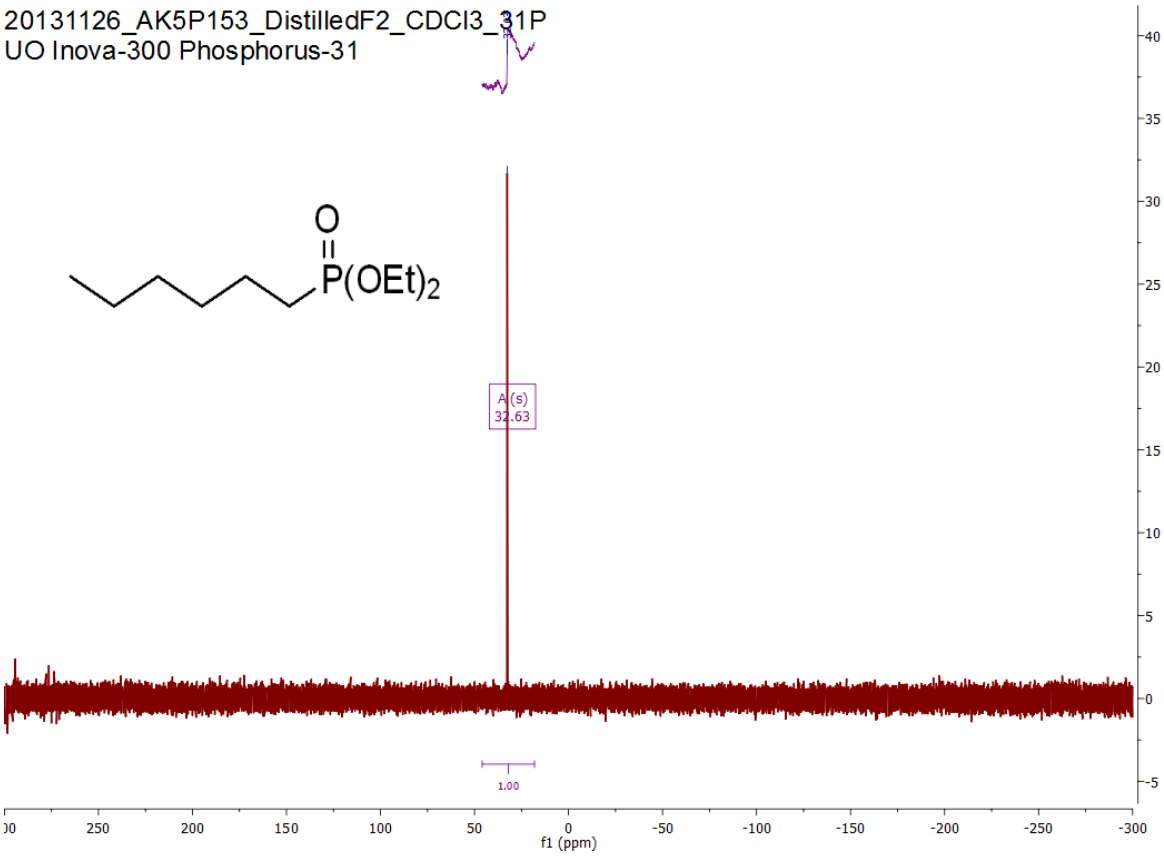

Figure A74. $^{31}P\{^{1}H\}$ NMR of diethyl *n*-hexylphosphonate.

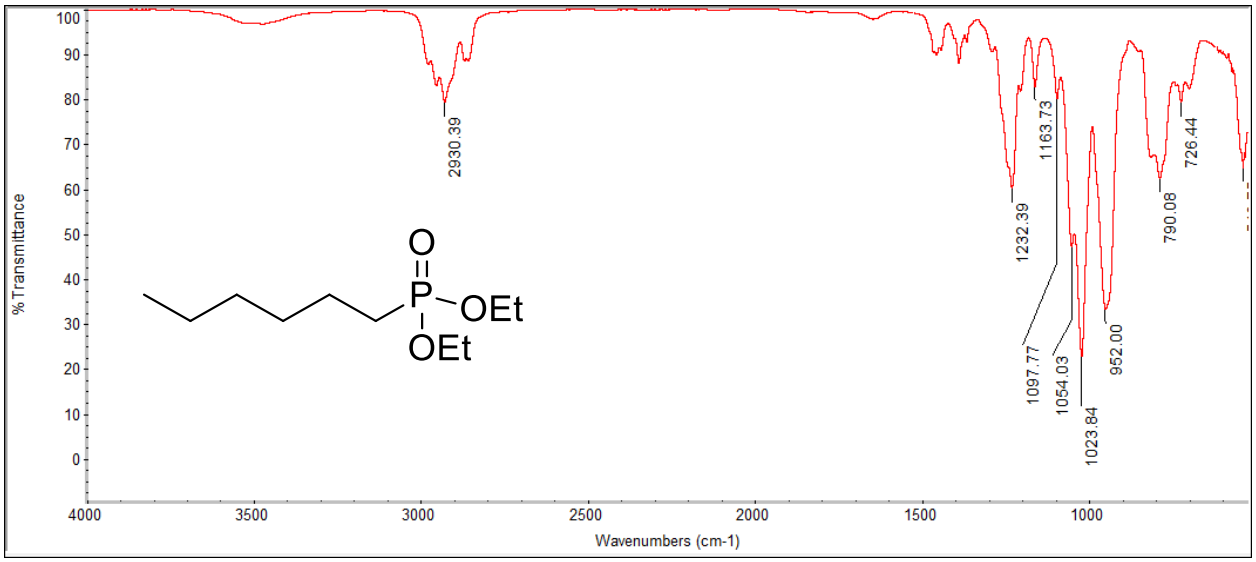

Figure A75. Infrared absorption spectrum of diethyl *n*-hexylphosphonate.

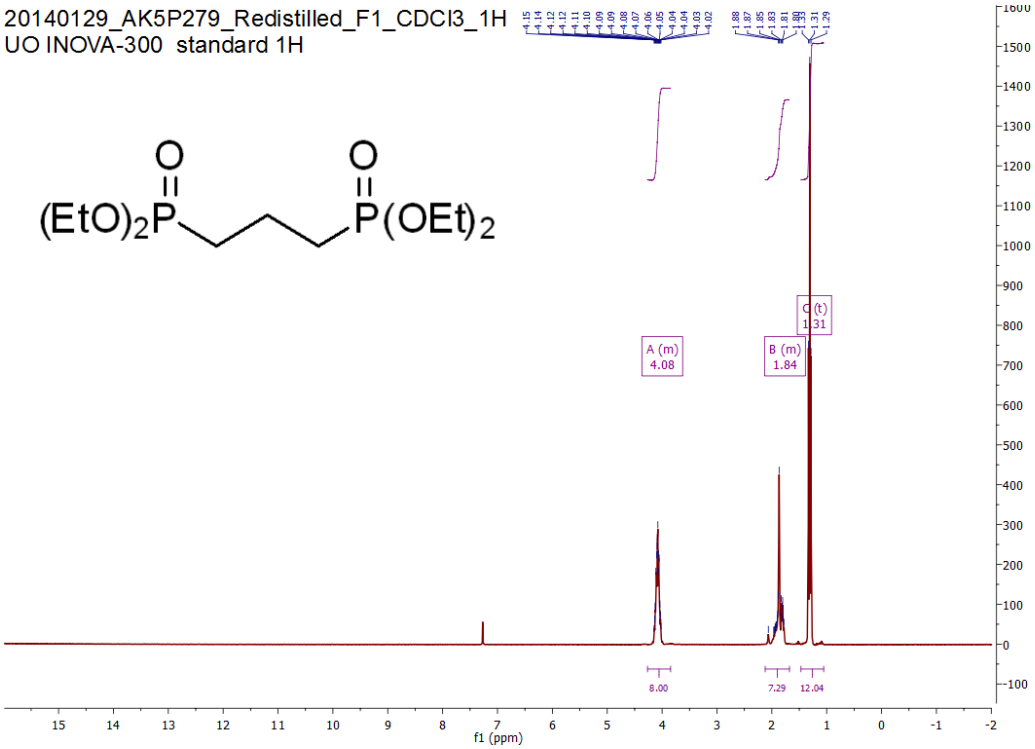

Figure A76. ^{1}H NMR of tetraethyl propane-1,3-diylbis(phosphonate).

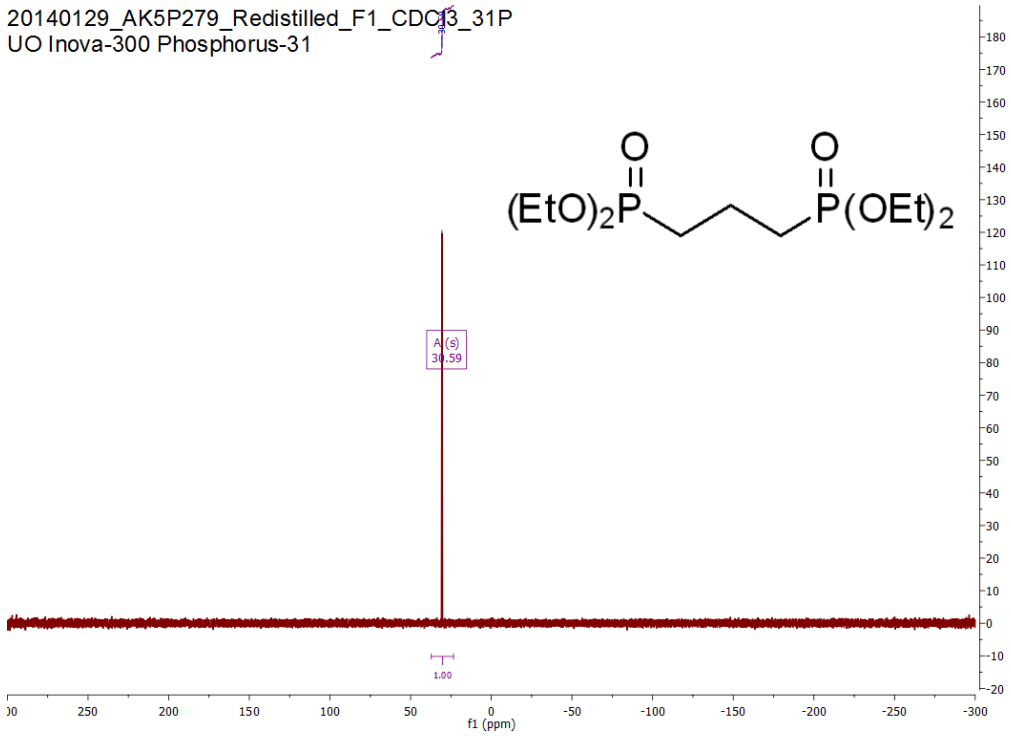

Figure A77. ^{31}P{^{1}H} of tetraethyl propane-1,3-diylbis(phosphonate).

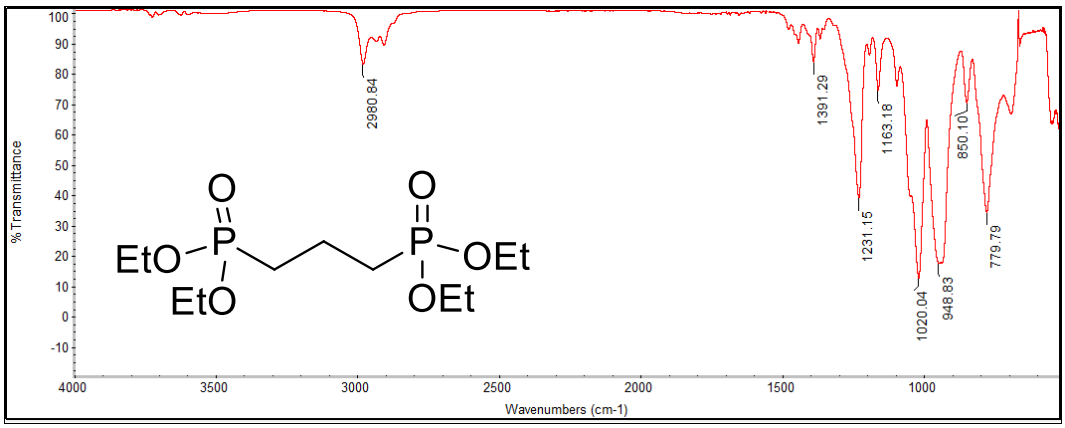

Figure A78. Infrared absorption spectrum of tetraethyl propane-1,3-diylbis(phosphonate).

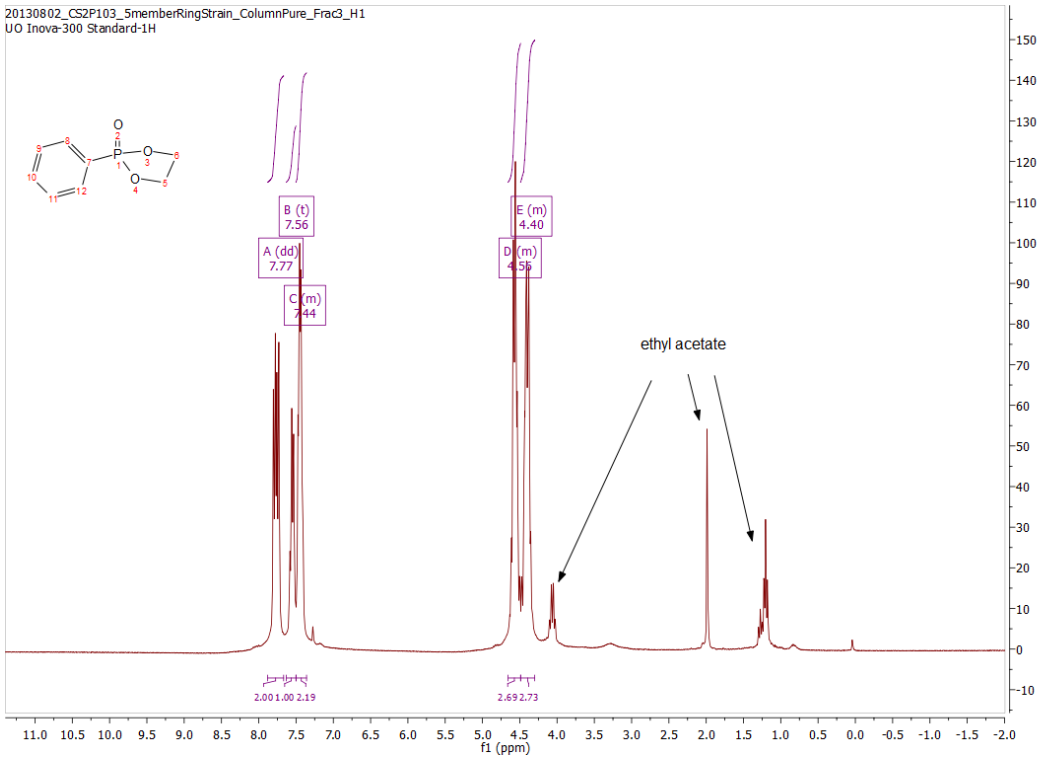

Figure A79. ^{1}H NMR of 2-phenyl-1,3,2-dioxaphospholane 2-oxide.

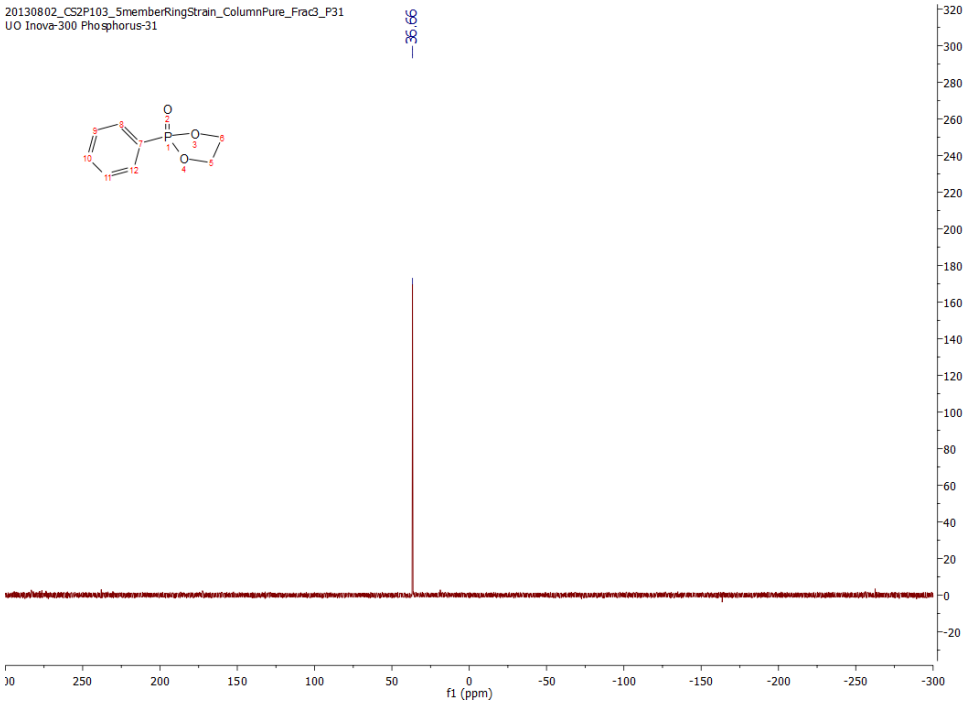

Figure A80. $^{31}P\{^{1}H\}$ NMR of 2-phenyl-1,3,2-dioxaphospholane 2-oxide.

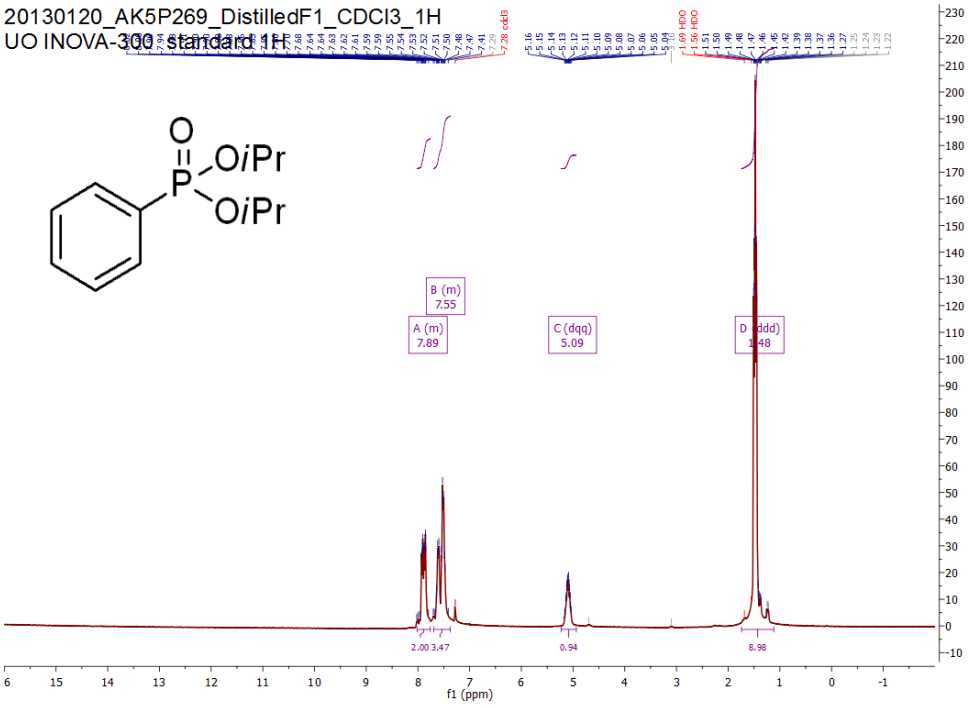

Figure A81. ^{1}H NMR of diisopropyl phenylphosphonate.

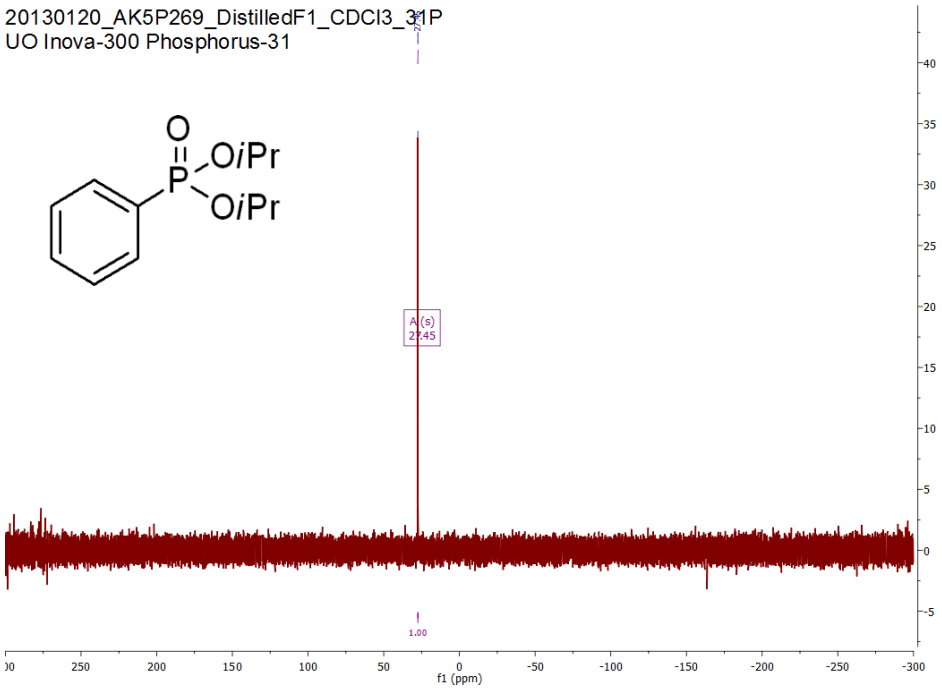

Figure A82. $^{31}P\{^{1}H\}$ NMR of diisopropyl phenylphosphonate.

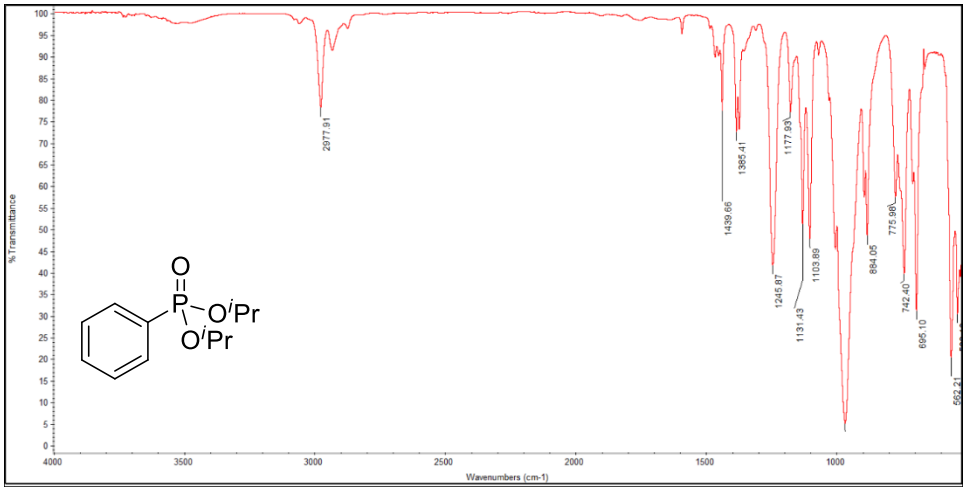

Figure A83. Infrared absorption spectrum of diisopropyl phenylphosphonate.

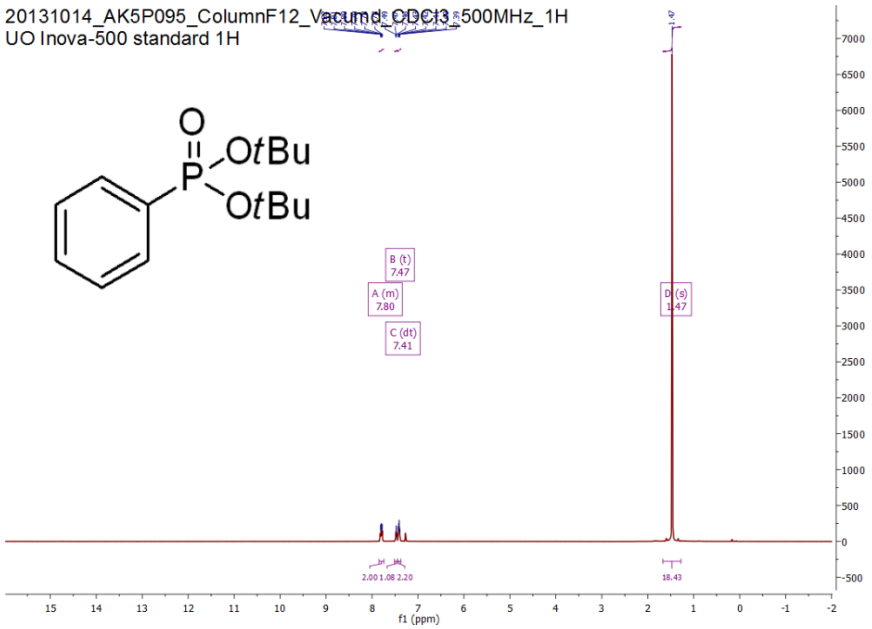

Figure A84. ^{1}H NMR of di(*tert*-butyl) phenylphosphonate.

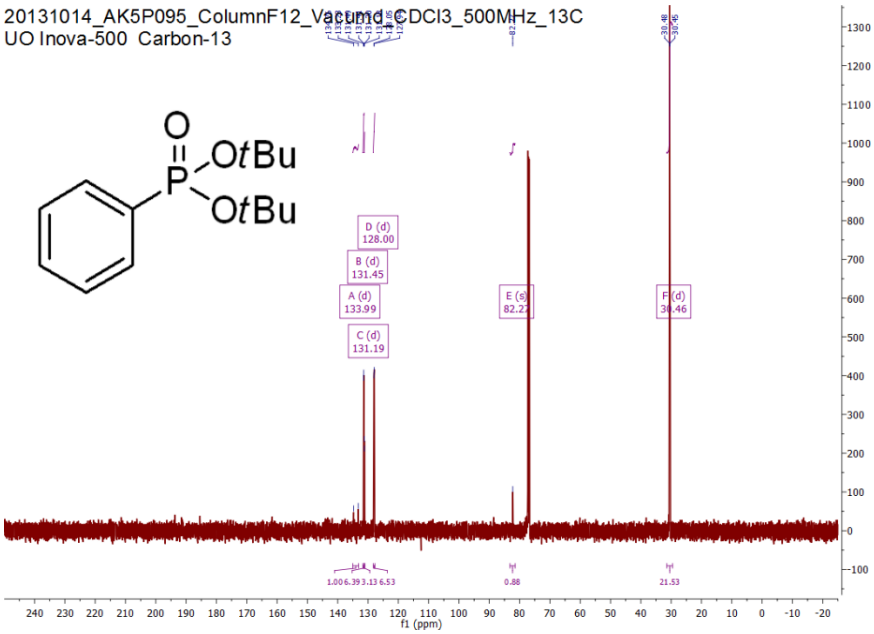

Figure A85. ^{13}C NMR of di(*tert*-butyl) phenylphosphonate.

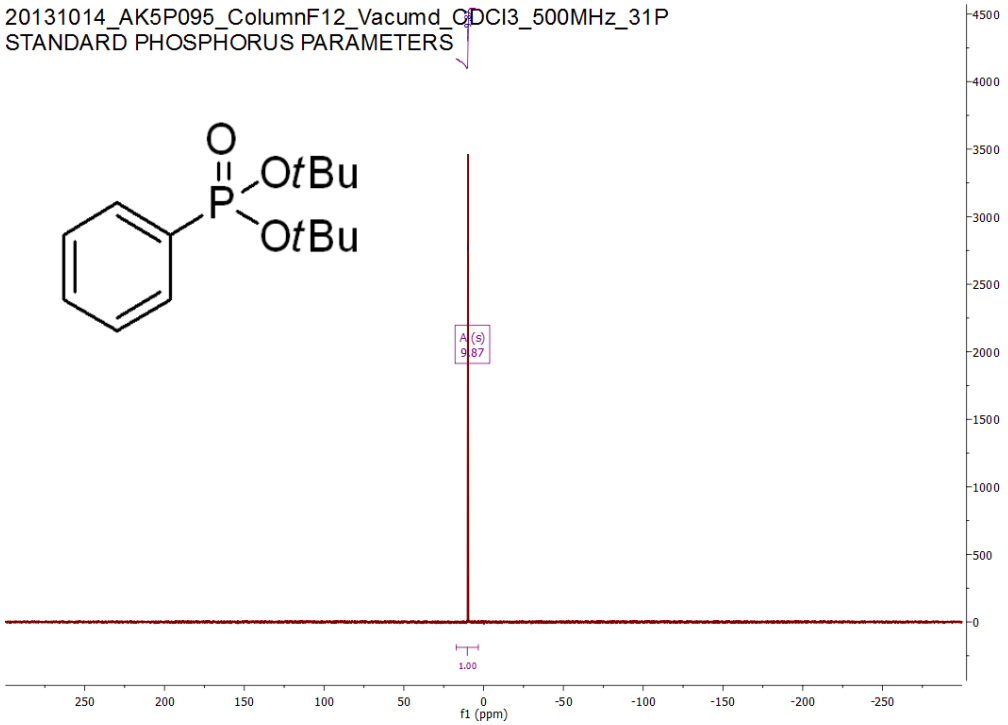

Figure A86. $^{31}P\{^{1}H\}$ NMR of di(*tert*-butyl) phenylphosphonate.

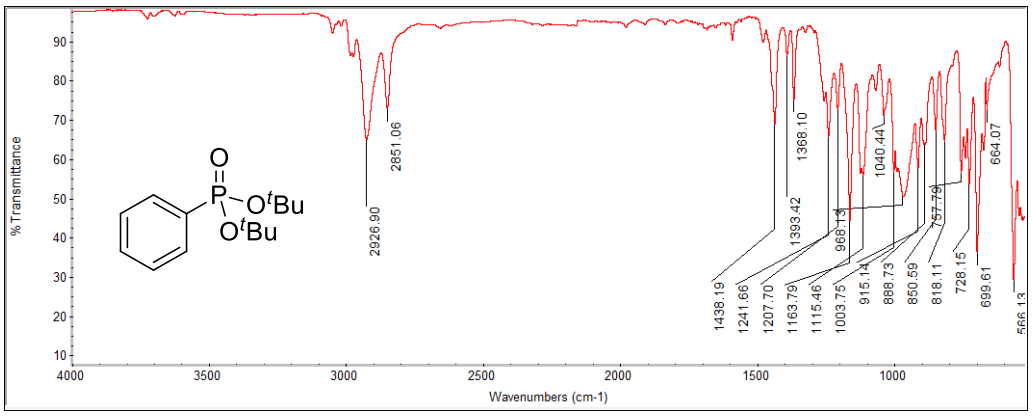

Figure A87. Infrared absorption spectrum of di(*tert*-butyl) phenylphosphonate.

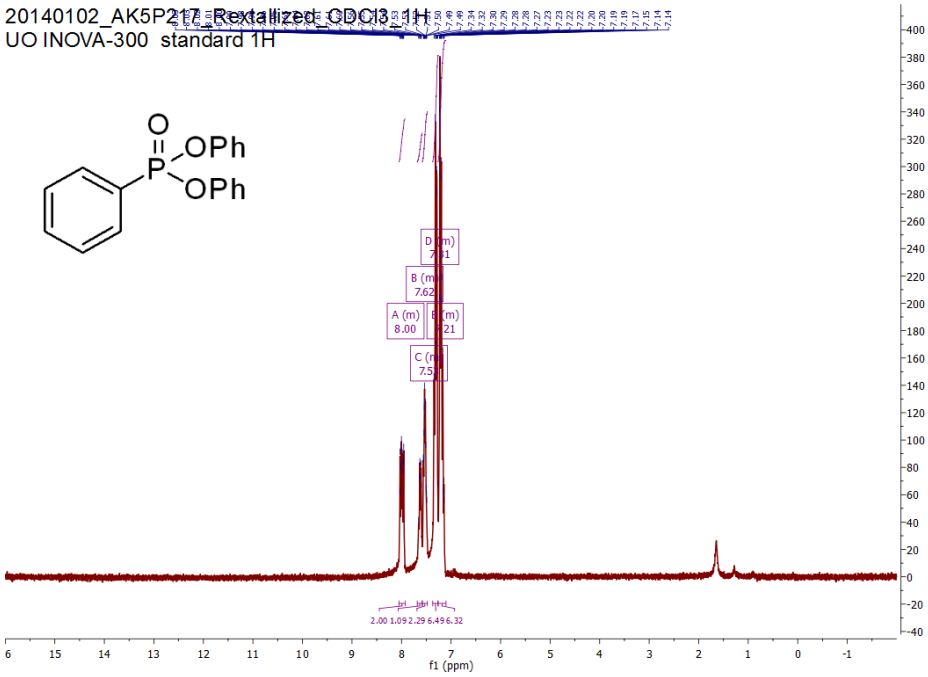

Figure A88. ^{1}H NMR of diphenyl phenylphosphonate.

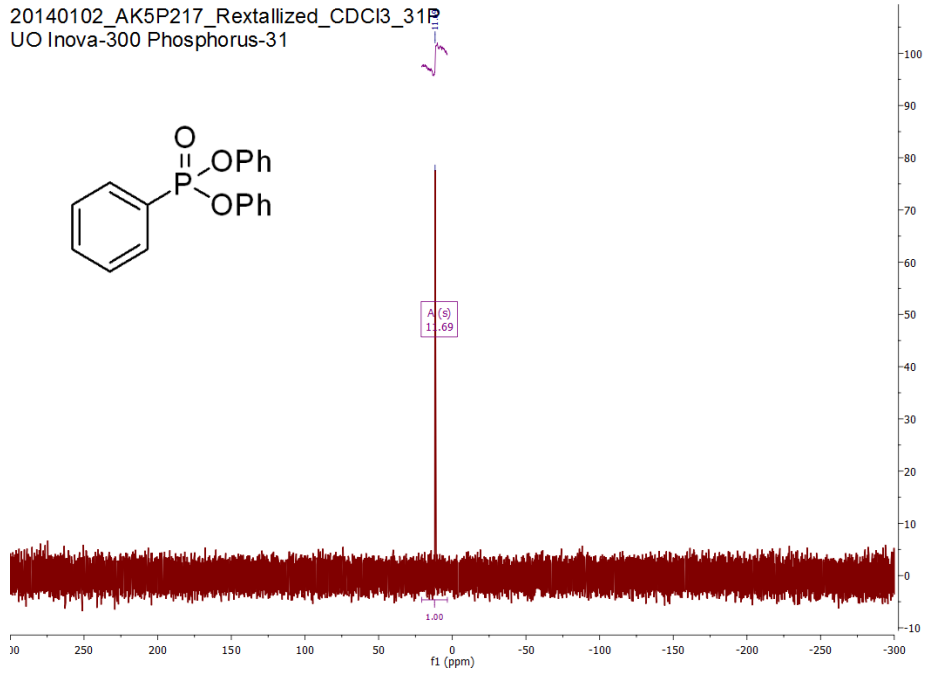

Figure A89. ^{31}P{^{1}H} NMR of diphenyl phenylphosphonate.

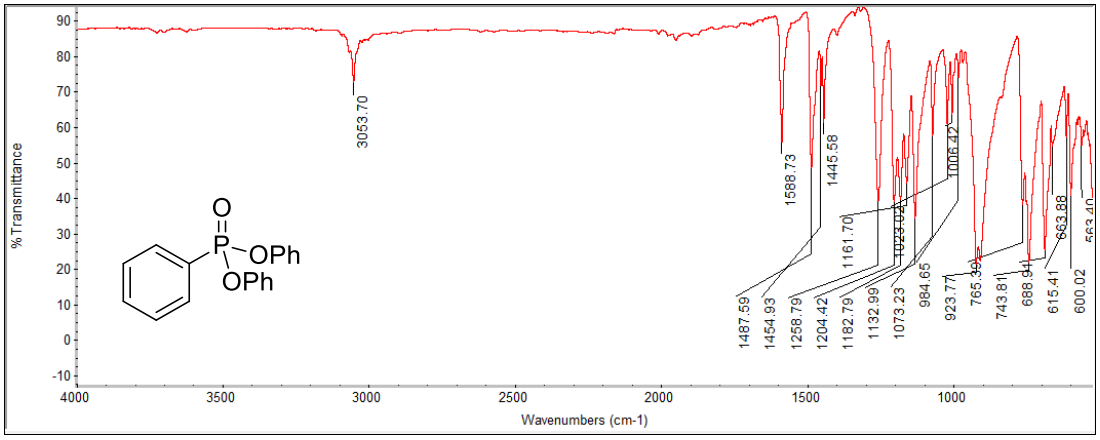

Figure A90. Infrared absorption spectrum of diphenyl phenylphosphonate.

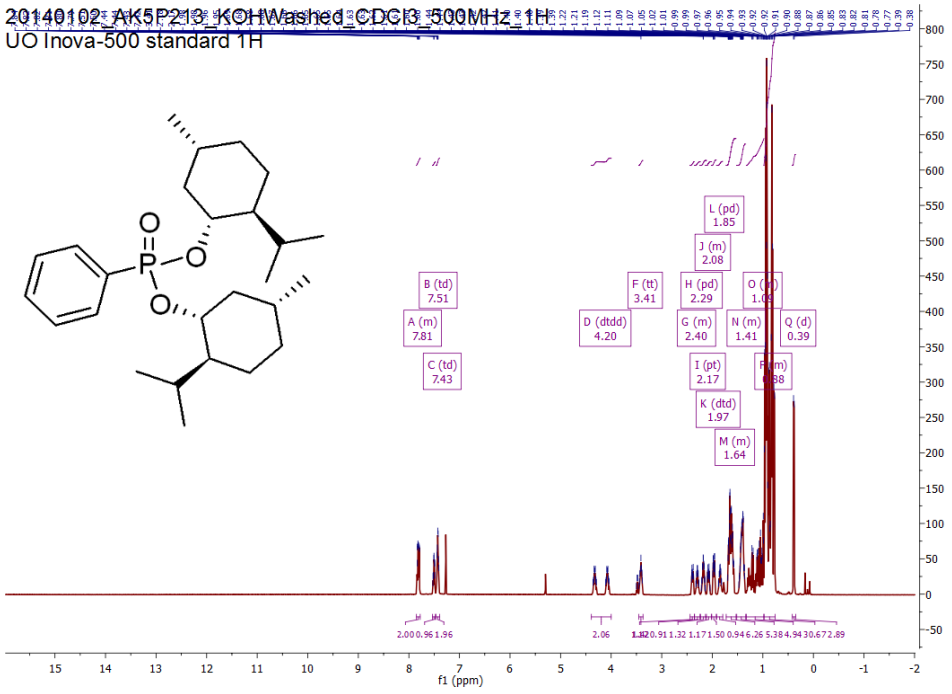

Figure A91. ^{1}H NMR of bis((1R,2S,5R)-2-isopropyl-5-methylcyclohexyl) phenylphosphonate.

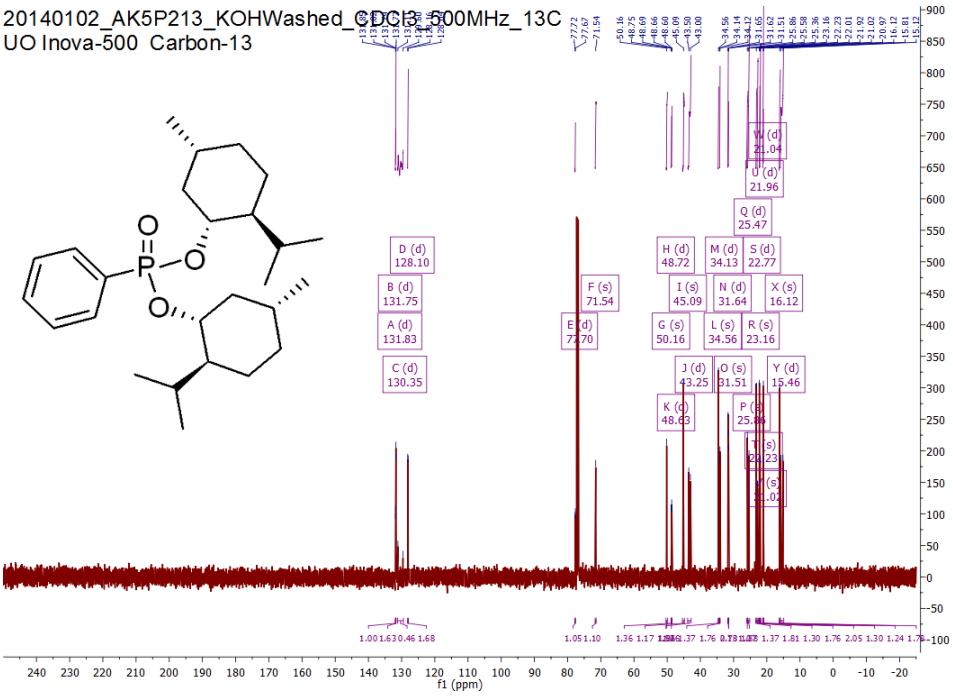

Figure A92. ^{13}C NMR of bis((1R,2S,5R)-2-isopropyl-5-methylcyclohexyl) phenylphosphonate.

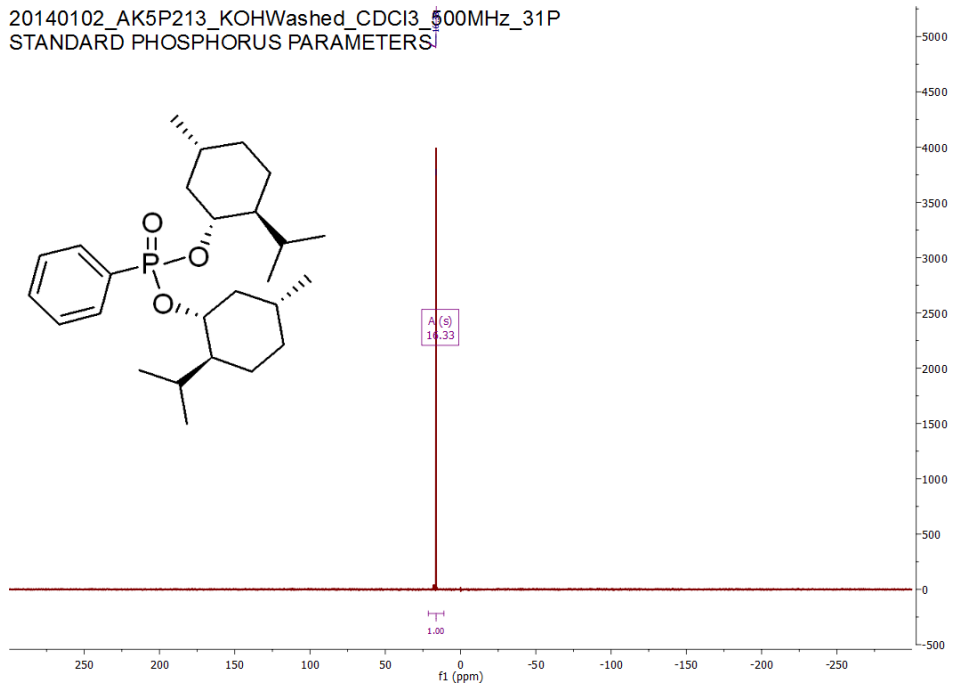

Figure A93. $^{31}P\{^{1}H\}$ NMR of bis((1R,2S,5R)-2-isopropyl-5-methylcyclohexyl) phenylphosphonate.

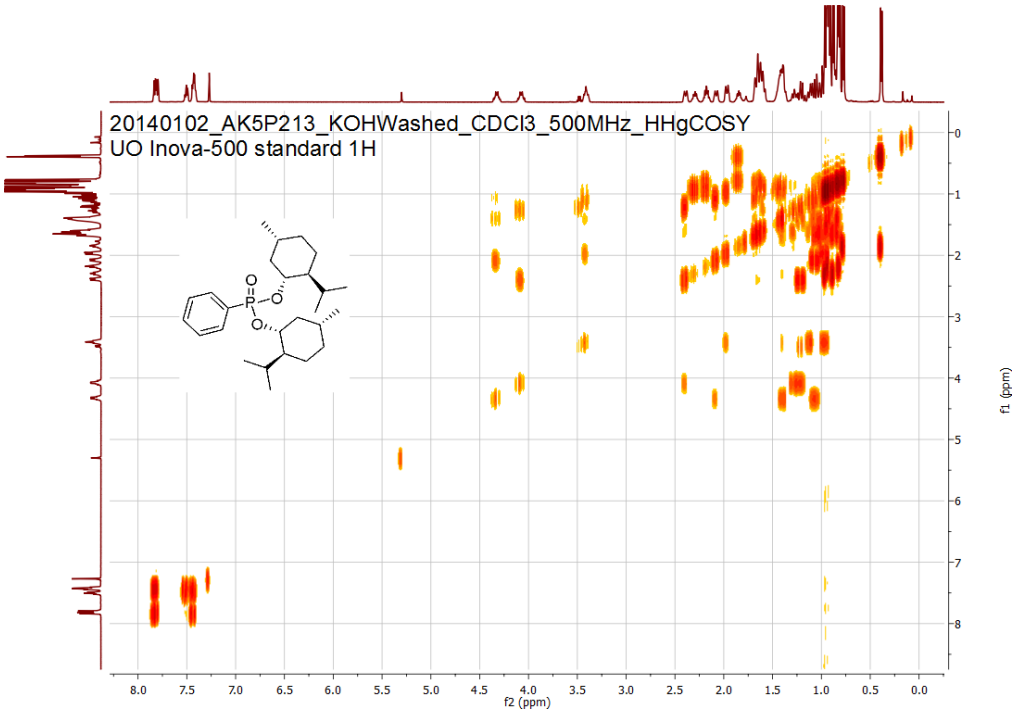

Figure A94. ^{1}H-^{1}H gradient COSY NMR of bis((1R,2S,5R)-2-isopropyl-5-methylcyclohexyl) phenylphosphonate.

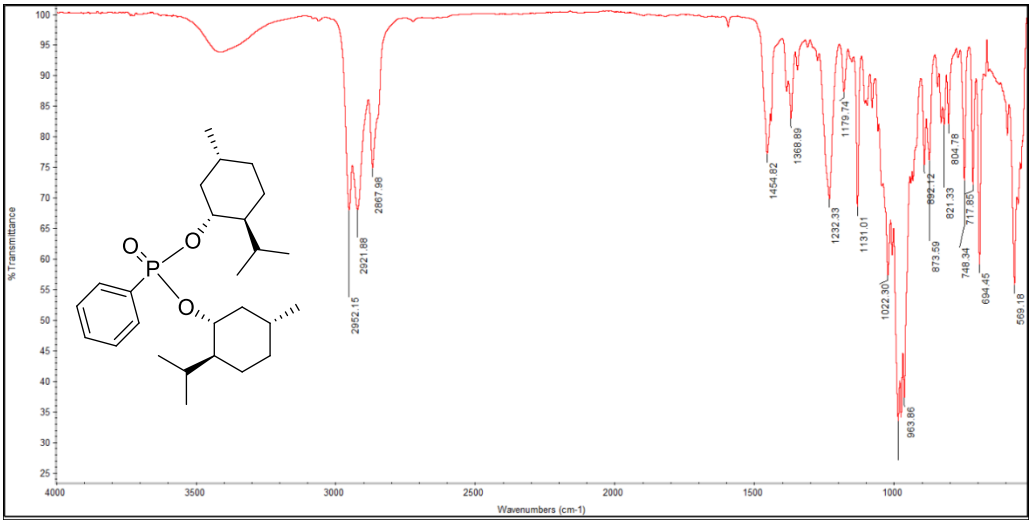

Figure A95. Infrared absorption spectrum of bis((1R,2S,5R)-2-isopropyl-5-methylcyclohexyl) phenylphosphonate.

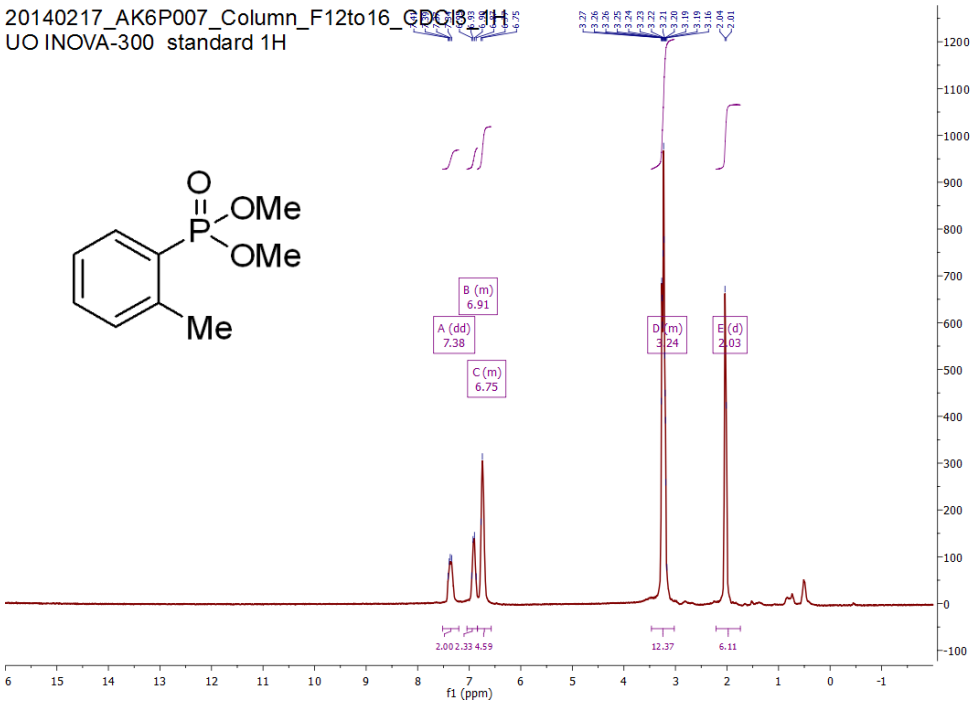

Figure A96. ^{1}H NMR of dimethyl *o*-tolylphosphonate.

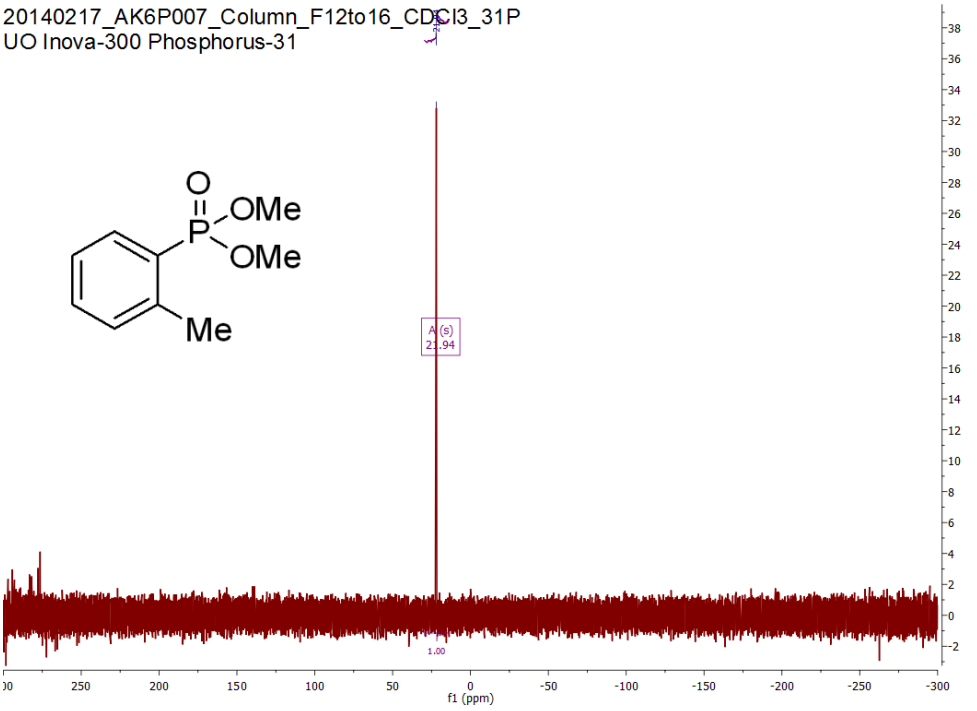

Figure A97. ^{31}P{^{1}H} NMR of dimethyl *o*-tolylphosphonate.

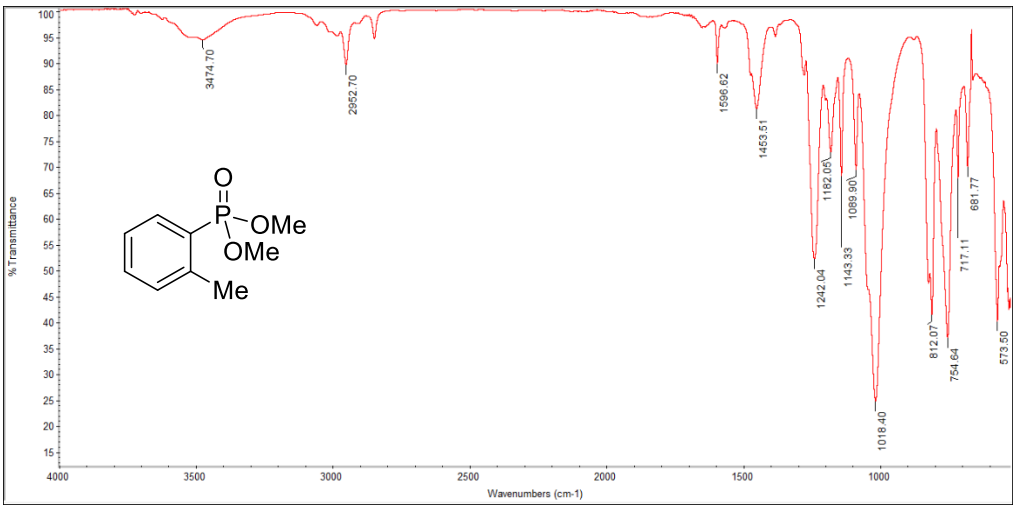

Figure A98. Infrared absorption spectrum of dimethyl *o*-tolylphosphonate.

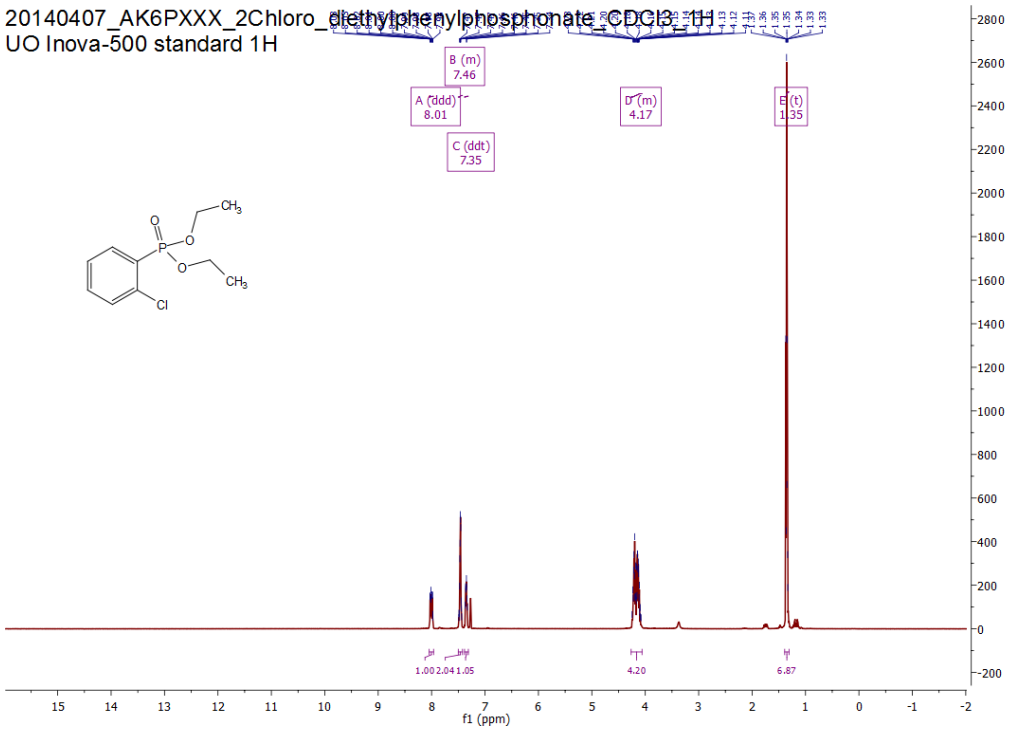

Figure A99. ^{1}H NMR of diethyl (*o*-chloro)phenylhosphonate.

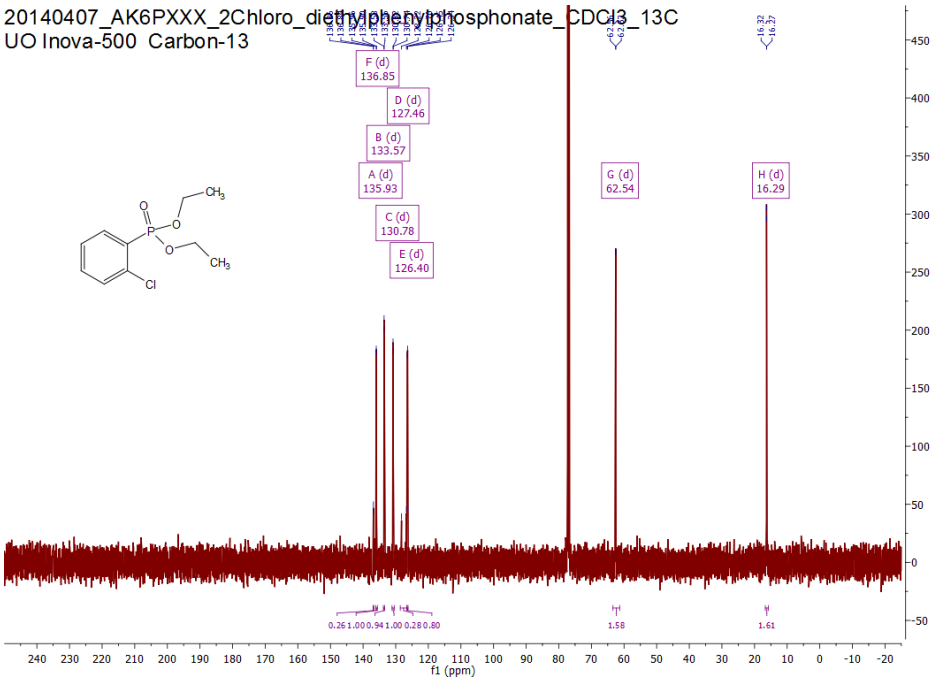

Figure A100. ^{13}C NMR of diethyl (*o*-chloro)phenylhosphonate.

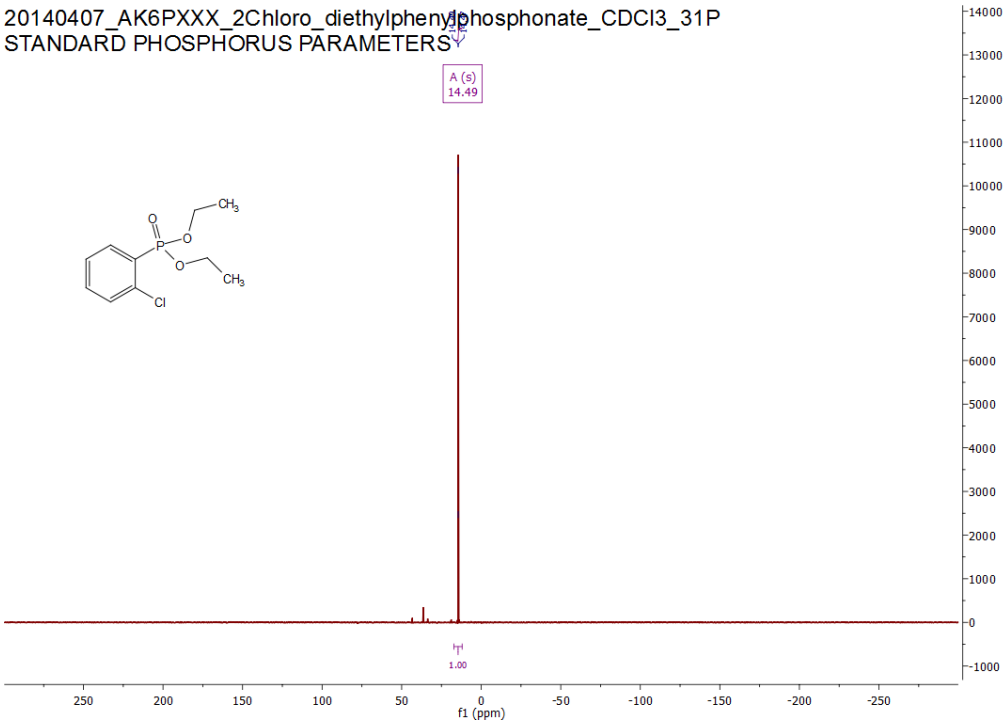

Figure A101. ^{31}P{^{1}H} NMR of diethyl (*o*-chloro)phenylhosphonate.

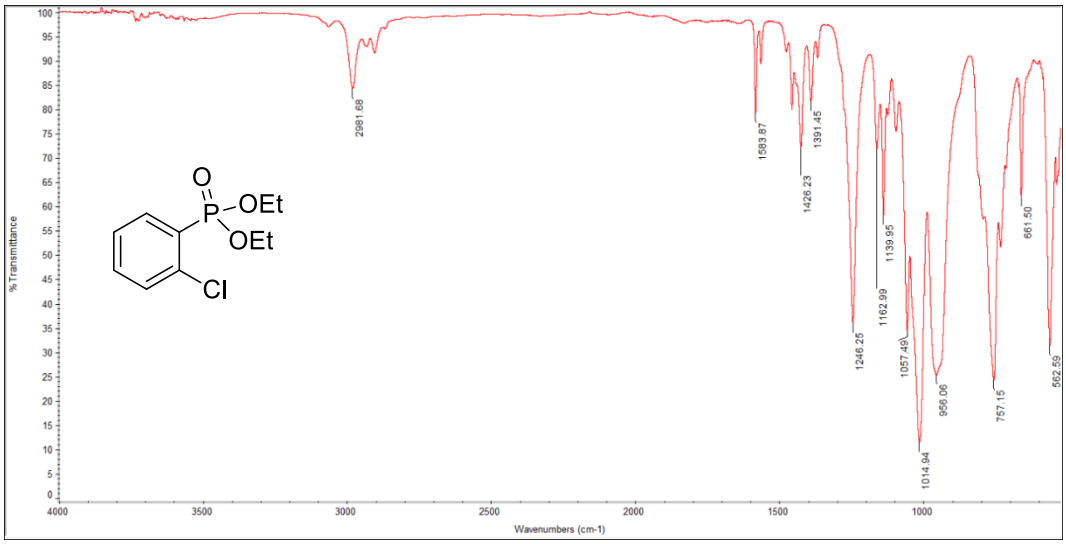

Figure A102. Infrared absorption spectrum of diethyl (*o*-chloro)phenylhosphonate.

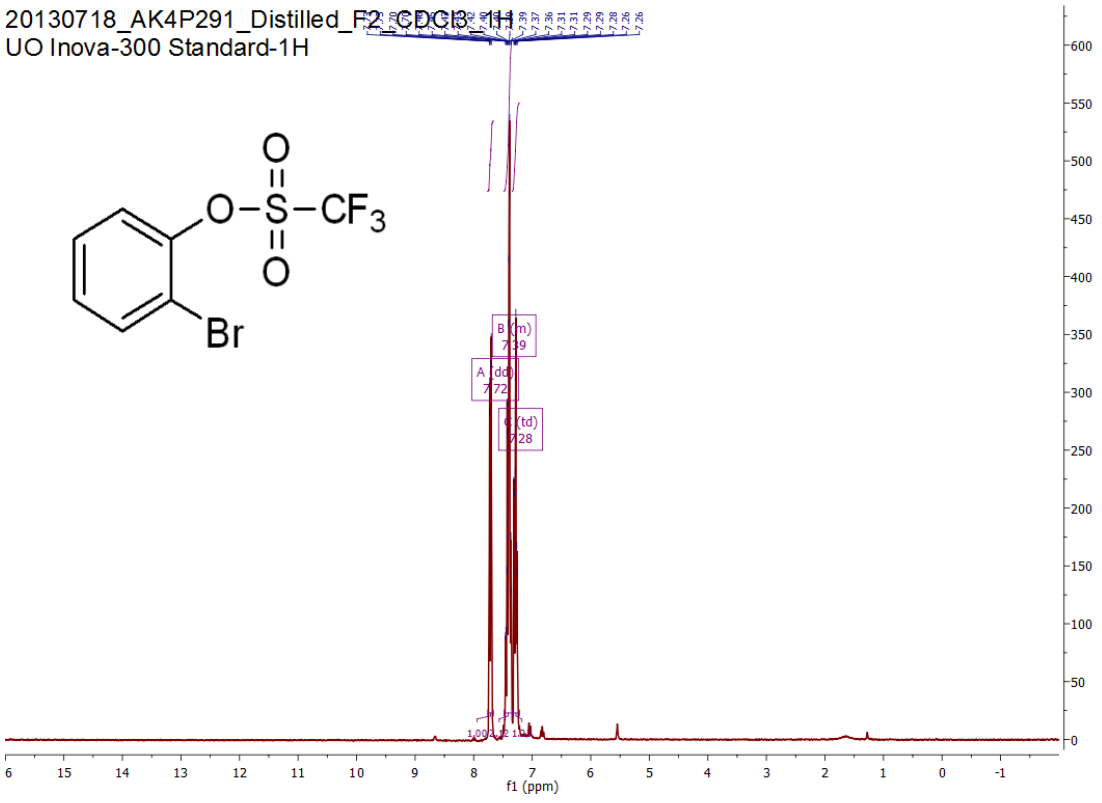

Figure A103. ^{1}H NMR of 2-bromophenyl trifluoromethanesulfonate.

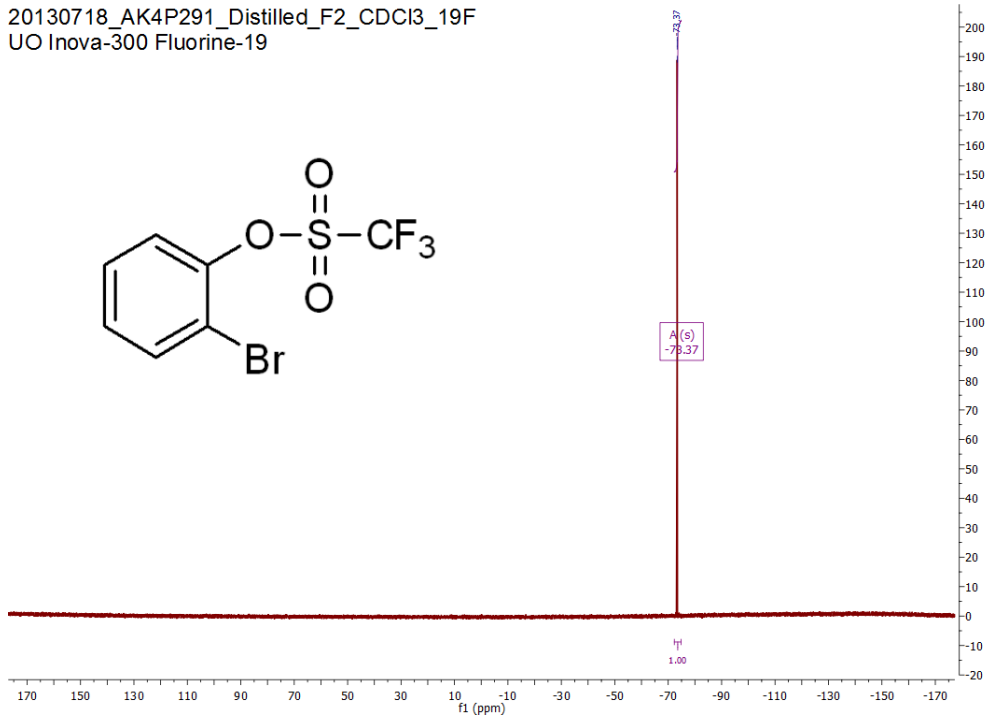

Figure A104. $^{31}P\{^{1}H\}$ NMR of 2-bromophenyl trifluoromethanesulfonate.

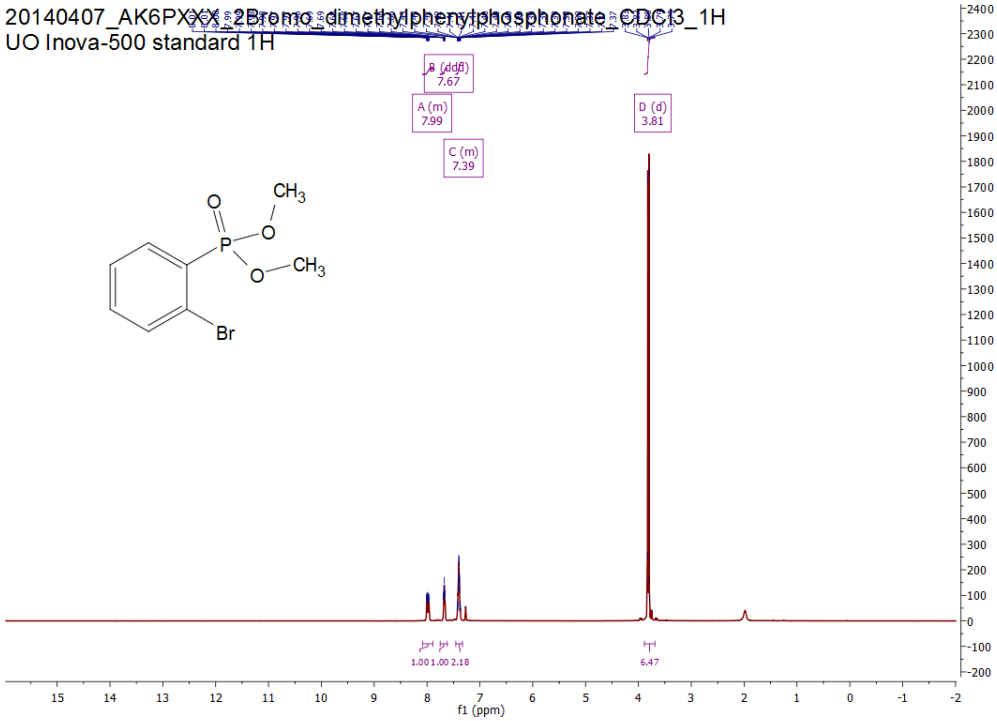

Figure A105. ^{1}H NMR of dimethyl *o*-(bromophenyl)phosphonate.

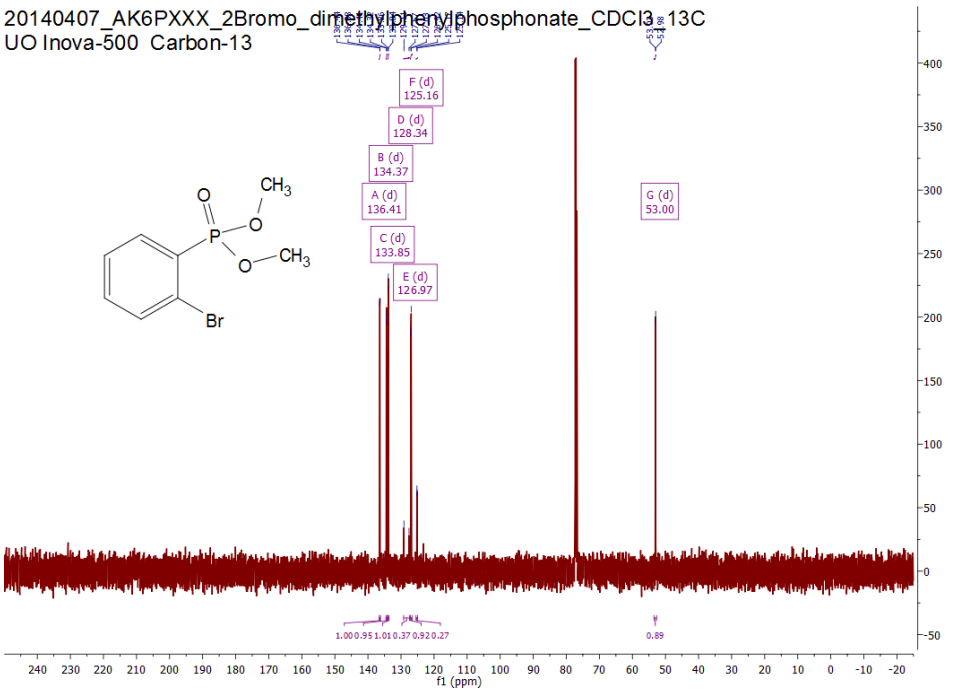

Figure A106. ^{13}C NMR of dimethyl *o*-(bromophenyl)phosphonate.

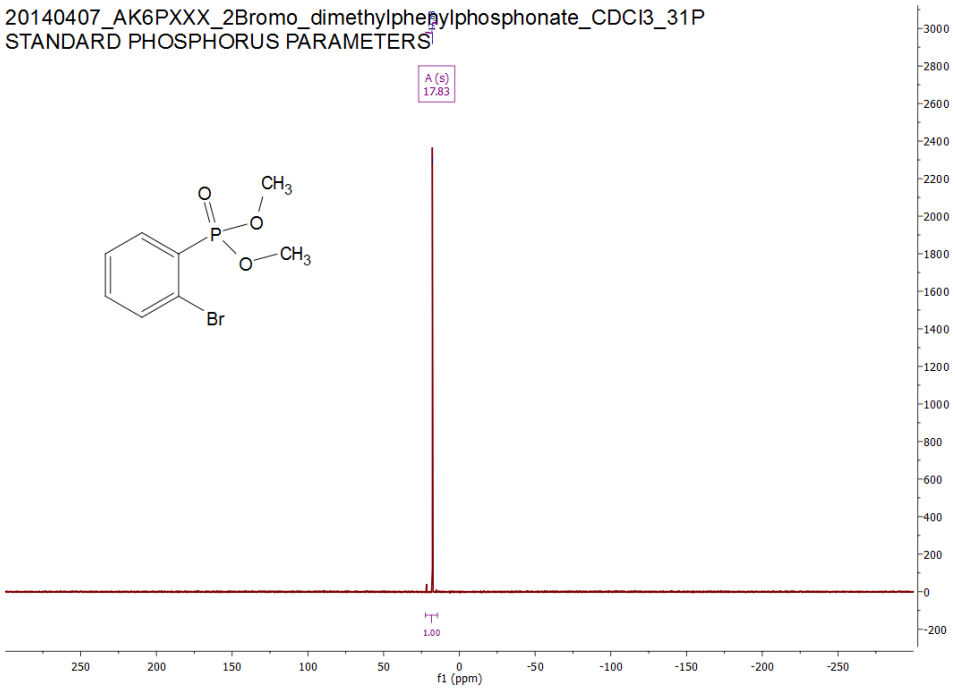

Figure A107. $^{31}P\{^{1}H\}$ NMR of dimethyl *o*-(bromophenyl)phosphonate.

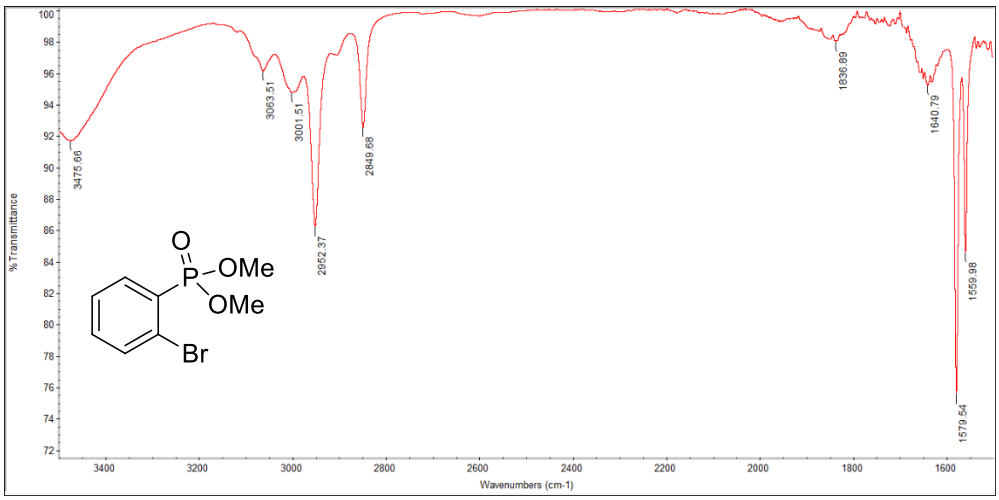

Figure A108. Infrared absorption spectrum of dimethyl *o*-(bromophenyl)phosphonate.

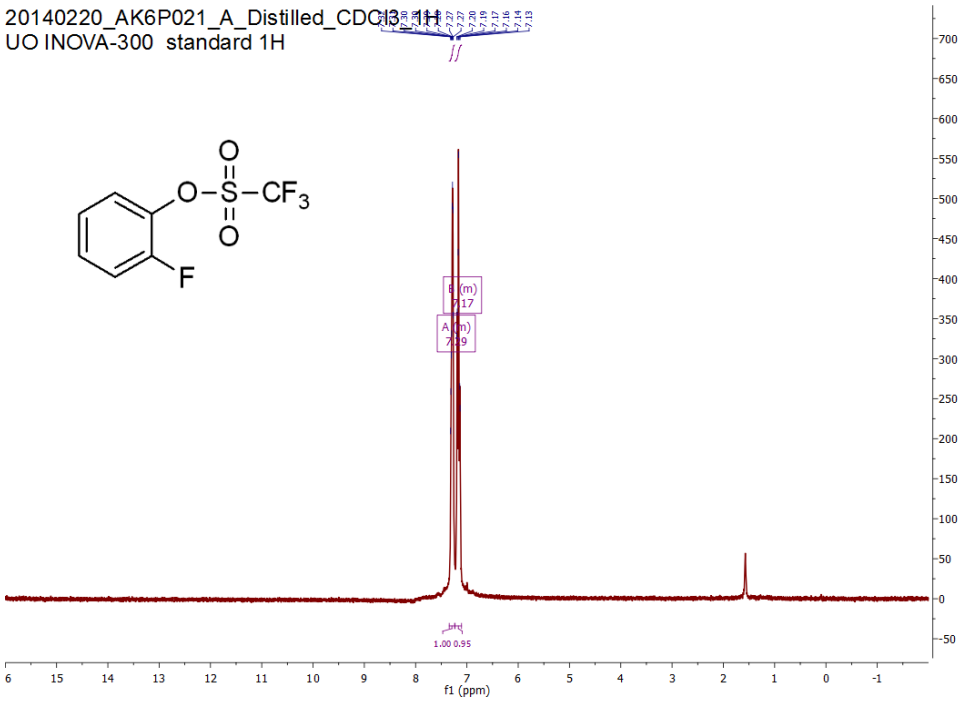

Figure A109. ^{1}H NMR of 2-fluorophenyl trifluoromethanesulfonate.

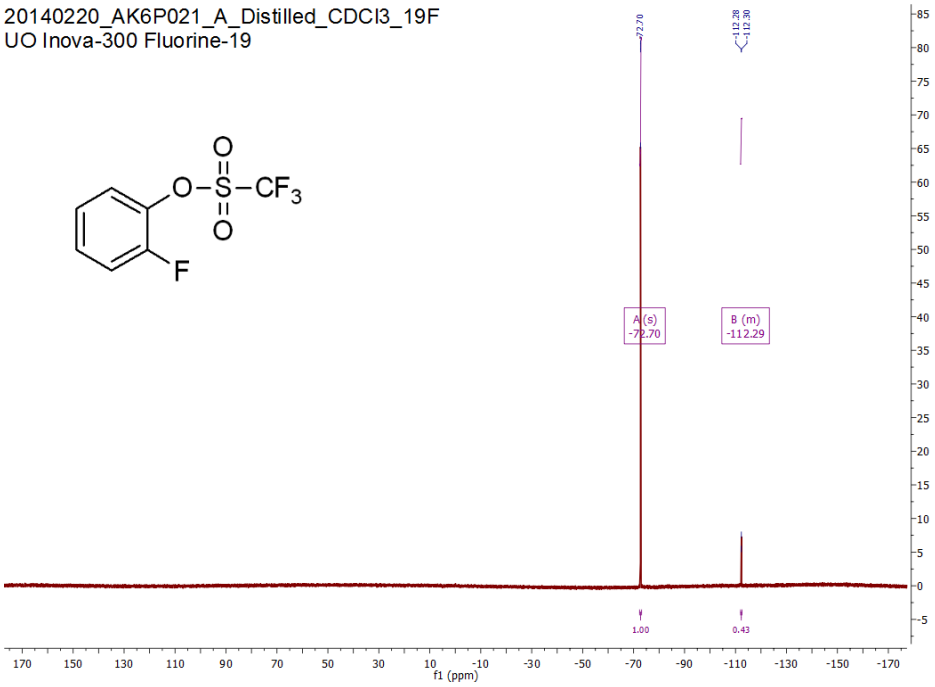

Figure A110. ^{19}F NMR of 2-fluorophenyl trifluoromethanesulfonate.

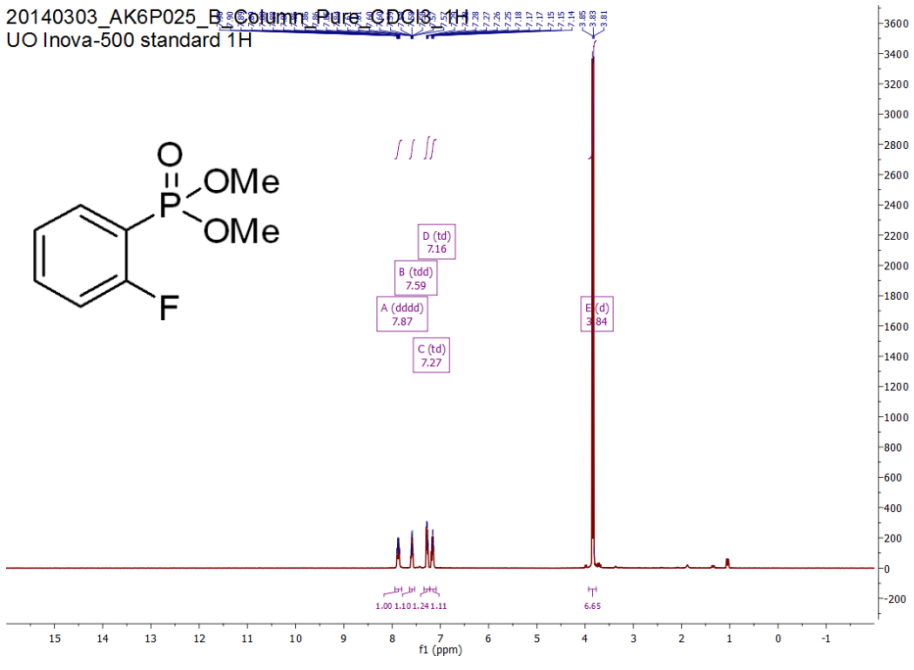

Figure A111. ^{1}H NMR of dimethyl *o*-(fluorophenyl)phosphonate.

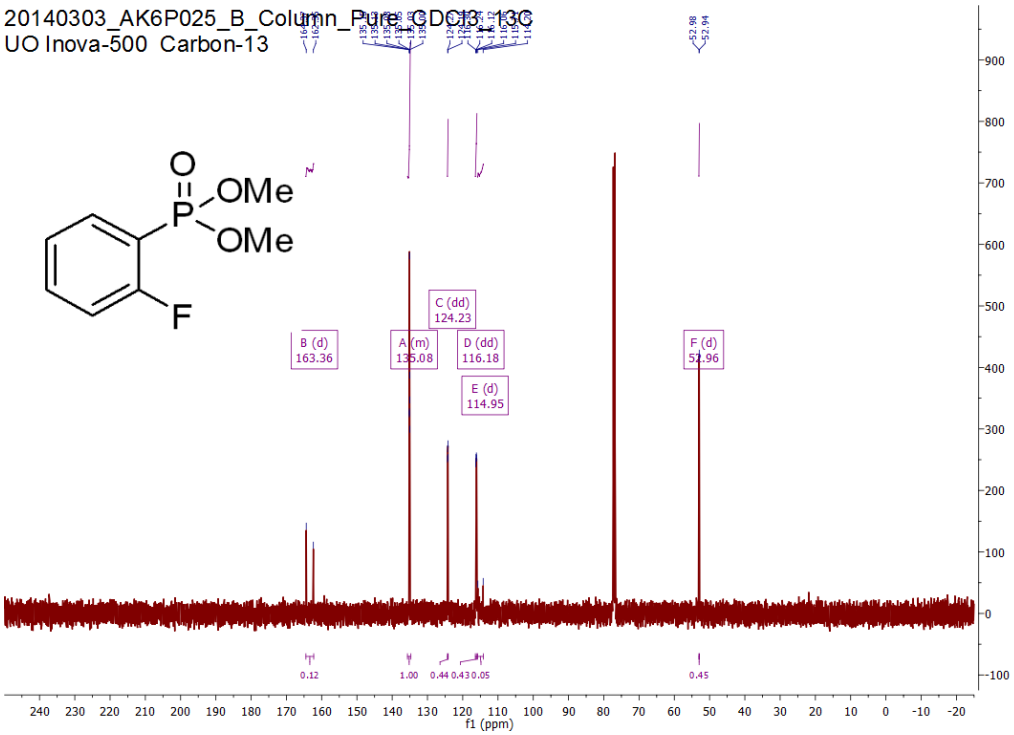

Figure A112. ^{1}H NMR of dimethyl *o*-(fluorophenyl)phosphonate.

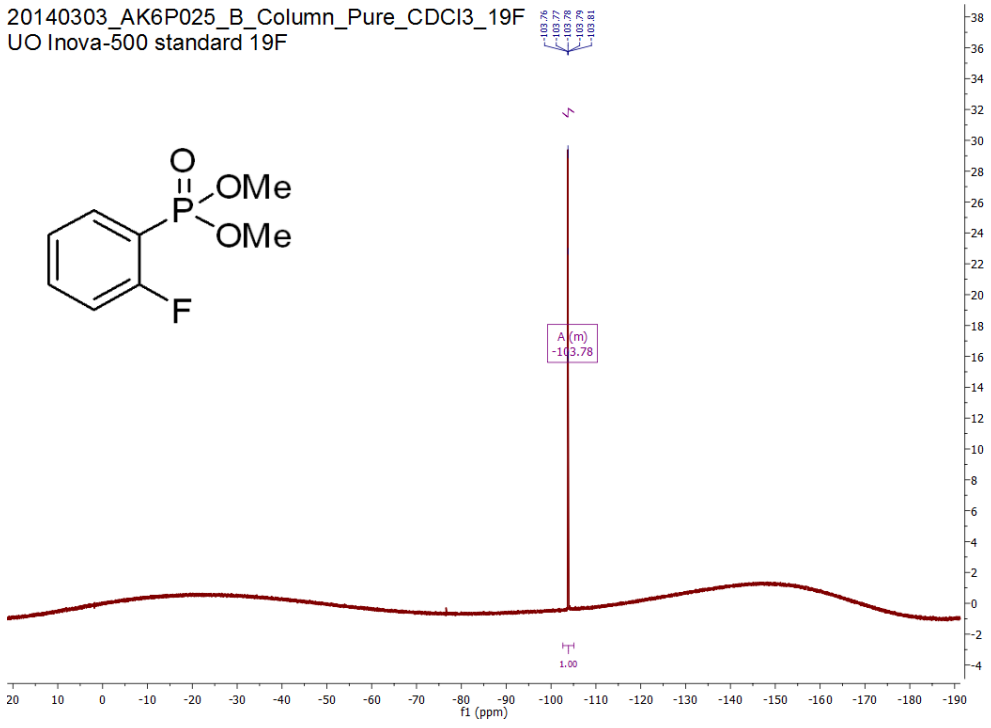

Figure A113. ^{19}F NMR of dimethyl *o*-(fluorophenyl)phosphonate.

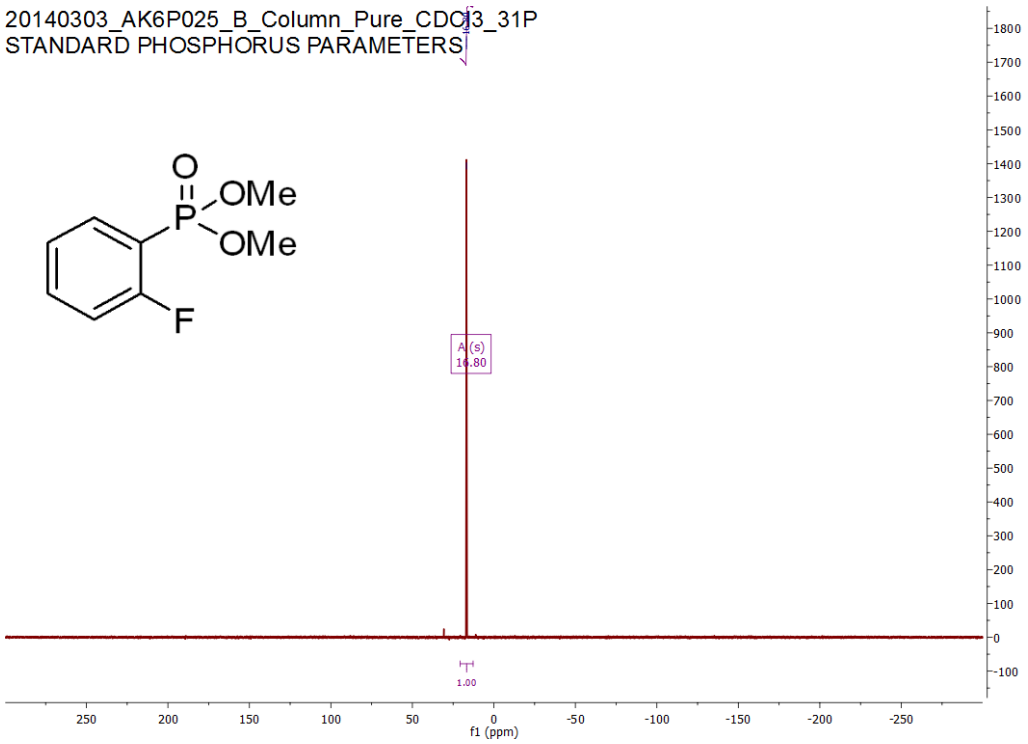

Figure A114. $^{31}P\{^{1}H\}$ NMR of dimethyl *o*-(fluorophenyl)phosphonate.

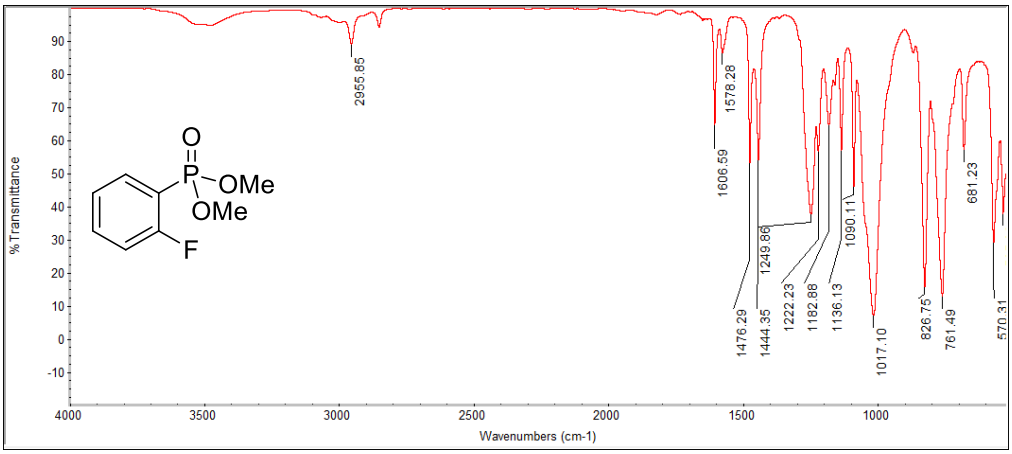

Figure A115. Infrared absorption spectrum of dimethyl *o*-(fluorophenyl)phosphonate.

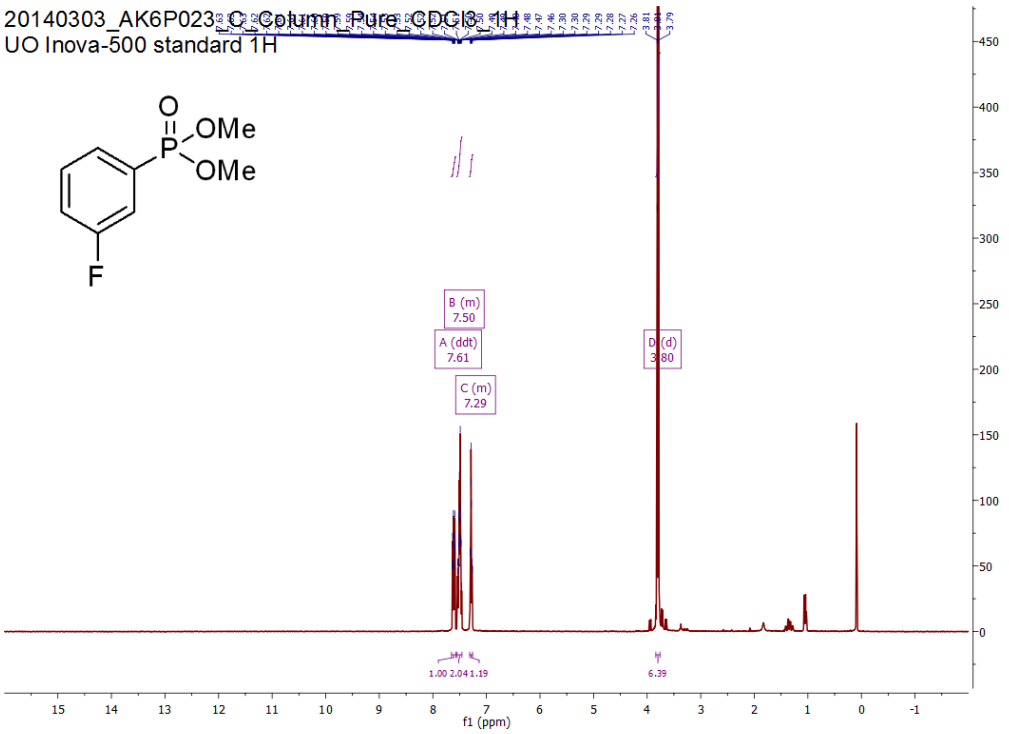

Figure A116. ^{1}H NMR of dimethyl *m*-(fluorophenyl)phosphonate.

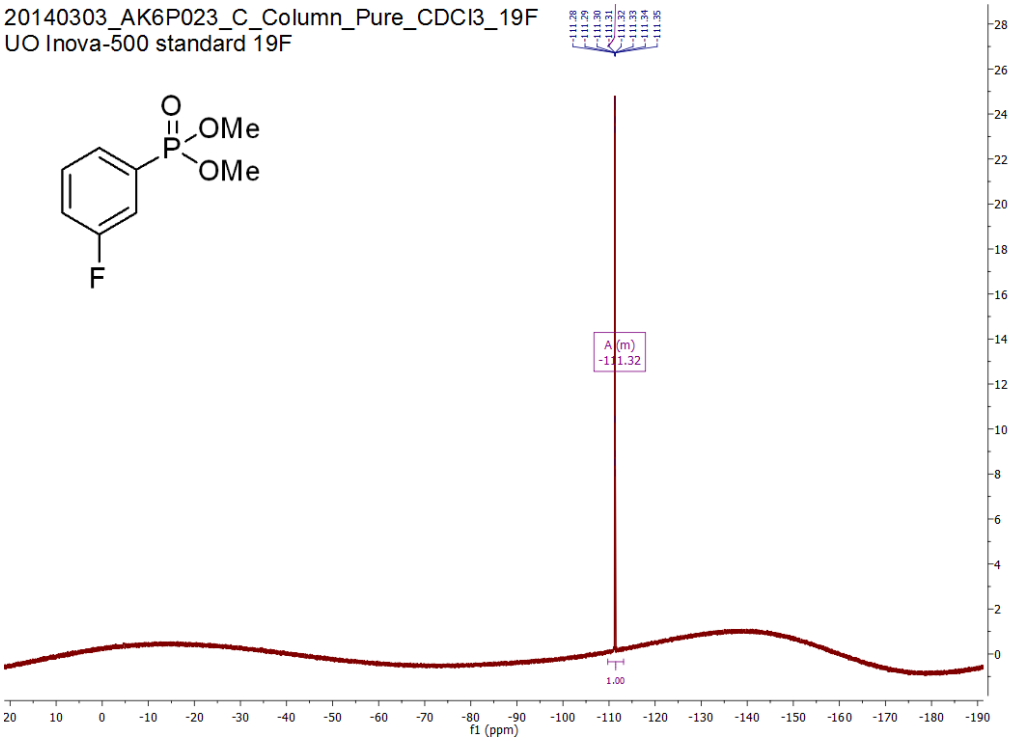

Figure A117. ^{31}P{^{1}H} NMR of dimethyl *m*-(fluorophenyl)phosphonate.

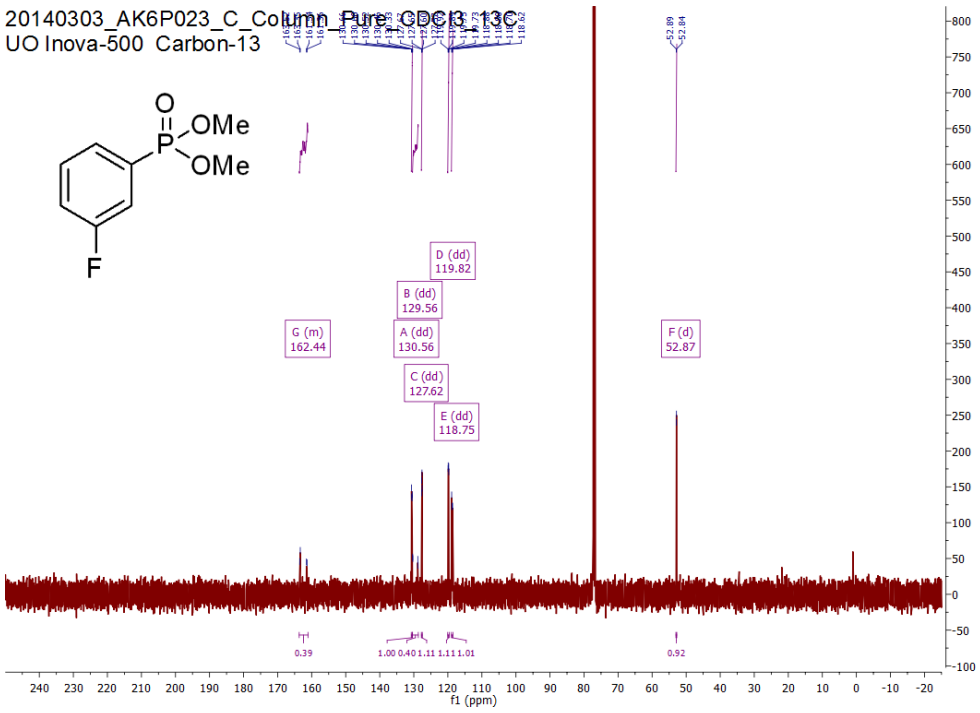

Figure A118. ^{13}C NMR of dimethyl *m*-(fluorophenyl)phosphonate.

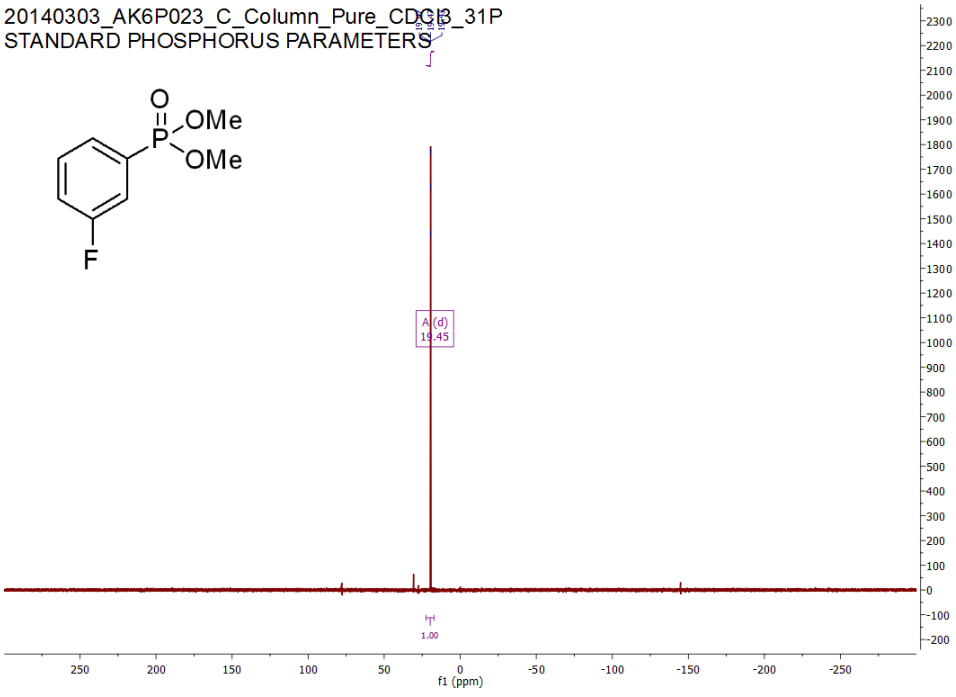

Figure A119. $^{31}P\{^{1}H\}$ NMR of dimethyl *m*-(fluorophenyl)phosphonate.

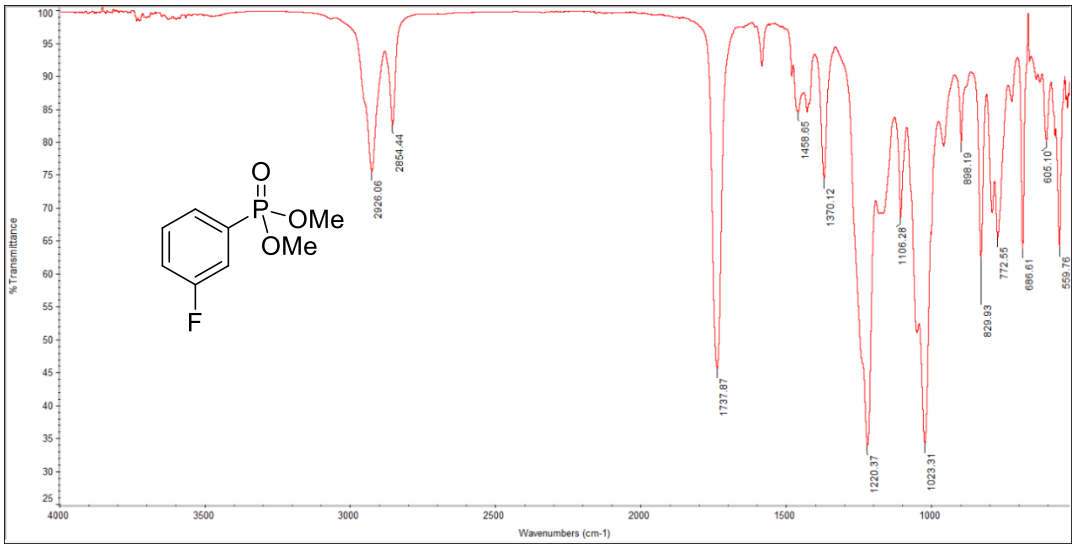

Figure A120. Infrared absorption spectrum of dimethyl *m*-(fluorophenyl)phosphonate.

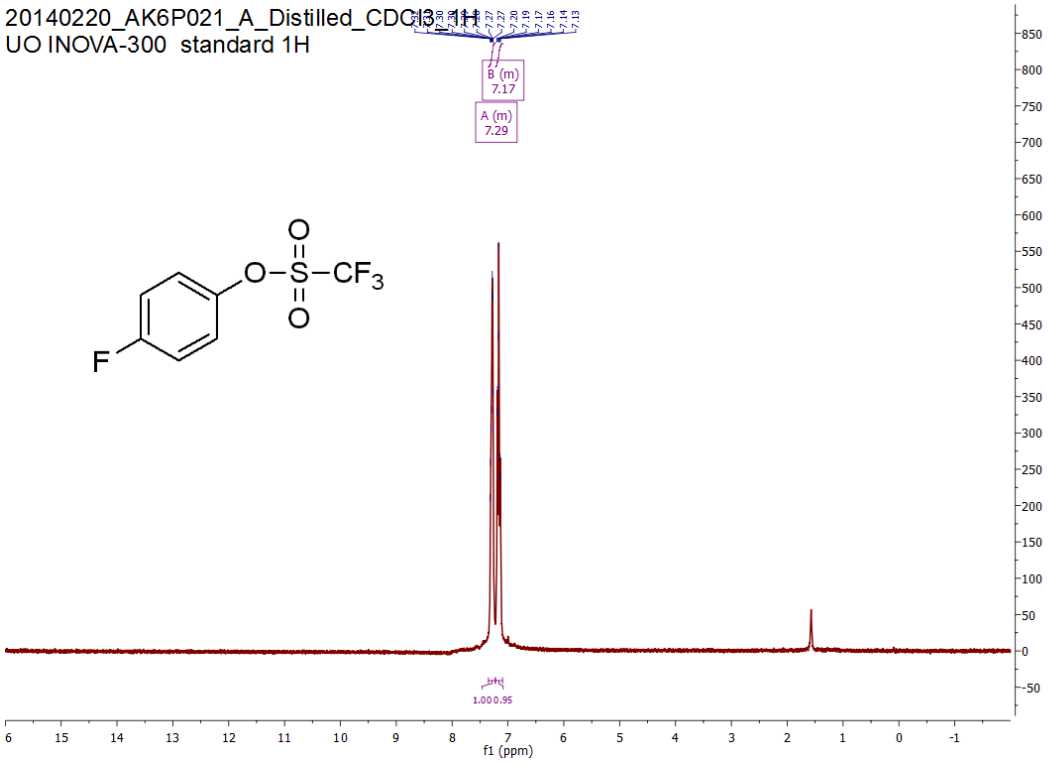

Figure A121. ^{1}H NMR of 4-fluorophenyl trifluoromethanesulfonate.

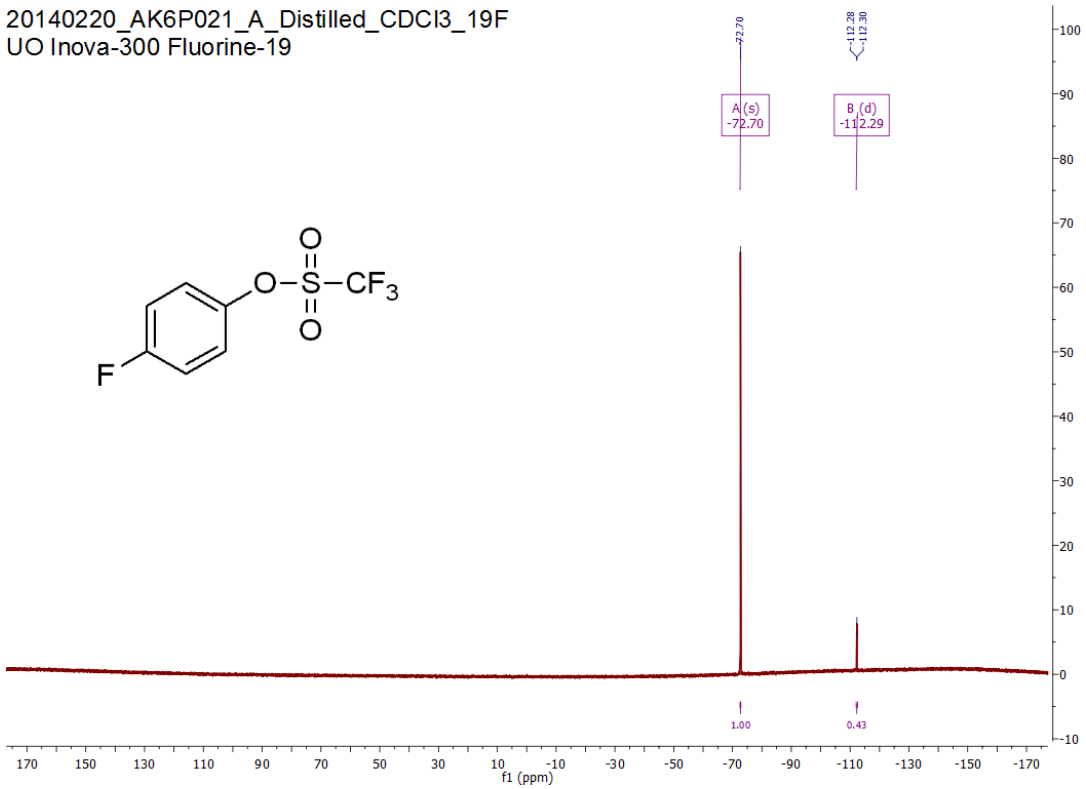

Figure A122. ^{19}F NMR of 4-fluorophenyl trifluoromethanesulfonate.

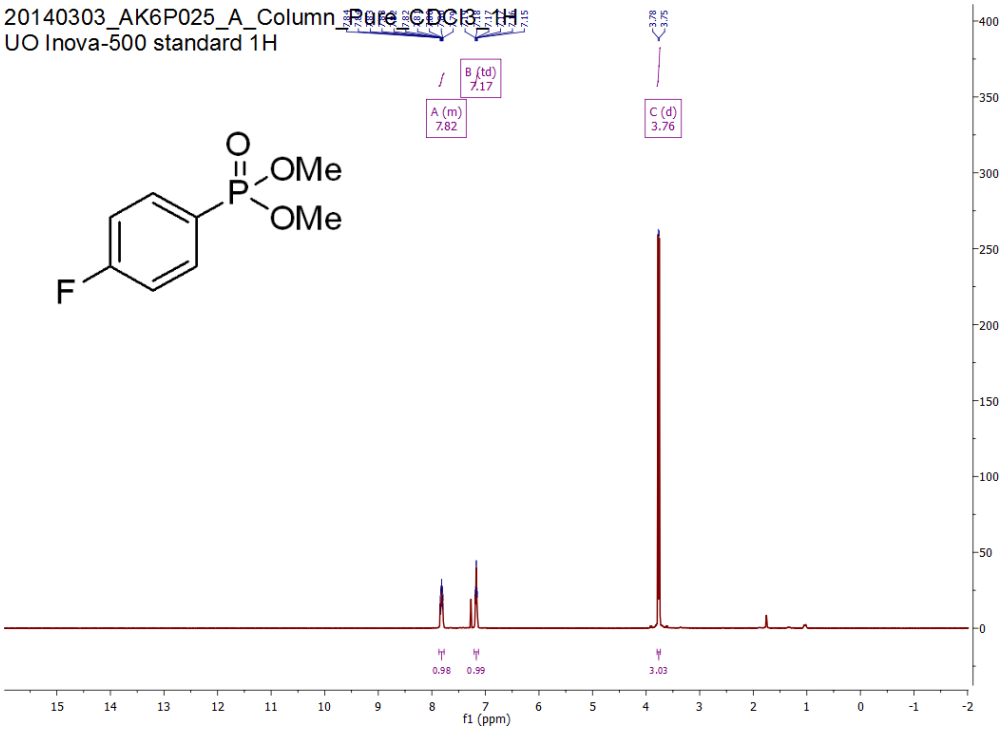

Figure A123. ^{1}H NMR of dimethyl *p*-(fluorophenyl)phosphonate.

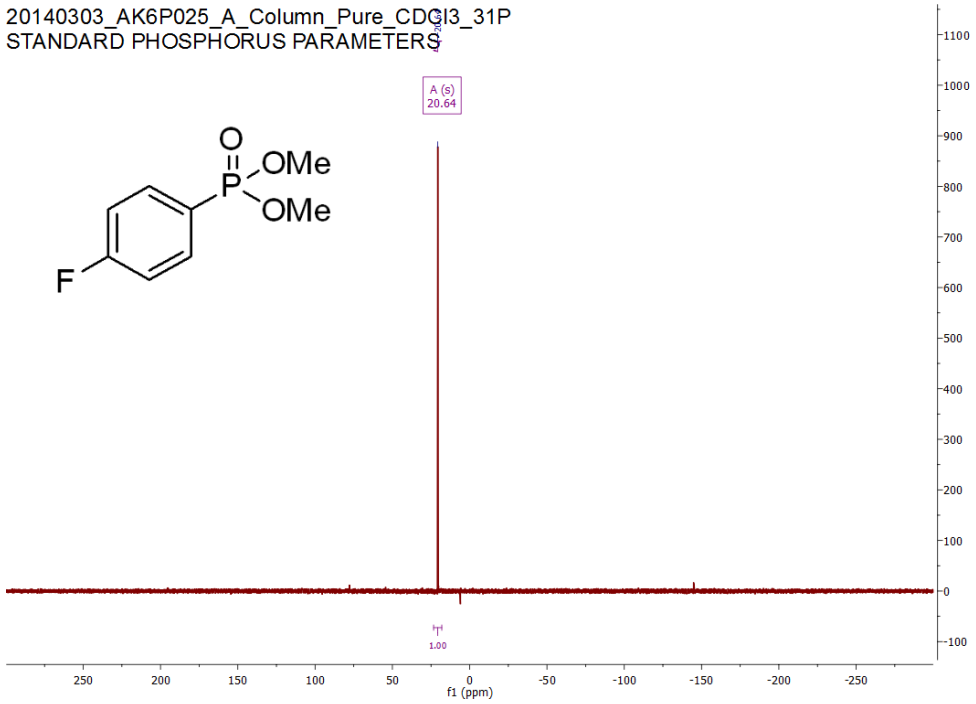

Figure A124. $^{31}P\{^{1}H\}$ NMR of dimethyl *p*-(fluorophenyl)phosphonate.

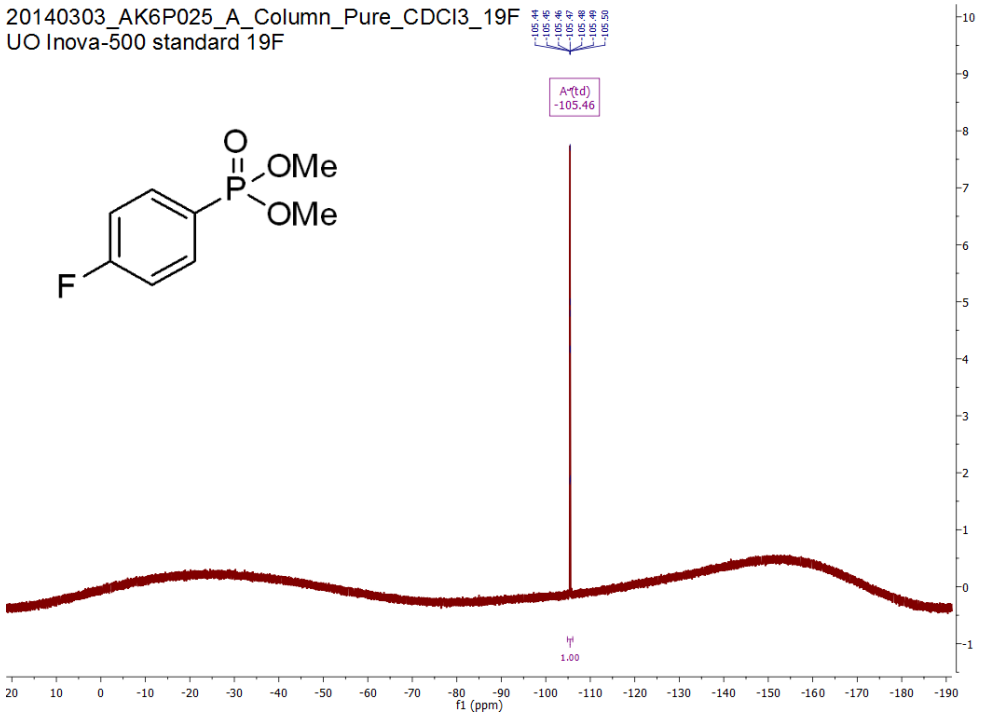

Figure A125. ^{19}F NMR of dimethyl *p*-(fluorophenyl)phosphonate.

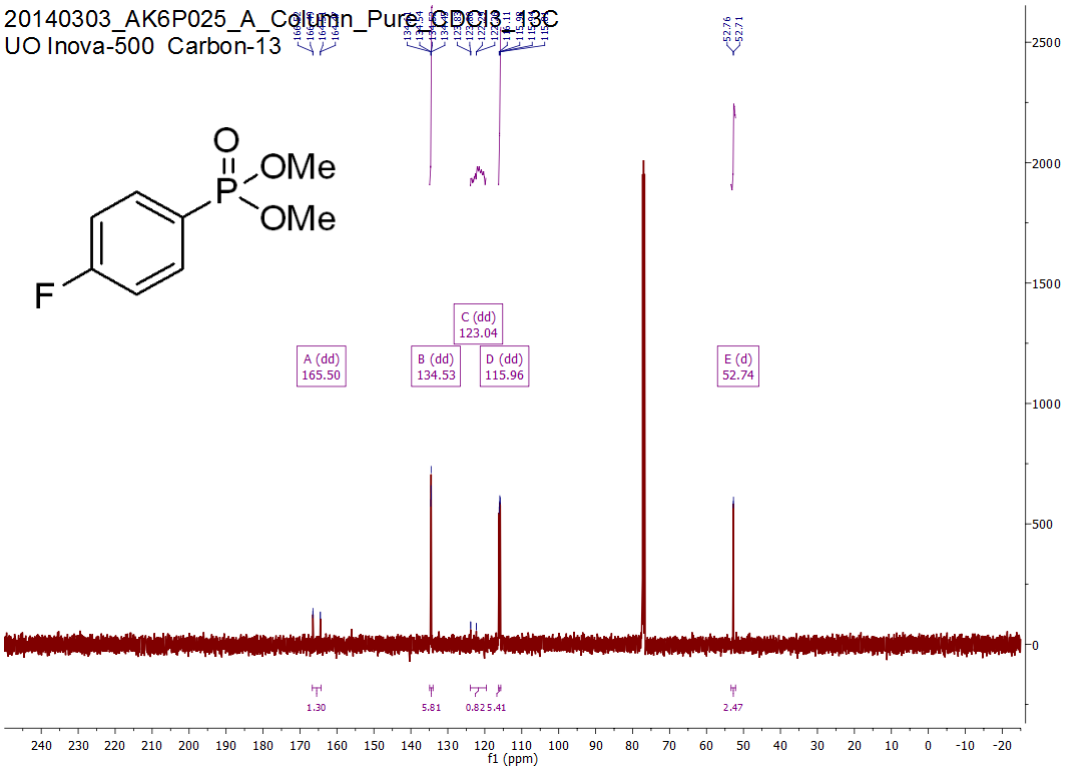

Figure A126. ^{13}C NMR of dimethyl *p*-(fluorophenyl)phosphonate.

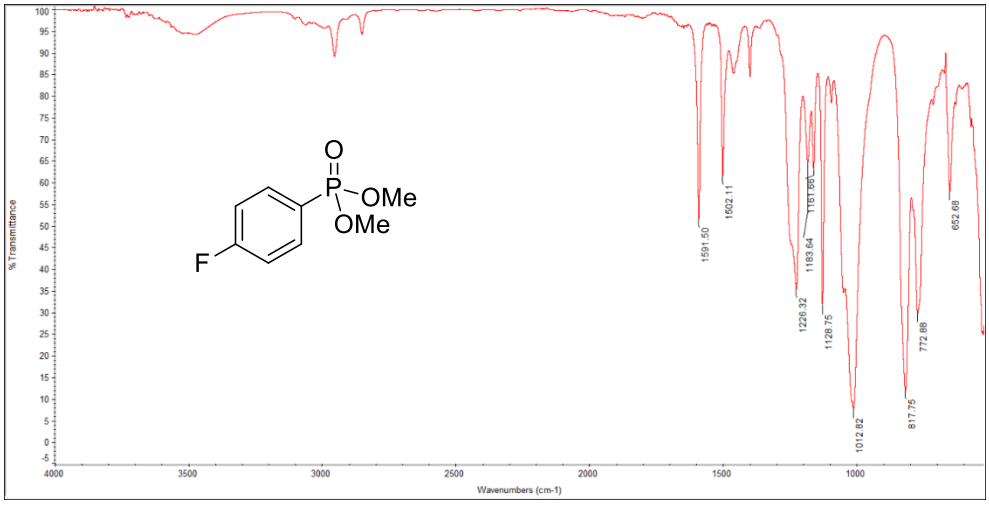

Figure A127. Infrared absorption spectrum of dimethyl *p*-(fluorophenyl)phosphonate.

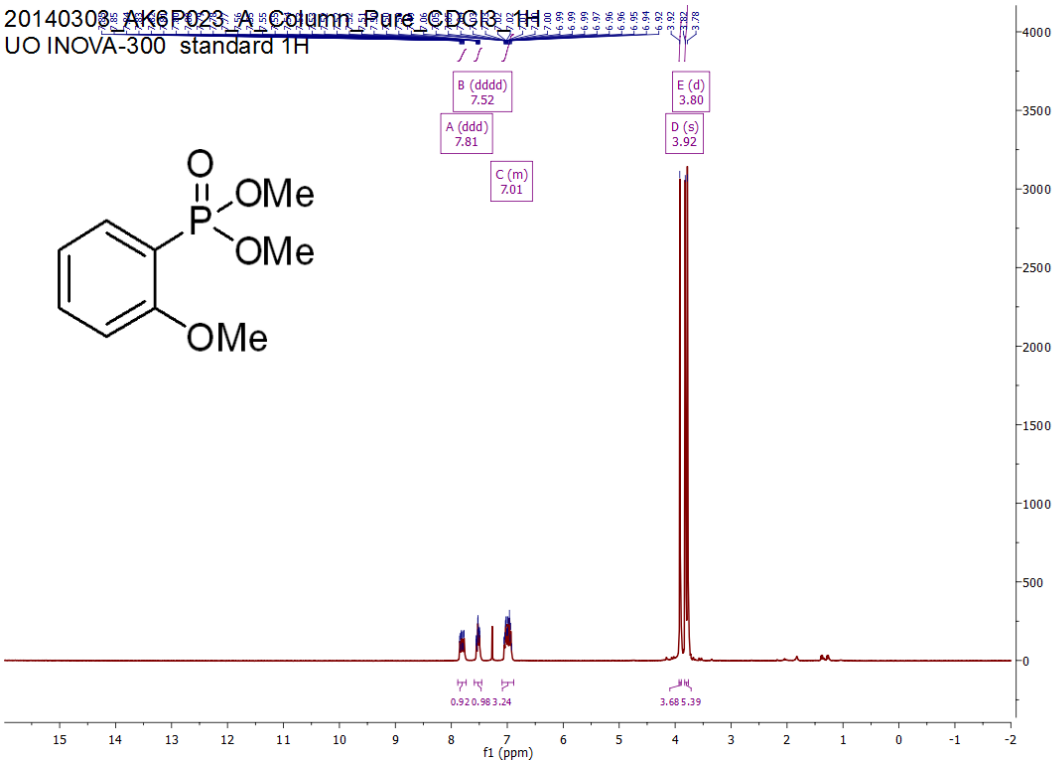

Figure A128. ^{1}H NMR of dimethyl *o*-(methoxyphenyl)phosphonate.

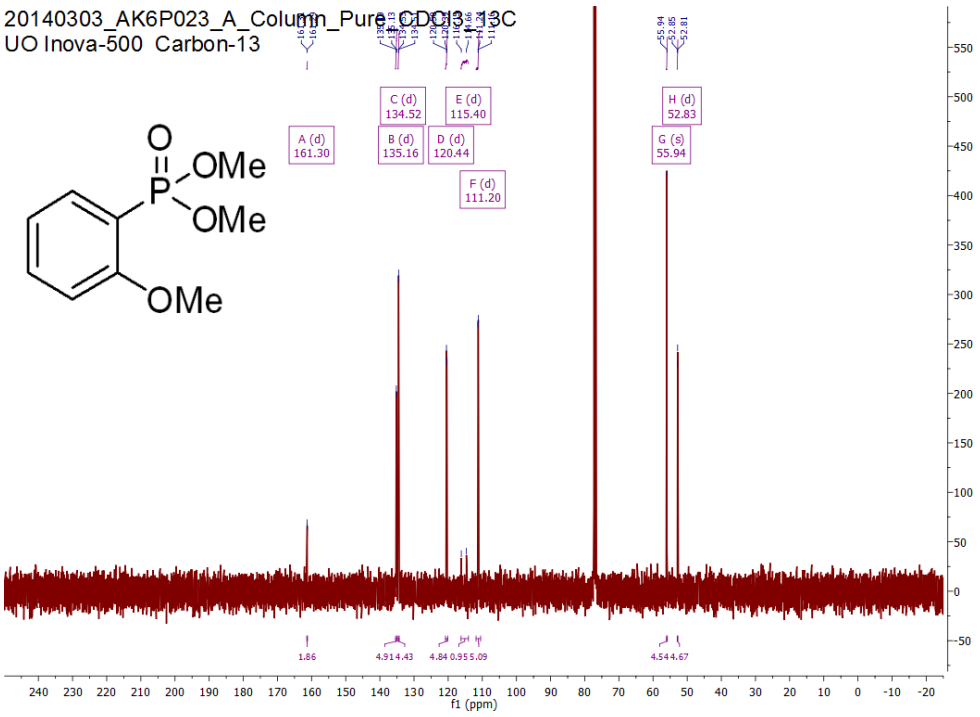

Figure A129. ^{13}C NMR of dimethyl *o*-(methoxyphenyl)phosphonate.

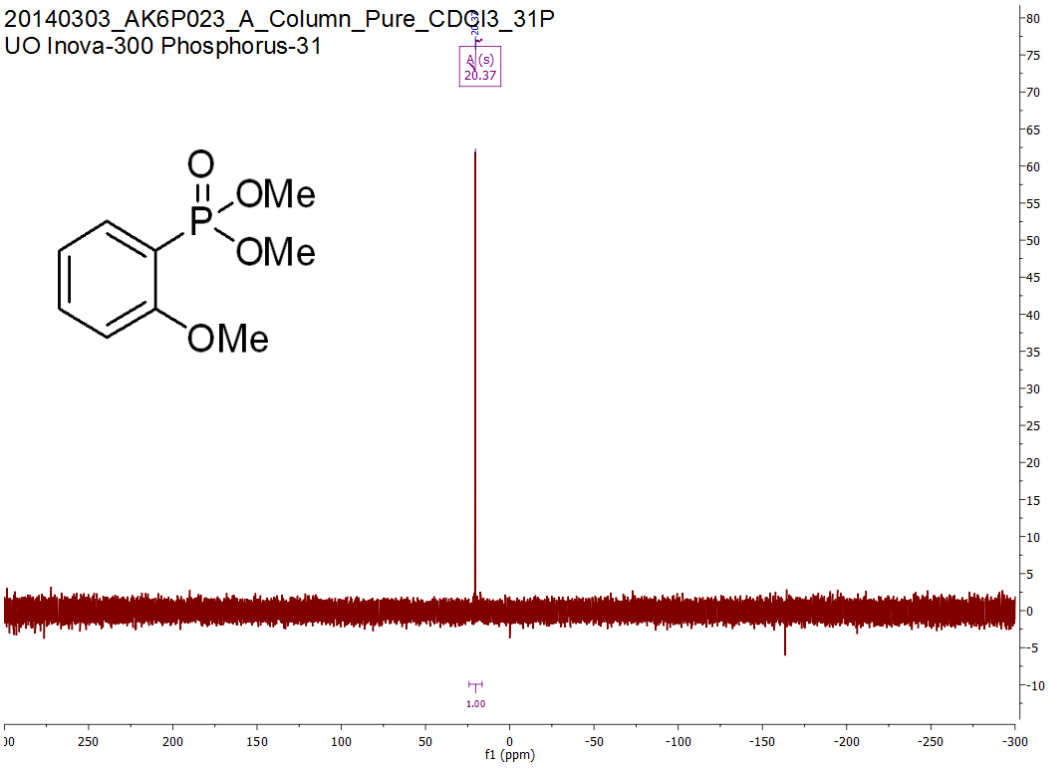

Figure A130. $^{31}P\{^{1}H\}$ NMR of dimethyl *o*-(methoxyphenyl)phosphonate.

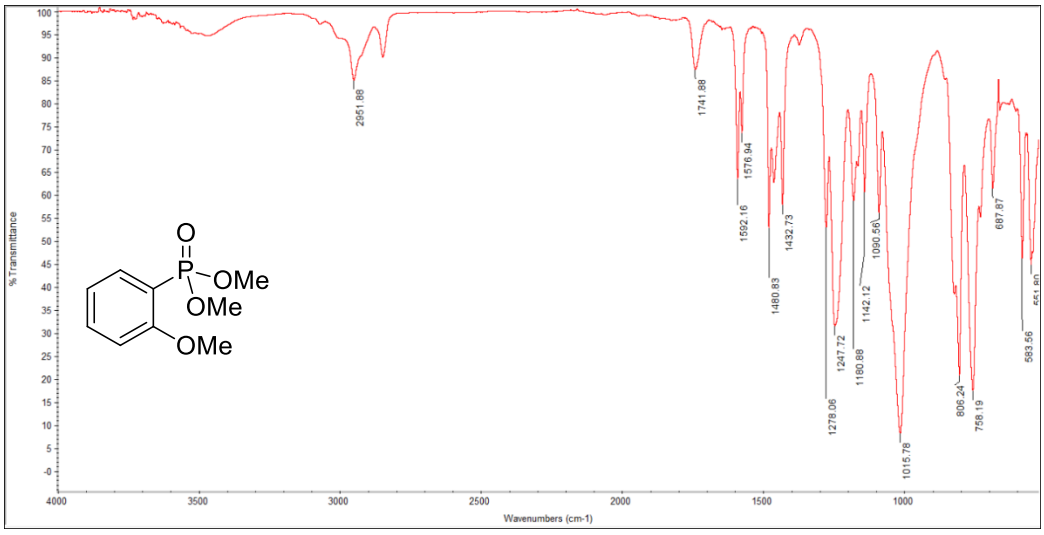

Figure A131. Infrared absorption spectrum of dimethyl *o*-(methoxyphenyl)phosphonate.

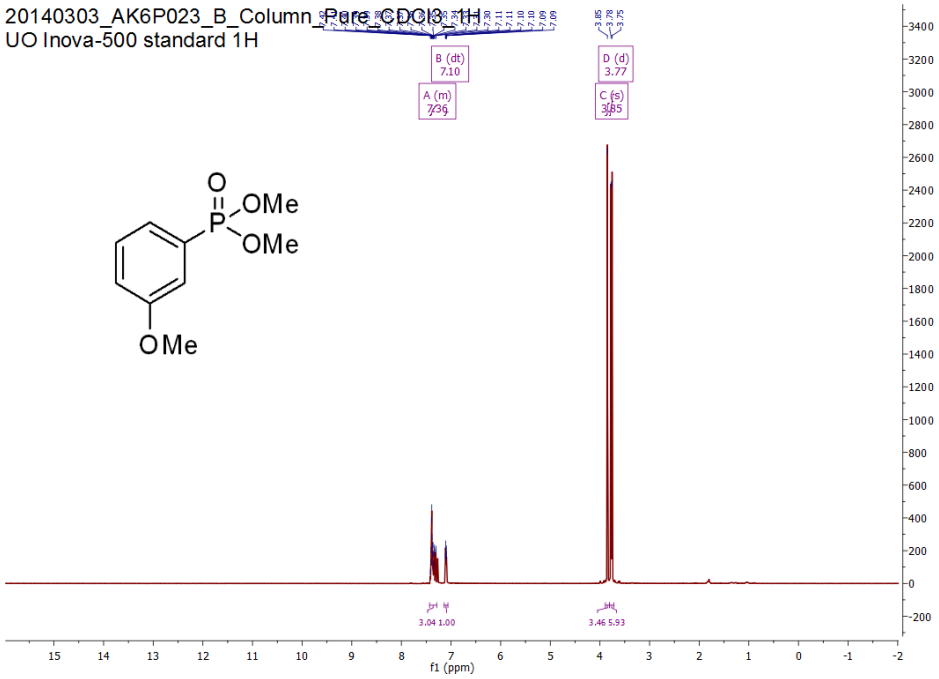

Figure A132. ^{1}H NMR of dimethyl *m*-(methoxyphenyl)phosphonate.

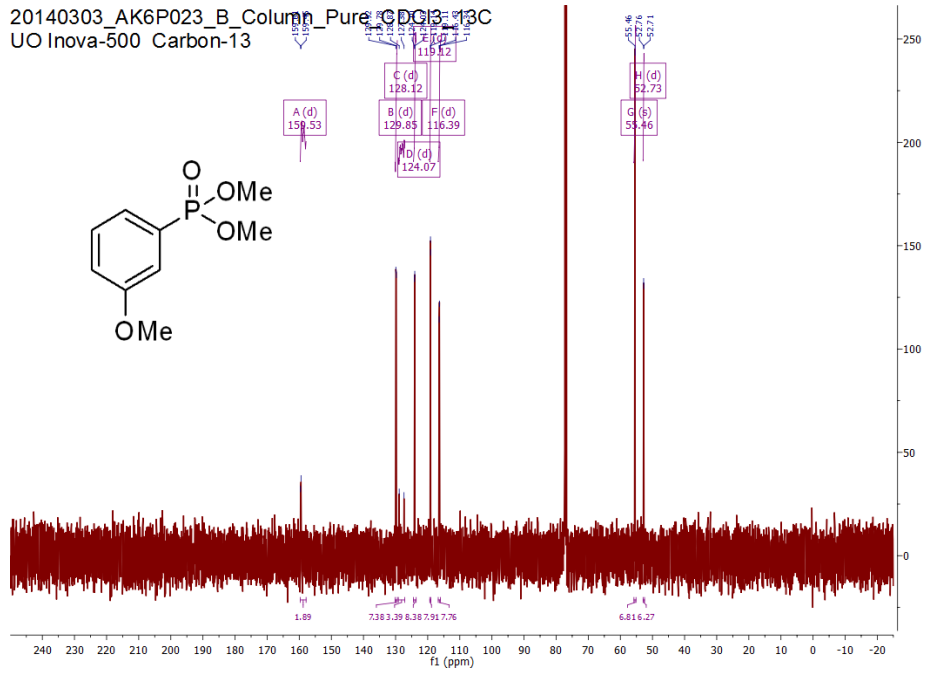

Figure A133. ^{13}C NMR of dimethyl *m*-(methoxyphenyl)phosphonate.

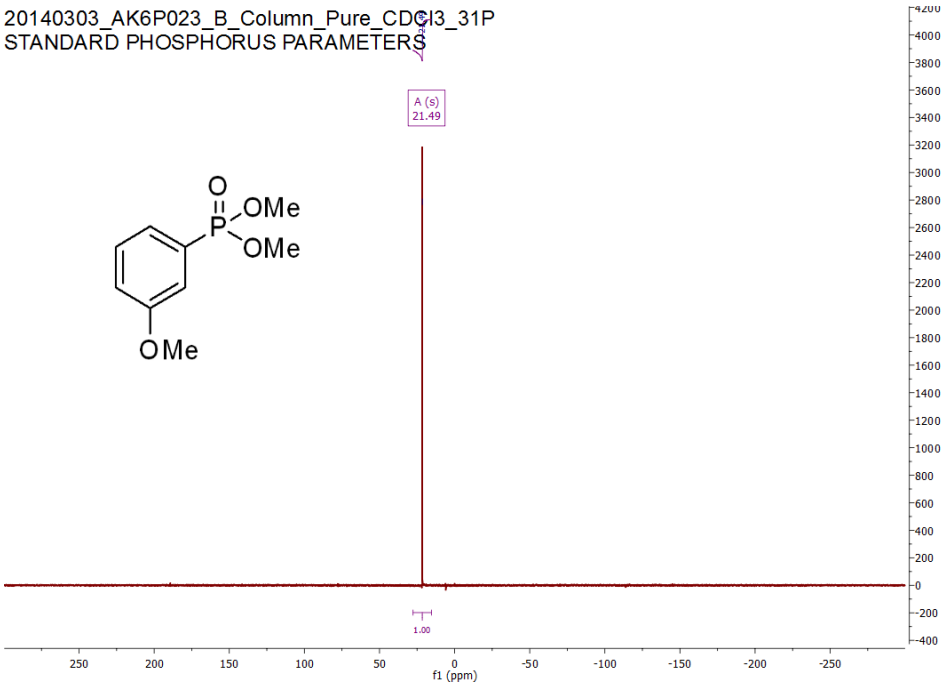

Figure A134. $^{31}P\{^{1}H\}$ NMR of dimethyl *m*-(methoxyphenyl)phosphonate.

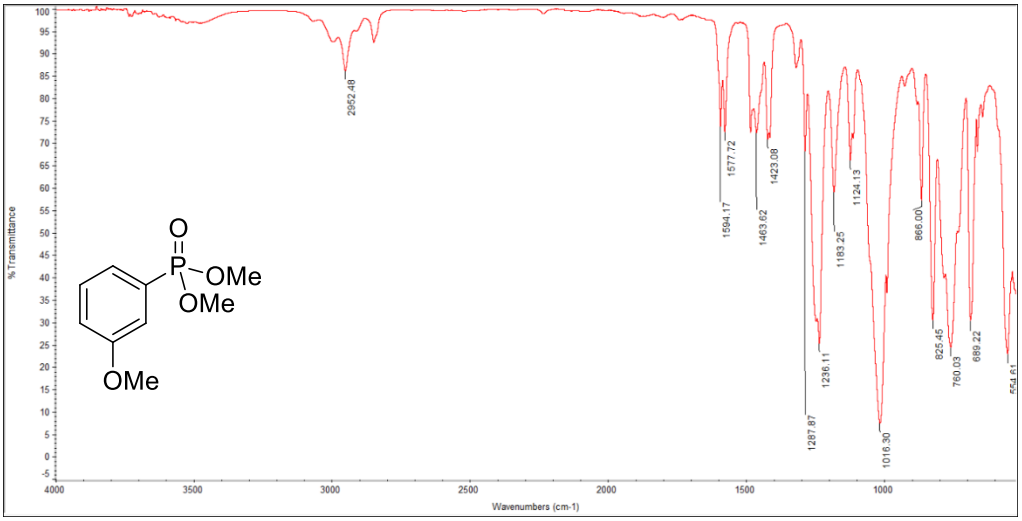

Figure A135. Infrared absorption spectrum of dimethyl *m*-(methoxyphenyl)phosphonate.

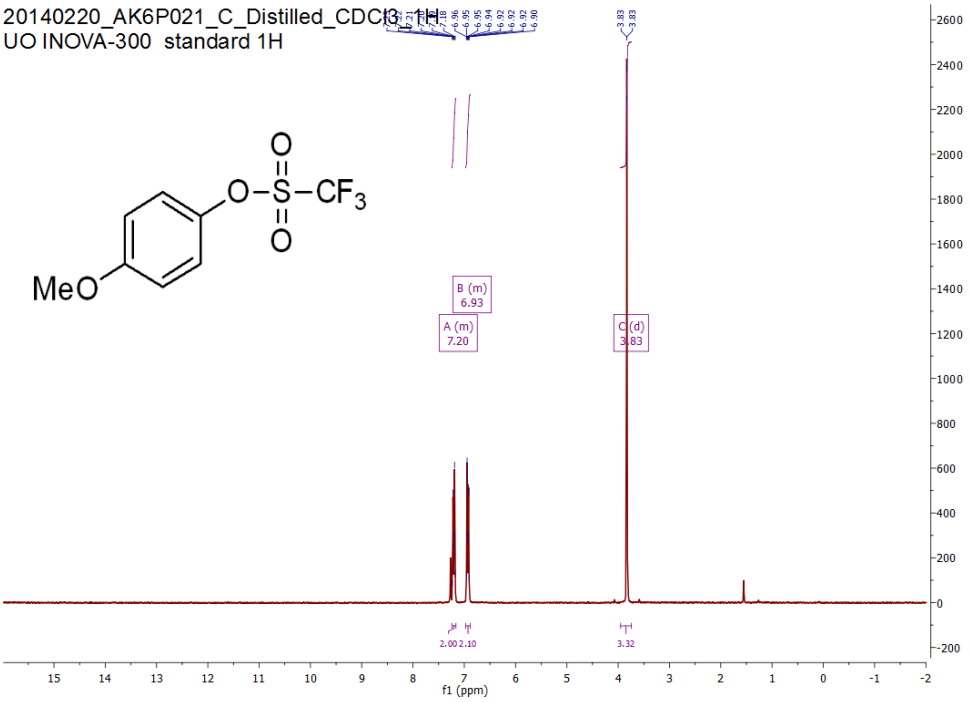

Figure A136. ^{1}H NMR of 4-methoxyphenyl trifluoromethanesulfonate.

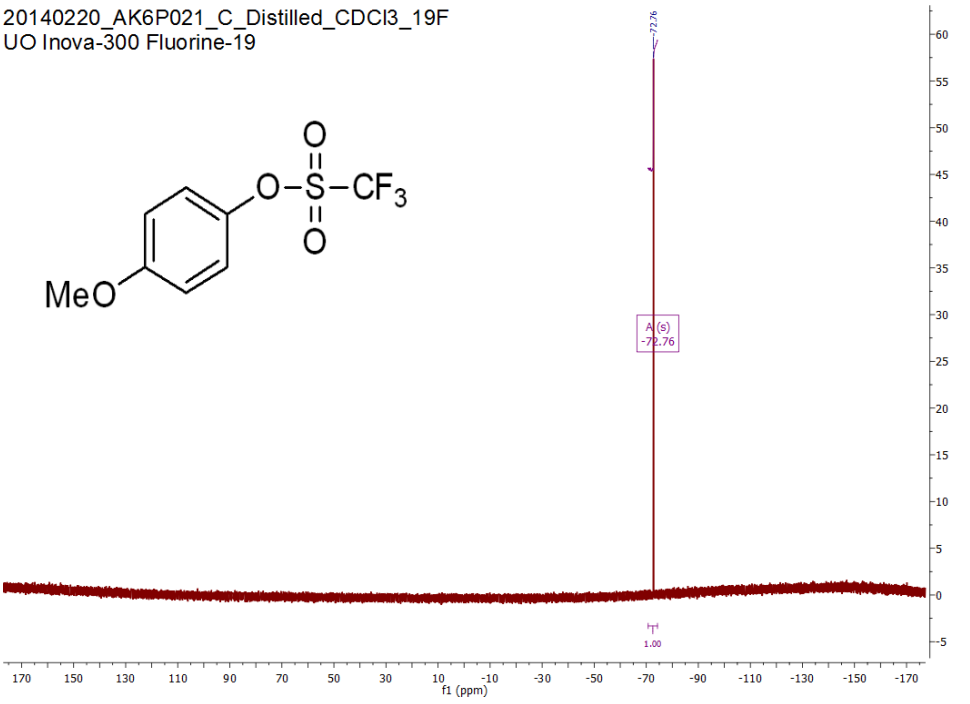

Figure A137. ^{19}F NMR of 4-methoxyphenyl trifluoromethanesulfonate.

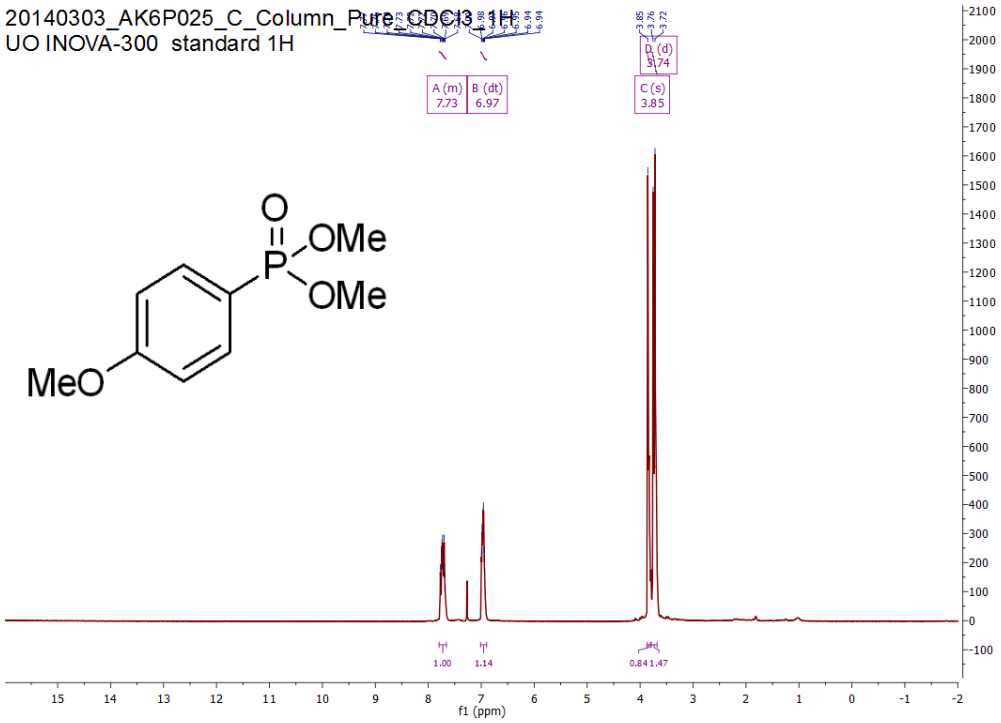

Figure A138. ^{1}H NMR of dimethyl *p*-(methoxyphenyl)phosphonate.

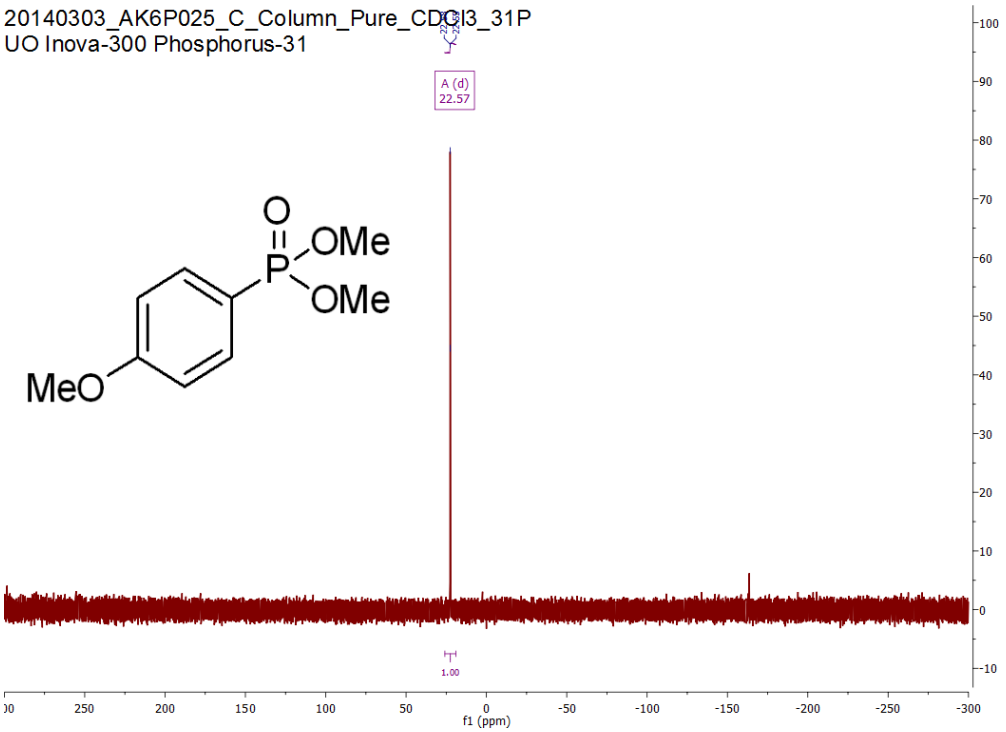

Figure A139. ^{31}P{^{1}H} NMR of dimethyl *p*-(methoxyphenyl)phosphonate.

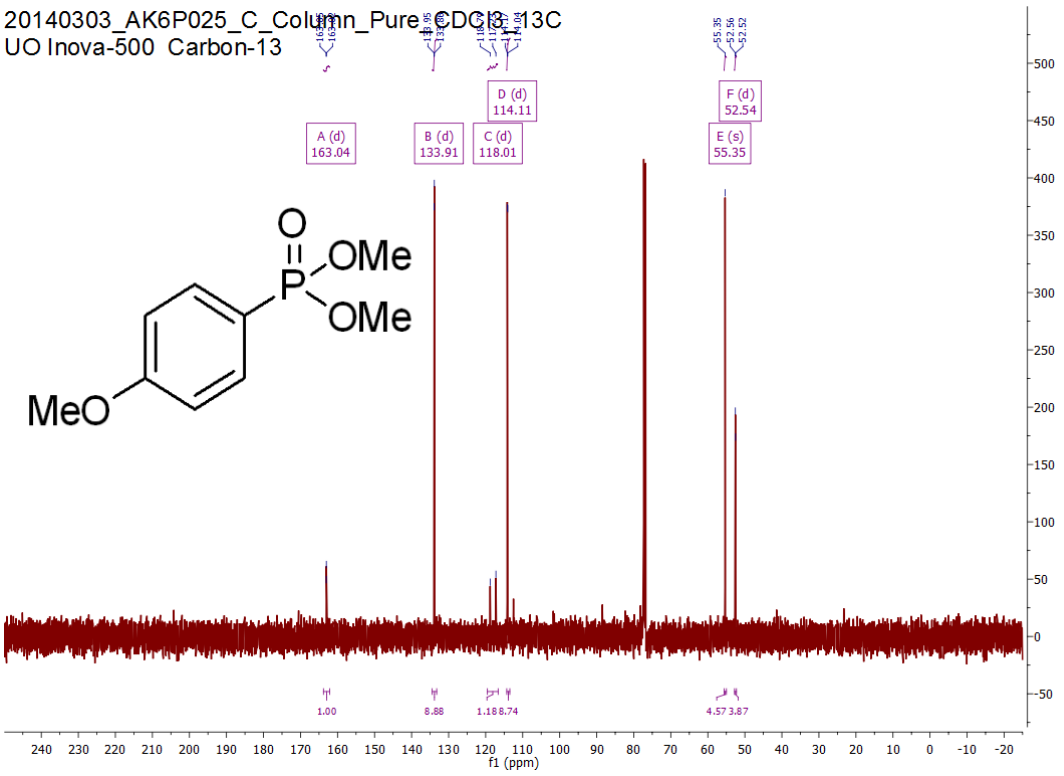

Figure A140. ^{13}C NMR of dimethyl *p*-(methoxyphenyl)phosphonate.

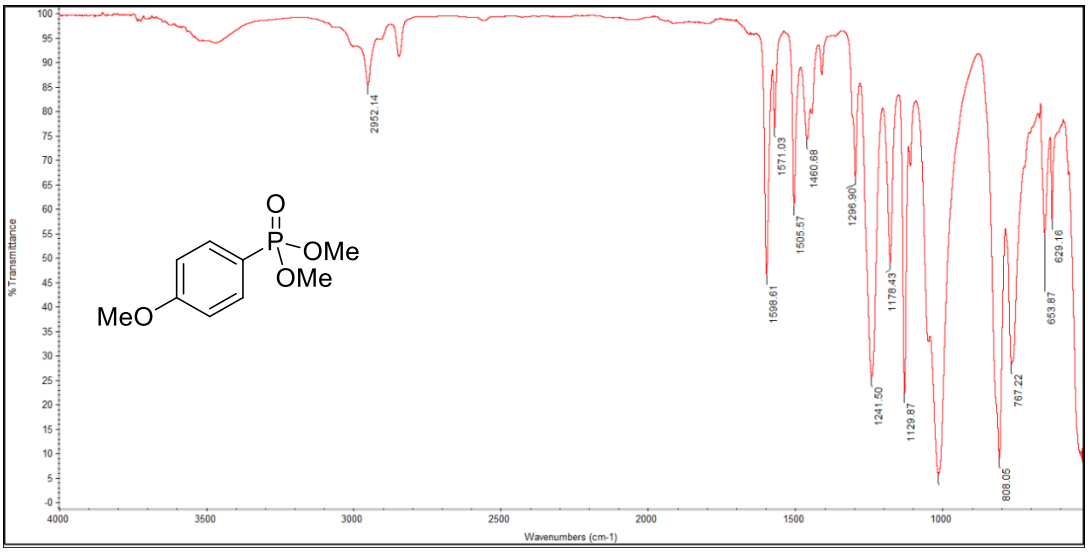

Figure A141. Infrared absorption spectrum of dimethyl *m*-(methoxyphenyl)phosphonate.

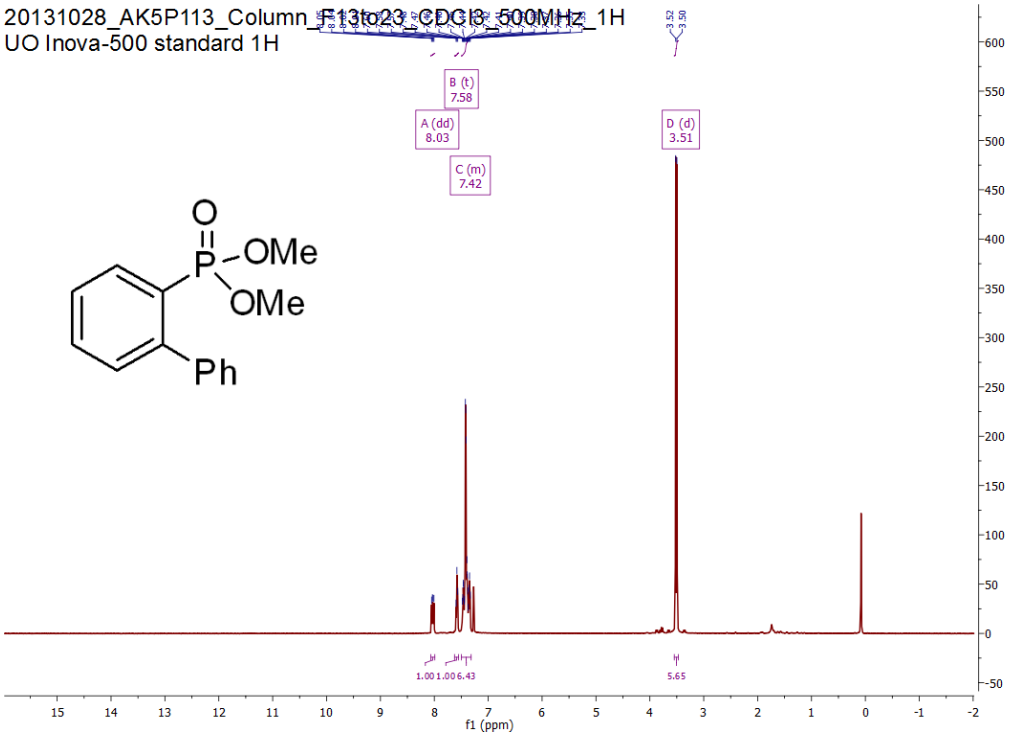

Figure A142. ^{1}H NMR of dimethyl *o*-(biphenyl)phosphonate.

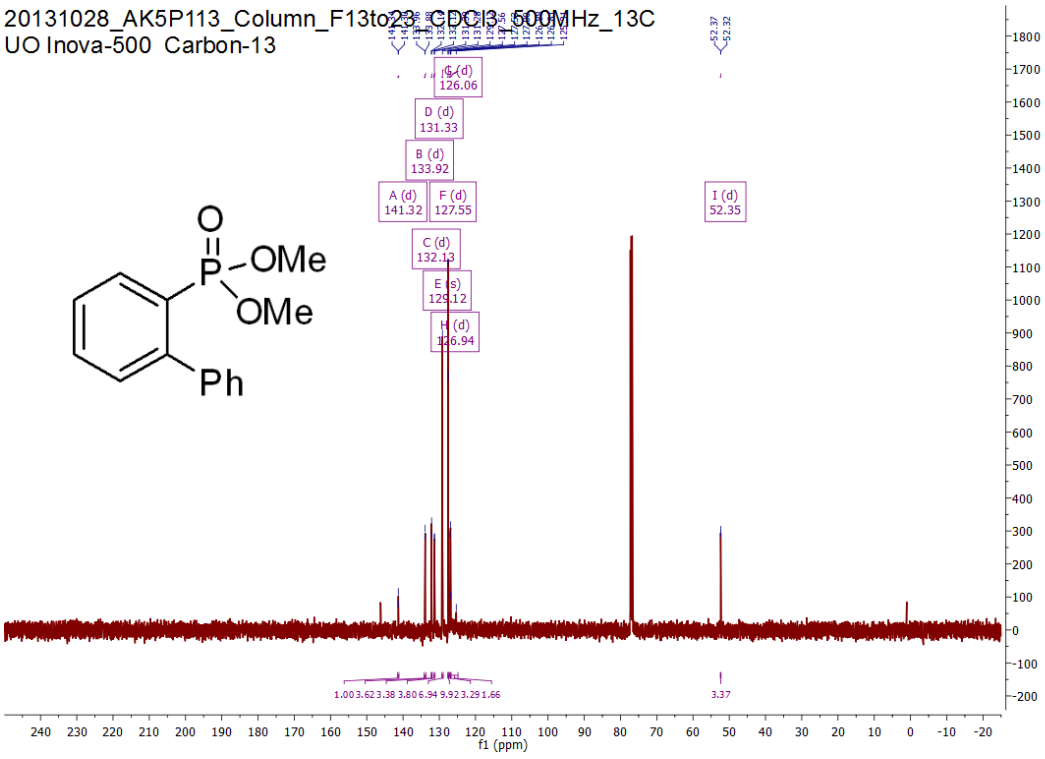

Figure A143. ^{13}C NMR of dimethyl *o*-(biphenyl)phosphonate.

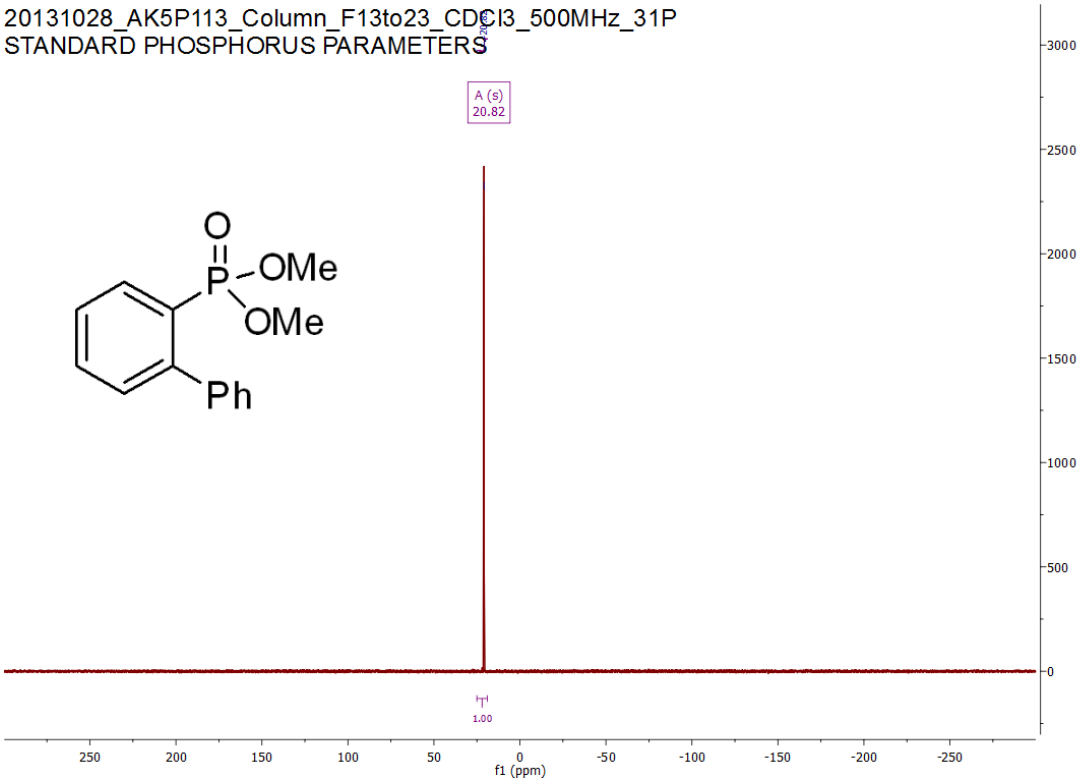

Figure A144. $^{31}P\{^{1}H\}$ NMR of dimethyl *o*-(biphenyl)phosphonate.

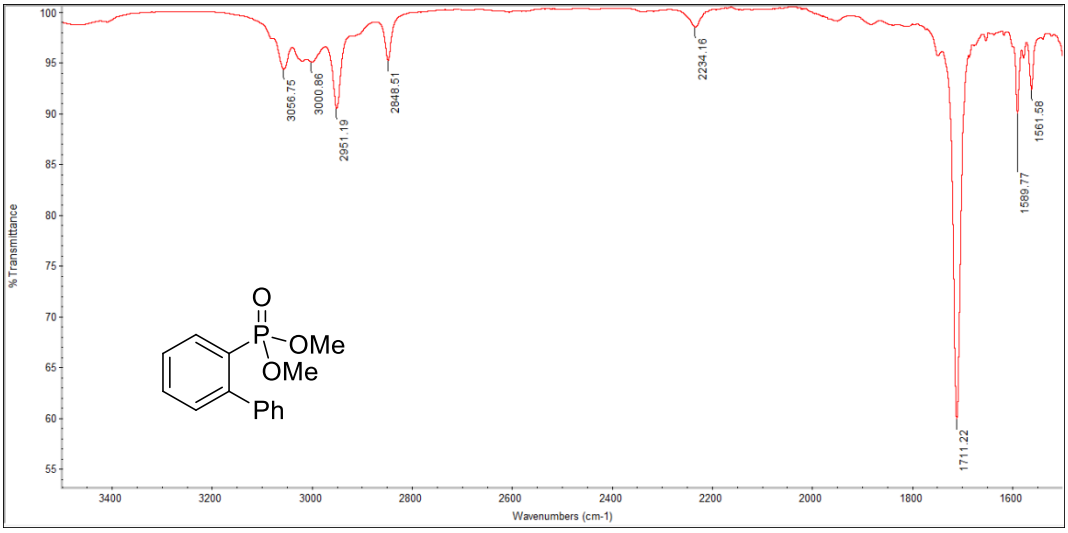

Figure A145. Infrared absorption spectrum of dimethyl *o*-(biphenyl)phosphonate.

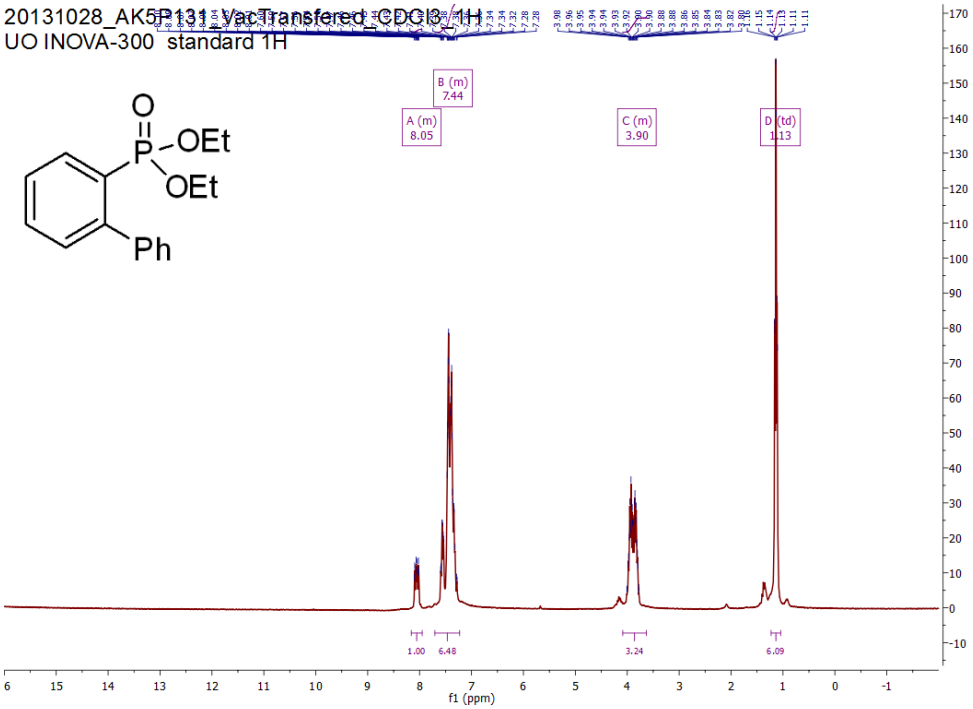

Figure A146. ^{1}H NMR of diethyl *o*-(biphenyl)phosphonate.

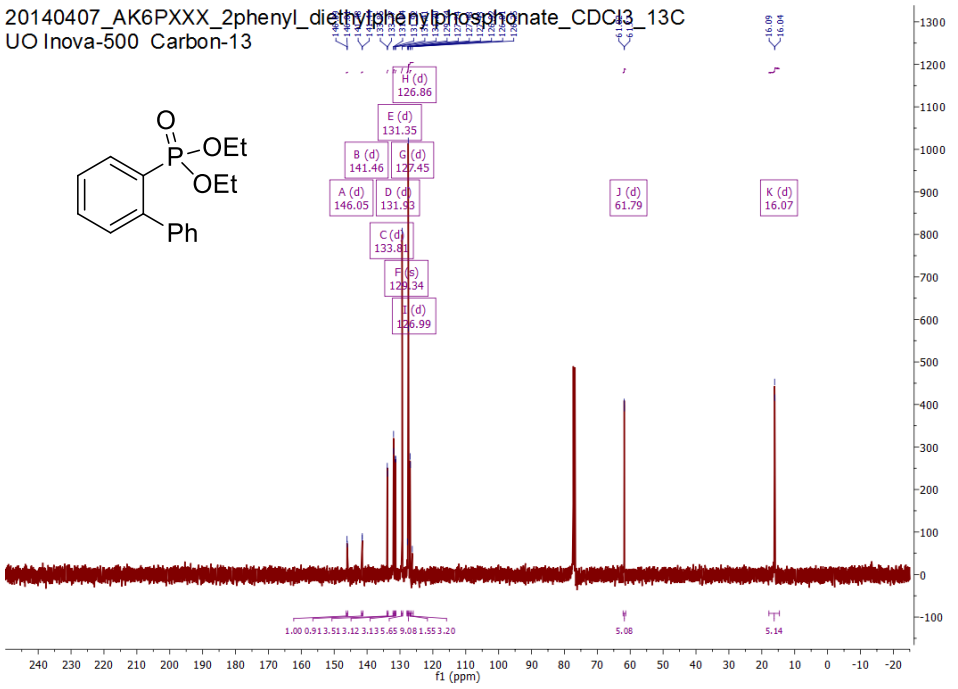

Figure A147. ^{13}C NMR of diethyl *o*-(biphenyl)phosphonate.

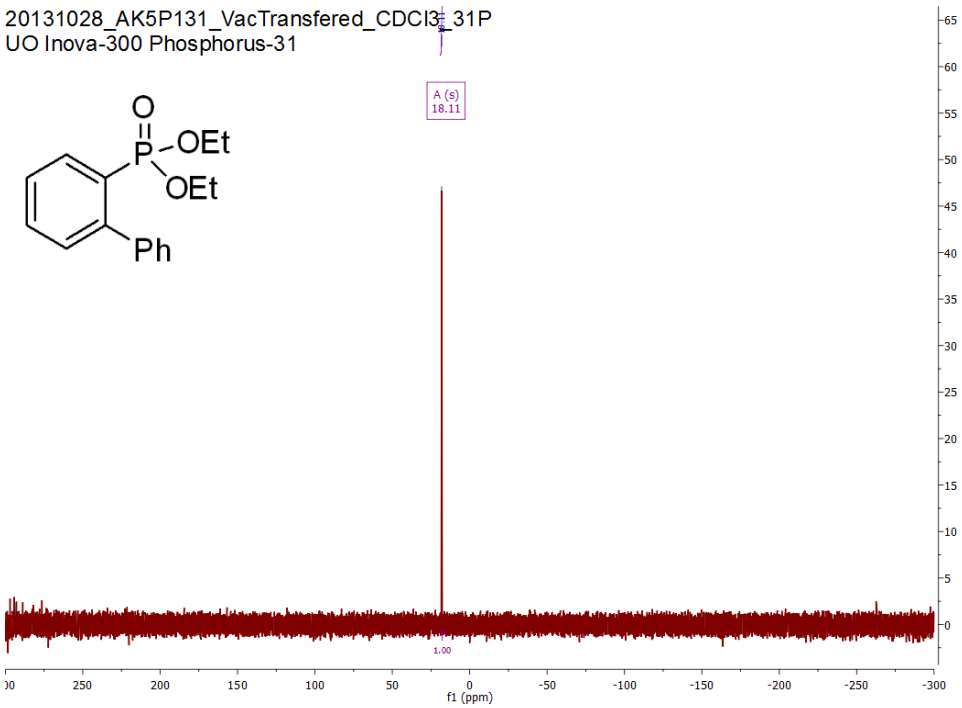

Figure A148. $^{31}P\{^{1}H\}$ NMR of diethyl *o*-(biphenyl)phosphonate.

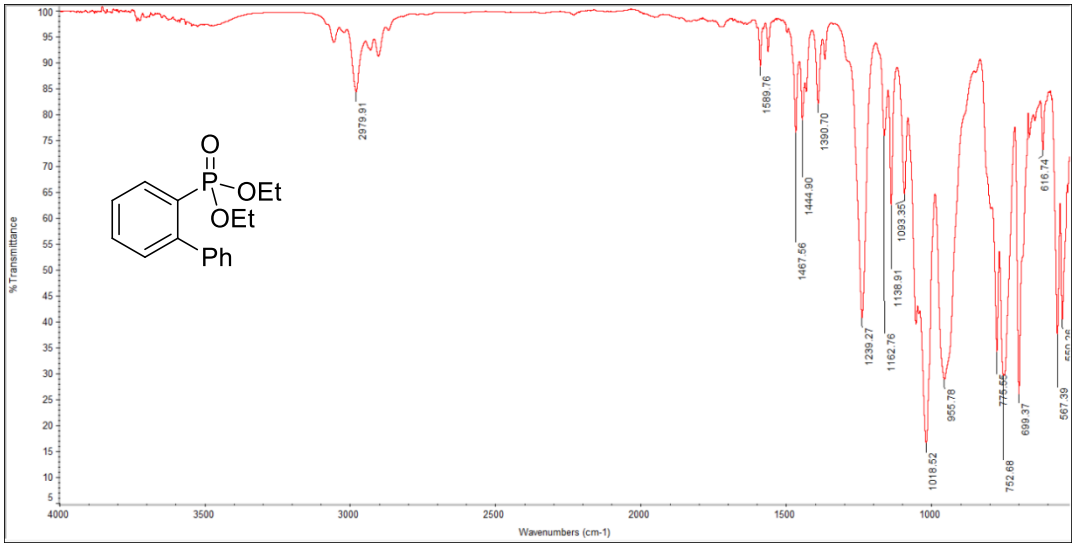

Figure A149. Infrared absorption spectrum of diethyl *o*-(biphenyl)phosphonate.

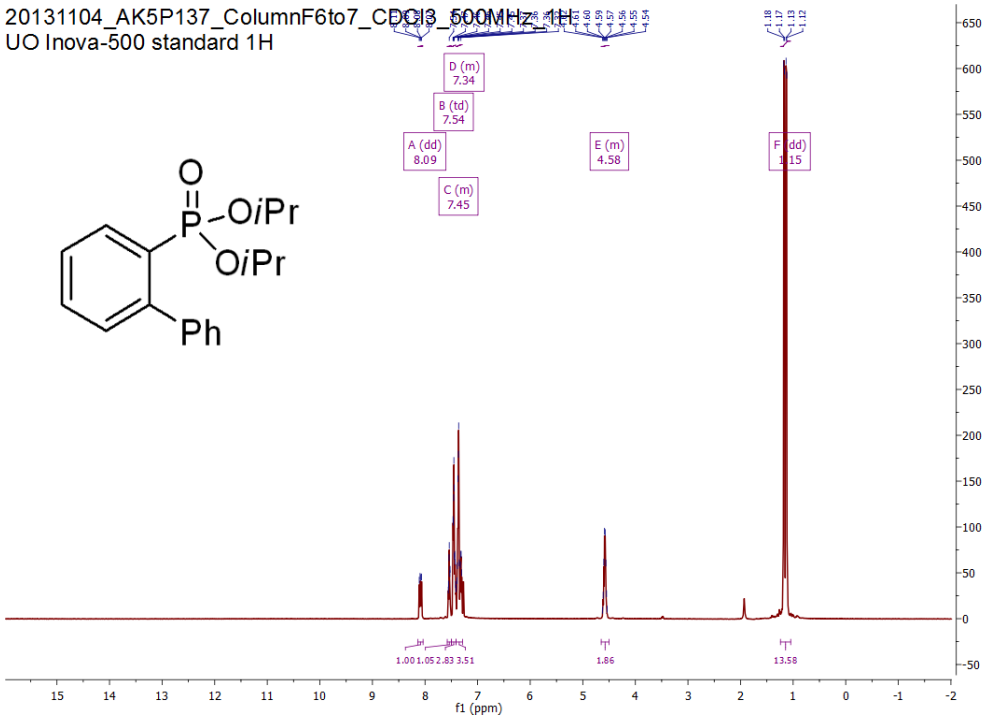

Figure A150. ^{1}H NMR of diisopropyl *o*-(biphenyl)phosphonate.

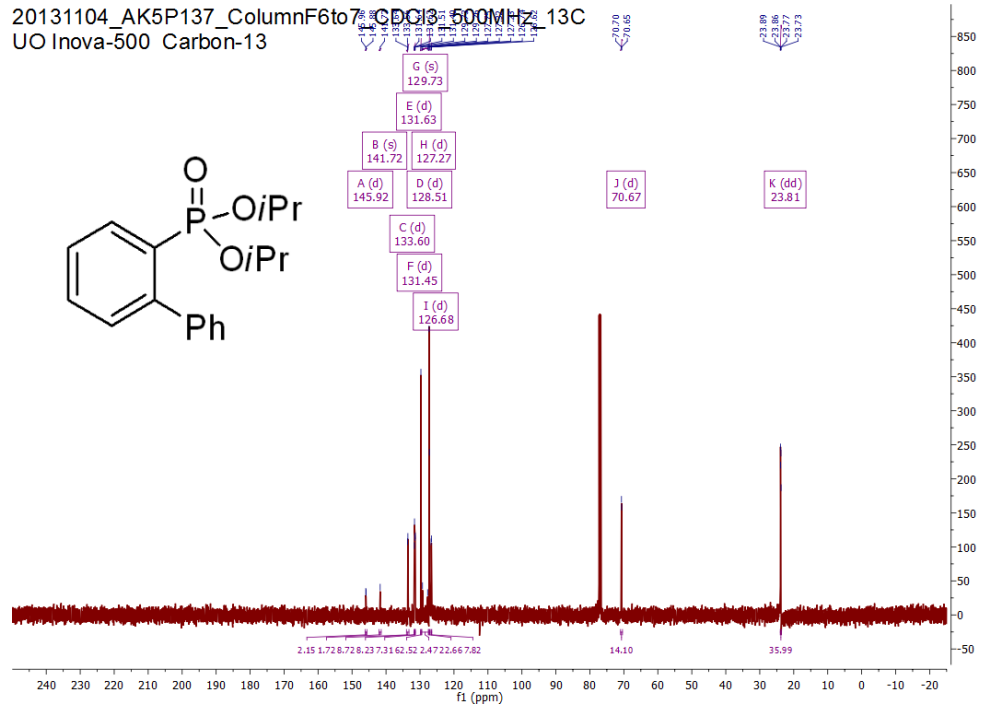

Figure A151. ^{13}C NMR of diisopropyl *o*-(biphenyl)phosphonate.

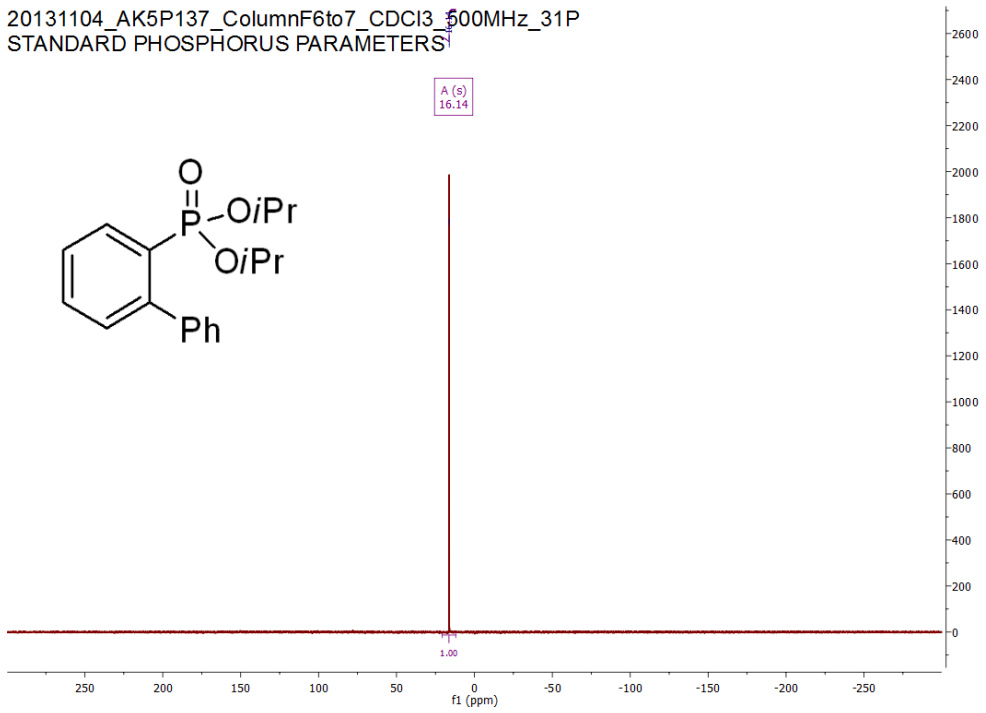

Figure A152. $^{31}P\{^{1}H\}$ NMR of diisopropyl *o*-(biphenyl)phosphonate.

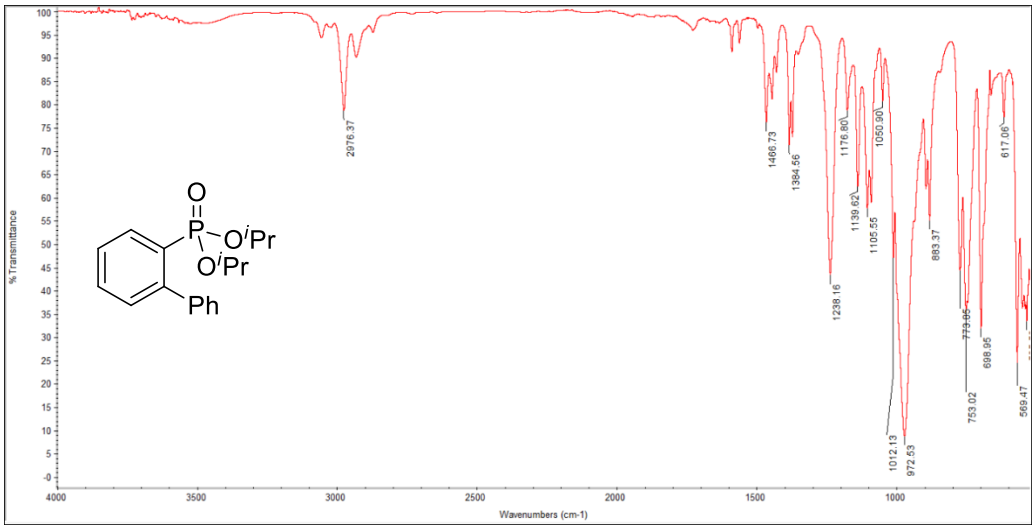

Figure A153. Infrared absorption spectrum of diisopropyl *o*-(biphenyl)phosphonate.

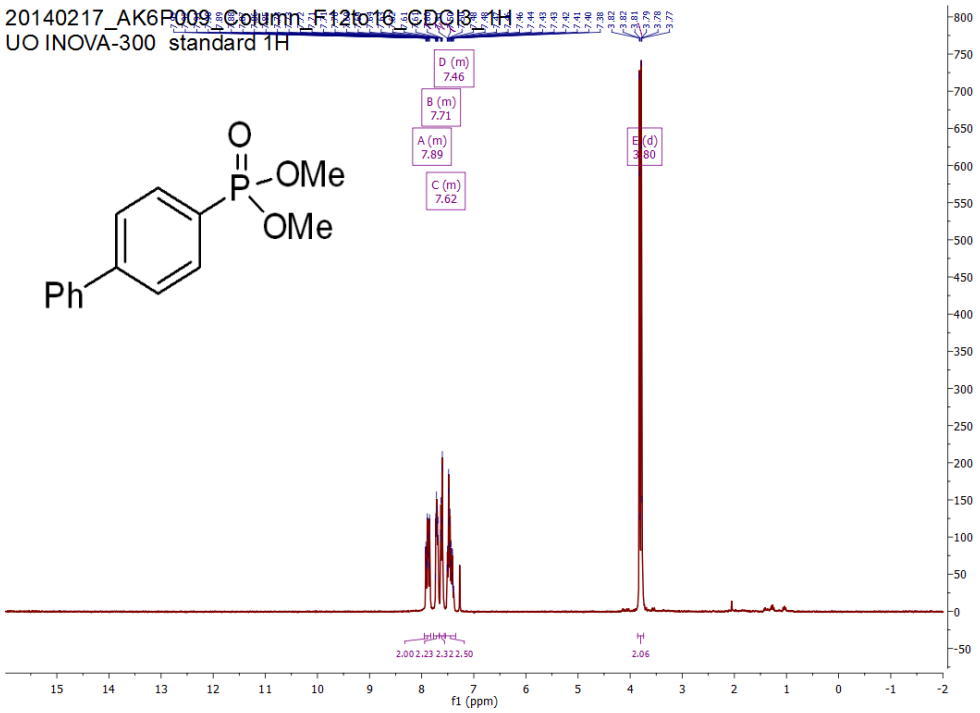

Figure A154. ^{1}H NMR of dimethyl *p*-(biphenyl)phosphonate.

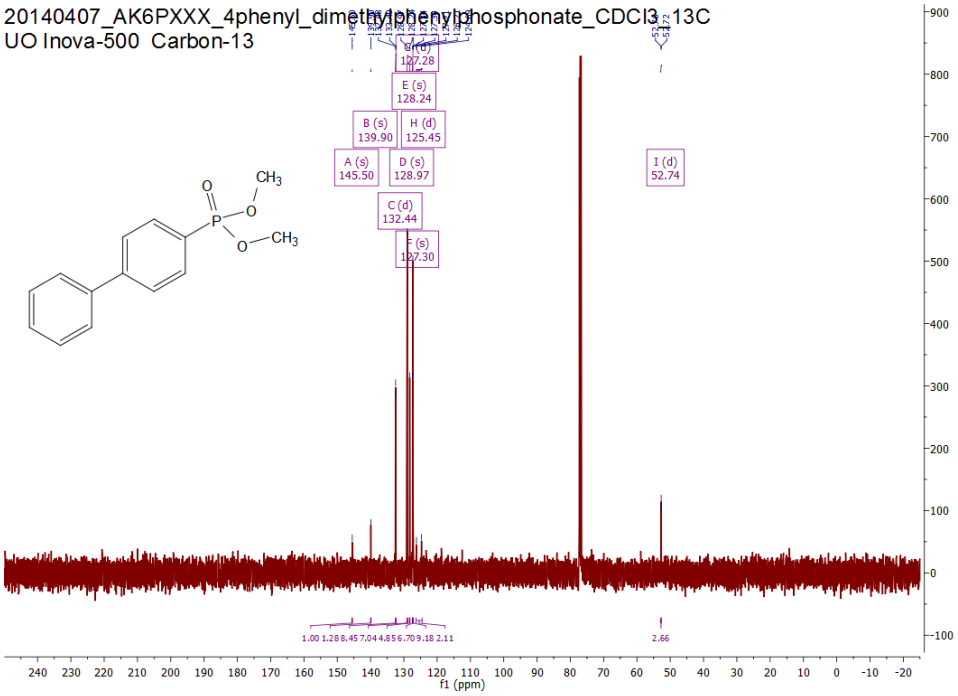

Figure A155. ^{13}C NMR of dimethyl *p*-(biphenyl)phosphonate.

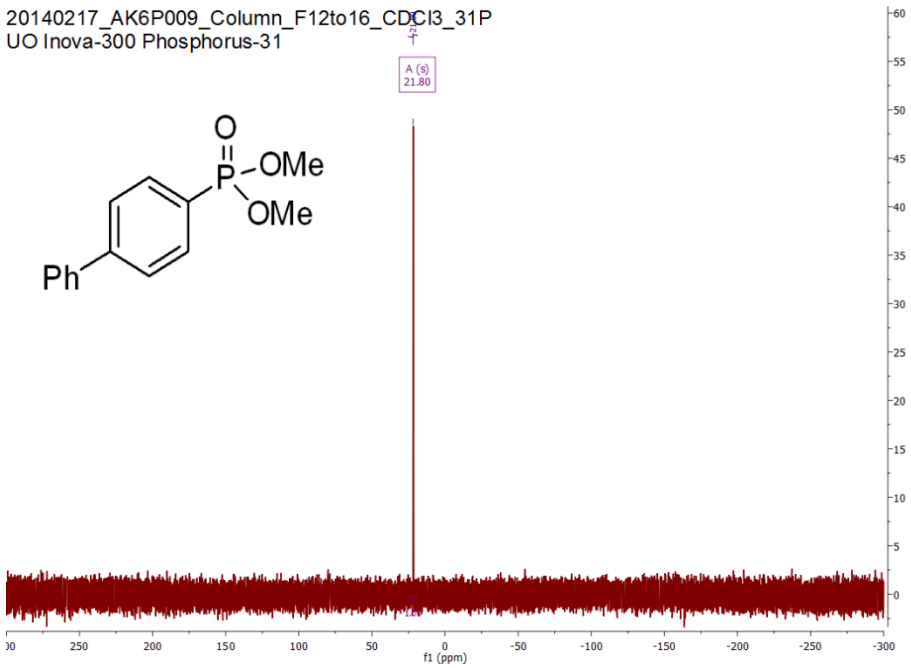

Figure A156. $^{31}P\{^{1}H\}$ NMR of dimethyl *p*-(biphenyl)phosphonate.

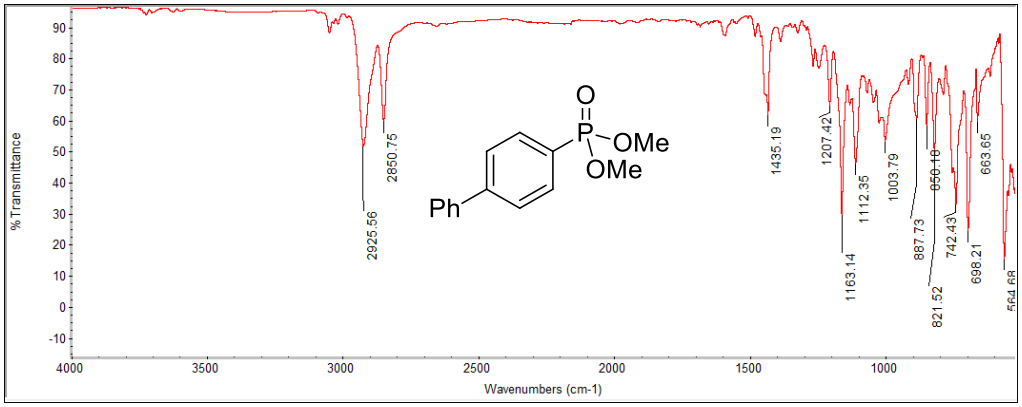

Figure A157. Infrared absorption spectrum of dimethyl *p*-(biphenyl)phosphonate.

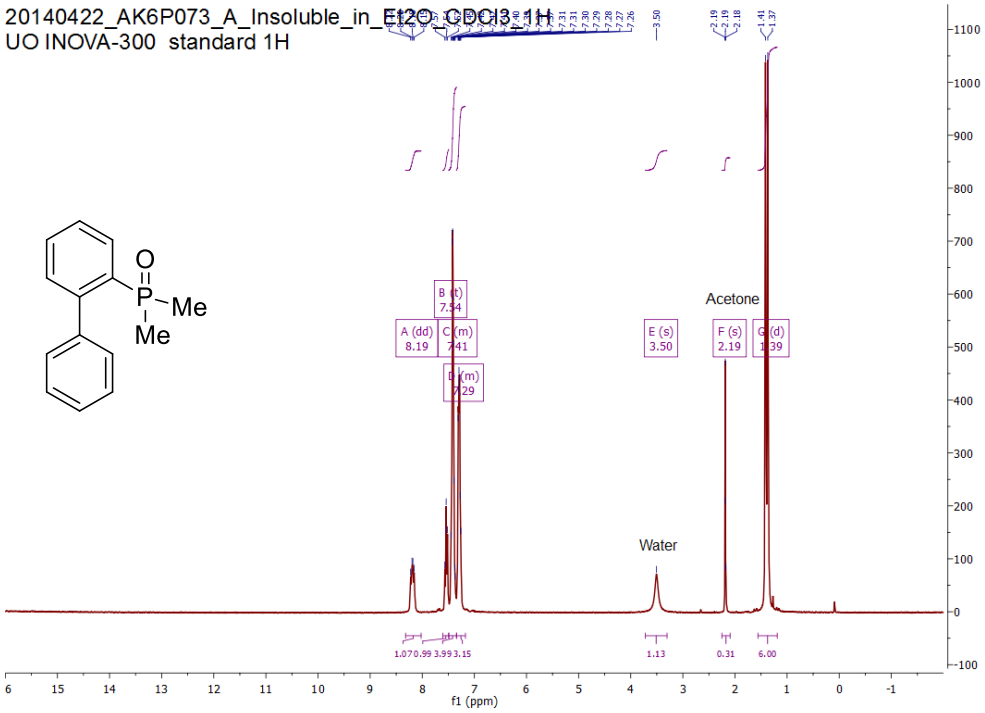

Figure A158. ^{1}H NMR of [1,1'-biphenyl]-2-yldimethylphosphine oxide.

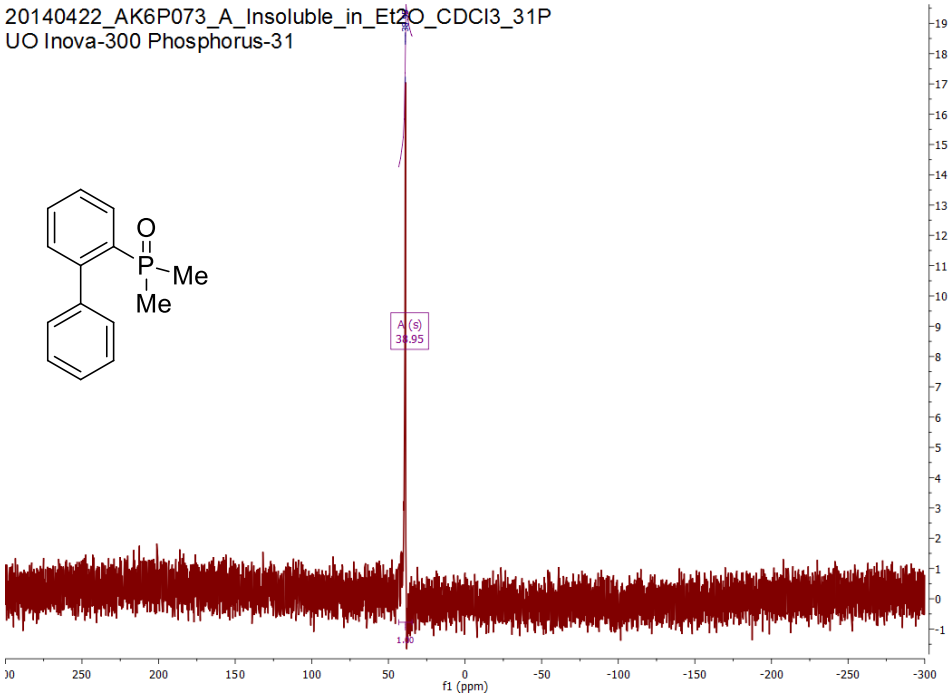

Figure A159. ^{31}P{^{1}H} NMR of [1,1'-biphenyl]-2-yldimethylphosphine oxide.

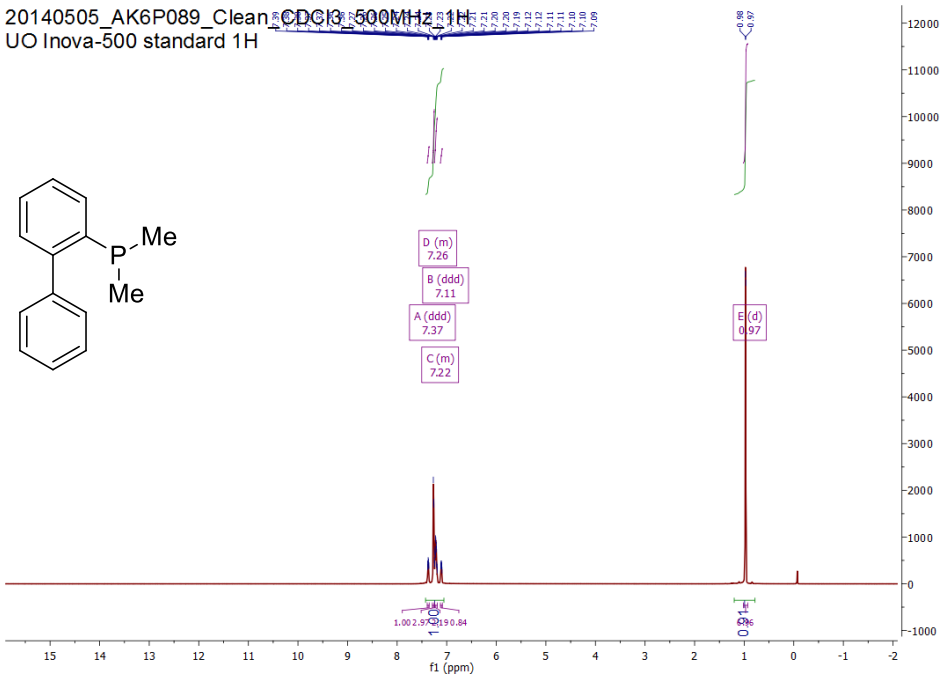

Figure A160. ^{1}H NMR of [1,1'-biphenyl]-2-yldimethylphosphine.

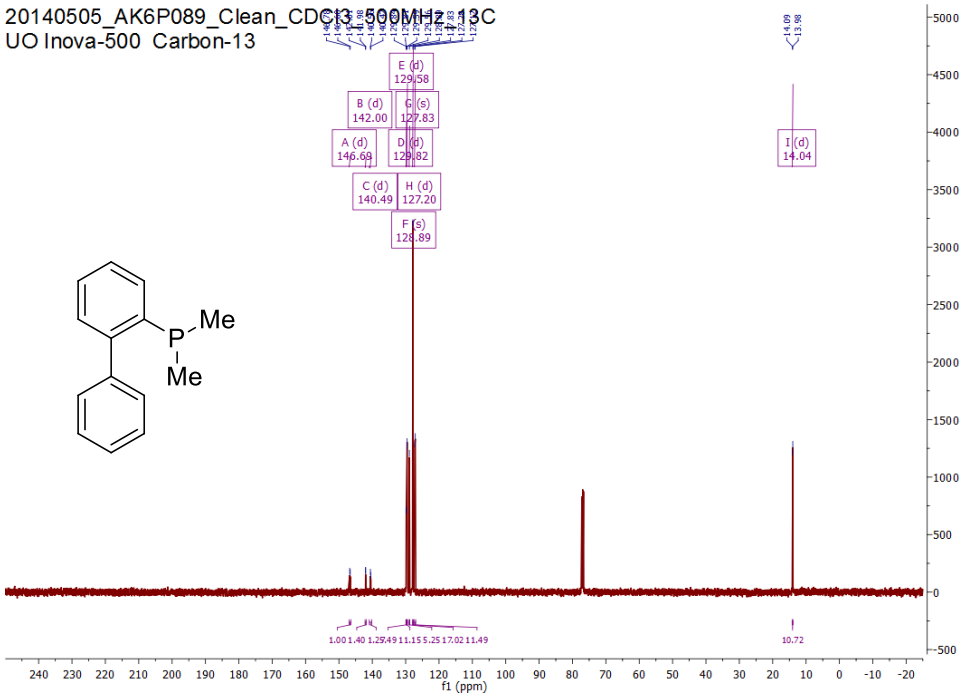

Figure A161. ^{13}C NMR of [1,1'-biphenyl]-2-yldimethylphosphine.

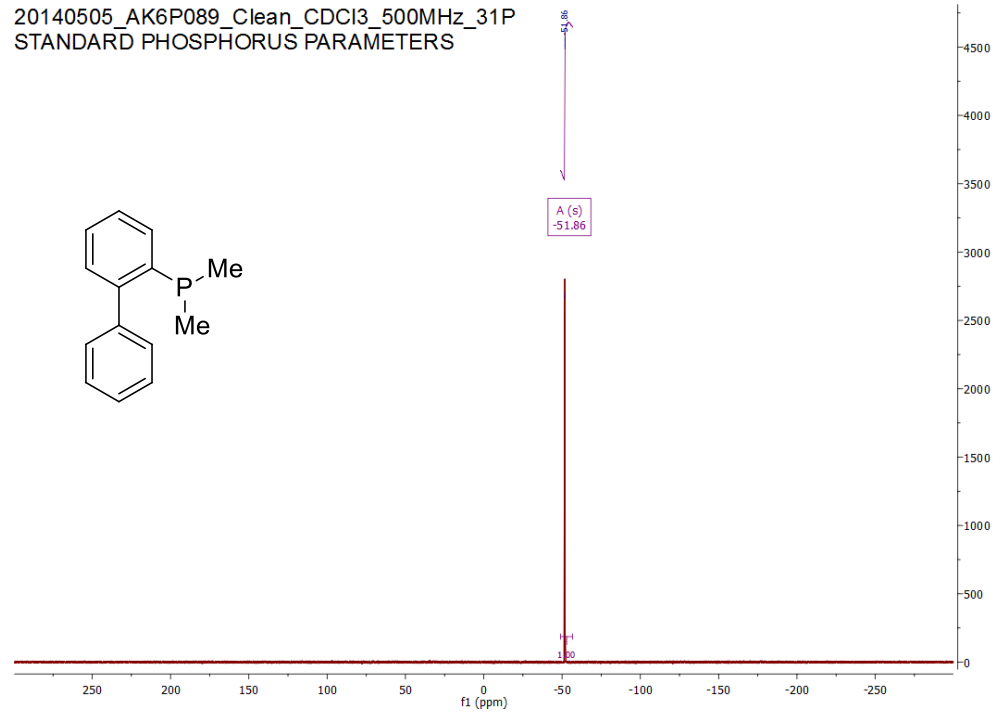

Figure A162. $^{31}P\{^{1}H\}$ NMR of [1,1'-biphenyl]-2-yldimethylphosphine.

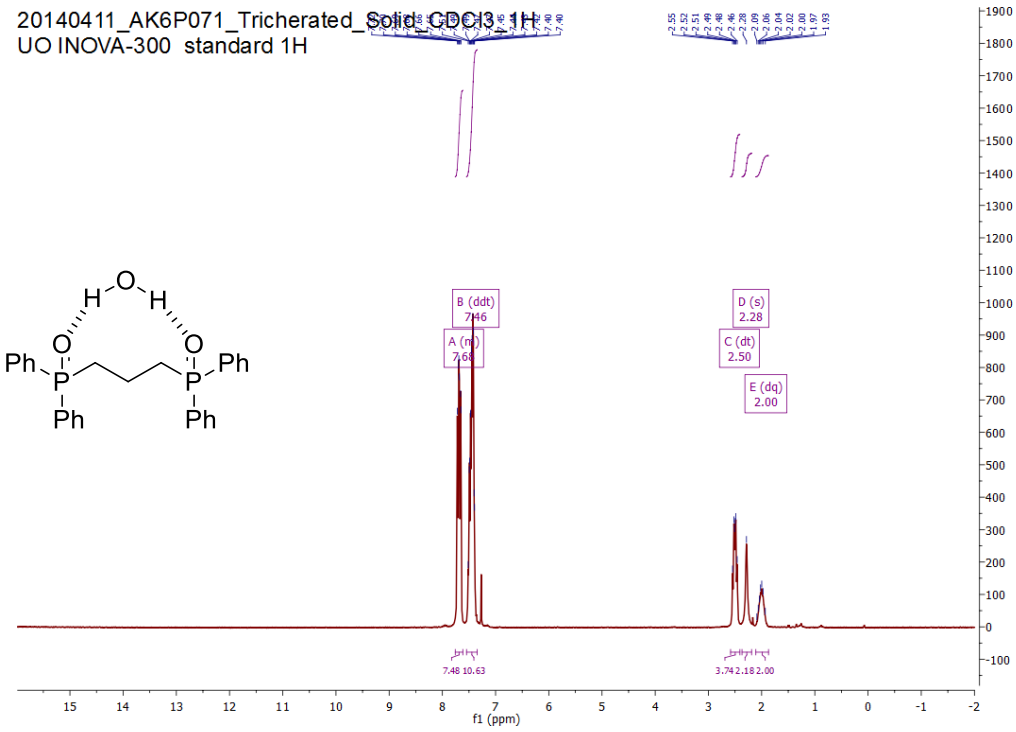

Figure A163. ^{1}H NMR of propane-1,3-diylbis(diphenylphosphine oxide) monohydrate.

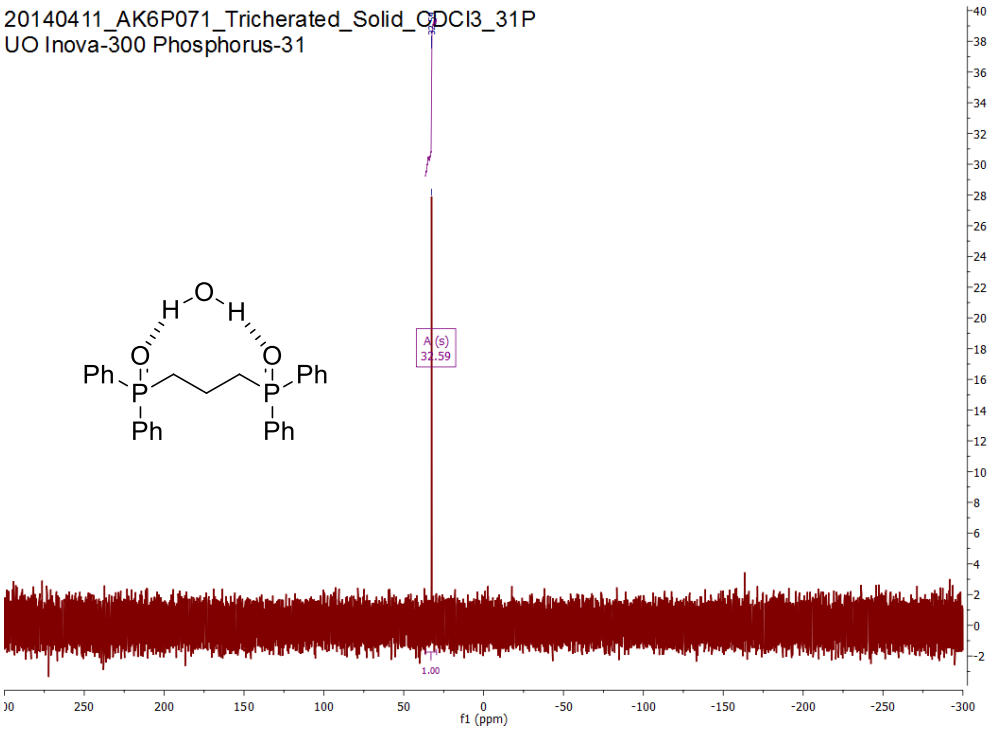

Figure A164. $^{31}P\{^{1}H\}$ NMR of propane-1,3-diylbis(diphenylphosphine oxide) monohydrate.

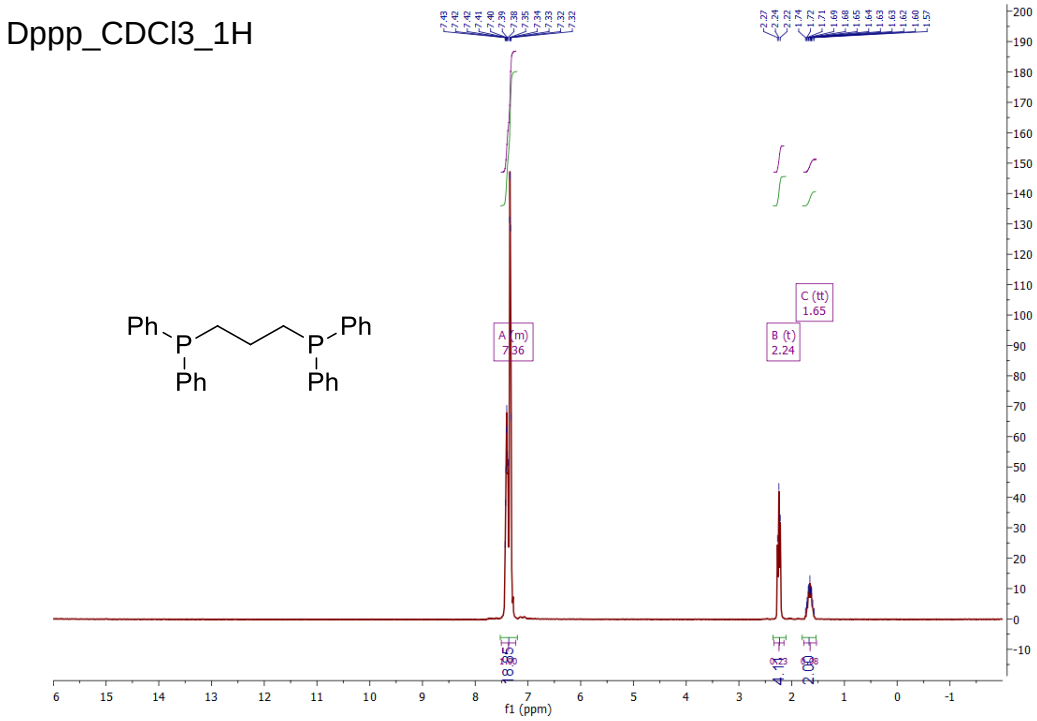

Figure A165. ^{1}H NMR of propane-1,3-diylbis(diphenylphosphine).

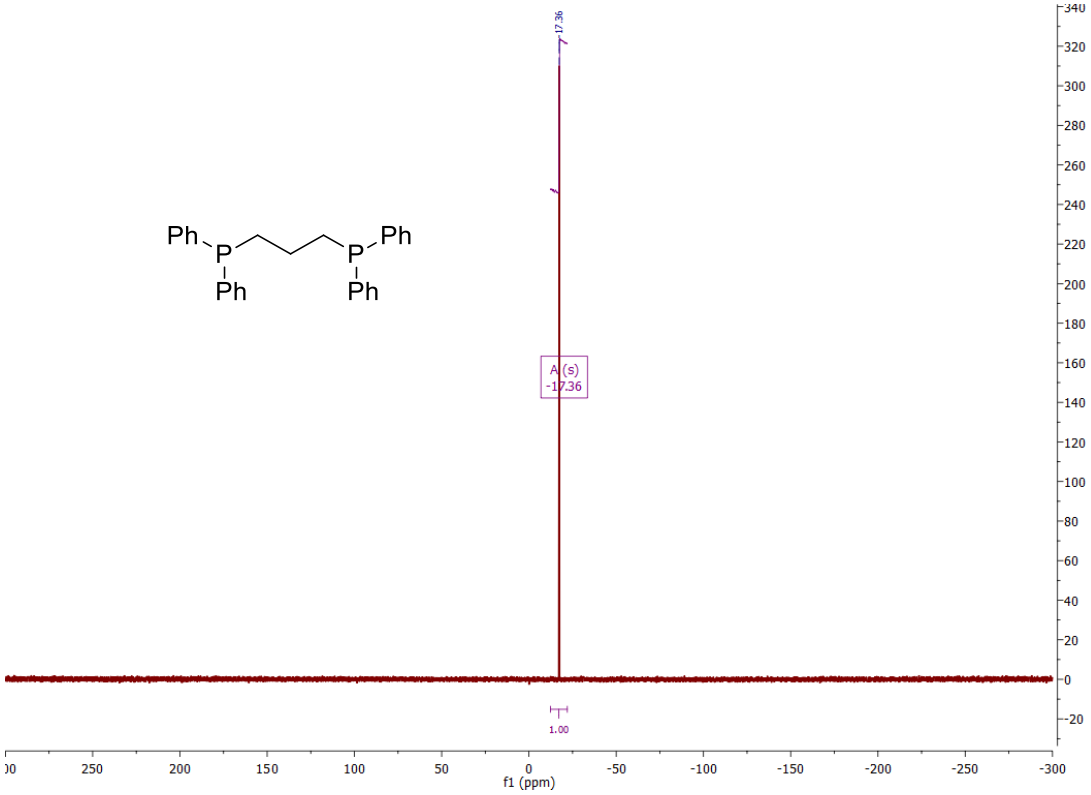

Figure A166. $^{31}P\{^{1}H\}$ NMR of propane-1,3-diylbis(diphenylphosphine).

APPENDIX B

SUPPORTING INFORMATION FOR CHAPTER III

B.1. Synthesis

The Doyle modified preparation of Hays original synthesis was used.[1,2] Several notes on the reactions and SPOs:

(1) A large Buchner funnel is recommended to filter the quenched reaction mixture – the $MgCO_3$ cake slows filtration considerably.

(2) Serial rinses of the cake with boiling methanol is strongly recommended.

(3) All of the SPOs thermally disproportionate to dialkylphosphines and dialkyl phosphonus acids at temperatures above their boiling points, so careful control over heating should be observed when distilling.

(4) Dimethylphosphine oxide should be distilled with care because it has a melting point very close to its boiling point.

(5) Dimethylphosphine oxide (solid with a very low melting point) is very hygroscopic but air-stable over several months on the benchtop.

(6) Diethylphosphine oxide and diisopropylphosphine oxide are easily stored and handled on the benchtop.

(7) Di-*tert*-butylphoshine oxide is slightly air sensitive (oxidizes over several weeks) and must be stored under an inert atmosphere.

B.2. Additional spectra

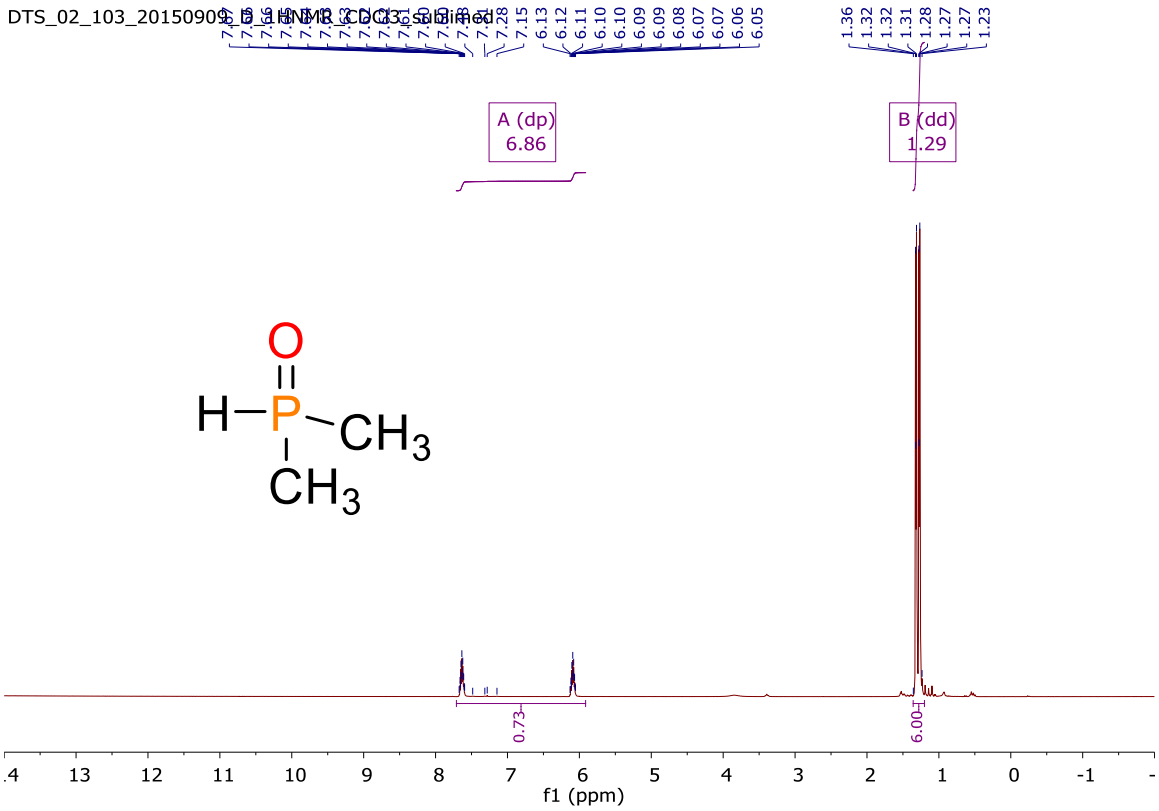

Figure B1. ^{1}H NMR of dimethylphopshine oxide.

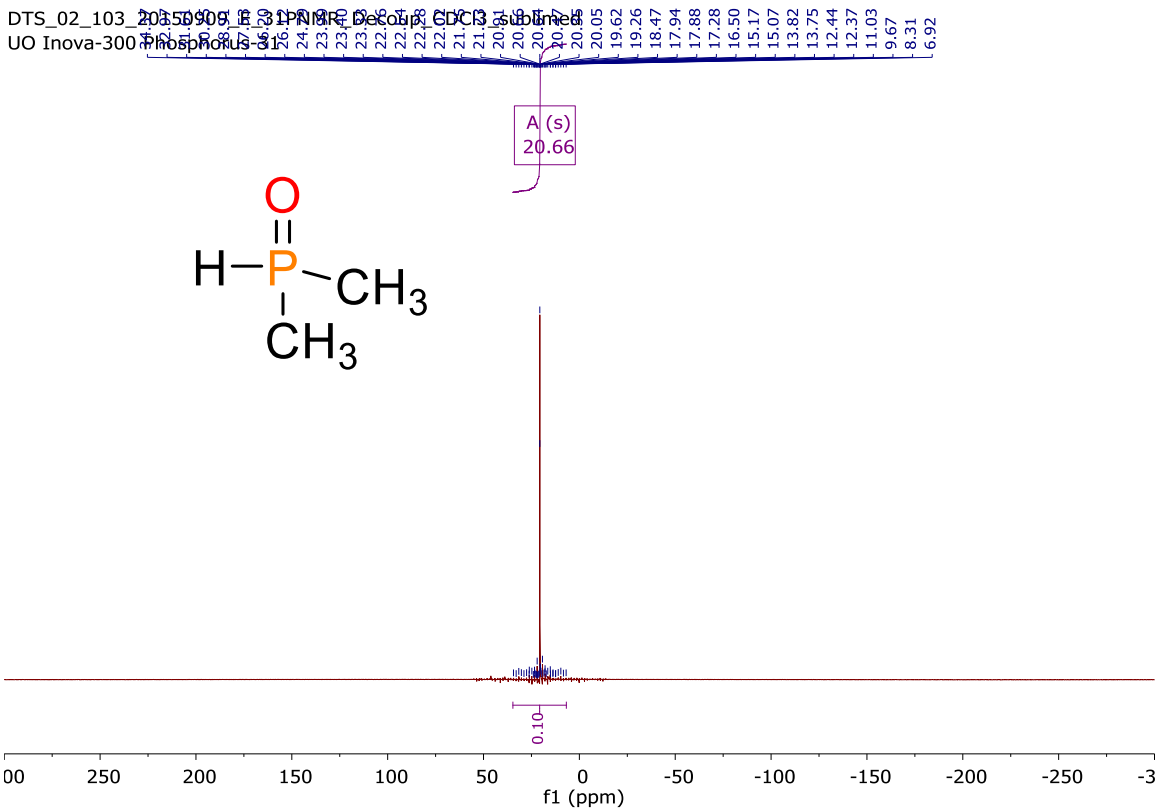

Figure B2. $^{31}P\{^{1}H\}$ NMR of dimethylphopshine oxide.

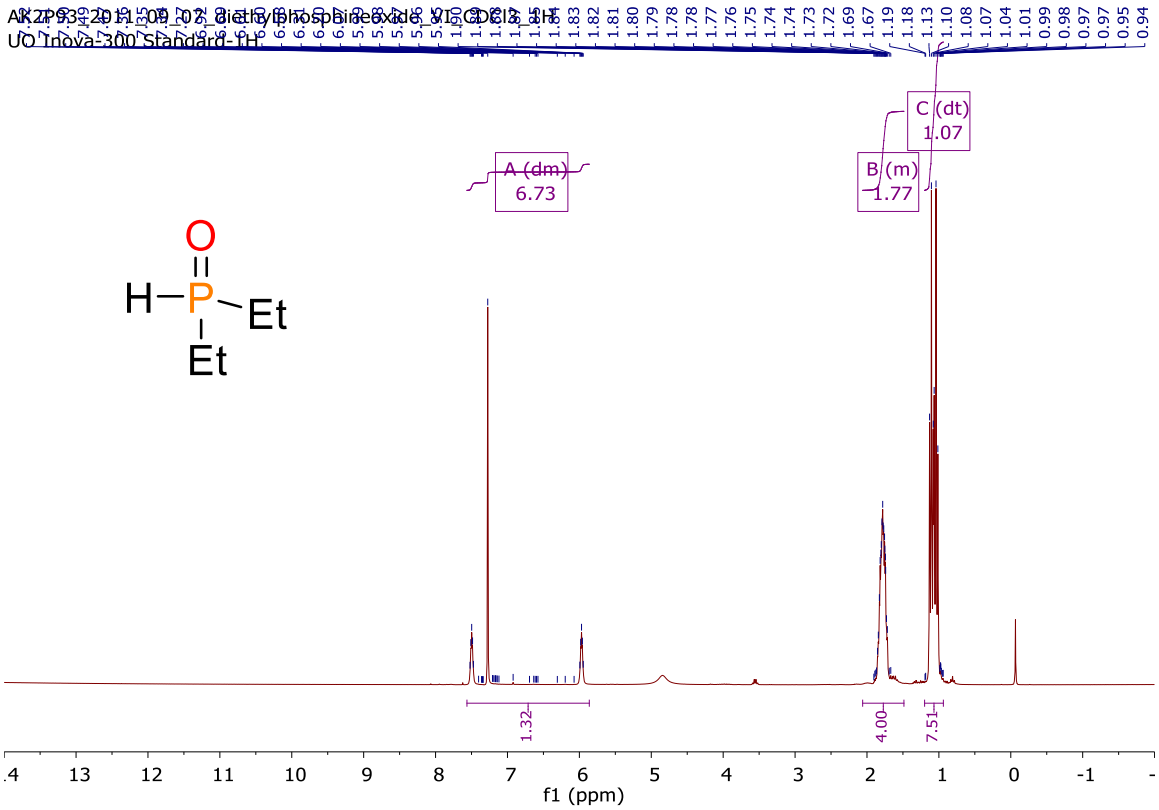

Figure B3. ^{1}H NMR of diethylphopshine oxide.

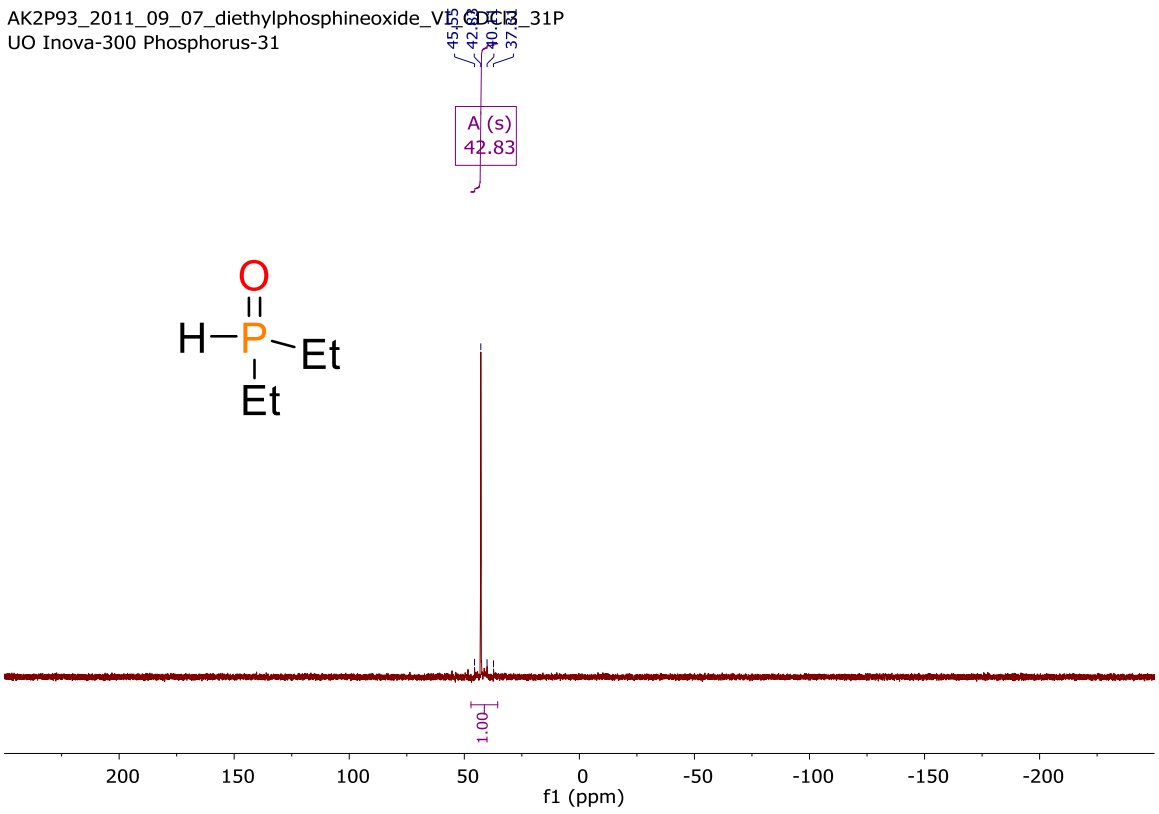

Figure B4. $^{31}P\{^{1}H\}$ NMR of diethylphopshine oxide.

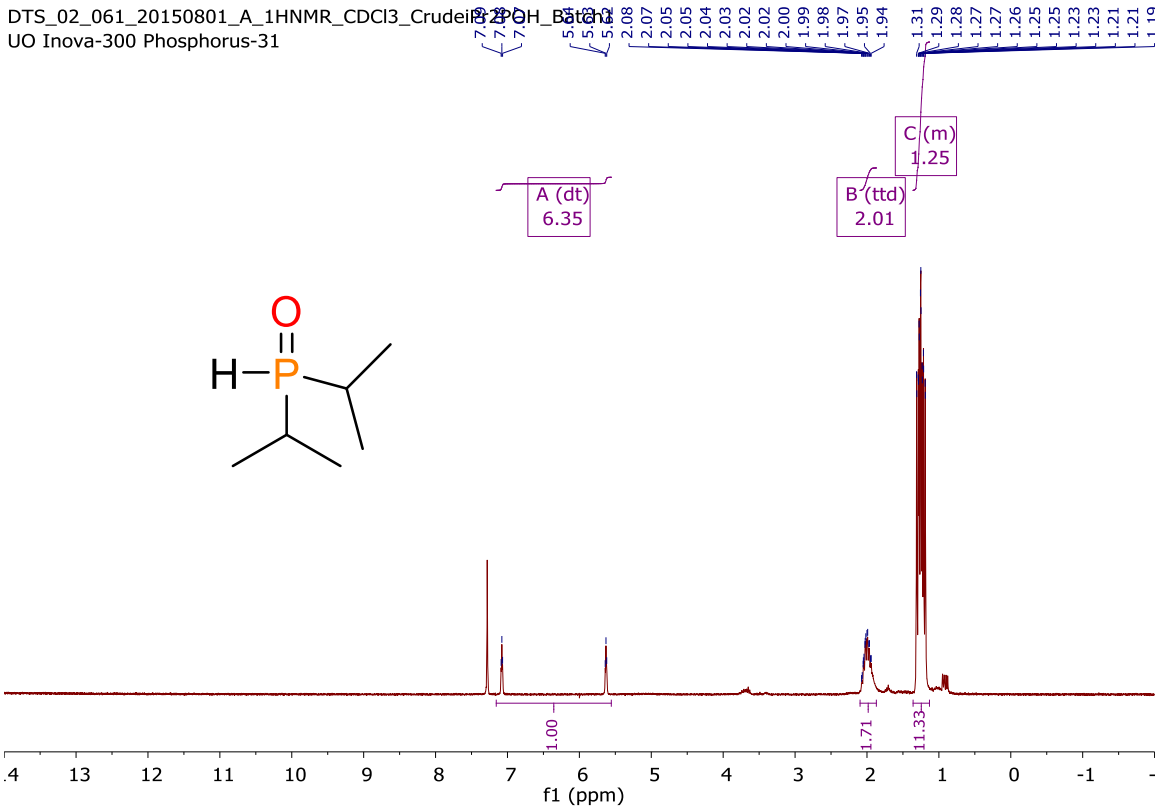

Figure B5. ^{1}H NMR of diisopropylphopshine oxide.

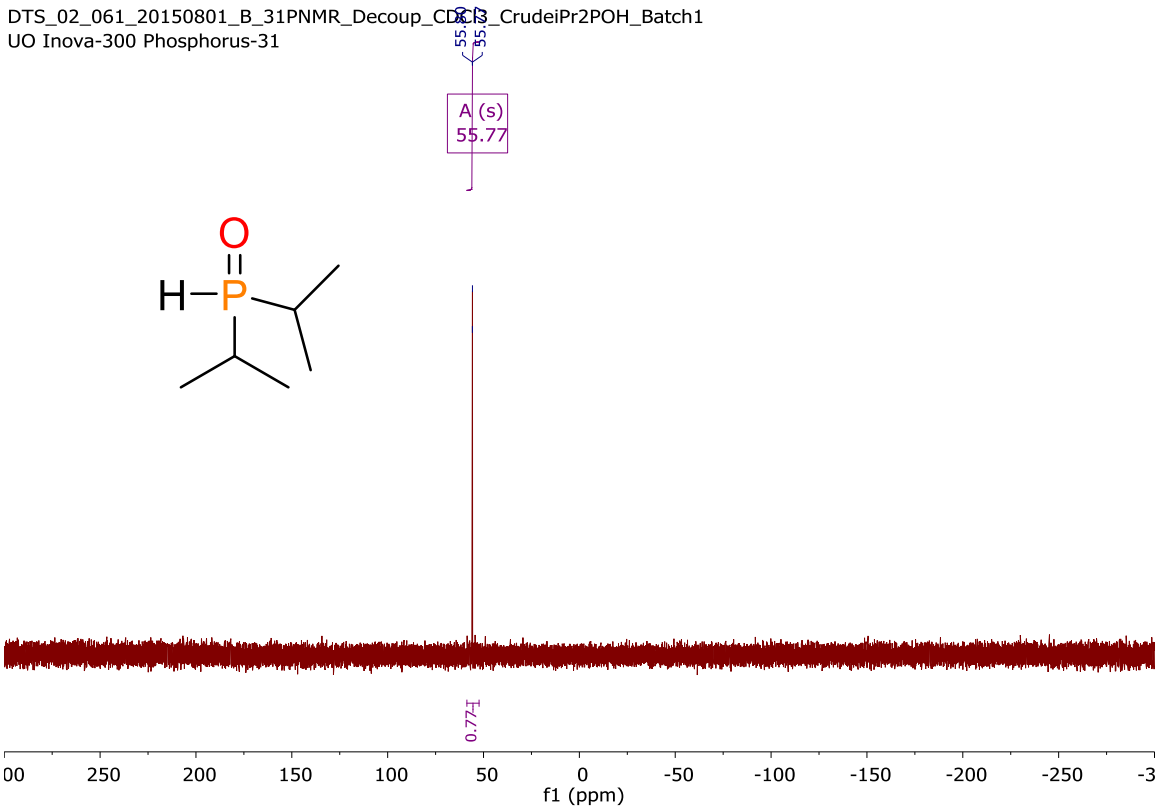

Figure B6. $^{31}P\{^{1}H\}$ NMR of diisopropylphopshine oxide.

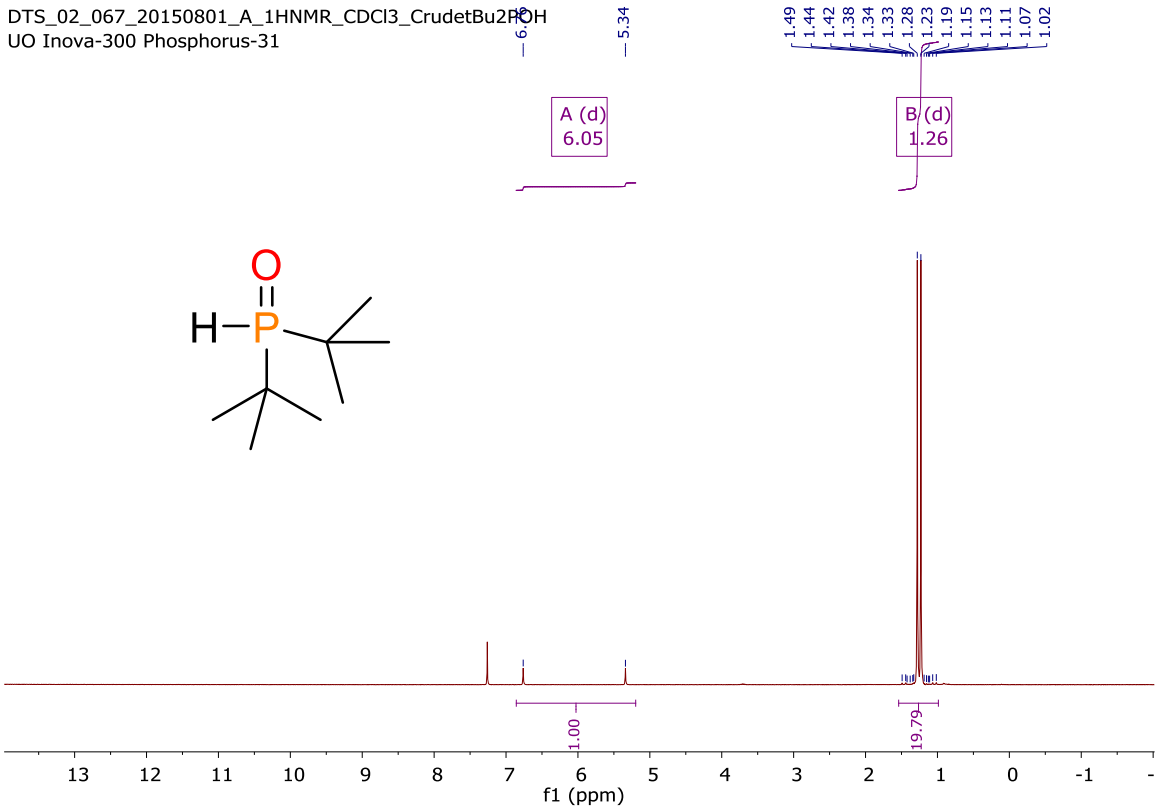

Figure B7. ^{1}H NMR of di-*tert*-butylphopshine oxide.

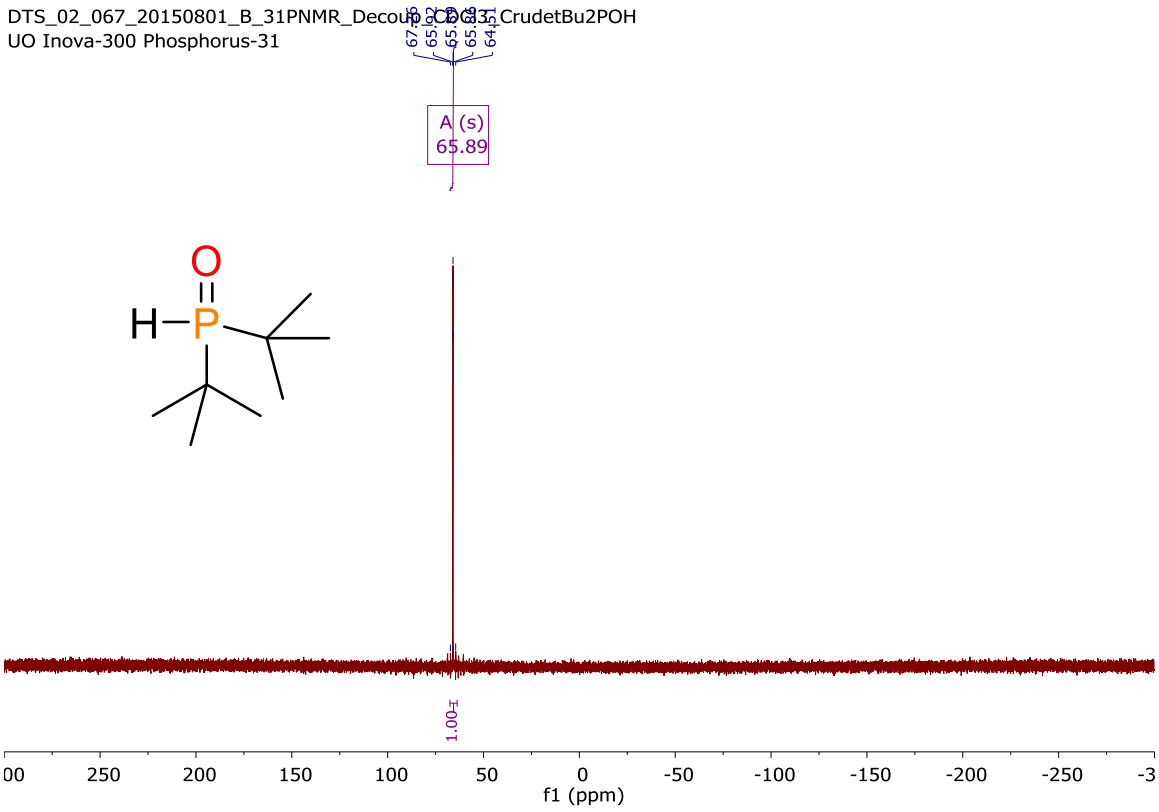

Figure B8. $^{31}P\{^{1}H\}$ NMR of di-*tert*-butylphopshine oxide.

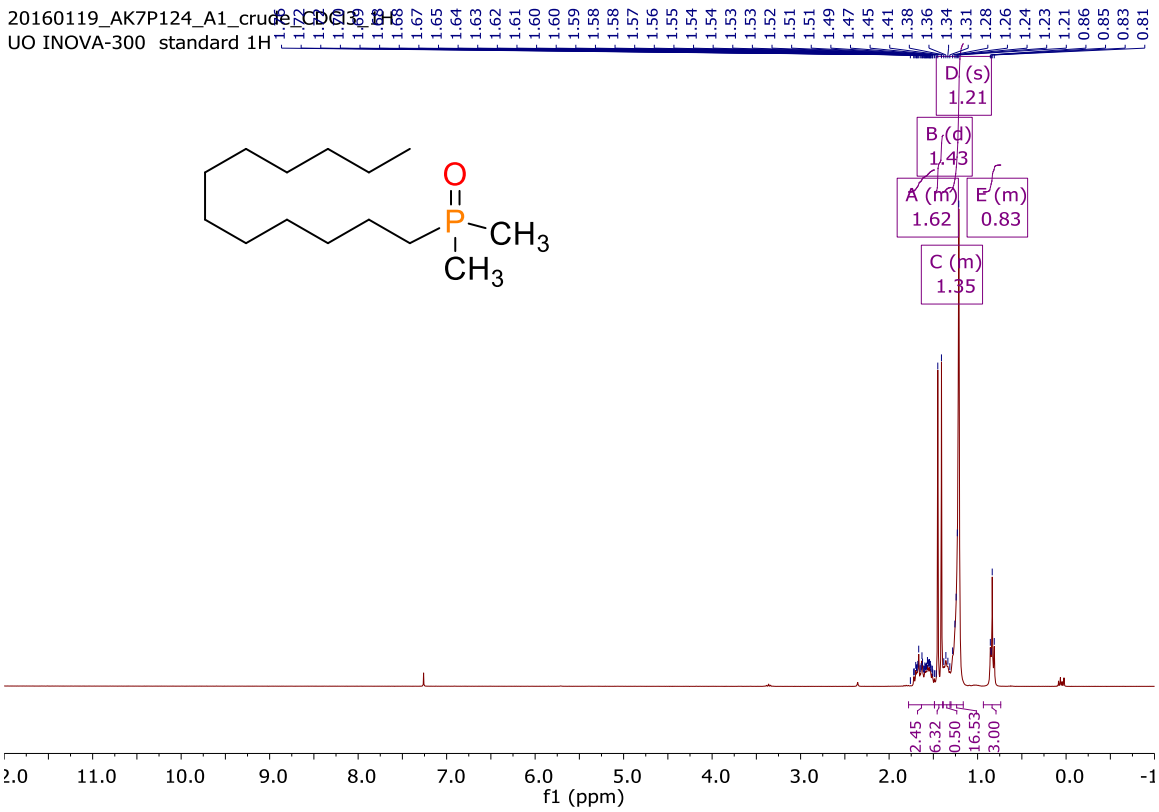

Figure B9. ^{1}H NMR of dodecyldimethylphosphine oxide.

.

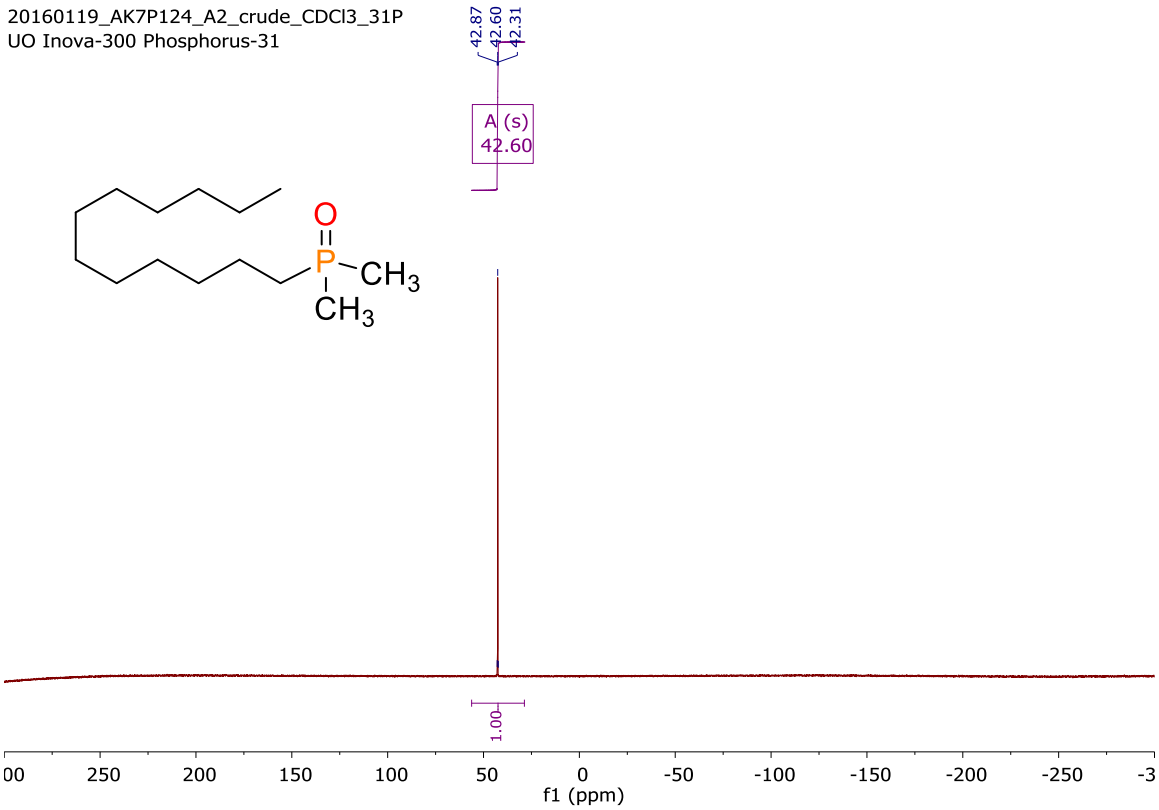

Figure B10. $^{31}P\{^{1}H\}$ NMR of dodecyldimethylphosphine oxide.

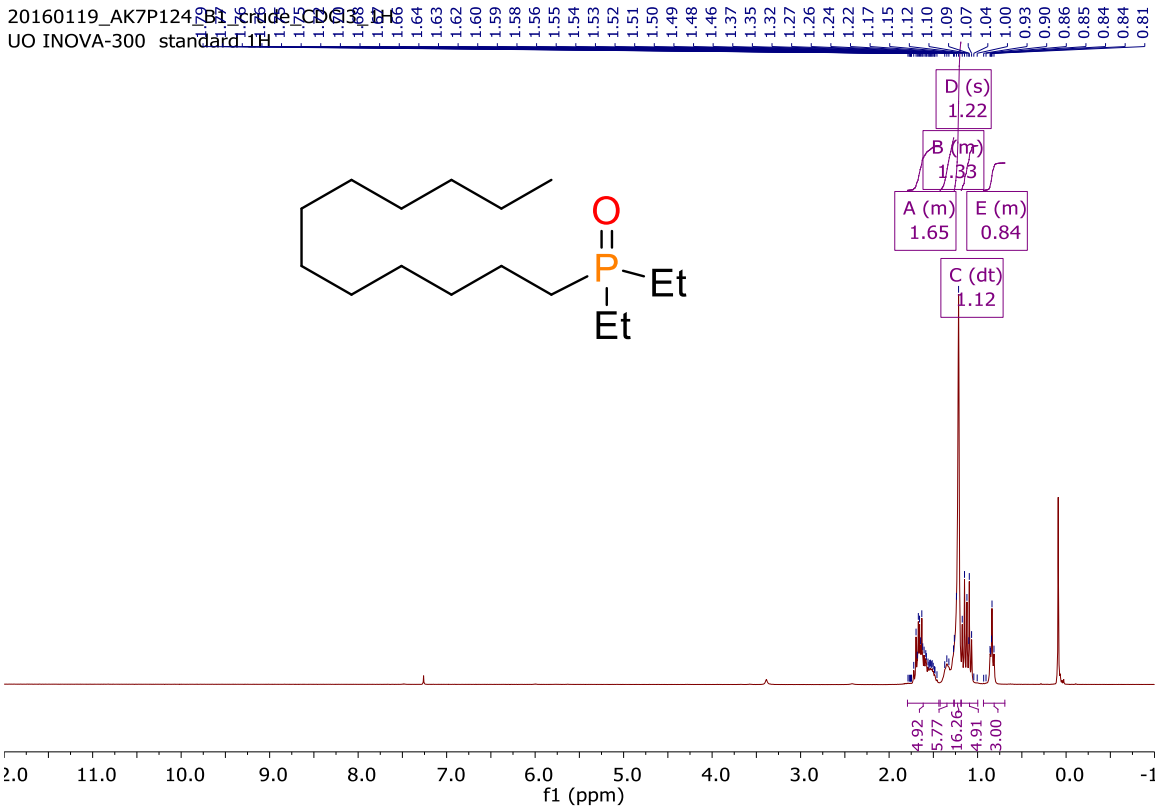

Figure B11. ^{1}H NMR of dodecyldiethylphosphine oxide.

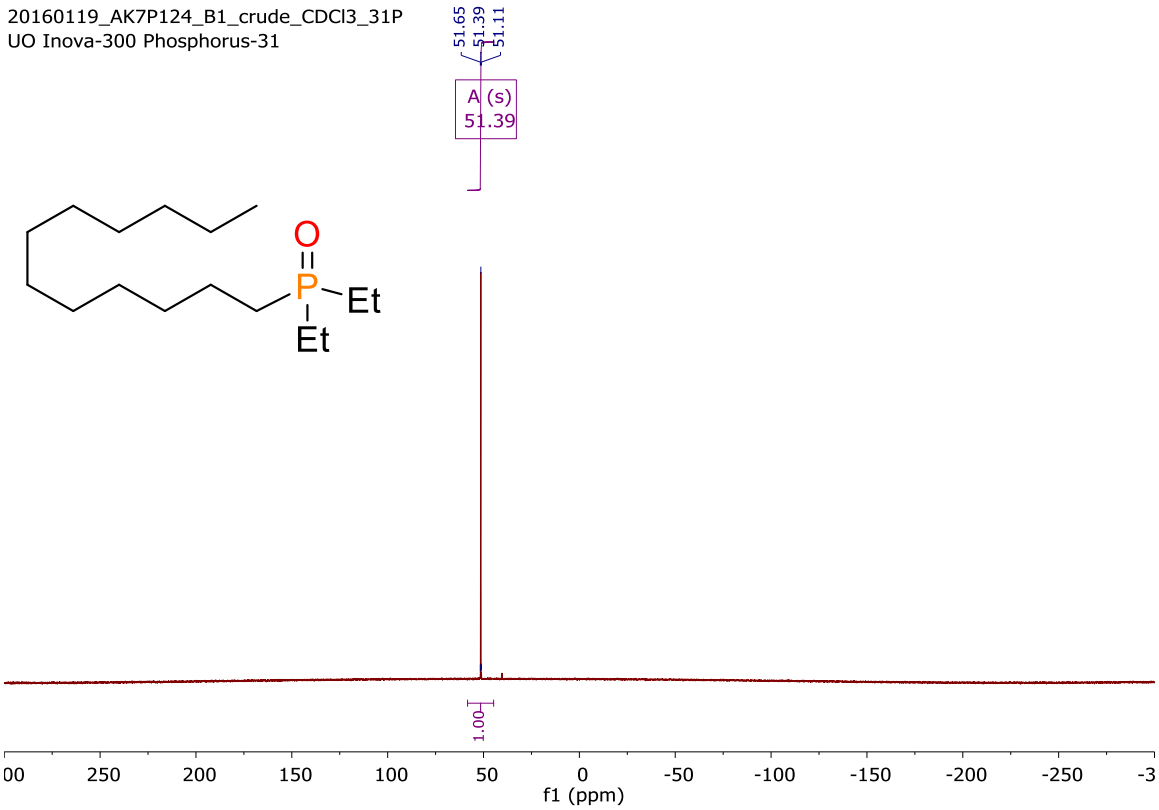

Figure B12. $^{31}P\{^{1}H\}$ NMR of dodecyldiethylphosphine oxide.

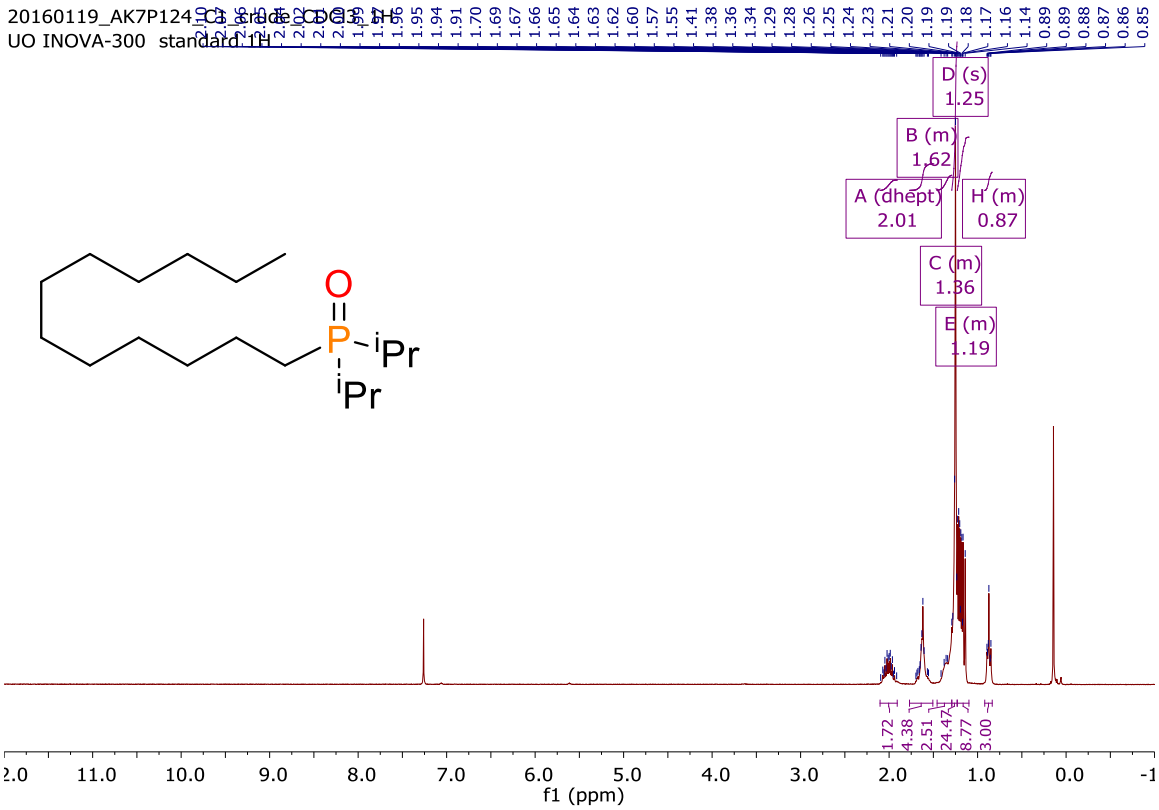

Figure B13. ^{1}H NMR of dodecyldiisopropylphsopine oxide.

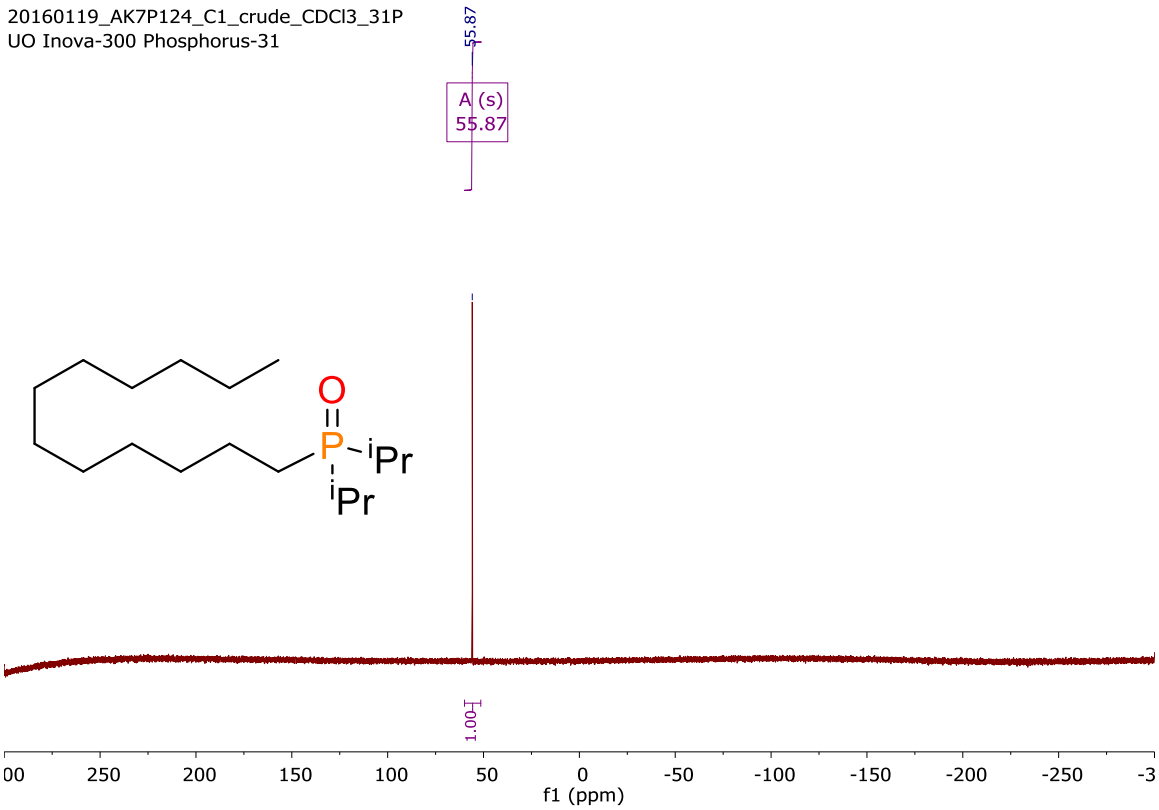

Figure B14. $^{31}P\{^{1}H\}$ NMR of dodecyldiisopropylphsopine oxide.

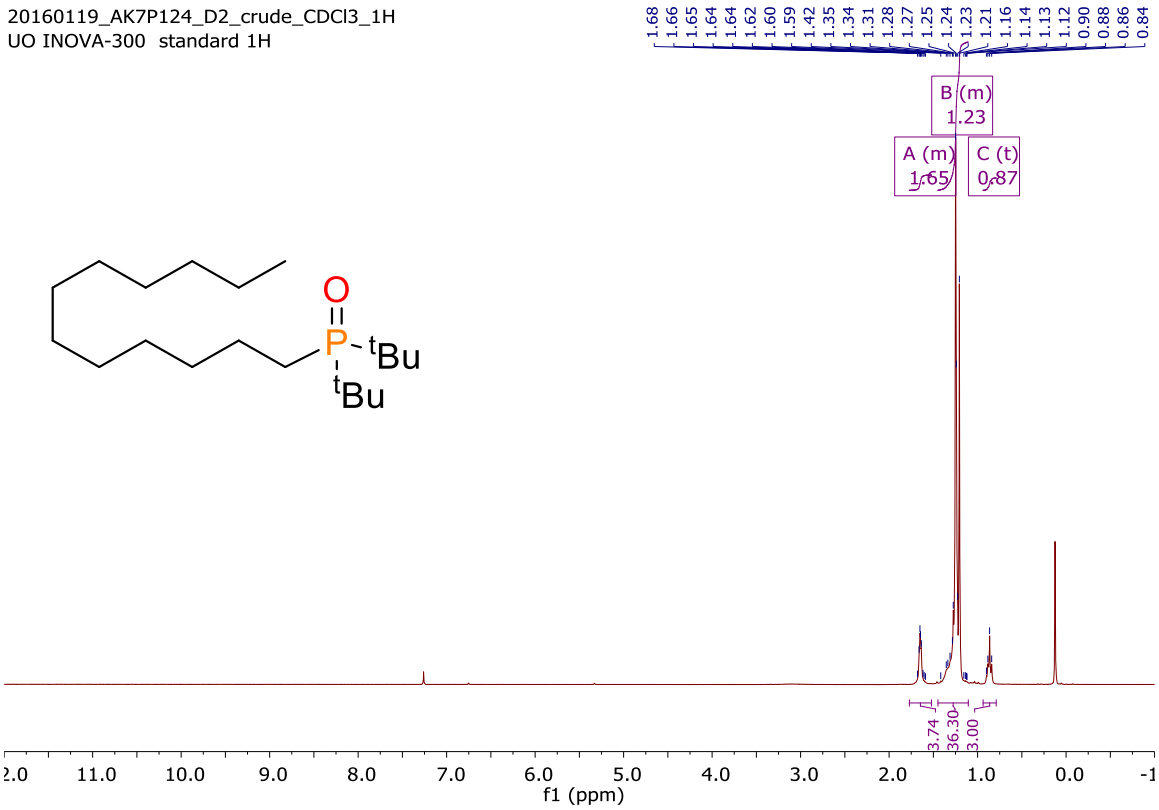

Figure B15. ^{1}H NMR of di-*tert*-butyl(dodecyl)phosphine oxide.

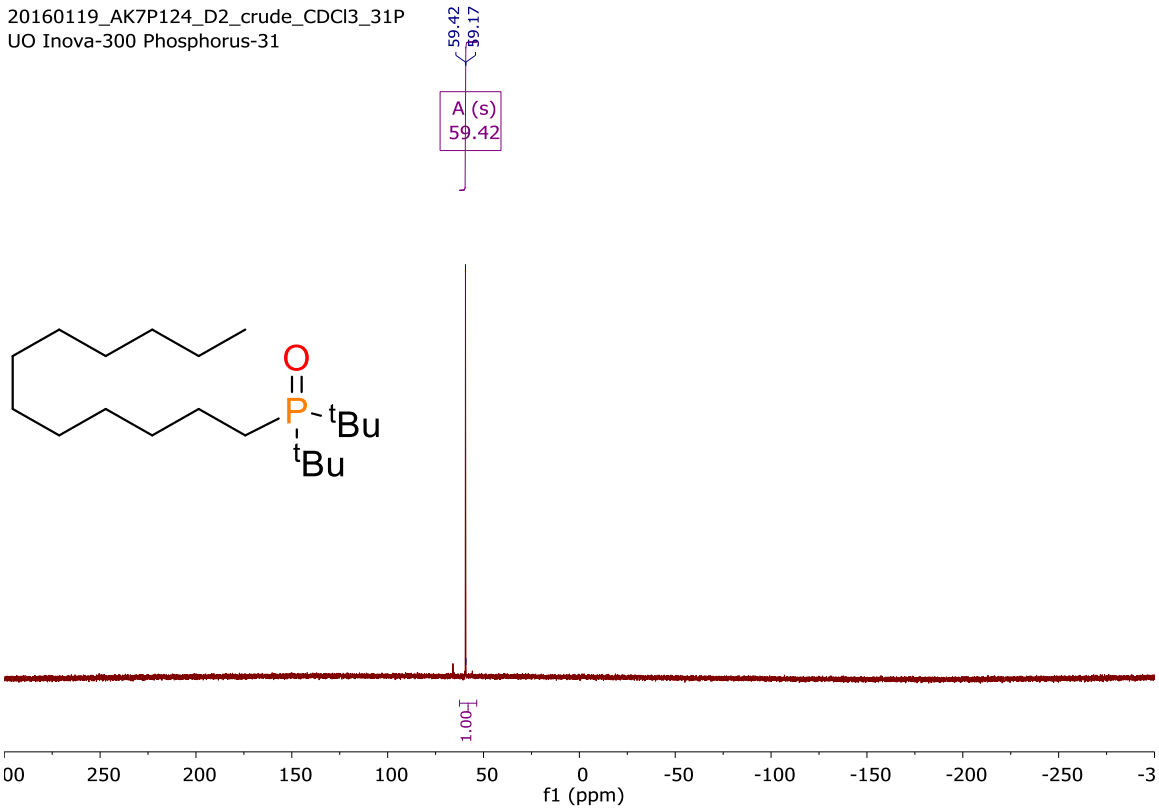

Figure B16. $^{31}P\{^{1}H\}$ NMR of di-*tert*-butyl(dodecyl)phosphine oxide.

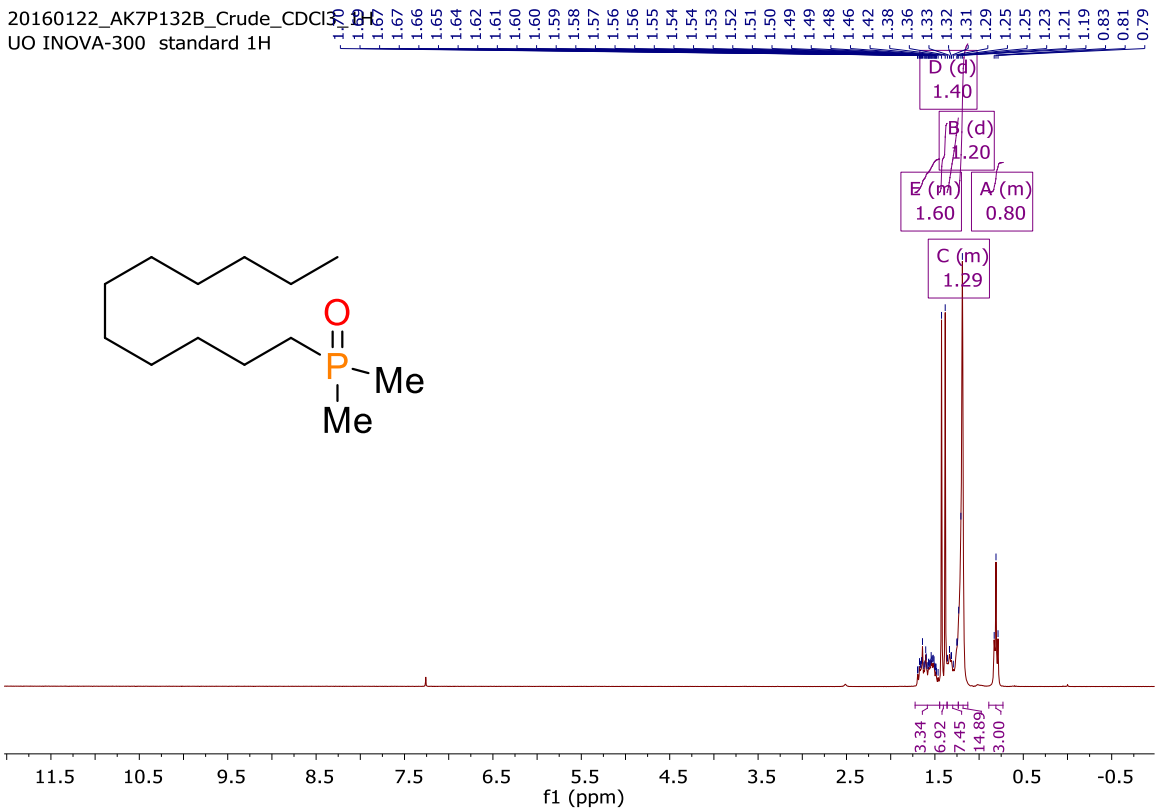

Figure B17. ^{1}H NMR of undecyldimethylphosphine oxide.

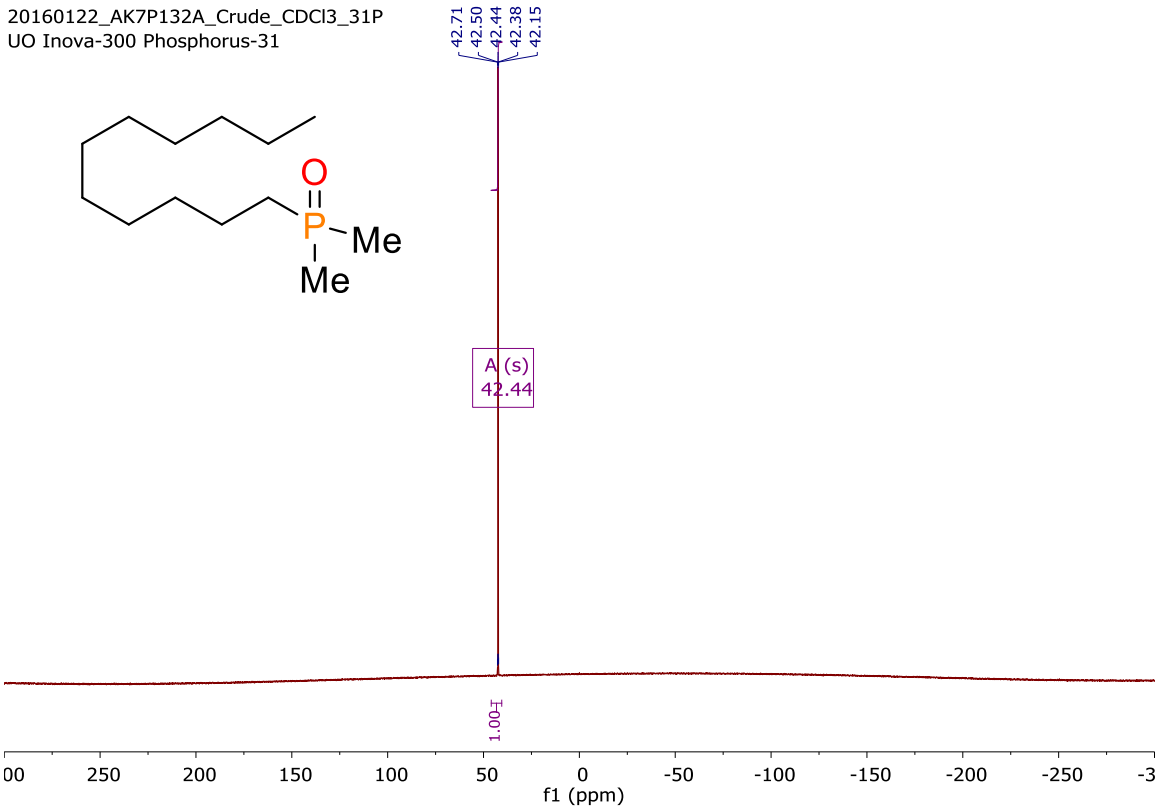

Figure B18. $^{31}P\{^{1}H\}$ NMR of undecyldimethylphosphine oxide.

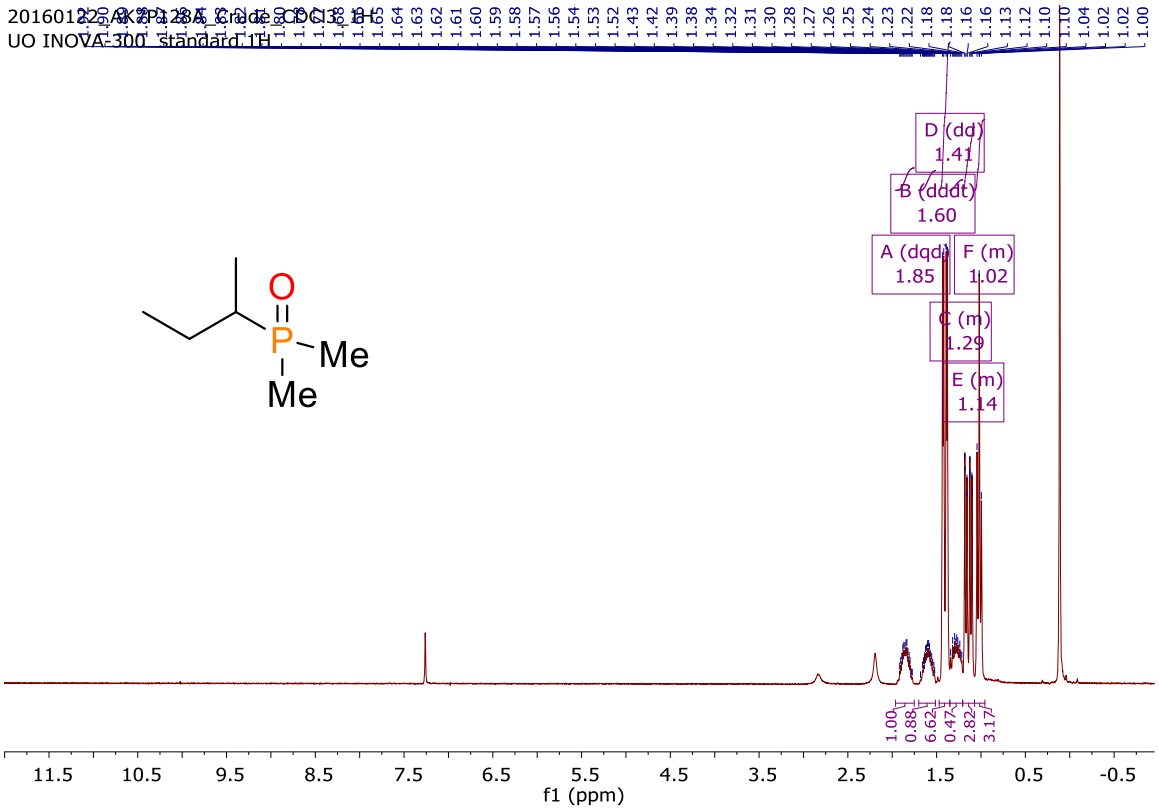

Figure B19. ^{1}H NMR of *sec*-Butyldimethylphosphine oxide.

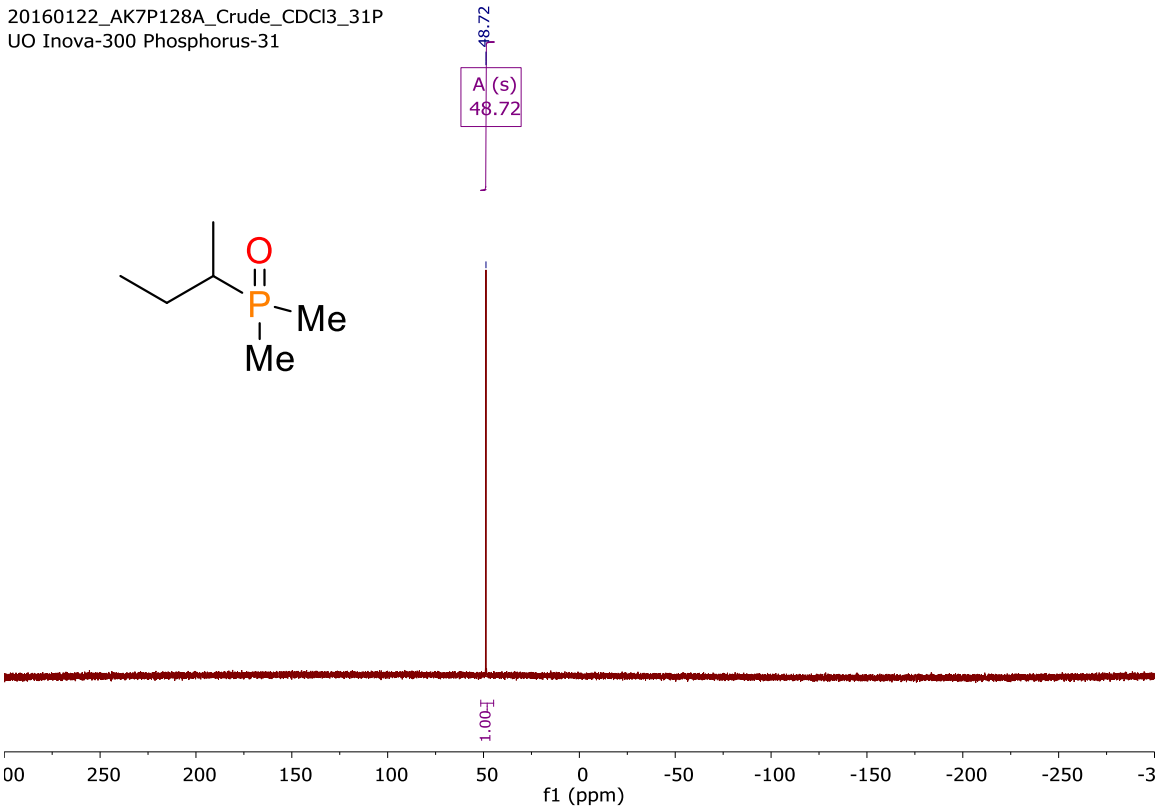

Figure B20. $^{31}P\{^{1}H\}$ NMR of *sec*-Butyldimethylphosphine oxide.

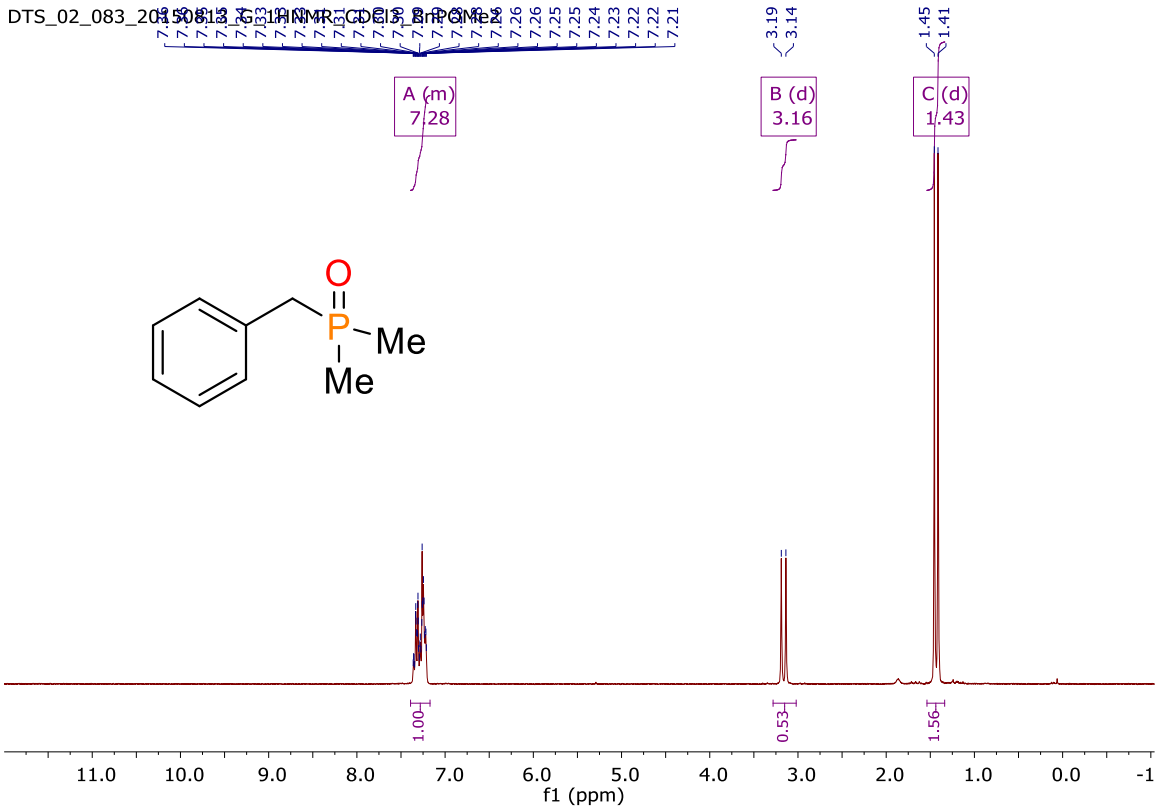

Figure B21. ^{1}H NMR of benzyldimethylphosphine oxide.

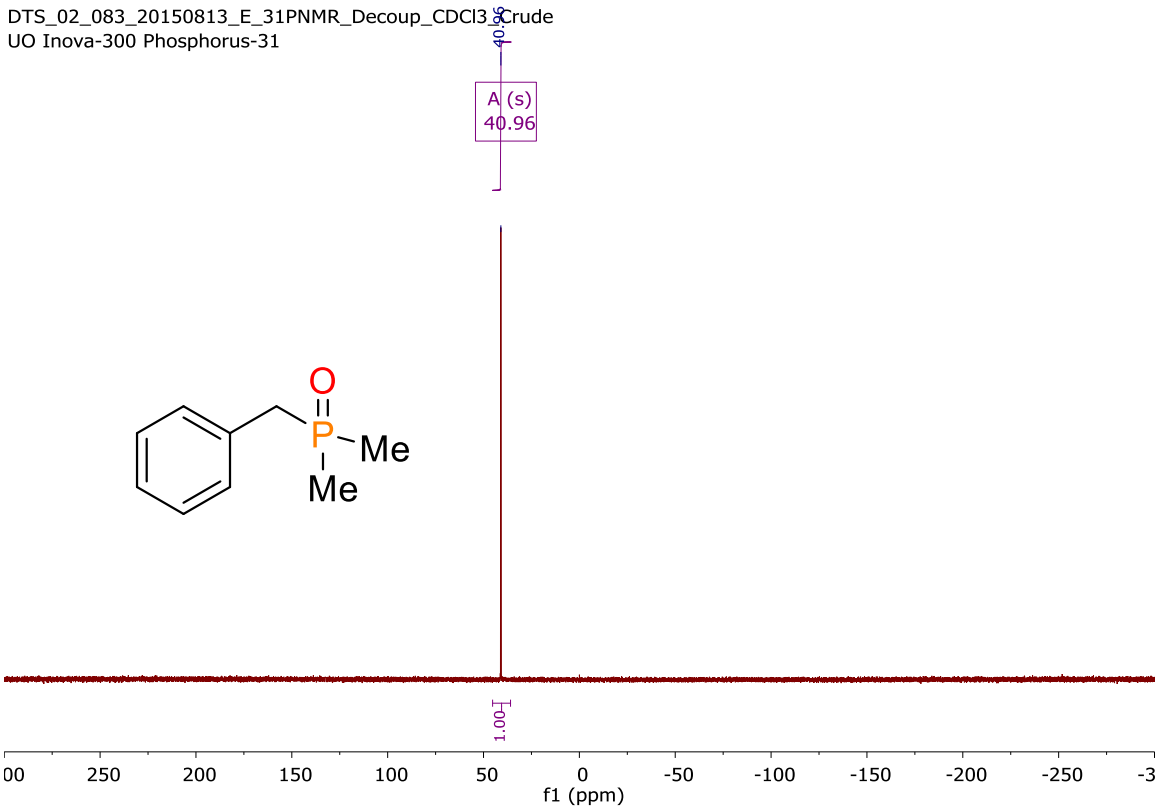

Figure B22. $^{31}P\{^{1}H\}$ NMR of benzyldimethylphosphine oxide.

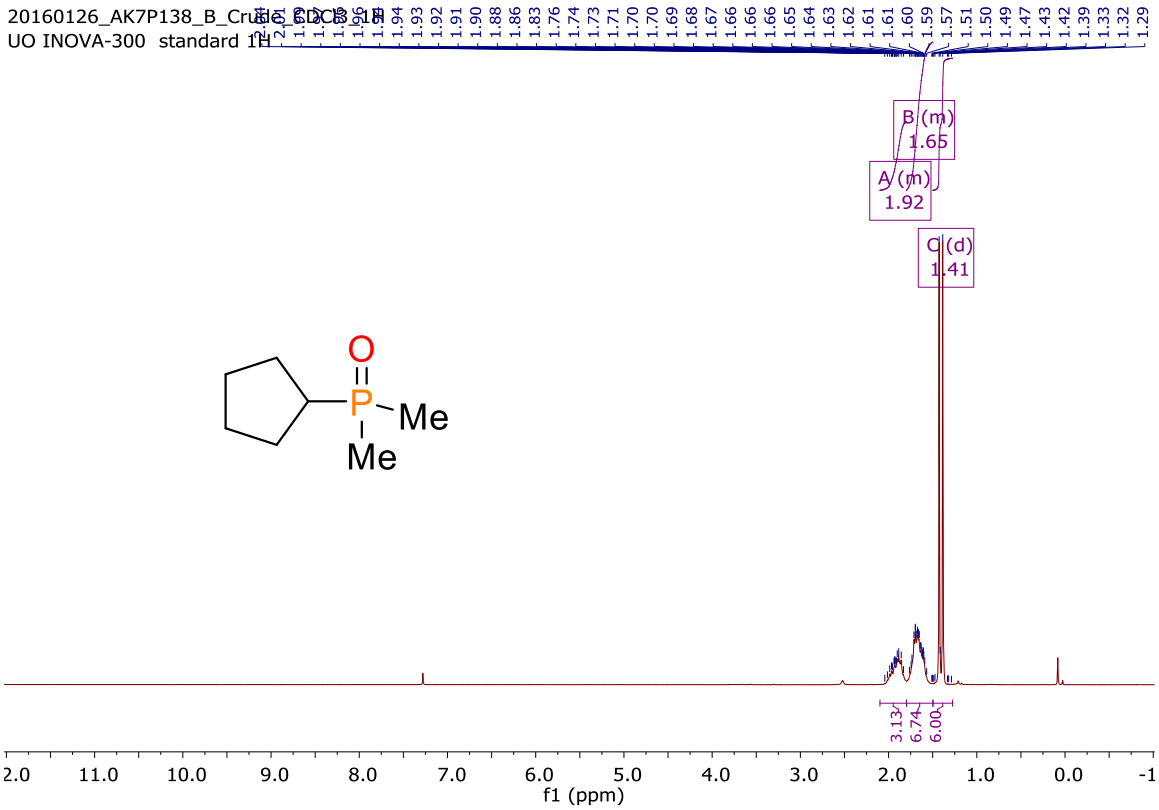

Figure B23. ^{1}H NMR of cyclopentyldimethylphosphine oxide.

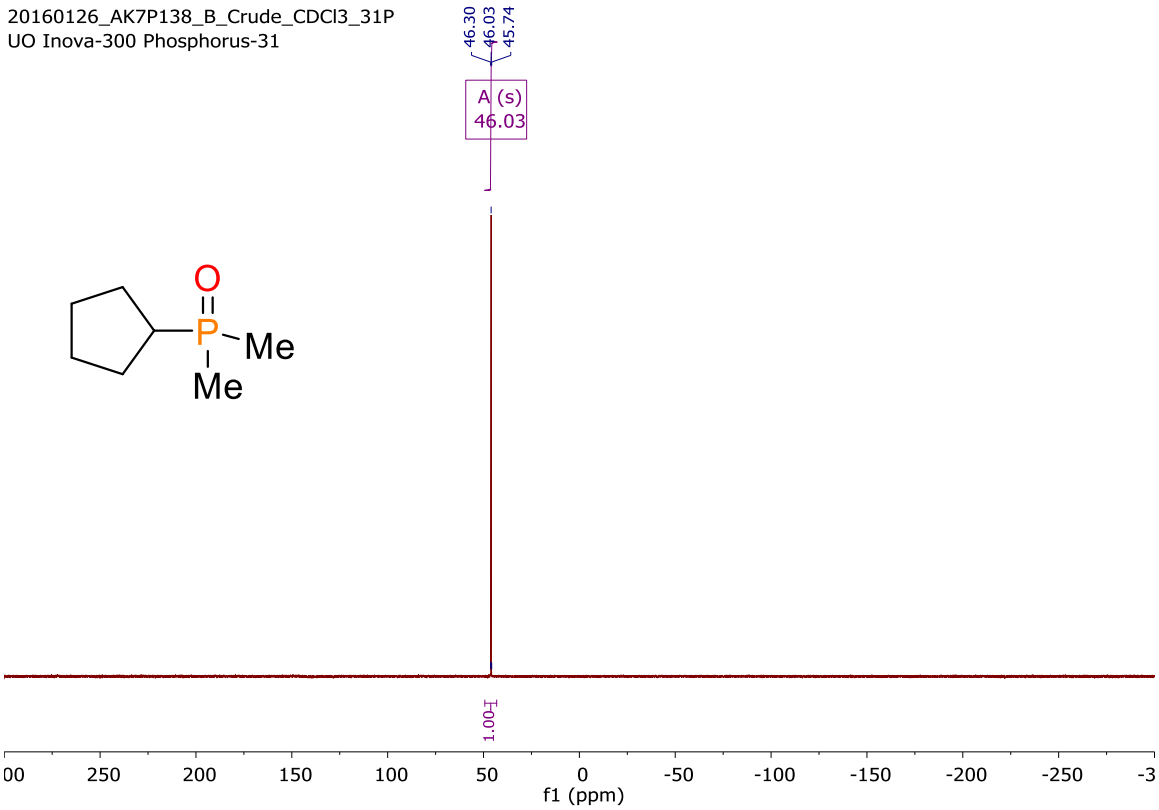

Figure B24. $^{31}P\{^{1}H\}$ NMR of cyclopentyldimethylphosphine oxide.

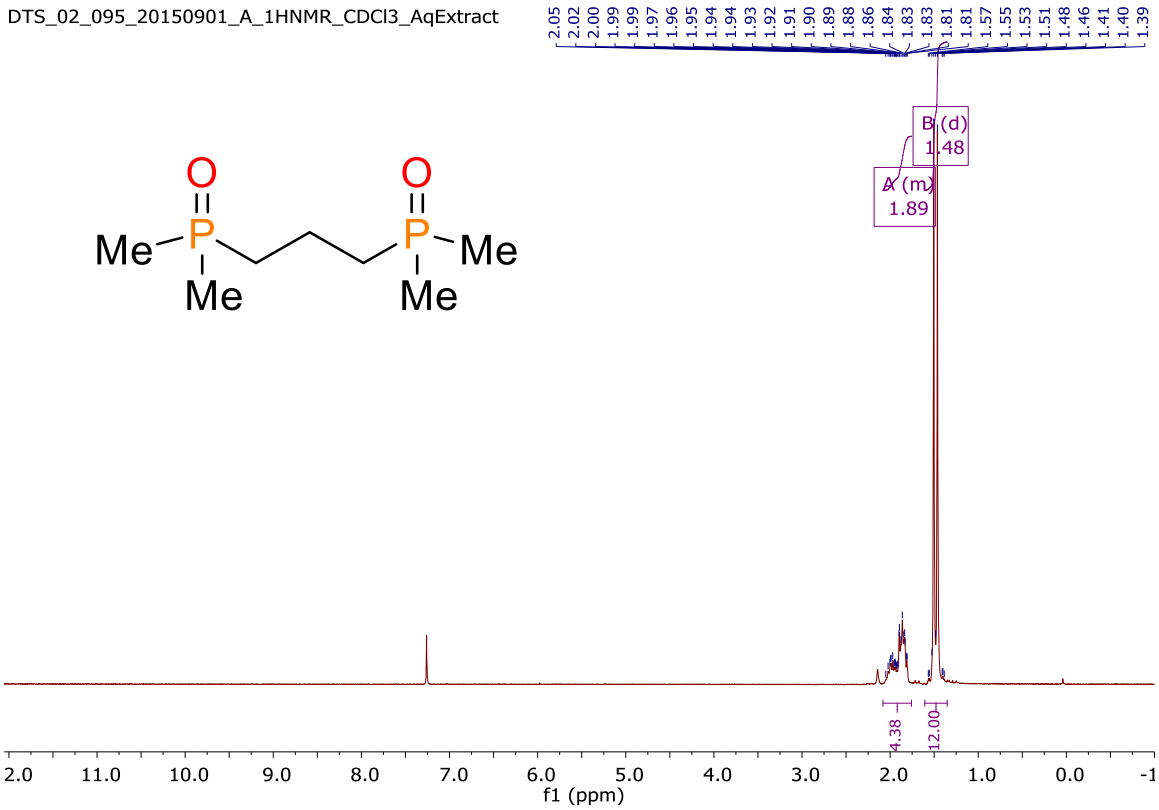

Figure B25. ^{1}H NMR of propane-1,3-diylbis(dimethylphosphine oxide).

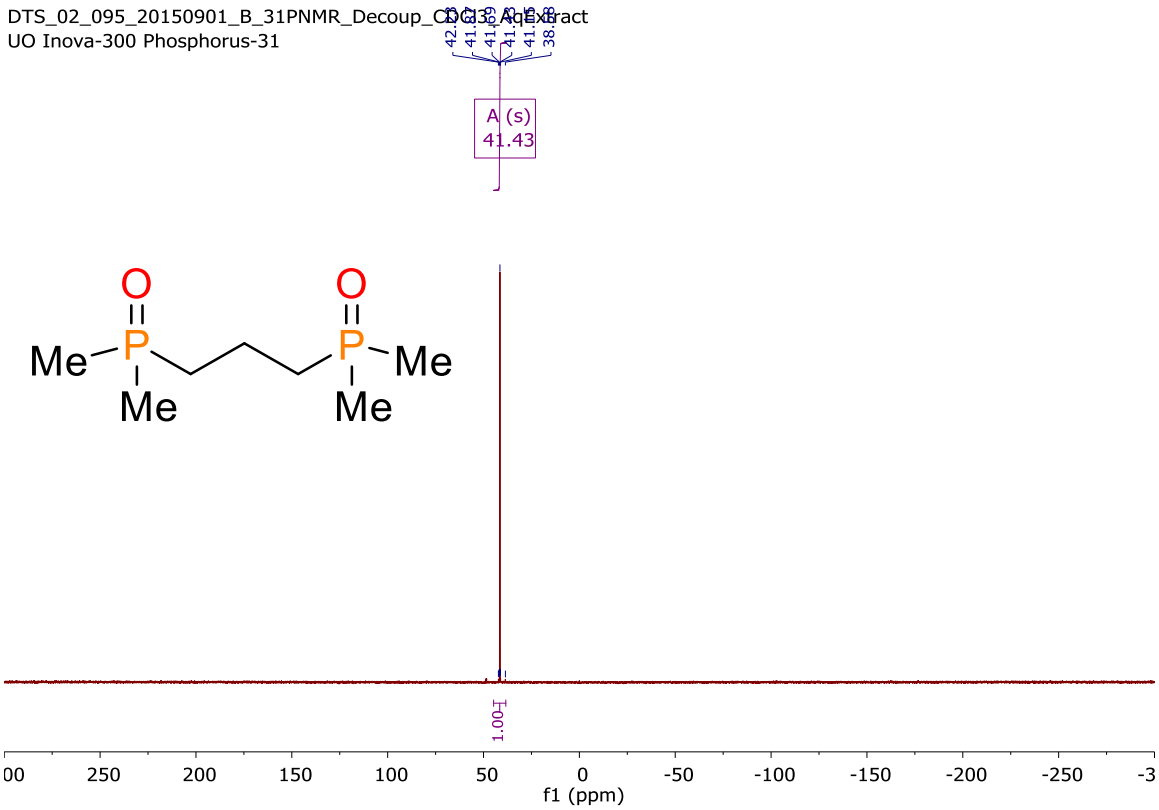

Figure B26. $^{31}P\{^{1}H\}$ NMR of propane-1,3-diylbis(dimethylphosphine oxide).

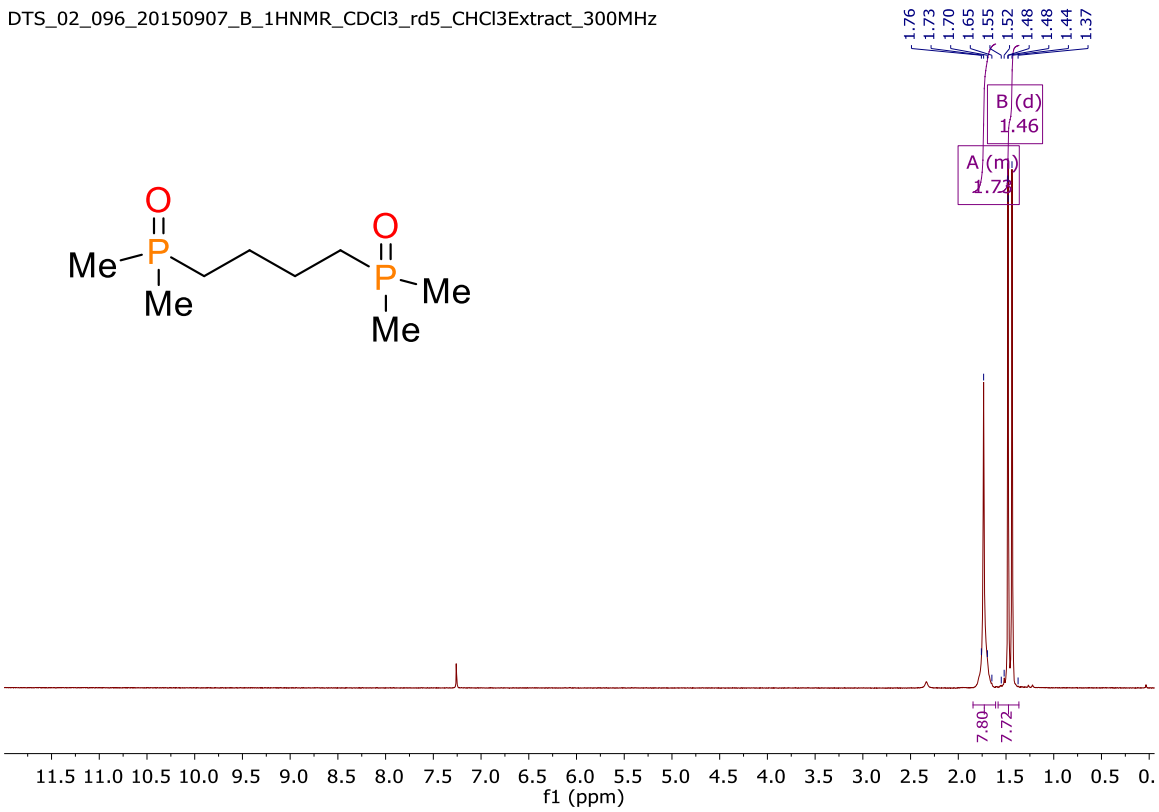

Figure B27. ^{1}H NMR of butane-1,4-diylbis(dimethylphosphine oxide).

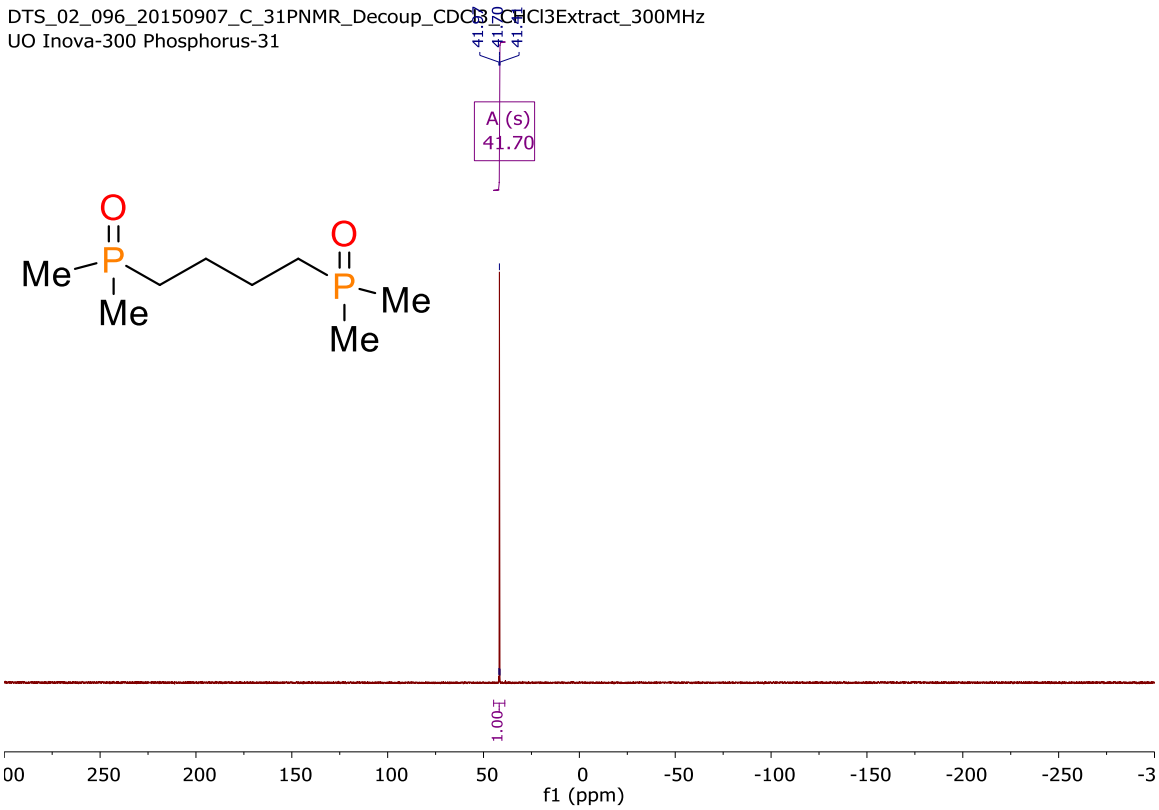

Figure B28. $^{31}P\{^{1}H\}$ NMR of butane-1,4-diylbis(dimethylphosphine oxide).

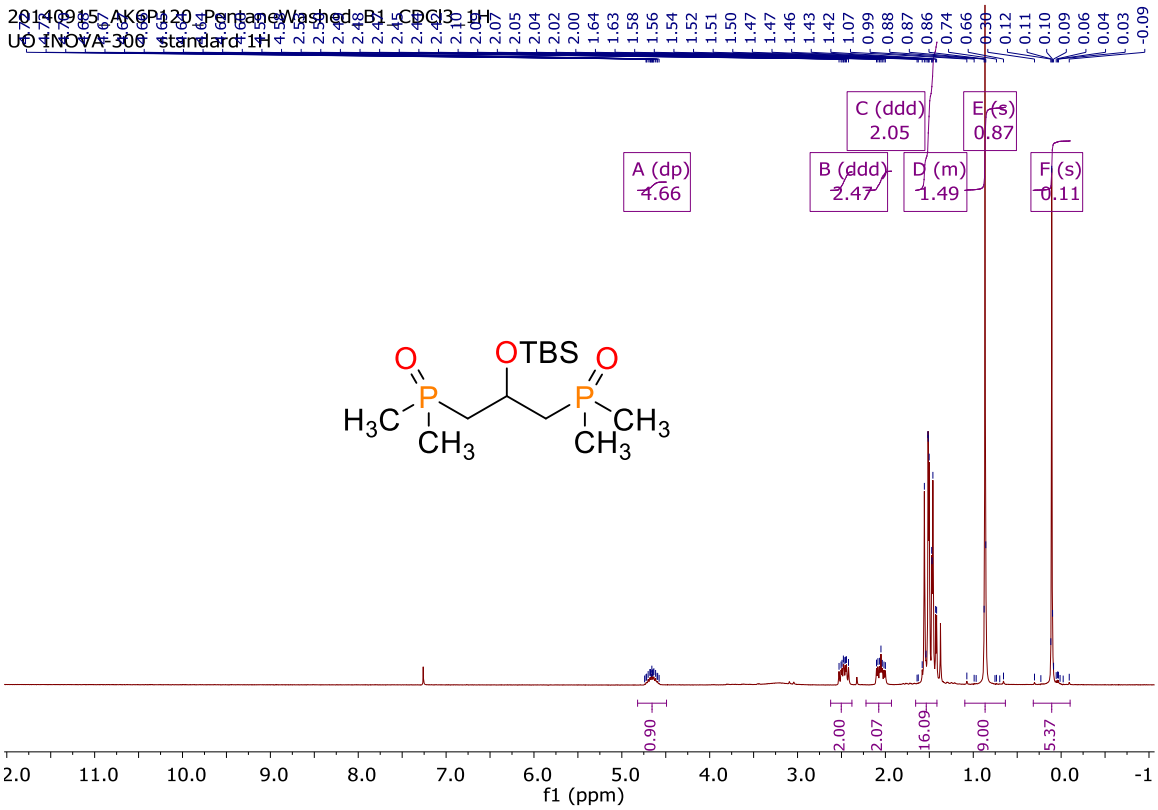

Figure B29. ^{1}H NMR of (2-((tert-butyldimethylsilyl)oxy)propane-1,3-diyl)bis(dimethylphosphine oxide).

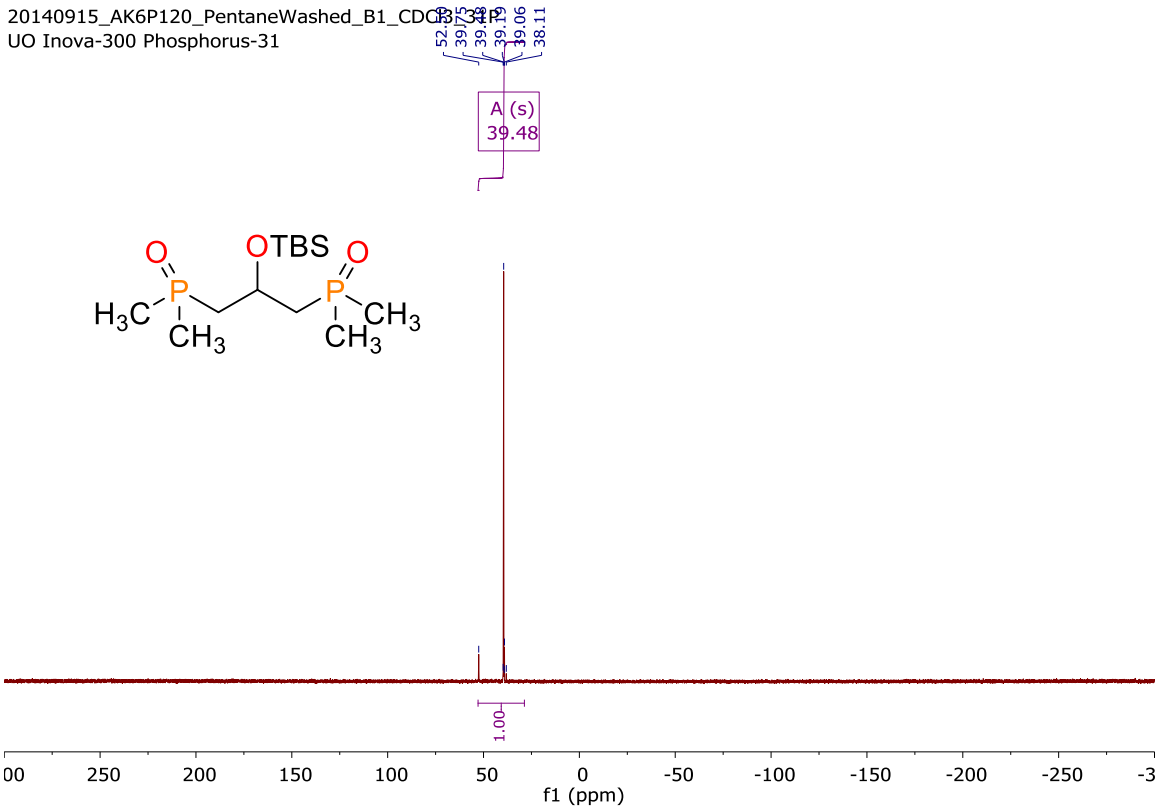

Figure B30. $^{31}P\{^{1}H\}$ NMR of (2-((tert-butyldimethylsilyl)oxy)propane-1,3-diyl)bis(dimethylphosphine oxide).

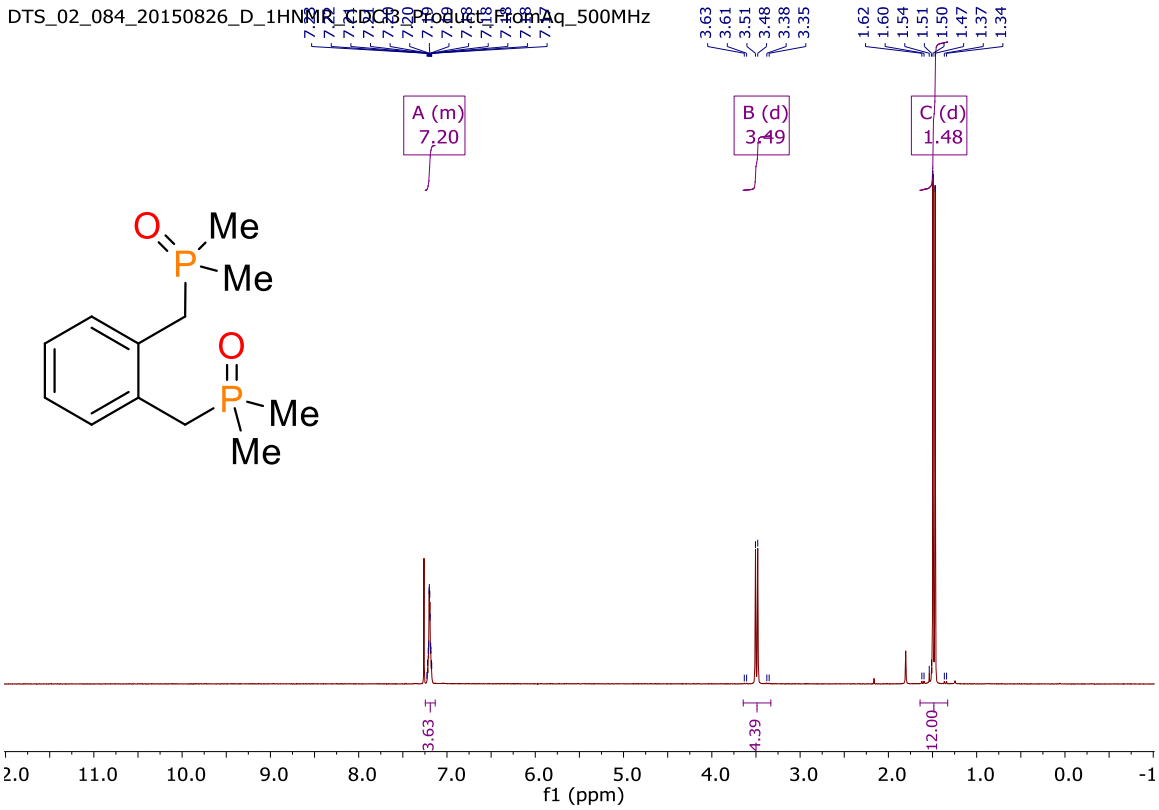

Figure B31. ^{1}H NMR of (1,2-phenylenebis(methylene))bis(dimethylphosphine oxide).

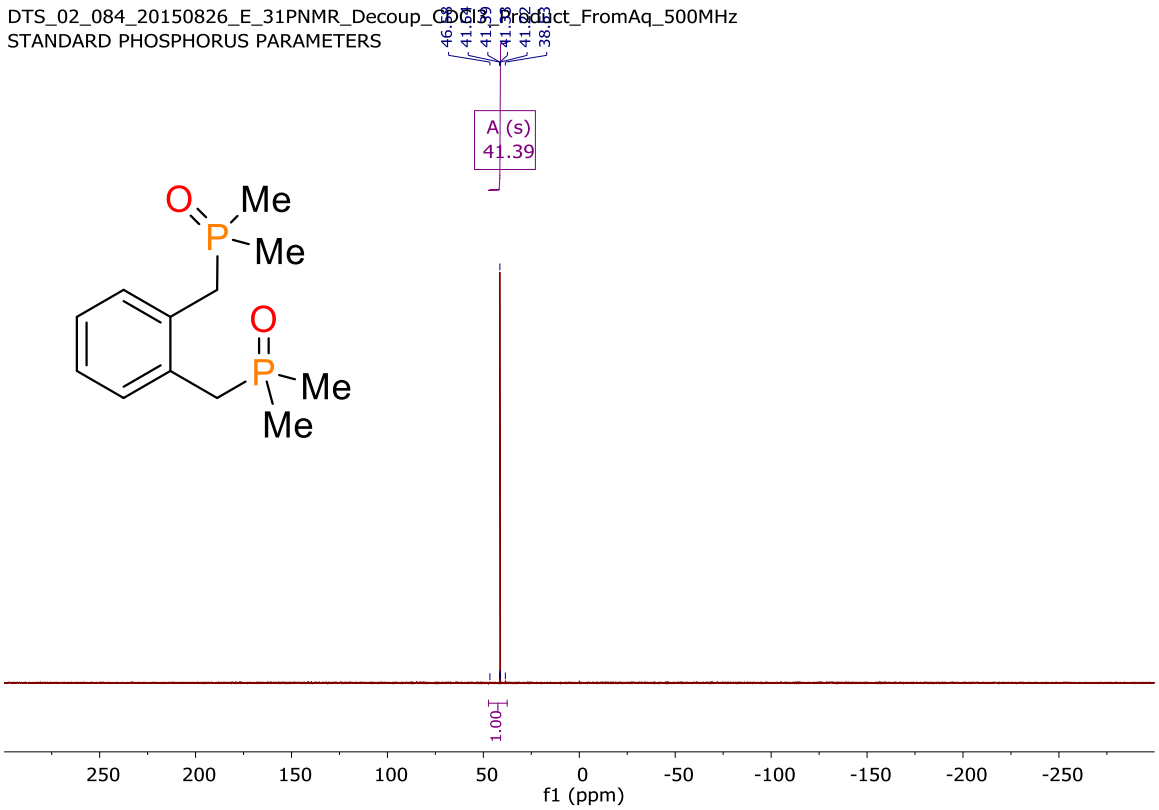

Figure B32. $^{31}P\{^{1}H\}$ NMR of (1,2-phenylenebis(methylene))bis(dimethylphosphine oxide).

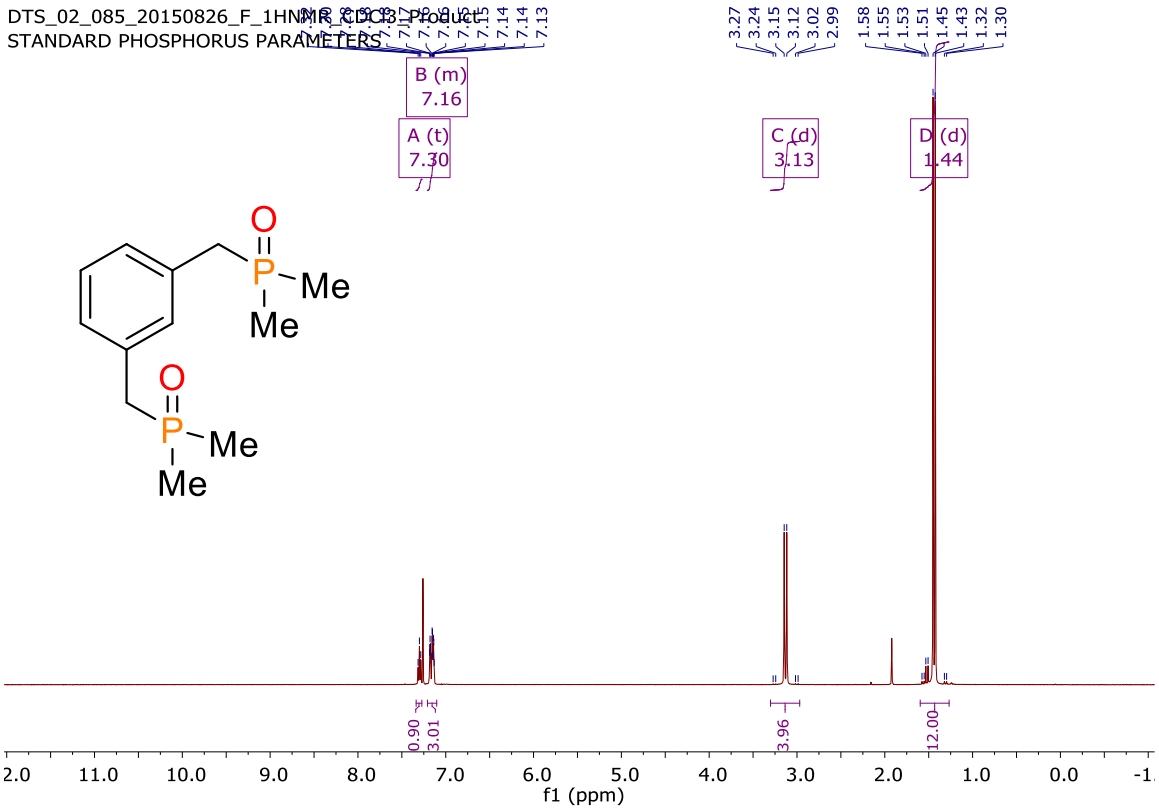

Figure B33. ^{1}H NMR of (1,3-phenylenebis(methylene))bis(dimethylphosphine oxide).

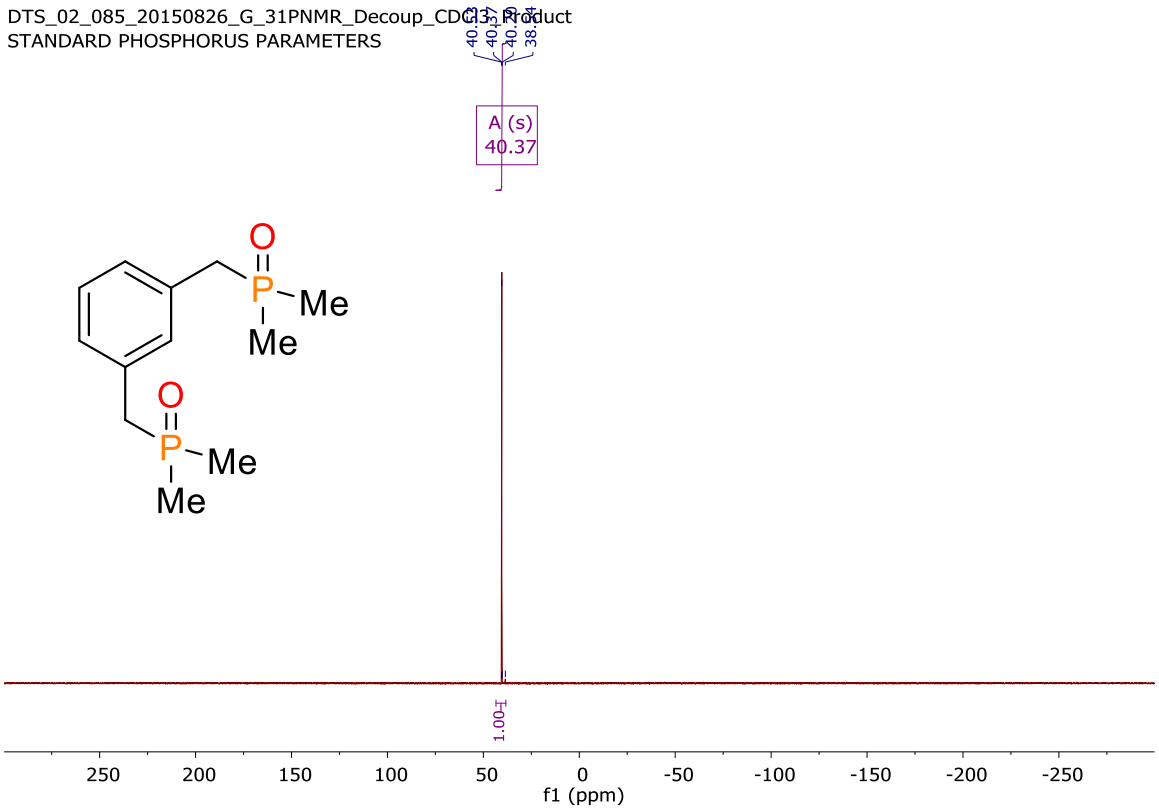

Figure B34. $^{31}P\{^{1}H\}$ NMR of (1,3-phenylenebis(methylene))bis(dimethylphosphine oxide).

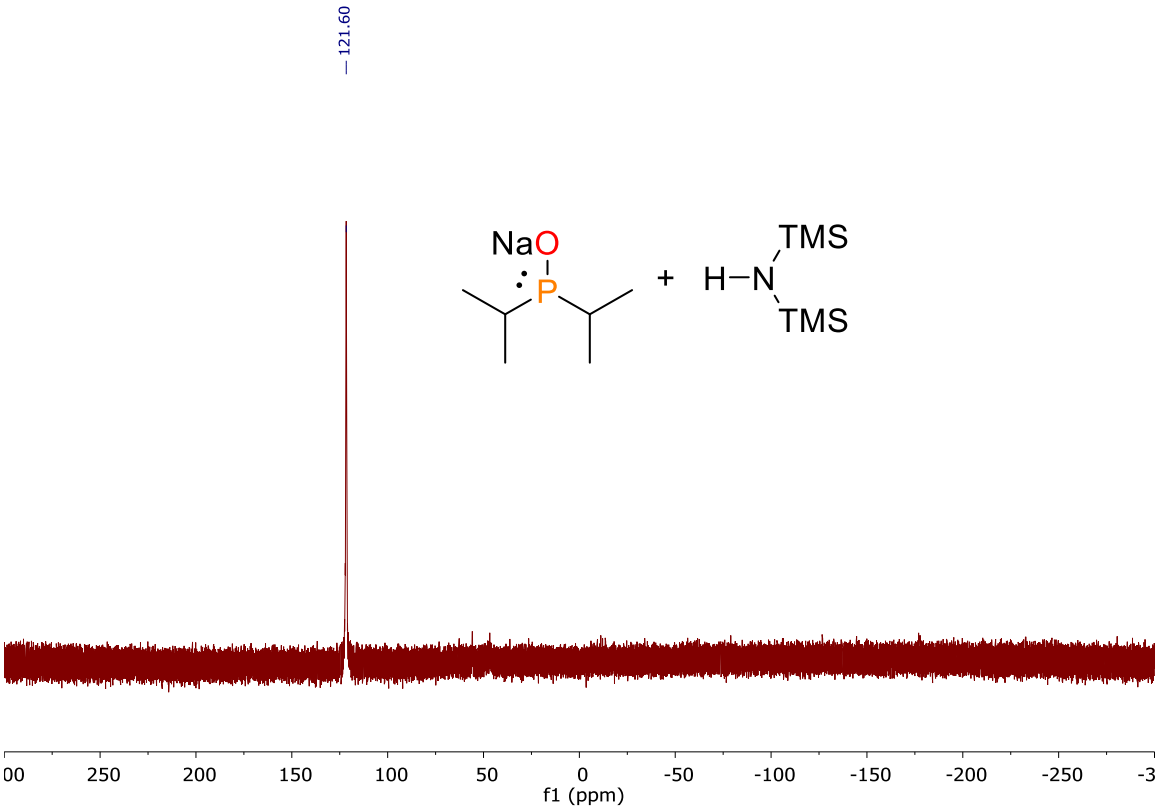

Figure B35. $^{31}P\{^{1}H\}$ of the intermediate formed by deprotonation of SPO with NaHMDS in THF.

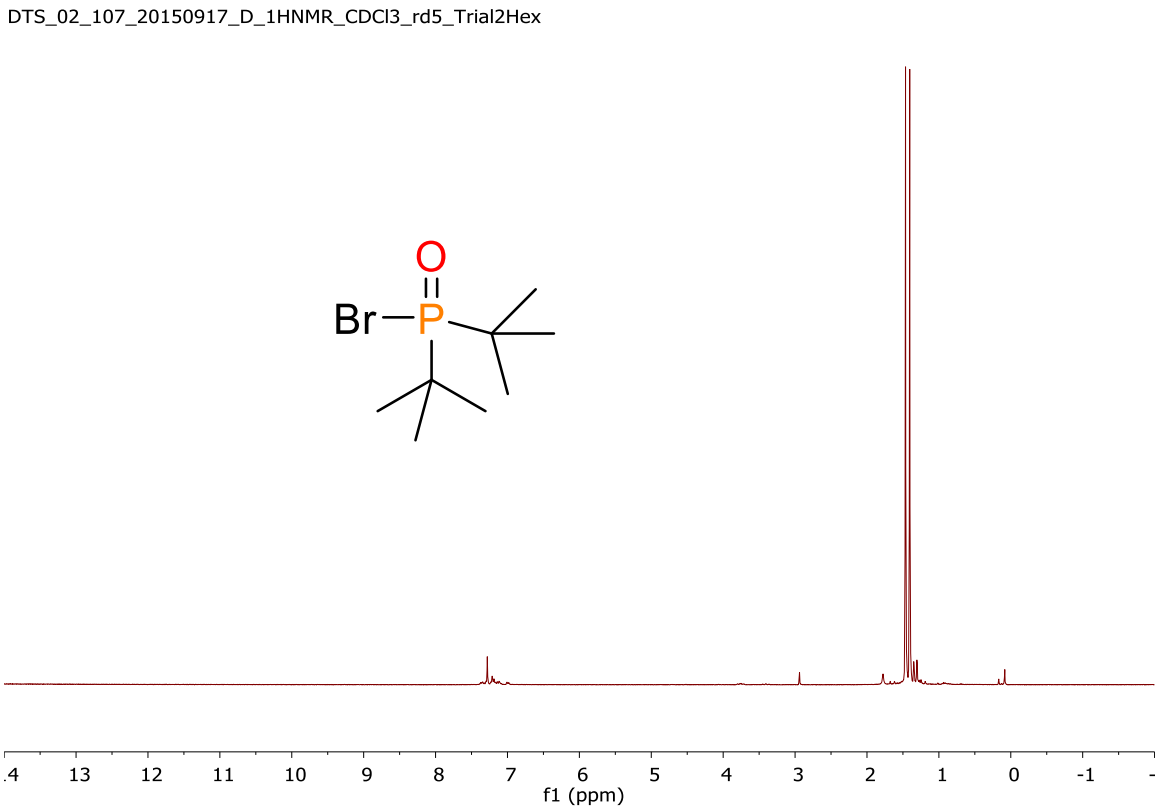

Figure B36. ^{1}H NMR of di-*tert*-butylphosphinic bromide.

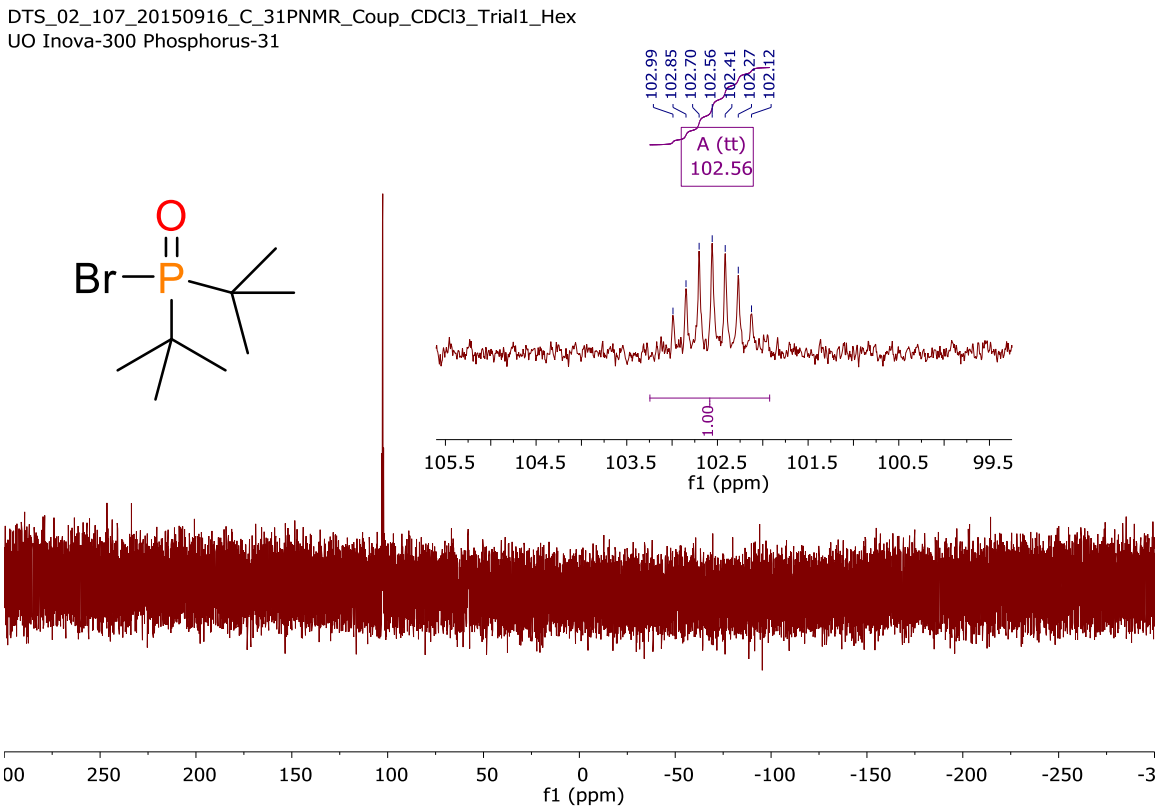

Figure B37. ^{31}P NMR of di-*tert*-butylphosphinic bromide.

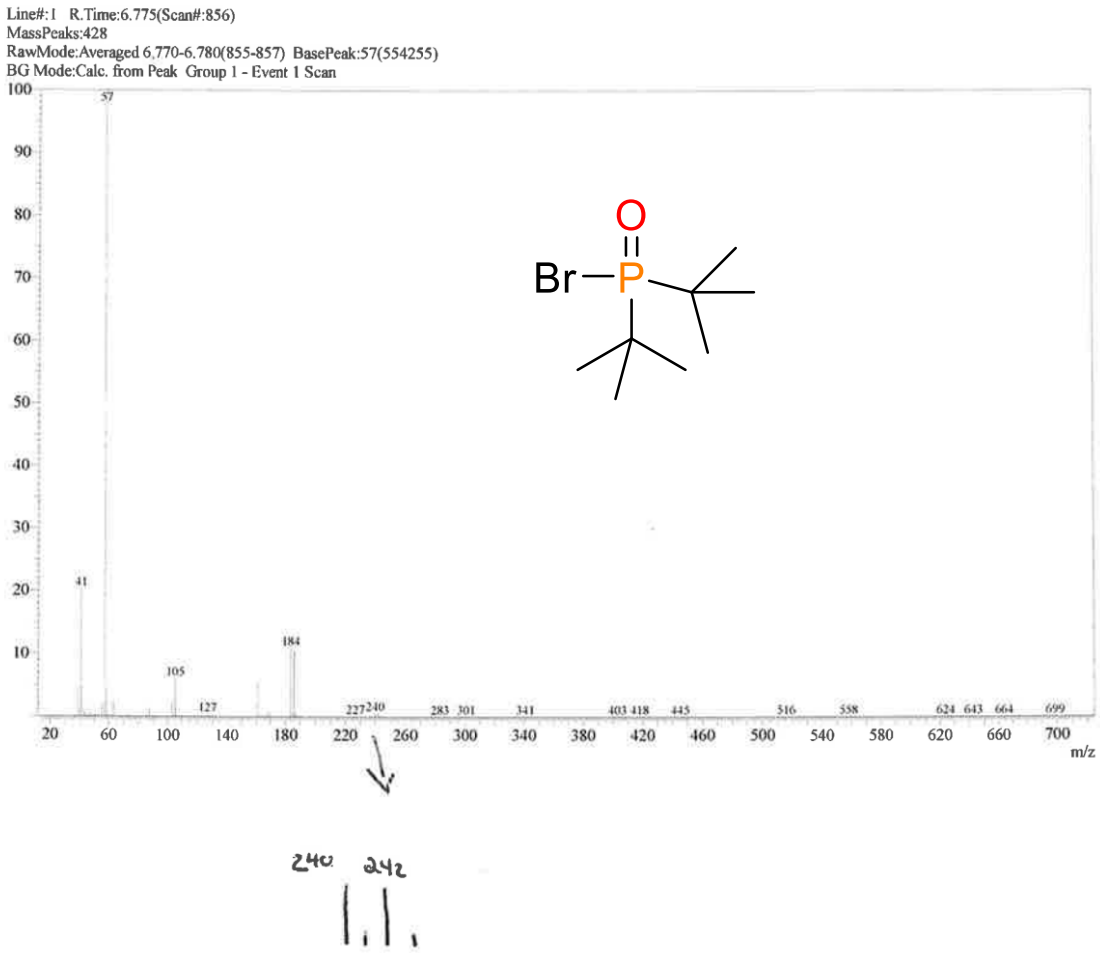

Figure B38. Mass spectrum of di-*tert*-butylphosphinic bromide with parent peak highlighted.

APPENDIX C

SUPPORTING INFORMATION FOR CHAPTER IV

C.1. Oxidation of MeJPhos

Under an atmosphere of N_2, MeJPhos (14.4 mg, 67 μmol) was added to a J-Young adapted NMR tube along with 442 μL C_6D_6 (c.a. 150 mM). ^1H and $^{31}P\{^1H\}$ NMRs were taken of the unreacted MeJPhos (d_1 = 10). The J-Young adapted NMR tube was frozen and the headspace exchanged with dry O_2 (1 atm). The sample was then warmed and vigorously shaken. The reaction progress was monitored via NMR (both ^1H and ^{31}P) to determine the ratio of oxidation over time.

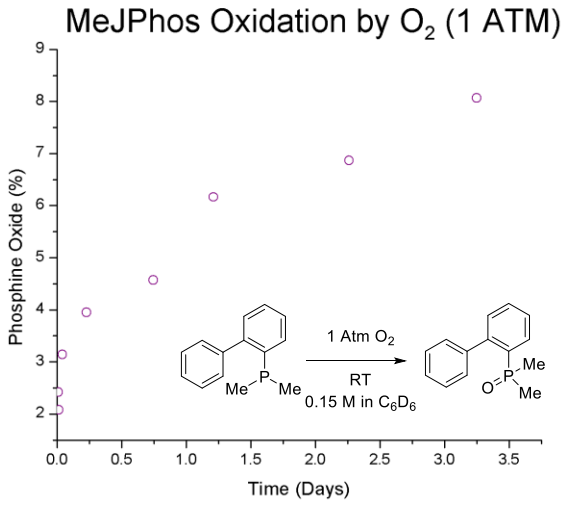

Figure C1. Oxidation of Methyl JohnPhos with molecular oxygen at room temperature.

C.2. Calculations of Steric and Electronic Parameters

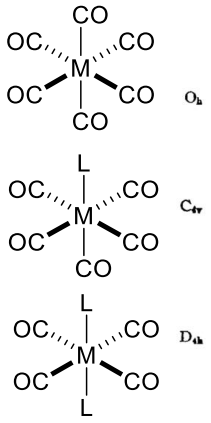

A_{1g}	Raman	$\lambda = \mu(k + k_t + 4k_c)$	$\lambda = \mu(k + 6k_i)$
E_g	Raman	$\lambda = \mu(k + k_t - 2k_c)$	$\lambda = \mu k$
T_{1u}	Infrared	$\lambda = \mu(k - k_t)$	$\lambda = \mu(k - 2k_i)$
$A_1^{(1)}$	Infrared and Raman	$\begin{vmatrix} \mu k_1 - \lambda & 2\mu k_c \\ 2\mu k_c & \mu(k_2 + k_t + 2k_c') - \lambda \end{vmatrix} = 0$	$\begin{vmatrix} \mu k_1 - \lambda & 2\mu k_i \\ 2\mu k_i & \mu(k_2 + 4k_i) - \lambda \end{vmatrix} = 0$
$A_1^{(2)}$			
B_1	Raman	$\lambda = \mu(k_2 + k_t - 2k_c')$	$\lambda = \mu k_2$
E	Infrared and Raman	$\lambda = \mu(k_2 - k_t)$	$\lambda = \mu(k_2 - 2k_i)$
A_{1g}	Raman	$\lambda = \mu(k + k_t + 2k_c)$	$\lambda = \mu(k + 4k_i)$
B_{1g}	Raman	$\lambda = \mu(k + k_t - 2k_c)$	$\lambda = \mu k$
E_u	Infrared	$\lambda = \mu(k - k_t)$	$\lambda = \mu(k - 2k_i)$

Figure C2. Determination of observed carbonyl absorbencies based on symmetry assignments and their mathematical relationship to the force constants of the carbonyls. Figure modified from: Cotton, F. A.; Kraihanzel, C. S. *J. Am. Chem. Soc.* **1962**, *84* (23), 4432–4438.

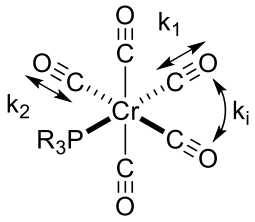

Figure C3. Visual representation of force constants for $Cr(0)(CO)_5(PR_3)$ complexes.

MeJPhos ChromiumCarbonyl Calculations

P-Cr(CO)5

General Factors

v1=A1 absorbtion in cm-1, v2=B1 absorbtion in cm-1, v3=E absorbtion in cm-1, u=inverse of reduced mass of CO in AMU-1, k2= k2; force constant, k=ki force constant, q=k1 force constant, all force constants in dynes/cm

Calculated from Cotton, A; Kraihanzel, C. S. J. Am. Chem. Soc. 1964, 84, 4432-4438.

Variables

```
v1
```

v1

```
v1 = 2059.6
```

2059.6

```
v2
```

v2

```
v2 = 2003.2
```

2003.2

```
v3
```

v3

```
v3 = 1937.5
```

1937.5

1937.5

```
u
```

0.14583

B1 CO stretch and k2

$$k2 = \frac{(5.8890 * 10^{-2})\ (v2)^2}{u}$$

```
1.620478605455668`*^6
```

1.62048×10^6

```
k2
```

1.62048×10^6

E CO stretch and ki

```
Solve[(5.8890 * 10^-2) (v3)^2 == u (k2 - 2 * k), k]
```

```
{{k → 52276.129641020416`}}
```

{{k → 52276.1}}

```
k = 52276.129641020416
```

52276.1

```
k
```

52276.1

A1 CO Stretch and k1

```
Solve[Det[{{u * q - (5.889 * 10^-2 * (v3)^2), 2 * u * k}, {2 * u * k, u (k2 + 4 * k) - (5.889 * 10^-2 * (v3)^2)}}] == 0, q]
```

{{q → 1.55078×10^6}}

Figure C4. Calculation of force constants for $Cr(0)(CO)_5$(MeJPhos) complexes using Wolfram Mathematica® 10 Student Ed. Version 10.0.2.0.

EtJPhos ChromiumCarbonyl Calculations

P-Cr(CO)5

General Factors

v1=A1 absorbtion in cm-1, v2=B1 absorbtion in cm-1, v3=E absorbtion in cm-1, u=inverse of reduced mass of CO in AMU-1, k2= k2; force constant, k=ki force constant, q=k1 force constant, all force constants in dynes/cm

Calculated from Cotton, A; Kraihanzel, C. S. J. Am. Chem. Soc. 1964, 84, 4432-4438.

Variables

```
v1
```

```
v1
```

```
v1 = 2072.5
```

```
2072.5
```

```
v2
```

```
v2
```

```
v2 = 2058.5
```

```
2058.5
```

```
v3
```

```
v3
```

```
v3 = 1935.3
```

```
1935.3
```

```
u = 0.14583`
```

```
0.14583
```

B1 CO stretch and k2

```
k2 = (5.8890*10^-2) (v2)^2 / u
```

$$\frac{249541.7963025`}{u}$$

$$1.71118\times10^{6}$$

```
k2 = 1.7111828588253448`*^6
```

$$1.71118\times10^{6}$$

E CO stretch and ki

```
Solve[(5.8890*10^-2) (v3)^2 == u (k2 - 2*k), k]
```

```
{{k → 99348.6}}
```

```
k = 99348.58898169099`
```

```
99348.6
```

```
k
```

```
99348.6
```

A1 CO Stretch and k1

```
Solve[Det[{{u*q - (5.889*10^-2*(v3)^2), 2*u*k}, {2*u*k, u (k2 + 4*k) - (5.889*10^-2*(v3)^2)}}] == 0, q]
```

$$\{\{q \to 1.57872\times10^{6}\}\}$$

Figure C5. Calculation of force constants for Cr(0)$(CO)_5$(EtJPhos) complexes using Wolfram Mathematica® 10 Student Ed. Version 10.0.2.0.

iPrJPhos ChromiumCarbonyl Calculations

P-Cr(CO)5

General Factors

v1=A1 absorbtion in cm-1, v2=B1 absorbtion in cm-1, v3=E absorbtion in cm-1, u=inverse of reduced mass of CO in AMU-1, k2= k2; force constant, k=ki force constant, q=k1 force constant, all force constants in dynes/cm

Calculated from Cotton, A; Kraihanzel, C. S. J. Am. Chem. Soc. 1964, 84, 4432-4438.

Variables

```
v1
```
v1

```
v1 = 2072.78
```
2072.78

```
v2
```
v2

```
v2 = 2057.58
```
2057.58

```
v3
```
v3

```
v3 = 1936.44
```
1936.44

```
u = 0.14583
```
0.14583

B1 CO stretch and k2

```
k2 = (5.8890*10^-2) (v2)^2 / u
```
$$\frac{249318.792027396`}{u}$$

1.70965×10^{6}

```
k2 = 1.7096536516998974`*^6
```
1.70965×10^{6}

E CO stretch and ki

```
Solve[(5.8890*10^-2) (v3)^2 == u (k2 - 2*k), k]
```
{{k → 97692.8}}

```
k = 97692.7843073853`
```
97692.8

A1 CO Stretch and k1

```
Solve[Det[{{u*q - (5.889*10^-2*(v3)^2), 2*u*k}, {2*u*k, u (k2 + 4*k) - (5.889*10^-2*(v3)^2)}}] == 0, q]
```
{{q → 1.5794×10^{6}}}

Figure C6. Calculation of force constants for Cr(0)$(CO)_5$(^{i}PrJPhos) complexes using Wolfram Mathematica® 10 Student Ed. Version 10.0.2.0.

CyHexJPhos ChromiumCarbonyl Calculations

P-Cr(CO)5

General Factors

v1=A1 absorbtion in cm-1, v2=B1 absorbtion in cm-1, v3=E absorbtion in cm-1, u=inverse of reduced mass of CO in AMU-1, k2= k2; force constant, k=ki force constant, q=k1 force constant, all force constants in dynes/cm

Calculated from Cotton, A; Kraihanzel, C. S. J. Am. Chem. Soc. 1964, 84, 4432-4438.

Variables

```
v1
```
v1

```
v1 = 2072.1
```
2072.1

```
v2
```
v2

```
v2 = 2056.7
```
2056.7

```
v3
```
v3

```
v3 = 1937.1
```
1937.1

1937.5

1937.5

```
u = 0.14583`
```
0.14583

B1 CO stretch and k2

$$k2 = \frac{(5.8890 * 10^{-2})\ (v2)^2}{u}$$

1.70819×10^6

```
k2 = 1.7081915715017489`*^6
```
1.70819×10^6

E CO stretch and ki

```
Solve[(5.8890 * 10^-2) (v3)^2 == u (k2 - 2 * k), k]
```
{{k → 96445.5}}

```
k = 96445.5457971611`
```
96445.5

A1 CO Stretch and k1

$$\text{Solve}\left[\text{Det}\left[\begin{pmatrix} u * q - (5.889 * 10^{-2} * (v3)^2) & 2 * u * k \\ 2 * u * k & u\ (k2 + 4 * k) - (5.889 * 10^{-2} * (v3)^2) \end{pmatrix}\right] == 0,\ q\right]$$

$\{\{q \to 1.5796 \times 10^6\}\}$

Figure C7. Calculation of force constants for $Cr(0)(CO)_5$(CyJPhos) complexes using Wolfram Mathematica® 10 Student Ed. Version 10.0.2.0.

tBuJPhos ChromiumCarbonyl Calculations

P-Cr(CO)5

General Factors

v1=A1 absorbtion in cm-1, v2=B1 absorbtion in cm-1, v3=E absorbtion in cm-1, u=inverse of reduced mass of CO in AMU-1, k2= k2; force constant, k=ki force constant, q=k1 force constant, all force constants in dynes/cm

Calculated from Cotton, A; Kraihanzel, C. S. J. Am. Chem. Soc. 1964, 84, 4432-4438.

Variables

```
v1
```

v1

```
v1 = 2072.1
```

2072.1

```
v2
```

v2

```
v2 = 2062.5
```

2062.5

2062.5

2062.5

```
v3
```

v3

```
v3 = 1937.1
```

1937.1

1937.5

```
u = 0.14583`
```

0.14583

B1 CO stretch and k2

$$k2 = \frac{(5.8890 * 10^{-2}) (v2)^2}{u}$$

$$\frac{250512.53906250003`}{u}$$

$$1.71784 \times 10^6$$

```
k2 = 1.7178395327607493`*^6
```

1.71784×10^6

E CO stretch and ki

```
Solve[(5.8890*10^-2) (v3)^2 == u (k2 - 2*k), k]
```

{{k → 101230.41331850443`}}

k = 101230.41331850443

{{k → 101230.}}

101230.

A1 CO Stretch and k1

$$\text{Solve}\left[\text{Det}\left[\begin{pmatrix} u*q - (5.889*10^{-2}*(v3)^2) & 2*u*k \\ 2*u*k & u\,(k2 + 4*k) - (5.889*10^{-2}*(v3)^2) \end{pmatrix}\right] == 0,\ q\right]$$

$$\left\{\left\{q \to \frac{6.5246307356908844`*^9 + 128906.53158082509`\,k + 0.08506555559999998`\,k^2}{4305.610676278108` + 0.08506555559999998`\,k}\right\}\right\}$$

$\{\{q \to 1.58287 \times 10^6\}\}$

Figure C8. Calculation of force constants for $Cr(0)(CO)_5$(^{t}BuJPhos) complexes using Wolfram Mathematica® 10 Student Ed. Version 10.0.2.0.

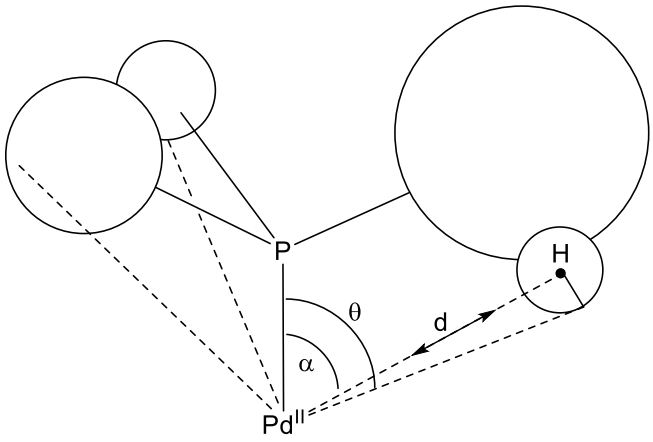

Figure C9. Definition of the van der Waals surface for phosphine ligands which results in the calculation of the Tolman cone angles directly from crystallographic data. Figure modified from: Müller, T. E.; Mingos, D. M. P. *Transit. Met. Chem.* **1995**, *20* (6), 533–539.

$$\theta_i = \alpha + \frac{180}{\pi}\left(\sin^{-1}\left(\frac{r_H}{d}\right)\right) \qquad \text{(C1)}$$

$$\Theta = \frac{2}{3}\sum_i \theta_i \qquad \text{(C2)}$$

For equations C1 and C2: Θ = crystalographically determined Tolman cone angle (°), θ = Hydrogen atom corrected partial cone angle (°), α = uncorrected crystallographic partial cone angle (°), r_H = radius of hydrogen (Å), d = distance from Pd to centroid of lowest hydrogen atom (Å).

Table C1. Compiled data from crystal structures used to calculate steric parameters S4' (°),[1] Tolman cone angle (°),[2] percent buried volume (%BV),[3] and Pd-P bond distances (Å). Note that the actual Pd-P bond distances were used in lieu of an artificial constant bond length for the steric calculations (as is typically reported).

t-Pd(II)Cl_2P_2	P-Pd bond length (Å)	∠Pd-P-C_1(°)	∠Pd-P-C_2(°)	∠Pd-P-C_3(°)	∠C_3-P-C_1(°)	∠C_1-P-C_2(°)	∠C_2-P-C_3(°)	α ∠Pd-P-H_1(°)	α ∠Pd-P-H_2(°)	α ∠Pd-P-H_3(°)
Methyl JohnPhos	2.319	105.42	117.94	118.24	105.57	104.74	103.33	91.25	38.75	43.43
Ethyl JohnPhos	2.325	107.37	117.87	117	103.79	105.21	103.98	93.97	39.44	60.4
iso-Propyl JohnPhos	2.356	113.74	115.96	107.81	109.52	105.04	104.1	66.51	54.96	96.11
CycloHexyl JohnPhos	2.38	108.46	112.34	115.78	108.62	106.13	104.92	64.51	54.68	84.86
tert-Butyl JohnPhos	-	-	-	-	-	-	-	-	-	-
Phenyl JohnPhos	2.34	115.74	119.32	108.23	104.02	102.2	105.61	63.84	60.23	83.78
DimethylPhenyl Phosphine	2.259	112.05	120.25	111.65	103.7	99.95	107.49	42.78	42.98	49.62
DiethylPhenyl Phosphine	2.319	113.68	109.44	116.97	105.93	106.1	103.75	62.76	39.36	54.56
DicyclohexylPhenyl Phosphine	2.334	110.96	114.66	115.03	107.36	104.6	103.31	55.87	59.43	68.65
Di-isopropyl-Phenyl Phosphine	2.337	116.35	118.13	106.91	106.59	102.63	104.8	57.71	63.79	55.38
Di-tertbutyl-Phenyl Phosphine	2.398	112.31	117.26	107.83	99.41	111.21	108.42	67.59	62.09	76.26
Trimethyl Phosphine	2.26	109.97	123.34	112.04	102.68	106.55	100.79	39.04	40.87	38.65
Triethyl Phosphine	2.186	109.65	116.37	113.41	106.1	105.63	104.91	61.51	40.5	62.79
Tri-isopropyl Phosphine	2.36	113.06	113.18	109.81	104.83	104.48	110.77	62.08	57.75	59.2
TriCycloHexyl Phosphine	2.363	114.26	112.49	110.99	104.86	103.06	110.38	68.75	52.6	60.77
Tri-tertbutyl Phosphine	2.361	108.6	113.7	110.33	109.36	108.06	106.64	67.55	63.17	55.42
TriPhenyl Phosphine	2.337	111.48	112.37	117.23	103.6	106.71	104.54	58.15	47.56	64.57

Table C2. Compiled data (continued) from crystal structures used to calculate steric parameters S4' (°),[1] Tolman cone angle (°),[2] percent buried volume (%BV),[3] and Pd-P bond distances (Å). Note that the actual Pd-P bond distances were used in lieu of an artificial constant bond length for the steric calculations (as is typically reported).

t-Pd(II)Cl_2P_2	Pd-H_1 distance (Å)	Pd-H_2 distance (Å)	Pd-H_3 distance (Å)	θ ∠Pd-P-H_1 (°)	θ ∠Pd-P-H_2 (°)	θ ∠Pd-P-H_3 (°)	S4' (°)	Cone Angle (Θ) (°)	%BV (%)
Methyl JohnPhos	4.106	3.62	3.291	105.34592	54.786108	61.119532	27.96	147.5	32.8
Ethyl JohnPhos	4.182	3.612	3.221	107.80461	55.512586	78.48711	29.26	161.2	33.8
iso-Propyl JohnPhos	2.988	3.634	4.354	86.062595	70.932674	109.38787	18.85	177.59	35
CycloHexyl JohnPhos	2.969	3.461	4.643	84.192868	71.474137	97.297704	16.91	168.64	32.7
tert-Butyl JohnPhos	-	-	-	-	-	-	-	-	-
Phenyl JohnPhos	2.847	3.242	4.601	84.403602	78.19594	96.333084	29.77	172.62	33.9
DimethylPhenyl Phosphine	3.559	3.549	3.684	59.098572	59.345843	65.370216	32.81	122.54	25.2
DiethylPhenyl Phosphine	3.069	3.614	3.665	81.776415	55.423451	70.394006	24.31	138.4	27.2
DicyclohexylPhenyl Phosphine	3.424	3.179	5.167	72.85109	77.764515	79.809208	25.38	153.62	30.3
Di-isopropyl-Phenyl Phosphine	3.684	3.223	3.477	73.460216	81.865499	72.094581	27.37	151.61	30.7
Di-tertbutyl-Phenyl Phosphine	2.799	3.161	3.367	88.52266	80.532669	93.537523	18.36	175.06	34.1
Trimethyl Phosphine	3.553	3.512	3.61	55.386901	57.413191	54.731732	35.33	111.69	23.6
Triethyl Phosphine	2.941	3.328	3.004	81.388117	57.986482	82.234249	22.79	147.74	30.7
Tri-isopropyl Phosphine	3.155	3.261	3.203	80.559009	75.607724	77.392303	15.97	155.71	31.3
TriCycloHexyl Phosphine	5.098	3.604	3.176	80.062224	68.709233	79.122451	19.44	151.93	30
Tri-tertbutyl Phosphine	2.804	3.104	3.438	88.443584	81.963902	72.329856	8.57	161.82	36.5
TriPhenyl Phosphine	3.218	3.845	2.906	76.254557	62.634692	84.697819	26.23	149.06	29

Table C3. Notes and references for Tables C1 and C2.

***t*-Pd(II)Cl_2P_2**	**Notes**	**Reference**
Methyl JohnPhos		This work
Ethyl JohnPhos	Br, Cl complex	4
iso-Propyl JohnPhos		This work
CycloHexyl JohnPhos	Br	5
tert-Butyl JohnPhos	Not crystalized	Not crystalized
Phenyl JohnPhos		6
DimethylPhenyl Phosphine	*cis*-complex	7
DiethylPhenyl Phosphine	2-Et (structurally edited out)	4
DicyclohexylPhenyl Phosphine	2-iPr (structurally edited out)	4
Di-isopropyl-Phenyl Phosphine		8
Di-tertbutyl-Phenyl Phosphine		9
Trimethyl Phosphine	*cis*-complex	10
Triethyl Phosphine		11
Tri-isopropyl Phosphine		12
TriCycloHexyl Phosphine		13
Tri-tertbutyl Phosphine	H,Cl complex	14
TriPhenyl Phosphine		15

C.3. Additional Spectra

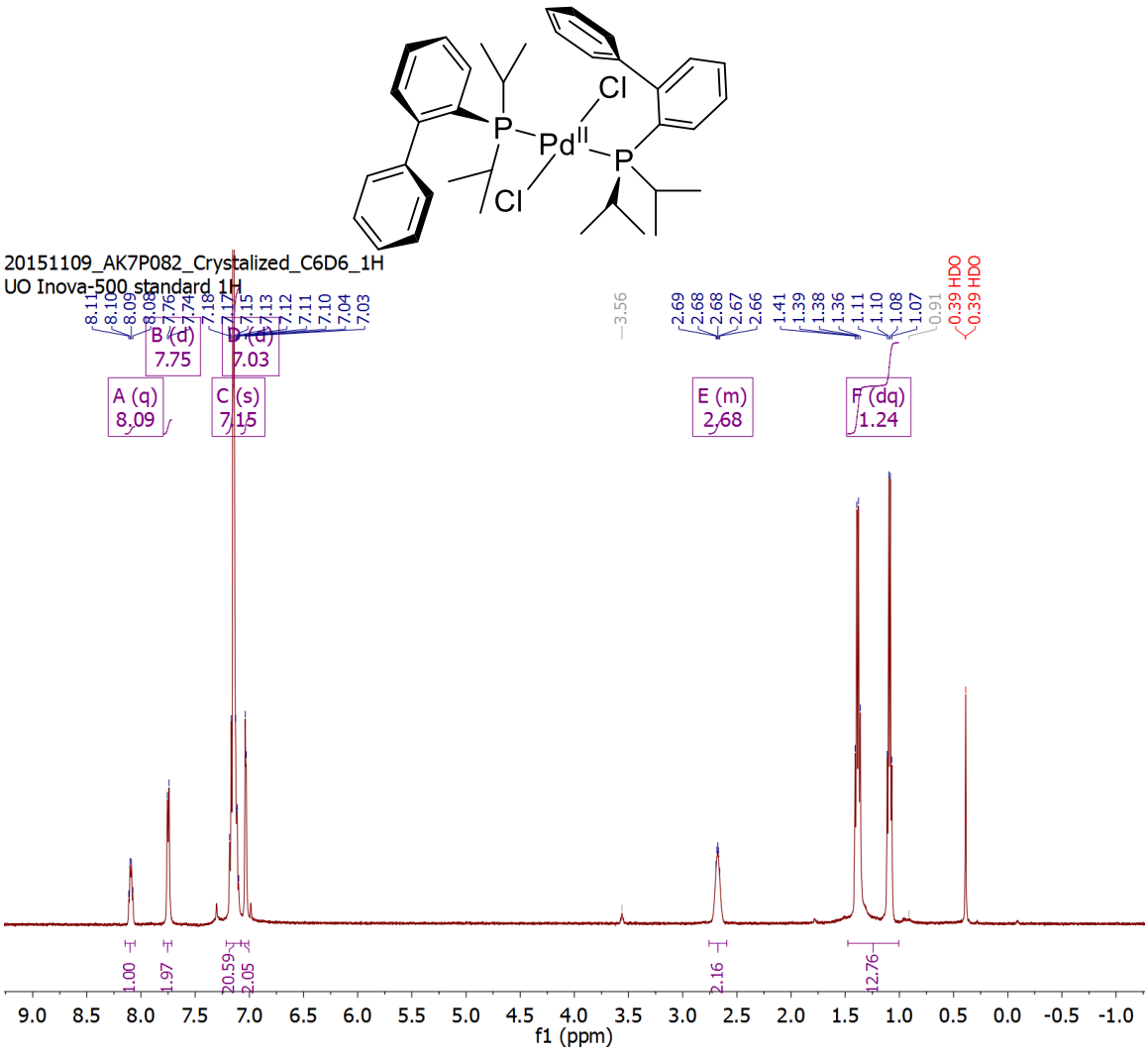

Figure C10. ^{1}H NMR of *trans*-Pd(II)(^{i}PrJPhos)$_2$(Cl)$_2$

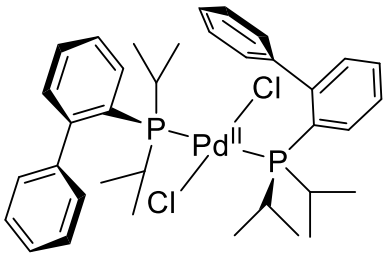

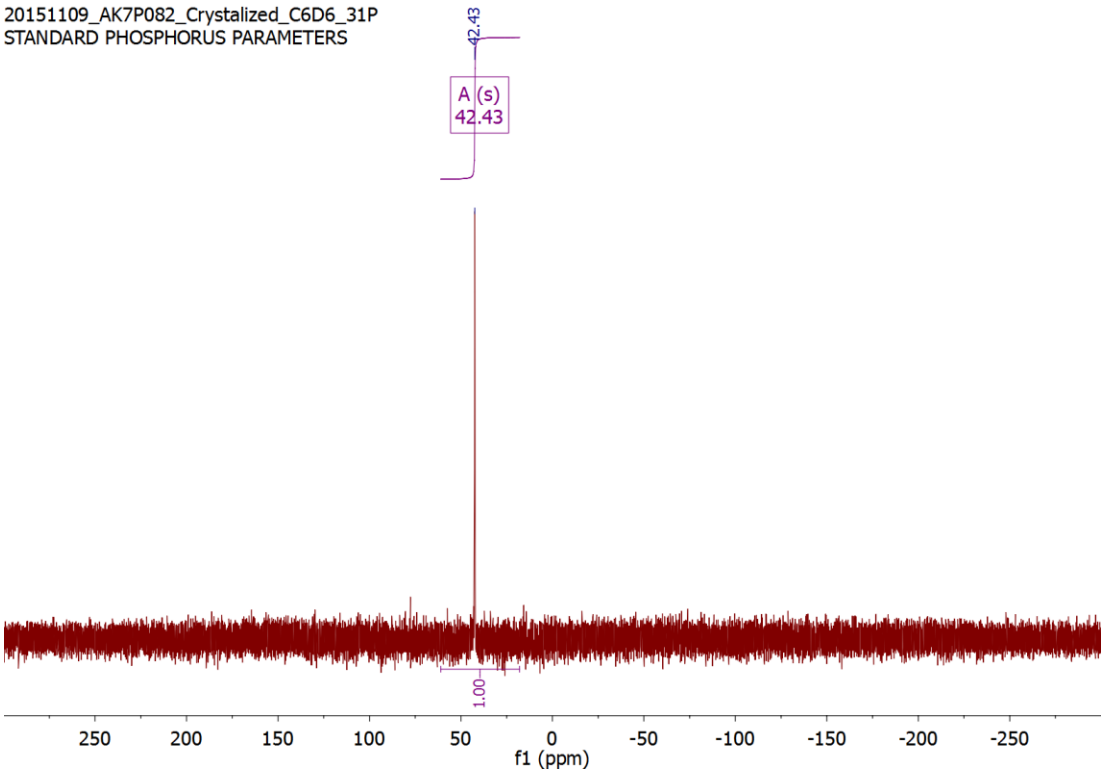

Figure C11. $^{31}P\{^{1}H\}$ NMR of *trans*-Pd(II)(^{i}PrJPhos)$_2$(Cl)$_2$

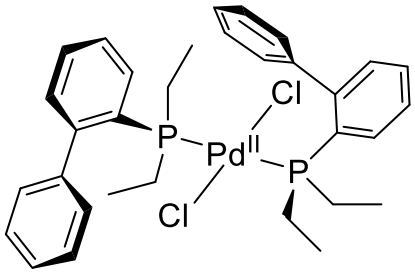

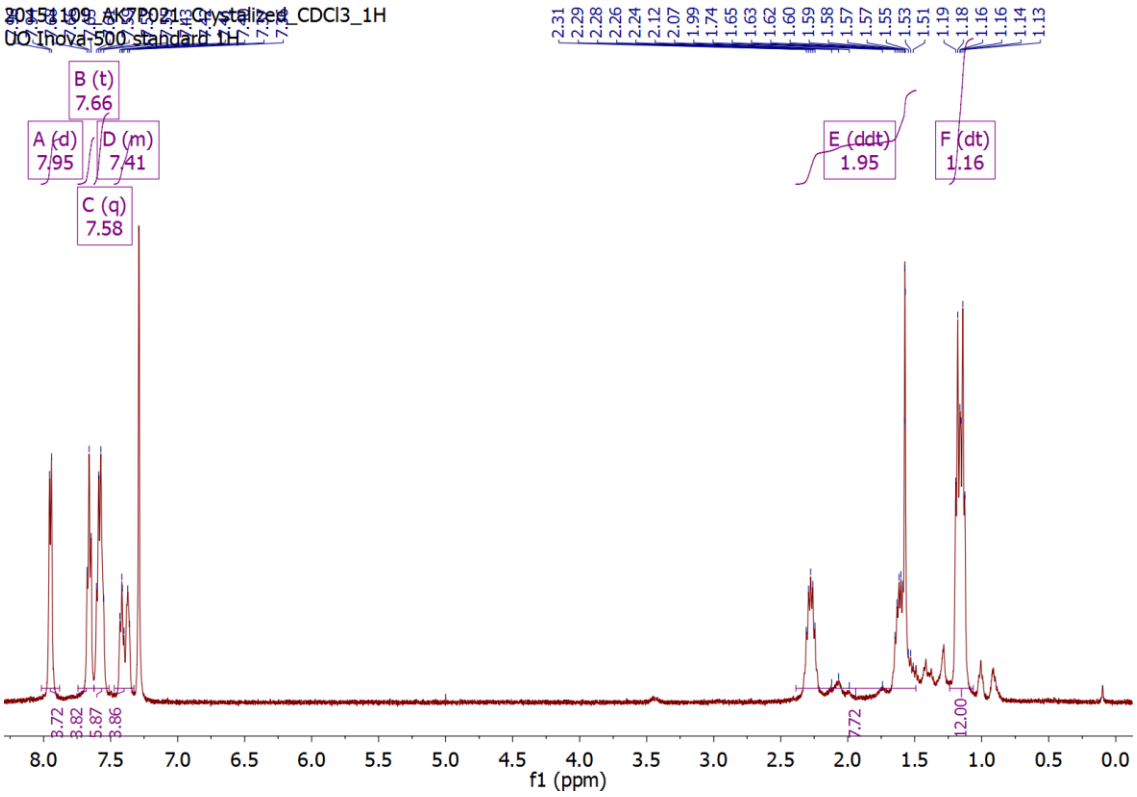

Figure C12. ^{1}H NMR of *trans*-Pd(II)(EtJPhos)$_2$(Cl)$_2$

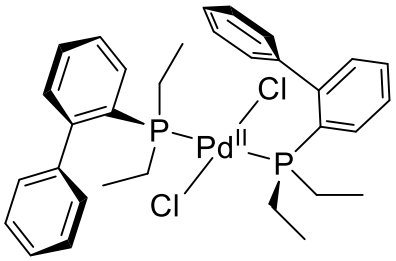

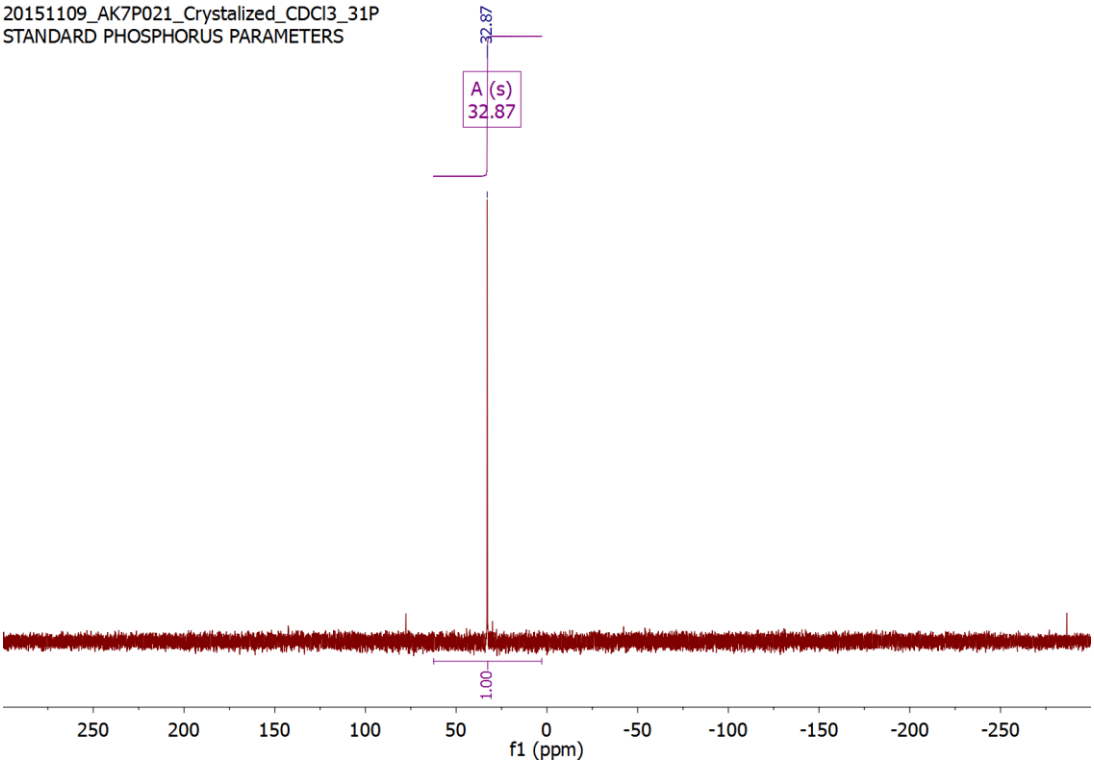

Figure C13. $^{31}P\{^{1}H\}$ NMR of *trans*-Pd(II)(EtJPhos)$_2$(Cl)$_2$

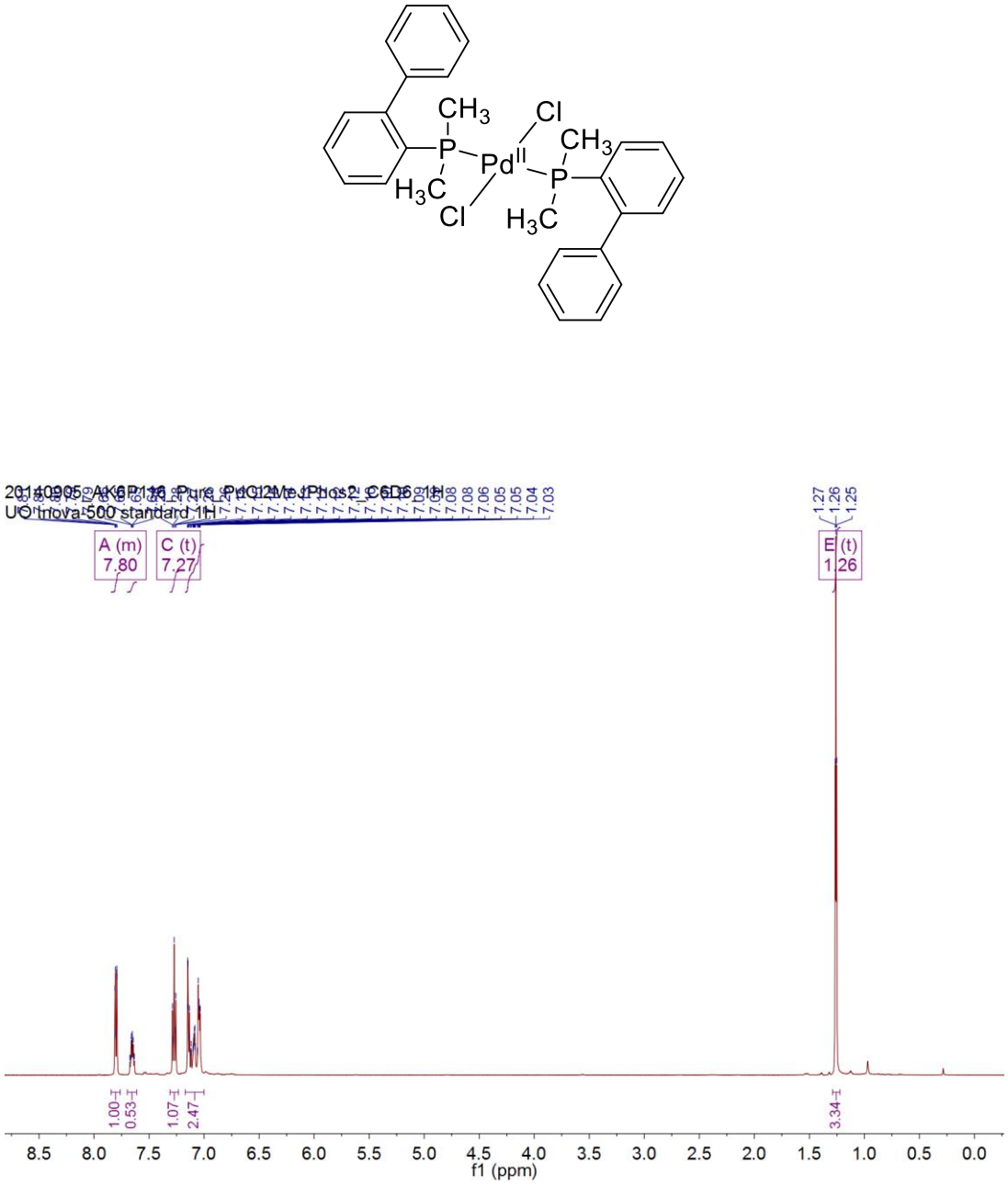

Figure C14. ^{1}H NMR of *trans*-Pd(II)(MeJPhos)$_2$(Cl)$_2$

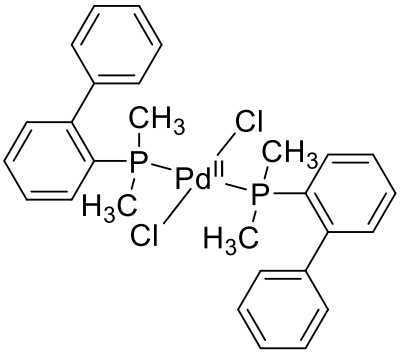

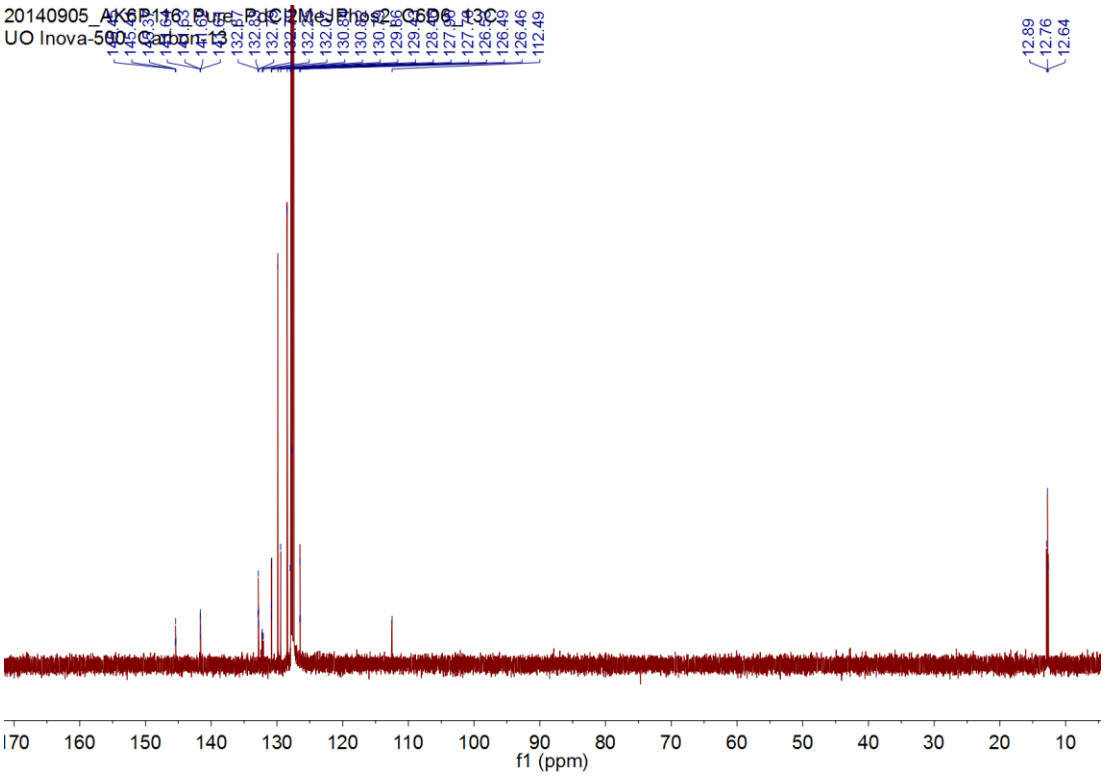

Figure C15. ^{13}C NMR of *trans*-Pd(II)(MeJPhos)$_2$(Cl)$_2$

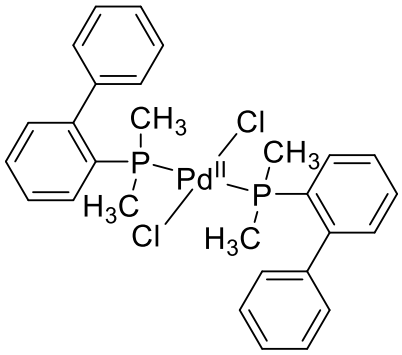

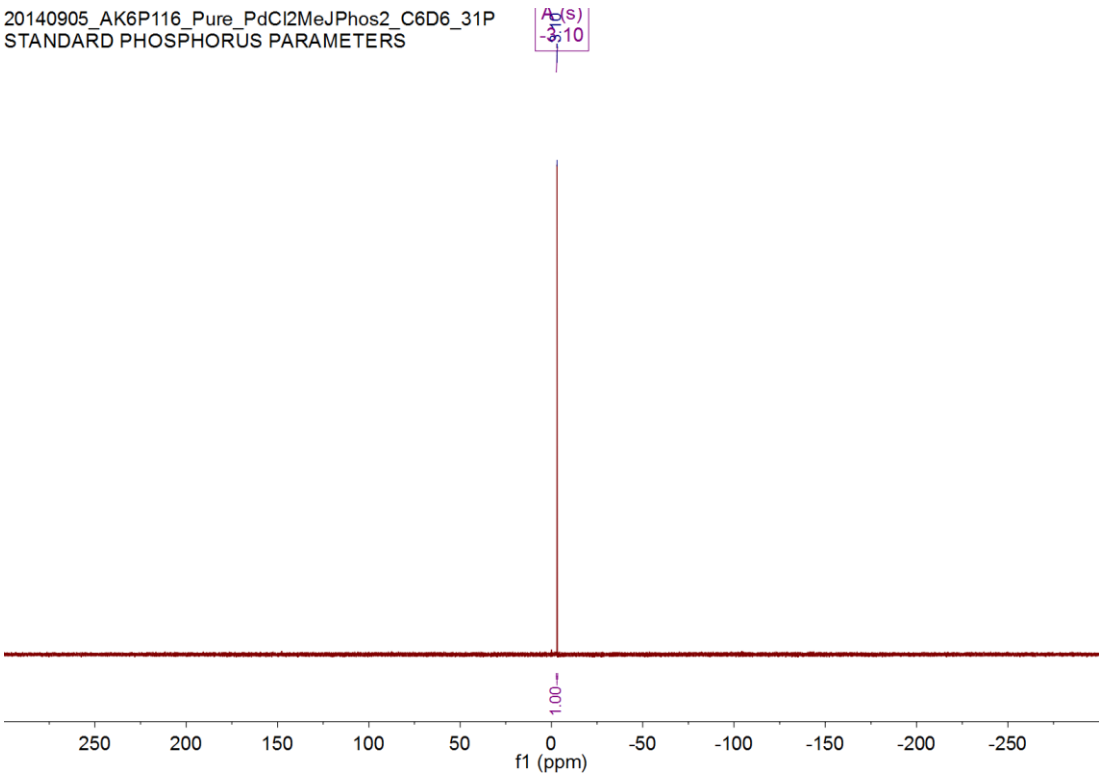

Figure C16. $^{31}P\{^{1}H\}$ NMR of *trans*-Pd(II)(MeJPhos)$_2$(Cl)$_2$

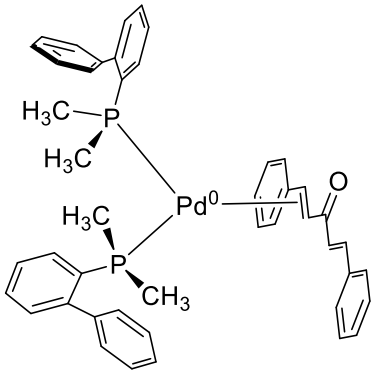

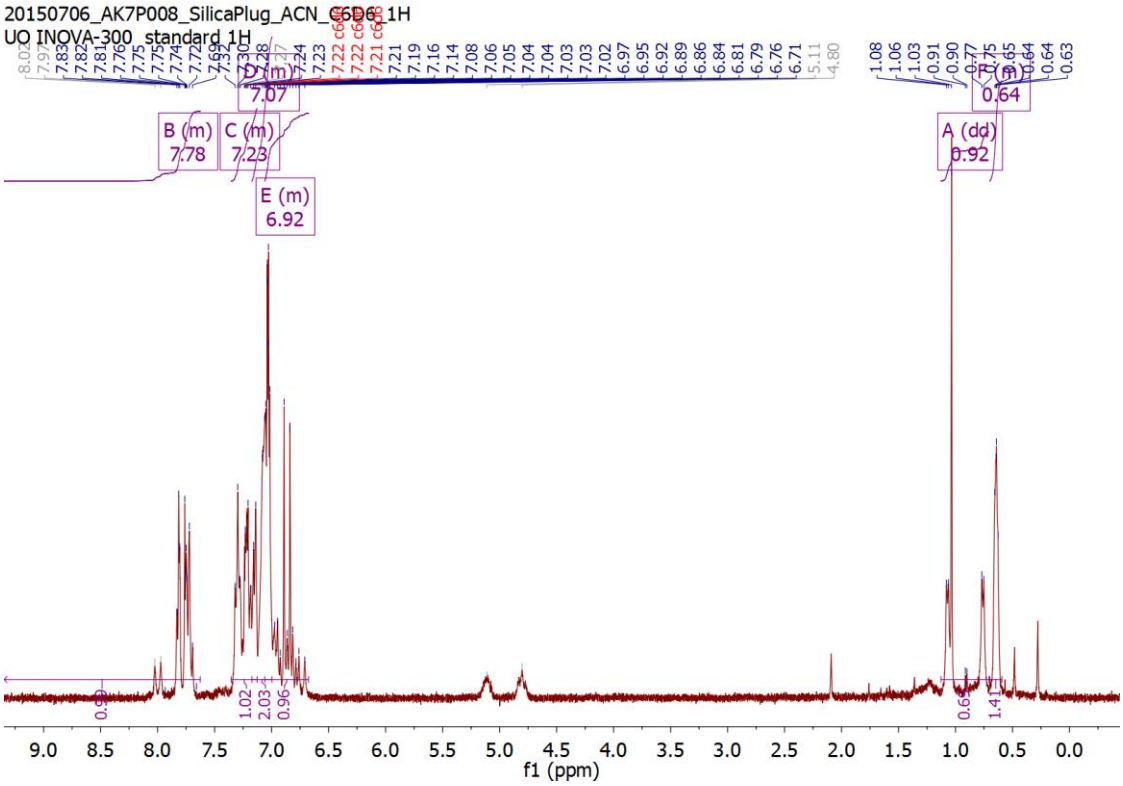

Figure C17. ^{1}H NMR of Pd(0)(MeJPhos)$_2$(η^2-dba)

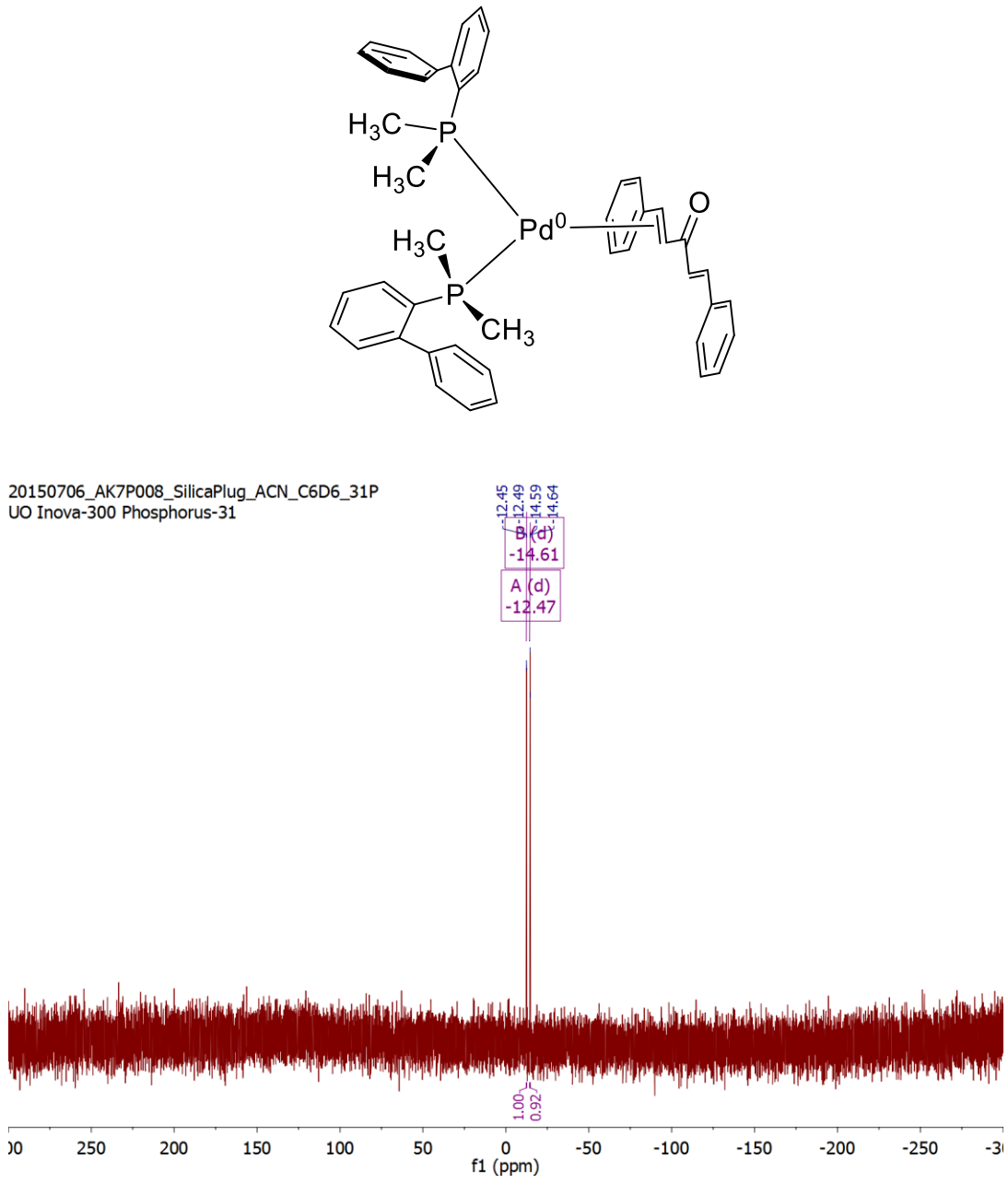

Figure C18. $^{31}P\{^{1}H\}$ NMR of Pd(0)(MeJPhos)$_2$(η^2-dba)

APPENDIX D

SUPPORTING INFORMATION FOR CHAPTER V

D.1. Additional spectra

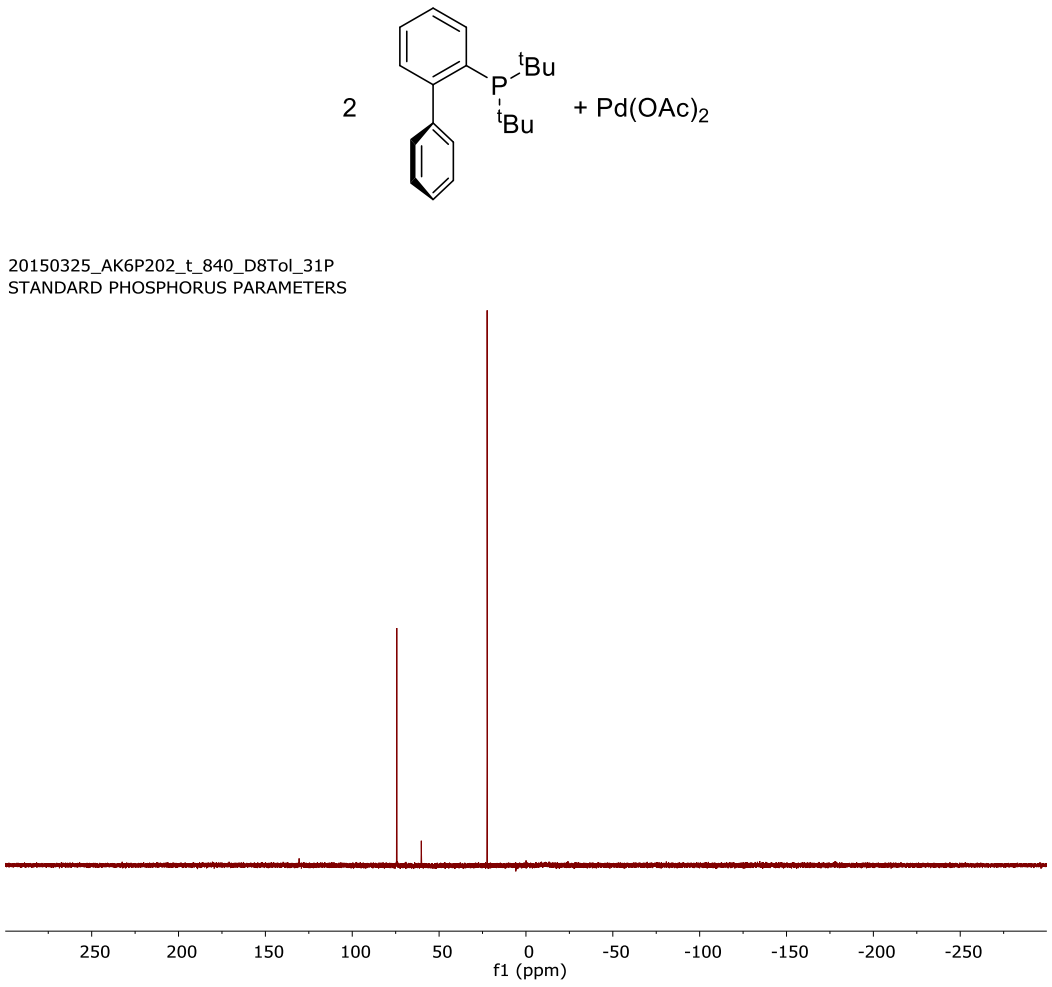

Figure D1. $^{31}P\{^{1}H\}$ NMR of ^{t}BuJPhos reacting with $Pd(OAc)_2$.

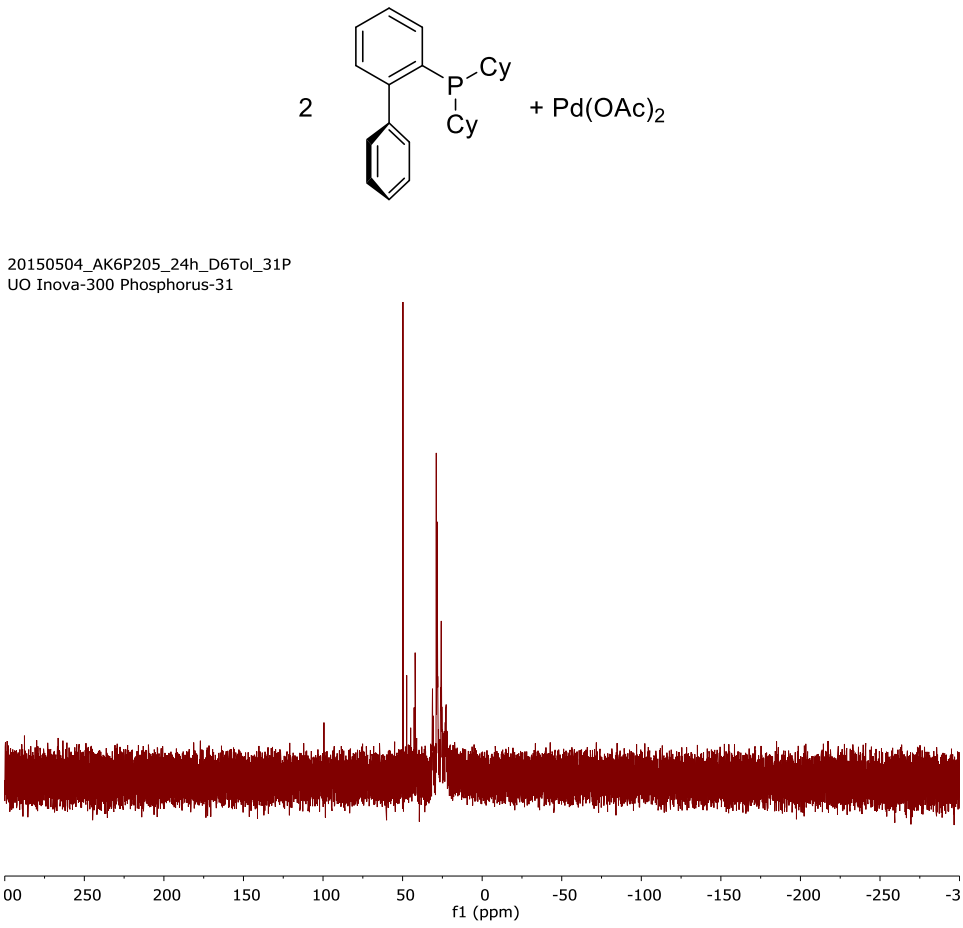

Figure D2. $^{31}P\{^{1}H\}$ NMR of CyJPhos reacting with $Pd(OAc)_2$.

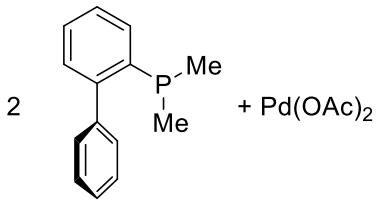

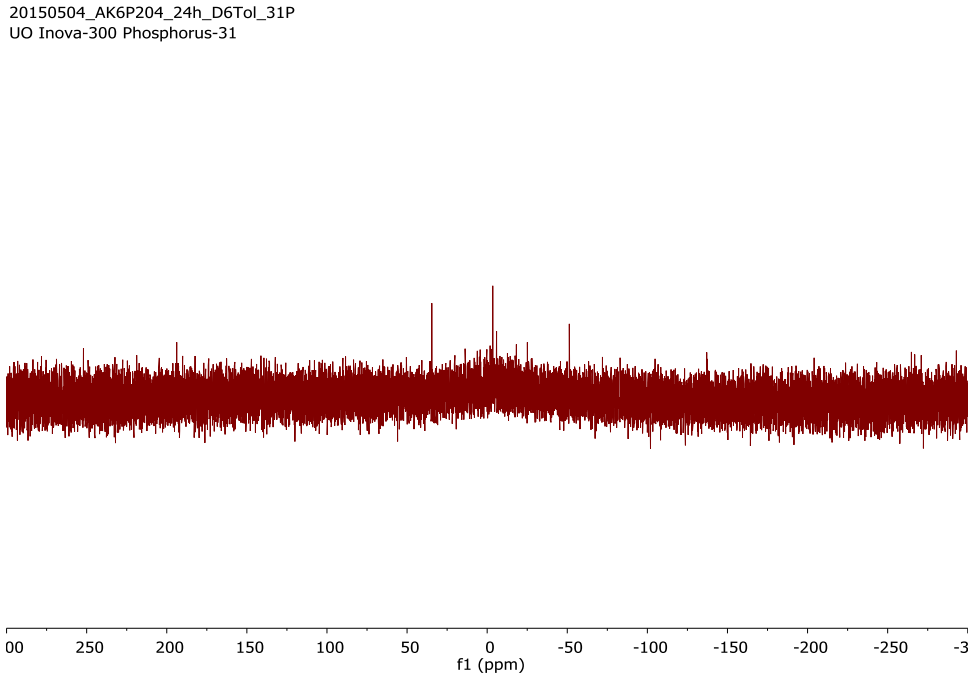

Figure D3. $^{31}P\{^{1}H\}$ NMR of MeJPhos reacting with $Pd(OAc)_2$. Note that most of the sample precipitated.

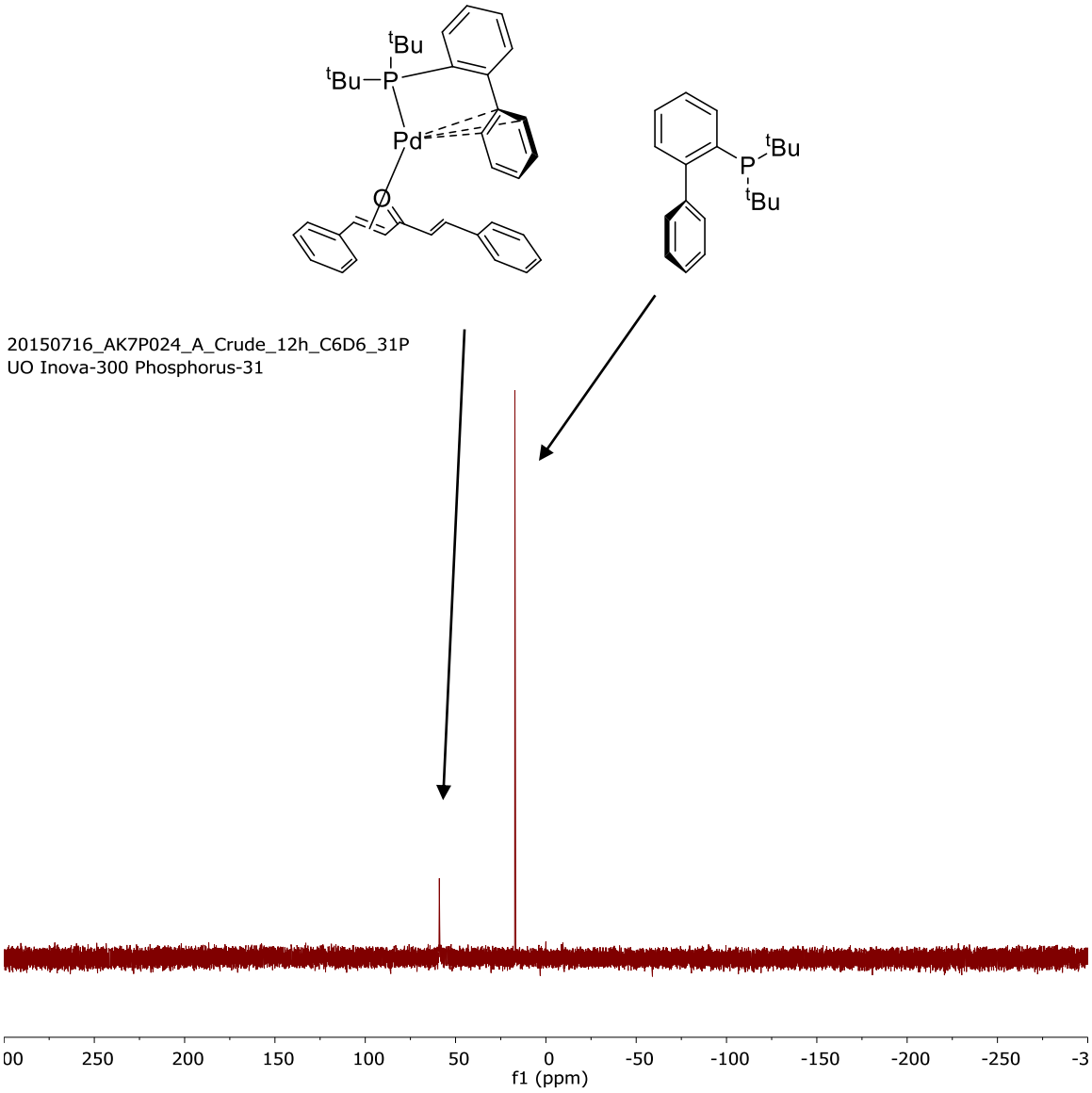

Figure D4. $^{31}P\{^{1}H\}$ NMR of ^{t}BuJPhos reacting with $Pd_2(dba)_3$.

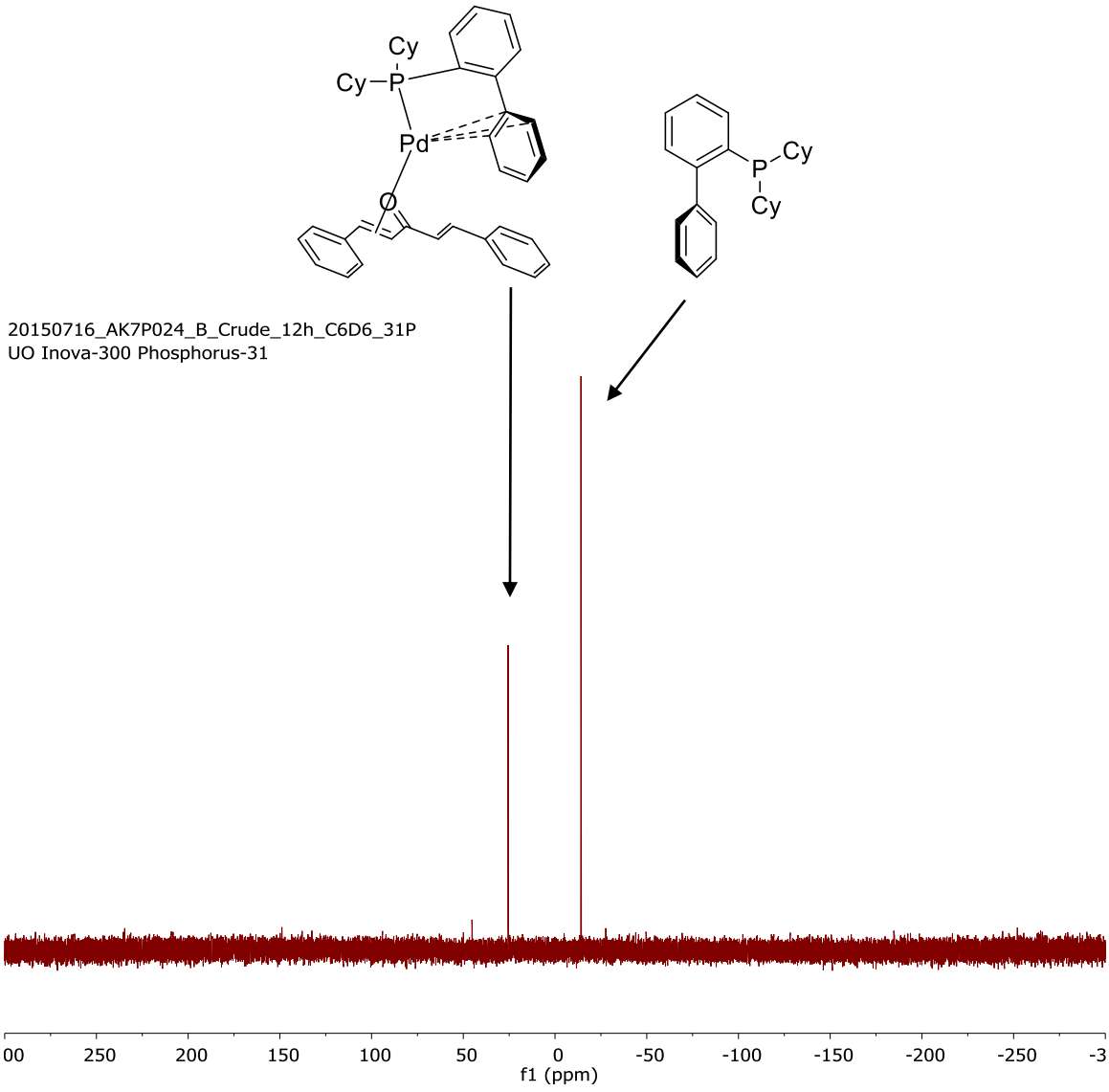

Figure D5. $^{31}P\{^{1}H\}$ NMR of CyJPhos reacting with $Pd_2(dba)_3$.

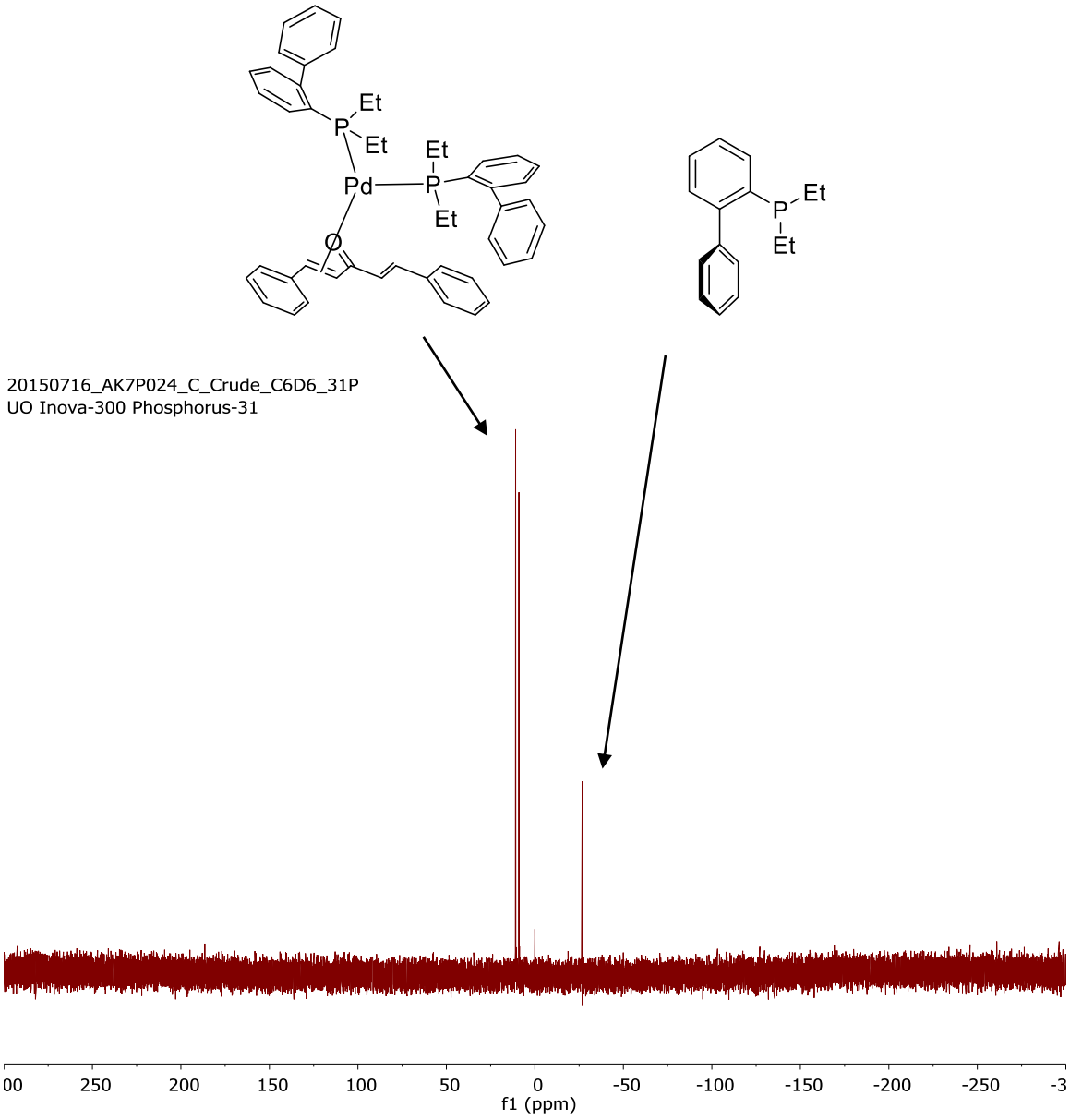

Figure D6. $^{31}P\{^{1}H\}$ NMR of EtJPhos reacting with $Pd_2(dba)_3$.

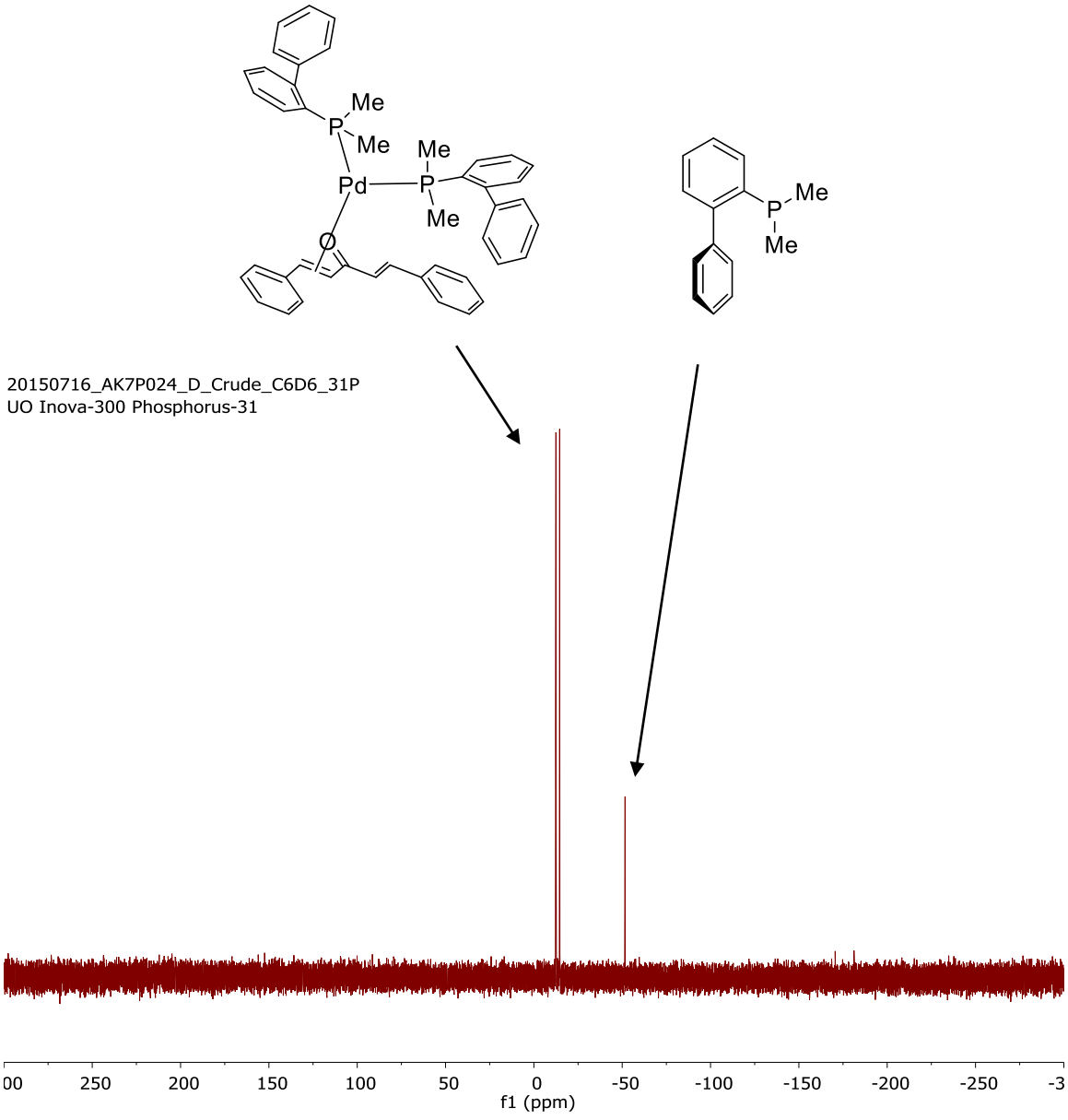

Figure D7. $^{31}P\{^{1}H\}$ NMR of MeJPhos reacting with $Pd_2(dba)_3$.

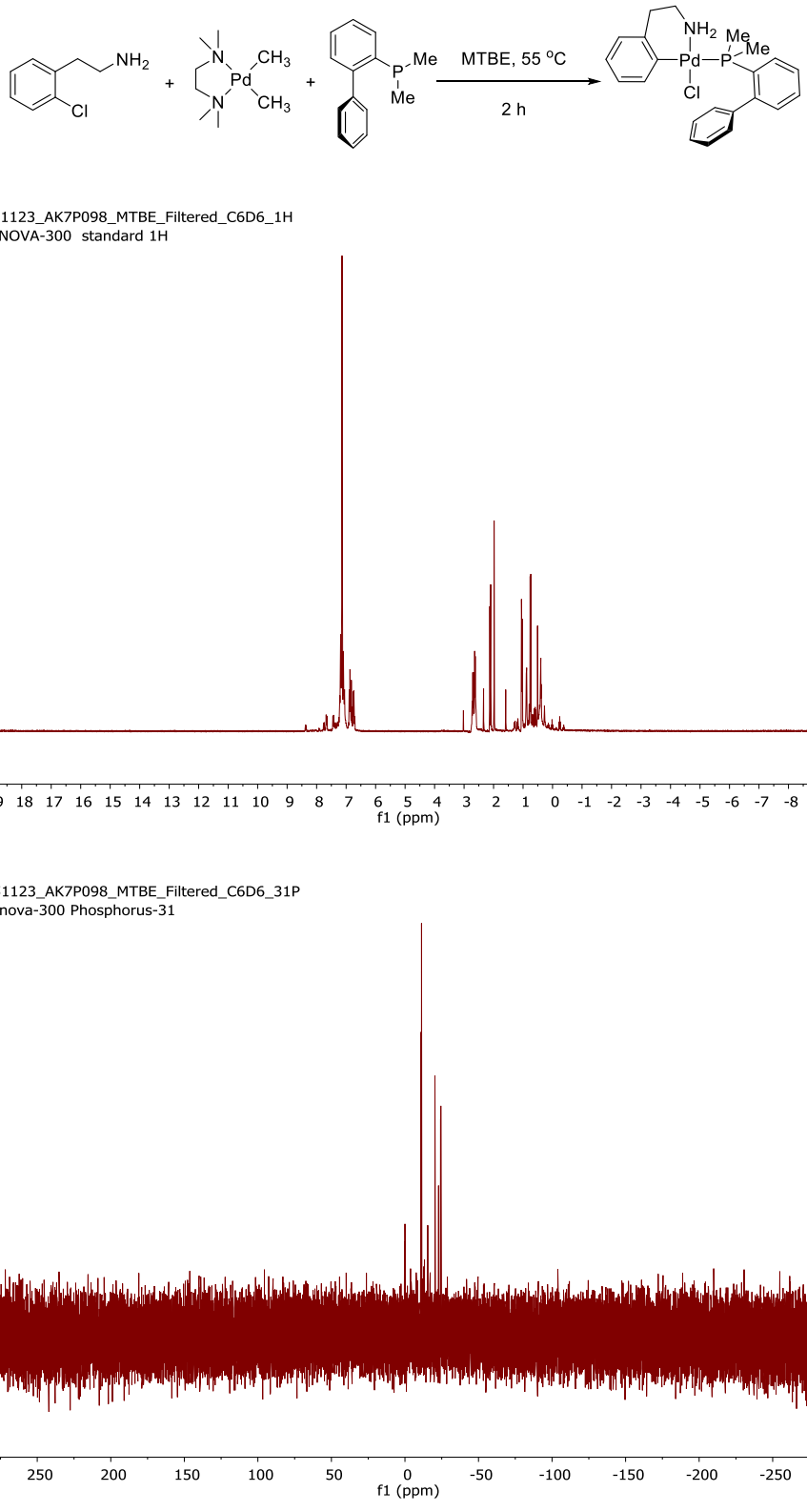

Figure D8. ^{1}H and $^{31}P\{^{1}H\}$ NMR of MeJPhos Buchwald precatalyst synthesis.

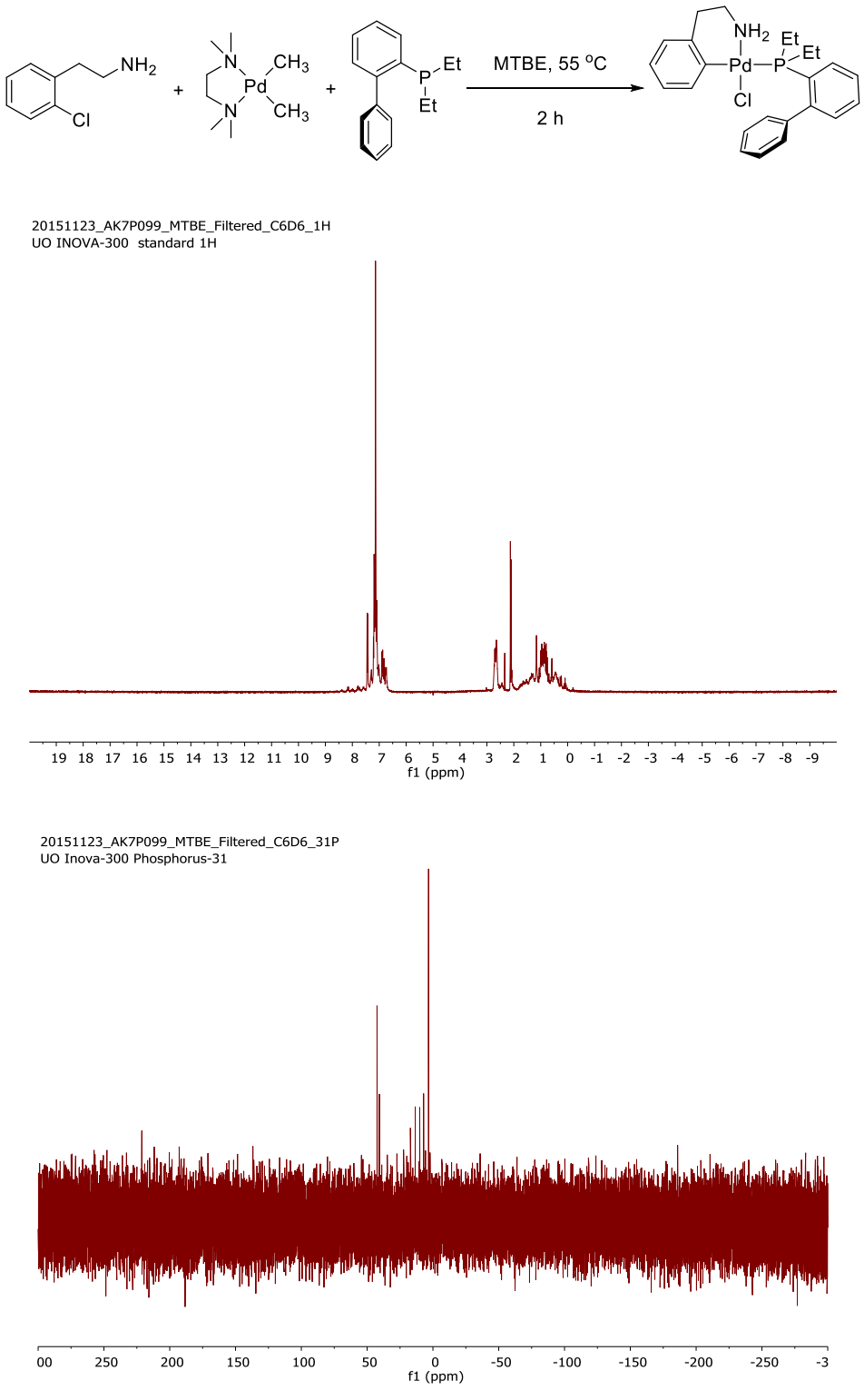

Figure D9. ^{1}H and $^{31}P\{^{1}H\}$ NMR of EtJPhos Buchwald precatalyst synthesis.

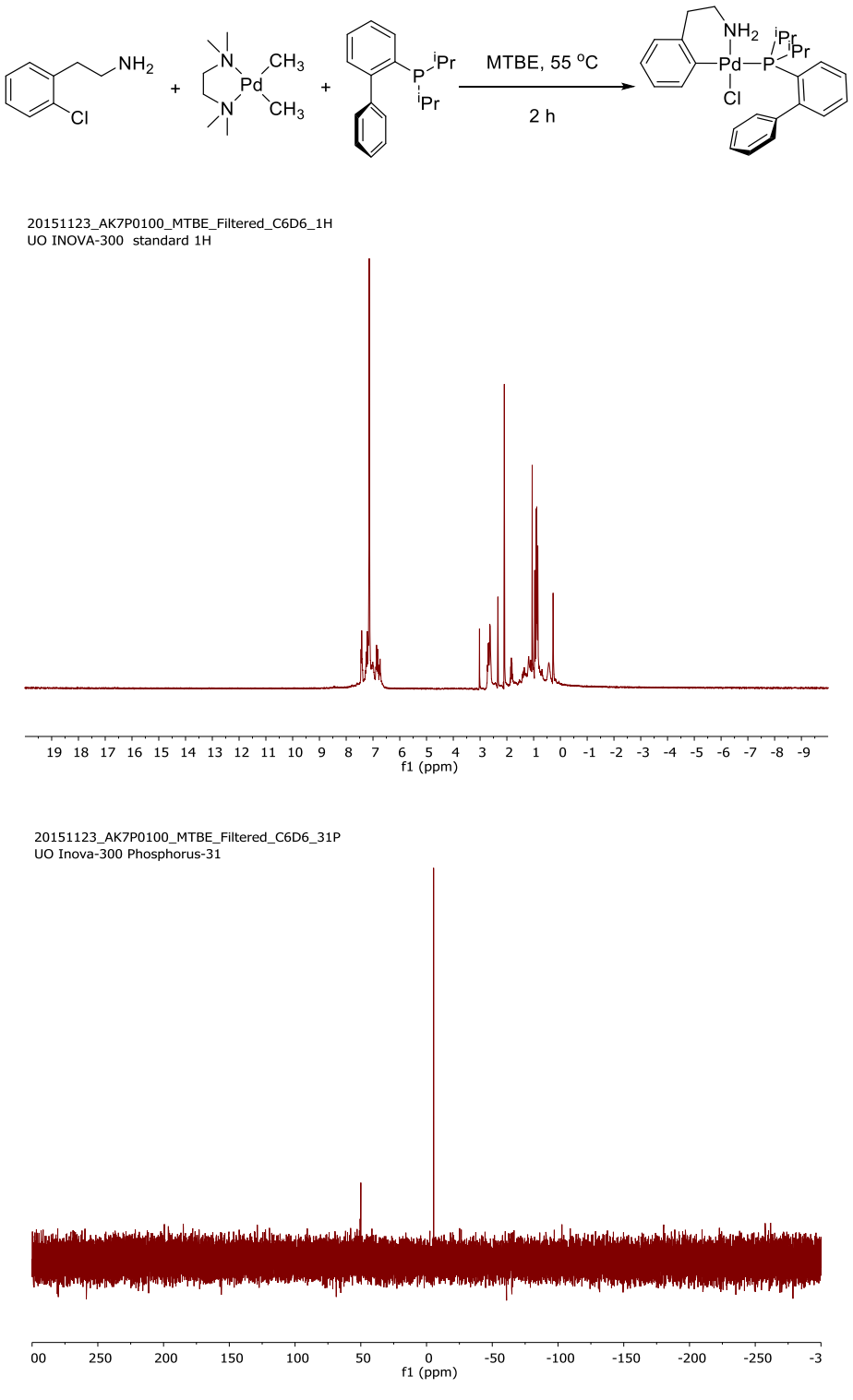

Figure D10. ^{1}H and $^{31}P\{^{1}H\}$ NMR of ^{i}PrJPhos Buchwald precatalyst synthesis.

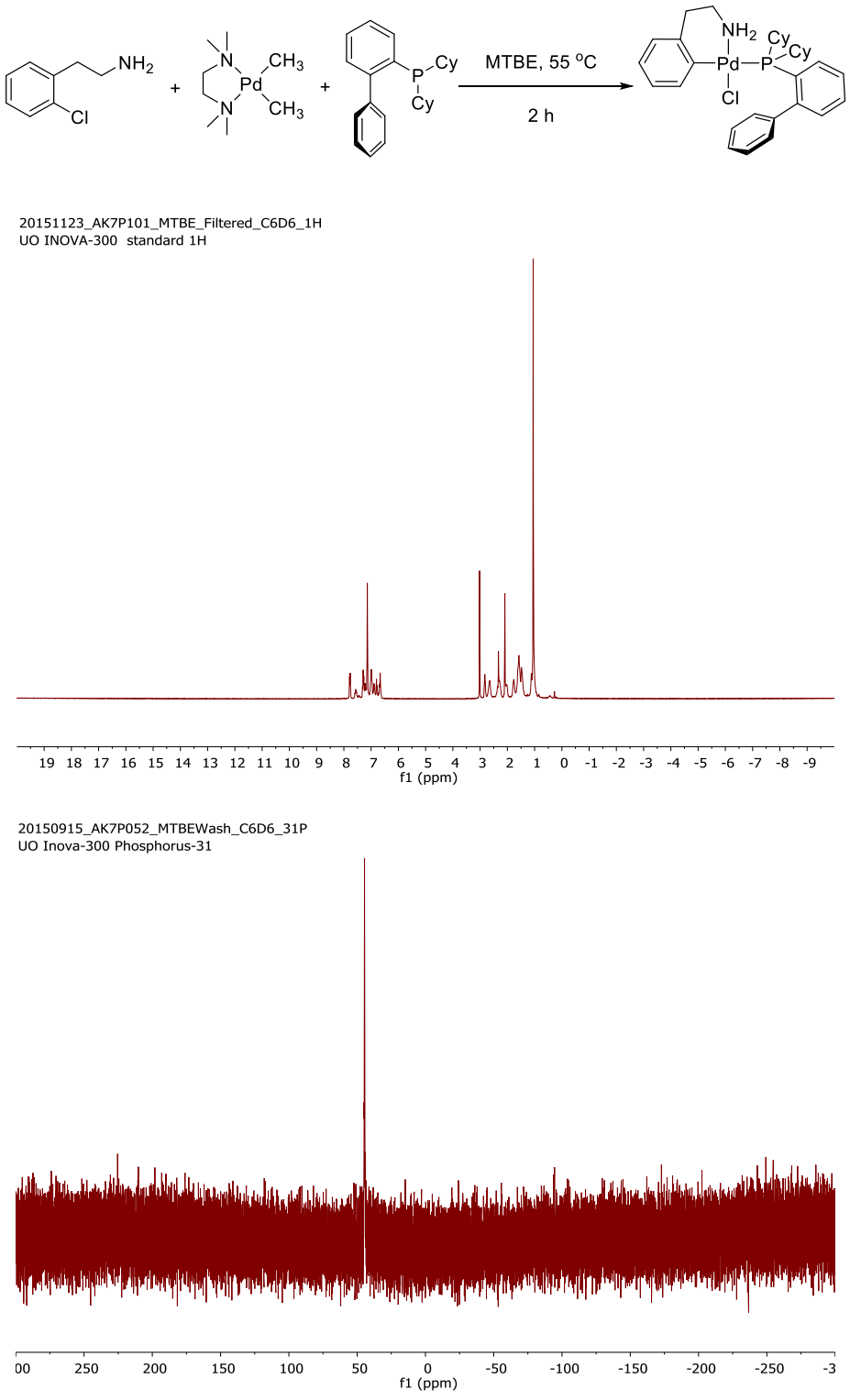

Figure D11. ^{1}H and $^{31}P\{^{1}H\}$ NMR of CyJPhos Buchwald precatalyst synthesis.

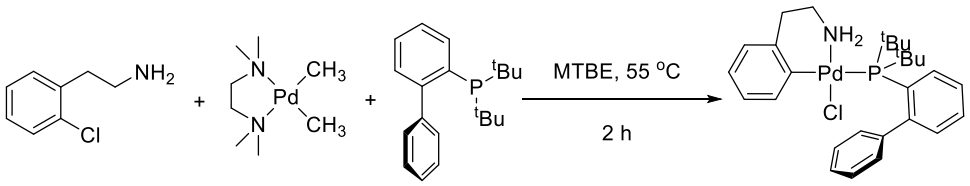

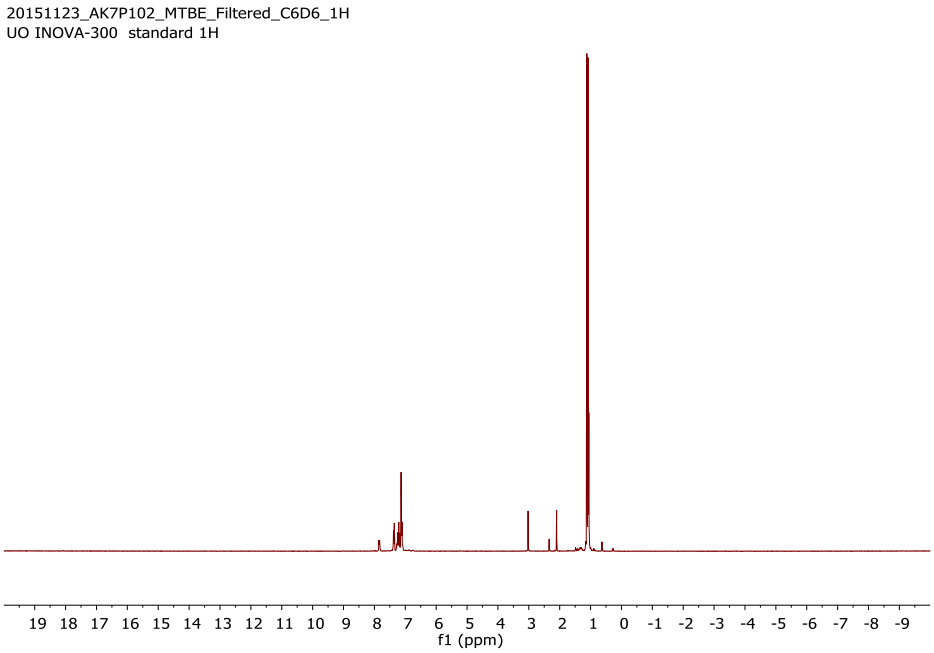

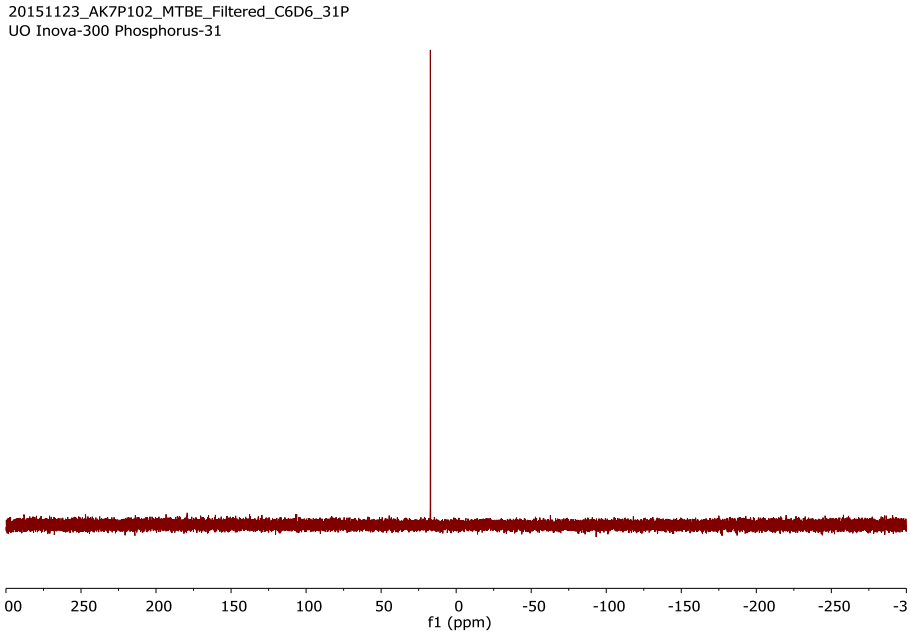

Figure D12. ^{1}H and $^{31}P\{^{1}H\}$ NMR of ^{t}BuJPhos Buchwald precatalyst synthesis. Note that no reaction is observed.

APPENDIX E

SUPPORTING INFORMATION FOR CHAPTER VI

E.1. Detailed KinetiChem Synthetron™ S3T1 continuous flow reactor diagram

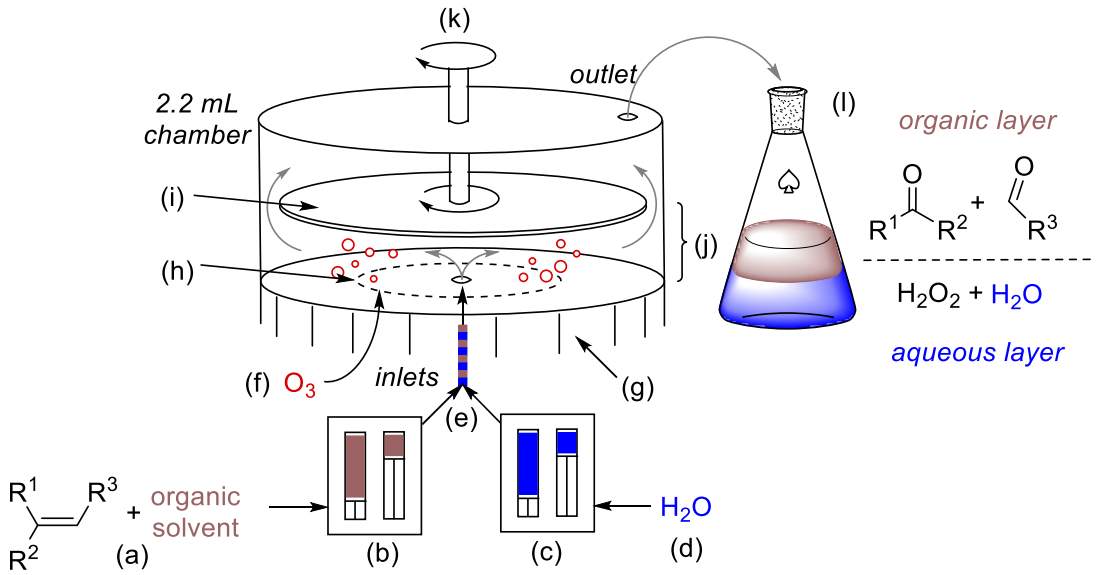

Figure E1. Detailed KinetiChem Synthetron™ S3T1 continuous flow reactor diagram. (a) 0.10 M in EtOAc ~0 °C, (b) Model 2250 J-Kem® Scientific Dual Syringe Pump run at 10 mL/min., (c) Model 2250 J-Kem® Scientific Dual Syringe Pump run at 10 mL/min., (d) deionized water ~0 °C, (e) PTFE tubing (1 mm ø) and check valve T joint for plug-flow, (f) Welsbach T-408 ozone generator operating at 0.8 L/min., 77 mg O_3/L, 1.4 mmol/min., (g) heat-exchange regulated using a recirculating cooling bath at 0 °C, (h) circular metal frit for sparging ozone through reaction mixture, (i) rotor (2.5" ø polyether ether ketone disk) spinning at 2000-3600 rpm, (j) gap size between rotor and stator (100 µm), (k) electric motor with rpm monitored using a Monarch Instrument Pocket Tach (PT99) non-contact tachometer, (l) collection flask with Na_2SO_3 to quench H_2O_2 in aqueous layer.

E.2. Titration of Ozone

The ozone generator was titrated following the protocol developed by Rakness et al.[1] Volume output of the generator was measured using water displacement. The volume

of water displaced in an upturned graduated cylinder was said to be equal to the volume of gas output by the generator in a given period of time at a given pressure, temperature, and instrument output. Stock solutions were prepared as dictated exactly in the guidelines. Vacuum-oven dried reagent grade anhydrous $K_2Cr_2O_7$ was used as the analytical standard. To a flask was added, 150 mL of deionized water, 1.0 mL of conc. H_2SO_4, 20.0 mL of the dichromate solution, and 2.0 g KI. The mixture was stirred and covered with aluminum foil for 6 minutes. A buret was charged with the sodium thiosulfate solution and used to titrate the prepared solution in triplicate.

For the titration of ozone, two 150 mL gas sparging bottles were connected in series to the generator using Tygon® tubing. The bottles were washed and stocked with 2% KI solution. The last bottle vented into a beaker full of KI solution through Tygon® tubing to ensure all ozone was consumed. A three-way valve allowed ozone to be generated without passing through the bottles, which was done for 2 minutes prior to the test. Ozone was allowed to pass through the bottles for approximately 2 minutes (the exact time noted). The ozone generator was then switched off and O_2 flushed through the system. The bottles were emptied into a beaker, washed three times with KI, and 10 mL 2.0 M H_2SO_4 was added. The solutions were then titrated using the thiosulfate solution analyzed above. These data were used to calculate the ozone generation in mg/L, which was found to be 67 ± 3 mg/L for our generator. This was measured twice and the results averaged. The titration was conducted each time maintenance was done on the ozone generator, and was found to vary between 67 mg/L at 1.1 L/min. at 0˚C to 77 ± 2 mg/L at 0.5 L/min. at -30°C.

E.3. Optimization of method

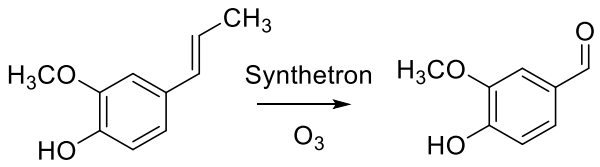

Figure E2. Optimization of method varying organic flow rate and alkene concentration for the ozonolysis of isoeugenol: (a) 100 µm gap conversion (%)[a], (b) 100 µm gap yield (%)[a], (c) 1000 µm gap conversion (%)[a], (d) 1000 µm gap yield(%)[a]. [a] Yields and conversions determined using ^{1}H NMR with an internal standard of hexamethyl benzene. Optimizations run in EtOAc with a flow rate of 10 mL/min. of H_2O. Ozone was set to a flow rate of 0.4 L/min. Note that increasing ozone flow rate to 0.8 L/min. provided quantitative conversions for optimized conditions (0.1 M alkene at 10 mL/min. and 10 mL/min. H_2O). All other parameters of the run were identical to the general procedure in the manuscript.

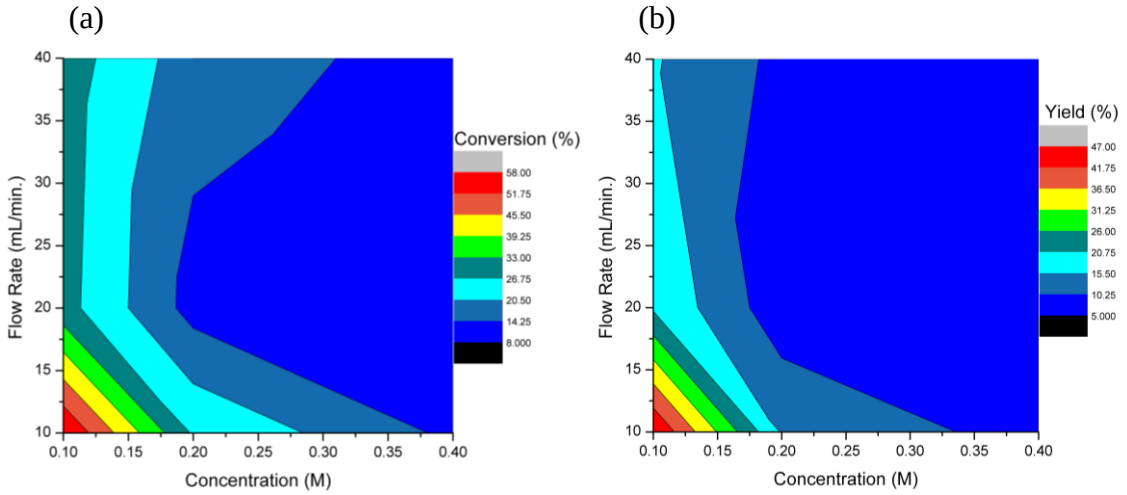

9 trials each

Figure E2. (continued).

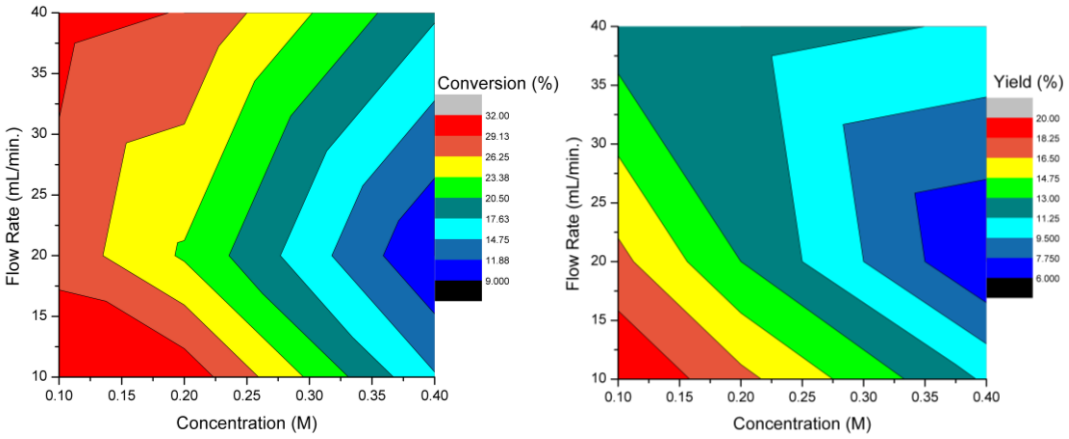

(c) *9 trials each* (d)

E.4. Isolated and NMR yields

E.4.1. Phenanthrene to [1,1'-biphenyl]-2,2'-dicarbaldehyde

0.9977 g (5.60 mmol) phenanthrene yielded a yellow waxy substance that was purified by flash chromatography using 1:1 diethyl ether to hexanes. The yellow crystals afforded were recrystallized using ether/hexanes and dried on high vac. to yield [1,1'-biphenyl]-2,2'-dicarbaldehyde (0.7580 g, 64% isolated). ^{1}H NMR (300 MHz, Chloroform-*d*) δ 9.84 (d, *J* = 0.8 Hz, 2H), 8.12 – 8.00 (m, 2H), 7.73 – 7.54 (m, 4H), 7.42 – 7.30 (m, 2H).

E.4.2. Trans-stilbene to benzaldehyde

1.1147 g (6.18 mmol) trans-stilbene yielded a clear liquid, benzaldehyde (1.0319 g, 79% yield isolated). ^{1}H NMR (300 MHz, Chloroform-*d*) δ 10.03 (s, 1H), 7.89 (d, *J* = 6.9 2H), 7.63 (t, *J* = 7.3 Hz, 1H), 7.54 (t, *J* = 7.4 Hz, 2H).

E.4.3. Trans-stilbene to benzaldehyde multi-gram scale

11.9676g (66.394mmol) of trans-stilbene yielded a clear liquid, which was distilled to purity (8.8801 g, 63% yield isolated). ^{1}H NMR (300 MHz, Chloroform-*d*) δ 10.03 (s, 1H), 7.89 (d, *J* = 6.9 2H), 7.63 (t, *J* = 7.3 Hz, 1H), 7.54 (t, *J* = 7.4 Hz, 2H).

E.4.4. Styrene to benzaldehyde

1.0040 g (9.60 mmol) styrene yielded a slightly yellow oil, benzaldehyde (72% yield isolated). ^{1}H NMR (300 MHz, Chloroform-*d*) δ 10.03 (s, 1H), 7.89 (d, *J* = 6.9 2H), 7.63 (t, *J* = 7.3 Hz, 1H), 7.54 (t, *J* = 7.4 Hz, 2H).

E.4.5. Anethole to 4-anisaldehyde

1.0030 g (6.77 mmol) anethole afforded 4-anisaldehyde (0.5970 g, 65% isolated). ^{1}H NMR (300 MHz, Chloroform-*d*) δ 9.89 (s, 1H), 7.84 (d, *J* = 8.8 Hz, 2H), 7.01 (d, *J* = 8.8 Hz, 2H), 3.89 (s, 3H).

E.4.6. Isoeugenol to vanillin

1.0013 g (6.09 mmol) isoeugenol afforded vanillin (0.4550 g, 49% isolated). ^{1}H NMR (300 MHz, Chloroform-*d*) δ 9.82 (s, 1H), 7.42 (dq, *J* = 3.2, 1.8 Hz, 2H), 7.04 (d, *J* = 8.5 Hz, 1H), 6.29 (s, 1H), 3.96 (s, 3H).

E.4.7. 1,1-Diphenylethylene to benzophenone

1.0140g 1,1-diphenylethylene afforded benzophenone (0.3542 g, 35% yield isolated). ^{1}H NMR (500 MHz, Chloroform-*d*) δ 7.89 – 7.78 (m, 2H), 7.65 – 7.56 (m, 1H), 7.55 – 7.45 (m, 2H).

E.5. NMR assignments of SOZ to carbonyl ratios

(Table 6.3, manuscript) Ratios were obtained by taking crude product ^{1}H NMR and integrating peaks specific to both the carbonyl and ozonide based on literature references (Table E1).

Table E1. References for ^{1}H NMR data regarding SOZ and carbonyl species. [a]Purchased standard used as references for ^{1}H NMRs. [b]No reference is available, however ^{1}H peak for SOZ is expected to be very close to the anethole ozonide from reference 2 (note that no SOZ was observed).

Alkene	Secondary Ozonide	Ref.	Carbonyl Product	Ref.
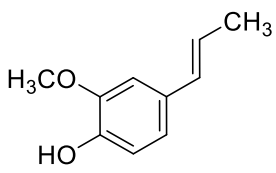	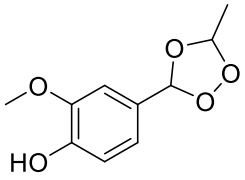	b	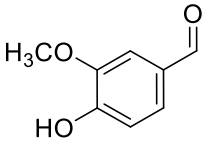	a
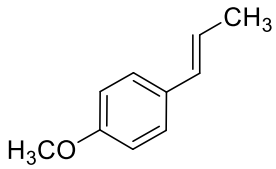	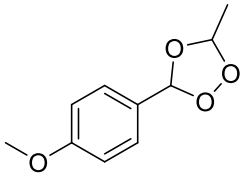	2	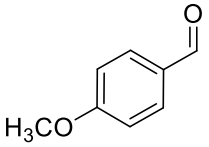	a
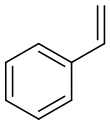	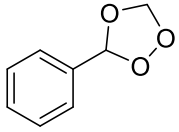	3	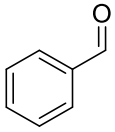	a

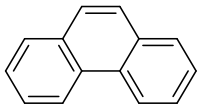	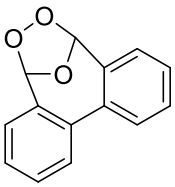	4	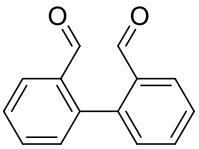	5
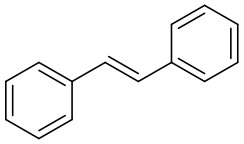	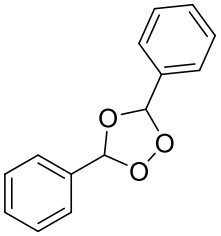	6	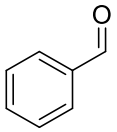	a
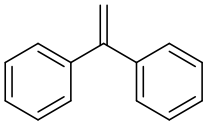	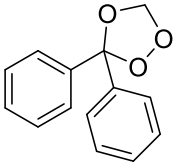	7	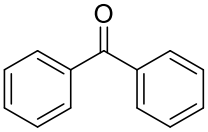	a
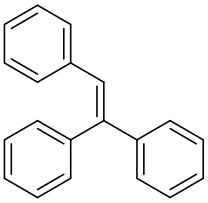	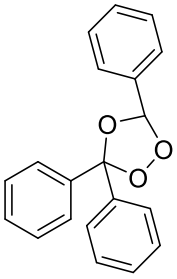	6	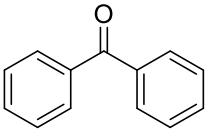	a
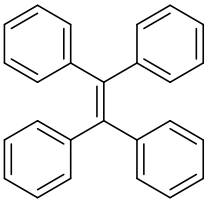	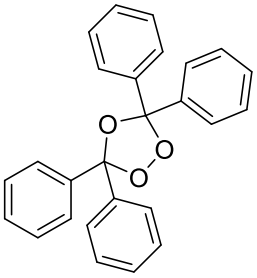	8	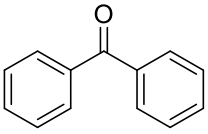	a
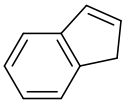	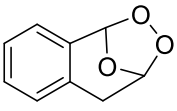	9	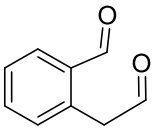	9

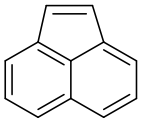	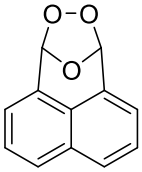	10	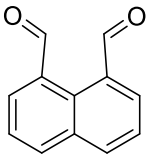	10

E.6. Additional spectra

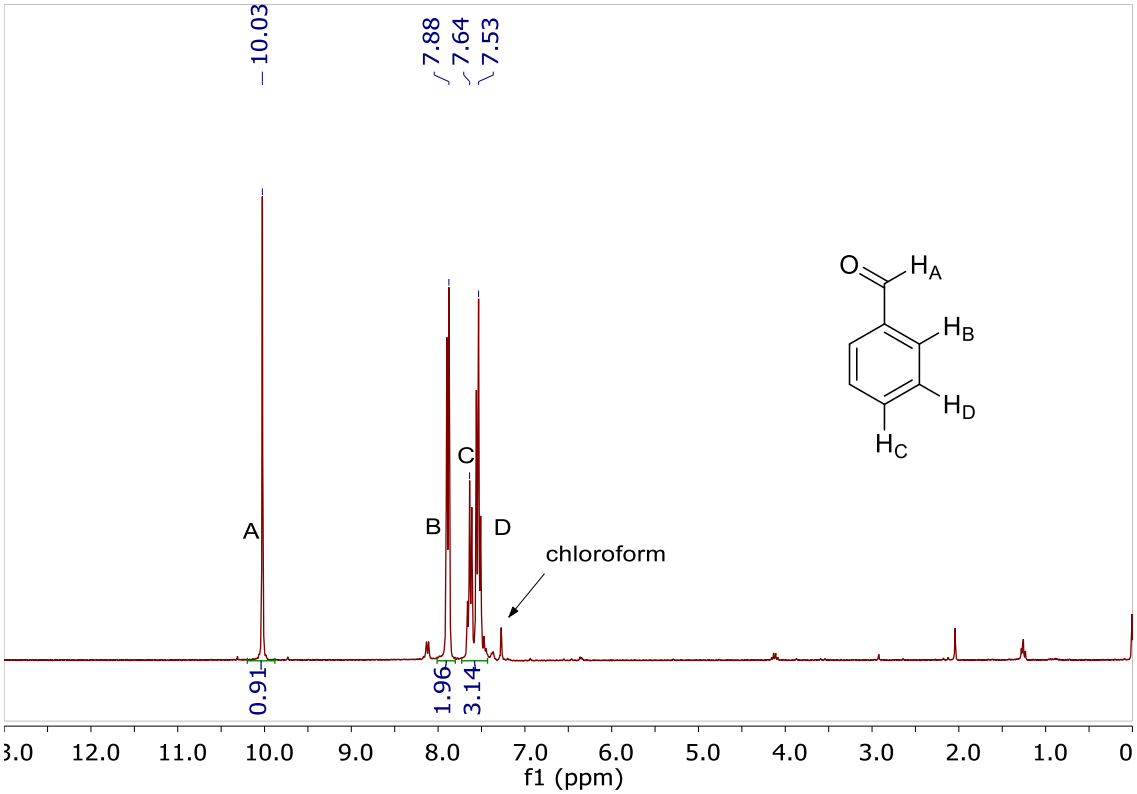

Figure E3. ^{1}H NMR of *trans*-stilbene to benzaldehyde.

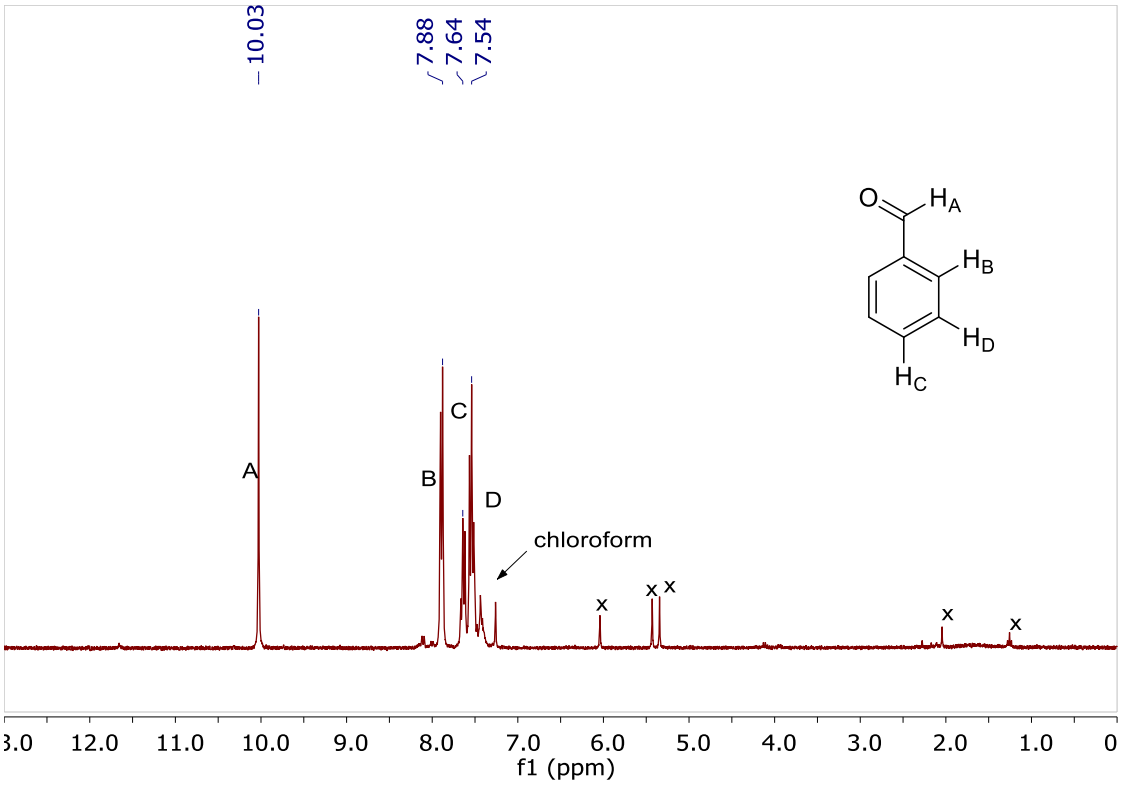

Figure E4. ^{1}H NMR of Styrene to benzaldehyde (NMR yield).

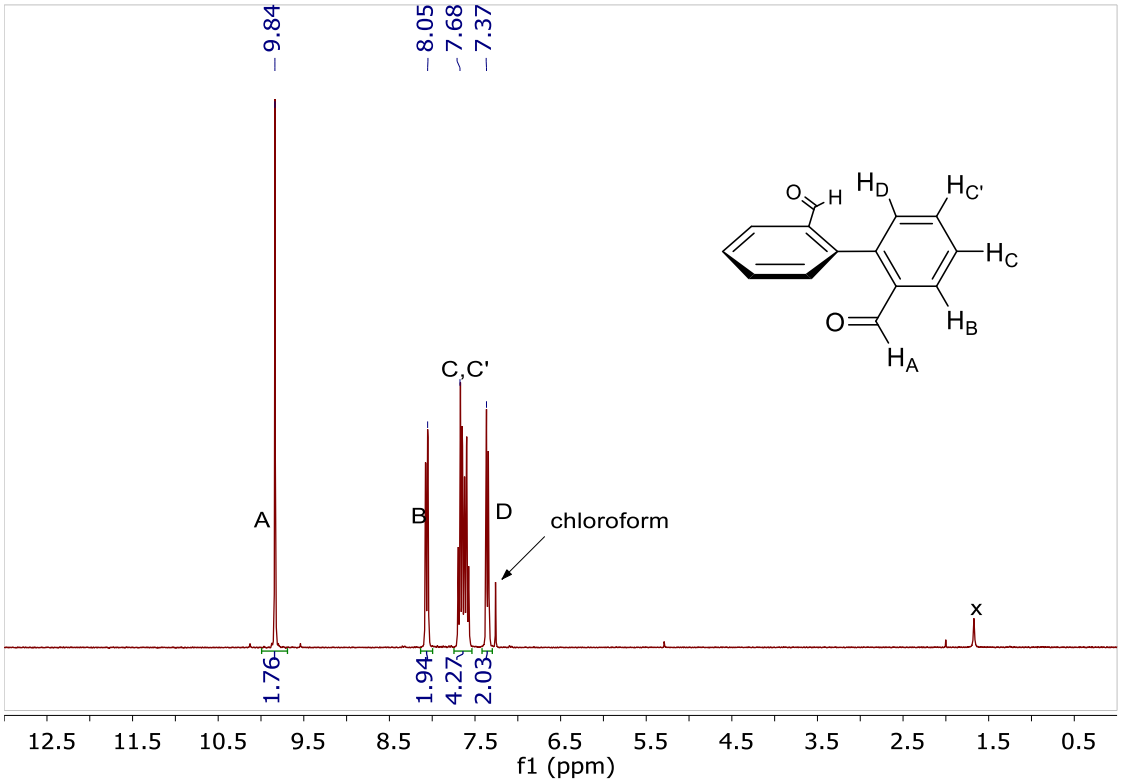

Figure E5. ^{1}H NMR of Phenanthrene to [1,1'-biphenyl]-2,2'-dicarbaldehyde.

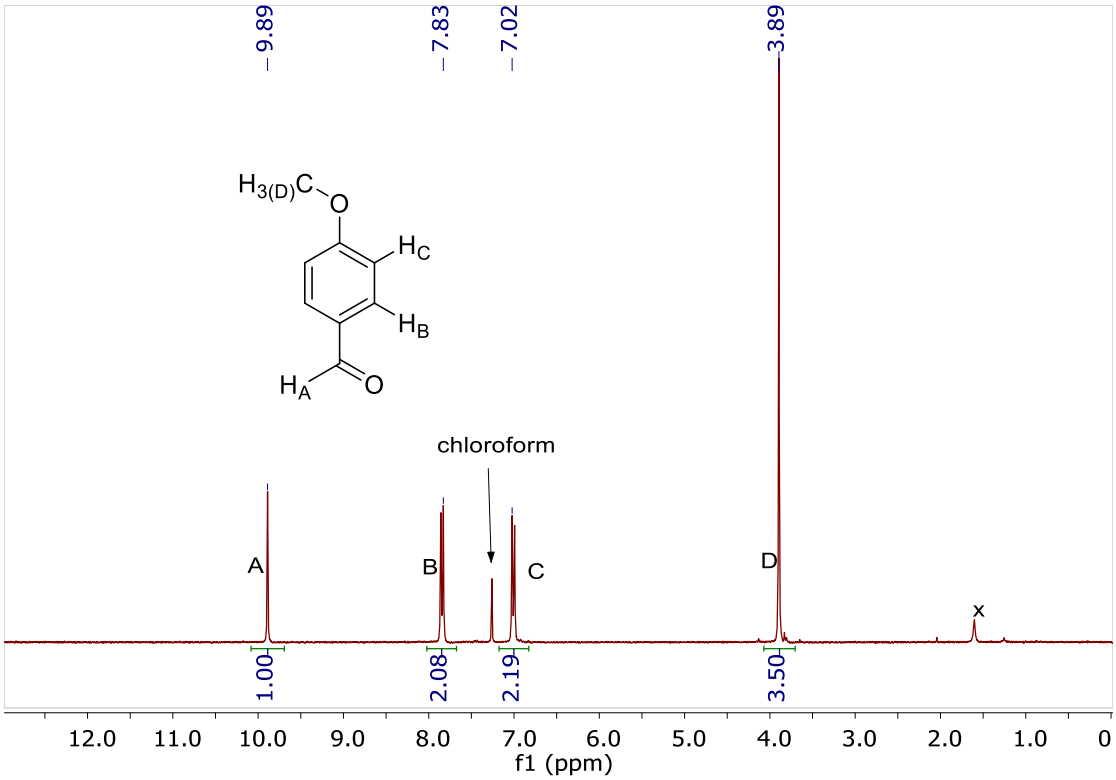

Figure E6. ^{1}H NMR of Anthole to 4-anisaldehyde.

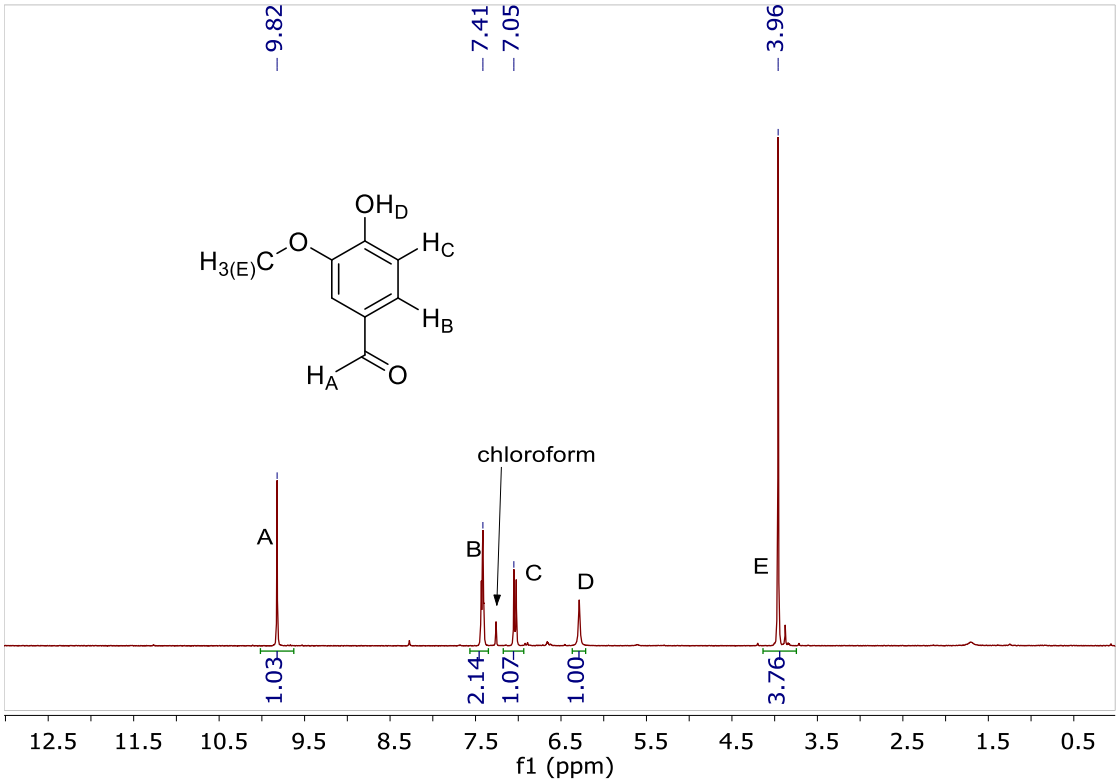

Figure E7. ^{1}H NMR of Isoeugenol to vanillin.

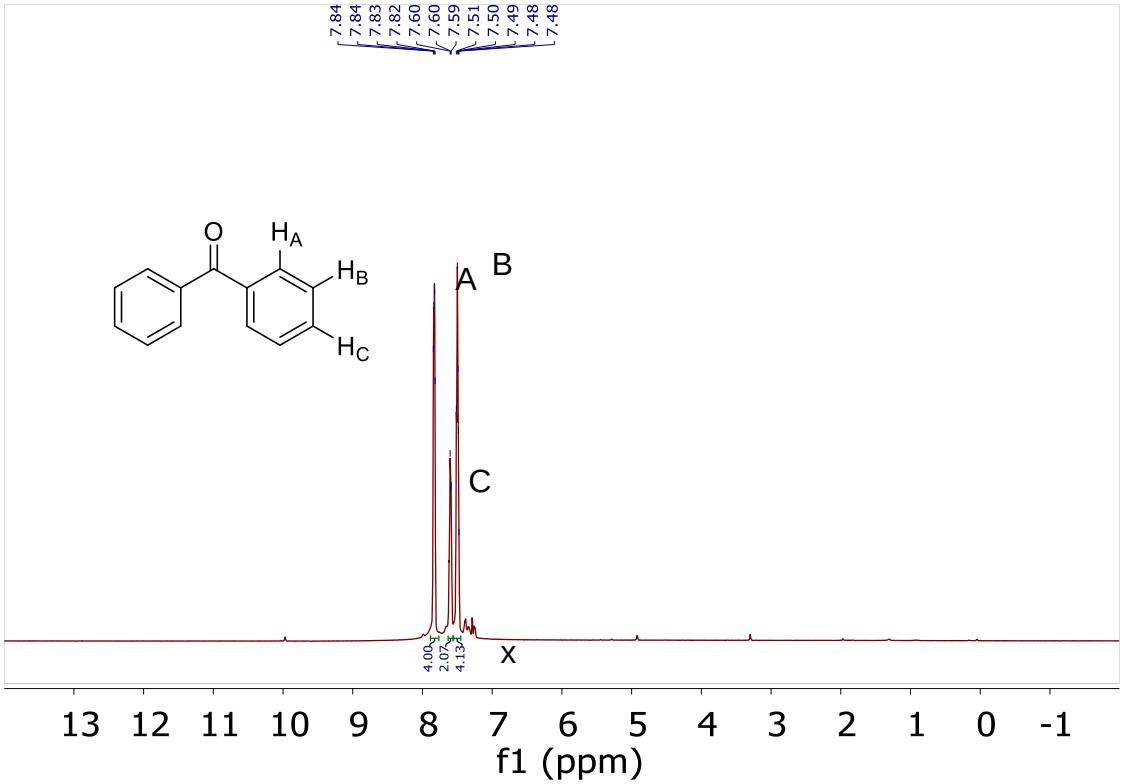

Figure E8. ^{1}H NMR of 1,1-Diphenylethylene to benzophenone.

E.7. Crude ozonolysis mixtures for carbonyl:SOZ ratios

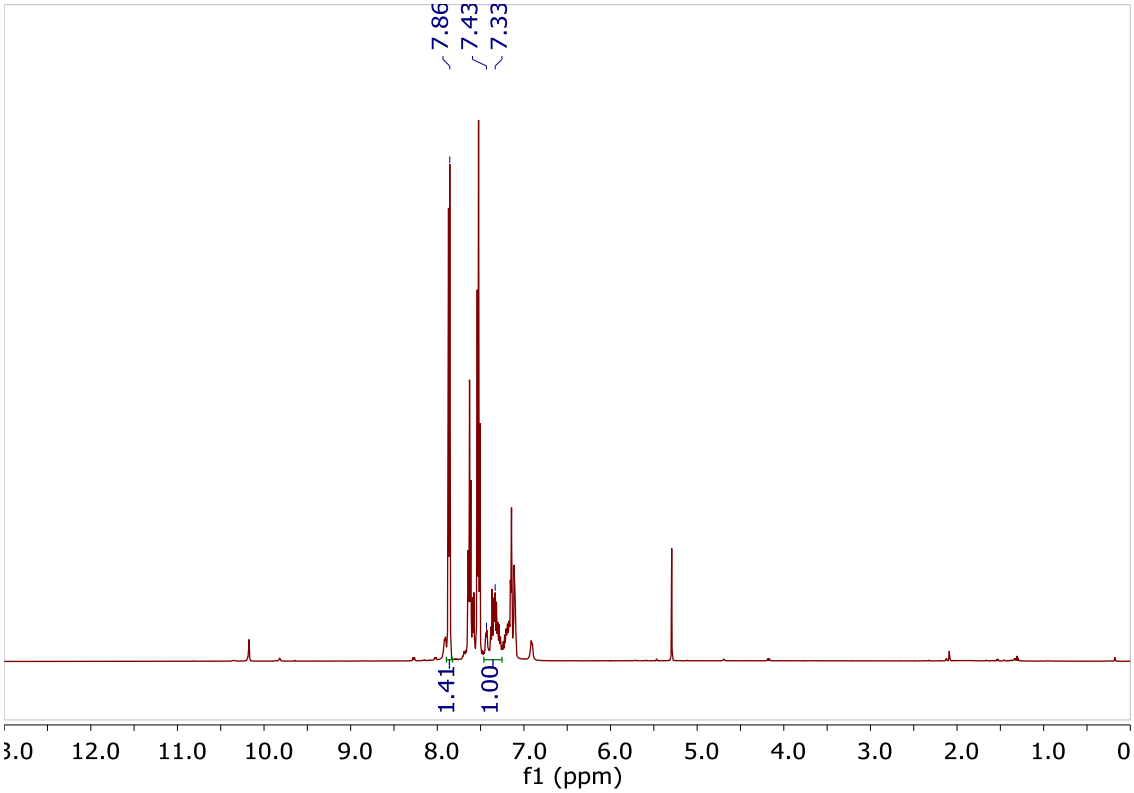

Figure E9. ^{1}H NMR of Crude ozonolysis of tetraphenylethylene. SOZ at 7.44-7.37(m) and also 7.33-7.27(m).[8]

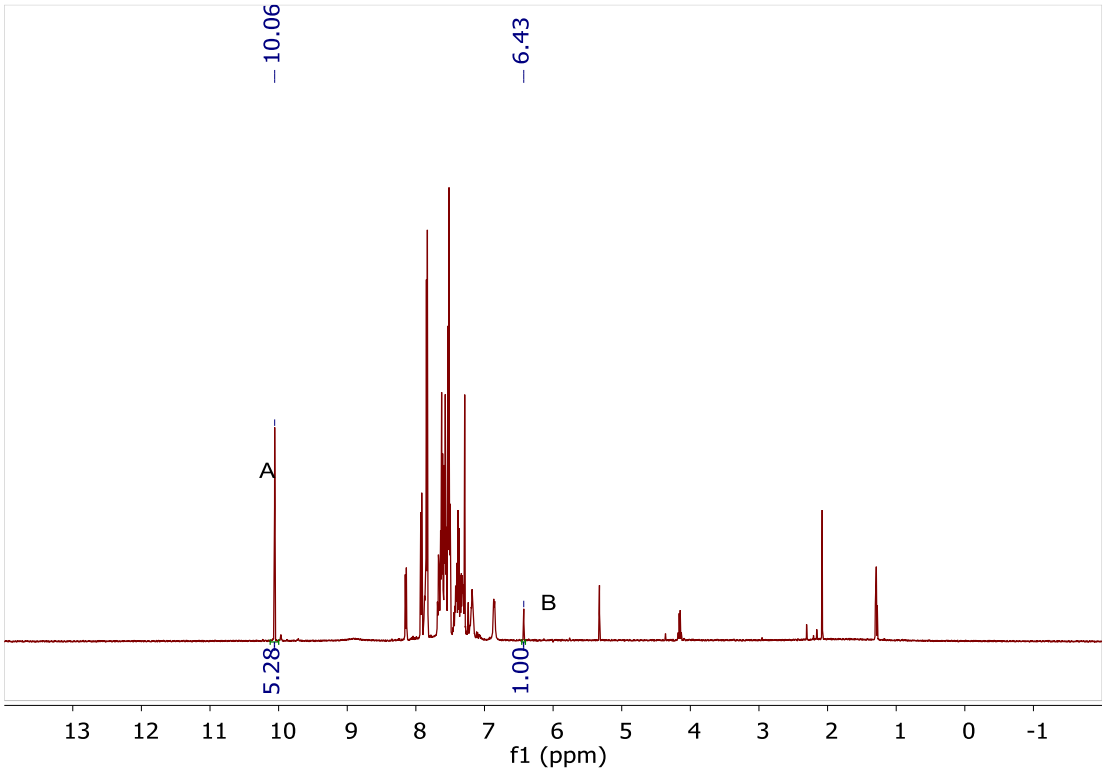

Figure E10. [1]H NMR of crude ozonolysis of triphenylethylene. SOZ at 6.33(s).[6]

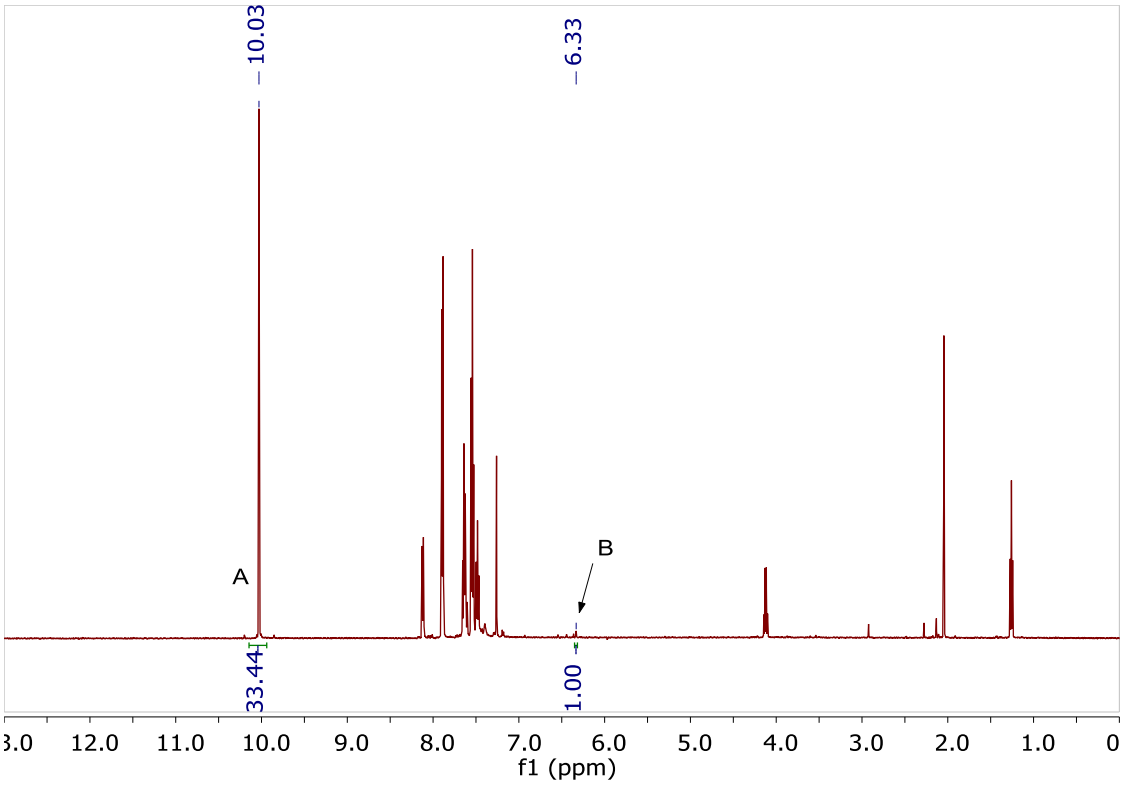

Figure E11. ^{1}H NMR of crude ozonolysis of stilbene. SOZ at 6.33(s) (*cis*-isomer) and 6.36(s) (*trans*-isomer).[6]

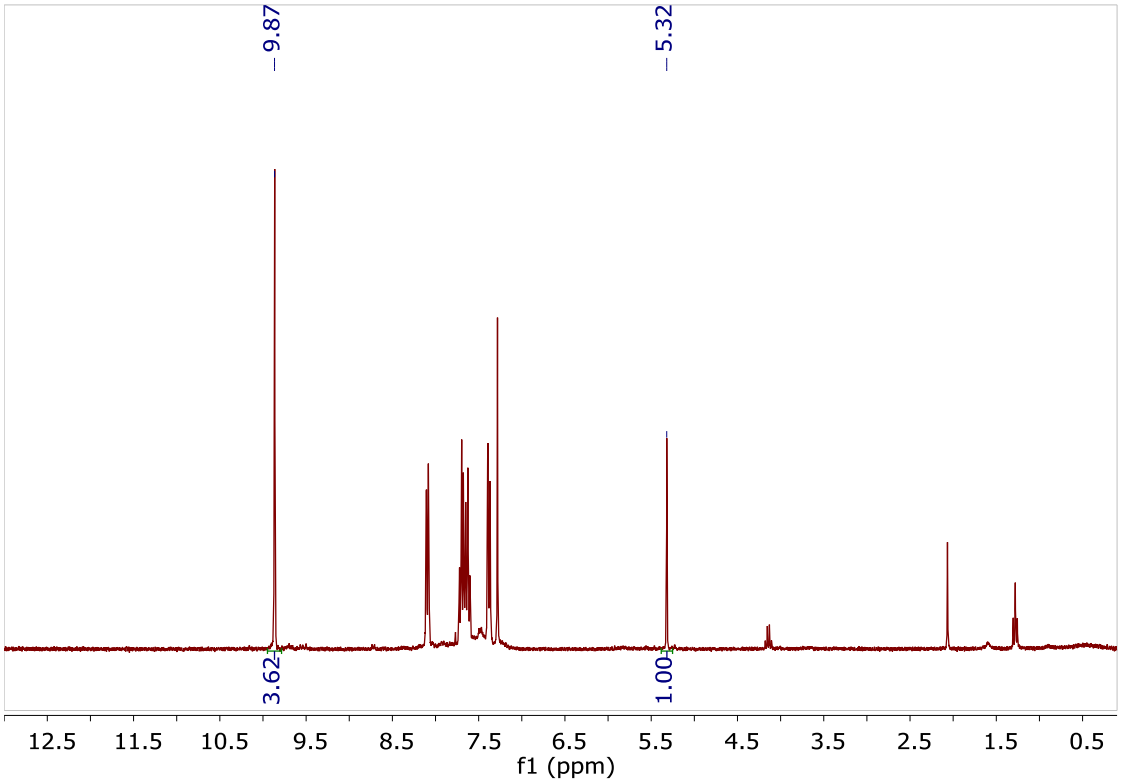

Figure E12. ^{1}H NMR of crude ozonolysis of phenanthrene. SOZ at 5.32(s).[4]

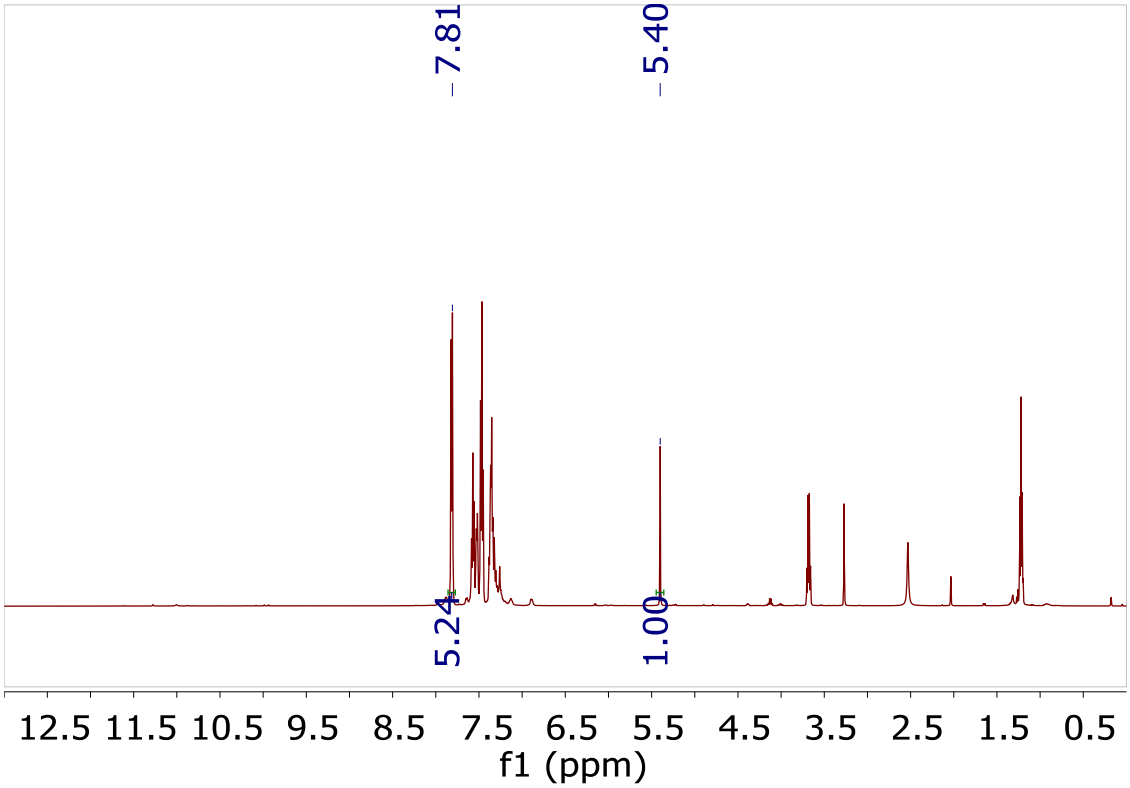

Figure E13. ^{1}H NMR of crude ozonolysis of 1,1'-diphenylethylene. SOZ at 5.37(s).[7]

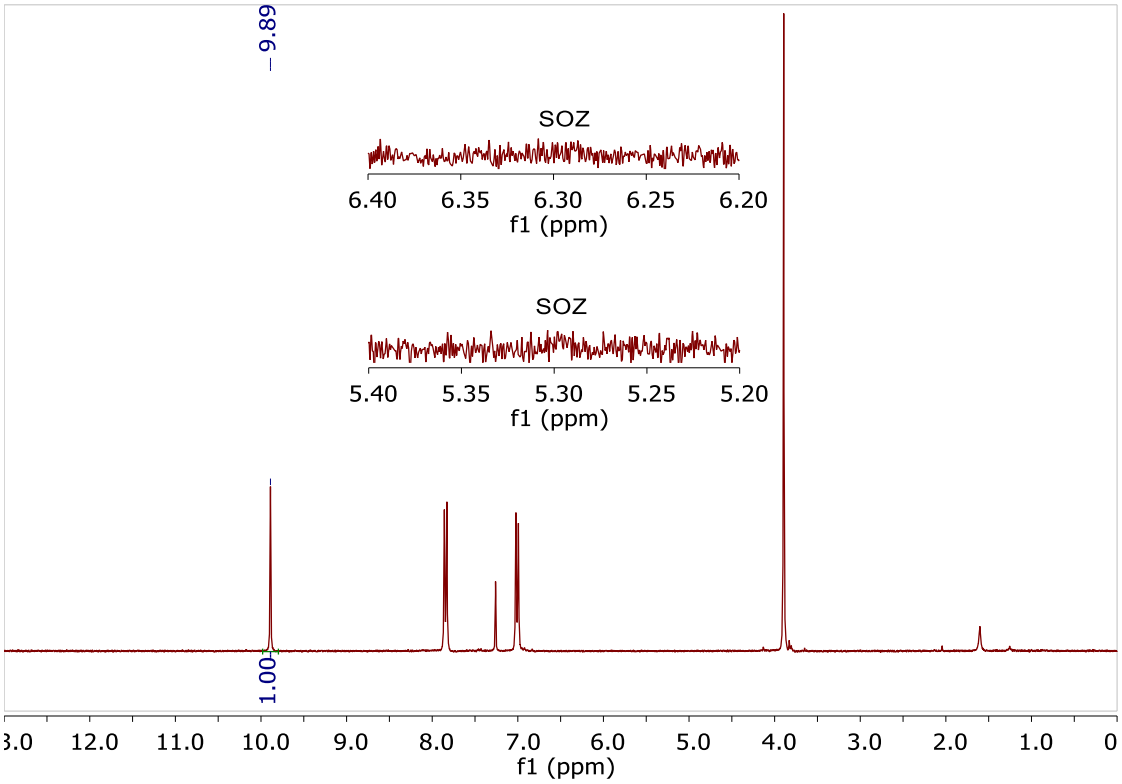

Figure E14. [1]H NMR of crude ozonolysis of anethole. SOZ at 6.3(s) and 5.3(q).[2]

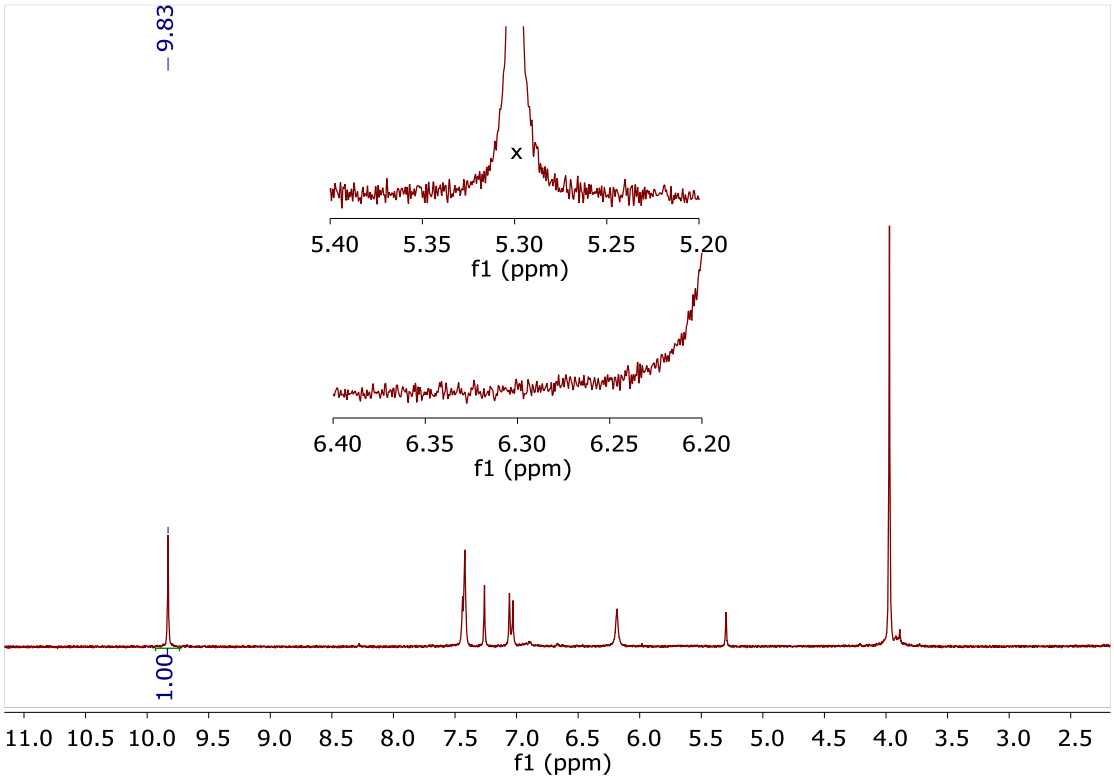

Figure E15. [1]H NMR of crude ozonolysis of isoeugenol. SOZ (anethole) 6.3(s) and 5.3(q).[2]

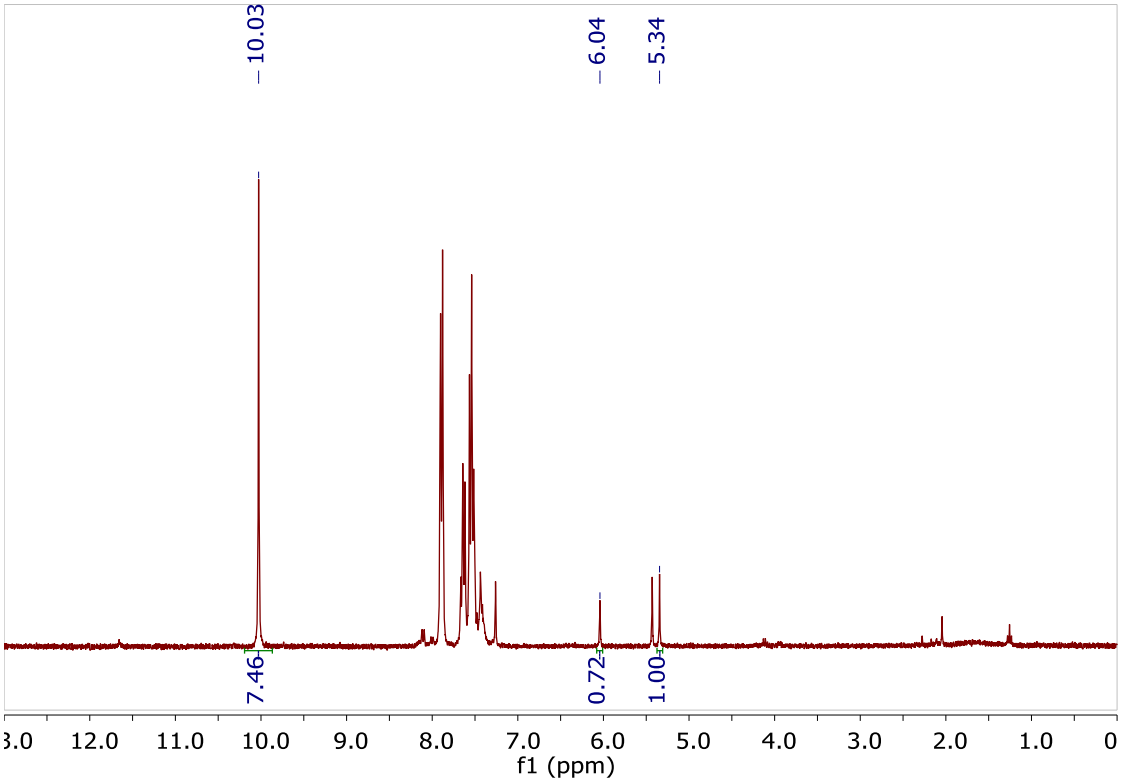

Figure E16. ^{1}H NMR of crude ozonolysis of styrene. SOZ at 6.05(s) and also 5.35(s).[3]

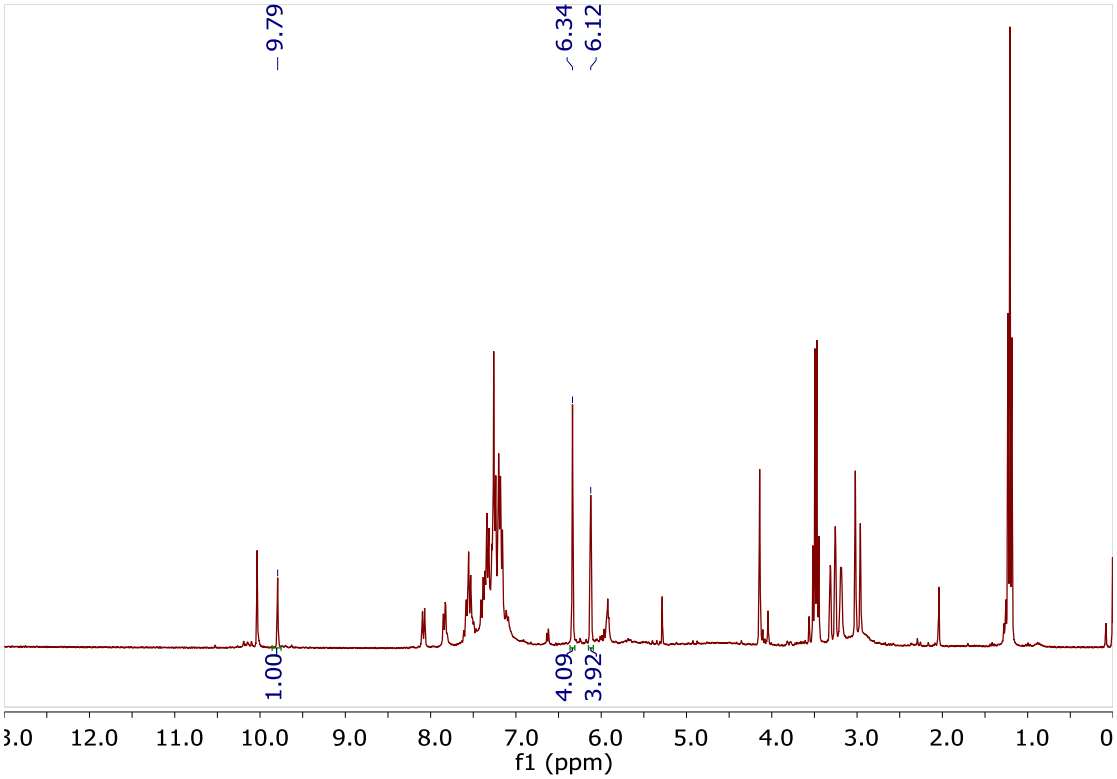

Figure E17. [1]H NMR of crude ozonolysis of indene. SOZ at 6.13(s) and also 6.34(s).[9]

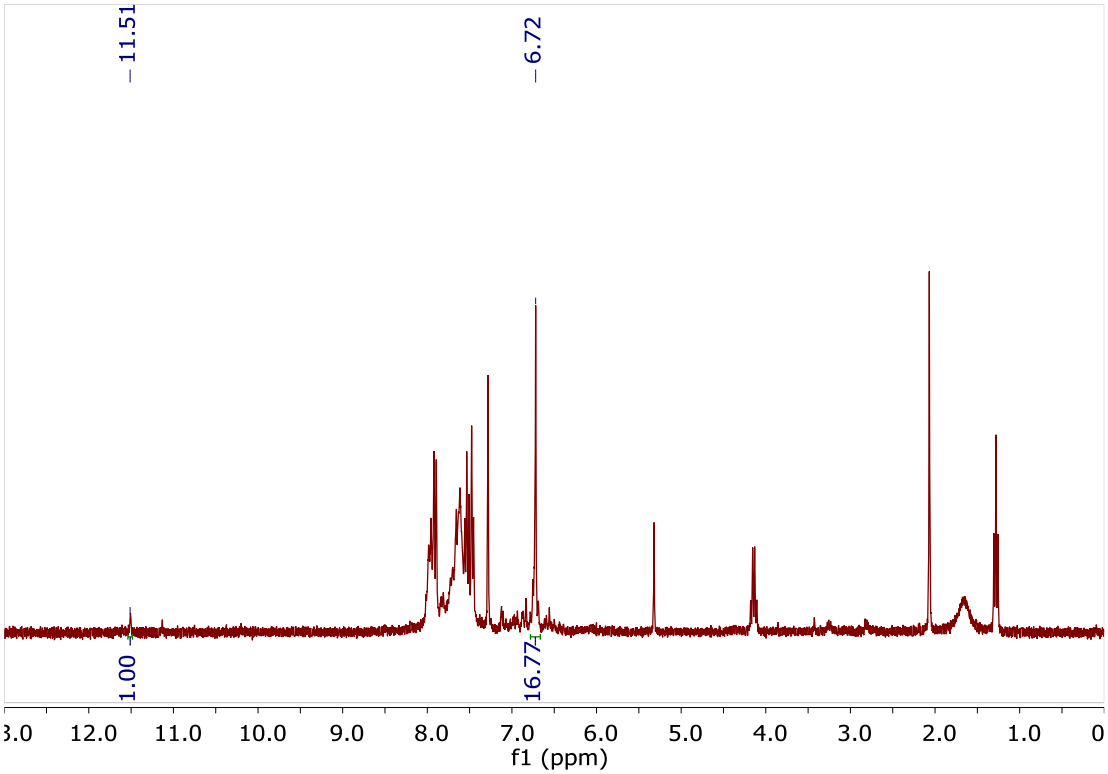

Figure E18. ^{1}H NMR of crude ozonolysis of acenaphthylene. SOZ at 6.69(s).[10]

APPENDIX F

TABULATED CRYSTALLOGRAPHIC DATA

F.1. Crystallographic data for (μ-DpPSMePE-κ*P*:κ*P′*)$_2$(FeCl$_2$)$_2$

Table F1. Crystal data and structure refinement for (μ-DpPSMePE-κ*P*:κ*P′*)$_2$(FeCl$_2$)$_2$.

Identification code	(μ-DpPSMePE-κ*P*:κ*P′*)$_2$(FeCl$_2$)$_2$	
Empirical formula	C62 H68 Cl8 Fe2 P4 S8	
Formula weight	1588.82	
Temperature	173(2) K	
Wavelength	0.71073 Å	
Crystal system	Monoclinic	
Space group	C2/c	
Unit cell dimensions	a = 20.0248(17) Å	α= 90°.
	b = 14.5159(12) Å	β= 104.0440(10)°.
	c = 25.819(2) Å	γ = 90°.
Volume	7280.6(10) Å^3	
Z	4	
Density (calculated)	1.450 Mg/m^3	
Absorption coefficient	1.047 mm^{-1}	
F(000)	3264	
Crystal size	0.25 x 0.13 x 0.07 mm^3	
Theta range for data collection	1.63 to 27.00°.	
Index ranges	-25<=h<=25, -18<=k<=18, -32<=l<=32	
Reflections collected	40434	
Independent reflections	7959 [R(int) = 0.0309]	
Completeness to theta = 27.00°	100.0 %	
Absorption correction	Semi-empirical from equivalents	
Max. and min. transmission	0.9303 and 0.7798	
Refinement method	Full-matrix least-squares on F^2	
Data / restraints / parameters	7959 / 0 / 380	
Goodness-of-fit on F^2	1.040	
Final R indices [I>2sigma(I)]	R1 = 0.0496, wR2 = 0.1531	
R indices (all data)	R1 = 0.0609, wR2 = 0.1669	
Largest diff. peak and hole	1.049 and -1.138 e.Å^{-3}	

Table F2. Atomic coordinates (x 10^4) and equivalent isotropic displacement parameters ($Å^2$x 10^3) for (μ-DpPSMePE-κ*P*:κ*P′*)$_2$(FeCl$_2$)$_2$. U(eq) is defined as one third of the trace of the orthogonalized U^{ij} tensor.

	x	y	z	U(eq)
Fe(1)	1138(1)	8522(1)	394(1)	29(1)
Cl(1)	633(1)	8142(1)	-451(1)	39(1)
Cl(2)	2008(1)	7720(1)	897(1)	49(1)
S(1)	2587(1)	11921(1)	2686(1)	44(1)
S(2)	3836(1)	10799(1)	-860(1)	52(1)
S(3)	1264(1)	15152(1)	-1160(1)	59(1)
S(4)	-1463(1)	10135(1)	-3272(1)	45(1)
P(1)	1485(1)	10141(1)	378(1)	27(1)
P(2)	-221(1)	11371(1)	-864(1)	27(1)
C(1)	822(2)	10931(2)	8(1)	29(1)
C(2)	484(2)	10597(2)	-557(1)	29(1)
C(3)	1769(2)	10700(2)	1025(1)	29(1)
C(4)	2159(2)	10190(2)	1447(1)	31(1)
C(5)	2400(2)	10582(2)	1944(1)	36(1)
C(6)	2257(2)	11498(2)	2034(1)	33(1)
C(7)	1861(2)	12009(2)	1620(1)	42(1)
C(8)	1621(2)	11612(2)	1119(1)	41(1)
C(9)	2221(3)	13052(3)	2663(2)	63(1)
C(10)	2176(2)	10315(2)	43(1)	29(1)
C(11)	2546(2)	11137(2)	84(1)	40(1)
C(12)	3043(2)	11261(3)	-190(2)	43(1)
C(13)	3181(2)	10575(2)	-528(1)	36(1)
C(14)	2824(2)	9755(2)	-567(1)	39(1)
C(15)	2330(2)	9625(2)	-280(1)	35(1)
C(16)	3636(3)	10009(4)	-1412(2)	65(1)
C(17)	217(2)	12448(2)	-921(1)	30(1)
C(18)	17(2)	13257(2)	-712(1)	37(1)
C(19)	327(2)	14091(2)	-773(2)	42(1)
C(20)	851(2)	14131(2)	-1037(2)	39(1)
C(21)	1070(2)	13315(2)	-1231(2)	41(1)
C(22)	756(2)	12489(2)	-1175(1)	37(1)
C(23)	988(3)	15982(3)	-748(2)	70(1)
C(24)	-515(2)	10974(2)	-1550(1)	28(1)
C(25)	-857(2)	11596(2)	-1934(1)	38(1)
C(26)	-1122(2)	11320(2)	-2453(1)	41(1)
C(27)	-1070(2)	10405(2)	-2603(1)	33(1)
C(28)	-749(2)	9780(2)	-2219(1)	36(1)
C(29)	-471(2)	10062(2)	-1697(1)	33(1)
C(30)	-1236(2)	8949(3)	-3331(2)	55(1)
Cl(1S)	9326(1)	6005(1)	2599(1)	104(1)

C(1S)	10000	6671(7)	2500	94(3)
Cl(2S)	9766(1)	2971(2)	2986(1)	136(1)
C(2S)	10000	3670(9)	2500	137(5)

Table F3. Bond lengths [Å] and angles [°] for (μ-DpPSMePE-κ*P*:κ*P′*)$_2$(FeCl$_2$)$_2$.

Fe(1)-Cl(2)	2.2308(9)
Fe(1)-Cl(1)	2.2401(9)
Fe(1)-P(2)#1	2.4403(9)
Fe(1)-P(1)	2.4543(9)
S(1)-C(6)	1.762(3)
S(1)-C(9)	1.794(4)
S(2)-C(13)	1.761(3)
S(2)-C(16)	1.797(5)
S(3)-C(20)	1.763(4)
S(3)-C(23)	1.783(5)
S(4)-C(27)	1.761(3)
S(4)-C(30)	1.796(5)
P(1)-C(3)	1.820(3)
P(1)-C(10)	1.820(3)
P(1)-C(1)	1.836(3)
P(2)-C(17)	1.816(3)
P(2)-C(24)	1.819(3)
P(2)-C(2)	1.828(3)
P(2)-Fe(1)#1	2.4403(9)
C(1)-C(2)	1.531(4)
C(3)-C(8)	1.391(4)
C(3)-C(4)	1.390(4)
C(4)-C(5)	1.380(4)
C(5)-C(6)	1.392(4)
C(6)-C(7)	1.383(5)
C(7)-C(8)	1.392(5)
C(10)-C(15)	1.385(4)
C(10)-C(11)	1.395(5)
C(11)-C(12)	1.367(5)
C(12)-C(13)	1.396(5)
C(13)-C(14)	1.381(5)
C(14)-C(15)	1.384(5)
C(17)-C(18)	1.391(4)
C(17)-C(22)	1.394(5)
C(18)-C(19)	1.386(5)
C(19)-C(20)	1.386(5)
C(20)-C(21)	1.397(5)
C(21)-C(22)	1.377(5)
C(24)-C(29)	1.387(4)
C(24)-C(25)	1.391(4)
C(25)-C(26)	1.377(5)
C(26)-C(27)	1.394(5)
C(27)-C(28)	1.381(5)
C(28)-C(29)	1.389(4)

Cl(1S)-C(1S)	1.729(6)
C(1S)-Cl(1S)#2	1.729(6)
Cl(2S)-C(2S)	1.763(8)
C(2S)-Cl(2S)#2	1.763(8)

Cl(2)-Fe(1)-Cl(1)	122.92(4)
Cl(2)-Fe(1)-P(2)#1	108.60(4)
Cl(1)-Fe(1)-P(2)#1	106.46(3)
Cl(2)-Fe(1)-P(1)	109.00(4)
Cl(1)-Fe(1)-P(1)	106.40(3)
P(2)#1-Fe(1)-P(1)	101.37(3)
C(6)-S(1)-C(9)	103.38(18)
C(13)-S(2)-C(16)	102.6(2)
C(20)-S(3)-C(23)	103.5(2)
C(27)-S(4)-C(30)	103.58(18)
C(3)-P(1)-C(10)	105.65(14)
C(3)-P(1)-C(1)	102.97(13)
C(10)-P(1)-C(1)	101.78(14)
C(3)-P(1)-Fe(1)	116.03(10)
C(10)-P(1)-Fe(1)	113.04(10)
C(1)-P(1)-Fe(1)	115.77(10)
C(17)-P(2)-C(24)	103.99(14)
C(17)-P(2)-C(2)	103.13(14)
C(24)-P(2)-C(2)	105.12(14)
C(17)-P(2)-Fe(1)#1	114.99(11)
C(24)-P(2)-Fe(1)#1	113.59(10)
C(2)-P(2)-Fe(1)#1	114.74(11)
C(2)-C(1)-P(1)	113.2(2)
C(1)-C(2)-P(2)	109.6(2)
C(8)-C(3)-C(4)	118.3(3)
C(8)-C(3)-P(1)	123.5(2)
C(4)-C(3)-P(1)	118.2(2)
C(5)-C(4)-C(3)	120.8(3)
C(4)-C(5)-C(6)	120.6(3)
C(7)-C(6)-C(5)	119.1(3)
C(7)-C(6)-S(1)	124.3(3)
C(5)-C(6)-S(1)	116.6(2)
C(6)-C(7)-C(8)	120.1(3)
C(3)-C(8)-C(7)	121.1(3)
C(15)-C(10)-C(11)	118.3(3)
C(15)-C(10)-P(1)	119.5(2)
C(11)-C(10)-P(1)	122.2(2)
C(12)-C(11)-C(10)	120.8(3)
C(11)-C(12)-C(13)	120.7(3)
C(14)-C(13)-C(12)	118.9(3)
C(14)-C(13)-S(2)	123.9(3)

C(12)-C(13)-S(2)	117.1(3)
C(13)-C(14)-C(15)	120.2(3)
C(10)-C(15)-C(14)	121.1(3)
C(18)-C(17)-C(22)	118.4(3)
C(18)-C(17)-P(2)	120.3(3)
C(22)-C(17)-P(2)	121.3(2)
C(19)-C(18)-C(17)	121.0(3)
C(20)-C(19)-C(18)	120.3(3)
C(19)-C(20)-C(21)	118.8(3)
C(19)-C(20)-S(3)	124.6(3)
C(21)-C(20)-S(3)	116.5(3)
C(22)-C(21)-C(20)	120.6(3)
C(21)-C(22)-C(17)	120.8(3)
C(29)-C(24)-C(25)	118.5(3)
C(29)-C(24)-P(2)	122.8(2)
C(25)-C(24)-P(2)	118.4(2)
C(26)-C(25)-C(24)	120.8(3)
C(25)-C(26)-C(27)	120.6(3)
C(28)-C(27)-C(26)	118.8(3)
C(28)-C(27)-S(4)	125.2(3)
C(26)-C(27)-S(4)	116.0(2)
C(27)-C(28)-C(29)	120.5(3)
C(24)-C(29)-C(28)	120.7(3)
Cl(1S)#2-C(1S)-Cl(1S)	112.0(6)
Cl(2S)#2-C(2S)-Cl(2S)	109.8(7)

Symmetry transformations used to generate equivalent atoms:
#1 -x,-y+2,-z #2 -x+2,y,-z+1/2

Table F4. Anisotropic displacement parameters ($Å^2 x\ 10^3$)for (μ-DpPSMePE-κ*P*:κ*P*′)$_2$(FeCl$_2$)$_2$. The anisotropic displacement factor exponent takes the form: $-2\pi^2[\ h^2 a^{*2} U^{11} + ... + 2\ h\ k\ a^*\ b^*\ U^{12}\ ]$

	U^{11}	U^{22}	U^{33}	U^{23}	U^{13}	U^{12}
Fe(1)	38(1)	26(1)	23(1)	-1(1)	5(1)	4(1)
Cl(1)	54(1)	34(1)	26(1)	-9(1)	6(1)	6(1)
Cl(2)	57(1)	36(1)	44(1)	1(1)	-4(1)	17(1)
S(1)	58(1)	40(1)	27(1)	-8(1)	-4(1)	-5(1)
S(2)	49(1)	48(1)	68(1)	2(1)	31(1)	5(1)
S(3)	54(1)	29(1)	92(1)	-2(1)	16(1)	-4(1)
S(4)	50(1)	57(1)	23(1)	-4(1)	1(1)	-9(1)
P(1)	32(1)	26(1)	20(1)	-1(1)	2(1)	4(1)
P(2)	34(1)	25(1)	20(1)	1(1)	3(1)	4(1)
C(1)	34(2)	28(1)	21(1)	0(1)	2(1)	5(1)
C(2)	35(2)	26(1)	23(1)	0(1)	0(1)	5(1)
C(3)	30(2)	31(2)	23(1)	-1(1)	3(1)	2(1)
C(4)	37(2)	26(2)	26(2)	-1(1)	1(1)	1(1)
C(5)	44(2)	32(2)	27(2)	3(1)	-2(1)	1(1)
C(6)	37(2)	34(2)	24(1)	-5(1)	3(1)	-5(1)
C(7)	58(2)	32(2)	30(2)	-6(1)	2(2)	8(2)
C(8)	59(2)	35(2)	24(2)	-1(1)	1(2)	12(2)
C(9)	83(3)	54(3)	43(2)	-19(2)	-4(2)	10(2)
C(10)	31(2)	28(1)	24(1)	-1(1)	1(1)	5(1)
C(11)	46(2)	32(2)	43(2)	-7(1)	15(2)	1(1)
C(12)	45(2)	34(2)	53(2)	-4(2)	15(2)	-4(2)
C(13)	33(2)	36(2)	39(2)	4(1)	9(1)	7(1)
C(14)	44(2)	35(2)	38(2)	-8(1)	12(2)	5(1)
C(15)	40(2)	30(2)	35(2)	-3(1)	8(1)	1(1)
C(16)	66(3)	88(4)	50(3)	-5(2)	28(2)	4(2)
C(17)	36(2)	24(1)	24(1)	-1(1)	-1(1)	2(1)
C(18)	38(2)	32(2)	40(2)	-7(1)	7(1)	5(1)
C(19)	43(2)	29(2)	53(2)	-9(2)	6(2)	6(1)
C(20)	36(2)	26(2)	50(2)	-2(1)	0(2)	1(1)
C(21)	44(2)	33(2)	46(2)	-3(2)	13(2)	1(2)
C(22)	45(2)	29(2)	36(2)	-5(1)	12(1)	4(1)
C(23)	74(3)	30(2)	101(4)	-17(2)	10(3)	-1(2)
C(24)	29(1)	32(2)	21(1)	2(1)	4(1)	1(1)
C(25)	48(2)	33(2)	28(2)	1(1)	1(1)	5(1)
C(26)	49(2)	40(2)	27(2)	7(1)	-3(1)	2(2)
C(27)	31(2)	44(2)	22(1)	-2(1)	5(1)	-7(1)
C(28)	40(2)	35(2)	30(2)	-7(1)	5(1)	-1(1)
C(29)	42(2)	32(2)	24(2)	0(1)	5(1)	6(1)
C(30)	63(3)	67(3)	35(2)	-18(2)	11(2)	-11(2)
Cl(1S)	116(1)	97(1)	114(1)	6(1)	59(1)	0(1)

C(1S)	84(6)	107(7)	85(6)	0	6(5)	0
Cl(2S)	118(2)	108(2)	176(2)	-4(2)	23(2)	-10(1)
C(2S)	154(11)	109(9)	178(13)	0	96(10)	0

Table F5. Hydrogen coordinates (x 10^4) and isotropic displacement parameters ($Å^2$x 10^3) for (μ-DpPSMePE-κ*P*:κ*P′*)$_2$(FeCl$_2$)$_2$.

	x	y	z	U(eq)
H(1A)	462	11007	209	34
H(1B)	1033	11542	-14	34
H(2A)	305	9964	-542	35
H(2B)	829	10584	-774	35
H(4A)	2261	9564	1392	38
H(5A)	2667	10223	2228	43
H(7A)	1752	12632	1678	50
H(8A)	1351	11970	836	49
H(9A)	2377	13348	3012	95
H(9B)	1718	13006	2571	95
H(9C)	2367	13421	2392	95
H(11A)	2451	11617	306	48
H(12A)	3298	11820	-150	52
H(14A)	2916	9277	-792	46
H(15A)	2093	9053	-305	42
H(16A)	3974	10077	-1627	98
H(16B)	3174	10141	-1632	98
H(16C)	3650	9377	-1276	98
H(18A)	-338	13238	-526	44
H(19A)	179	14638	-632	51
H(21A)	1438	13329	-1404	49
H(22A)	909	11941	-1311	44
H(23A)	1194	16581	-790	105
H(23B)	1132	15787	-374	105
H(23C)	485	16034	-853	105
H(25A)	-908	12218	-1836	46
H(26A)	-1344	11757	-2712	49
H(28A)	-717	9151	-2314	43
H(29A)	-249	9625	-1438	40
H(30A)	-1435	8735	-3696	83
H(30B)	-1416	8575	-3079	83
H(30C)	-734	8890	-3250	83

Table F6. Torsion angles [°] for (μ-DpPSMePE-κ*P*:κ*P*′)$_2$(FeCl$_2$)$_2$.

Cl(2)-Fe(1)-P(1)-C(3)	-56.34(12)
Cl(1)-Fe(1)-P(1)-C(3)	169.21(11)
P(2)#1-Fe(1)-P(1)-C(3)	58.07(11)
Cl(2)-Fe(1)-P(1)-C(10)	65.94(11)
Cl(1)-Fe(1)-P(1)-C(10)	-68.52(11)
P(2)#1-Fe(1)-P(1)-C(10)	-179.65(10)
Cl(2)-Fe(1)-P(1)-C(1)	-177.20(11)
Cl(1)-Fe(1)-P(1)-C(1)	48.34(11)
P(2)#1-Fe(1)-P(1)-C(1)	-62.79(11)
C(3)-P(1)-C(1)-C(2)	-178.7(2)
C(10)-P(1)-C(1)-C(2)	71.9(2)
Fe(1)-P(1)-C(1)-C(2)	-51.1(2)
P(1)-C(1)-C(2)-P(2)	174.55(16)
C(17)-P(2)-C(2)-C(1)	65.4(2)
C(24)-P(2)-C(2)-C(1)	174.1(2)
Fe(1)#1-P(2)-C(2)-C(1)	-60.4(2)
C(10)-P(1)-C(3)-C(8)	91.5(3)
C(1)-P(1)-C(3)-C(8)	-14.9(3)
Fe(1)-P(1)-C(3)-C(8)	-142.4(3)
C(10)-P(1)-C(3)-C(4)	-88.1(3)
C(1)-P(1)-C(3)-C(4)	165.6(3)
Fe(1)-P(1)-C(3)-C(4)	38.0(3)
C(8)-C(3)-C(4)-C(5)	-0.8(5)
P(1)-C(3)-C(4)-C(5)	178.8(3)
C(3)-C(4)-C(5)-C(6)	0.1(5)
C(4)-C(5)-C(6)-C(7)	0.9(5)
C(4)-C(5)-C(6)-S(1)	179.6(3)
C(9)-S(1)-C(6)-C(7)	4.9(4)
C(9)-S(1)-C(6)-C(5)	-173.8(3)
C(5)-C(6)-C(7)-C(8)	-1.1(6)
S(1)-C(6)-C(7)-C(8)	-179.8(3)
C(4)-C(3)-C(8)-C(7)	0.6(5)
P(1)-C(3)-C(8)-C(7)	-179.0(3)
C(6)-C(7)-C(8)-C(3)	0.4(6)
C(3)-P(1)-C(10)-C(15)	143.8(3)
C(1)-P(1)-C(10)-C(15)	-108.9(3)
Fe(1)-P(1)-C(10)-C(15)	15.9(3)
C(3)-P(1)-C(10)-C(11)	-38.4(3)
C(1)-P(1)-C(10)-C(11)	68.8(3)
Fe(1)-P(1)-C(10)-C(11)	-166.3(2)
C(15)-C(10)-C(11)-C(12)	0.5(5)
P(1)-C(10)-C(11)-C(12)	-177.3(3)
C(10)-C(11)-C(12)-C(13)	1.5(6)
C(11)-C(12)-C(13)-C(14)	-2.3(6)

C(11)-C(12)-C(13)-S(2)	-179.6(3)
C(16)-S(2)-C(13)-C(14)	23.6(4)
C(16)-S(2)-C(13)-C(12)	-159.3(3)
C(12)-C(13)-C(14)-C(15)	0.9(5)
S(2)-C(13)-C(14)-C(15)	178.0(3)
C(11)-C(10)-C(15)-C(14)	-1.9(5)
P(1)-C(10)-C(15)-C(14)	176.0(3)
C(13)-C(14)-C(15)-C(10)	1.2(5)
C(24)-P(2)-C(17)-C(18)	123.9(3)
C(2)-P(2)-C(17)-C(18)	-126.6(3)
Fe(1)#1-P(2)-C(17)-C(18)	-1.0(3)
C(24)-P(2)-C(17)-C(22)	-55.8(3)
C(2)-P(2)-C(17)-C(22)	53.7(3)
Fe(1)#1-P(2)-C(17)-C(22)	179.4(2)
C(22)-C(17)-C(18)-C(19)	2.4(5)
P(2)-C(17)-C(18)-C(19)	-177.3(3)
C(17)-C(18)-C(19)-C(20)	-0.9(5)
C(18)-C(19)-C(20)-C(21)	-1.3(5)
C(18)-C(19)-C(20)-S(3)	177.6(3)
C(23)-S(3)-C(20)-C(19)	12.5(4)
C(23)-S(3)-C(20)-C(21)	-168.6(3)
C(19)-C(20)-C(21)-C(22)	1.9(5)
S(3)-C(20)-C(21)-C(22)	-177.1(3)
C(20)-C(21)-C(22)-C(17)	-0.3(5)
C(18)-C(17)-C(22)-C(21)	-1.8(5)
P(2)-C(17)-C(22)-C(21)	177.9(3)
C(17)-P(2)-C(24)-C(29)	137.9(3)
C(2)-P(2)-C(24)-C(29)	29.9(3)
Fe(1)#1-P(2)-C(24)-C(29)	-96.4(3)
C(17)-P(2)-C(24)-C(25)	-48.4(3)
C(2)-P(2)-C(24)-C(25)	-156.5(3)
Fe(1)#1-P(2)-C(24)-C(25)	77.3(3)
C(29)-C(24)-C(25)-C(26)	-2.6(5)
P(2)-C(24)-C(25)-C(26)	-176.5(3)
C(24)-C(25)-C(26)-C(27)	1.7(6)
C(25)-C(26)-C(27)-C(28)	0.2(5)
C(25)-C(26)-C(27)-S(4)	177.4(3)
C(30)-S(4)-C(27)-C(28)	-7.4(3)
C(30)-S(4)-C(27)-C(26)	175.6(3)
C(26)-C(27)-C(28)-C(29)	-1.3(5)
S(4)-C(27)-C(28)-C(29)	-178.2(3)
C(25)-C(24)-C(29)-C(28)	1.5(5)
P(2)-C(24)-C(29)-C(28)	175.2(3)
C(27)-C(28)-C(29)-C(24)	0.4(5)

Symmetry transformations used to generate equivalent atoms: #1 -x,-y+2,-z #2 -x+2,y,-z+1/2

F.2. Crystallographic data for *trans*-$FeCl_2(DpPSMePE)_2$

Table F7. Crystal data and structure refinement for *trans*-$FeCl_2(DpPSMePE)_2$.

Identification code	*trans*-$FeCl_2(DpPSMePE)_2$	
Empirical formula	C61 H66 Cl4 Fe P4 S8	
Formula weight	1377.15	
Temperature	173(2) K	
Wavelength	0.71073 Å	
Crystal system	Triclinic	
Space group	P-1	
Unit cell dimensions	a = 10.5589(13) Å	α= 92.397(2)°.
	b = 11.7579(14) Å	β= 97.465(2)°.
	c = 28.178(3) Å	γ = 110.261(2)°.
Volume	3239.8(7) $Å^3$	
Z	2	
Density (calculated)	1.412 Mg/m^3	
Absorption coefficient	0.793 mm^{-1}	
F(000)	1428	
Crystal size	0.38 x 0.14 x 0.07 mm^3	
Theta range for data collection	1.46 to 26.00°.	
Index ranges	-13<=h<=13, -14<=k<=14, -34<=l<=34	
Reflections collected	33856	
Independent reflections	12677 [R(int) = 0.0428]	
Completeness to theta = 26.00°	99.5 %	
Absorption correction	Semi-empirical from equivalents	
Max. and min. transmission	0.9466 and 0.7527	
Refinement method	Full-matrix least-squares on F^2	
Data / restraints / parameters	12677 / 0 / 706	
Goodness-of-fit on F^2	1.085	
Final R indices [I>2sigma(I)]	R1 = 0.0583, wR2 = 0.1308	
R indices (all data)	R1 = 0.0843, wR2 = 0.1465	
Largest diff. peak and hole	0.964 and -0.866 $e.Å^{-3}$	

Table F8. Atomic coordinates (x 10^4) and equivalent isotropic displacement parameters ($Å^2$x 10^3) for *trans*-$FeCl_2(DpPSMePE)_2$. U(eq) is defined as one third of the trace of the orthogonalized U^{ij} tensor.

	x	y	z	U(eq)
Fe(1)	5000	5000	5000	22(1)
Cl(1)	5131(1)	3311(1)	4588(1)	29(1)
P(1)	6754(1)	6429(1)	4493(1)	23(1)
P(2)	7350(1)	5151(1)	5521(1)	22(1)
S(1)	6902(2)	3712(1)	2503(1)	54(1)
S(2)	7021(1)	11746(1)	3971(1)	49(1)
S(3)	8552(1)	449(1)	6211(1)	36(1)
S(4)	9888(1)	8807(1)	7430(1)	47(1)
C(1)	8443(4)	6781(4)	4857(1)	27(1)
C(2)	8573(4)	5675(4)	5094(1)	28(1)
C(3)	6917(4)	5743(4)	3924(1)	25(1)
C(4)	5836(4)	5506(4)	3552(2)	33(1)
C(5)	5801(4)	4901(4)	3114(2)	34(1)
C(6)	6854(5)	4505(4)	3040(2)	32(1)
C(7)	7949(5)	4758(4)	3405(2)	38(1)
C(8)	7982(4)	5366(4)	3841(2)	31(1)
C(9)	5406(5)	3683(5)	2114(2)	52(1)
C(10)	6815(4)	7940(4)	4335(1)	27(1)
C(11)	5776(5)	8351(4)	4409(2)	41(1)
C(12)	5807(5)	9487(4)	4290(2)	46(1)
C(13)	6870(4)	10245(4)	4094(2)	34(1)
C(14)	7919(5)	9834(4)	4016(2)	50(1)
C(15)	7883(5)	8701(4)	4135(2)	48(1)
C(16)	5352(5)	11550(5)	3664(2)	48(1)
C(17)	7750(4)	3832(4)	5714(1)	23(1)
C(18)	7726(4)	2914(4)	5371(1)	27(1)
C(19)	7953(4)	1878(4)	5509(2)	28(1)
C(20)	8238(4)	1722(4)	5990(2)	27(1)
C(21)	8275(4)	2636(4)	6333(2)	32(1)
C(22)	8025(4)	3664(4)	6197(2)	29(1)
C(23)	8281(5)	-551(4)	5681(2)	46(1)
C(24)	8132(4)	6256(3)	6048(1)	21(1)
C(25)	9527(4)	6709(4)	6205(1)	27(1)
C(26)	10091(4)	7486(4)	6620(2)	30(1)
C(27)	9265(4)	7843(4)	6891(2)	30(1)
C(28)	7863(4)	7408(4)	6735(2)	34(1)
C(29)	7304(4)	6624(4)	6322(1)	29(1)
C(30)	11688(5)	9122(4)	7500(2)	48(1)
Fe(1')	10000	10000	10000	23(1)
Cl(1')	10512(1)	8491(1)	10392(1)	29(1)

P(1')	8113(1)	10053(1)	10522(1)	21(1)
P(2')	7775(1)	8304(1)	9485(1)	26(1)
S(1')	7225(1)	7286(1)	12423(1)	44(1)
S(2')	7675(1)	15142(1)	11219(1)	37(1)
S(3')	7039(1)	2755(1)	8934(1)	44(1)
S(4')	5453(2)	10244(2)	7598(1)	60(1)
C(1')	6504(4)	9310(4)	10103(1)	25(1)
C(2')	6453(4)	8091(4)	9872(2)	28(1)
C(3')	7831(4)	9196(3)	11048(1)	22(1)
C(4')	8925(4)	8987(3)	11311(1)	25(1)
C(5')	8791(4)	8396(4)	11731(1)	29(1)
C(6')	7541(4)	7996(3)	11891(1)	28(1)
C(7')	6429(4)	8178(4)	11625(1)	28(1)
C(8')	6573(4)	8768(3)	11214(1)	24(1)
C(9')	8890(5)	7395(5)	12707(2)	57(2)
C(10')	7904(4)	11474(3)	10713(1)	22(1)
C(11')	8201(4)	11929(4)	11198(1)	28(1)
C(12')	8115(4)	13040(4)	11339(2)	31(1)
C(13')	7741(4)	13742(4)	10998(2)	26(1)
C(14')	7475(4)	13309(4)	10517(2)	27(1)
C(15')	7556(4)	12196(4)	10377(1)	25(1)
C(16')	7402(6)	15858(4)	10687(2)	47(1)
C(17')	7583(4)	6725(4)	9319(2)	29(1)
C(18')	8703(4)	6359(4)	9377(2)	38(1)
C(19')	8566(4)	5166(4)	9253(2)	40(1)
C(20')	7300(4)	4305(4)	9075(2)	31(1)
C(21')	6173(4)	4669(4)	9014(2)	42(1)
C(22')	6320(4)	5855(4)	9132(2)	41(1)
C(23')	8506(5)	2813(4)	8664(2)	40(1)
C(24')	7010(4)	8723(4)	8930(2)	29(1)
C(25')	5782(4)	8930(4)	8874(2)	33(1)
C(26')	5334(5)	9360(4)	8464(2)	37(1)
C(27')	6107(5)	9619(4)	8098(2)	41(1)
C(28')	7294(5)	9379(4)	8132(2)	46(1)
C(29')	7749(5)	8921(4)	8548(2)	39(1)
C(30')	6861(6)	10746(8)	7322(2)	97(3)
C(1S)	1874(7)	4601(7)	2207(3)	106(3)
Cl(1S)	512(2)	4851(2)	2438(1)	94(1)
Cl(2S)	3357(2)	5950(3)	2359(1)	134(1)

Table F9. Bond lengths [Å] and angles [°] for *trans*-$FeCl_2(DpPSMePE)_2$.

Fe(1)-Cl(1)#1	2.3123(10)
Fe(1)-Cl(1)	2.3123(10)
Fe(1)-P(1)	2.6518(10)
Fe(1)-P(1)#1	2.6518(10)
Fe(1)-P(2)#1	2.6590(10)
Fe(1)-P(2)	2.6590(10)
P(1)-C(3)	1.820(4)
P(1)-C(10)	1.830(4)
P(1)-C(1)	1.840(4)
P(2)-C(17)	1.829(4)
P(2)-C(24)	1.832(4)
P(2)-C(2)	1.847(4)
S(1)-C(6)	1.761(4)
S(1)-C(9)	1.790(5)
S(2)-C(13)	1.769(4)
S(2)-C(16)	1.793(5)
S(3)-C(20)	1.762(4)
S(3)-C(23)	1.791(5)
S(4)-C(27)	1.762(4)
S(4)-C(30)	1.788(5)
C(1)-C(2)	1.526(6)
C(1)-H(1A)	0.9900
C(1)-H(1B)	0.9900
C(2)-H(2A)	0.9900
C(2)-H(2B)	0.9900
C(3)-C(8)	1.385(6)
C(3)-C(4)	1.387(6)
C(4)-C(5)	1.388(6)
C(4)-H(4A)	0.9500
C(5)-C(6)	1.381(6)
C(5)-H(5A)	0.9500
C(6)-C(7)	1.382(6)
C(7)-C(8)	1.386(6)
C(7)-H(7A)	0.9500
C(8)-H(8A)	0.9500
C(9)-H(9A)	0.9800
C(9)-H(9B)	0.9800
C(9)-H(9C)	0.9800
C(10)-C(11)	1.378(6)
C(10)-C(15)	1.379(6)
C(11)-C(12)	1.382(6)
C(11)-H(11A)	0.9500
C(12)-C(13)	1.366(6)
C(12)-H(12A)	0.9500

C(13)-C(14)	1.391(6)
C(14)-C(15)	1.376(6)
C(14)-H(14A)	0.9500
C(15)-H(15A)	0.9500
C(16)-H(16A)	0.9800
C(16)-H(16B)	0.9800
C(16)-H(16C)	0.9800
C(17)-C(22)	1.392(6)
C(17)-C(18)	1.410(5)
C(18)-C(19)	1.382(6)
C(18)-H(18A)	0.9500
C(19)-C(20)	1.385(6)
C(19)-H(19A)	0.9500
C(20)-C(21)	1.401(6)
C(21)-C(22)	1.383(6)
C(21)-H(21A)	0.9500
C(22)-H(22A)	0.9500
C(23)-H(23A)	0.9800
C(23)-H(23B)	0.9800
C(23)-H(23C)	0.9800
C(24)-C(25)	1.384(5)
C(24)-C(29)	1.398(5)
C(25)-C(26)	1.382(5)
C(25)-H(25A)	0.9500
C(26)-C(27)	1.386(6)
C(26)-H(26A)	0.9500
C(27)-C(28)	1.391(6)
C(28)-C(29)	1.382(6)
C(28)-H(28A)	0.9500
C(29)-H(29A)	0.9500
C(30)-H(30A)	0.9800
C(30)-H(30B)	0.9800
C(30)-H(30C)	0.9800
Fe(1')-Cl(1')#2	2.3091(10)
Fe(1')-Cl(1')	2.3091(10)
Fe(1')-P(1')#2	2.6423(10)
Fe(1')-P(1')	2.6423(10)
Fe(1')-P(2')	2.6888(11)
Fe(1')-P(2')#2	2.6888(11)
P(1')-C(3')	1.825(4)
P(1')-C(10')	1.827(4)
P(1')-C(1')	1.846(4)
P(2')-C(17')	1.831(4)
P(2')-C(24')	1.831(4)
P(2')-C(2')	1.839(4)
S(1')-C(6')	1.760(4)

S(1')-C(9')	1.794(5)
S(2')-C(13')	1.763(4)
S(2')-C(16')	1.789(5)
S(3')-C(20')	1.766(4)
S(3')-C(23')	1.794(5)
S(4')-C(30')	1.701(7)
S(4')-C(27')	1.784(5)
C(1')-C(2')	1.530(5)
C(1')-H(1'A)	0.9900
C(1')-H(1'B)	0.9900
C(2')-H(2'A)	0.9900
C(2')-H(2'B)	0.9900
C(3')-C(4')	1.391(5)
C(3')-C(8')	1.397(5)
C(4')-C(5')	1.394(6)
C(4')-H(4'A)	0.9500
C(5')-C(6')	1.383(6)
C(5')-H(5'A)	0.9500
C(6')-C(7')	1.393(6)
C(7')-C(8')	1.375(5)
C(7')-H(7'A)	0.9500
C(8')-H(8'A)	0.9500
C(9')-H(9'A)	0.9800
C(9')-H(9'B)	0.9800
C(9')-H(9'C)	0.9800
C(10')-C(15')	1.396(5)
C(10')-C(11')	1.401(5)
C(11')-C(12')	1.386(6)
C(11')-H(11B)	0.9500
C(12')-C(13')	1.398(6)
C(12')-H(12B)	0.9500
C(13')-C(14')	1.385(6)
C(14')-C(15')	1.384(5)
C(14')-H(14B)	0.9500
C(15')-H(15B)	0.9500
C(16')-H(16D)	0.9800
C(16')-H(16E)	0.9800
C(16')-H(16F)	0.9800
C(17')-C(18')	1.384(6)
C(17')-C(22')	1.389(6)
C(18')-C(19')	1.385(6)
C(18')-H(18B)	0.9500
C(19')-C(20')	1.382(6)
C(19')-H(19B)	0.9500
C(20')-C(21')	1.391(6)
C(21')-C(22')	1.370(6)

C(21')-H(21B)	0.9500
C(22')-H(22B)	0.9500
C(23')-H(23D)	0.9800
C(23')-H(23E)	0.9800
C(23')-H(23F)	0.9800
C(24')-C(29')	1.390(6)
C(24')-C(25')	1.391(6)
C(25')-C(26')	1.374(6)
C(25')-H(25B)	0.9500
C(26')-C(27')	1.377(6)
C(26')-H(26B)	0.9500
C(27')-C(28')	1.369(7)
C(28')-C(29')	1.408(7)
C(28')-H(28B)	0.9500
C(29')-H(29B)	0.9500
C(30')-H(30D)	0.9800
C(30')-H(30E)	0.9800
C(30')-H(30F)	0.9800
C(1S)-Cl(1S)	1.760(8)
C(1S)-Cl(2S)	1.789(8)
C(1S)-H(1SA)	0.9900
C(1S)-H(1SB)	0.9900

Cl(1)#1-Fe(1)-Cl(1)	180.0
Cl(1)#1-Fe(1)-P(1)	90.35(4)
Cl(1)-Fe(1)-P(1)	89.65(4)
Cl(1)#1-Fe(1)-P(1)#1	89.65(4)
Cl(1)-Fe(1)-P(1)#1	90.35(4)
P(1)-Fe(1)-P(1)#1	180.0
Cl(1)#1-Fe(1)-P(2)#1	85.66(3)
Cl(1)-Fe(1)-P(2)#1	94.34(3)
P(1)-Fe(1)-P(2)#1	100.23(3)
P(1)#1-Fe(1)-P(2)#1	79.77(3)
Cl(1)#1-Fe(1)-P(2)	94.34(3)
Cl(1)-Fe(1)-P(2)	85.66(3)
P(1)-Fe(1)-P(2)	79.77(3)
P(1)#1-Fe(1)-P(2)	100.23(3)
P(2)#1-Fe(1)-P(2)	180.0
C(3)-P(1)-C(10)	101.61(18)
C(3)-P(1)-C(1)	103.60(19)
C(10)-P(1)-C(1)	101.79(19)
C(3)-P(1)-Fe(1)	116.50(13)
C(10)-P(1)-Fe(1)	125.53(13)
C(1)-P(1)-Fe(1)	105.02(13)
C(17)-P(2)-C(24)	101.69(17)
C(17)-P(2)-C(2)	99.87(18)

C(24)-P(2)-C(2)	103.18(18)
C(17)-P(2)-Fe(1)	123.92(13)
C(24)-P(2)-Fe(1)	121.77(13)
C(2)-P(2)-Fe(1)	102.38(14)
C(6)-S(1)-C(9)	103.8(2)
C(13)-S(2)-C(16)	102.8(2)
C(20)-S(3)-C(23)	103.7(2)
C(27)-S(4)-C(30)	103.1(2)
C(2)-C(1)-P(1)	111.9(3)
C(2)-C(1)-H(1A)	109.2
P(1)-C(1)-H(1A)	109.2
C(2)-C(1)-H(1B)	109.2
P(1)-C(1)-H(1B)	109.2
H(1A)-C(1)-H(1B)	107.9
C(1)-C(2)-P(2)	111.9(3)
C(1)-C(2)-H(2A)	109.2
P(2)-C(2)-H(2A)	109.2
C(1)-C(2)-H(2B)	109.2
P(2)-C(2)-H(2B)	109.2
H(2A)-C(2)-H(2B)	107.9
C(8)-C(3)-C(4)	117.5(4)
C(8)-C(3)-P(1)	125.6(3)
C(4)-C(3)-P(1)	116.8(3)
C(5)-C(4)-C(3)	121.8(4)
C(5)-C(4)-H(4A)	119.1
C(3)-C(4)-H(4A)	119.1
C(6)-C(5)-C(4)	120.1(4)
C(6)-C(5)-H(5A)	120.0
C(4)-C(5)-H(5A)	120.0
C(5)-C(6)-C(7)	118.5(4)
C(5)-C(6)-S(1)	123.8(3)
C(7)-C(6)-S(1)	117.6(3)
C(6)-C(7)-C(8)	121.1(4)
C(6)-C(7)-H(7A)	119.4
C(8)-C(7)-H(7A)	119.4
C(7)-C(8)-C(3)	120.9(4)
C(7)-C(8)-H(8A)	119.5
C(3)-C(8)-H(8A)	119.5
S(1)-C(9)-H(9A)	109.5
S(1)-C(9)-H(9B)	109.5
H(9A)-C(9)-H(9B)	109.5
S(1)-C(9)-H(9C)	109.5
H(9A)-C(9)-H(9C)	109.5
H(9B)-C(9)-H(9C)	109.5
C(11)-C(10)-C(15)	117.5(4)
C(11)-C(10)-P(1)	120.7(3)

C(15)-C(10)-P(1)	121.8(3)
C(10)-C(11)-C(12)	121.3(4)
C(10)-C(11)-H(11A)	119.3
C(12)-C(11)-H(11A)	119.3
C(13)-C(12)-C(11)	121.1(4)
C(13)-C(12)-H(12A)	119.4
C(11)-C(12)-H(12A)	119.4
C(12)-C(13)-C(14)	118.0(4)
C(12)-C(13)-S(2)	123.2(3)
C(14)-C(13)-S(2)	118.8(3)
C(15)-C(14)-C(13)	120.6(4)
C(15)-C(14)-H(14A)	119.7
C(13)-C(14)-H(14A)	119.7
C(14)-C(15)-C(10)	121.4(4)
C(14)-C(15)-H(15A)	119.3
C(10)-C(15)-H(15A)	119.3
S(2)-C(16)-H(16A)	109.5
S(2)-C(16)-H(16B)	109.5
H(16A)-C(16)-H(16B)	109.5
S(2)-C(16)-H(16C)	109.5
H(16A)-C(16)-H(16C)	109.5
H(16B)-C(16)-H(16C)	109.5
C(22)-C(17)-C(18)	117.6(4)
C(22)-C(17)-P(2)	122.1(3)
C(18)-C(17)-P(2)	120.2(3)
C(19)-C(18)-C(17)	121.2(4)
C(19)-C(18)-H(18A)	119.4
C(17)-C(18)-H(18A)	119.4
C(18)-C(19)-C(20)	120.8(4)
C(18)-C(19)-H(19A)	119.6
C(20)-C(19)-H(19A)	119.6
C(19)-C(20)-C(21)	118.3(4)
C(19)-C(20)-S(3)	125.1(3)
C(21)-C(20)-S(3)	116.7(3)
C(22)-C(21)-C(20)	121.2(4)
C(22)-C(21)-H(21A)	119.4
C(20)-C(21)-H(21A)	119.4
C(21)-C(22)-C(17)	120.9(4)
C(21)-C(22)-H(22A)	119.5
C(17)-C(22)-H(22A)	119.5
S(3)-C(23)-H(23A)	109.5
S(3)-C(23)-H(23B)	109.5
H(23A)-C(23)-H(23B)	109.5
S(3)-C(23)-H(23C)	109.5
H(23A)-C(23)-H(23C)	109.5
H(23B)-C(23)-H(23C)	109.5

C(25)-C(24)-C(29)	117.7(4)
C(25)-C(24)-P(2)	122.4(3)
C(29)-C(24)-P(2)	119.8(3)
C(26)-C(25)-C(24)	121.6(4)
C(26)-C(25)-H(25A)	119.2
C(24)-C(25)-H(25A)	119.2
C(25)-C(26)-C(27)	120.4(4)
C(25)-C(26)-H(26A)	119.8
C(27)-C(26)-H(26A)	119.8
C(26)-C(27)-C(28)	118.6(4)
C(26)-C(27)-S(4)	123.7(3)
C(28)-C(27)-S(4)	117.7(3)
C(29)-C(28)-C(27)	120.7(4)
C(29)-C(28)-H(28A)	119.7
C(27)-C(28)-H(28A)	119.7
C(28)-C(29)-C(24)	121.0(4)
C(28)-C(29)-H(29A)	119.5
C(24)-C(29)-H(29A)	119.5
S(4)-C(30)-H(30A)	109.5
S(4)-C(30)-H(30B)	109.5
H(30A)-C(30)-H(30B)	109.5
S(4)-C(30)-H(30C)	109.5
H(30A)-C(30)-H(30C)	109.5
H(30B)-C(30)-H(30C)	109.5
Cl(1')#2-Fe(1')-Cl(1')	180.000(1)
Cl(1')#2-Fe(1')-P(1')#2	94.80(3)
Cl(1')-Fe(1')-P(1')#2	85.20(3)
Cl(1')#2-Fe(1')-P(1')	85.20(3)
Cl(1')-Fe(1')-P(1')	94.80(3)
P(1')#2-Fe(1')-P(1')	180.000(1)
Cl(1')#2-Fe(1')-P(2')	90.17(4)
Cl(1')-Fe(1')-P(2')	89.83(4)
P(1')#2-Fe(1')-P(2')	100.50(3)
P(1')-Fe(1')-P(2')	79.50(3)
Cl(1')#2-Fe(1')-P(2')#2	89.83(4)
Cl(1')-Fe(1')-P(2')#2	90.17(4)
P(1')#2-Fe(1')-P(2')#2	79.50(3)
P(1')-Fe(1')-P(2')#2	100.50(3)
P(2')-Fe(1')-P(2')#2	180.0
C(3')-P(1')-C(10')	102.86(17)
C(3')-P(1')-C(1')	103.03(19)
C(10')-P(1')-C(1')	100.53(18)
C(3')-P(1')-Fe(1')	121.52(13)
C(10')-P(1')-Fe(1')	122.18(13)
C(1')-P(1')-Fe(1')	103.06(13)
C(17')-P(2')-C(24')	102.13(19)

C(17')-P(2')-C(2')	101.24(19)
C(24')-P(2')-C(2')	102.8(2)
C(17')-P(2')-Fe(1')	125.74(14)
C(24')-P(2')-Fe(1')	117.83(14)
C(2')-P(2')-Fe(1')	103.71(13)
C(6')-S(1')-C(9')	103.6(2)
C(13')-S(2')-C(16')	103.7(2)
C(20')-S(3')-C(23')	103.3(2)
C(30')-S(4')-C(27')	100.0(3)
C(2')-C(1')-P(1')	110.9(3)
C(2')-C(1')-H(1'A)	109.5
P(1')-C(1')-H(1'A)	109.5
C(2')-C(1')-H(1'B)	109.5
P(1')-C(1')-H(1'B)	109.5
H(1'A)-C(1')-H(1'B)	108.1
C(1')-C(2')-P(2')	111.4(3)
C(1')-C(2')-H(2'A)	109.4
P(2')-C(2')-H(2'A)	109.4
C(1')-C(2')-H(2'B)	109.4
P(2')-C(2')-H(2'B)	109.4
H(2'A)-C(2')-H(2'B)	108.0
C(4')-C(3')-C(8')	117.5(4)
C(4')-C(3')-P(1')	119.0(3)
C(8')-C(3')-P(1')	123.4(3)
C(3')-C(4')-C(5')	121.7(4)
C(3')-C(4')-H(4'A)	119.1
C(5')-C(4')-H(4'A)	119.1
C(6')-C(5')-C(4')	119.7(4)
C(6')-C(5')-H(5'A)	120.1
C(4')-C(5')-H(5'A)	120.1
C(5')-C(6')-C(7')	119.1(4)
C(5')-C(6')-S(1')	125.0(3)
C(7')-C(6')-S(1')	115.8(3)
C(8')-C(7')-C(6')	120.8(4)
C(8')-C(7')-H(7'A)	119.6
C(6')-C(7')-H(7'A)	119.6
C(7')-C(8')-C(3')	121.2(4)
C(7')-C(8')-H(8'A)	119.4
C(3')-C(8')-H(8'A)	119.4
S(1')-C(9')-H(9'A)	109.5
S(1')-C(9')-H(9'B)	109.5
H(9'A)-C(9')-H(9'B)	109.5
S(1')-C(9')-H(9'C)	109.5
H(9'A)-C(9')-H(9'C)	109.5
H(9'B)-C(9')-H(9'C)	109.5
C(15')-C(10')-C(11')	117.5(4)

C(15')-C(10')-P(1')	121.0(3)
C(11')-C(10')-P(1')	121.3(3)
C(12')-C(11')-C(10')	121.2(4)
C(12')-C(11')-H(11B)	119.4
C(10')-C(11')-H(11B)	119.4
C(11')-C(12')-C(13')	120.5(4)
C(11')-C(12')-H(12B)	119.7
C(13')-C(12')-H(12B)	119.7
C(14')-C(13')-C(12')	118.5(4)
C(14')-C(13')-S(2')	124.9(3)
C(12')-C(13')-S(2')	116.5(3)
C(13')-C(14')-C(15')	120.8(4)
C(13')-C(14')-H(14B)	119.6
C(15')-C(14')-H(14B)	119.6
C(14')-C(15')-C(10')	121.4(4)
C(14')-C(15')-H(15B)	119.3
C(10')-C(15')-H(15B)	119.3
S(2')-C(16')-H(16D)	109.5
S(2')-C(16')-H(16E)	109.5
H(16D)-C(16')-H(16E)	109.5
S(2')-C(16')-H(16F)	109.5
H(16D)-C(16')-H(16F)	109.5
H(16E)-C(16')-H(16F)	109.5
C(18')-C(17')-C(22')	117.8(4)
C(18')-C(17')-P(2')	120.7(3)
C(22')-C(17')-P(2')	121.6(3)
C(17')-C(18')-C(19')	121.0(4)
C(17')-C(18')-H(18B)	119.5
C(19')-C(18')-H(18B)	119.5
C(20')-C(19')-C(18')	120.6(4)
C(20')-C(19')-H(19B)	119.7
C(18')-C(19')-H(19B)	119.7
C(19')-C(20')-C(21')	118.5(4)
C(19')-C(20')-S(3')	123.1(3)
C(21')-C(20')-S(3')	118.4(3)
C(22')-C(21')-C(20')	120.5(4)
C(22')-C(21')-H(21B)	119.8
C(20')-C(21')-H(21B)	119.8
C(21')-C(22')-C(17')	121.5(4)
C(21')-C(22')-H(22B)	119.2
C(17')-C(22')-H(22B)	119.2
S(3')-C(23')-H(23D)	109.5
S(3')-C(23')-H(23E)	109.5
H(23D)-C(23')-H(23E)	109.5
S(3')-C(23')-H(23F)	109.5
H(23D)-C(23')-H(23F)	109.5

H(23E)-C(23')-H(23F)	109.5
C(29')-C(24')-C(25')	117.8(4)
C(29')-C(24')-P(2')	117.7(3)
C(25')-C(24')-P(2')	124.4(3)
C(26')-C(25')-C(24')	121.4(4)
C(26')-C(25')-H(25B)	119.3
C(24')-C(25')-H(25B)	119.3
C(25')-C(26')-C(27')	120.6(4)
C(25')-C(26')-H(26B)	119.7
C(27')-C(26')-H(26B)	119.7
C(28')-C(27')-C(26')	119.5(5)
C(28')-C(27')-S(4')	124.3(4)
C(26')-C(27')-S(4')	116.2(4)
C(27')-C(28')-C(29')	120.2(4)
C(27')-C(28')-H(28B)	119.9
C(29')-C(28')-H(28B)	119.9
C(24')-C(29')-C(28')	120.4(4)
C(24')-C(29')-H(29B)	119.8
C(28')-C(29')-H(29B)	119.8
S(4')-C(30')-H(30D)	109.5
S(4')-C(30')-H(30E)	109.5
H(30D)-C(30')-H(30E)	109.5
S(4')-C(30')-H(30F)	109.5
H(30D)-C(30')-H(30F)	109.5
H(30E)-C(30')-H(30F)	109.5
Cl(1S)-C(1S)-Cl(2S)	108.1(5)
Cl(1S)-C(1S)-H(1SA)	110.1
Cl(2S)-C(1S)-H(1SA)	110.1
Cl(1S)-C(1S)-H(1SB)	110.1
Cl(2S)-C(1S)-H(1SB)	110.1
H(1SA)-C(1S)-H(1SB)	108.4

Symmetry transformations used to generate equivalent atoms:
#1 -x+1,-y+1,-z+1 #2 -x+2,-y+2,-z+2

Table F10. Anisotropic displacement parameters ($Å^2 x\ 10^3$) for *trans*-$FeCl_2(DpPSMePE)_2$. The anisotropic displacement factor exponent takes the form: $-2\pi^2[h^2a^{*2}U^{11} + ... + 2\ h\ k\ a^*\ b^*\ U^{12}]$

	U^{11}	U^{22}	U^{33}	U^{23}	U^{13}	U^{12}
Fe(1)	22(1)	22(1)	22(1)	-3(1)	3(1)	9(1)
Cl(1)	33(1)	28(1)	27(1)	-7(1)	1(1)	16(1)
P(1)	23(1)	24(1)	24(1)	2(1)	6(1)	9(1)
P(2)	20(1)	23(1)	21(1)	-2(1)	1(1)	8(1)
S(1)	78(1)	60(1)	33(1)	-8(1)	11(1)	38(1)
S(2)	38(1)	32(1)	87(1)	21(1)	24(1)	17(1)
S(3)	43(1)	28(1)	43(1)	7(1)	10(1)	17(1)
S(4)	47(1)	49(1)	40(1)	-23(1)	-7(1)	18(1)
C(1)	21(2)	29(2)	26(2)	1(2)	5(2)	2(2)
C(2)	26(2)	31(2)	27(2)	1(2)	6(2)	11(2)
C(3)	26(2)	25(2)	26(2)	4(2)	8(2)	8(2)
C(4)	29(2)	41(3)	31(2)	-2(2)	5(2)	14(2)
C(5)	32(2)	37(3)	28(2)	-2(2)	1(2)	8(2)
C(6)	47(3)	28(2)	24(2)	5(2)	11(2)	15(2)
C(7)	50(3)	47(3)	30(2)	9(2)	14(2)	31(2)
C(8)	35(2)	41(3)	25(2)	7(2)	5(2)	21(2)
C(9)	61(4)	44(3)	37(3)	-11(2)	3(2)	5(3)
C(10)	27(2)	24(2)	27(2)	1(2)	6(2)	7(2)
C(11)	27(2)	34(3)	62(3)	17(2)	18(2)	7(2)
C(12)	32(3)	38(3)	78(4)	19(3)	24(3)	19(2)
C(13)	33(2)	27(2)	46(3)	8(2)	14(2)	13(2)
C(14)	40(3)	35(3)	86(4)	29(3)	34(3)	16(2)
C(15)	37(3)	42(3)	80(4)	23(3)	33(3)	23(2)
C(16)	63(3)	47(3)	40(3)	-3(2)	-1(2)	31(3)
C(17)	18(2)	25(2)	25(2)	-1(2)	1(2)	7(2)
C(18)	28(2)	33(2)	22(2)	1(2)	2(2)	13(2)
C(19)	26(2)	27(2)	31(2)	-3(2)	2(2)	11(2)
C(20)	20(2)	24(2)	38(2)	3(2)	6(2)	7(2)
C(21)	39(3)	29(2)	25(2)	3(2)	5(2)	10(2)
C(22)	32(2)	24(2)	30(2)	-2(2)	5(2)	11(2)
C(23)	61(3)	26(2)	55(3)	2(2)	10(3)	19(2)
C(24)	23(2)	21(2)	20(2)	3(2)	4(2)	8(2)
C(25)	24(2)	27(2)	28(2)	-1(2)	4(2)	8(2)
C(26)	23(2)	28(2)	30(2)	-3(2)	-4(2)	4(2)
C(27)	34(2)	24(2)	29(2)	-6(2)	-1(2)	11(2)
C(28)	34(2)	40(3)	31(2)	-10(2)	2(2)	19(2)
C(29)	23(2)	34(2)	29(2)	-2(2)	0(2)	12(2)
C(30)	46(3)	41(3)	43(3)	-19(2)	-16(2)	11(2)
Fe(1')	22(1)	22(1)	25(1)	1(1)	2(1)	9(1)
Cl(1')	36(1)	30(1)	29(1)	7(1)	9(1)	19(1)

P(1')	21(1)	21(1)	21(1)	1(1)	3(1)	9(1)
P(2')	21(1)	21(1)	33(1)	-6(1)	1(1)	7(1)
S(1')	48(1)	45(1)	33(1)	16(1)	5(1)	7(1)
S(2')	46(1)	24(1)	44(1)	-2(1)	9(1)	15(1)
S(3')	29(1)	24(1)	75(1)	-10(1)	2(1)	9(1)
S(4')	61(1)	76(1)	40(1)	14(1)	10(1)	17(1)
C(1')	20(2)	28(2)	27(2)	0(2)	1(2)	9(2)
C(2')	25(2)	25(2)	30(2)	0(2)	1(2)	6(2)
C(3')	27(2)	16(2)	22(2)	-2(2)	4(2)	6(2)
C(4')	23(2)	24(2)	28(2)	-2(2)	5(2)	9(2)
C(5')	35(2)	30(2)	25(2)	0(2)	0(2)	16(2)
C(6')	38(2)	18(2)	24(2)	0(2)	2(2)	7(2)
C(7')	25(2)	25(2)	28(2)	-1(2)	4(2)	1(2)
C(8')	20(2)	24(2)	25(2)	-1(2)	2(2)	6(2)
C(9')	57(3)	58(4)	43(3)	22(3)	-11(3)	7(3)
C(10')	17(2)	19(2)	27(2)	1(2)	5(2)	4(2)
C(11')	34(2)	24(2)	26(2)	4(2)	5(2)	12(2)
C(12')	33(2)	33(2)	28(2)	-2(2)	6(2)	12(2)
C(13')	24(2)	22(2)	32(2)	-1(2)	7(2)	6(2)
C(14')	25(2)	26(2)	34(2)	7(2)	6(2)	11(2)
C(15')	26(2)	28(2)	22(2)	-1(2)	2(2)	10(2)
C(16')	62(3)	25(2)	57(3)	5(2)	9(3)	21(2)
C(17')	23(2)	25(2)	37(2)	-7(2)	0(2)	6(2)
C(18')	21(2)	25(2)	59(3)	-11(2)	-3(2)	3(2)
C(19')	22(2)	30(2)	66(3)	-10(2)	-2(2)	12(2)
C(20')	23(2)	20(2)	45(3)	-7(2)	-2(2)	7(2)
C(21')	23(2)	26(2)	69(3)	-16(2)	-6(2)	6(2)
C(22')	22(2)	28(2)	69(3)	-12(2)	-3(2)	10(2)
C(23')	50(3)	39(3)	39(3)	1(2)	6(2)	27(2)
C(24')	30(2)	22(2)	29(2)	-6(2)	0(2)	4(2)
C(25')	36(3)	36(2)	27(2)	-2(2)	2(2)	15(2)
C(26')	40(3)	40(3)	33(3)	-4(2)	2(2)	18(2)
C(27')	40(3)	32(3)	40(3)	-6(2)	-1(2)	1(2)
C(28')	43(3)	47(3)	31(3)	-7(2)	17(2)	-6(2)
C(29')	28(2)	40(3)	39(3)	-8(2)	5(2)	1(2)
C(30')	55(4)	147(7)	64(4)	-35(5)	-1(3)	14(4)
C(1S)	72(5)	111(7)	140(7)	70(6)	25(5)	30(5)
Cl(1S)	75(1)	125(2)	81(1)	10(1)	13(1)	33(1)
Cl(2S)	69(1)	150(2)	177(3)	75(2)	5(1)	29(1)

Table F11. Hydrogen coordinates (x 10^4) and isotropic displacement parameters ($Å^2$x 10^3) for *trans*-$FeCl_2(DpPSMePE)_2$.

	x	y	z	U(eq)
H(1A)	9158	7067	4649	33
H(1B)	8595	7447	5109	33
H(2A)	9515	5887	5266	33
H(2B)	8409	5005	4842	33
H(4A)	5099	5766	3598	40
H(5A)	5052	4759	2864	41
H(7A)	8693	4510	3356	45
H(8A)	8745	5527	4086	38
H(9A)	5347	3251	1802	78
H(9B)	5458	4519	2069	78
H(9C)	4593	3263	2259	78
H(11A)	5024	7843	4544	49
H(12A)	5075	9746	4344	55
H(14A)	8668	10341	3878	60
H(15A)	8610	8439	4078	57
H(16A)	5323	12342	3580	71
H(16B)	4672	11201	3874	71
H(16C)	5150	11001	3370	71
H(18A)	7550	3009	5038	33
H(19A)	7913	1265	5270	34
H(21A)	8475	2547	6665	38
H(22A)	8041	4264	6437	34
H(23A)	8434	-1295	5769	70
H(23B)	8920	-145	5465	70
H(23C)	7341	-760	5517	70
H(25A)	10111	6479	6023	32
H(26A)	11052	7778	6720	35
H(28A)	7283	7652	6915	41
H(29A)	6343	6330	6222	34
H(30A)	12136	9660	7794	72
H(30B)	12052	9520	7223	72
H(30C)	11863	8358	7520	72
H(1'A)	5720	9175	10279	30
H(1'B)	6430	9851	9849	30
H(2'A)	5541	7668	9679	33
H(2'B)	6587	7572	10128	33
H(4'A)	9786	9254	11202	30
H(5'A)	9555	8269	11905	35
H(7'A)	5563	7890	11730	34
H(8'A)	5804	8887	11039	29

H(9'A)	8816	7019	13011	86
H(9'B)	9481	8254	12770	86
H(9'C)	9284	6971	12495	86
H(11B)	8467	11469	11434	33
H(12B)	8312	13327	11670	37
H(14B)	7234	13781	10280	33
H(15B)	7370	11919	10045	30
H(16D)	7348	16653	10776	70
H(16E)	6545	15344	10487	70
H(16F)	8162	15969	10506	70
H(18B)	9578	6937	9503	45
H(19B)	9350	4937	9291	48
H(21B)	5295	4091	8890	50
H(22B)	5540	6088	9084	49
H(23D)	8454	1983	8572	59
H(23E)	9338	3228	8895	59
H(23F)	8528	3260	8378	59
H(25B)	5242	8771	9125	40
H(26B)	4483	9479	8432	44
H(28B)	7811	9522	7874	55
H(29B)	8567	8746	8568	47
H(30D)	6654	11127	7034	145
H(30E)	7127	10057	7231	145
H(30F)	7613	11345	7543	145
H(1SA)	1648	4417	1854	127
H(1SB)	2046	3900	2348	127

Table F12. Torsion angles [°] for *trans*-$FeCl_2(DpPSMePE)_2$.

Cl(1)#1-Fe(1)-P(1)-C(3)	-158.96(15)
Cl(1)-Fe(1)-P(1)-C(3)	21.04(15)
P(1)#1-Fe(1)-P(1)-C(3)	35(100)
P(2)#1-Fe(1)-P(1)-C(3)	-73.31(15)
P(2)-Fe(1)-P(1)-C(3)	106.69(15)
Cl(1)#1-Fe(1)-P(1)-C(10)	-29.74(17)
Cl(1)-Fe(1)-P(1)-C(10)	150.26(17)
P(1)#1-Fe(1)-P(1)-C(10)	165(100)
P(2)#1-Fe(1)-P(1)-C(10)	55.91(17)
P(2)-Fe(1)-P(1)-C(10)	-124.09(17)
Cl(1)#1-Fe(1)-P(1)-C(1)	87.10(14)
Cl(1)-Fe(1)-P(1)-C(1)	-92.90(14)
P(1)#1-Fe(1)-P(1)-C(1)	-79(100)
P(2)#1-Fe(1)-P(1)-C(1)	172.75(14)
P(2)-Fe(1)-P(1)-C(1)	-7.25(14)
Cl(1)#1-Fe(1)-P(2)-C(17)	140.96(15)
Cl(1)-Fe(1)-P(2)-C(17)	-39.04(15)
P(1)-Fe(1)-P(2)-C(17)	-129.47(16)
P(1)#1-Fe(1)-P(2)-C(17)	50.53(16)
P(2)#1-Fe(1)-P(2)-C(17)	-38(100)
Cl(1)#1-Fe(1)-P(2)-C(24)	6.24(15)
Cl(1)-Fe(1)-P(2)-C(24)	-173.76(15)
P(1)-Fe(1)-P(2)-C(24)	95.81(15)
P(1)#1-Fe(1)-P(2)-C(24)	-84.19(15)
P(2)#1-Fe(1)-P(2)-C(24)	-172(100)
Cl(1)#1-Fe(1)-P(2)-C(2)	-108.00(14)
Cl(1)-Fe(1)-P(2)-C(2)	72.00(14)
P(1)-Fe(1)-P(2)-C(2)	-18.43(14)
P(1)#1-Fe(1)-P(2)-C(2)	161.57(14)
P(2)#1-Fe(1)-P(2)-C(2)	73(100)
C(3)-P(1)-C(1)-C(2)	-82.9(3)
C(10)-P(1)-C(1)-C(2)	172.0(3)
Fe(1)-P(1)-C(1)-C(2)	39.8(3)
P(1)-C(1)-C(2)-P(2)	-62.9(3)
C(17)-P(2)-C(2)-C(1)	178.3(3)
C(24)-P(2)-C(2)-C(1)	-77.1(3)
Fe(1)-P(2)-C(2)-C(1)	50.2(3)
C(10)-P(1)-C(3)-C(8)	117.1(4)
C(1)-P(1)-C(3)-C(8)	11.7(4)
Fe(1)-P(1)-C(3)-C(8)	-103.0(4)
C(10)-P(1)-C(3)-C(4)	-67.4(4)
C(1)-P(1)-C(3)-C(4)	-172.7(3)
Fe(1)-P(1)-C(3)-C(4)	72.5(3)
C(8)-C(3)-C(4)-C(5)	0.9(6)

P(1)-C(3)-C(4)-C(5)	-175.0(3)
C(3)-C(4)-C(5)-C(6)	0.7(7)
C(4)-C(5)-C(6)-C(7)	-2.0(7)
C(4)-C(5)-C(6)-S(1)	179.1(3)
C(9)-S(1)-C(6)-C(5)	3.7(4)
C(9)-S(1)-C(6)-C(7)	-175.3(4)
C(5)-C(6)-C(7)-C(8)	1.7(7)
S(1)-C(6)-C(7)-C(8)	-179.3(4)
C(6)-C(7)-C(8)-C(3)	-0.2(7)
C(4)-C(3)-C(8)-C(7)	-1.1(6)
P(1)-C(3)-C(8)-C(7)	174.4(3)
C(3)-P(1)-C(10)-C(11)	124.1(4)
C(1)-P(1)-C(10)-C(11)	-129.2(4)
Fe(1)-P(1)-C(10)-C(11)	-10.8(4)
C(3)-P(1)-C(10)-C(15)	-55.2(4)
C(1)-P(1)-C(10)-C(15)	51.5(4)
Fe(1)-P(1)-C(10)-C(15)	169.8(3)
C(15)-C(10)-C(11)-C(12)	-0.4(7)
P(1)-C(10)-C(11)-C(12)	-179.8(4)
C(10)-C(11)-C(12)-C(13)	0.0(8)
C(11)-C(12)-C(13)-C(14)	0.5(8)
C(11)-C(12)-C(13)-S(2)	-175.7(4)
C(16)-S(2)-C(13)-C(12)	-47.8(5)
C(16)-S(2)-C(13)-C(14)	136.1(4)
C(12)-C(13)-C(14)-C(15)	-0.4(8)
S(2)-C(13)-C(14)-C(15)	175.9(5)
C(13)-C(14)-C(15)-C(10)	0.0(9)
C(11)-C(10)-C(15)-C(14)	0.5(8)
P(1)-C(10)-C(15)-C(14)	179.8(4)
C(24)-P(2)-C(17)-C(22)	23.3(4)
C(2)-P(2)-C(17)-C(22)	129.1(3)
Fe(1)-P(2)-C(17)-C(22)	-118.6(3)
C(24)-P(2)-C(17)-C(18)	-159.7(3)
C(2)-P(2)-C(17)-C(18)	-53.9(4)
Fe(1)-P(2)-C(17)-C(18)	58.4(4)
C(22)-C(17)-C(18)-C(19)	0.7(6)
P(2)-C(17)-C(18)-C(19)	-176.5(3)
C(17)-C(18)-C(19)-C(20)	-1.3(6)
C(18)-C(19)-C(20)-C(21)	0.7(6)
C(18)-C(19)-C(20)-S(3)	-179.7(3)
C(23)-S(3)-C(20)-C(19)	-4.2(4)
C(23)-S(3)-C(20)-C(21)	175.4(3)
C(19)-C(20)-C(21)-C(22)	0.5(6)
S(3)-C(20)-C(21)-C(22)	-179.2(3)
C(20)-C(21)-C(22)-C(17)	-1.1(6)
C(18)-C(17)-C(22)-C(21)	0.5(6)

P(2)-C(17)-C(22)-C(21)	177.6(3)
C(17)-P(2)-C(24)-C(25)	64.1(4)
C(2)-P(2)-C(24)-C(25)	-39.1(4)
Fe(1)-P(2)-C(24)-C(25)	-152.9(3)
C(17)-P(2)-C(24)-C(29)	-112.6(3)
C(2)-P(2)-C(24)-C(29)	144.2(3)
Fe(1)-P(2)-C(24)-C(29)	30.3(4)
C(29)-C(24)-C(25)-C(26)	0.7(6)
P(2)-C(24)-C(25)-C(26)	-176.1(3)
C(24)-C(25)-C(26)-C(27)	-0.4(6)
C(25)-C(26)-C(27)-C(28)	-0.4(6)
C(25)-C(26)-C(27)-S(4)	178.8(3)
C(30)-S(4)-C(27)-C(26)	-0.1(4)
C(30)-S(4)-C(27)-C(28)	179.0(4)
C(26)-C(27)-C(28)-C(29)	0.8(7)
S(4)-C(27)-C(28)-C(29)	-178.4(3)
C(27)-C(28)-C(29)-C(24)	-0.5(7)
C(25)-C(24)-C(29)-C(28)	-0.3(6)
P(2)-C(24)-C(29)-C(28)	176.6(3)
Cl(1')#2-Fe(1')-P(1')-C(3')	-172.29(15)
Cl(1')-Fe(1')-P(1')-C(3')	7.71(15)
P(1')#2-Fe(1')-P(1')-C(3')	25(100)
P(2')-Fe(1')-P(1')-C(3')	96.64(15)
P(2')#2-Fe(1')-P(1')-C(3')	-83.36(15)
Cl(1')#2-Fe(1')-P(1')-C(10')	-38.30(15)
Cl(1')-Fe(1')-P(1')-C(10')	141.70(15)
P(1')#2-Fe(1')-P(1')-C(10')	159(100)
P(2')-Fe(1')-P(1')-C(10')	-129.37(15)
P(2')#2-Fe(1')-P(1')-C(10')	50.63(15)
Cl(1')#2-Fe(1')-P(1')-C(1')	73.26(14)
Cl(1')-Fe(1')-P(1')-C(1')	-106.74(14)
P(1')#2-Fe(1')-P(1')-C(1')	-89(100)
P(2')-Fe(1')-P(1')-C(1')	-17.81(14)
P(2')#2-Fe(1')-P(1')-C(1')	162.19(14)
Cl(1')#2-Fe(1')-P(2')-C(17')	150.87(18)
Cl(1')-Fe(1')-P(2')-C(17')	-29.13(18)
P(1')#2-Fe(1')-P(2')-C(17')	55.95(18)
P(1')-Fe(1')-P(2')-C(17')	-124.05(18)
P(2')#2-Fe(1')-P(2')-C(17')	46(100)
Cl(1')#2-Fe(1')-P(2')-C(24')	18.58(16)
Cl(1')-Fe(1')-P(2')-C(24')	-161.42(16)
P(1')#2-Fe(1')-P(2')-C(24')	-76.33(16)
P(1')-Fe(1')-P(2')-C(24')	103.67(16)
P(2')#2-Fe(1')-P(2')-C(24')	-86(100)
Cl(1')#2-Fe(1')-P(2')-C(2')	-94.13(14)
Cl(1')-Fe(1')-P(2')-C(2')	85.87(14)

P(1')#2-Fe(1')-P(2')-C(2')	170.95(14)
P(1')-Fe(1')-P(2')-C(2')	-9.05(14)
P(2')#2-Fe(1')-P(2')-C(2')	161(100)
C(3')-P(1')-C(1')-C(2')	-76.3(3)
C(10')-P(1')-C(1')-C(2')	177.7(3)
Fe(1')-P(1')-C(1')-C(2')	50.9(3)
P(1')-C(1')-C(2')-P(2')	-65.5(3)
C(17')-P(2')-C(2')-C(1')	174.2(3)
C(24')-P(2')-C(2')-C(1')	-80.5(3)
Fe(1')-P(2')-C(2')-C(1')	42.8(3)
C(10')-P(1')-C(3')-C(4')	-111.3(3)
C(1')-P(1')-C(3')-C(4')	144.6(3)
Fe(1')-P(1')-C(3')-C(4')	30.1(3)
C(10')-P(1')-C(3')-C(8')	66.4(3)
C(1')-P(1')-C(3')-C(8')	-37.7(4)
Fe(1')-P(1')-C(3')-C(8')	-152.2(3)
C(8')-C(3')-C(4')-C(5')	-1.3(6)
P(1')-C(3')-C(4')-C(5')	176.5(3)
C(3')-C(4')-C(5')-C(6')	0.4(6)
C(4')-C(5')-C(6')-C(7')	0.9(6)
C(4')-C(5')-C(6')-S(1')	-177.7(3)
C(9')-S(1')-C(6')-C(5')	6.4(4)
C(9')-S(1')-C(6')-C(7')	-172.3(3)
C(5')-C(6')-C(7')-C(8')	-1.3(6)
S(1')-C(6')-C(7')-C(8')	177.4(3)
C(6')-C(7')-C(8')-C(3')	0.4(6)
C(4')-C(3')-C(8')-C(7')	0.9(6)
P(1')-C(3')-C(8')-C(7')	-176.8(3)
C(3')-P(1')-C(10')-C(15')	-156.9(3)
C(1')-P(1')-C(10')-C(15')	-50.8(3)
Fe(1')-P(1')-C(10')-C(15')	62.1(3)
C(3')-P(1')-C(10')-C(11')	28.8(4)
C(1')-P(1')-C(10')-C(11')	134.9(3)
Fe(1')-P(1')-C(10')-C(11')	-112.3(3)
C(15')-C(10')-C(11')-C(12')	1.8(6)
P(1')-C(10')-C(11')-C(12')	176.3(3)
C(10')-C(11')-C(12')-C(13')	-0.7(6)
C(11')-C(12')-C(13')-C(14')	-0.7(6)
C(11')-C(12')-C(13')-S(2')	-179.7(3)
C(16')-S(2')-C(13')-C(14')	-6.5(4)
C(16')-S(2')-C(13')-C(12')	172.4(3)
C(12')-C(13')-C(14')-C(15')	1.0(6)
S(2')-C(13')-C(14')-C(15')	179.9(3)
C(13')-C(14')-C(15')-C(10')	0.1(6)
C(11')-C(10')-C(15')-C(14')	-1.5(6)
P(1')-C(10')-C(15')-C(14')	-176.1(3)

C(24')-P(2')-C(17')-C(18')	125.8(4)
C(2')-P(2')-C(17')-C(18')	-128.4(4)
Fe(1')-P(2')-C(17')-C(18')	-12.2(5)
C(24')-P(2')-C(17')-C(22')	-54.3(4)
C(2')-P(2')-C(17')-C(22')	51.5(4)
Fe(1')-P(2')-C(17')-C(22')	167.7(3)
C(22')-C(17')-C(18')-C(19')	-0.1(7)
P(2')-C(17')-C(18')-C(19')	179.8(4)
C(17')-C(18')-C(19')-C(20')	-1.0(8)
C(18')-C(19')-C(20')-C(21')	1.2(7)
C(18')-C(19')-C(20')-S(3')	-177.2(4)
C(23')-S(3')-C(20')-C(19')	-39.7(5)
C(23')-S(3')-C(20')-C(21')	141.9(4)
C(19')-C(20')-C(21')-C(22')	-0.4(8)
S(3')-C(20')-C(21')-C(22')	178.1(4)
C(20')-C(21')-C(22')-C(17')	-0.7(8)
C(18')-C(17')-C(22')-C(21')	0.9(7)
P(2')-C(17')-C(22')-C(21')	-179.0(4)
C(17')-P(2')-C(24')-C(29')	-73.7(4)
C(2')-P(2')-C(24')-C(29')	-178.3(3)
Fe(1')-P(2')-C(24')-C(29')	68.4(3)
C(17')-P(2')-C(24')-C(25')	110.6(4)
C(2')-P(2')-C(24')-C(25')	5.9(4)
Fe(1')-P(2')-C(24')-C(25')	-107.3(4)
C(29')-C(24')-C(25')-C(26')	-2.4(6)
P(2')-C(24')-C(25')-C(26')	173.4(3)
C(24')-C(25')-C(26')-C(27')	-1.2(7)
C(25')-C(26')-C(27')-C(28')	3.8(7)
C(25')-C(26')-C(27')-S(4')	-176.9(3)
C(30')-S(4')-C(27')-C(28')	-14.7(5)
C(30')-S(4')-C(27')-C(26')	166.1(4)
C(26')-C(27')-C(28')-C(29')	-2.8(7)
S(4')-C(27')-C(28')-C(29')	178.0(4)
C(25')-C(24')-C(29')-C(28')	3.4(6)
P(2')-C(24')-C(29')-C(28')	-172.7(3)
C(27')-C(28')-C(29')-C(24')	-0.8(7)

Symmetry transformations used to generate equivalent atoms:
#1 -x+1,-y+1,-z+1 #2 -x+2,-y+2,-z+2

F.3. Crystallographic data for DpPSMePE(BH_3)$_2$

Table F13. Crystal data and structure refinement for DpPSMePE(BH_3)$_2$.

Identification code	DpPSMePE(BH_3)$_2$	
Empirical formula	C30 H38 B2 P2 S4	
Formula weight	610.40	
Temperature	173(2) K	
Wavelength	0.71073 Å	
Crystal system	Monoclinic	
Space group	P2(1)/c	
Unit cell dimensions	a = 11.9406(14) Å	α= 90°.
	b = 19.391(2) Å	β= 101.172(2)°.
	c = 14.1165(17) Å	γ = 90°.
Volume	3206.6(7) Å^3	
Z	4	
Density (calculated)	1.264 Mg/m^3	
Absorption coefficient	0.415 mm^{-1}	
F(000)	1288	
Crystal size	0.37 x 0.21 x 0.09 mm^3	
Theta range for data collection	1.74 to 25.00°.	
Index ranges	-14<=h<=14, -23<=k<=23, -16<=l<=16	
Reflections collected	30662	
Independent reflections	5640 [R(int) = 0.0295]	
Completeness to theta = 25.00°	99.9 %	
Absorption correction	Semi-empirical from equivalents	
Max. and min. transmission	0.9636 and 0.8615	
Refinement method	Full-matrix least-squares on F^2	
Data / restraints / parameters	5640 / 0 / 367	
Goodness-of-fit on F^2	1.024	
Final R indices [I>2sigma(I)]	R1 = 0.0594, wR2 = 0.1528	
R indices (all data)	R1 = 0.0709, wR2 = 0.1646	
Largest diff. peak and hole	1.724 and -0.764 e.Å^{-3}	

Table F14. Atomic coordinates (x 10^4) and equivalent isotropic displacement parameters ($Å^2$x 10^3) for DpPSMePE(BH_3)$_2$. U(eq) is defined as one third of the trace of the orthogonalized U^{ij} tensor.

	x	y	z	U(eq)
S(1)	-3805(1)	1997(1)	7036(1)	63(1)
S(2)	4676(1)	1700(1)	9146(1)	59(1)
S(3)	-1999(1)	83(1)	0(1)	42(1)
S(4)	6433(1)	885(1)	2002(1)	67(1)
P(1)	813(1)	2202(1)	5421(1)	25(1)
P(2)	1897(1)	512(1)	3702(1)	27(1)
B(1)	1018(4)	3018(2)	4713(3)	36(1)
B(2)	1976(4)	-184(2)	4667(3)	41(1)
C(1)	711(3)	1440(2)	4655(2)	28(1)
C(2)	1781(3)	1364(2)	4214(2)	28(1)
C(3)	-499(3)	2192(2)	5887(2)	26(1)
C(4)	-510(3)	2107(2)	6870(2)	31(1)
C(5)	-1529(3)	2068(2)	7187(3)	38(1)
C(6)	-2567(3)	2110(2)	6542(3)	37(1)
C(7)	-2561(3)	2223(2)	5573(3)	38(1)
C(8)	-1534(3)	2262(2)	5254(2)	33(1)
C(9)	-4841(4)	1762(4)	6030(4)	95(2)
C(10)	1942(3)	2025(2)	6439(2)	28(1)
C(11)	2624(3)	2562(2)	6868(3)	40(1)
C(12)	3451(3)	2449(2)	7693(3)	47(1)
C(13)	3622(3)	1793(2)	8090(2)	41(1)
C(14)	2965(3)	1249(2)	7658(3)	41(1)
C(15)	2133(3)	1369(2)	6842(2)	35(1)
C(16)	4840(4)	784(3)	9269(4)	70(1)
C(17)	733(3)	432(2)	2690(2)	26(1)
C(18)	306(3)	992(2)	2113(2)	31(1)
C(19)	-541(3)	906(2)	1304(2)	34(1)
C(20)	-969(3)	253(2)	1042(2)	30(1)
C(21)	-559(3)	-308(2)	1621(2)	35(1)
C(22)	274(3)	-219(2)	2434(2)	33(1)
C(23)	-2151(4)	895(2)	-620(3)	55(1)
C(24)	3180(3)	587(2)	3207(2)	30(1)
C(25)	3161(3)	659(2)	2225(3)	41(1)
C(26)	4155(3)	759(2)	1882(3)	51(1)
C(27)	5208(3)	778(2)	2515(3)	44(1)
C(28)	5234(3)	706(2)	3493(3)	45(1)
C(29)	4235(3)	611(2)	3836(3)	42(1)
C(30)	7475(4)	1182(3)	2977(3)	69(1)

Table F15. Bond lengths [Å] and angles [°] for DpPSMePE(BH_3)$_2$.

S(1)-C(9)	1.753(5)
S(1)-C(6)	1.765(3)
S(2)-C(13)	1.763(3)
S(2)-C(16)	1.792(6)
S(3)-C(20)	1.755(3)
S(3)-C(23)	1.794(4)
S(4)-C(30)	1.764(5)
S(4)-C(27)	1.766(4)
P(1)-C(10)	1.803(3)
P(1)-C(3)	1.814(3)
P(1)-C(1)	1.820(3)
P(1)-B(1)	1.913(4)
P(2)-C(17)	1.797(3)
P(2)-C(24)	1.809(3)
P(2)-C(2)	1.819(3)
P(2)-B(2)	1.907(4)
B(1)-H(1)	1.03(4)
B(1)-H(2)	1.05(4)
B(1)-H(3)	1.14(4)
B(2)-H(4)	1.08(4)
B(2)-H(5)	1.06(5)
B(2)-H(6)	1.09(5)
C(1)-C(2)	1.534(4)
C(1)-H(1A)	0.9900
C(1)-H(1B)	0.9900
C(2)-H(2A)	0.9900
C(2)-H(2B)	0.9900
C(3)-C(8)	1.385(4)
C(3)-C(4)	1.399(4)
C(4)-C(5)	1.378(5)
C(4)-H(4A)	0.9500
C(5)-C(6)	1.390(5)
C(5)-H(5A)	0.9500
C(6)-C(7)	1.388(5)
C(7)-C(8)	1.388(5)
C(7)-H(7A)	0.9500
C(8)-H(8A)	0.9500
C(9)-H(9A)	0.9800
C(9)-H(9B)	0.9800
C(9)-H(9C)	0.9800
C(10)-C(11)	1.387(5)
C(10)-C(15)	1.394(5)
C(11)-C(12)	1.391(5)
C(11)-H(11A)	0.9500

C(12)-C(13)	1.388(6)
C(12)-H(12A)	0.9500
C(13)-C(14)	1.385(5)
C(14)-C(15)	1.388(5)
C(14)-H(14A)	0.9500
C(15)-H(15A)	0.9500
C(16)-H(16A)	0.9800
C(16)-H(16B)	0.9800
C(16)-H(16C)	0.9800
C(17)-C(18)	1.393(4)
C(17)-C(22)	1.396(4)
C(18)-C(19)	1.382(5)
C(18)-H(18A)	0.9500
C(19)-C(20)	1.389(5)
C(19)-H(19A)	0.9500
C(20)-C(21)	1.391(5)
C(21)-C(22)	1.376(5)
C(21)-H(21A)	0.9500
C(22)-H(22A)	0.9500
C(23)-H(23A)	0.9800
C(23)-H(23B)	0.9800
C(23)-H(23C)	0.9800
C(24)-C(25)	1.389(5)
C(24)-C(29)	1.394(5)
C(25)-C(26)	1.380(5)
C(25)-H(25A)	0.9500
C(26)-C(27)	1.394(5)
C(26)-H(26A)	0.9500
C(27)-C(28)	1.382(6)
C(28)-C(29)	1.385(5)
C(28)-H(28A)	0.9500
C(29)-H(29A)	0.9500
C(30)-H(30B)	0.9800
C(30)-H(30C)	0.9800
C(30)-H(30D)	0.9800

C(9)-S(1)-C(6)	103.0(2)
C(13)-S(2)-C(16)	103.3(2)
C(20)-S(3)-C(23)	103.48(17)
C(30)-S(4)-C(27)	103.5(2)
C(10)-P(1)-C(3)	105.89(14)
C(10)-P(1)-C(1)	105.84(15)
C(3)-P(1)-C(1)	104.11(14)
C(10)-P(1)-B(1)	114.99(18)
C(3)-P(1)-B(1)	113.92(16)
C(1)-P(1)-B(1)	111.19(17)

C(17)-P(2)-C(24)	106.39(15)
C(17)-P(2)-C(2)	106.76(14)
C(24)-P(2)-C(2)	102.47(14)
C(17)-P(2)-B(2)	115.50(18)
C(24)-P(2)-B(2)	113.82(18)
C(2)-P(2)-B(2)	110.87(18)
P(1)-B(1)-H(1)	100(2)
P(1)-B(1)-H(2)	103(2)
H(1)-B(1)-H(2)	116(3)
P(1)-B(1)-H(3)	107(2)
H(1)-B(1)-H(3)	116(3)
H(2)-B(1)-H(3)	111(3)
P(2)-B(2)-H(4)	106(2)
P(2)-B(2)-H(5)	109(3)
H(4)-B(2)-H(5)	121(3)
P(2)-B(2)-H(6)	98(3)
H(4)-B(2)-H(6)	103(3)
H(5)-B(2)-H(6)	117(4)
C(2)-C(1)-P(1)	110.7(2)
C(2)-C(1)-H(1A)	109.5
P(1)-C(1)-H(1A)	109.5
C(2)-C(1)-H(1B)	109.5
P(1)-C(1)-H(1B)	109.5
H(1A)-C(1)-H(1B)	108.1
C(1)-C(2)-P(2)	112.5(2)
C(1)-C(2)-H(2A)	109.1
P(2)-C(2)-H(2A)	109.1
C(1)-C(2)-H(2B)	109.1
P(2)-C(2)-H(2B)	109.1
H(2A)-C(2)-H(2B)	107.8
C(8)-C(3)-C(4)	118.3(3)
C(8)-C(3)-P(1)	119.3(2)
C(4)-C(3)-P(1)	122.4(2)
C(5)-C(4)-C(3)	120.4(3)
C(5)-C(4)-H(4A)	119.8
C(3)-C(4)-H(4A)	119.8
C(4)-C(5)-C(6)	121.1(3)
C(4)-C(5)-H(5A)	119.5
C(6)-C(5)-H(5A)	119.5
C(7)-C(6)-C(5)	118.7(3)
C(7)-C(6)-S(1)	125.0(3)
C(5)-C(6)-S(1)	116.3(3)
C(6)-C(7)-C(8)	120.2(3)
C(6)-C(7)-H(7A)	119.9
C(8)-C(7)-H(7A)	119.9
C(3)-C(8)-C(7)	121.2(3)

C(3)-C(8)-H(8A)	119.4
C(7)-C(8)-H(8A)	119.4
S(1)-C(9)-H(9A)	109.5
S(1)-C(9)-H(9B)	109.5
H(9A)-C(9)-H(9B)	109.5
S(1)-C(9)-H(9C)	109.5
H(9A)-C(9)-H(9C)	109.5
H(9B)-C(9)-H(9C)	109.5
C(11)-C(10)-C(15)	118.2(3)
C(11)-C(10)-P(1)	119.3(3)
C(15)-C(10)-P(1)	122.5(2)
C(10)-C(11)-C(12)	120.5(4)
C(10)-C(11)-H(11A)	119.7
C(12)-C(11)-H(11A)	119.7
C(13)-C(12)-C(11)	120.5(3)
C(13)-C(12)-H(12A)	119.7
C(11)-C(12)-H(12A)	119.7
C(14)-C(13)-C(12)	119.6(3)
C(14)-C(13)-S(2)	123.0(3)
C(12)-C(13)-S(2)	117.4(3)
C(13)-C(14)-C(15)	119.4(4)
C(13)-C(14)-H(14A)	120.3
C(15)-C(14)-H(14A)	120.3
C(14)-C(15)-C(10)	121.7(3)
C(14)-C(15)-H(15A)	119.1
C(10)-C(15)-H(15A)	119.1
S(2)-C(16)-H(16A)	109.5
S(2)-C(16)-H(16B)	109.5
H(16A)-C(16)-H(16B)	109.5
S(2)-C(16)-H(16C)	109.5
H(16A)-C(16)-H(16C)	109.5
H(16B)-C(16)-H(16C)	109.5
C(18)-C(17)-C(22)	118.3(3)
C(18)-C(17)-P(2)	122.4(2)
C(22)-C(17)-P(2)	119.2(2)
C(19)-C(18)-C(17)	121.0(3)
C(19)-C(18)-H(18A)	119.5
C(17)-C(18)-H(18A)	119.5
C(18)-C(19)-C(20)	120.2(3)
C(18)-C(19)-H(19A)	119.9
C(20)-C(19)-H(19A)	119.9
C(19)-C(20)-C(21)	119.1(3)
C(19)-C(20)-S(3)	123.8(3)
C(21)-C(20)-S(3)	117.1(2)
C(22)-C(21)-C(20)	120.5(3)
C(22)-C(21)-H(21A)	119.7

C(20)-C(21)-H(21A)	119.7
C(21)-C(22)-C(17)	120.8(3)
C(21)-C(22)-H(22A)	119.6
C(17)-C(22)-H(22A)	119.6
S(3)-C(23)-H(23A)	109.5
S(3)-C(23)-H(23B)	109.5
H(23A)-C(23)-H(23B)	109.5
S(3)-C(23)-H(23C)	109.5
H(23A)-C(23)-H(23C)	109.5
H(23B)-C(23)-H(23C)	109.5
C(25)-C(24)-C(29)	118.1(3)
C(25)-C(24)-P(2)	122.8(3)
C(29)-C(24)-P(2)	119.0(3)
C(26)-C(25)-C(24)	121.0(3)
C(26)-C(25)-H(25A)	119.5
C(24)-C(25)-H(25A)	119.5
C(25)-C(26)-C(27)	120.6(4)
C(25)-C(26)-H(26A)	119.7
C(27)-C(26)-H(26A)	119.7
C(28)-C(27)-C(26)	118.8(3)
C(28)-C(27)-S(4)	124.1(3)
C(26)-C(27)-S(4)	117.1(3)
C(27)-C(28)-C(29)	120.5(3)
C(27)-C(28)-H(28A)	119.7
C(29)-C(28)-H(28A)	119.7
C(28)-C(29)-C(24)	121.0(3)
C(28)-C(29)-H(29A)	119.5
C(24)-C(29)-H(29A)	119.5
S(4)-C(30)-H(30B)	109.5
S(4)-C(30)-H(30C)	109.5
H(30B)-C(30)-H(30C)	109.5
S(4)-C(30)-H(30D)	109.5
H(30B)-C(30)-H(30D)	109.5
H(30C)-C(30)-H(30D)	109.5

Symmetry transformations used to generate equivalent atoms:

Table F16. Anisotropic displacement parameters ($Å^2 x\ 10^3$)for DpPSMePE(BH_3)$_2$. The anisotropic displacement factor exponent takes the form: $-2\pi^2[\ h^2 a^{*2} U^{11} + ... + 2\ h\ k\ a^*\ b^*\ U^{12}\ ]$

	U^{11}	U^{22}	U^{33}	U^{23}	U^{13}	U^{12}
S(1)	41(1)	95(1)	62(1)	-15(1)	28(1)	-10(1)
S(2)	41(1)	87(1)	43(1)	-6(1)	-9(1)	3(1)
S(3)	39(1)	45(1)	36(1)	-6(1)	-3(1)	-9(1)
S(4)	36(1)	114(1)	56(1)	-26(1)	20(1)	-16(1)
P(1)	24(1)	28(1)	25(1)	-2(1)	6(1)	0(1)
P(2)	24(1)	27(1)	30(1)	-2(1)	4(1)	2(1)
B(1)	41(2)	32(2)	38(2)	5(2)	16(2)	-1(2)
B(2)	42(2)	38(2)	42(2)	9(2)	5(2)	6(2)
C(1)	24(2)	32(2)	30(2)	-7(1)	7(1)	-2(1)
C(2)	25(2)	31(2)	28(2)	-5(1)	6(1)	-2(1)
C(3)	28(2)	23(2)	30(2)	0(1)	8(1)	1(1)
C(4)	32(2)	33(2)	29(2)	-3(1)	6(1)	2(1)
C(5)	40(2)	44(2)	31(2)	-5(2)	15(2)	-1(2)
C(6)	33(2)	39(2)	44(2)	-7(2)	17(2)	1(2)
C(7)	25(2)	42(2)	46(2)	1(2)	4(2)	2(1)
C(8)	30(2)	39(2)	31(2)	2(1)	6(1)	0(1)
C(9)	48(3)	167(7)	76(4)	-11(4)	26(3)	-39(3)
C(10)	22(2)	35(2)	29(2)	-6(1)	7(1)	1(1)
C(11)	32(2)	36(2)	48(2)	-10(2)	1(2)	0(2)
C(12)	30(2)	56(2)	49(2)	-24(2)	-3(2)	-3(2)
C(13)	27(2)	66(3)	31(2)	-5(2)	5(1)	6(2)
C(14)	32(2)	54(2)	35(2)	8(2)	4(2)	0(2)
C(15)	30(2)	41(2)	34(2)	2(2)	2(1)	-2(1)
C(16)	52(3)	87(4)	63(3)	24(3)	-9(2)	-3(2)
C(17)	23(2)	27(2)	30(2)	-4(1)	7(1)	-1(1)
C(18)	29(2)	25(2)	37(2)	-3(1)	3(1)	-4(1)
C(19)	30(2)	32(2)	38(2)	3(1)	2(1)	-1(1)
C(20)	25(2)	37(2)	29(2)	-6(1)	7(1)	-4(1)
C(21)	37(2)	28(2)	40(2)	-6(1)	6(2)	-8(1)
C(22)	36(2)	26(2)	36(2)	0(1)	7(1)	-2(1)
C(23)	53(2)	56(3)	48(2)	6(2)	-11(2)	-6(2)
C(24)	24(2)	30(2)	36(2)	-6(1)	6(1)	4(1)
C(25)	29(2)	58(2)	36(2)	-16(2)	4(2)	-1(2)
C(26)	39(2)	79(3)	36(2)	-17(2)	12(2)	-4(2)
C(27)	31(2)	56(2)	48(2)	-18(2)	13(2)	-5(2)
C(28)	28(2)	57(2)	48(2)	-2(2)	4(2)	1(2)
C(29)	30(2)	57(2)	37(2)	6(2)	4(2)	2(2)
C(30)	36(2)	114(4)	58(3)	9(3)	10(2)	-20(2)

Table F17. Hydrogen coordinates (x 10^4) and isotropic displacement parameters ($Å^2$x 10^3) for DpPSMePE$(BH_3)_2$.

	x	y	z	U(eq)
H(1A)	620	1025	5042	34
H(1B)	29	1478	4132	34
H(2A)	2466	1452	4720	34
H(2B)	1763	1715	3703	34
H(4A)	190	2075	7321	37
H(5A)	-1523	2013	7856	45
H(7A)	-3262	2275	5127	46
H(8A)	-1542	2339	4588	40
H(9A)	-5572	1686	6230	143
H(9B)	-4604	1337	5748	143
H(9C)	-4926	2132	5548	143
H(11A)	2526	3011	6595	48
H(12A)	3902	2823	7988	56
H(14A)	3083	797	7918	49
H(15A)	1681	994	6550	42
H(16A)	5417	679	9845	105
H(16B)	5083	596	8697	105
H(16C)	4110	577	9332	105
H(18A)	603	1440	2278	37
H(19A)	-832	1295	926	41
H(21A)	-857	-755	1455	42
H(22A)	541	-607	2826	39
H(23A)	-2717	851	-1221	83
H(23B)	-1415	1032	-771	83
H(23C)	-2405	1246	-209	83
H(25A)	2452	640	1782	50
H(26A)	4123	816	1209	61
H(28A)	5944	723	3934	54
H(29A)	4268	560	4511	50
H(30B)	8195	1258	2759	104
H(30C)	7589	837	3494	104
H(30D)	7218	1616	3220	104
H(1)	280(40)	3010(20)	4200(30)	57(12)
H(2)	1780(40)	2920(20)	4470(30)	59(12)
H(3)	1120(30)	3470(20)	5240(30)	56(12)
H(4)	1170(40)	-170(20)	4910(30)	51(11)
H(5)	2270(40)	-650(30)	4410(30)	71(14)
H(6)	2560(40)	80(30)	5240(40)	80(15)

Table F18. Torsion angles [°] for DpPSMePE(BH_3)$_2$.

C(10)-P(1)-C(1)-C(2)	-67.5(2)
C(3)-P(1)-C(1)-C(2)	-178.9(2)
B(1)-P(1)-C(1)-C(2)	58.1(3)
P(1)-C(1)-C(2)-P(2)	165.30(16)
C(17)-P(2)-C(2)-C(1)	66.2(3)
C(24)-P(2)-C(2)-C(1)	177.9(2)
B(2)-P(2)-C(2)-C(1)	-60.3(3)
C(10)-P(1)-C(3)-C(8)	-175.3(3)
C(1)-P(1)-C(3)-C(8)	-63.9(3)
B(1)-P(1)-C(3)-C(8)	57.4(3)
C(10)-P(1)-C(3)-C(4)	4.0(3)
C(1)-P(1)-C(3)-C(4)	115.3(3)
B(1)-P(1)-C(3)-C(4)	-123.4(3)
C(8)-C(3)-C(4)-C(5)	2.4(5)
P(1)-C(3)-C(4)-C(5)	-176.8(3)
C(3)-C(4)-C(5)-C(6)	0.3(5)
C(4)-C(5)-C(6)-C(7)	-3.0(5)
C(4)-C(5)-C(6)-S(1)	176.1(3)
C(9)-S(1)-C(6)-C(7)	20.1(4)
C(9)-S(1)-C(6)-C(5)	-158.9(4)
C(5)-C(6)-C(7)-C(8)	2.9(5)
S(1)-C(6)-C(7)-C(8)	-176.0(3)
C(4)-C(3)-C(8)-C(7)	-2.5(5)
P(1)-C(3)-C(8)-C(7)	176.8(3)
C(6)-C(7)-C(8)-C(3)	-0.2(5)
C(3)-P(1)-C(10)-C(11)	-103.2(3)
C(1)-P(1)-C(10)-C(11)	146.7(3)
B(1)-P(1)-C(10)-C(11)	23.5(3)
C(3)-P(1)-C(10)-C(15)	74.3(3)
C(1)-P(1)-C(10)-C(15)	-35.9(3)
B(1)-P(1)-C(10)-C(15)	-159.0(3)
C(15)-C(10)-C(11)-C(12)	-1.9(5)
P(1)-C(10)-C(11)-C(12)	175.7(3)
C(10)-C(11)-C(12)-C(13)	1.3(6)
C(11)-C(12)-C(13)-C(14)	0.1(6)
C(11)-C(12)-C(13)-S(2)	-179.2(3)
C(16)-S(2)-C(13)-C(14)	12.5(4)
C(16)-S(2)-C(13)-C(12)	-168.2(3)
C(12)-C(13)-C(14)-C(15)	-0.9(5)
S(2)-C(13)-C(14)-C(15)	178.3(3)
C(13)-C(14)-C(15)-C(10)	0.3(5)
C(11)-C(10)-C(15)-C(14)	1.1(5)
P(1)-C(10)-C(15)-C(14)	-176.4(3)
C(24)-P(2)-C(17)-C(18)	-75.8(3)

C(2)-P(2)-C(17)-C(18)	33.1(3)
B(2)-P(2)-C(17)-C(18)	156.8(3)
C(24)-P(2)-C(17)-C(22)	100.6(3)
C(2)-P(2)-C(17)-C(22)	-150.5(3)
B(2)-P(2)-C(17)-C(22)	-26.8(3)
C(22)-C(17)-C(18)-C(19)	-0.5(5)
P(2)-C(17)-C(18)-C(19)	175.9(3)
C(17)-C(18)-C(19)-C(20)	-1.2(5)
C(18)-C(19)-C(20)-C(21)	2.1(5)
C(18)-C(19)-C(20)-S(3)	-177.1(3)
C(23)-S(3)-C(20)-C(19)	6.9(3)
C(23)-S(3)-C(20)-C(21)	-172.2(3)
C(19)-C(20)-C(21)-C(22)	-1.2(5)
S(3)-C(20)-C(21)-C(22)	178.0(3)
C(20)-C(21)-C(22)-C(17)	-0.5(5)
C(18)-C(17)-C(22)-C(21)	1.4(5)
P(2)-C(17)-C(22)-C(21)	-175.1(3)
C(17)-P(2)-C(24)-C(25)	7.8(3)
C(2)-P(2)-C(24)-C(25)	-104.1(3)
B(2)-P(2)-C(24)-C(25)	136.1(3)
C(17)-P(2)-C(24)-C(29)	-175.8(3)
C(2)-P(2)-C(24)-C(29)	72.3(3)
B(2)-P(2)-C(24)-C(29)	-47.4(3)
C(29)-C(24)-C(25)-C(26)	-0.7(6)
P(2)-C(24)-C(25)-C(26)	175.8(3)
C(24)-C(25)-C(26)-C(27)	1.1(6)
C(25)-C(26)-C(27)-C(28)	-1.1(6)
C(25)-C(26)-C(27)-S(4)	178.3(3)
C(30)-S(4)-C(27)-C(28)	-20.5(4)
C(30)-S(4)-C(27)-C(26)	160.1(4)
C(26)-C(27)-C(28)-C(29)	0.6(6)
S(4)-C(27)-C(28)-C(29)	-178.7(3)
C(27)-C(28)-C(29)-C(24)	-0.2(6)
C(25)-C(24)-C(29)-C(28)	0.3(5)
P(2)-C(24)-C(29)-C(28)	-176.4(3)

Symmetry transformations used to generate equivalent atoms:

F.4. Crystallographic data for DpPSMePE

Table F19. Crystal data and structure refinement for DpPSMePE.

Identification code	DpPSMePE	
Empirical formula	C30 H32 P2 S4	
Formula weight	582.74	
Temperature	173(2) K	
Wavelength	0.71073 Å	
Crystal system	Monoclinic	
Space group	P2(1)/c	
Unit cell dimensions	a = 11.6057(19) Å	α= 90°.
	b = 5.2265(9) Å	β= 94.509(3)°.
	c = 24.290(4) Å	γ = 90°.
Volume	1468.8(4) $Å^3$	
Z	2	
Density (calculated)	1.318 Mg/m^3	
Absorption coefficient	0.451 mm^{-1}	
F(000)	612	
Crystal size	0.41 x 0.09 x 0.08 mm^3	
Theta range for data collection	1.68 to 27.00°.	
Index ranges	-14<=h<=14, -6<=k<=6, -30<=l<=30	
Reflections collected	15581	
Independent reflections	3203 [R(int) = 0.0333]	
Completeness to theta = 27.00°	99.8 %	
Absorption correction	Semi-empirical from equivalents	
Max. and min. transmission	0.9648 and 0.8366	
Refinement method	Full-matrix least-squares on F^2	
Data / restraints / parameters	3203 / 0 / 227	
Goodness-of-fit on F^2	1.071	
Final R indices [I>2sigma(I)]	R1 = 0.0432, wR2 = 0.1003	
R indices (all data)	R1 = 0.0573, wR2 = 0.1093	
Largest diff. peak and hole	0.380 and -0.181 $e.Å^{-3}$	

Table F20. Atomic coordinates (x 10^4) and equivalent isotropic displacement parameters ($Å^2$x 10^3) for DpPSMePE. U(eq) is defined as one third of the trace of the orthogonalized U^{ij} tensor.

	x	y	z	U(eq)
P(1)	3831(1)	2697(1)	499(1)	30(1)
S(1)	7340(1)	4612(2)	2616(1)	68(1)
S(2)	-1111(1)	6518(2)	1163(1)	61(1)
C(1)	4377(2)	5258(4)	62(1)	33(1)
C(2)	4753(2)	3192(4)	1135(1)	32(1)
C(3)	5660(2)	1510(4)	1248(1)	37(1)
C(4)	6470(2)	1856(5)	1696(1)	44(1)
C(5)	6370(2)	3915(5)	2042(1)	42(1)
C(6)	5436(2)	5583(5)	1944(1)	48(1)
C(7)	4645(2)	5230(4)	1498(1)	43(1)
C(8)	8482(3)	2335(8)	2554(2)	86(1)
C(9)	2455(2)	4028(4)	681(1)	32(1)
C(10)	1869(2)	2759(5)	1077(1)	44(1)
C(11)	798(2)	3557(5)	1213(1)	50(1)
C(12)	258(2)	5635(4)	957(1)	39(1)
C(13)	817(2)	6885(5)	556(1)	51(1)
C(14)	1902(2)	6096(5)	423(1)	50(1)
C(15)	-1565(2)	8987(7)	682(1)	62(1)

Table F21. Bond lengths [Å] and angles [°] for DpPSMePE.

P(1)-C(2)	1.827(2)
P(1)-C(9)	1.8284(19)
P(1)-C(1)	1.850(2)
S(1)-C(5)	1.759(2)
S(1)-C(8)	1.797(4)
S(2)-C(12)	1.765(2)
S(2)-C(15)	1.792(3)
C(1)-C(1)#1	1.525(4)
C(1)-H(1A)	0.93(2)
C(1)-H(1B)	0.96(2)
C(2)-C(3)	1.383(3)
C(2)-C(7)	1.395(3)
C(3)-C(4)	1.392(3)
C(3)-H(3)	0.92(2)
C(4)-C(5)	1.376(3)
C(4)-H(4)	0.94(3)
C(5)-C(6)	1.397(3)
C(6)-C(7)	1.376(3)
C(6)-H(6)	0.92(3)
C(7)-H(7)	0.96(2)
C(8)-H(8A)	0.90(4)
C(8)-H(8B)	0.93(4)
C(8)-H(8C)	1.07(4)
C(9)-C(14)	1.382(3)
C(9)-C(10)	1.388(3)
C(10)-C(11)	1.377(3)
C(10)-H(10)	0.89(3)
C(11)-C(12)	1.378(3)
C(11)-H(11)	0.86(3)
C(12)-C(13)	1.376(3)
C(13)-C(14)	1.388(3)
C(13)-H(13)	0.95(2)
C(14)-H(14)	0.93(3)
C(15)-H(15A)	1.03(4)
C(15)-H(15B)	0.96(3)
C(15)-H(15C)	0.99(3)
C(2)-P(1)-C(9)	101.89(9)
C(2)-P(1)-C(1)	100.22(9)
C(9)-P(1)-C(1)	102.05(9)
C(5)-S(1)-C(8)	103.15(14)
C(12)-S(2)-C(15)	103.18(12)
C(1)#1-C(1)-P(1)	111.03(18)
C(1)#1-C(1)-H(1A)	109.2(13)

P(1)-C(1)-H(1A)	106.8(12)
C(1)#1-C(1)-H(1B)	113.3(12)
P(1)-C(1)-H(1B)	108.4(11)
H(1A)-C(1)-H(1B)	107.9(17)
C(3)-C(2)-C(7)	117.63(19)
C(3)-C(2)-P(1)	117.70(15)
C(7)-C(2)-P(1)	124.57(16)
C(2)-C(3)-C(4)	122.0(2)
C(2)-C(3)-H(3)	119.2(14)
C(4)-C(3)-H(3)	118.7(14)
C(5)-C(4)-C(3)	119.7(2)
C(5)-C(4)-H(4)	120.7(15)
C(3)-C(4)-H(4)	119.7(15)
C(4)-C(5)-C(6)	119.0(2)
C(4)-C(5)-S(1)	124.51(19)
C(6)-C(5)-S(1)	116.49(17)
C(7)-C(6)-C(5)	120.8(2)
C(7)-C(6)-H(6)	117.9(16)
C(5)-C(6)-H(6)	121.1(16)
C(6)-C(7)-C(2)	120.9(2)
C(6)-C(7)-H(7)	119.3(14)
C(2)-C(7)-H(7)	119.8(14)
S(1)-C(8)-H(8A)	102(2)
S(1)-C(8)-H(8B)	110(3)
H(8A)-C(8)-H(8B)	110(3)
S(1)-C(8)-H(8C)	105(2)
H(8A)-C(8)-H(8C)	112(3)
H(8B)-C(8)-H(8C)	116(3)
C(14)-C(9)-C(10)	116.93(19)
C(14)-C(9)-P(1)	124.80(16)
C(10)-C(9)-P(1)	118.05(16)
C(11)-C(10)-C(9)	121.5(2)
C(11)-C(10)-H(10)	118.9(16)
C(9)-C(10)-H(10)	119.6(16)
C(10)-C(11)-C(12)	121.2(2)
C(10)-C(11)-H(11)	117.5(18)
C(12)-C(11)-H(11)	121.2(18)
C(13)-C(12)-C(11)	118.1(2)
C(13)-C(12)-S(2)	124.19(18)
C(11)-C(12)-S(2)	117.73(17)
C(12)-C(13)-C(14)	120.7(2)
C(12)-C(13)-H(13)	121.0(14)
C(14)-C(13)-H(13)	118.3(14)
C(9)-C(14)-C(13)	121.6(2)
C(9)-C(14)-H(14)	120.0(16)
C(13)-C(14)-H(14)	118.1(16)

S(2)-C(15)-H(15A)	115.4(19)
S(2)-C(15)-H(15B)	103.1(18)
H(15A)-C(15)-H(15B)	114(3)
S(2)-C(15)-H(15C)	110.3(17)
H(15A)-C(15)-H(15C)	103(2)
H(15B)-C(15)-H(15C)	111(2)

Symmetry transformations used to generate equivalent atoms:
#1 -x+1,-y+1,-z

Table F22. Anisotropic displacement parameters ($Å^2 x\ 10^3$) for DpPSMePE. The anisotropic displacement factor exponent takes the form: $-2\pi^2[\ h^2 a^{*2} U^{11} + ... + 2\ h\ k\ a^*\ b^*\ U^{12}\ ]$

	U^{11}	U^{22}	U^{33}	U^{23}	U^{13}	U^{12}
P(1)	29(1)	28(1)	34(1)	-1(1)	3(1)	2(1)
S(1)	70(1)	94(1)	37(1)	-3(1)	-10(1)	-30(1)
S(2)	36(1)	85(1)	62(1)	-1(1)	18(1)	11(1)
C(1)	31(1)	33(1)	35(1)	-1(1)	7(1)	5(1)
C(2)	31(1)	31(1)	34(1)	1(1)	6(1)	-2(1)
C(3)	37(1)	39(1)	36(1)	-4(1)	2(1)	3(1)
C(4)	38(1)	55(1)	39(1)	4(1)	-1(1)	1(1)
C(5)	43(1)	54(1)	29(1)	1(1)	4(1)	-17(1)
C(6)	56(2)	49(1)	41(1)	-13(1)	8(1)	-9(1)
C(7)	43(1)	39(1)	46(1)	-7(1)	5(1)	2(1)
C(8)	76(2)	109(3)	66(2)	20(2)	-37(2)	-18(2)
C(9)	30(1)	32(1)	33(1)	-3(1)	3(1)	-1(1)
C(10)	40(1)	53(1)	40(1)	13(1)	7(1)	8(1)
C(11)	41(1)	68(2)	42(1)	14(1)	15(1)	4(1)
C(12)	28(1)	50(1)	39(1)	-8(1)	3(1)	2(1)
C(13)	38(1)	49(1)	66(2)	14(1)	12(1)	13(1)
C(14)	40(1)	47(1)	64(2)	18(1)	20(1)	10(1)
C(15)	36(1)	87(2)	63(2)	-15(2)	-1(1)	21(1)

Table F23. Hydrogen coordinates (x 10^4) and isotropic displacement parameters ($Å^2$x 10^3) for DpPSMePE.

	x	y	z	U(eq)
H(1A)	3909(18)	5260(40)	-267(9)	32(5)
H(1B)	4277(16)	6870(40)	242(8)	27(5)
H(3)	5717(19)	80(40)	1030(10)	45(6)
H(4)	7090(20)	690(50)	1757(10)	57(7)
H(6)	5360(20)	7020(50)	2156(11)	55(7)
H(7)	4010(20)	6400(50)	1439(9)	49(7)
H(8A)	9000(30)	2790(70)	2834(16)	106(12)
H(8B)	8800(30)	2550(80)	2219(18)	124(16)
H(8C)	8100(30)	510(80)	2624(15)	116(13)
H(10)	2190(20)	1370(50)	1243(10)	55(7)
H(11)	470(20)	2680(50)	1457(12)	66(8)
H(13)	480(20)	8350(50)	373(9)	50(7)
H(14)	2290(20)	7110(50)	180(11)	67(8)
H(15A)	-1050(30)	10590(70)	691(13)	96(11)
H(15B)	-2340(30)	9320(60)	765(12)	83(9)
H(15C)	-1540(20)	8360(60)	298(13)	74(9)

Table F24. Torsion angles [°] for DpPSMePE.

C(2)-P(1)-C(1)-C(1)#1	66.1(2)
C(9)-P(1)-C(1)-C(1)#1	170.7(2)
C(9)-P(1)-C(2)-C(3)	151.80(16)
C(1)-P(1)-C(2)-C(3)	-103.45(16)
C(9)-P(1)-C(2)-C(7)	-31.88(19)
C(1)-P(1)-C(2)-C(7)	72.88(19)
C(7)-C(2)-C(3)-C(4)	-2.3(3)
P(1)-C(2)-C(3)-C(4)	174.29(17)
C(2)-C(3)-C(4)-C(5)	0.6(3)
C(3)-C(4)-C(5)-C(6)	1.6(3)
C(3)-C(4)-C(5)-S(1)	-178.99(16)
C(8)-S(1)-C(5)-C(4)	7.4(2)
C(8)-S(1)-C(5)-C(6)	-173.2(2)
C(4)-C(5)-C(6)-C(7)	-2.1(3)
S(1)-C(5)-C(6)-C(7)	178.50(18)
C(5)-C(6)-C(7)-C(2)	0.3(3)
C(3)-C(2)-C(7)-C(6)	1.8(3)
P(1)-C(2)-C(7)-C(6)	-174.48(18)
C(2)-P(1)-C(9)-C(14)	117.8(2)
C(1)-P(1)-C(9)-C(14)	14.5(2)
C(2)-P(1)-C(9)-C(10)	-67.67(18)
C(1)-P(1)-C(9)-C(10)	-170.98(17)
C(14)-C(9)-C(10)-C(11)	-1.2(4)
P(1)-C(9)-C(10)-C(11)	-176.20(19)
C(9)-C(10)-C(11)-C(12)	0.8(4)
C(10)-C(11)-C(12)-C(13)	0.4(4)
C(10)-C(11)-C(12)-S(2)	-179.6(2)
C(15)-S(2)-C(12)-C(13)	6.5(2)
C(15)-S(2)-C(12)-C(11)	-173.4(2)
C(11)-C(12)-C(13)-C(14)	-1.1(4)
S(2)-C(12)-C(13)-C(14)	179.0(2)
C(10)-C(9)-C(14)-C(13)	0.5(4)
P(1)-C(9)-C(14)-C(13)	175.1(2)
C(12)-C(13)-C(14)-C(9)	0.7(4)

Symmetry transformations used to generate equivalent atoms:
#1 -x+1,-y+1,-z

F.5. Crystal Structure Report for *trans*-$Pd^{II}(Cl)_2(^iPrJPhos)_2$

Table F25. Data collection details for *trans*-$Pd^{II}(Cl)_2(^iPrJPhos)_2$. A yellow block-like specimen of $C_{36}H_{46}Cl_2P_2Pd$, approximate dimensions 0.070 mm x 0.130 mm x 0.140 mm, was used for the X-ray crystallographic analysis. The X-ray intensity data were measured.

Axis	dx/mm	2θ/°	ω/°	φ/°	χ/°	Width/°	Frames	Time/s	Wavelength/Å	Voltage/kV	Current/mA	Temperature/K
Omega	49.853	26.56	13.62	0.00	-54.74	1.00	133	5.00	0.71073	50	30.0	296.15
Omega	49.853	26.56	13.62	-105.00	-54.74	1.00	133	5.00	0.71073	50	30.0	296.15
Omega	49.853	26.56	13.62	102.00	-54.74	1.00	133	5.00	0.71073	50	30.0	296.15
Omega	49.853	26.56	13.62	153.00	-54.74	1.00	133	5.00	0.71073	50	30.0	296.15
Omega	49.853	26.56	-51.34	0.00	64.88	1.00	89	5.00	0.71073	50	30.0	296.15
Phi	49.853	26.56	281.38	0.00	23.00	1.00	360	5.00	0.71073	50	30.0	296.15
Omega	49.853	26.56	13.62	51.00	-54.74	1.00	133	5.00	0.71073	50	30.0	296.15

A total of 1114 frames were collected. The total exposure time was 1.55 hours. The frames were integrated with the Bruker SAINT software package using a narrow-frame algorithm. The integration of the data using a triclinic unit cell yielded a total of 35568 reflections to a maximum θ angle of 28.16° (0.75 Å resolution), of which 8457 were independent (average redundancy 4.206, completeness = 99.5%, R_{int} = 9.71%, R_{sig} = 9.64%) and 5329 (63.01%) were greater than $2\sigma(F^2)$. The final cell constants of $\underline{a}$ = 11.0565(18) Å, $\underline{b}$ = 12.827(2) Å, $\underline{c}$ = 13.891(2) Å, α = 71.824(3)°, β = 73.300(3)°, γ = 70.806(3)°, volume = 1729.8(5) $Å^3$, are based upon the refinement of the XYZ-centroids of 3365 reflections above 20 σ(I) with 4.542° < 2θ < 44.20°. Data were corrected for absorption effects using the multi-scan method (SADABS). The ratio of minimum to

maximum apparent transmission was 0.945. The calculated minimum and maximum transmission coefficients (based on crystal size) are 0.8950 and 0.9460.

The final anisotropic full-matrix least-squares refinement on F^2 with 370 variables converged at R1 = 4.66%, for the observed data and wR2 = 9.84% for all data. The goodness-of-fit was 1.017. The largest peak in the final difference electron density synthesis was 0.559 $e^-/Å^3$ and the largest hole was -0.986 $e^-/Å^3$ with an RMS deviation of 0.113 $e^-/Å^3$. On the basis of the final model, the calculated density was 1.378 g/cm^3 and F(000), 744 e^-.

Table F26. Sample and crystal data for *trans*-$Pd^{II}(Cl)_2(^iPrJPhos)_2$.

Identification code	*trans*-$Pd^{II}(Cl)_2(^iPrJPhos)_2$	
Chemical formula	$C_{36}H_{46}Cl_2P_2Pd$	
Formula weight	717.97	
Temperature	173(2) K	
Wavelength	0.71073 Å	
Crystal size	0.070 x 0.130 x 0.140 mm	
Crystal habit	yellow block	
Crystal system	triclinic	
Space group	P -1	
Unit cell dimensions	a = 11.0565(18) Å	α = 71.824(3)°
	b = 12.827(2) Å	β = 73.300(3)°
	c = 13.891(2) Å	γ = 70.806(3)°
Volume	1729.8(5) $Å^3$	
Z	2	

Density (calculated)	1.378 g/cm^3
Absorption coefficient	0.807 mm^{-1}
F(000)	744

Table F27. Data collection and structure refinement for *trans*-Pd^{II}(Cl)$_2$(^{i}PrJPhos)$_2$.

Theta range for data collection	1.58 to 28.16°	
Index ranges	-14<=h<=14, -17<=k<=16, -18<=l<=18	
Reflections collected	35568	
Independent reflections	8457 [R(int) = 0.0971]	
Coverage of independent reflections	99.5%	
Absorption correction	multi-scan	
Max. and min. transmission	0.9460 and 0.8950	
Refinement method	Full-matrix least-squares on F^2	
Refinement program	SHELXL-2013 (Sheldrick, 2013)	
Function minimized	$\Sigma\, w(F_o^2 - F_c^2)^2$	
Data / restraints / parameters	8457 / 0 / 370	
Goodness-of-fit on F^2	1.017	
Final R indices	5329 data; I>2σ(I)	R1 = 0.0466, wR2 = 0.0820
	all data	R1 = 0.0955, wR2 = 0.0984
Weighting scheme	$w=1/[\sigma^2(F_o^2)+(0.0309P)^2]$ where $P=(F_o^2+2F_c^2)/3$	

Largest diff. peak and hole	0.559 and -0.986 eÅ^{-3}
R.M.S. deviation from mean	0.113 eÅ^{-3}

Table F28. Atomic coordinates and equivalent isotropic atomic displacement parameters (Å^2) for *trans*-Pd^{II}(Cl)$_2$(^{i}PrJPhos)$_2$. U(eq) is defined as one third of the trace of the orthogonalized U_{ij} tensor.

	x/a	y/b	z/c	U(eq)
Pd1	0.22964(3)	0.19559(3)	0.76900(2)	0.01848(9)
Cl1	0.05096(9)	0.19132(8)	0.90700(7)	0.0259(2)
Cl2	0.41019(9)	0.19678(8)	0.63404(7)	0.0277(2)
P1	0.27304(9)	0.34226(8)	0.81095(7)	0.0179(2)
P2	0.19222(9)	0.03792(8)	0.74079(7)	0.0182(2)
C1	0.3413(3)	0.4428(3)	0.6985(3)	0.0213(8)
C2	0.2684(3)	0.4785(3)	0.6206(3)	0.0233(9)
C3	0.2848(4)	0.5697(3)	0.5363(3)	0.0254(9)
C4	0.3759(3)	0.6274(3)	0.5275(3)	0.0237(9)
C5	0.4513(3)	0.5910(3)	0.6027(3)	0.0224(8)
C6	0.4372(3)	0.4996(3)	0.6875(3)	0.0183(8)
C7	0.5319(3)	0.4651(3)	0.7577(3)	0.0198(8)
C8	0.5222(4)	0.5305(3)	0.8251(3)	0.0269(9)
C9	0.6159(4)	0.5006(4)	0.8844(3)	0.0322(10)
C10	0.7220(4)	0.4065(4)	0.8764(3)	0.0301(10)
C11	0.7352(4)	0.3415(3)	0.8088(3)	0.0295(9)
C12	0.6409(3)	0.3720(3)	0.7495(3)	0.0244(9)
C13	0.3772(3)	0.2756(3)	0.9097(3)	0.0229(8)

	x/a	y/b	z/c	U(eq)
C14	0.4839(4)	0.1714(3)	0.8793(3)	0.0338(10)
C15	0.2966(4)	0.2401(4)	0.0186(3)	0.0382(11)
C16	0.1289(3)	0.4406(3)	0.8731(3)	0.0257(9)
C17	0.0214(4)	0.4967(4)	0.8093(3)	0.0361(11)
C18	0.1671(4)	0.5316(4)	0.8999(3)	0.0369(11)
C19	0.0264(3)	0.0650(3)	0.7177(3)	0.0190(8)
C20	0.9334(3)	0.0166(3)	0.7953(3)	0.0253(9)
C21	0.8118(4)	0.0264(3)	0.7793(3)	0.0314(10)
C22	0.7797(4)	0.0845(3)	0.6838(3)	0.0309(10)
C23	0.8675(3)	0.1371(3)	0.6071(3)	0.0255(9)
C24	0.9909(3)	0.1298(3)	0.6226(3)	0.0189(8)
C25	0.0729(4)	0.1959(4)	0.5342(3)	0.0325(10)
C26	0.1116(5)	0.1692(4)	0.4374(3)	0.0481(13)
C27	0.1793(5)	0.2331(5)	0.3531(4)	0.0696(18)
C28	0.2082(5)	0.3245(6)	0.3640(4)	0.080(2)
C29	0.1688(7)	0.3527(6)	0.4578(5)	0.088(2)
C30	0.1010(5)	0.2881(5)	0.5437(4)	0.0587(16)
C31	0.3068(3)	0.9805(3)	0.6301(3)	0.0240(9)
C32	0.2583(4)	0.9055(3)	0.5891(3)	0.0319(10)
C33	0.4449(3)	0.9178(3)	0.6515(3)	0.0329(10)
C34	0.1979(4)	0.9240(3)	0.8619(3)	0.0240(9)
C35	0.1941(4)	0.8075(3)	0.8539(3)	0.0312(10)
C36	0.3119(4)	0.9087(4)	0.9116(3)	0.0376(11)

Table F29. Bond lengths (Å) for *trans*-$Pd^{II}(Cl)_2(^{i}PrJPhos)_2$.

Pd1-Cl2	2.3133(10)	Pd1-Cl1	2.3260(10)
Pd1-P1	2.3553(10)	Pd1-P2	2.3564(10)
P1-C1	1.838(4)	P1-C16	1.855(4)
P1-C13	1.863(4)	P2-C19	1.853(3)
P2-C34	1.854(4)	P2-C31	1.867(4)
C1-C2	1.407(5)	C1-C6	1.422(5)
C2-C3	1.391(5)	C2-H2A	0.95
C3-C4	1.393(5)	C3-H3A	0.95
C4-C5	1.394(5)	C4-H4A	0.95
C5-C6	1.393(5)	C5-H5A	0.95
C6-C7	1.502(5)	C7-C8	1.402(5)
C7-C12	1.397(5)	C8-C9	1.391(5)
C8-H8A	0.95	C9-C10	1.387(6)
C9-H9A	0.95	C10-C11	1.388(5)
C10-H10A	0.95	C11-C12	1.394(5)
C11-H11A	0.95	C12-H12A	0.95
C13-C15	1.534(5)	C13-C14	1.544(5)
C13-H13A	1.0	C14-H14A	0.98
C14-H14B	0.98	C14-H14C	0.98
C15-H15A	0.98	C15-H15B	0.98
C15-H15C	0.98	C16-C18	1.538(5)

C16-C17	1.537(5)	C16-H16A	1.0
C17-H17A	0.98	C17-H17B	0.98
C17-H17C	0.98	C18-H18A	0.98
C18-H18B	0.98	C18-H18C	0.98
C19-C20	1.404(5)	C19-C24	1.411(5)
C20-C21	1.384(5)	C20-H20A	0.95
C21-C22	1.386(5)	C21-H21A	0.95
C22-C23	1.386(5)	C22-H22A	0.95
C23-C24	1.410(5)	C23-H23A	0.95
C24-C25	1.505(5)	C25-C30	1.371(6)
C25-C26	1.403(6)	C26-C27	1.380(6)
C26-H26A	0.95	C27-C28	1.372(8)
C27-H27A	0.95	C28-C29	1.372(8)
C28-H28A	0.95	C29-C30	1.396(7)
C29-H29A	0.95	C30-H30A	0.95
C31-C32	1.548(5)	C31-C33	1.540(5)
C31-H31A	1.0	C32-H32A	0.98
C32-H32B	0.98	C32-H32C	0.98

C33-H33A	0.98	C33-H33B	0.98
C33-H33C	0.98	C34-C36	1.535(5)
C34-C35	1.548(5)	C34-H34A	1.0
C35-H35A	0.98	C35-H35B	0.98
C35-H35C	0.98	C36-H36A	0.98
C36-H36B	0.98	C36-H36C	0.98

Table F30. Bond angles (°) for *trans*-$Pd^{II}(Cl)_2(^{i}PrJPhos)_2$.

Cl2-Pd1-Cl1	178.76(4)	Cl2-Pd1-P1	88.85(3)
Cl1-Pd1-P1	91.21(4)	Cl2-Pd1-P2	92.87(4)
Cl1-Pd1-P2	86.97(3)	P1-Pd1-P2	174.84(4)
C1-P1-C16	101.02(17)	C1-P1-C13	113.23(17)
C16-P1-C13	104.02(17)	C1-P1-Pd1	114.25(12)
C16-P1-Pd1	115.95(12)	C13-P1-Pd1	107.95(12)
C19-P2-C34	104.10(16)	C19-P2-C31	105.04(16)
C34-P2-C31	109.52(17)	C19-P2-Pd1	113.74(12)
C34-P2-Pd1	107.81(12)	C31-P2-Pd1	115.96(12)
C2-C1-C6	118.4(3)	C2-C1-P1	110.7(3)
C6-C1-P1	130.1(3)	C3-C2-C1	121.7(3)
C3-C2-H2A	119.2	C1-C2-H2A	119.2
C4-C3-C2	119.8(3)	C4-C3-H3A	120.1
C2-C3-H3A	120.1	C3-C4-C5	119.1(3)

C3-C4-H4A	120.5	C5-C4-H4A	120.5
C4-C5-C6	122.2(3)	C4-C5-H5A	118.9
C6-C5-H5A	118.9	C5-C6-C1	118.8(3)
C5-C6-C7	116.0(3)	C1-C6-C7	125.1(3)
C8-C7-C12	117.9(3)	C8-C7-C6	121.8(3)
C12-C7-C6	120.0(3)	C9-C8-C7	120.7(4)
C9-C8-H8A	119.7	C7-C8-H8A	119.7
C10-C9-C8	120.3(4)	C10-C9-H9A	119.8
C8-C9-H9A	119.8	C9-C10-C11	120.1(4)
C9-C10-H10A	120.0	C11-C10-H10A	120.0
C12-C11-C10	119.3(4)	C12-C11-H11A	120.4
C10-C11-H11A	120.4	C11-C12-C7	121.7(4)
C11-C12-H12A	119.1	C7-C12-H12A	119.1
C15-C13-C14	110.2(3)	C15-C13-P1	111.9(3)
C14-C13-P1	109.3(2)	C15-C13-H13A	108.4
C14-C13-H13A	108.4	P1-C13-H13A	108.4
C13-C14-H14A	109.5	C13-C14-H14B	109.5
H14A-C14-H14B	109.5	C13-C14-H14C	109.5
H14A-C14-H14C	109.5	H14B-C14-H14C	109.5
C13-C15-H15A	109.5	C13-C15-H15B	109.5

H15A-C15-H15B	109.5	C13-C15-H15C	109.5
H15A-C15-H15C	109.5	H15B-C15-H15C	109.5
C18-C16-C17	110.3(3)	C18-C16-P1	112.2(2)
C17-C16-P1	113.2(3)	C18-C16-H16A	106.9
C17-C16-H16A	106.9	P1-C16-H16A	106.9
C16-C17-H17A	109.5	C16-C17-H17B	109.5
H17A-C17-H17B	109.5	C16-C17-H17C	109.5
H17A-C17-H17C	109.5	H17B-C17-H17C	109.5
C16-C18-H18A	109.5	C16-C18-H18B	109.5
H18A-C18-H18B	109.5	C16-C18-H18C	109.5
H18A-C18-H18C	109.5	H18B-C18-H18C	109.5
C20-C19-C24	118.1(3)	C20-C19-P2	119.7(3)
C24-C19-P2	122.2(3)	C21-C20-C19	122.1(4)
C21-C20-H20A	118.9	C19-C20-H20A	118.9
C20-C21-C22	119.8(4)	C20-C21-H21A	120.1
C22-C21-H21A	120.1	C21-C22-C23	119.4(3)
C21-C22-H22A	120.3	C23-C22-H22A	120.3

C22-C23-C24	121.5(4)	C22-C23-H23A	119.2
C24-C23-H23A	119.2	C23-C24-C19	118.9(3)
C23-C24-C25	115.4(3)	C19-C24-C25	125.6(3)
C30-C25-C26	119.0(4)	C30-C25-C24	121.2(4)
C26-C25-C24	119.6(4)	C27-C26-C25	120.8(5)
C27-C26-H26A	119.6	C25-C26-H26A	119.6
C28-C27-C26	119.6(5)	C28-C27-H27A	120.2
C26-C27-H27A	120.2	C27-C28-C29	120.2(5)
C27-C28-H28A	119.9	C29-C28-H28A	119.9
C28-C29-C30	120.7(5)	C28-C29-H29A	119.6
C30-C29-H29A	119.6	C25-C30-C29	119.6(5)
C25-C30-H30A	120.2	C29-C30-H30A	120.2
C32-C31-C33	109.6(3)	C32-C31-P2	115.8(2)
C33-C31-P2	112.9(3)	C32-C31-H31A	106.0
C33-C31-H31A	106.0	P2-C31-H31A	106.0
C31-C32-H32A	109.5	C31-C32-H32B	109.5
H32A-C32-H32B	109.5	C31-C32-H32C	109.5
H32A-C32-H32C	109.5	H32B-C32-H32C	109.5

C31-C33-H33A	109.5	C31-C33-H33B	109.5
H33A-C33-H33B	109.5	C31-C33-H33C	109.5
H33A-C33-H33C	109.5	H33B-C33-H33C	109.5
C36-C34-C35	110.1(3)	C36-C34-P2	113.2(3)
C35-C34-P2	115.3(3)	C36-C34-H34A	105.8
C35-C34-H34A	105.8	P2-C34-H34A	105.8
C34-C35-H35A	109.5	C34-C35-H35B	109.5
H35A-C35-H35B	109.5	C34-C35-H35C	109.5
H35A-C35-H35C	109.5	H35B-C35-H35C	109.5
C34-C36-H36A	109.5	C34-C36-H36B	109.5
H36A-C36-H36B	109.5	C34-C36-H36C	109.5
H36A-C36-H36C	109.5	H36B-C36-H36C	109.5

Table F31. Torsion angles (°) for *trans*-$Pd^{II}(Cl)_2(^{i}PrJPhos)_2$.

C16-P1-C1-C2	-77.4(3)	C13-P1-C1-C2	172.0(2)
Pd1-P1-C1-C2	47.8(3)	C16-P1-C1-C6	91.5(4)
C13-P1-C1-C6	-19.1(4)	Pd1-P1-C1-C6	-143.3(3)

C6-C1-C2-C3	-2.4(5)	P1-C1-C2-C3	168.0(3)
C1-C2-C3-C4	0.4(6)	C2-C3-C4-C5	1.3(5)
C3-C4-C5-C6	-0.9(5)	C4-C5-C6-C1	-1.1(5)
C4-C5-C6-C7	175.7(3)	C2-C1-C6-C5	2.7(5)
P1-C1-C6-C5	-165.5(3)	C2-C1-C6-C7	-173.8(3)
P1-C1-C6-C7	18.1(5)	C5-C6-C7-C8	73.3(4)
C1-C6-C7-C8	-110.2(4)	C5-C6-C7-C12	-100.1(4)
C1-C6-C7-C12	76.4(5)	C12-C7-C8-C9	-2.3(5)
C6-C7-C8-C9	-175.9(3)	C7-C8-C9-C10	1.2(6)
C8-C9-C10-C11	0.0(6)	C9-C10-C11-C12	0.0(6)
C10-C11-C12-C7	-1.3(6)	C8-C7-C12-C11	2.4(6)
C6-C7-C12-C11	176.1(3)	C1-P1-C13-C15	152.9(3)
C16-P1-C13-C15	44.1(3)	Pd1-P1-C13-C15	-79.6(3)
C1-P1-C13-C14	-84.7(3)	C16-P1-C13-C14	166.5(3)
Pd1-P1-C13-C14	42.8(3)	C1-P1-C16-C18	-57.3(3)
C13-P1-C16-C18	60.3(3)	Pd1-P1-C16-C18	178.7(2)
C1-P1-C16-C17	68.4(3)	C13-P1-C16-C17	-174.0(3)
Pd1-P1-C16-C17	-55.6(3)	C34-P2-C19-C20	10.4(3)

C31-P2-C19-C20	125.5(3)	Pd1-P2-C19-C20	-106.6(3)
C34-P2-C19-C24	-167.1(3)	C31-P2-C19-C24	-52.0(3)
Pd1-P2-C19-C24	75.8(3)	C24-C19-C20-C21	3.0(5)
P2-C19-C20-C21	-174.7(3)	C19-C20-C21-C22	0.7(6)
C20-C21-C22-C23	-3.2(6)	C21-C22-C23-C24	2.1(6)
C22-C23-C24-C19	1.6(5)	C22-C23-C24-C25	-177.2(4)
C20-C19-C24-C23	-4.0(5)	P2-C19-C24-C23	173.6(3)
C20-C19-C24-C25	174.6(4)	P2-C19-C24-C25	-7.8(5)
C23-C24-C25-C30	112.9(4)	C19-C24-C25-C30	-65.8(6)
C23-C24-C25-C26	-61.4(5)	C19-C24-C25-C26	120.0(4)
C30-C25-C26-C27	1.3(7)	C24-C25-C26-C27	175.7(4)
C25-C26-C27-C28	-0.6(8)	C26-C27-C28-C29	-0.6(9)
C27-C28-C29-C30	1.1(10)	C26-C25-C30-C29	-0.8(7)
C24-C25-C30-C29	-175.1(5)	C28-C29-C30-C25	-0.4(9)
C19-P2-C31-C32	-34.4(3)	C34-P2-C31-C32	76.9(3)
Pd1-P2-C31-C32	-160.9(2)	C19-P2-C31-C33	-161.8(3)

C34-P2-C31-C33	-50.5(3)	Pd1-P2-C31-C33	71.7(3)
C19-P2-C34-C36	-165.1(3)	C31-P2-C34-C36	83.0(3)
Pd1-P2-C34-C36	-44.0(3)	C19-P2-C34-C35	66.8(3)
C31-P2-C34-C35	-45.0(3)	Pd1-P2-C34-C35	-172.0(2)

Table F32. Anisotropic atomic displacement parameters ($Å^2$) for *trans*-$Pd^{II}(Cl)_2(^{i}PrJPhos)_2$. The anisotropic atomic displacement factor exponent takes the form: $-2\pi^2[h^2 a^{*2} U_{11} + ... + 2 h k a^* b^* U_{12}]$**.**

	U_{11}	**U_{22}**	**U_{33}**	**U_{23}**	**U_{13}**	**U_{12}**
Pd1	0.01876(14)	0.01810(17)	0.01940(15)	-0.00369(12)	-0.00308(11)	-0.00740(12)
Cl1	0.0240(5)	0.0260(6)	0.0267(5)	-0.0075(5)	0.0031(4)	-0.0114(4)
Cl2	0.0257(5)	0.0298(6)	0.0279(5)	-0.0105(5)	0.0048(4)	-0.0135(4)
P1	0.0190(5)	0.0168(5)	0.0189(5)	-0.0039(4)	-0.0032(4)	-0.0069(4)
P2	0.0185(5)	0.0162(5)	0.0211(5)	-0.0040(4)	-0.0055(4)	-0.0052(4)
C1	0.0201(19)	0.020(2)	0.021(2)	-0.0077(17)	-0.0021(15)	-0.0016(16)
C2	0.024(2)	0.021(2)	0.026(2)	-0.0026(18)	-0.0084(16)	-0.0076(17)
C3	0.030(2)	0.024(2)	0.022(2)	-0.0006(18)	-0.0112(17)	-0.0063(18)
C4	0.025(2)	0.018(2)	0.024(2)	-0.0021(17)	-0.0033(16)	-0.0053(17)
C5	0.0215(19)	0.020(2)	0.027(2)	-0.0062(18)	-0.0025(16)	-0.0101(17)
C6	0.0174(18)	0.017(2)	0.0209(19)	-0.0061(17)	-0.0031(15)	-0.0038(15)
C7	0.0219(19)	0.020(2)	0.0192(19)	-0.0022(17)	-0.0023(15)	-0.0120(16)
C8	0.027(2)	0.027(2)	0.028(2)	-0.0055(19)	-0.0035(17)	-0.0107(18)
C9	0.043(3)	0.036(3)	0.027(2)	-0.009(2)	-0.0085(19)	-0.020(2)

	U_{11}	U_{22}	U_{33}	U_{23}	U_{13}	U_{12}
C10	0.029(2)	0.036(3)	0.028(2)	0.004(2)	-0.0131(18)	-0.016(2)
C11	0.023(2)	0.025(2)	0.034(2)	-0.002(2)	-0.0071(18)	-0.0025(18)
C12	0.0223(19)	0.023(2)	0.027(2)	-0.0049(18)	-0.0066(16)	-0.0048(17)
C13	0.028(2)	0.022(2)	0.021(2)	-0.0010(17)	-0.0102(16)	-0.0097(17)
C14	0.028(2)	0.030(3)	0.045(3)	-0.008(2)	-0.021(2)	0.0004(19)
C15	0.043(3)	0.051(3)	0.021(2)	0.004(2)	-0.0086(19)	-0.023(2)
C16	0.0219(19)	0.025(2)	0.026(2)	-0.0084(19)	0.0046(16)	-0.0067(17)
C17	0.026(2)	0.032(3)	0.044(3)	-0.009(2)	0.0004(19)	-0.0066(19)
C18	0.034(2)	0.034(3)	0.048(3)	-0.027(2)	0.007(2)	-0.013(2)
C19	0.0200(18)	0.015(2)	0.023(2)	-0.0060(17)	-0.0044(15)	-0.0044(16)
C20	0.0215(19)	0.027(2)	0.024(2)	-0.0029(18)	-0.0048(16)	-0.0053(17)
C21	0.021(2)	0.029(3)	0.042(3)	-0.005(2)	-0.0034(18)	-0.0106(18)
C22	0.019(2)	0.033(3)	0.043(3)	-0.012(2)	-0.0089(18)	-0.0069(18)
C23	0.026(2)	0.021(2)	0.032(2)	-0.0088(19)	-0.0160(17)	0.0003(17)
C24	0.0220(19)	0.015(2)	0.024(2)	-0.0092(17)	-0.0041(15)	-0.0061(16)
C25	0.024(2)	0.035(3)	0.033(2)	0.004(2)	-0.0126(18)	-0.0074(19)
C26	0.057(3)	0.038(3)	0.032(3)	0.002(2)	-0.007(2)	-0.003(2)
C27	0.052(3)	0.082(5)	0.037(3)	0.011(3)	0.004(3)	-0.004(3)
C28	0.057(4)	0.128(6)	0.049(4)	0.040(4)	-0.024(3)	-0.063(4)
C29	0.140(6)	0.100(5)	0.063(4)	0.033(4)	-0.057(4)	-0.099(5)
C30	0.100(4)	0.064(4)	0.035(3)	0.015(3)	-0.035(3)	-0.057(3)
C31	0.024(2)	0.021(2)	0.024(2)	-0.0028(18)	-0.0043(16)	-0.0058(17)
C32	0.035(2)	0.031(3)	0.034(2)	-0.014(2)	-0.0074(19)	-0.008(2)
C33	0.022(2)	0.029(3)	0.040(3)	-0.009(2)	-0.0003(18)	-0.0027(18)
C34	0.027(2)	0.021(2)	0.025(2)	-0.0009(18)	-0.0108(17)	-0.0079(17)

	U_{11}	U_{22}	U_{33}	U_{23}	U_{13}	U_{12}
C35	0.038(2)	0.020(2)	0.035(2)	-0.003(2)	-0.0120(19)	-0.0070(19)
C36	0.039(2)	0.033(3)	0.041(3)	0.004(2)	-0.023(2)	-0.009(2)

Table F33. Hydrogen atomic coordinates and isotropic atomic displacement parameters ($Å^2$) for *trans*-$Pd^{II}(Cl)_2(^{i}PrJPhos)_2$.

	x/a	y/b	z/c	U(eq)
H2A	0.2065	0.4394	0.6257	0.028
H3A	0.2341	0.5925	0.4849	0.031
H4A	0.3866	0.6908	0.4709	0.028
H5A	0.5142	0.6298	0.5959	0.027
H8A	0.4508	0.5960	0.8302	0.032
H9A	0.6073	0.5449	0.9308	0.039
H10A	0.7857	0.3865	0.9172	0.036
H11A	0.8076	0.2770	0.8031	0.035
H12A	0.6511	0.3283	0.7023	0.029
H13A	0.4211	0.3322	0.9103	0.027
H14A	0.5392	0.1364	0.9309	0.051
H14B	0.5378	0.1958	0.8112	0.051
H14C	0.4424	0.1160	0.8764	0.051
H15A	0.3546	0.2063	1.0683	0.057
H15B	0.2532	0.1843	1.0195	0.057
H15C	0.2305	0.3071	1.0377	0.057
H16A	0.0901	0.3938	0.9400	0.031
H17A	-0.0520	0.5471	0.8460	0.054
H17B	-0.0090	0.4378	0.7995	0.054

	x/a	y/b	z/c	U(eq)
H17C	0.0567	0.5410	0.7416	0.054
H18A	0.0884	0.5812	0.9329	0.055
H18B	0.2096	0.5771	0.8364	0.055
H18C	0.2276	0.4946	0.9475	0.055
H20A	-0.0454	-0.0242	0.8608	0.03
H21A	-0.2495	-0.0066	0.8336	0.038
H22A	-0.3018	0.0883	0.6711	0.037
H23A	-0.1559	0.1790	0.5425	0.031
H26A	0.0908	0.1064	0.4297	0.058
H27A	0.2058	0.2140	0.2881	0.084
H28A	0.2556	0.3683	0.3065	0.096
H29A	0.1878	0.4169	0.4643	0.106
H30A	0.0746	0.3080	0.6085	0.07
H31A	0.3171	0.0482	0.5716	0.029
H32A	0.3247	-0.1199	0.5312	0.048
H32B	0.1766	-0.0503	0.5656	0.048
H32C	0.2427	-0.1609	0.6447	0.048
H33A	0.5009	-0.1102	0.5911	0.049
H33B	0.4398	-0.1465	0.7120	0.049
H33C	0.4820	-0.0298	0.6651	0.049
H34A	0.1164	-0.0498	0.9123	0.029
H35A	0.1962	-0.2467	0.9215	0.047
H35B	0.2701	-0.2209	0.8027	0.047
H35C	0.1136	-0.1837	0.8324	0.047
H36A	0.3092	-0.1517	0.9755	0.056

	x/a	y/b	z/c	U(eq)
H36B	0.3044	-0.0200	0.9276	0.056
H36C	0.3950	-0.1120	0.8633	0.056

F.6. Crystal Structure Report for $Pd^0(MeJPhos)_2(\eta^2\text{-dba})$

Table F34. Data collection details for $Pd^0(MeJPhos)_2(\eta^2\text{-dba})$. A orange plate-like specimen of $C_{45}H_{44}OP_2Pd$, approximate dimensions 0.020 mm x 0.040 mm x 0.070 mm, was used for the X-ray crystallographic analysis. The X-ray intensity data were measured.

Axis	dx/mm	2θ/°	ω/°	φ/°	χ/°	Width/°	Frames	Time/s	Wavelength/Å	Voltage/kV	Current/mA	Temperature/K
Phi	44.944	104.92	82.48	0.00	-23.00	1.00	360	2.00	1.54184	45	0.7	296.15
Omega	44.944	104.59	-16.71	108.00	64.88	1.00	129	2.00	1.54184	45	0.7	296.15
Omega	44.944	104.59	-16.71	-90.00	64.88	1.00	129	2.00	1.54184	45	0.7	296.15
Phi	44.944	-36.55	345.89	0.00	23.00	1.00	360	2.00	1.54184	45	0.7	296.15
Omega	44.944	-39.59	-47.38	135.00	-64.88	1.00	99	2.00	1.54184	45	0.7	296.15
Omega	44.944	104.59	-16.71	54.00	64.88	1.00	129	2.00	1.54184	45	0.7	296.15
Omega	44.944	-39.59	-47.38	0.00	-64.88	1.00	99	2.00	1.54184	45	0.7	296.15
Phi	44.944	104.92	4.83	0.00	23.00	1.00	360	2.00	1.54184	45	0.7	296.15
Omega	44.944	-39.59	-47.38	-90.00	-64.88	1.00	99	2.00	1.54184	45	0.7	296.15
Omega	44.944	104.59	-16.71	-144.00	64.88	1.00	129	2.00	1.54184	45	0.7	296.15
Omega	44.944	-39.59	-154.12	-135.00	54.74	1.00	123	2.00	1.54184	45	0.7	296.15
Omega	44.944	-39.59	-154.12	135.00	54.74	1.00	123	2.00	1.54184	45	0.7	296.15
Omega	44.944	104.59	-16.71	0.00	64.88	1.00	129	2.00	1.54184	45	0.7	296.15
Omega	44.944	104.59	-16.71	-171.00	64.88	1.00	129	2.00	1.54184	45	0.7	296.15
Omega	44.944	104.59	96.11	-90.00	-54.74	1.00	123	2.00	1.54184	45	0.7	296.15

Axis	dx/mm	2θ/°	ω/°	φ/°	χ/°	Width/°	Frames	Time/s	Wavelength/Å	Voltage/kV	Current/mA	Temperature/K
Omega	44.944	-39.59	-154.12	-90.00	54.74	1.00	123	2.00	1.54184	45	0.7	296.15
Omega	44.944	-39.59	-154.12	0.00	54.74	1.00	123	2.00	1.54184	45	0.7	296.15
Omega	44.944	104.59	96.11	108.00	-54.74	1.00	123	2.00	1.54184	45	0.7	296.15
Omega	44.944	104.59	-16.71	-117.00	64.88	1.00	129	2.00	1.54184	45	0.7	296.15

A total of 3018 frames were collected. The total exposure time was 1.68 hours. The frames were integrated with the Bruker SAINT software package using a narrow-frame algorithm. The integration of the data using a triclinic unit cell yielded a total of 11800 reflections to a maximum θ angle of 55.00° (0.94 Å resolution), of which 4684 were independent (average redundancy 2.519, completeness = 99.2%, R_{int} = 6.50%, R_{sig} = 8.24%) and 3506 (74.85%) were greater than $2\sigma(F^2)$. The final cell constants of a = 11.1180(6) Å, b = 11.4477(6) Å, c = 15.4317(9) Å, α = 81.426(2)°, β = 78.935(2)°, γ = 79.538(2)°, volume = 1882.20(18) $Å^3$, are based upon the refinement of the XYZ-centroids of 2322 reflections above 20 σ(I) with 5.877° < 2θ < 101.1°. Data were corrected for absorption effects using the multi-scan method (SADABS). The ratio of minimum to maximum apparent transmission was 0.829. The calculated minimum and maximum transmission coefficients (based on crystal size) are 0.7200 and 0.9060.

The final anisotropic full-matrix least-squares refinement on F^2 with 442 variables converged at R1 = 7.00%, for the observed data and wR2 = 17.55% for all data. The goodness-of-fit was 1.023. The largest peak in the final difference electron density synthesis was 0.450 $e^-/Å^3$ and the largest hole was -1.114 $e^-/Å^3$ with an RMS deviation of 0.111 $e^-/Å^3$. On the basis of the final model, the calculated density was 1.357 g/cm^3 and F(000), 796 e^-.

Table F35. Sample and crystal data for $Pd^0(MeJPhos)_2(\eta^2\text{-dba})$.

Identification code	$Pd^0(MeJPhos)_2(\eta^2\text{-dba})$	
Chemical formula	$C_{45}H_{44}OP_2Pd$	
Formula weight	769.14	
Temperature	173(2) K	
Wavelength	1.54178 Å	
Crystal size	0.020 x 0.040 x 0.070 mm	
Crystal habit	orange plate	
Crystal system	triclinic	
Space group	P -1	
Unit cell dimensions	a = 11.1180(6) Å	α = 81.426(2)°
	b = 11.4477(6) Å	β = 78.935(2)°
	c = 15.4317(9) Å	γ = 79.538(2)°
Volume	1882.20(18) $Å^3$	
Z	2	
Density (calculated)	1.357 g/cm^3	
Absorption coefficient	5.030 mm^{-1}	
F(000)	796	

Table F36. Data collection and structure refinement for $Pd^0(MeJPhos)_2(\eta^2\text{-dba})$.

Theta range for data collection	2.94 to 55.00°
Index ranges	-8<=h<=11, -12<=k<=12, -16<=l<=16
Reflections collected	11800
Independent reflections	4684 [R(int) = 0.0650]

Coverage of independent reflections	99.2%	
Absorption correction	multi-scan	
Max. and min. transmission	0.9060 and 0.7200	
Refinement method	Full-matrix least-squares on F^2	
Refinement program	SHELXL-2013 (Sheldrick, 2013)	
Function minimized	$\Sigma\, w(F_o^2 - F_c^2)^2$	
Data / restraints / parameters	4684 / 0 / 442	
Goodness-of-fit on F^2	1.023	
Final R indices	3506 data; $I>2\sigma(I)$	R1 = 0.0700, wR2 = 0.1649
	all data	R1 = 0.0889, wR2 = 0.1755
Weighting scheme	$w=1/[\sigma^2(F_o^2)+(0.1014P)^2]$ where $P=(F_o^2+2F_c^2)/3$	
Largest diff. peak and hole	0.450 and -1.114 eÅ^{-3}	
R.M.S. deviation from mean	0.111 eÅ^{-3}	

Table F37. Atomic coordinates and equivalent isotropic atomic displacement parameters (Å^2) for $Pd^0(MeJPhos)_2(\eta^2$-dba). U(eq) is defined as one third of the trace of the orthogonalized U_{ij} tensor.

	x/a	**y/b**	**z/c**	**U(eq)**
Pd1	0.41498(5)	0.32294(6)	0.30233(4)	0.0466(3)
P1	0.5963(2)	0.2049(2)	0.33347(15)	0.0523(6)
P2	0.3821(2)	0.2675(2)	0.17275(15)	0.0495(6)
O1	0.3865(5)	0.6155(5)	0.2640(4)	0.0624(17)

	x/a	y/b	z/c	U(eq)
C1	0.3593(7)	0.4261(7)	0.4108(5)	0.050(2)
C2	0.2753(7)	0.4651(7)	0.3501(6)	0.051(2)
C3	0.2949(8)	0.5645(8)	0.2802(6)	0.057(2)
C4	0.1937(8)	0.6008(8)	0.2256(6)	0.054(2)
C5	0.2034(8)	0.6832(7)	0.1553(6)	0.052(2)
C6	0.1109(7)	0.7357(7)	0.0986(6)	0.050(2)
C7	0.9891(8)	0.7129(8)	0.1185(6)	0.059(2)
C8	0.9034(9)	0.7668(9)	0.0640(7)	0.069(3)
C9	0.9371(9)	0.8426(8)	0.9875(6)	0.062(2)
C10	0.0573(9)	0.8648(8)	0.9680(6)	0.066(3)
C11	0.1426(9)	0.8128(8)	0.0229(7)	0.065(3)
C12	0.3253(8)	0.3580(7)	0.4988(6)	0.053(2)
C13	0.4018(9)	0.3460(9)	0.5622(6)	0.066(3)
C14	0.3729(10)	0.2842(9)	0.6457(7)	0.073(3)
C15	0.2657(11)	0.2364(10)	0.6690(7)	0.082(3)
C16	0.1886(10)	0.2472(9)	0.6064(7)	0.077(3)
C17	0.2169(9)	0.3075(9)	0.5218(6)	0.067(3)
C18	0.6929(8)	0.2588(8)	0.3990(6)	0.053(2)
C19	0.6959(9)	0.2099(9)	0.4878(6)	0.070(3)
C20	0.7733(11)	0.2446(12)	0.5367(7)	0.085(4)
C21	0.8462(11)	0.3280(11)	0.4977(8)	0.086(4)
C22	0.8459(8)	0.3782(9)	0.4110(7)	0.068(3)
C23	0.7709(8)	0.3444(8)	0.3607(6)	0.056(2)
C24	0.7747(8)	0.4003(8)	0.2660(6)	0.054(2)
C25	0.8830(9)	0.3805(9)	0.2062(7)	0.068(3)

	x/a	y/b	z/c	U(eq)
C26	0.8873(10)	0.4245(9)	0.1171(7)	0.074(3)
C27	0.7828(10)	0.4888(9)	0.0875(7)	0.078(3)
C28	0.6739(9)	0.5135(8)	0.1480(7)	0.061(2)
C29	0.6688(8)	0.4690(7)	0.2361(6)	0.052(2)
C30	0.5606(9)	0.0650(8)	0.3979(7)	0.076(3)
C31	0.7108(7)	0.1488(9)	0.2409(6)	0.062(3)
C32	0.4330(7)	0.1100(7)	0.1544(5)	0.045(2)
C37	0.3737(8)	0.0142(8)	0.2004(5)	0.050(2)
C36	0.4266(8)	0.8975(8)	0.1878(6)	0.060(2)
C35	0.5376(9)	0.8720(9)	0.1298(7)	0.068(3)
C34	0.5953(9)	0.9641(9)	0.0813(6)	0.067(3)
C33	0.5430(8)	0.0802(8)	0.0947(6)	0.057(2)
C38	0.2512(8)	0.0320(7)	0.2604(6)	0.050(2)
C39	0.1543(8)	0.9839(7)	0.2404(6)	0.056(2)
C40	0.0397(8)	0.9937(8)	0.2943(7)	0.064(3)
C41	0.0184(9)	0.0519(9)	0.3694(7)	0.070(3)
C42	0.1138(8)	0.0972(8)	0.3924(6)	0.064(3)
C43	0.2293(8)	0.0896(8)	0.3362(6)	0.056(2)
C44	0.2252(7)	0.3006(8)	0.1460(6)	0.061(2)
C45	0.4630(9)	0.3497(8)	0.0743(6)	0.067(3)

Table F38. Bond lengths (Å) for $Pd^0(MeJPhos)_2(\eta^2\text{-dba})$.

Pd1-C1	2.122(8)	Pd1-C2	2.146(7)
Pd1-P2	2.297(2)	Pd1-P1	2.305(2)

P1-C30	1.821(9)	P1-C31	1.830(8)
P1-C18	1.843(9)	P2-C44	1.830(8)
P2-C45	1.833(9)	P2-C32	1.837(8)
O1-C3	1.231(10)	C1-C2	1.416(11)
C1-C12	1.479(11)	C1-H1A	1.0
C2-C3	1.463(12)	C2-H2A	1.0
C3-C4	1.497(12)	C4-C5	1.328(11)
C4-H4A	0.95	C5-C6	1.466(11)
C5-H5A	0.95	C6-C11	1.385(12)
C6-C7	1.394(11)	C7-C8	1.390(12)
C7-H7A	0.95	C8-C9	1.390(12)
C8-H8A	0.95	C9-C10	1.374(12)
C9-H9A	0.95	C10-C11	1.387(12)
C10-H10A	0.95	C11-H11A	0.95
C12-C13	1.391(12)	C12-C17	1.394(12)
C13-C14	1.384(13)	C13-H13A	0.95
C14-C15	1.365(14)	C14-H14A	0.95
C15-C16	1.388(13)	C15-H15A	0.95
C16-C17	1.390(12)	C16-H16A	0.95
C17-H17A	0.95	C18-C19	1.406(12)
C18-C23	1.415(12)	C19-C20	1.389(14)
C19-H19A	0.95	C20-C21	1.361(15)
C20-H20A	0.95	C21-C22	1.377(14)
C21-H21A	0.95	C22-C23	1.380(12)
C22-H22A	0.95	C23-C24	1.501(12)
C24-C25	1.375(12)	C24-C29	1.408(11)

C25-C26	1.387(13)	C25-H25A	0.95
C26-C27	1.375(13)	C26-H26A	0.95
C27-C28	1.392(13)	C27-H27A	0.95
C28-C29	1.374(11)	C28-H28A	0.95
C29-H29A	0.95	C30-H30A	0.98
C30-H30B	0.98	C30-H30C	0.98
C31-H31A	0.98	C31-H31B	0.98
C31-H31C	0.98	C32-C33	1.404(11)
C32-C37	1.411(11)	C37-C36	1.384(12)
C37-C38	1.492(11)	C36-C35	1.390(12)
C36-H36A	0.95	C35-C34	1.382(13)
C35-H35A	0.95	C34-C33	1.380(13)
C34-H34A	0.95	C33-H33A	0.95
C38-C43	1.386(12)	C38-C39	1.398(11)
C39-C40	1.377(12)	C39-H39A	0.95
C40-C41	1.382(13)	C40-H40A	0.95
C41-C42	1.385(13)	C41-H41A	0.95
C42-C43	1.401(12)	C42-H42A	0.95
C43-H43A	0.95	C44-H44A	0.98
C44-H44B	0.98	C44-H44C	0.98
C45-H45A	0.98	C45-H45B	0.98
C45-H45C	0.98		

Table F39. Bond angles (°) for $Pd^0(MeJPhos)_2(\eta^2\text{-dba})$.

C1-Pd1-C2	38.8(3)	C1-Pd1-P2	151.0(2)

C2-Pd1-P2	112.4(2)	C1-Pd1-P1	103.2(2)
C2-Pd1-P1	141.8(2)	P2-Pd1-P1	105.72(9)
C30-P1-C31	100.8(5)	C30-P1-C18	103.6(4)
C31-P1-C18	102.6(4)	C30-P1-Pd1	109.3(3)
C31-P1-Pd1	118.4(3)	C18-P1-Pd1	119.8(3)
C44-P2-C45	99.0(4)	C44-P2-C32	103.7(4)
C45-P2-C32	103.8(4)	C44-P2-Pd1	118.8(3)
C45-P2-Pd1	111.9(3)	C32-P2-Pd1	117.1(3)
C2-C1-C12	123.0(8)	C2-C1-Pd1	71.5(5)
C12-C1-Pd1	115.6(6)	C2-C1-H1A	113.4
C12-C1-H1A	113.4	Pd1-C1-H1A	113.4
C1-C2-C3	120.9(8)	C1-C2-Pd1	69.7(4)
C3-C2-Pd1	102.5(5)	C1-C2-H2A	117.4
C3-C2-H2A	117.4	Pd1-C2-H2A	117.4
O1-C3-C2	124.9(8)	O1-C3-C4	120.5(9)
C2-C3-C4	114.6(8)	C5-C4-C3	121.2(8)
C5-C4-H4A	119.4	C3-C4-H4A	119.4
C4-C5-C6	128.6(8)	C4-C5-H5A	115.7
C6-C5-H5A	115.7	C11-C6-C7	117.5(8)
C11-C6-C5	120.0(8)	C7-C6-C5	122.5(8)
C8-C7-C6	120.6(9)	C8-C7-H7A	119.7
C6-C7-H7A	119.7	C7-C8-C9	121.2(9)
C7-C8-H8A	119.4	C9-C8-H8A	119.4
C10-C9-C8	118.0(9)	C10-C9-H9A	121.0
C8-C9-H9A	121.0	C9-C10-C11	121.1(9)

C9-C10-H10A	119.5	C11-C10-H10A	119.5
C6-C11-C10	121.6(9)	C6-C11-H11A	119.2
C10-C11-H11A	119.2	C13-C12-C17	118.2(9)
C13-C12-C1	119.5(9)	C17-C12-C1	122.2(8)
C14-C13-C12	121.4(10)	C14-C13-H13A	119.3
C12-C13-H13A	119.3	C15-C14-C13	120.5(10)
C15-C14-H14A	119.8	C13-C14-H14A	119.8
C14-C15-C16	118.7(10)	C14-C15-H15A	120.6
C16-C15-H15A	120.6	C15-C16-C17	121.6(10)
C15-C16-H16A	119.2	C17-C16-H16A	119.2
C16-C17-C12	119.4(9)	C16-C17-H17A	120.3
C12-C17-H17A	120.3	C19-C18-C23	118.2(8)
C19-C18-P1	120.2(8)	C23-C18-P1	121.5(6)
C20-C19-C18	120.9(11)	C20-C19-H19A	119.5
C18-C19-H19A	119.5	C21-C20-C19	119.2(11)
C21-C20-H20A	120.4	C19-C20-H20A	120.4
C20-C21-C22	121.7(10)	C20-C21-H21A	119.2

C22-C21-H21A	119.2	C21-C22-C23	120.3(11)
C21-C22-H22A	119.9	C23-C22-H22A	119.9
C22-C23-C18	119.7(9)	C22-C23-C24	118.5(9)
C18-C23-C24	121.8(8)	C25-C24-C29	119.1(9)
C25-C24-C23	119.3(8)	C29-C24-C23	121.6(8)
C24-C25-C26	120.6(9)	C24-C25-H25A	119.7
C26-C25-H25A	119.7	C27-C26-C25	120.2(10)
C27-C26-H26A	119.9	C25-C26-H26A	119.9
C26-C27-C28	119.8(10)	C26-C27-H27A	120.1
C28-C27-H27A	120.1	C29-C28-C27	120.2(9)
C29-C28-H28A	119.9	C27-C28-H28A	119.9
C28-C29-C24	120.1(8)	C28-C29-H29A	120.0
C24-C29-H29A	120.0	P1-C30-H30A	109.5
P1-C30-H30B	109.5	H30A-C30-H30B	109.5
P1-C30-H30C	109.5	H30A-C30-H30C	109.5
H30B-C30-H30C	109.5	P1-C31-H31A	109.5
P1-C31-H31B	109.5	H31A-C31-H31B	109.5

P1-C31-H31C	109.5	H31A-C31-H31C	109.5
H31B-C31-H31C	109.5	C33-C32-C37	116.8(8)
C33-C32-P2	118.4(6)	C37-C32-P2	124.7(7)
C36-C37-C32	120.0(8)	C36-C37-C38	117.0(8)
C32-C37-C38	123.0(8)	C37-C36-C35	121.3(9)
C37-C36-H36A	119.3	C35-C36-H36A	119.3
C34-C35-C36	120.0(9)	C34-C35-H35A	120.0
C36-C35-H35A	120.0	C33-C34-C35	118.5(9)
C33-C34-H34A	120.7	C35-C34-H34A	120.7
C34-C33-C32	123.4(9)	C34-C33-H33A	118.3
C32-C33-H33A	118.3	C43-C38-C39	118.4(8)
C43-C38-C37	123.9(7)	C39-C38-C37	117.7(8)
C40-C39-C38	120.9(9)	C40-C39-H39A	119.6
C38-C39-H39A	119.6	C39-C40-C41	120.4(9)
C39-C40-H40A	119.8	C41-C40-H40A	119.8
C40-C41-C42	119.9(9)	C40-C41-H41A	120.0
C42-C41-H41A	120.0	C41-C42-C43	119.4(10)
C41-C42-H42A	120.3	C43-C42-H42A	120.3

C38-C43-C42	120.9(9)	C38-C43-H43A	119.5
C42-C43-H43A	119.5	P2-C44-H44A	109.5
P2-C44-H44B	109.5	H44A-C44-H44B	109.5
P2-C44-H44C	109.5	H44A-C44-H44C	109.5
H44B-C44-H44C	109.5	P2-C45-H45A	109.5
P2-C45-H45B	109.5	H45A-C45-H45B	109.5
P2-C45-H45C	109.5	H45A-C45-H45C	109.5
H45B-C45-H45C	109.5		

Table F40. Torsion angles (°) for $Pd^0(MeJPhos)_2(\eta^2\text{-dba})$.

C12-C1-C2-C3	158.3(8)	Pd1-C1-C2-C3	-92.7(7)
C12-C1-C2-Pd1	-109.0(8)	C1-C2-C3-O1	5.3(14)
Pd1-C2-C3-O1	-68.3(10)	C1-C2-C3-C4	-175.8(8)
Pd1-C2-C3-C4	110.5(7)	O1-C3-C4-C5	4.4(14)
C2-C3-C4-C5	-174.5(8)	C3-C4-C5-C6	-175.0(8)
C4-C5-C6-C11	-173.9(9)	C4-C5-C6-C7	7.1(14)
C11-C6-C7-C8	-0.5(13)	C5-C6-C7-C8	178.5(9)
C6-C7-C8-C9	1.5(15)	C7-C8-C9-C10	-1.3(15)
C8-C9-C10-C11	0.2(14)	C7-C6-C11-C10	-0.6(14)

C5-C6-C11-C10	-179.6(8)	C9-C10-C11-C6	0.8(15)
C2-C1-C12-C13	-165.7(8)	Pd1-C1-C12-C13	110.5(8)
C2-C1-C12-C17	12.6(13)	Pd1-C1-C12-C17	-71.2(10)
C17-C12-C13-C14	0.9(14)	C1-C12-C13-C14	179.3(8)
C12-C13-C14-C15	-2.1(15)	C13-C14-C15-C16	2.3(16)
C14-C15-C16-C17	-1.4(17)	C15-C16-C17-C12	0.3(16)
C13-C12-C17-C16	0.0(14)	C1-C12-C17-C16	-178.3(8)
C30-P1-C18-C19	-15.7(8)	C31-P1-C18-C19	-120.3(7)
Pd1-P1-C18-C19	106.2(7)	C30-P1-C18-C23	160.5(7)
C31-P1-C18-C23	56.0(8)	Pd1-P1-C18-C23	-77.5(7)
C23-C18-C19-C20	0.0(13)	P1-C18-C19-C20	176.4(7)
C18-C19-C20-C21	0.6(15)	C19-C20-C21-C22	-0.5(17)
C20-C21-C22-C23	-0.2(15)	C21-C22-C23-C18	0.8(13)
C21-C22-C23-C24	-179.3(8)	C19-C18-C23-C22	-0.7(12)
P1-C18-C23-C22	-177.0(6)	C19-C18-C23-C24	179.3(8)
P1-C18-C23-C24	3.0(11)	C22-C23-C24-C25	63.7(11)

C18-C23-C24-C25	-116.4(10)	C22-C23-C24-C29	-118.8(9)
C18-C23-C24-C29	61.2(12)	C29-C24-C25-C26	-1.8(14)
C23-C24-C25-C26	175.9(9)	C24-C25-C26-C27	0.0(15)
C25-C26-C27-C28	2.5(15)	C26-C27-C28-C29	-3.3(15)
C27-C28-C29-C24	1.5(13)	C25-C24-C29-C28	1.0(13)
C23-C24-C29-C28	-176.5(8)	C44-P2-C32-C33	123.7(7)
C45-P2-C32-C33	20.6(7)	Pd1-P2-C32-C33	-103.2(6)
C44-P2-C32-C37	-60.5(8)	C45-P2-C32-C37	-163.6(7)
Pd1-P2-C32-C37	72.6(7)	C33-C32-C37-C36	2.3(12)
P2-C32-C37-C36	-173.6(6)	C33-C32-C37-C38	-175.0(7)
P2-C32-C37-C38	9.2(11)	C32-C37-C36-C35	-0.5(13)
C38-C37-C36-C35	176.9(8)	C37-C36-C35-C34	-2.0(14)
C36-C35-C34-C33	2.7(14)	C35-C34-C33-C32	-0.9(14)
C37-C32-C33-C34	-1.6(13)	P2-C32-C33-C34	174.5(7)
C36-C37-C38-C43	121.7(9)	C32-C37-C38-C43	-61.0(12)
C36-C37-C38-C39	-56.0(11)	C32-C37-C38-C39	121.3(9)

C43-C38-C39-C40	0.2(12)	C37-C38-C39-C40	178.1(8)
C38-C39-C40-C41	0.2(13)	C39-C40-C41-C42	-2.1(14)
C40-C41-C42-C43	3.7(14)	C39-C38-C43-C42	1.4(13)
C37-C38-C43-C42	-176.3(8)	C41-C42-C43-C38	-3.3(14)

Table F41. Anisotropic atomic displacement parameters ($Å^2$) for $Pd^0(MeJPhos)_2(\eta^2$-dba). The anisotropic atomic displacement factor exponent takes the form: $-2\pi^2[h^2 a^{*2} U_{11} + ... + 2 h k a^* b^* U_{12}]$.

	U_{11}	U_{22}	U_{33}	U_{23}	U_{13}	U_{12}
Pd1	0.0432(4)	0.0453(4)	0.0512(4)	-0.0026(3)	-0.0109(3)	-0.0061(3)
P1	0.0493(13)	0.0508(14)	0.0541(14)	0.0001(11)	-0.0115(11)	-0.0035(11)
P2	0.0468(13)	0.0475(13)	0.0553(14)	0.0008(11)	-0.0134(11)	-0.0109(10)
O1	0.056(4)	0.052(4)	0.080(5)	0.003(3)	-0.021(3)	-0.010(3)
C1	0.050(5)	0.046(5)	0.053(6)	-0.015(4)	-0.010(4)	-0.001(4)
C2	0.035(5)	0.043(5)	0.068(6)	-0.008(5)	-0.005(4)	0.010(4)
C3	0.049(6)	0.054(6)	0.070(6)	-0.014(5)	-0.010(5)	-0.002(5)
C4	0.053(5)	0.049(5)	0.059(6)	-0.008(5)	-0.009(4)	-0.007(4)
C5	0.044(5)	0.049(5)	0.064(6)	-0.007(5)	-0.009(4)	-0.009(4)
C6	0.040(5)	0.048(5)	0.061(6)	-0.011(5)	-0.007(4)	-0.005(4)
C7	0.067(6)	0.049(6)	0.060(6)	0.004(5)	-0.013(5)	-0.015(5)
C8	0.055(6)	0.068(7)	0.086(8)	0.000(6)	-0.020(5)	-0.015(5)
C9	0.061(6)	0.060(6)	0.067(7)	-0.008(5)	-0.018(5)	-0.005(5)

	U_{11}	U_{22}	U_{33}	U_{23}	U_{13}	U_{12}
C10	0.080(7)	0.053(6)	0.055(6)	-0.002(5)	-0.002(5)	0.003(5)
C11	0.050(6)	0.060(6)	0.080(7)	-0.004(6)	-0.004(5)	-0.005(5)
C12	0.064(6)	0.045(5)	0.054(6)	-0.019(5)	-0.018(5)	0.004(4)
C13	0.062(6)	0.070(7)	0.063(7)	-0.005(5)	-0.010(5)	-0.007(5)
C14	0.083(8)	0.066(7)	0.074(8)	-0.010(6)	-0.024(6)	-0.010(6)
C15	0.098(9)	0.075(8)	0.067(7)	-0.001(6)	-0.015(7)	-0.009(7)
C16	0.071(7)	0.072(7)	0.088(8)	-0.005(6)	-0.009(6)	-0.020(6)
C17	0.062(6)	0.080(7)	0.063(7)	0.006(6)	-0.021(5)	-0.025(5)
C18	0.044(5)	0.057(6)	0.054(6)	-0.006(5)	-0.014(4)	0.006(4)
C19	0.066(6)	0.080(7)	0.054(6)	-0.010(5)	-0.019(5)	0.027(5)
C20	0.083(8)	0.108(10)	0.062(7)	-0.021(7)	-0.035(6)	0.026(7)
C21	0.082(8)	0.092(9)	0.091(9)	-0.042(8)	-0.051(7)	0.030(7)
C22	0.053(6)	0.075(7)	0.085(8)	-0.039(6)	-0.026(5)	0.011(5)
C23	0.048(5)	0.058(6)	0.060(6)	-0.015(5)	-0.016(4)	0.008(4)
C24	0.046(5)	0.050(5)	0.067(6)	-0.018(5)	-0.011(4)	-0.003(4)
C25	0.058(6)	0.066(7)	0.082(8)	-0.019(6)	-0.014(5)	-0.007(5)
C26	0.074(8)	0.062(7)	0.081(8)	-0.004(6)	0.003(6)	-0.019(6)
C27	0.088(8)	0.070(7)	0.075(8)	0.005(6)	-0.008(6)	-0.027(6)
C28	0.064(6)	0.045(5)	0.076(7)	0.008(5)	-0.023(5)	-0.013(5)
C29	0.044(5)	0.047(5)	0.064(6)	-0.003(5)	-0.005(4)	-0.013(4)
C30	0.084(7)	0.051(6)	0.088(8)	0.025(5)	-0.027(6)	-0.011(5)
C31	0.045(5)	0.078(7)	0.065(6)	-0.033(5)	-0.009(4)	0.006(5)
C32	0.047(5)	0.039(5)	0.056(5)	-0.008(4)	-0.022(4)	-0.009(4)
C37	0.046(5)	0.056(6)	0.050(5)	-0.005(5)	-0.012(4)	-0.008(4)
C36	0.059(6)	0.057(6)	0.069(6)	-0.003(5)	-0.023(5)	-0.011(5)

	U_{11}	U_{22}	U_{33}	U_{23}	U_{13}	U_{12}
C35	0.066(7)	0.068(7)	0.076(7)	-0.033(6)	-0.023(6)	0.006(5)
C34	0.058(6)	0.080(8)	0.061(6)	-0.027(6)	-0.002(5)	0.001(6)
C33	0.055(6)	0.058(6)	0.060(6)	-0.007(5)	-0.008(5)	-0.013(5)
C38	0.061(6)	0.037(5)	0.057(6)	-0.001(4)	-0.021(5)	-0.011(4)
C39	0.054(6)	0.043(5)	0.073(6)	0.005(5)	-0.019(5)	-0.008(4)
C40	0.049(6)	0.060(6)	0.084(7)	0.004(6)	-0.023(5)	-0.011(5)
C41	0.054(6)	0.063(7)	0.088(8)	0.009(6)	-0.010(5)	-0.007(5)
C42	0.063(6)	0.065(6)	0.056(6)	0.005(5)	0.004(5)	-0.017(5)
C43	0.053(6)	0.058(6)	0.057(6)	0.003(5)	-0.002(4)	-0.024(5)
C44	0.047(5)	0.063(6)	0.076(7)	-0.001(5)	-0.023(5)	-0.009(4)
C45	0.075(7)	0.067(6)	0.062(6)	-0.003(5)	-0.013(5)	-0.022(5)

Table F42. Hydrogen atomic coordinates and isotropic atomic displacement parameters ($Å^2$) for $Pd^0(MeJPhos)_2(\eta^2\text{-dba})$.

	x/a	y/b	z/c	U(eq)
H1A	0.4157	0.4847	0.4112	0.06
H2A	0.1887	0.4476	0.3696	0.061
H4A	0.1210	0.5644	0.2415	0.064
H5A	0.2807	0.7117	0.1396	0.063
H7A	-0.0357	0.6599	0.1697	0.07
H8A	-0.1797	0.7516	0.0794	0.083
H9A	-0.1212	0.8781	-0.0502	0.075
H10A	0.0824	0.9165	-0.0838	0.079
H11A	0.2248	0.8306	0.0081	0.078
H13A	0.4754	0.3810	0.5479	0.079

	x/a	y/b	z/c	U(eq)
H14A	0.4281	0.2750	0.6871	0.088
H15A	0.2442	0.1965	0.7270	0.098
H16A	0.1148	0.2126	0.6218	0.093
H17A	0.1627	0.3141	0.4800	0.08
H19A	0.6443	0.1522	0.5149	0.084
H20A	0.7753	0.2106	0.5965	0.102
H21A	0.8986	0.3522	0.5313	0.103
H22A	0.8977	0.4364	0.3856	0.082
H25A	0.9556	0.3362	0.2261	0.081
H26A	0.9627	0.4103	0.0764	0.088
H27A	0.7850	0.5161	0.0261	0.093
H28A	0.6029	0.5614	0.1282	0.073
H29A	0.5937	0.4845	0.2769	0.062
H30A	0.6375	0.0146	0.4112	0.114
H30B	0.5199	0.0232	0.3635	0.114
H30C	0.5050	0.0820	0.4536	0.114
H31A	0.7827	0.1004	0.2638	0.093
H31B	0.7375	0.2164	0.1994	0.093
H31C	0.6735	0.0995	0.2100	0.093
H36A	0.3863	-0.1663	0.2194	0.072
H35A	0.5738	-0.2088	0.1235	0.082
H34A	0.6694	-0.0522	0.0396	0.081
H33A	0.5835	0.1433	0.0618	0.069
H39A	0.1676	-0.0561	0.1889	0.068
H40A	-0.0250	-0.0397	0.2798	0.077

	x/a	y/b	z/c	U(eq)
H41A	-0.0616	0.0608	0.4053	0.084
H42A	0.1011	0.1332	0.4457	0.077
H43A	0.2935	0.1244	0.3501	0.068
H44A	0.2256	0.2719	0.0892	0.092
H44B	0.1970	0.3872	0.1414	0.092
H44C	0.1688	0.2605	0.1930	0.092
H45A	0.4468	0.3236	0.0205	0.1
H45B	0.5524	0.3338	0.0751	0.1
H45C	0.4330	0.4357	0.0746	0.1

F.7.Crystal Structure Report for *trans*-$Pd^{II}(Cl)_2(MeJPhos)_2$

Table F43. Data collection details for *trans*-$Pd^{II}(Cl)_2(MeJPhos)_2$. A specimen of $C_{14}H_{15}ClPPd$, approximate dimensions 0.080 mm x 0.160 mm x 0.270 mm, was used for the X-ray crystallographic analysis. The X-ray intensity data were measured.

Axis	dx/mm	2θ/°	ω/°	φ/°	χ/°	Width/°	Frames	Time/s	Wavelength/Å	Voltage/kV	Current/mA	Temperature/K
Omega	59.960	35.60	15.29	0.00	-54.74	1.00	150	2.00	0.71073	50	30.0	296.15
Phi	59.960	35.60	280.80	0.00	23.00	1.00	360	2.00	0.71073	50	30.0	296.15
Phi	59.960	35.60	14.89	0.00	-57.06	1.00	360	2.00	0.71073	50	30.0	296.15
Omega	59.960	14.32	-5.99	0.00	-54.74	1.00	150	2.00	0.71073	50	30.0	296.15

A total of 1020 frames were collected. The total exposure time was 0.57 hours. The frames were integrated with the Bruker SAINT software package using a narrow-frame algorithm. The integration of the data using a monoclinic unit cell yielded a total of 19508 reflections to a maximum θ angle of 30.54° (0.70 Å resolution), of which 4177 were independent (average redundancy 4.670, completeness = 99.7%, R_{int} = 5.09%, R_{sig} =

4.25%) and 3182 (76.18%) were greater than $2\sigma(F^2)$. The final cell constants of a = 11.6418(13) Å, b = 7.1671(8) Å, c = 16.4230(17) Å, β = 92.638(5)°, volume = 1368.8(3) $Å^3$, are based upon the refinement of the XYZ-centroids of 118 reflections above 20 σ(I) with 7.092° < 2θ < 51.62°. Data were corrected for absorption effects using the multi-scan method (SADABS). The ratio of minimum to maximum apparent transmission was 0.917. The calculated minimum and maximum transmission coefficients (based on crystal size) are 0.6660 and 0.8800.

The final anisotropic full-matrix least-squares refinement on F^2 with 211 variables converged at R1 = 3.76%, for the observed data and wR2 = 9.30% for all data. The goodness-of-fit was 1.023. The largest peak in the final difference electron density synthesis was 0.799 $e^-/Å^3$ and the largest hole was -0.703 $e^-/Å^3$ with an RMS deviation of 0.080 $e^-/Å^3$. On the basis of the final model, the calculated density was 1.728 g/cm^3 and F(000), 708 e^-.

Table F44. Sample and crystal data for *trans*-$Pd^{II}(Cl)_2(MeJPhos)_2$.

Identification code	*trans*-$Pd^{II}(Cl)_2(MeJPhos)_2$
Chemical formula	$C_{14}H_{15}ClPPd$
Formula weight	356.08
Temperature	200(2) K
Wavelength	0.71073 Å
Crystal size	0.080 x 0.160 x 0.270 mm
Crystal system	monoclinic

Space group	P 1 21/n 1	
Unit cell dimensions	a = 11.6418(13) Å	α = 90°
	b = 7.1671(8) Å	β = 92.638(5)°
	c = 16.4230(17) Å	γ = 90°
Volume	1368.8(3) $Å^3$	
Z	4	
Density (calculated)	1.728 g/cm^3	
Absorption coefficient	1.642 mm^{-1}	
F(000)	708	

Table F45. Data collection and structure refinement for *trans*-$Pd^{II}(Cl)_2(MeJPhos)_2$.

Theta range for data collection	2.10 to 30.54°
Index ranges	-16<=h<=16, -7<=k<=10, -23<=l<=23
Reflections collected	19508
Independent reflections	4177 [R(int) = 0.0509]
Coverage of independent reflections	99.7%
Absorption correction	multi-scan
Max. and min. transmission	0.8800 and 0.6660
Refinement method	Full-matrix least-squares on F^2
Refinement program	SHELXL-2013 (Sheldrick, 2013)
Function minimized	$\Sigma w(F_o^2 - F_c^2)^2$
Data / restraints / parameters	4177 / 0 / 211

Goodness-of-fit on F^2	1.023	
Final R indices	3182 data; $I>2\sigma(I)$	R1 = 0.0376, wR2 = 0.0818
	all data	R1 = 0.0583, wR2 = 0.0930
Weighting scheme	$w=1/[\sigma^2(F_o^2)+(0.0369P)^2+0.8398P]$ where $P=(F_o^2+2F_c^2)/3$	
Largest diff. peak and hole	0.799 and -0.703 eÅ^{-3}	
R.M.S. deviation from mean	0.080 eÅ^{-3}	

Table F46. Atomic coordinates and equivalent isotropic atomic displacement parameters (Å^2) for *trans*-$Pd^{II}(Cl)_2(MeJPhos)_2$. U(eq) is defined as one third of the trace of the orthogonalized U_{ij} tensor.

	x/a	y/b	z/c	U(eq)
Pd1	0.0	0.0	0.0	0.03434(9)
Cl1	0.02039(7)	0.15757(14)	0.12210(5)	0.0681(3)
P1	0.18332(6)	0.87814(9)	0.02212(4)	0.03534(15)
C1	0.1645(4)	0.6657(5)	0.0797(3)	0.0619(9)
C2	0.2597(3)	0.8002(5)	0.93456(19)	0.0438(6)
C3	0.2882(2)	0.0162(3)	0.08203(15)	0.0352(5)
C4	0.3178(3)	0.9635(5)	0.16243(17)	0.0492(7)
C5	0.3997(3)	0.0605(6)	0.20848(19)	0.0566(8)
C6	0.4526(3)	0.2131(5)	0.17747(19)	0.0566(8)
C7	0.4243(2)	0.2684(5)	0.09822(18)	0.0458(6)
C8	0.3431(2)	0.1724(4)	0.04920(14)	0.0339(5)
C9	0.3198(2)	0.2383(3)	0.96398(15)	0.0352(5)

	x/a	y/b	z/c	U(eq)
C10	0.4095(3)	0.2474(4)	0.91054(18)	0.0462(6)
C11	0.3886(4)	0.3070(5)	0.8313(2)	0.0618(9)
C12	0.2799(4)	0.3583(5)	0.8041(2)	0.0678(11)
C13	0.1907(3)	0.3506(4)	0.8560(2)	0.0555(8)
C14	0.2100(2)	0.2918(4)	0.93583(18)	0.0405(6)

Table F47. Bond lengths (Å) for *trans*-$Pd^{II}(Cl)_2(MeJPhos)_2$.

Pd1-Cl1	2.3041(7)	Pd1-Cl1	2.3041(7)
Pd1-P1	2.3191(7)	Pd1-P1	2.3191(7)
P1-C1	1.811(3)	P1-C2	1.813(3)
P1-C3	1.824(3)	C1-H1A	1.00(5)
C1-H1B	0.91(4)	C1-H1C	0.97(4)
C2-H2A	0.96(4)	C2-H2B	0.88(4)
C2-H2C	0.97(4)	C3-C4	1.401(4)
C3-C8	1.409(4)	C4-C5	1.378(5)
C4-H4	0.96(4)	C5-C6	1.365(5)
C5-H5	0.88(4)	C6-C7	1.386(4)
C6-H6	0.92(4)	C7-C8	1.395(4)
C7-H7	0.90(3)	C8-C9	1.490(3)
C9-C14	1.392(4)	C9-C10	1.396(4)
C10-C11	1.380(4)	C10-H10	0.97(3)
C11-C12	1.373(6)	C11-H11	0.79(4)
C12-C13	1.374(5)	C12-H12	0.90(4)
C13-C14	1.386(4)	C13-H13	0.91(3)

C14-H14 0.95(3)

Table F48. Bond angles (°) for *trans*-$Pd^{II}(Cl)_2(MeJPhos)_2$.

Cl1-Pd1-Cl1	180.00(4)	Cl1-Pd1-P1	89.49(3)
Cl1-Pd1-P1	90.51(3)	Cl1-Pd1-P1	90.51(3)
Cl1-Pd1-P1	89.49(3)	P1-Pd1-P1	180.0
C1-P1-C2	103.33(17)	C1-P1-C3	105.57(18)
C2-P1-C3	104.73(13)	C1-P1-Pd1	105.43(15)
C2-P1-Pd1	118.23(12)	C3-P1-Pd1	117.94(8)
P1-C1-H1A	109.(3)	P1-C1-H1B	109.(3)
H1A-C1-H1B	102.(3)	P1-C1-H1C	109.(2)
H1A-C1-H1C	113.(3)	H1B-C1-H1C	114.(3)
P1-C2-H2A	109.(2)	P1-C2-H2B	107.(3)
H2A-C2-H2B	113.(3)	P1-C2-H2C	110.(2)
H2A-C2-H2C	114.(3)	H2B-C2-H2C	104.(3)
C4-C3-C8	118.6(2)	C4-C3-P1	119.4(2)
C8-C3-P1	121.92(19)	C5-C4-C3	121.0(3)
C5-C4-H4	121.(2)	C3-C4-H4	118.(2)
C6-C5-C4	120.8(3)	C6-C5-H5	121.(3)
C4-C5-H5	117.(2)	C5-C6-C7	119.2(3)
C5-C6-H6	128.(2)	C7-C6-H6	113.(2)
C6-C7-C8	121.8(3)	C6-C7-H7	120.1(17)
C8-C7-H7	118.1(17)	C7-C8-C3	118.6(2)

C7-C8-C9	118.4(2)	C3-C8-C9	123.0(2)
C14-C9-C10	118.7(3)	C14-C9-C8	121.6(2)
C10-C9-C8	119.7(2)	C11-C10-C9	120.2(3)
C11-C10-H10	121.6(17)	C9-C10-H10	117.8(17)
C12-C11-C10	120.6(3)	C12-C11-H11	122.(3)
C10-C11-H11	117.(3)	C11-C12-C13	119.9(3)
C11-C12-H12	120.(2)	C13-C12-H12	120.(2)
C12-C13-C14	120.3(3)	C12-C13-H13	123.(2)
C14-C13-H13	116.(2)	C13-C14-C9	120.3(3)
C13-C14-H14	118.4(17)	C9-C14-H14	121.4(17)

Table F49. Torsion angles (°) for *trans*-$Pd^{II}(Cl)_2(MeJPhos)_2$.

C1-P1-C3-C4	-12.1(3)	C2-P1-C3-C4	-120.8(2)
Pd1-P1-C3-C4	105.3(2)	C1-P1-C3-C8	166.2(2)
C2-P1-C3-C8	57.5(2)	Pd1-P1-C3-C8	-76.4(2)
C8-C3-C4-C5	-0.7(4)	P1-C3-C4-C5	177.6(2)
C3-C4-C5-C6	1.3(5)	C4-C5-C6-C7	-1.0(5)
C5-C6-C7-C8	0.0(5)	C6-C7-C8-C3	0.6(4)
C6-C7-C8-C9	-178.5(3)	C4-C3-C8-C7	-0.2(4)
P1-C3-C8-C7	-178.52(19)	C4-C3-C8-C9	178.8(2)
P1-C3-C8-C9	0.5(3)	C7-C8-C9-C14	-121.8(3)
C3-C8-C9-C14	59.2(3)	C7-C8-C9-C10	58.2(3)

C3-C8-C9-C10	-120.8(3)	C14-C9-C10-C11	-0.5(4)
C8-C9-C10-C11	179.6(3)	C9-C10-C11-C12	0.1(5)
C10-C11-C12-C13	0.1(5)	C11-C12-C13-C14	0.2(5)
C12-C13-C14-C9	-0.6(4)	C10-C9-C14-C13	0.7(4)
C8-C9-C14-C13	-179.3(2)		

Table F50. Anisotropic atomic displacement parameters ($Å^2$) for *trans*-$Pd^{II}(Cl)_2(MeJPhos)_2$. The anisotropic atomic displacement factor exponent takes the form: $-2\pi^2[h^2 a^{*2} U_{11} + ... + 2 h k a^* b^* U_{12}]$

	U_{11}	U_{22}	U_{33}	U_{23}	U_{13}	U_{12}
Pd1	0.03449(14)	0.03724(15)	0.03209(14)	-0.01055(11)	0.01000(10)	-0.00730(11)
Cl1	0.0475(4)	0.1036(7)	0.0532(4)	-0.0462(5)	0.0041(3)	0.0031(4)
P1	0.0379(3)	0.0360(3)	0.0329(3)	-0.0042(3)	0.0108(3)	-0.0033(3)
C1	0.078(3)	0.0462(18)	0.064(2)	0.0080(16)	0.024(2)	-0.0039(18)
C2	0.0430(15)	0.0468(16)	0.0429(15)	-0.0130(13)	0.0145(12)	-0.0025(13)
C3	0.0363(12)	0.0431(14)	0.0266(11)	-0.0039(10)	0.0048(9)	0.0047(10)
C4	0.0555(17)	0.0629(19)	0.0300(13)	0.0023(13)	0.0095(12)	0.0057(14)
C5	0.0611(19)	0.081(2)	0.0274(14)	-0.0050(15)	-0.0044(13)	0.0140(17)
C6	0.0517(17)	0.073(2)	0.0436(17)	-0.0171(16)	-0.0128(14)	0.0012(16)
C7	0.0391(14)	0.0528(17)	0.0451(16)	-0.0056(13)	-0.0026(12)	-0.0025(13)
C8	0.0317(11)	0.0403(13)	0.0296(12)	-0.0044(10)	0.0009(9)	0.0032(10)
C9	0.0436(13)	0.0305(12)	0.0316(12)	-0.0041(10)	0.0018(10)	-0.0060(10)

	U_{11}	U_{22}	U_{33}	U_{23}	U_{13}	U_{12}
C10	0.0528(17)	0.0462(16)	0.0406(15)	0.0000(12)	0.0107(13)	-0.0030(13)
C11	0.093(3)	0.0526(18)	0.0412(17)	0.0007(14)	0.0232(18)	-0.0057(19)
C12	0.122(3)	0.0485(18)	0.0314(16)	0.0026(14)	-0.0089(19)	-0.006(2)
C13	0.075(2)	0.0400(16)	0.0492(18)	0.0021(13)	-0.0241(17)	-0.0023(15)
C14	0.0445(14)	0.0310(12)	0.0450(15)	-0.0010(11)	-0.0088(12)	-0.0043(11)

Table F51. Hydrogen atomic coordinates and isotropic atomic displacement parameters ($Å^2$) for *trans*-$Pd^{II}(Cl)_2(MeJPhos)_2$.

	x/a	y/b	z/c	U(eq)
H1A	0.110(4)	-0.419(7)	0.048(3)	0.095(14)
H1B	0.125(3)	-0.307(5)	0.124(3)	0.083(12)
H1C	0.239(3)	-0.392(5)	0.091(2)	0.066(11)
H2A	0.211(3)	-0.283(5)	-0.098(2)	0.069(10)
H2B	0.324(4)	-0.253(6)	-0.047(2)	0.089(14)
H2C	0.286(3)	-0.093(5)	-0.096(2)	0.064(10)
H4	0.281(3)	-0.146(5)	0.183(2)	0.066(10)
H5	0.423(3)	0.012(5)	0.255(3)	0.074(12)
H6	0.507(3)	0.288(5)	0.203(2)	0.073(11)
H7	0.457(2)	0.371(4)	0.0773(16)	0.035(7)
H10	0.483(2)	0.198(4)	-0.0710(16)	0.044(8)

	x/a	y/b	z/c	U(eq)
H11	0.441(3)	0.307(5)	-0.197(2)	0.068(11)
H12	0.268(3)	0.404(6)	-0.247(2)	0.076(11)
H13	0.119(3)	0.392(5)	-0.1578(19)	0.058(9)
H14	0.146(2)	0.287(4)	-0.0298(17)	0.042(8)

Table F52. Hydrogen bond distances (Å) and angles (°) for *trans*-$Pd^{II}(Cl)_2(MeJPhos)_2$.

	Donor-H	Acceptor-H	Donor-Acceptor	Angle
C2-H2A···Cl1	0.96(4)	2.85(3)	3.363(4)	114.0
C2-H2A···Cl1	0.96(4)	2.85(3)	3.363(4)	114.0
C2-H2A···Cl1	0.96(4)	2.85(3)	3.363(4)	114.0

F.8. Crystal Structure Report for *trans*-$Cr^0(CO)_4(MeJPhos)_2$

Table F53. Data collection details for *trans*-$Cr^0(CO)_4(MeJPhos)_2$. A specimen of $C_{32}H_{30}CrO_4P_2$, approximate dimensions 0.020 mm x 0.070 mm x 0.100 mm, was used for the X-ray crystallographic analysis. The X-ray intensity data were measured.

Axis	dx/mm	2θ/°	ω/°	φ/°	χ/°	Width/°	Frames	Time/s	Wavelength/Å	Voltage/kV	Current/mA	Temperature/K
Phi	44.948	104.92	82.48	0.00	-23.00	1.00	360	5.00	1.54184	45	0.7	296.15
Omega	44.948	104.59	-16.71	108.00	64.88	1.00	129	5.00	1.54184	45	0.7	296.15
Omega	44.948	104.59	-16.71	-90.00	64.88	1.00	129	5.00	1.54184	45	0.7	296.15
Phi	44.948	-36.55	345.89	0.00	23.00	1.00	360	2.00	1.54184	45	0.7	296.15

Axis	dx/mm	2θ/°	ω/°	φ/°	χ/°	Width/°	Frames	Time/s	Wavelength/Å	Voltage/kV	Current/mA	Temperature/K
Omega	44.948	-39.59	-47.38	-180.00	-64.88	1.00	99	2.00	1.54184	45	0.7	296.15
Omega	44.948	104.59	-16.71	54.00	64.88	1.00	129	5.00	1.54184	45	0.7	296.15
Omega	44.948	-39.59	-47.38	0.00	-64.88	1.00	99	2.00	1.54184	45	0.7	296.15
Omega	44.948	104.59	-16.71	-144.00	64.88	1.00	129	5.00	1.54184	45	0.7	296.15
Phi	44.948	104.92	4.83	0.00	23.00	1.00	360	5.00	1.54184	45	0.7	296.15
Omega	44.948	-39.59	-154.12	-135.00	54.74	1.00	123	2.00	1.54184	45	0.7	296.15
Omega	44.948	-39.59	-154.12	0.00	54.74	1.00	123	2.00	1.54184	45	0.7	296.15
Omega	44.948	-39.59	-154.12	90.00	54.74	1.00	123	2.00	1.54184	45	0.7	296.15
Omega	44.948	104.59	-16.71	0.00	64.88	1.00	129	5.00	1.54184	45	0.7	296.15
Omega	44.948	-39.59	-154.12	-45.00	54.74	1.00	123	2.00	1.54184	45	0.7	296.15
Omega	44.948	104.59	-16.71	162.00	64.88	1.00	129	5.00	1.54184	45	0.7	296.15
Omega	44.948	104.59	96.11	81.00	-54.74	1.00	123	5.00	1.54184	45	0.7	296.15
Omega	44.948	-39.59	-154.12	45.00	54.74	1.00	123	2.00	1.54184	45	0.7	296.15

A total of 2790 frames were collected. The total exposure time was 2.90 hours. The frames were integrated with the Bruker SAINT software package using a narrow-frame algorithm. The integration of the data using a triclinic unit cell yielded a total of 8026 reflections to a maximum θ angle of 66.66° (0.84 Å resolution), of which 2550 were independent (average redundancy 3.147, completeness = 99.0%, R_{int} = 4.32%, R_{sig} = 4.29%) and 2268 (88.94%) were greater than $2\sigma(F^2)$. The final cell constants of $\underline{a}$ = 7.3216(3) Å, $\underline{b}$ = 9.6435(4) Å, $\underline{c}$ = 11.8158(4) Å, α = 67.621(2)°, β = 72.584(2)°, γ = 76.173(2)°, volume = 728.64(5) $Å^3$, are based upon the refinement of the XYZ-centroids of 3694 reflections above 20 σ(I) with 8.319° < 2θ < 133.1°. Data were corrected for

absorption effects using the multi-scan method (SADABS). The ratio of minimum to maximum apparent transmission was 0.847. The calculated minimum and maximum transmission coefficients (based on crystal size) are 0.6590 and 0.9140.

The final anisotropic full-matrix least-squares refinement on F^2 with 238 variables converged at R1 = 3.54%, for the observed data and wR2 = 9.34% for all data. The goodness-of-fit was 1.057. The largest peak in the final difference electron density synthesis was 0.290 $e^-/Å^3$ and the largest hole was -0.262 $e^-/Å^3$ with an RMS deviation of 0.052 $e^-/Å^3$. On the basis of the final model, the calculated density was 1.350 g/cm^3 and F(000), 308 e^-.

Table F54. Sample and crystal data for *trans*-$Cr^0(CO)_4(MeJPhos)_2$.

Identification code	*trans*-$Cr^0(CO)_4(MeJPhos)_2$	
Chemical formula	$C_{32}H_{30}CrO_4P_2$	
Formula weight	592.50	
Temperature	173(2) K	
Wavelength	1.54178 Å	
Crystal size	0.020 x 0.070 x 0.100 mm	
Crystal system	triclinic	
Space group	P -1	
Unit cell dimensions	a = 7.3216(3) Å	α = 67.621(2)°
	b = 9.6435(4) Å	β = 72.584(2)°
	c = 11.8158(4) Å	γ = 76.173(2)°
Volume	728.64(5) $Å^3$	
Z	1	

Density (calculated)	1.350 g/cm^3
Absorption coefficient	4.553 mm^{-1}
F(000)	308

Table F55. Data collection and structure refinement for *trans*-$Cr^0(CO)_4(MeJPhos)_2$.

Theta range for data collection	4.16 to 66.66°	
Index ranges	-8<=h<=8, -11<=k<=11, -13<=l<=14	
Reflections collected	8026	
Independent reflections	2550 [R(int) = 0.0432]	
Coverage of independent reflections	99.0%	
Absorption correction	multi-scan	
Max. and min. transmission	0.9140 and 0.6590	
Refinement method	Full-matrix least-squares on F^2	
Refinement program	SHELXL-2013 (Sheldrick, 2013)	
Function minimized	$\Sigma\ w(F_o^2 - F_c^2)^2$	
Data / restraints / parameters	2550 / 0 / 238	
Goodness-of-fit on F^2	1.057	
Final R indices	2268 data; I>2σ(I)	R1 = 0.0354, wR2 = 0.0908
	all data	R1 = 0.0395, wR2 = 0.0934

Weighting scheme	$w=1/[\sigma^2(F_o^2)+(0.0511P)^2+0.0877P]$ where $P=(F_o^2+2F_c^2)/3$
Largest diff. peak and hole	0.290 and -0.262 eÅ^{-3}
R.M.S. deviation from mean	0.052 eÅ^{-3}

Table F56. Atomic coordinates and equivalent isotropic atomic displacement parameters (Å^2) for *trans*-$Cr^0(CO)_4(MeJPhos)_2$. U(eq) is defined as one third of the trace of the orthogonalized U_{ij} tensor.

	x/a	y/b	z/c	U(eq)
Cr1	0.5	0.5	0.0	0.02098(15)
P1	0.56114(7)	0.71657(5)	0.82739(5)	0.02283(16)
O1	0.5079(3)	0.6762(2)	0.16250(17)	0.0485(5)
O2	0.0679(2)	0.60425(19)	0.04781(17)	0.0408(4)
C1	0.7353(4)	0.8191(3)	0.8359(2)	0.0332(5)
C2	0.6860(3)	0.6858(3)	0.6773(2)	0.0306(5)
C3	0.3603(3)	0.8724(2)	0.79448(19)	0.0246(4)
C4	0.3122(4)	0.9669(3)	0.8673(2)	0.0348(5)
C5	0.1723(4)	0.0929(3)	0.8480(3)	0.0401(6)
C6	0.0782(4)	0.1288(3)	0.7529(3)	0.0402(6)
C7	0.1199(3)	0.0354(2)	0.6816(2)	0.0314(5)
C8	0.2562(3)	0.9043(2)	0.70291(19)	0.0244(4)
C9	0.2734(3)	0.8038(2)	0.6299(2)	0.0260(5)
C10	0.2273(3)	0.6572(3)	0.6903(2)	0.0307(5)
C11	0.2335(4)	0.5661(3)	0.6223(3)	0.0388(6)
C12	0.2880(4)	0.6212(3)	0.4918(3)	0.0482(7)

	x/a	y/b	z/c	U(eq)
C13	0.3376(4)	0.7642(3)	0.4311(2)	0.0462(7)
C14	0.3292(4)	0.8554(3)	0.4988(2)	0.0365(6)
C15	0.5080(3)	0.6068(2)	0.1022(2)	0.0305(5)
C16	0.2314(3)	0.5636(2)	0.02830(19)	0.0259(5)

Table F57. Bond lengths (Å) for *trans*-$Cr^0(CO)_4(MeJPhos)_2$.

Cr1-C15	1.881(2)	Cr1-C15	1.881(2)
Cr1-C16	1.882(2)	Cr1-C16	1.882(2)
Cr1-P1	2.3192(5)	Cr1-P1	2.3192(5)
P1-C2	1.835(2)	P1-C1	1.835(2)
P1-C3	1.848(2)	O1-C15	1.149(3)
O2-C16	1.149(3)	C1-H1A	1.00(3)
C1-H1B	0.93(3)	C1-H1C	1.00(3)
C2-H2A	0.98(3)	C2-H2B	0.96(3)
C2-H2C	0.96(3)	C3-C4	1.399(3)
C3-C8	1.405(3)	C4-C5	1.383(3)
C4-H4	0.97(3)	C5-C6	1.382(4)
C5-H5	0.86(3)	C6-C7	1.380(4)
C6-H6	0.91(3)	C7-C8	1.401(3)
C7-H7	0.97(2)	C8-C9	1.487(3)
C9-C10	1.393(3)	C9-C14	1.395(3)
C10-C11	1.384(3)	C10-H10	0.91(2)
C11-C12	1.388(4)	C11-H11	0.94(3)
C12-C13	1.371(4)	C12-H12	0.89(3)

C13-C14 1.377(4) C13-H13 0.95(3)

C14-H14 0.94(3)

Table F58. Bond angles (°) for *trans*-$Cr^0(CO)_4(MeJPhos)_2$.

C15-Cr1-C15	180.0	C15-Cr1-C16	87.51(10)
C15-Cr1-C16	92.49(10)	C15-Cr1-C16	92.49(10)
C15-Cr1-C16	87.51(10)	C16-Cr1-C16	180.0
C15-Cr1-P1	88.16(6)	C15-Cr1-P1	91.84(6)
C16-Cr1-P1	92.13(6)	C16-Cr1-P1	87.88(6)
C15-Cr1-P1	91.84(6)	C15-Cr1-P1	88.16(6)
C16-Cr1-P1	87.88(6)	C16-Cr1-P1	92.12(6)
P1-Cr1-P1	180.00(3)	C2-P1-C1	98.66(12)
C2-P1-C3	106.53(10)	C1-P1-C3	100.17(10)
C2-P1-Cr1	115.85(8)	C1-P1-Cr1	113.85(8)
C3-P1-Cr1	118.89(7)	P1-C1-H1A	113.0(16)
P1-C1-H1B	109.5(17)	H1A-C1-H1B	106.(2)
P1-C1-H1C	106.5(16)	H1A-C1-H1C	113.(2)
H1B-C1-H1C	108.(2)	P1-C2-H2A	112.5(15)
P1-C2-H2B	104.7(15)	H2A-C2-H2B	112.(2)
P1-C2-H2C	110.2(15)	H2A-C2-H2C	110.(2)
H2B-C2-H2C	108.(2)	C4-C3-C8	118.3(2)
C4-C3-P1	115.82(17)	C8-C3-P1	125.89(16)
C5-C4-C3	122.0(2)	C5-C4-H4	119.0(16)
C3-C4-H4	119.0(16)	C4-C5-C6	119.5(2)
C4-C5-H5	120.9(18)	C6-C5-H5	119.7(18)

C7-C6-C5	119.6(2)	C7-C6-H6	120.7(18)
C5-C6-H6	119.7(18)	C6-C7-C8	121.7(2)
C6-C7-H7	120.0(15)	C8-C7-H7	118.3(15)
C7-C8-C3	118.8(2)	C7-C8-C9	116.80(19)
C3-C8-C9	124.33(19)	C10-C9-C14	117.9(2)
C10-C9-C8	120.93(19)	C14-C9-C8	121.1(2)
C11-C10-C9	121.1(2)	C11-C10-H10	124.9(16)
C9-C10-H10	114.0(16)	C10-C11-C12	119.6(2)
C10-C11-H11	117.9(17)	C12-C11-H11	122.6(17)
C13-C12-C11	120.1(2)	C13-C12-H12	121.9(19)
C11-C12-H12	118.(2)	C12-C13-C14	120.3(2)
C12-C13-H13	115.7(18)	C14-C13-H13	124.0(18)
C13-C14-C9	121.0(2)	C13-C14-H14	120.4(18)
C9-C14-H14	118.6(18)	O1-C15-Cr1	177.4(2)
O2-C16-Cr1	178.13(19)		

Table F59. Torsion angles (°) for *trans*-$Cr^0(CO)_4(MeJPhos)_2$.

C2-P1-C3-C4	-147.38(18)	C1-P1-C3-C4	-45.1(2)
Cr1-P1-C3-C4	79.53(18)	C2-P1-C3-C8	31.7(2)
C1-P1-C3-C8	133.95(19)	Cr1-P1-C3-C8	-101.43(18)
C8-C3-C4-C5	-2.8(4)	P1-C3-C4-C5	176.3(2)
C3-C4-C5-C6	-0.9(4)	C4-C5-C6-C7	2.4(4)

C5-C6-C7-C8	-0.1(4)	C6-C7-C8-C3	-3.6(3)
C6-C7-C8-C9	173.5(2)	C4-C3-C8-C7	5.0(3)
P1-C3-C8-C7	-174.04(16)	C4-C3-C8-C9	-171.9(2)
P1-C3-C8-C9	9.1(3)	C7-C8-C9-C10	-115.9(2)
C3-C8-C9-C10	61.1(3)	C7-C8-C9-C14	61.7(3)
C3-C8-C9-C14	-121.4(2)	C14-C9-C10-C11	-1.0(3)
C8-C9-C10-C11	176.6(2)	C9-C10-C11-C12	0.5(4)
C10-C11-C12-C13	0.8(4)	C11-C12-C13-C14	-1.5(4)
C12-C13-C14-C9	1.0(4)	C10-C9-C14-C13	0.3(4)
C8-C9-C14-C13	-177.3(2)		

Table F60. Anisotropic atomic displacement parameters ($Å^2$) for *trans*-$Cr^0(CO)_4(MeJPhos)_2$. The anisotropic atomic displacement factor exponent takes the form: $-2\pi^2[h^2 a^{*2} U_{11} + ... + 2 h k a^* b^* U_{12}]$

	U_{11}	**U_{22}**	**U_{33}**	**U_{23}**	**U_{13}**	**U_{12}**
Cr1	0.0233(3)	0.0183(2)	0.0222(3)	-0.00774(19)	-0.00683(19)	-0.00083(19)
P1	0.0227(3)	0.0209(3)	0.0245(3)	-0.0072(2)	-0.0064(2)	-0.0018(2)
O1	0.0723(14)	0.0431(10)	0.0433(10)	-0.0255(9)	-0.0161(9)	-0.0101(9)
O2	0.0282(10)	0.0380(9)	0.0548(11)	-0.0192(8)	-0.0087(8)	0.0028(7)
C1	0.0292(13)	0.0304(12)	0.0414(13)	-0.0101(11)	-0.0097(10)	-0.0079(10)

	U_{11}	U_{22}	U_{33}	U_{23}	U_{13}	U_{12}
C2	0.0264(13)	0.0327(12)	0.0280(11)	-0.0099(10)	-0.0033(9)	0.0005(10)
C3	0.0256(11)	0.0182(9)	0.0273(10)	-0.0055(8)	-0.0040(8)	-0.0043(8)
C4	0.0350(14)	0.0348(13)	0.0397(13)	-0.0181(11)	-0.0118(11)	-0.0006(10)
C5	0.0405(15)	0.0311(12)	0.0545(15)	-0.0258(12)	-0.0105(12)	0.0030(11)
C6	0.0312(14)	0.0233(11)	0.0617(16)	-0.0129(11)	-0.0119(12)	0.0032(10)
C7	0.0265(12)	0.0265(11)	0.0388(12)	-0.0071(10)	-0.0114(10)	-0.0010(9)
C8	0.0220(11)	0.0218(10)	0.0258(10)	-0.0045(8)	-0.0030(8)	-0.0056(8)
C9	0.0206(11)	0.0279(11)	0.0289(11)	-0.0090(9)	-0.0099(8)	0.0021(8)
C10	0.0265(12)	0.0302(12)	0.0358(12)	-0.0126(10)	-0.0076(9)	-0.0014(9)
C11	0.0313(14)	0.0348(13)	0.0581(16)	-0.0232(12)	-0.0158(11)	0.0009(10)
C12	0.0470(17)	0.0559(17)	0.0598(17)	-0.0404(15)	-0.0290(14)	0.0164(13)
C13	0.0531(17)	0.0529(16)	0.0327(13)	-0.0205(12)	-0.0161(12)	0.0103(13)
C14	0.0370(14)	0.0381(13)	0.0324(12)	-0.0095(11)	-0.0128(10)	0.0006(11)
C15	0.0365(13)	0.0268(11)	0.0278(11)	-0.0075(9)	-0.0093(9)	-0.0042(9)
C16	0.0287(13)	0.0212(10)	0.0270(10)	-0.0075(8)	-0.0062(9)	-0.0030(9)

Table F61. Hydrogen atomic coordinates and isotropic atomic displacement parameters ($Å^2$) for *trans*-$Cr^0(CO)_4(MeJPhos)_2$.

	x/a	y/b	z/c	U(eq)
H1A	0.757(4)	0.914(3)	0.763(3)	0.049(8)
H1B	0.689(4)	0.848(3)	0.907(3)	0.046(8)
H1C	0.856(4)	0.745(3)	0.846(3)	0.050(8)
H2A	0.703(4)	0.781(3)	0.607(2)	0.039(7)
H2B	0.808(4)	0.627(3)	0.691(2)	0.035(7)
H2C	0.617(4)	0.626(3)	0.660(2)	0.040(7)

	x/a	y/b	z/c	U(eq)
H4	0.378(4)	0.943(3)	0.934(2)	0.043(7)
H5	0.141(4)	1.147(3)	0.896(2)	0.042(8)
H6	-0.015(4)	1.212(3)	0.740(3)	0.047(8)
H7	0.051(4)	1.058(3)	0.617(2)	0.033(6)
H10	0.193(4)	0.630(3)	0.776(2)	0.035(7)
H11	0.202(4)	0.468(3)	0.667(3)	0.048(8)
H12	0.290(4)	0.561(3)	0.450(3)	0.057(9)
H13	0.374(4)	0.795(3)	0.342(3)	0.050(8)
H14	0.362(4)	0.954(3)	0.457(3)	0.057(9)

F.9. Crystal Structure Report for Me-JohnPhos

Table F62. Data collection details for Me-JohnPhos. A specimen of $C_{28}H_{30}P_2$, approximate dimensions 0.140 mm x 0.210 mm x 0.250 mm, was used for the X-ray crystallographic analysis. The X-ray intensity data were measured.

Axis	dx/mm	2θ/°	ω/°	φ/°	χ/°	Width/°	Frames	Time/s	Wavelength/Å	Voltage/kV	Current/mA	Temperature/K
Phi	49.988	43.02	11.36	0.00	-23.00	1.00	360	2.00	0.71073	50	30.0	296.15
Omega	49.988	43.02	-51.61	40.00	64.88	1.00	106	2.00	0.71073	50	30.0	296.15
Omega	49.988	43.02	-51.61	-160.00	64.88	1.00	106	2.00	0.71073	50	30.0	296.15
Phi	49.988	43.02	29.46	0.00	-57.06	1.00	360	2.00	0.71073	50	30.0	296.15
Phi	49.988	15.59	-16.08	0.00	-23.00	1.00	360	2.00	0.71073	50	30.0	296.15
Omega	49.988	43.02	-51.61	0.00	64.88	1.00	106	2.00	0.71073	50	30.0	296.15
Omega	49.988	15.59	2.65	-120.00	-54.74	1.00	133	2.00	0.71073	50	30.0	296.15

A total of 1531 frames were collected. The total exposure time was 0.85 hours. The frames were integrated with the Bruker SAINT software package using a narrow-frame algorithm. The integration of the data using a triclinic unit cell yielded a total of 26879 reflections to a maximum θ angle of 28.00° (0.76 Å resolution), of which 5817 were independent (average redundancy 4.621, completeness = 100.0%, R_{int} = 5.56%, R_{sig} = 4.52%) and 4507 (77.48%) were greater than $2\sigma(F^2)$. The final cell constants of a = 7.9111(5) Å, b = 11.4369(8) Å, c = 13.9141(9) Å, α = 78.752(3)°, β = 80.116(3)°, γ = 79.644(3)°, volume = 1202.40(14) $Å^3$, are based upon the refinement of the XYZ-centroids of 8260 reflections above 20 σ(I) with 4.339° < 2θ < 69.11°. Data were corrected for absorption effects using the multi-scan method (SADABS). The ratio of minimum to maximum apparent transmission was 0.943. The calculated minimum and maximum transmission coefficients (based on crystal size) are 0.9530 and 0.9730.

The final anisotropic full-matrix least-squares refinement on F^2 with 392 variables converged at R1 = 3.90%, for the observed data and wR2 = 10.45% for all data. The goodness-of-fit was 1.012. The largest peak in the final difference electron density synthesis was 0.277 $e^-/Å^3$ and the largest hole was -0.258 $e^-/Å^3$ with an RMS deviation of 0.044 $e^-/Å^3$. On the basis of the final model, the calculated density was 1.183 g/cm^3 and F(000), 456 e^-.

Table F63. Sample and crystal data for Me-JohnPhos.

Identification code	Me-JohnPhos
Chemical formula	$C_{28}H_{30}P_2$
Formula weight	428.46

Temperature	200(2) K	
Wavelength	0.71073 Å	
Crystal size	0.140 x 0.210 x 0.250 mm	
Crystal system	triclinic	
Space group	P -1	
Unit cell dimensions	a = 7.9111(5) Å	α = 78.752(3)°
	b = 11.4369(8) Å	β = 80.116(3)°
	c = 13.9141(9) Å	γ = 79.644(3)°
Volume	1202.40(14) $Å^3$	
Z	2	
Density (calculated)	1.183 g/cm^3	
Absorption coefficient	0.193 mm^{-1}	
F(000)	456	

Table F64. Data collection and structure refinement for Me-JohnPhos.

Theta range for data collection	1.51 to 28.00°
Index ranges	-10<=h<=10, -15<=k<=15, -18<=l<=18
Reflections collected	26879
Independent reflections	5817 [R(int) = 0.0556]
Coverage of independent reflections	100.0%
Absorption correction	multi-scan
Max. and min. transmission	0.9730 and 0.9530
Refinement method	Full-matrix least-squares on F^2

Refinement program	SHELXL-2013 (Sheldrick, 2013)	
Function minimized	$\Sigma\ w(F_o^2 - F_c^2)^2$	
Data / restraints / parameters	5817 / 0 / 392	
Goodness-of-fit on F^2	1.012	
Δ/σ_{max}	0.001	
Final R indices	4507 data; $I>2\sigma(I)$	R1 = 0.0390, wR2 = 0.0922
	all data	R1 = 0.0563, wR2 = 0.1045
Weighting scheme	$w=1/[\sigma^2(F_o^2)+(0.0416P)^2+0.3931P]$ where $P=(F_o^2+2F_c^2)/3$	
Extinction coefficient	0.0430(30)	
Largest diff. peak and hole	0.277 and -0.258 eÅ^{-3}	
R.M.S. deviation from mean	0.044 eÅ^{-3}	

Table F65. Atomic coordinates and equivalent isotropic atomic displacement parameters (Å^2) for Me-JohnPhos. U(eq) is defined as one third of the trace of the orthogonalized U_{ij} tensor.

	x/a	y/b	z/c	U(eq)
P1	0.64162(5)	0.90611(4)	0.78515(3)	0.03241(13)
C1	0.5317(3)	0.0243(2)	0.85562(18)	0.0516(5)
C2	0.6710(3)	0.78225(19)	0.88922(15)	0.0455(5)
C3	0.85933(18)	0.95056(13)	0.75102(11)	0.0267(3)
C4	0.0037(2)	0.88190(15)	0.79068(12)	0.0327(3)
C5	0.1683(2)	0.91434(15)	0.76068(12)	0.0351(4)
C6	0.1912(2)	0.01656(16)	0.69229(12)	0.0364(4)

	x/a	y/b	z/c	U(eq)
C7	0.0498(2)	0.08612(15)	0.65239(12)	0.0340(4)
C8	0.88364(18)	0.05399(13)	0.67938(10)	0.0265(3)
C9	0.73790(18)	0.12988(13)	0.62998(10)	0.0274(3)
C10	0.6777(2)	0.09247(15)	0.55414(11)	0.0331(3)
C11	0.5463(2)	0.16469(17)	0.50627(13)	0.0393(4)
C12	0.4727(2)	0.27412(17)	0.53358(13)	0.0427(4)
C13	0.5307(2)	0.31291(17)	0.60875(14)	0.0447(4)
C14	0.6630(2)	0.24087(15)	0.65607(13)	0.0370(4)
P1'	0.03968(5)	0.41910(4)	0.29319(3)	0.03349(13)
C1'	0.0264(4)	0.5467(2)	0.35675(18)	0.0568(6)
C2'	0.0069(3)	0.30147(18)	0.40192(14)	0.0420(4)
C3'	0.82710(17)	0.45229(13)	0.24993(10)	0.0249(3)
C4'	0.6987(2)	0.37874(14)	0.28775(12)	0.0310(3)
C5'	0.5384(2)	0.40347(15)	0.25504(12)	0.0359(4)
C6'	0.5006(2)	0.50361(16)	0.18484(13)	0.0385(4)
C7'	0.6259(2)	0.57771(15)	0.14571(12)	0.0338(4)
C8'	0.78979(18)	0.55234(13)	0.17579(10)	0.0258(3)
C9'	0.91984(18)	0.63441(13)	0.12779(10)	0.0258(3)
C10'	0.07008(19)	0.59342(15)	0.06758(11)	0.0294(3)
C11'	0.1857(2)	0.67157(16)	0.01989(12)	0.0372(4)
C12'	0.1548(2)	0.79009(16)	0.03342(13)	0.0421(4)
C13'	0.0078(3)	0.83140(16)	0.09420(14)	0.0438(4)
C14'	0.8904(2)	0.75406(15)	0.14032(12)	0.0369(4)

Table F66. Bond lengths (Å) for Me-JohnPhos.

P1-C1	1.830(2)	P1-C2	1.8315(18)
P1-C3	1.8412(14)	C1-H1A	1.01(2)
C1-H1C	0.94(2)	C1-H2B	0.99(2)
C2-H2A	0.98(2)	C2-H2B	0.95(2)
C2-H2C	0.97(2)	C3-C4	1.397(2)
C3-C8	1.409(2)	C4-C5	1.391(2)
C4-H4	0.968(18)	C5-C6	1.374(2)
C5-H5	0.981(19)	C6-C7	1.383(2)
C6-H6	0.938(18)	C7-C8	1.398(2)
C7-H7	0.97(2)	C8-C9	1.495(2)
C9-C14	1.389(2)	C9-C10	1.395(2)
C10-C11	1.386(2)	C10-H10	0.960(18)
C11-C12	1.378(3)	C11-H11	0.96(2)
C12-C13	1.386(3)	C12-H12	0.96(2)
C13-C14	1.387(2)	C13-H13	0.97(2)
C14-H14	0.937(19)	P1'-C1'	1.827(2)
P1'-C3'	1.8340(14)	P1'-C2'	1.8337(18)
C1'-H1D	0.94(2)	C1'-H1E	0.96(2)
C1'-H1F	0.96(3)	C2'-H2D	0.98(2)
C2'-H2E	0.95(2)	C2'-H2F	0.97(2)
C3'-C4'	1.4029(19)	C3'-C8'	1.408(2)
C4'-C5'	1.383(2)	C4'-H4'	0.963(17)
C5'-C6'	1.377(2)	C5'-H5'	0.971(19)
C6'-C7'	1.390(2)	C6'-H6'	0.937(19)
C7'-C8'	1.395(2)	C7'-H7'	0.99(2)

C8'-C9'	1.5008(18)	C9'-C14'	1.386(2)
C9'-C10'	1.395(2)	C10'-C11'	1.389(2)
C10'-H10'	0.940(16)	C11'-C12'	1.377(3)
C11'-H11'	0.965(19)	C12'-C13'	1.383(3)
C12'-H12'	0.957(19)	C13'-C14'	1.388(2)
C13'-H13'	0.922(19)	C14'-H14'	0.97(2)

Table F67. Bond angles (°) for Me-JohnPhos.

C1-P1-C2	98.34(11)	C1-P1-C3	100.33(8)
C2-P1-C3	102.70(8)	P1-C1-H1A	111.0(13)
P1-C1-H1C	110.8(13)	H1A-C1-H1C	109.0(19)
P1-C1-H2B	109.6(12)	H1A-C1-H2B	108.6(18)
H1C-C1-H2B	107.7(18)	P1-C2-H2A	109.8(12)
P1-C2-H2B	106.2(13)	H2A-C2-H2B	109.3(17)
P1-C2-H2C	112.2(12)	H2A-C2-H2C	110.8(18)
H2B-C2-H2C	108.3(17)	C4-C3-C8	118.55(13)
C4-C3-P1	122.06(11)	C8-C3-P1	119.33(11)
C5-C4-C3	121.11(15)	C5-C4-H4	119.3(11)
C3-C4-H4	119.6(11)	C6-C5-C4	120.24(15)
C6-C5-H5	121.6(10)	C4-C5-H5	118.2(10)
C5-C6-C7	119.58(14)	C5-C6-H6	118.5(11)
C7-C6-H6	121.9(11)	C6-C7-C8	121.37(15)

C6-C7-H7	119.8(12)	C8-C7-H7	118.8(12)
C7-C8-C3	119.12(14)	C7-C8-C9	118.69(13)
C3-C8-C9	122.19(12)	C14-C9-C10	118.39(15)
C14-C9-C8	120.99(14)	C10-C9-C8	120.59(14)
C11-C10-C9	120.54(16)	C11-C10-H10	120.3(11)
C9-C10-H10	119.2(11)	C12-C11-C10	120.30(17)
C12-C11-H11	119.9(12)	C10-C11-H11	119.8(12)
C11-C12-C13	120.04(17)	C11-C12-H12	119.9(12)
C13-C12-H12	120.0(12)	C14-C13-C12	119.55(18)
C14-C13-H13	120.4(12)	C12-C13-H13	120.0(12)
C13-C14-C9	121.18(17)	C13-C14-H14	120.5(11)
C9-C14-H14	118.3(11)	C1'-P1'-C3'	100.31(10)
C1'-P1'-C2'	98.74(10)	C3'-P1'-C2'	102.65(8)
P1'-C1'-H1D	110.0(15)	P1'-C1'-H1E	109.2(14)
H1D-C1'-H1E	110.(2)	P1'-C1'-H1F	106.5(14)
H1D-C1'-H1F	110.(2)	H1E-C1'-H1F	110.3(19)
P1'-C2'-H2D	106.7(13)	P1'-C2'-H2E	111.4(13)
H2D-C2'-H2E	108.4(18)	P1'-C2'-H2F	111.2(11)
H2D-C2'-H2F	105.7(17)	H2E-C2'-H2F	113.1(17)
C4'-C3'-C8'	118.08(13)	C4'-C3'-P1'	121.61(11)
C8'-C3'-P1'	120.30(10)	C5'-C4'-C3'	121.69(14)
C5'-C4'-H4'	119.7(10)	C3'-C4'-H4'	118.6(10)
C6'-C5'-C4'	119.96(14)	C6'-C5'-H5'	121.6(11)
C4'-C5'-H5'	118.3(11)	C5'-C6'-C7'	119.54(15)
C5'-C6'-H6'	120.2(11)	C7'-C6'-H6'	120.2(11)
C6'-C7'-C8'	121.28(15)	C6'-C7'-H7'	118.7(11)

C8'-C7'-H7'	120.0(11)	C7'-C8'-C3'	119.38(13)
C7'-C8'-C9'	118.14(13)	C3'-C8'-C9'	122.48(12)
C14'-C9'-C10'	118.52(13)	C14'-C9'-C8'	120.41(13)
C10'-C9'-C8'	121.05(13)	C11'-C10'-C9'	120.59(15)
C11'-C10'-H10'	119.0(10)	C9'-C10'-H10'	120.4(10)
C12'-C11'-C10'	120.14(16)	C12'-C11'-H11'	120.4(11)
C10'-C11'-H11'	119.5(11)	C11'-C12'-C13'	119.85(15)
C11'-C12'-H12'	120.2(11)	C13'-C12'-H12'	119.9(11)
C12'-C13'-C14'	120.07(17)	C12'-C13'-H13'	120.7(12)
C14'-C13'-H13'	119.2(12)	C9'-C14'-C13'	120.81(16)
C9'-C14'-H14'	119.9(11)	C13'-C14'-H14'	119.3(11)

Table F68. Torsion angles (°) for Me-JohnPhos.

C1-P1-C3-C4	111.04(15)	C2-P1-C3-C4	9.97(16)
C1-P1-C3-C8	-71.88(14)	C2-P1-C3-C8	-172.96(13)
C8-C3-C4-C5	0.1(2)	P1-C3-C4-C5	177.20(12)
C3-C4-C5-C6	1.2(2)	C4-C5-C6-C7	-0.9(3)
C5-C6-C7-C8	-0.7(3)	C6-C7-C8-C3	2.0(2)

C6-C7-C8-C9	-177.15(14)	C4-C3-C8-C7	-1.7(2)
P1-C3-C8-C7	-178.83(11)	C4-C3-C8-C9	177.44(14)
P1-C3-C8-C9	0.26(19)	C7-C8-C9-C14	-76.33(18)
C3-C8-C9-C14	104.57(17)	C7-C8-C9-C10	101.54(17)
C3-C8-C9-C10	-77.56(18)	C14-C9-C10-C11	0.0(2)
C8-C9-C10-C11	-177.95(14)	C9-C10-C11-C12	-0.4(2)
C10-C11-C12-C13	0.5(3)	C11-C12-C13-C14	0.0(3)
C12-C13-C14-C9	-0.5(3)	C10-C9-C14-C13	0.5(2)
C8-C9-C14-C13	178.40(15)	C1'-P1'-C3'-C4'	-112.58(14)
C2'-P1'-C3'-C4'	-11.10(15)	C1'-P1'-C3'-C8'	68.54(14)
C2'-P1'-C3'-C8'	170.02(13)	C8'-C3'-C4'-C5'	-0.9(2)
P1'-C3'-C4'-C5'	-179.84(13)	C3'-C4'-C5'-C6'	-1.1(3)
C4'-C5'-C6'-C7'	1.5(3)	C5'-C6'-C7'-C8'	0.3(3)
C6'-C7'-C8'-C3'	-2.4(2)	C6'-C7'-C8'-C9'	178.10(15)
C4'-C3'-C8'-C7'	2.7(2)	P1'-C3'-C8'-C7'	-178.42(12)
C4'-C3'-C8'-C9'	-177.86(13)	P1'-C3'-C8'-C9'	1.05(19)

C7'-C8'-C9'-C14'	64.50(19)	C3'-C8'-C9'-C14'	-114.97(17)
C7'-C8'-C9'-C10'	-113.69(17)	C3'-C8'-C9'-C10'	66.84(19)
C14'-C9'-C10'-C11'	-1.2(2)	C8'-C9'-C10'-C11'	177.06(14)
C9'-C10'-C11'-C12'	1.4(2)	C10'-C11'-C12'-C13'	-0.3(3)
C11'-C12'-C13'-C14'	-0.9(3)	C10'-C9'-C14'-C13'	-0.1(2)
C8'-C9'-C14'-C13'	-178.37(15)	C12'-C13'-C14'-C9'	1.2(3)

Table F69. Anisotropic atomic displacement parameters (Å^2) for Me-JohnPhos. The anisotropic atomic displacement factor exponent takes the form: $-2\pi^2[h^2 a^{*2} U_{11} + ... + 2 h k a^* b^* U_{12}]$.

	U_{11}	**U_{22}**	**U_{33}**	**U_{23}**	**U_{13}**	**U_{12}**
P1	0.0253(2)	0.0367(2)	0.0352(2)	0.00204(17)	-0.00656(16)	-0.01138(16)
C1	0.0349(10)	0.0512(12)	0.0611(13)	-0.0073(10)	0.0116(9)	-0.0069(9)
C2	0.0409(10)	0.0457(11)	0.0456(10)	0.0083(9)	-0.0040(8)	-0.0145(9)
C3	0.0239(7)	0.0296(8)	0.0283(7)	-0.0068(6)	-0.0046(6)	-0.0058(6)
C4	0.0280(8)	0.0314(8)	0.0394(9)	-0.0035(7)	-0.0096(6)	-0.0043(6)
C5	0.0245(7)	0.0408(9)	0.0418(9)	-0.0112(7)	-0.0103(7)	0.0000(7)
C6	0.0233(7)	0.0491(10)	0.0383(9)	-0.0109(7)	0.0000(6)	-0.0095(7)
C7	0.0298(8)	0.0408(9)	0.0306(8)	-0.0019(7)	-0.0007(6)	-0.0115(7)
C8	0.0256(7)	0.0296(8)	0.0250(7)	-0.0064(6)	-0.0027(6)	-0.0045(6)
C9	0.0258(7)	0.0305(8)	0.0252(7)	-0.0013(6)	-0.0014(5)	-0.0077(6)
C10	0.0354(8)	0.0337(9)	0.0312(8)	-0.0034(7)	-0.0051(6)	-0.0094(7)

	U_{11}	U_{22}	U_{33}	U_{23}	U_{13}	U_{12}
C11	0.0384(9)	0.0478(10)	0.0336(8)	-0.0003(7)	-0.0112(7)	-0.0124(8)
C12	0.0325(9)	0.0489(11)	0.0417(9)	0.0058(8)	-0.0105(7)	-0.0028(8)
C13	0.0432(10)	0.0385(10)	0.0481(10)	-0.0049(8)	-0.0076(8)	0.0039(8)
C14	0.0392(9)	0.0365(9)	0.0365(9)	-0.0083(7)	-0.0084(7)	-0.0036(7)
P1'	0.0228(2)	0.0443(3)	0.0315(2)	0.00260(17)	-0.00794(15)	-0.00623(17)
C1'	0.0722(15)	0.0531(13)	0.0559(13)	0.0013(10)	-0.0338(12)	-0.0255(11)
C2'	0.0442(10)	0.0435(11)	0.0379(9)	0.0034(8)	-0.0163(8)	-0.0066(8)
C3'	0.0211(6)	0.0265(7)	0.0272(7)	-0.0057(6)	-0.0028(5)	-0.0033(5)
C4'	0.0288(7)	0.0293(8)	0.0337(8)	-0.0006(6)	-0.0040(6)	-0.0068(6)
C5'	0.0275(8)	0.0398(9)	0.0420(9)	-0.0043(7)	-0.0036(7)	-0.0136(7)
C6'	0.0231(7)	0.0512(10)	0.0425(9)	-0.0029(8)	-0.0114(7)	-0.0080(7)
C7'	0.0276(8)	0.0373(9)	0.0347(8)	0.0014(7)	-0.0087(6)	-0.0039(6)
C8'	0.0231(7)	0.0279(7)	0.0264(7)	-0.0051(6)	-0.0028(5)	-0.0041(6)
C9'	0.0263(7)	0.0289(7)	0.0229(7)	-0.0014(6)	-0.0066(5)	-0.0059(6)
C10'	0.0295(8)	0.0314(8)	0.0281(7)	-0.0051(6)	-0.0065(6)	-0.0049(6)
C11'	0.0309(8)	0.0490(10)	0.0315(8)	-0.0044(7)	0.0000(7)	-0.0120(7)
C12'	0.0466(10)	0.0453(10)	0.0369(9)	-0.0011(7)	-0.0010(7)	-0.0250(8)
C13'	0.0570(11)	0.0298(9)	0.0458(10)	-0.0063(7)	-0.0023(8)	-0.0145(8)
C14'	0.0387(9)	0.0327(9)	0.0381(9)	-0.0074(7)	0.0003(7)	-0.0059(7)

Table F70. Hydrogen atomic coordinates and isotropic atomic displacement parameters ($Å^2$) for Me-JohnPhos.

	x/a	y/b	z/c	U(eq)
H1A	0.514(3)	0.105(2)	0.8108(18)	0.076(7)

	x/a	y/b	z/c	U(eq)
H1C	0.596(3)	0.0303(19)	0.9045(16)	0.056(6)
H1D	0.924(3)	0.553(2)	0.4020(18)	0.071(8)
H1E	1.029(3)	0.619(2)	0.3089(18)	0.076(7)
H1F	1.126(3)	0.531(2)	0.3909(17)	0.071(7)
H2A	0.740(3)	-0.289(2)	0.8651(16)	0.061(6)
H2B	0.417(3)	0.0044(19)	0.8889(16)	0.064(6)
H2B	0.558(3)	-0.2348(18)	0.9176(15)	0.057(6)
H2C	0.724(3)	-0.1958(19)	0.9395(16)	0.058(6)
H2D	1.108(3)	0.2916(19)	0.4368(16)	0.064(6)
H2E	1.002(3)	0.2267(19)	0.3834(15)	0.056(6)
H2F	0.907(3)	0.3274(17)	0.4482(15)	0.050(5)
H4	0.990(2)	-0.1909(17)	0.8384(13)	0.042(5)
H4'	0.724(2)	0.3093(15)	0.3377(12)	0.032(4)
H5	1.266(2)	-0.1371(16)	0.7902(13)	0.042(5)
H5'	0.453(3)	0.3509(17)	0.2851(14)	0.049(5)
H6	1.303(2)	0.0368(16)	0.6738(13)	0.041(5)
H6'	0.390(2)	0.5232(16)	0.1651(13)	0.042(5)
H7	1.065(2)	0.1581(18)	0.6040(14)	0.049(5)
H7'	0.596(2)	0.6507(18)	0.0963(14)	0.049(5)
H10	0.730(2)	0.0165(17)	0.5347(13)	0.040(5)
H10'	1.095(2)	0.5123(15)	0.0591(12)	0.029(4)
H11	0.510(3)	0.1396(18)	0.4521(15)	0.053(6)

	x/a	y/b	z/c	U(eq)
H11'	1.287(3)	0.6424(17)	-0.0233(14)	0.049(5)
H12	0.384(3)	0.3248(19)	0.4988(15)	0.058(6)
H12'	1.235(2)	0.8437(16)	0.0015(13)	0.046(5)
H13	0.480(3)	0.3908(18)	0.6271(14)	0.054(6)
H13'	0.988(2)	0.9098(18)	0.1057(14)	0.048(5)
H14	0.704(2)	0.2662(16)	0.7067(14)	0.042(5)
H14'	0.788(3)	0.7841(17)	0.1834(15)	0.052(5)

REFERENCES CITED

Chapter I

(1) Allen, D. W.; Tebby, J. C.; Balczewski, P.; Loakes, D.; Keglevich, G.; Migaud, M. *Organophosphorus Chemistry*; Royal Society of Chemistry, 2011.

(2) Chatt, J.; Hart, F. A.; Fielding, H. C. Preparation of diphosphines. GB877592 (A), September 13, 1961.

(3) Jackson, I. K.; Jones, W. J. *J. Chem. Soc. Resumed* **1931**, No. 0, 575–578.

(4) Börner, A. *Phosphorus Ligands in Asymmetric Catalysis: Synthesis and Applications*; John Wiley & Sons Incorporated, 2008.

(5) Baumgartner, T. *Acc. Chem. Res.* **2014**, *47* (5), 1613–1622.

(6) Baszczyński, O.; Janeba, Z. *Med. Res. Rev.* **2013**, *33* (6), 1304–1344.

(7) Sereda, O.; Tabassum, S.; Wilhelm, R. In *Asymmetric Organocatalysis*; List, B., Ed.; Topics in Current Chemistry; Springer Berlin Heidelberg, 2010; pp 86–117.

(8) M. de los Santos, J.; Vicario, J.; Alonso, C.; Palacios, F. *Curr. Org. Chem.* **2011**, *15* (10), 1644–1660.

(9) Kolodiazhnyi, O. I. *Phosphorus Ylides: Chemistry and Applications in Organic Synthesis*; John Wiley & Sons, 2008.

(10) Thenard, P. *Jahresber.* **1847**, 645–646.

(11) Thenard, P. *Compt Rend* **1847**, *25*, 892–895.

(12) Kamer, P. C. J.; Leeuwen, P. W. N. M. van. *Phosphorus(III)Ligands in Homogeneous Catalysis: Design and Synthesis*; Wiley, 2012.

(13) Pignolet, L. H. *Homogeneous Catalysis With Metal Phosphine Complexes*; Plenum Publishing Corporation, 1983.

(14) Hitchcock, C. H. S.; Mann, F. G. *J. Chem. Soc. Resumed* **1958**, No. 0, 2081–2086.

(15) Bishop, J. J.; Davison, A.; Katcher, M. L.; Lichtenberg, D. W.; Merrill, R. E.; Smart, J. C. *J. Organomet. Chem.* **1971**, *27* (2), 241–249.

(16) Miyashita, A.; Yasuda, A.; Takaya, H.; Toriumi, K.; Ito, T.; Souchi, T.; Noyori, R. *J. Am. Chem. Soc.* **1980**, *102* (27), 7932–7934.

(17) Barder, T. E.; Walker, S. D.; Martinelli, J. R.; Buchwald, S. L. *J. Am. Chem. Soc.* **2005**, *127* (13), 4685–4696.

(18) Togni, A. *Chim. Int. J. Chem.* **1996**, *50* (3), 86–93.

(19) Kranenburg, M.; van der Burgt, Y. E. M.; Kamer, P. C. J.; van Leeuwen, P. W. N. M.; Goubitz, K.; Fraanje, J. *Organometallics* **1995**, *14* (6), 3081–3089.

(20) Surry, D. S.; Buchwald, S. L. *Chem. Sci. R. Soc. Chem. 2010* **2011**, *2* (1), 27–50.

(21) Littke, A. F.; Dai, C.; Fu, G. C. *J. Am. Chem. Soc.* **2000**, *122* (17), 4020–4028.

(22) Proutiere, F.; Lyngvi, E.; Aufiero, M.; Sanhueza, I. A.; Schoenebeck, F. *Organometallics* **2014**, *33* (23), 9879–6884.

(23) Lyngvi, E.; Sanhueza, I. A.; Schoenebeck, F. *Organometallics* **2014**, *34* (5), 805–812.

(24) Kölmel, C.; Ochsenfeld, C.; Ahlrichs, R. *Theor. Chim. Acta* **1992**, *82* (3-4), 271–284.

(25) Pietrusiewicz, K. M.; Zablocka, M. *Chem. Rev.* **1994**, *94* (5), 1375–1411.

(26) Montchamp, J.-L. *Phosphorus Chemistry I: Asymmetric Synthesis and Bioactive Compounds*; Springer, 2015.

(27) Han, Z. S.; Goyal, N.; Herbage, M. A.; Sieber, J. D.; Qu, B.; Xu, Y.; Li, Z.; Reeves, J. T.; Desrosiers, J.-N.; Ma, S.; Grinberg, N.; Lee, H.; Mangunuru, H. P. R.; Zhang, Y.; Krishnamurthy, D.; Lu, B. Z.; Song, J. J.; Wang, G.; Senanayake, C. H. *J. Am. Chem. Soc.* **2013**, *135* (7), 2474–2477.

(28) Corbridge, D. E. C. *Phosphorus: Chemistry, Biochemistry and Technology, Sixth Edition*; CRC Press, 2013.

(29) Gilheany, D. G. *Chem. Rev.* **1994**, *94* (5), 1339–1374.

(30) Drago, R. S.; Joerg, S. *J. Am. Chem. Soc.* **1996**, *118* (11), 2654–2663.

(31) Angelici, R. J. *Acc. Chem. Res.* **1995**, *28* (2), 51–60.

(32) Tolman, C. A. *Chem. Rev.* **1977**, *77* (3), 313–348.

(33) Orpen, A. G.; Connelly, N. G. *Organometallics* **1990**, *9* (4), 1206–1210.

(34) Henderson, W. A.; Streuli, C. A. *J. Am. Chem. Soc.* **1960**, *82* (22), 5791–5794.

(35) Barder, T. E.; Buchwald, S. L. *J. Am. Chem. Soc.* **2007**, *129* (16), 5096–5101.

(36) Nöth, H.; Vetter, H.-J. *Chem. Ber.* **1963**, *96* (4), 1109–1118.

(37) Li, J.-N.; Liu, L.; Fu, Y.; Guo, Q.-X. *Tetrahedron* **2006**, *62* (18), 4453–4462.

(38) Böhm, V. P. W.; Brookhart, M. *Angew. Chem. Int. Ed.* **2001**, *40* (24), 4694–4696.

(39) Masuda, J. D.; Hoskin, A. J.; Graham, T. W.; Beddie, C.; Fermin, M. C.; Etkin, N.; Stephan, D. W. *Chem. – Eur. J.* **2006**, *12* (34), 8696–8707.

(40) Ficks, A.; Clegg, W.; Harrington, R. W.; Higham, L. J. *Organometallics* **2014**, *33* (22), 6319–6329.

(41) Stewart, B.; Harriman, A.; Higham, L. J. *Organometallics* **2011**, *30* (20), 5338–5343.

(42) *Sigma-Aldrich MSDS of Phosphine*; MSDS 015-181-00-1 [Online]; Sigma-Aldrich: St. Louis, MO, 2015.

(43) Trofimov, B. A.; Brandsma, L.; Arbuzova, S. N.; Malysheva, S. F.; Gusarova, N. K. *Tetrahedron Lett.* **1994**, *35* (41), 7647–7650.

(44) Hayashi, M. *Chem. Rec.* **2009**, *9* (4), 236–245.

(45) Bhattacharya, A. K.; Thyagarajan, G. *Chem Rev* **1981**, *81* (4), 415–430.

(46) Renard, P.-Y.; Vayron, P.; Mioskowski, C. *Org. Lett.* **2003**, *5* (10), 1661–1664.

(47) Quin, L. D. *A Guide to Organophosphorus Chemistry*; John Wiley & Sons, 2000.

(48) Fu, T.; Qiao, H.; Peng, Z.; Hu, G.; Wu, X.; Gao, Y.; Zhao, Y. *Org. Biomol. Chem.* **2014**, *12* (18), 2895.

(49) Montchamp, J.-L. *Phosphorus Chemistry II: Synthetic Methods*; Springer, 2015.

(50) Antczak, M. I.; Montchamp, J.-L. *Org. Lett.* **2008**, *10* (5), 977–980.

(51) Li, Y.; Das, S.; Zhou, S.; Junge, K.; Beller, M. *J. Am. Chem. Soc.* **2012**, *134* (23), 9727–9732.

(52) Li, Y.; Lu, L.-Q.; Das, S.; Pisiewicz, S.; Junge, K.; Beller, M. *J. Am. Chem. Soc.* **2012**, *134* (44), 18325–18329.

(53) Rajendran, K. V.; Gilheany, D. G. *Chem. Commun.* **2012**, *48* (6), 817.

(54) Berlin, K. D.; Butler, G. B. *Chem. Rev.* **1960**, *60* (3), 243–260.

(55) Hays, H. R. *J. Org. Chem.* **1968**, *33* (11), 4201–4205.

(56) Kendall, A. J.; Salazar, C. A.; Martino, P. F.; Tyler, D. R. *Organometallics* **2014**, *33* (21), 6171–6178.

(57) Hays, H. R. *J Org Chem* **1968**, *33* (10), 3690–3694.

(58) Wauters, I.; Debrouwer, W.; Stevens, C. V. *Beilstein J. Org. Chem.* **2014**, *10*, 1064–1096.

(59) Zhao, D.; Mao, L.; Yang, D.; Wang, R. *J. Org. Chem.* **2010**, *75* (20), 6756–6763.

(60) Rulev, A. Y. *RSC Adv.* **2014**, *4* (49), 26002–26012.

(61) Zhang, H.; Sun, Y.-M.; Zhao, Y.; Zhou, Z.-Y.; Wang, J.-P.; Xin, N.; Nie, S.-Z.; Zhao, C.-Q.; Han, L.-B. *Org. Lett.* **2015**, *17* (1), 142–145.

(62) Byrne, L. T.; Engelhardt, L. M.; Jacobsen, G. E.; Leung, W.-P.; Papasergio, R. I.; Raston, C. L.; Skelton, B. W.; Twiss, P.; White, A. H. *J. Chem. Soc. Dalton Trans.* **1989**, No. 1, 105–113.

(63) Thomas, J. C.; Peters, J. C. *Inorg. Chem.* **2003**, *42* (17), 5055–5073.

(64) Zhou, S.-F.; Li, D.-P.; Liu, K.; Zou, J.-P.; Asekun, O. T. *J. Org. Chem.* **2014**, *80* (2), 1214–1220.

(65) Miao, T.; Wang, L. *Adv. Synth. Catal.* **2014**, *356* (5), 967–971.

(66) Xu, W.; Hu, G.; Xu, P.; Gao, Y.; Yin, Y.; Zhao, Y. *Adv. Synth. Catal.* **2014**, *356* (14-15), 2948–2954.

(67) Xu, K.; Hu, H.; Yang, F.; Wu, Y. *Eur. J. Org. Chem.* **2013**, *2013* (2), 319–325.

(68) Kalek, M.; Jezowska, M.; Stawinski, J. *Adv. Synth. Catal.* **2009**, *351* (18), 3207–3216.

(69) Kalek, M.; Ziadi, A.; Stawinski, J. *Org. Lett.* **2008**, *10* (20), 4637–4640.

(70) Zhou, A.-X.; Mao, L.-L.; Wang, G.-W.; Yang, S.-D. *Chem. Commun.* **2014**, *50* (62), 8529–8532.

(71) Deal, E. L.; Petit, C.; Montchamp, J.-L. *Org. Lett.* **2011**, *13* (12), 3270–3273.

(72) Wang, T.; Sang, S.; Liu, L.; Qiao, H.; Gao, Y.; Zhao, Y. *J. Org. Chem.* **2014**, *79* (2), 608–617.

(73) Mao, L.-L.; Zhou, A.-X.; Liu, N.; Yang, S.-D. *Synlett* **2014**, *25* (19), 2727–2732.

(74) McDougal, N. T.; Streuff, J.; Mukherjee, H.; Virgil, S. C.; Stoltz, B. M. *Tetrahedron Lett.* **2010**, *51* (42), 5550–5554.

(75) *Adv. Synth. Catal.* **2013**, *355* (7), 1227–1233.

(76) Yang, J.; Chen, T.; Han, L.-B. *J. Am. Chem. Soc.* **2015**, *137* (5), 1782–1785.

(77) Imamoto, T.; Oshiki, T.; Onozawa, T.; Kusumoto, T.; Sato, K. *J. Am. Chem. Soc.* **1990**, *112* (13), 5244–5252.

(78) Pellon, P. *Tetrahedron Lett.* **1992**, *33* (31), 4451–4452.

(79) Kenny, N. P.; Rajendran, K. V.; Jennings, E. V.; Gilheany, D. G. *Chem. – Eur. J.* **2013**, *19* (42), 14210–14214.

(80) Phelps, J. E.; Frawley, S. B.; Peters, R. G. *Heteroat. Chem.* **2009**, *20* (7), 393–397.

(81) Tavs, P. *Chem. Ber.* **1970**, *103* (8), 2428–2436.

Chapter II

(1) *Phosphorus(III)Ligands in Homogeneous Catalysis: Design and Synthesis*; Kamer, P. C. J.; Leeuwen, P. W. N. M. van, Eds.; 1st ed.; Wiley, 2012.

(2) Surry, D. S.; Buchwald, S. L. *Angew. Chem. Int. Ed.* **2008**, *47*, 6338–6361.

(3) Murphy, D. P. J. *Organophosphorus Reagents: A Practical Approach in Chemistry*; Oxford University Press, 2004.

(4) Allen, D. W.; Tebby, J. C. *Organophosphorus Chemistry*; Royal Society of Chemistry, 2000.

(5) Wauters, I.; Debrouwer, W.; Stevens, C. V. *Beilstein J. Org. Chem.* **2014**, *10*, 1064–1096.

(6) Ferron, J. *Nature* **1961**, *189*, 916.

(7) Möbus, J.; Kehr, G.; Daniliuc, C. G.; Fröhlich, R.; Erker, G. *Dalton Trans.* **2014**, *43*, 632.

(8) Reiter, S. A.; Nogai, S. D.; Karaghiosoff, K.; Schmidbaur, H. *J. Am. Chem. Soc.* **2004**, *126*, 15833–15843.

(9) Kilah, N. L.; Wild, S. B. *Organometallics* **2012**, *31*, 2658–2666.

(10) Surry, D. S.; Buchwald, S. L. *Chem. Sci. R. Soc. Chem. 2010* **2011**, *2*, 27–50.

(11) Sigma-Aldrich: Analytical, Biology, Chemistry & Materials Science products and services. https://www.sigmaaldrich.com/sigma-aldrich/home.html (accessed Sep 26, 2014).

(12) Barder, T. E.; Buchwald, S. L. *J. Am. Chem. Soc.* **2007**, *129*, 5096–5101.

(13) Drago, R. S.; Joerg, S. *J. Am. Chem. Soc.* **1996**, *118*, 2654–2663.

(14) Woska, D.; Prock, A.; Giering, W. P. *Organometallics* **2000**, *19*, 4629–4638.

(15) Tolman, C. A. *Chem. Rev.* **1977**, *77*, 313–348.

(16) Orpen, A. G.; Brammer, L.; Allen, F. H.; Kennard, O.; Watson, D. G.; Taylor, R. *J. Chem. Soc. Dalton Trans.* **1989**, S1.

(17) Jover, J.; Fey, N.; Harvey, J. N.; Lloyd-Jones, G. C.; Orpen, A. G.; Owen-Smith, G. J. J.; Murray, P.; Hose, D. R. J.; Osborne, R.; Purdie, M. *Organometallics* **2010**, *29*, 6245–6258.

(18) *Homogeneous Catalysis with Metal Phosphine Complexes*; Pignolet, L. M., Ed.; Softcover reprint of the original 1st ed. 1983 edition.; Springer: S.l., 2013.

(19) Bhattacharya, A. K.; Thyagarajan, G. *Chem Rev* **1981**, *81*, 415–430.

(20) Troev, K. D. *Chemistry And Application of H-phosphonates*; Elsevier, 2006.

(21) Berlin, K. D.; Butler, G. B. *Chem. Rev.* **1960**, *60*, 243–260.

(22) Hays, H. R. *J. Org. Chem.* **1968**, *33*, 4201–4205.

(23) Yang, J.-C.; Gorenstein, D. G. *Tetrahedron* **1987**, *43*, 479–486.

(24) Fulmer, G. R.; Miller, A. J. M.; Sherden, N. H.; Gottlieb, H. E.; Nudelman, A.; Stoltz, B. M.; Bercaw, J. E.; Goldberg, K. I. *Organometallics* **2010**, *29*, 2176–2179.

(25) Allred, A. L.; Rochow, E. G. *J. Am. Chem. Soc.* **1957**, *79*, 5361–5365.

(26) Mikulski, C. M.; Karayannis, N. M.; Minkiewicz, J. V.; Pytlewski, L. L.; Labes, M. M. *Inorganica Chim. Acta* **1969**, *3*, 523–526.

(27) Reetz, M. T.; Harmat, N.; Mahrwald, R. *Angew. Chem. Int. Ed. Engl.* **1992**, *31*, 342–344.

(28) Denney, D. B.; Denney, D. Z.; Chang, B. C.; Marsi, K. L. *J. Am. Chem. Soc.* **1969**, *91*, 5243–5246.

(29) Granoth, I.; Martin, J. C. *J. Am. Chem. Soc.* **1978**, *100*, 5229–5230.

(30) Granoth, I.; Martin, J. C. *J. Am. Chem. Soc.* **1978**, *100*, 7434–7436.

(31) Granoth, I.; Martin, J. C. *J. Am. Chem. Soc.* **1979**, *101*, 4618–4622.

(32) McClelland, R. A.; Cramm, D. A.; McGall, G. H. *J. Am. Chem. Soc.* **1986**, *108*, 2416–2420.

(33) Yoshida, T.; Iwamoto, M.; Yuguchi, S. JP 42011934.

(34) Sommer, K. *Z. Für Anorg. Allg. Chem.* **1970**, *376*, 37–43.

(35) Wissel, K.; Maase, M.; Huttenloch, O.; Flajs, T.; Kuhl, M. Method for Producing Tertiary Phosphines. US20080146850 A1, June 19, 2008.

(36) Vuoti, S.; Autio, J.; Laitila, M.; Haukka, M.; Pursiainen, J. *Eur. J. Inorg. Chem.* **2008**, *2008*, 397–407.

(37) Rajendran, K. V.; Gilheany, D. G. *Chem. Commun.* **2012**, *48*, 817.

(38) Berthod, M.; Favre-Réguillon, A.; Mohamad, J.; Mignani, G.; Docherty, G.; Lemaire, M. *Synlett* **2007**, *2007*, 1545–1548.

(39) Kenny, N. P.; Rajendran, K. V.; Jennings, E. V.; Gilheany, D. G. *Chem. – Eur. J.* **2013**, *19*, 14210–14214.

(40) Wu, H.-C.; Yu, J.-Q.; Spencer, J. B. *Org. Lett.* **2004**, *6*, 4675–4678.

(41) Li, Y.; Lu, L.-Q.; Das, S.; Pisiewicz, S.; Junge, K.; Beller, M. *J. Am. Chem. Soc.* **2012**, *134*, 18325–18329.

(42) Li, Y.; Das, S.; Zhou, S.; Junge, K.; Beller, M. *J. Am. Chem. Soc.* **2012**, *134*, 9727–9732.

(43) Armarego, W. L. F.; Chai, C. L. L. *Purification of Laboratory Chemicals*; Elsevier, 2003.

(44) Pirrung, M. C. *The Synthetic Organic Chemist's Companion*; 1 edition.; Wiley-Interscience: Hoboken, N.J, 2007.

(45) Hoye, T. R.; Eklov, B. M.; Voloshin, M. *Org. Lett.* **2004**, *6*, 2567–2570.

(46) Griffith, J. A.; McCauley, D. J.; Barrans, R. E.; Herlinger, A. W. *Synth. Commun.* **1998**, *28*, 4317–4323.

(47) Farnung, Winfried. Process for preparing phosphonic-acid esters, and phosphonic acid derivatives. DE3319795 (A1) Abstract of corresponding document: EP0127876 (A2), December 6, 1984.

Chapter III

(1) Kendall, A. J.; Tyler, D. R. Dalton Trans. 2015, 44 (28), 12473–12483.

(2) Homogeneous Catalysis with Metal Phosphine Complexes, Softcover reprint of the original 1st ed. 1983 edition.; Pignolet, L. M., Ed.; Springer: S.l., 2013.

(3) Phosphorus(III)Ligands in Homogeneous Catalysis: Design and Synthesis, 1st ed.; Kamer, P. C. J., Leeuwen, P. W. N. M. van, Eds.; Wiley, 2012.

(4) Honaker, M.; Hovland, J.; Nicholas Salvatore, R. Curr. Org. Synth. 2007, 4 (1), 31–45.

(5) Kendall, A. J.; Salazar, C. A.; Martino, P. F.; Tyler, D. R. Organometallics 2014, 33 (21), 6171–6178.

(6) Bloomfield, A. J.; Qian, J. M.; Herzon, S. B. Organometallics 2010, 29 (18), 4193–4195.

(7) Xu, Q.; Zhao, C.-Q.; Han, L.-B. J. Am. Chem. Soc. 2008, 130 (38), 12648–12655.

(8) Petit, C.; Favre-Réguillon, A.; Mignani, G.; Lemaire, M. Green Chem. 2010, 12 (2), 326–330.

(9) Bloomfield, A. J.; Herzon, S. B. Org. Lett. 2012, 14 (17), 4370–4373.

(10) Allen, D. W.; Tebby, J. C.; Balczewski, P.; Loakes, D.; Keglevich, G.; Migaud, M. Organophosphorus Chemistry; Royal Society of Chemistry, 2011.

(11) Hays, H. R. J Org Chem 1968, 33 (10), 3690–3694.

(12) Doyle, L. R.; Heath, A.; Low, C. H.; Ashley, A. E. Adv. Synth. Catal. 2014, 356 (2-3), 603–608.

(13) Li, J.-N.; Liu, L.; Fu, Y.; Guo, Q.-X. Tetrahedron 2006, 62 (18), 4453–4462.

(14) Creaser, C. S.; Kaska, W. C. Inorganica Chim. Acta 1978, 30, L325–L326.

(15) Bampos, N.; Field, L. D.; Hambley, T. W. Polyhedron 1992, 11 (10), 1213–1218.

(16) Kordosky, G.; Cook, B. R.; Jr, J. C.; Meek, D. W.; Parshall, G. W.; Wonchoba, E. R. In Inorganic Syntheses; Wold, A., Ruff, J. K., Eds.; John Wiley & Sons, Inc., 1973; pp 14–23.

(17) Müller, G.; Feustel, A. Organometallics 2003, 22 (15), 3049–3058.

(18) Rajendran, K. V.; Gilheany, D. G. Chem. Commun. 2012, 48 (6), 817.

(19) Berthod, M.; Favre-Réguillon, A.; Mohamad, J.; Mignani, G.; Docherty, G.; Lemaire, M. Synlett 2007, 2007 (10), 1545–1548.

(20) Wu, H.-C.; Yu, J.-Q.; Spencer, J. B. Org. Lett. 2004, 6 (25), 4675–4678.

(21) Armarego, W. L. F.; Chai, C. L. L. Purification of Laboratory Chemicals; Elsevier, 2003.

(22) Pirrung, M. C. The Synthetic Organic Chemist's Companion, 1 edition.; Wiley-Interscience: Hoboken, N.J, 2007.

(23) Hoye, T. R.; Eklov, B. M.; Voloshin, M. Org. Lett. 2004, 6 (15), 2567–2570.

Chapter IV

(1) Gildner, P. G.; Colacot, T. J. *Organometallics* **2015**, *34*, 5497–5508.

(2) Surry, D. S.; Buchwald, S. L. *Angew. Chem. Int. Ed.* **2008**, *47* (34), 6338–6361.

(3) Martin, R.; Buchwald, S. L. *Acc. Chem. Res.* **2008**, *41* (11), 1461–1473.

(4) Barder, T. E.; Biscoe, M. R.; Buchwald, S. L. *Organometallics* **2007**, *26* (9), 2183–2192.

(5) Kendall, A. J.; Tyler, D. R. *Dalton Trans.* **2015**, *44* (28), 12473–12483.

(6) Zuideveld, M. A.; Swennenhuis, B. H. G.; Boele, M. D. K.; Guari, Y.; Strijdonck, G. P. F. van; Reek, J. N. H.; Kamer, P. C. J.; Goubitz, K.; Fraanje, J.; Lutz, M.; Spek, A. L.; Leeuwen, P. W. N. M. van. *J. Chem. Soc. Dalton Trans.* **2002**, No. 11, 2308–2317.

(7) SciFinder https://scifinder.cas.org/(accessed Jan 12, 2016).

(8) Gathy, T.; Leyssens, T.; Peeters, D. *Comput. Theor. Chem.* **2011**, *970* (1–3), 23–29.

(9) Boz, E.; Haşlak, Z. P.; Tüzün, N. Ş.; Konuklar, F. A. S. *Organometallics* **2014**, *33* (19), 5111–5119.

(10) Jover, J.; Fey, N.; Harvey, J. N.; Lloyd-Jones, G. C.; Orpen, A. G.; Owen-Smith, G. J. J.; Murray, P.; Hose, D. R. J.; Osborne, R.; Purdie, M. *Organometallics* **2010**, *29* (23), 6245–6258.

(11) Pudasaini, B.; Janesko, B. G. *Organometallics* **2011**, *30* (17), 4564–4571.

(12) Kendall, A. J.; Salazar, C. A.; Martino, P. F.; Tyler, D. R. *Organometallics* **2014**, *33*, 6171–6178.

(13) Surry, D. S.; Buchwald, S. L. *Chem. Sci. R. Soc. Chem. 2010* **2011**, *2* (1), 27–50.

(14) Yang, Y.; Niedermann, K.; Han, C.; Buchwald, S. L. *Org. Lett.* **2014**, *16* (17), 4638–4641.

(15) Huang, X.; Anderson, K. W.; Zim, D.; Jiang, L.; Klapars, A.; Buchwald, S. L. *J. Am. Chem. Soc.* **2003**, *125* (22), 6653–6655.

(16) Vuoti, S.; Autio, J.; Laitila, M.; Haukka, M.; Pursiainen, J. *Eur. J. Inorg. Chem.* **2008**, *2008* (3), 397–407.

(17) Vuoti, S.; Autio, J.; Haukka, M.; Pursiainen, J. *Inorganica Chim. Acta* **2009**, *362* (13), 4685–4691.

(18) Hartwig, J. *Organotransition Metal Chemistry*; University Science Books: Sausalito, CA, 2010.

(19) Barder, T. E.; Buchwald, S. L. *J. Am. Chem. Soc.* **2007**, *129* (16), 5096–5101.

(20) Tolman, C. A. *Chem. Rev.* **1977**, *77* (3), 313–348.

(21) Bodner, G. M.; May, M. P.; McKinney, L. E. *Inorg. Chem.* **1980**, *19* (7), 1951–1958.

(22) Golovin, M. N.; Rahman, M. M.; Belmonte, J. E.; Giering, W. P. *Organometallics* **1985**, *4* (11), 1981–1991.

(23) Chatt, J.; Watson, H. R. *J. Chem. Soc. Resumed* **1961**, No. 0, 4980–4988.

(24) Cotton, F. A.; Kraihanzel, C. S. *J. Am. Chem. Soc.* **1962**, *84* (23), 4432–4438.

(25) Kraihanzel, C. S.; Cotton, F. A. *Inorg. Chem.* **1963**, *2* (3), 533–540.

(26) Cotton, F. A. *Inorg. Chem.* **1964**, *3* (5), 702–711.

(27) Graham, W. A. G. *Inorg. Chem.* **1968**, *7* (2), 315–321.

(28) Dunne, B. J.; Morris, R. B.; Orpen, A. G. *J. Chem. Soc. Dalton Trans.* **1991**, No. S, 653–661.

(29) Huheey, J. E.; Keiter, E. A.; Keiter, R. L.; Medhi, O. K. *Inorganic Chemistry: Principles of Structure and Reactivity*; Pearson Education, 2006.

(30) Suresh, C. H.; Koga, N. *Inorg. Chem.* **2002**, *41* (6), 1573–1578.

(31) Brown, H. C.; Cahn, A. *J. Am. Chem. Soc.* **1950**, *72* (7), 2939–2943.

(32) Allman, T.; Goel, R. G. *Can. J. Chem.* **1982**, *60* (6), 716–722.

(33) Clavier, H.; Nolan, S. P. *Chem. Commun.* **2010**, *46* (6), 841–861.

(34) Majchrzak, M.; Kostera, S.; Kubicki, M.; Kownacki, I. *Dalton Trans.* **2013**, *42* (44), 15535–15539.

(35) Anslyn, E. V.; Dougherty, D. A. *Modern Physical Organic Chemistry*; University Science Books: Sausalito, CA, 2006.

(36) Herrmann, W. A.; Thiel, W. R.; Broißmer, C.; Öfele, K.; Priermeier, T.; Scherer, W. *J. Organomet. Chem.* **1993**, *461* (1–2), 51–60.

(37) Reid, S. M.; Mague, J. T.; Fink, M. J. *J. Organomet. Chem.* **2000**, *616* (1–2), 10–18.

(38) Bellabarba, R. M.; Hammond, C.; Forman, G. S.; Tooze, R. P.; Slawin, A. M. Z. *Dalton Trans.* **2006**, No. 20, 2444–2449.

(39) Comanescu, C. C.; Iluc, V. M. *Inorg. Chem.* **2014**, *53* (16), 8517–8528.

(40) Agranat, I.; Rabinovitz, M.; Shaw, W.-C. *J. Org. Chem.* **1979**, *44* (12), 1936–1941.

(41) Fawcett, J.; Kemmitt, R. D. W.; Russell, D. R.; Serindag, O. *J. Organomet. Chem.* **1995**, *486* (1–2), 171–176.

(42) Cooney, K. D.; Cundari, T. R.; Hoffman, N. W.; Pittard, K. A.; Temple, M. D.; Zhao, Y. *J. Am. Chem. Soc.* **2003**, *125* (14), 4318–4324.

(43) Orpen, A. G.; Connelly, N. G. *Organometallics* **1990**, *9* (4), 1206–1210.

(44) Harper, K. C.; Bess, E. N.; Sigman, M. S. *Nat. Chem.* **2012**, *4* (5), 366–374.

(45) Poater, A.; Cosenza, B.; Correa, A.; Giudice, S.; Ragone, F.; Scarano, V.; Cavallo, L. *Eur. J. Inorg. Chem.* **2009**, *2009* (13), 1759–1766.

(46) SambVca@MoLNaC https://www.molnac.unisa.it/OMtools/sambvca.php (accessed Nov 13, 2015).

(47) Alcazar-Roman, L. M.; Hartwig, J. F. *J. Am. Chem. Soc.* **2001**, *123* (51), 12905–12906.

(48) Wolfe, J. P.; Buchwald, S. L. *Angew. Chem. Int. Ed.* **1999**, *38* (16), 2413–2416.

(49) Armarego, W. L. F.; Chai, C. L. L. *Purification of Laboratory Chemicals*; Elsevier, 2003.

(50) Pirrung, M. C. *The Synthetic Organic Chemist's Companion*, 1 edition.; Wiley-Interscience: Hoboken, N.J, 2007.

(51) Hoye, T. R.; Eklov, B. M.; Voloshin, M. *Org. Lett.* **2004**, *6* (15), 2567–2570.

(52) Hu, R.-B.; Zhang, H.; Zhang, X.-Y.; Yang, S.-D. *Chem. Commun.* **2014**, *50* (17), 2193–2195.

(53) Zalesskiy, S. S.; Ananikov, V. P. *Organometallics* **2012**, *31* (6), 2302–2309.

(54) G. M. Sheldrick, *Bruker/Siemens Area Detector Absorption Correction Program*, Bruker AXS, Madison, WI, 1998.

(55) Sheldrick, G. M. *Acta Cryst.* **2008**, *A64*, 112-122.

Chapter V

(1) Johansson Seechurn, C. C. C.; Kitching, M. O.; Colacot, T. J.; Snieckus, V. *Angew. Chem. Int. Ed.* **2012**, *51* (21), 5062–5085.

(2) Gildner, P. G.; Colacot, T. J. *Organometallics* **2015**, *34* (23), 5497-5508.

(3) Kosugi, M.; Kameyama, M.; Migita, T. *Chem. Lett.* **1983**, No. 6, 927–928.

(4) Kondratenko, N. V.; Kolomeitsev, A. A.; Mogilevskaya, V. O.; Varlamova, N. M.; Yagupol'skii, L. M. *Zh Org Khim* **1986**, *22*, 1721–1729.

(5) Guram, A. S.; Rennels, R. A.; Buchwald, S. L. *Angew. Chem.* **1995**, *107* (12), 1456–1459.

(6) Louie, J.; Hartwig, J. F. *Tetrahedron Lett.* **1995**, *36* (21), 3609–3612.

(7) Wang, Z. In *Comprehensive Organic Name Reactions and Reagents*; John Wiley & Sons, Inc., 2010.

(8) Barder, T. E.; Biscoe, M. R.; Buchwald, S. L. *Organometallics* **2007**, *26* (9), 2183–2192.

(9) Hartwig, J. *Organotransition Metal Chemistry*; University Science Books: Sausalito, CA, 2010.

(10) Surry, D. S.; Buchwald, S. L. *Chem. Sci. R. Soc. Chem. 2010* **2011**, *2* (1), 27–50.

(11) Collins, K. D.; Gensch, T.; Glorius, F. *Nat. Chem.* **2014**, *6* (10), 859–871.

(12) Amatore, C.; Jutand, A. *J. Organomet. Chem.* **1999**, *576* (1–2), 254–278.

(13) Crabtree, R. H. *Chem. Rev.* **2015**, *115* (1), 127–150.

(14) Wolfe, J. P.; Buchwald, S. L. *Angew. Chem. Int. Ed.* **1999**, *38* (16), 2413–2416.

(15) Alcazar-Roman, L. M.; Hartwig, J. F. *J. Am. Chem. Soc.* **2001**, *123* (51), 12905–12906.

(16) Barrios-Landeros, F.; Hartwig, J. F. *J. Am. Chem. Soc.* **2005**, *127* (19), 6944–6945.

(17) Amatore, C.; Carre, E.; Jutand, A.; M'Barki, M. A. *Organometallics* **1995**, *14* (4), 1818–1826.

(18) Zim, D.; Buchwald, S. L. *Org. Lett.* **2003**, *5* (14), 2413–2415.

(19) Christmann, U.; Vilar, R.; White, A. J. P.; Williams, D. J. *Chem. Commun.* **2004**, No. 11, 1294–1295.

(20) Biscoe, M. R.; Fors, B. P.; Buchwald, S. L. *J. Am. Chem. Soc.* **2008**, *130* (21), 6686–6687.

(21) Kaboudin, B.; Abedi, Y. *Synthesis* **2009**, *2009* (12), 2025–2028.

(22) Littke, A. F.; Fu, G. C. *Angew. Chem. Int. Ed.* **2002**, *41* (22), 4176–4211.

(23) Driver, M. S.; Hartwig, J. F. *J. Am. Chem. Soc.* **1996**, *118* (30), 7217–7218.

(24) Armarego, W. L. F.; Chai, C. L. L. *Purification of Laboratory Chemicals*; Elsevier, 2003.

Chapter VI

(1) Ishmuratov, G. Y.; Legostaeva, Y. V.; Garifullina, L. R.; Botsman, L. P.; Yakovleva, M. P.; Tolstikov, G. A. *Chem. Nat. Compd.* **2015**, *51* (2), 199–219.

(2) Van Ornum, S. G.; Champeau, R. M.; Pariza, R. *Chem. Rev.* **2006**, *106* (7), 2990–3001.

(3) Bailey, P. S. *Ozonation in Organic Chemistry: Olefinic Compounds*; Academic Press: New York, 1978; Vol. 1.

(4) Anderson, N. G. *Practical Process Research & Development.*, 2nd ed.; Academic Press: New York, 2012.

(5) Ayman Allian. In *Managing Hazardous Reactions and Compounds in Process Chemistry*; ACS Symposium Series; American Chemical Society, 2014; Vol. 1181, pp 353–382.

(6) Irfan, M.; Glasnov, T. N.; Kappe, C. O. *Org. Lett.* **2011**, *13* (5), 984–987.

(7) Allian, A. D.; Richter, S. M.; Kallemeyn, J. M.; Robbins, T. A.; Kishore, V. *Org. Process Res. Dev.* **2011**, *15* (1), 91–97.

(8) O'Brien, M.; Baxendale, I. R.; Ley, S. V. *Org. Lett.* **2010**, *12* (7), 1596–1598.

(9) Hübner, S.; Bentrup, U.; Budde, U.; Lovis, K.; Dietrich, T.; Freitag, A.; Küpper, L.; Jähnisch, K. *Org. Process Res. Dev.* **2009**, *13* (5), 952–960.

(10) Bogdan, A.; McQuade, D. T. *Beilstein J. Org. Chem.* **2009**, *5*.

(11) Schiaffo, C. E.; Dussault, P. H. *J. Org. Chem.* **2008**, *73* (12), 4688–4690.

(12) Willand-Charnley, R.; Dussault, P. H. *J. Org. Chem.* **2013**, *78* (1), 42–47.

(13) Criegee, R. *Angew. Chem. Int. Ed. Engl.* **1975**, *14* (11), 745–752.

(14) Schiaffo, C. I. An Improved Procedure for Alkene Ozonolysis. II. Exploring a New Structural Paradigm for Peroxide Antimalarials., University of Nebraska-Lincoln: Lincoln, NE, 2011.

(15) Kinetichem, Inc http://kinetichem.com/ (accessed Jan 3, 2016).

(16) Fox, B. R.; Brinich, B. L.; Male, J. L.; Hubbard, R. L.; Siddiqui, M. N.; Saleh, T. A.; Tyler, D. R. *Fuel* **2015**, *156*, 142–147.

(17) Ghanem, A.; Lemenand, T.; Della Valle, D.; Peerhossaini, H. *Chem. Eng. Res. Des.* **2014**, *92* (2), 205–228.

(18) Boodhoo, K. In *Process Intensification for Green Chemistry*; Boodhoo, K., Harvey, A., Eds.; John Wiley & Sons, Ltd, 2013; pp 59–90.

(19) Hampton, P. D.; Whealon, M. D.; Roberts, L. M.; Yaeger, A. A.; Boydson, R. *Org. Process Res. Dev.* **2008**, *12* (5), 946–949.

(20) Holl, Richard. *TCE* **2003**, *742*, 32–34.

(21) Sun, B.; Gao, M.; Arowo, M.; Wang, J.; Chen, J.; Meng, H.; Shao, L. *Ind. Eng. Chem. Res.* **2014**, *53* (49), 19071–19076.

(22) Steinfeldt, N.; Abdallah, R.; Dingerdissen, U.; Jähnisch, K. *Org. Process Res. Dev.* **2007**, *11* (6), 1025–1031.

(23) Wada, Y.; Schmidt, M. A.; Jensen, K. F. *Ind. Eng. Chem. Res.* **2006**, *45* (24), 8036–8042.

(24) Roydhouse, M. D.; Motherwell, W. B.; Constantinou, A.; Gavriilidis, A.; Wheeler, R.; Down, K.; Campbell, I. *RSC Adv.* **2013**, *3* (15), 5076–5082.

(25) Bunnelle, W. H. *Chem. Rev.* **1991**, *91* (3), 335–362.

(26) Leonard, J.; Lygo, B.; Procter, G. *Advanced Practical Organic Chemistry, Third Edition*, 3 edition.; CRC Press: Boca Raton, 2013.

(27) Bazhenova, T. A.; Shilov, A. E. *Coord. Chem. Rev.* **1995**, *144*, 69–145.

(28) Leigh, G. J. *J. Organomet. Chem.* **2004**, *689* (24), 3999.

(29) Gilbertson, J. D.; Szymczak, N. K.; Tyler, D. R. *J. Am. Chem. Soc.* **2005**, *127* (29), 10184–10185.

(30) Ciganda, R.; Li, N.; Deraedt, C.; Gatard, S.; Zhao, P.; Salmon, L.; Hernández, R.; Ruiz, J.; Astruc, D. *Chem. Commun.* **2014**, *50* (70), 10126.

(31) Hirao, T. *Redox Systems Under Nano-Space Control*; Springer Science & Business Media, 2006.

(32) Henglein, A. *Chem. Rev.* **1989**, *89* (8), 1861–1873.

(33) Joo, J.; Na, H. B.; Yu, T.; Yu, J. H.; Kim, Y. W.; Wu, F.; Zhang, J. Z.; Hyeon, T. *J. Am. Chem. Soc.* **2003**, *125* (36), 11100–11105.

(34) Leigh, G. J. *Acc. Chem. Res.* **1992**, *25* (4), 177–181.

(35) Armarego, W. L. F.; Chai, C. L. L. *Purification of Laboratory Chemicals*; Elsevier, 2003.

(36) Pirrung, M. C. *The Synthetic Organic Chemist's Companion*; John Wiley & Sons, 2007.

(37) G. M. Sheldrick, *Bruker/Siemens Area Detector Absorption Correction Program*, Bruker AXS, Madison, WI, 1998.

(38) Sheldrick, G. M. *Acta Cryst.* **2008**, *A64*, 112-122.

Appendix A

(1) Armarego, W. L. F.; Chai, C. L. L. *Purification of Laboratory Chemicals*; Elsevier, 2003.

(2) Pirrung, M. C. *The Synthetic Organic Chemist's Companion*; John Wiley & Sons, 2007.

(3) Hoye, T. R.; Eklov, B. M.; Voloshin, M. *Org. Lett.* **2004**, *6*, 2567–2570.

(4) Stankevič, M.; Włodarczyk, A.; Jaklińska, M.; Parcheta, R.; Pietrusiewicz, K. M. *Tetrahedron* **2011**, *67*, 8671–8678.

(5) Bisaro, F.; Gouverneur, V. *Tetrahedron* **2005**, *61*, 2395–2400.

(6) Keglevich, G.; Tamás, A.; Parlagh, G.; Tőke, L. *Heteroat. Chem.* **2001**, *12*, 38–41.

(7) Gray, G. A.; Cremer, S. E.; Marsi, K. L. *J. Am. Chem. Soc.* **1976**, *98*, 2109–2118.

(8) Stankevič, M.; Włodarczyk, A. *Tetrahedron* **2013**, *69*, 73–81.

(9) Simalty, M.; Le Van Chau. *Tetrahedron Lett.* **1970**, *11*, 4371–4373.

(10) Zhuang, R.; Xu, J.; Cai, Z.; Tang, G.; Fang, M.; Zhao, Y. *Org. Lett.* **2011**, *13*, 2110–2113.

(11) Fakhraian, H.; Mirzaei, A. *Org. Process Res. Dev.* **2004**, *8*, 401–404.

(12) Bergin, E.; O'Connor, C. T.; Robinson, S. B.; McGarrigle, E. M.; O'Mahony, C. P.; Gilheany, D. G. *J. Am. Chem. Soc.* **2007**, *129*, 9566–9567.

(13) Renard, P.-Y.; Vayron, P.; Mioskowski, C. *Org. Lett.* **2003**, *5*, 1661–1664.

(14) Canavan, A. E.; Dowden, B. F.; Eaborn, C. *J. Chem. Soc. Resumed* **1962**, 331–334.

(15) Griffith, J. A.; McCauley, D. J.; Barrans, R. E.; Herlinger, A. W. *Synth. Commun.* **1998**, *28*, 4317–4323.

(16) Yang, J.-C.; Gorenstein, D. G. *Tetrahedron* **1987**, *43*, 479–486.

(17) Williams, D. B. G.; Netshiozwi, T. E. *Tetrahedron* **2009**, *65*, 9973–9982.

(18) Yao, Q.; Levchik, S. *Tetrahedron Lett.* **2006**, *47*, 277–281.

(19) Zon, D. G.; Mislow, P. D. K. In *The Chemistry of Organophosphorus Compounds I*; Fortschritte der Chemischen Forschung; Springer Berlin Heidelberg, 1971; pp. 61–94.

(20) Chen, S.-Y.; Zeng, R.-S.; Zou, J.-P.; Asekun, O. T. *J. Org. Chem.* **2014**, *79*, 1449–1453.

(21) Berrino, R.; Cacchi, S.; Fabrizi, G.; Goggiamani, A.; Stabile, P. *Org. Biomol. Chem.* **2010**, *8*, 4518.

(22) Green, A. E.; Agouridas, V.; Deniau, E. *Tetrahedron Lett.* **2013**, *54*, 7078–7079.

(23) Obrycki, R.; Griffin, C. E. *Tetrahedron Lett.* **1966**, *7*, 5049–5052.

(24) Huang, Z.; Chen, Z.; Lim, L. H.; Quang, G. C. P.; Hirao, H.; Zhou, J. (Steve). *Angew. Chem. Int. Ed.* **2013**, *52*, 5807–5812.

(25) Obrycki, R.; Griffin, C. E. *J. Org. Chem.* **1968**, *33*, 632–636.

(26) Farnung, winfried. Process for preparing phosphonic-acid esters, and phosphonic acid derivatives. DE3319795 (A1) Abstract of corresponding document: EP0127876 (A2), December 6, 1984.

(27) Vedejs, E.; Daugulis, O.; Diver, S. T.; Powell, D. R. *J. Org. Chem.* **1998**, *63*, 2338–2341.

(28) Xu, K.; Hu, H.; Yang, F.; Wu, Y. *Eur. J. Org. Chem.* **2013**, *2013*, 319–325.

Appendix B

(1) Hays, H. R. *J Org Chem* **1968**, *33* (10), 3690–3694.

(2) Doyle, L. R.; Heath, A.; Low, C. H.; Ashley, A. E. *Adv. Synth. Catal.* **2014**, *356* (2-3), 603–608.

Appendix C

(1) Dunne, B. J.; Morris, R. B.; Orpen, A. G. *J. Chem. Soc. Dalton Trans.* **1991**, 653–661.

(2) Müller, T. E.; Mingos, D. M. P. *Transit. Met. Chem.* **1995**, *20*, 533–539.

(3) Clavier, H.; Nolan, S. P. *Chem. Commun.* **2010**, *46*, 841–861.

(4) Vuoti, S.; Autio, J.; Laitila, M.; Haukka, M.; Pursiainen, J. *Eur. J. Inorg. Chem.* **2008**, *2008*, 397–407.

(5) Xu, C.; Li, Y.-F.; Wang, Z.-Q.; Cen, F.-F.; Zhang, Y.-Q. *Acta Crystallogr. Sect. E Struct. Rep. Online* **2008**, *64*, m1349–m1349.

(6) Joshua J. Stone, R. A. S. J. *Inorganica Chim. Acta* **2003**, *342*, 236–240.

(7) Jacobson, R. A.; Martin, L. L. *Inorg. Chem.* **1971**, *10*, 1795–1798.

(8) Burgoyne, A. R.; Meijboom, R.; Ogutu, H. *Acta Crystallogr. Sect. E Struct. Rep. Online* **2012**, *68*, m404–m404.

(9) DiMeglio, C. M.; Luck, L. A.; Rithner, C. D.; Rheingold, A. L.; Elcesser, W. L.; Hubbard, J. L.; Bushweller, C. H. *J. Phys. Chem.* **1990**, *94*, 6255–6263.

(10) György Schultz, N. Y. S. *Inorganica Chim. Acta* **1992**, *191*, 85–90.

(11) Woisetschlager, E.; Beck, W.; Polborn, K.; Department Chemie, Universitat Munchen. Private Communication, 2005.

(12) Wisniewska, A.; Baranowska, K.; Pikies, J. *Acta Crystallogr. Sect. E Struct. Rep. Online* **2008**, *64* (Pt 7), m967.

(13) Grushin, V. V.; Bensimon, C.; Alper, H. *Inorg. Chem.* **1994**, *33*, 4804–4806.

(14) Hills, I. D.; Fu, G. C. *J. Am. Chem. Soc.* **2004**, *126*, 13178–13179.

(15) Ferguson, G.; McCrindle, R.; McAlees, A. J.; Parvez, M. *Acta Crystallogr. Sect. B* **1982**, *38*, 2679–2681.

Appendix E

(1) Rakness, K.; Gordon, G.; Langlais, B.; Masschelein, W.; Matsumoto, N.; Richard, Y.; Robson, C. M.; Somiya, I. *Ozone Sci. Eng.* **1996**, *18* (3), 209–229.

(2) Yu, Jing; Chengyong, H.; Minmin, S.; Lianli, D.; Lu, G. *Jingxi Huagong* **2010**, *27* (4), 374–378.

(3) Keul, H.; Kuczkowski, R. L.; Choi, H.-S. *J. Org. Chem.* **1985**, *50* (18), 3365–3371.

(4) Huh, T. S. *Bull. Korean Chem. Soc.* **2000**, *21* (4), 369–370.

(5) Xia, Y.; Liu, Z.; Xiao, Q.; Qu, P.; Ge, R.; Zhang, Y.; Wang, J. *Angew. Chem. Int. Ed.* **2012**, *51* (23), 5714–5717.

(6) Griesbaum, K.; Kim, W. S.; Nakamura, N.; Mori, M.; Nojima, M.; Kusabayashi, S. *J. Org. Chem.* **1990**, *55* (25), 6153–6161.

(7) McCullough, K. J.; Mori, M.; Tabuchi, T.; Yamakoshi, H.; Kusabayashi, S.; Nojima, M. *J. Chem. Soc. [Perkin 1]* **1995**, No. 1, 41–48.

(8) Schank, K.; Beck, H.; Buschlinger, M.; Eder, J.; Heisel, T.; Pistorius, S.; Wagner, C. *Helv. Chim. Acta* **2000**, *83* (4), 801–826.

(9) Lee, K.-R.; Lee, C. W.; Huh, T. S. *Bull. Korean Chem. Soc.* **1999**, *20* (12), 1437–1440.

(10) Lee, C. *Bull. Korean Chem. Soc.* **1999**, *20* (8), 969–972.